Stony Brook University

Drug discovery through combination of computational screening and design, chemical synthesis and biological evaluations

A Dissertation Presented

by

William T. Berger

to

The Graduate School

in Partial Fulfillment of the

Requirements

for the Degree of

Doctor of Philosophy

in

Chemistry

Stony Brook University

December 2013

Stony Brook University

The Graduate School

William T. Berger

We, the dissertation committee for the above candidate for the

Doctor of Philosophy degree, hereby recommend

acceptance of this dissertation.

Iwao Ojima – Dissertation Advisor
Distinguished Professor – Department of Chemistry

Carlos Simmerling - Chairperson of Defense
Professor – Department of Chemistry

Elizabeth Boon – 3rd Member
Associate Professor – Department of Chemistry

Dale G. Deutsch – Outside Member
Professor – Department of Biochemistry and Cellular Biology
Stony Brook University, Stony Brook, New York

This dissertation is accepted by the Graduate School

Charles Taber
Dean of the Graduate School

Abstract of the Dissertation

Drug discovery through combination of computational screening and design, chemical synthesis and biological evaluations

by

William T. Berger

Doctor of Philosophy

in

Chemistry

Stony Brook University

2013

A long-standing problem with the use of conventional cancer chemotherapy is the inherent lack of tumor specificity. Tumor-targeting drug-delivery systems (TTDS) have since been explored to overcome this deficiency. These drug conjugates can deliver potent cytotoxic drugs specifically to tumors and tumor cells with minimal systemic toxicity. Among various tumor-targeting molecules discussed, Designed Ankyrin Repeat Proteins (DARPins) represent a new approach to tumor targeting. In particular, DARPins targeting CD326 Epithelial Cell Adhesion Molecule (EpCAM) receptors provide an effective cancer target, as EpCAM is critical to the regulation of cellular matrix composition and overall cancer aggressiveness.

Botulism is a human illness caused by the bacterium *Clostridium botulinum* which results in fatal flaccid paralysis and eventual respiratory failure. *Clostridium botulinum* produces botulinum neurotoxins (BotNTs), which by themselves are considered by the CDC to be potential Category A bioterrorism weapons. The light chain protease domain of BotNTs efficiently cleaves SNARE proteins which in turn regulates neurotransmitter release in motor neurons, resulting in the inhibition of neuronal transmission. Discussed is the use of a novel footprint-based virtual screening to identify compounds with inhibitory activity against BotNTA-LC catalytic activity.

Fatty acid binding proteins (FABPs), have recently been identified as intracellular transporters for the endocannabinoid anadamide (AEA). Furthermore, animal studies by others have shown that elevated levels of endocannabinoids result in beneficial pharmacological effects on stress, pain and inflammation and also ameliorate the effects of drug withdrawal. Accordingly a novel α-truxillic acid derivative (SB-FI-26) was synthesized and assayed for its inhibitory activity against FABP5. Additionally, we found SB-FI-26 to act as a potent anti-nociceptive agent with mild anti-inflammatory activity in mice, which strongly supports our hypothesis that the inhibition of FABPs and subsequent elevation of anandamide is a promising new approach in drug discovery.

Table of Contents

Chapter 5: Development of Novel Small Molecule Inhibitors of Botulinum Neurotoxin A

Chapter 6: Targeting Fatty Acid Binding Protein (FABP) Anandamide Transport – A Novel Therapy for the Management of Pain and Inflammation

Appendixes

List of Figures

Figure Page

Chapter 1

Chapter 2

Chapter 3

Chapter 4

Chapter 5

Chapter 6

List of Schemes

Schemes Page

Chapter 1

Chapter 2

Chapter 3

Chapter 4

Chapter 5

Chapter 6

List of Tables

Tables Page

Chapter 1

Chapter 2

Chapter 3

Chapter 4

Chapter 5

Chapter 6

List of Equations

Equations Page

Chapter 2

List of Abbreviations

10-DAB III	10-Deacetylbaccatin III
°C	Degrees Celsius
µM	Micromolar
AEA	Anandamide
Ac	Acetyl
Arg	Arginine
Asp	Asparagine
ATP	Adenosine triphosphate
BotNT	Botulinum Neurotoxin
BOC	*tert*-Butyl carbonate
Bu	Butyl
BuLi	Butyl lithium
CAN	Ceric ammonium nitrate
CDI	Carbonyl-di-imidazole
CFM	Confocal microscopy
CSC	Cancer stem cell
D	Day
DCC	N,N'-Dicyclohexylcabodiimide
DCM	dichloromethane
DHA	Docosahexaenoic acid
DIC	Diisopropylcarbodiimide
DIPEA	N,N-Diisopropylethylamine
DMAP	4-Dimethylaminopyridine
DMF	Dimethylformamide
DMSO	Dimethyl sulfoxide
DNA	Deoxyribonucleic acid
DPBS	Dulbecco's Phosphate buffered saline
DR	Dorsal Raphe
EC50	Half maximal effective inhibitory concentration
EDC	1-Ethyl-3-(3-dimethylaminopropyl)carbodiimide
ee	Enantiomeric excess
EpCAM	Epithelial Cell Adhesion Molecule
EPSC	Excitatory postsynaptic current
ES	Electrostatic Energy (kilocalories per mole)
Et	Ethyl
EtOH	Ethanol
FA	Folic acid
FAAH	Fatty Acid Amid Hydrolase
FABP	Fatty Acid Binding Protein

FACS	Fluorescence-activated cell sorting
FBS	Fetal Bovine Serum
FDA	Food and drug administration
FITC	Fluorescein isothiocyanate
FR	Folate receptor
g	Gram
Glu	Glutamic acid
Gly	Glycine
gp60	glycoprotein 60
GSH	Glutathione
GSH-OEt	Glutathione ethyl ester
GTP	Guanosine-5'-triphosphate
h	Hours
HEPES	4-(2-hydroxyethyl)-1-piperazineethanesulfonic acid
HOAc	Acetic acid
HOSu/NHS	N-Hydroxysuccinimide
HPLC	High-performance liquid chromatography
HSA	Human serum albumin
Hz	Hertz
IC50	Half maximal inhibitory concentration
Ig	Immunoglobin
IPA	Isopropanol
k	Kilo
KOH	Potassium hydroxide
L	Liter
Leu	Leucine
LiHMDS	Lithium bis(trimethylsilyl)amide and lithium hexamethyldisilazide
LNA	α-Linolenic acid
Lys	Lysine
m	Meter
mAbs	Monoclonal antibodies
MALDI	Matrix-assisted laser desoprtion/ionization
MDR	Multidrug resistance
Me	Methyl
mM	Millimolar
mg	Milligram
MHz	Megahertz
min	Minutes
mL	Milliliter
mmol	Millimole

m.p.	Melting point
MTT	3-(4,5-Dimethylthiazol-2-yl)-2,5-diphenyltetrazolium bromide
NaH	Sodium Hydride
NaHMDS	Sodium bis(trimethylsilyl)amide and lithium hexamethyldisilazide
NCI	National Cancer Institute
nM	Nanomolar
NMR	Nuclear magnetic resonance
NSCLC	Non-small-cell lung carcinoma
PBS	Phosphate buffer solution
PEG	Polyethylene glycol
Pgp	P-glycoprotein
Ph	Phenyl
Phe	Phenylalanine
pM	Picomolar
PMA	Phosphomolybdic acid
PMP	*p*-Methoxyphenyl
pr	Propyl
PUFA	Polyunsaturated fatty acid
py	Pyridine
r.t.	Room temperature
RME	Receptor-mediated endocytosis
RPMI	Roswell Park Memorial Institute medium
s	Seconds
SAR	Structure-activity relationship
SB-FI	Stony Brook Fatty Acid Binding Protein Inhibitor
SB-T	Stony Brook taxoid
scFv	Single-chain variable fragment
SCID	Severe combined immune deficiency
SNAP-25	Synaptosomal-associated protein 25
SNARE	Soluble N-ethylmaleimide-sensitive factor Attachment Protein Receptor
TEA	Triethylamine
TES	Triethylsilyl
TESCl	Triethylsilyl chloride
TFA	Trifluoroacetic acid
THF	Tetrahydrofuran
TIPS	Triisopropyl
TLC	Thin layer chromatography
TIPS	Triisopropylsilyl
TIPSCl	Triisopropylsilyl chloride
TTM	Tumor-targeting module

µL	Microliter
µM	Micromolar
Val	Valine
VDW	Van der Waals Energy (kilocalories per mole)

Acknowledgments

First and foremost, I would like to thank my advisor, Distinguished Professor Iwao Ojima for giving me the opportunity to work with him on such a multitude of amazing projects. Professor Ojima has broadened my horizons, and personally has taught me what to expect from science and from myself. I thank him for sharing his knowledge and his wisdom and especially his company. Additionally, I would like to thank Mrs. Yoko Ojima for all the hospitality that she has shown over the years.

I would also like to thank my committee members, Professor Simmerling, and Professor Boon. I am truly lucky to have your insight on my committee.

I would like to thank my outside member Professor Deutsch who has inspired me in many ways and was gracious enough to be my outside member.

I would also like to thank Pat Marinaccio who always provided great emotional support throughout my ups and downs.

I would like to thank my colleagues. First and foremost, I would like to thank Professor Rizzo for welcoming me into his lab and group meetings. Without his help I would not have been able to finish my most significant projects. From the Rizzo laboratory, I would also like to thank Dr. Trent Balius and Dr. Sudipto Mukherjee for giving me insight and inspiring me to be a better computational chemist. From the Deutsch laboratory, I would like to thank Dr. Martin Kaczocha who inspired many of us not to overlook FABPs and has provided to best feedback of any person I know. From the Ojima laboratory, I would like to thank Dr. Eduard Melief who tirelessly helped me when my chemical biology skills needed a boost. I would also like to thank my group members: Joshua Seitz, Manisha Das, Edison Zuniga, Jacob Vineberg, Tao Wang, Longfei Wei (Cancer Team); Dr. Kunal Kumar, Divya Awasthi, Bora Park, Krupa Haranahalli, Simon Tong (TB Team); Gary Teng (FABP Team); Chih-Wei Chien, and Chi-Feng Lin.

Lastly, I would like to thank my wife Margaret, my family, and my friends for their emotional support.

Chapter 1

Second Generation Taxoid SB-T-1214 and the β-Lactam Synthon Method

Content

§1.0 Introduction:

§1.0.1 Cancer and Chemotherapy:

Despite advances in medicine, cancer continues to remain a major health concern throughout the world. In a 2005 study, cancer ranked 2nd among the leading causes of death in the US, exceeded only by heart disease.[1] Nonetheless, cancer related deaths have remained consistent, while heart disease mortality has declined over the past 30 years. Significant advances in cardiovascular medicine and nutritional awareness have contributed greatly to this decline, while treatments for cancer have remained only modestly effective. An estimated 1.44 million new cancer patients were recorded in the U.S. in 2008, an increase from 1.39 million in 2006.[2] What remains clear, is there will be a continual need to understand and develop effective treatments for cancer.

The collection of diseases referred to as cancer originates typically from both external (foreign substances, radiation damage, viruses, etc) as well as internal contributors (mutations, immune deficiencies, etc) which ultimately affect proper cell functionality. Among the many cellular abnormalities include, a dysregulation of growth signaling, altered apoptosis signaling, and amplified and uncontrolled replication.[3] Furthermore, cancer cells promote their cellular dysfunction by means of angiogenesis, metastasis, and the proliferation of normal tissues. Several of these intricate processes have been the focus of recent cancer research in an effort to limit the growth and spread of cancerous cells.

Specifically, cancer progression typically develops in a stepwise fashion. Cancer begins with the formation of agglomerates of abnormal cells inside normal tissues as shown in **Figure 1-1**.[4, 5] This benign mass, commonly referred to as a tumor, remains encapsulated by a membrane isolating it from the rest of the body. At this early stage of progression, the most effective treatment is typically surgery, but as time progresses; membrane rupture ensues leading to the invasion of surrounding tissues. The infiltration of healthy tissue is further exacerbated by the ability of cancer cells to actively promote angiogenesis, which both aids to increase the availability of nutrients to these rapidly dividing cells, and also to serve as a route for these malignant cells to invade both the lymphatic and circulatory systems. This process is promoted by the breakdown of the cellular matrix as malignant cells from the original tumor site can travel dormant in circulation until finally settling in a suitable niche environment. Once settled, these metastatic cells can proliferate healthy tissues in the surrounding environment leading to a disruption in normal organ function and eventually death.

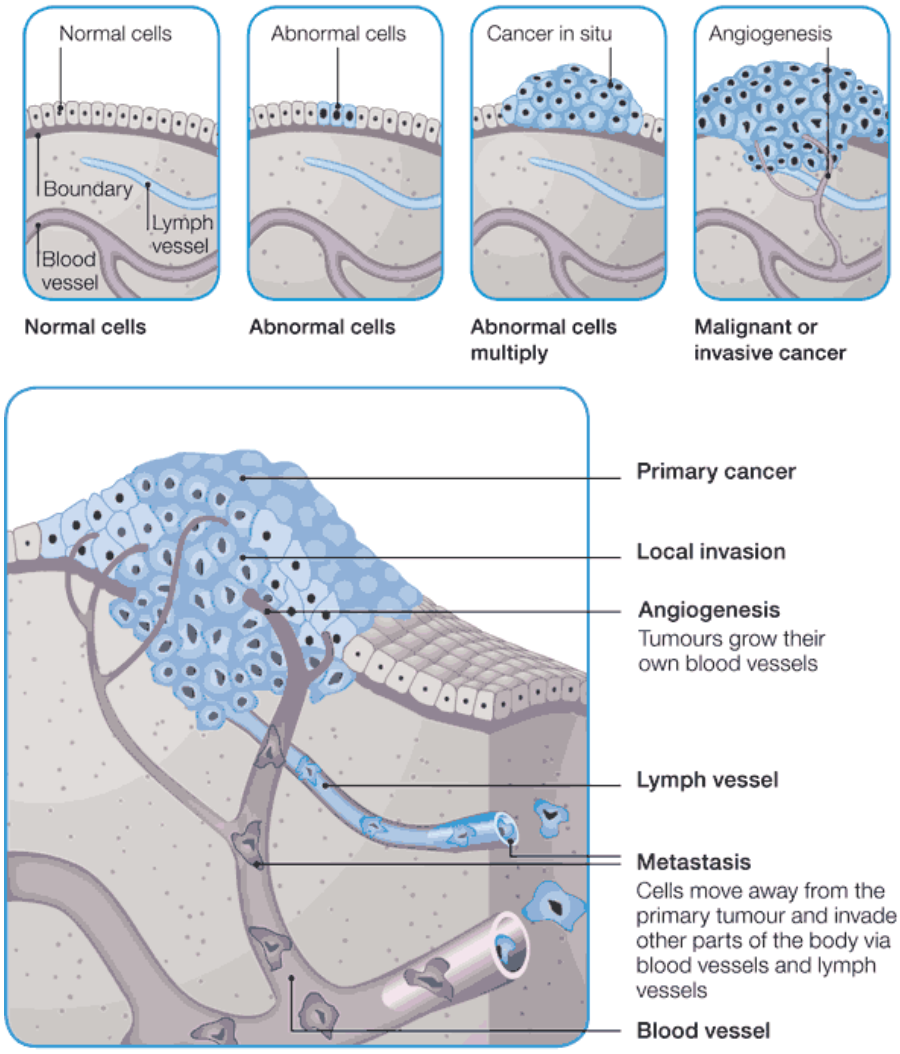

Figure 1-1: Cancer progression. Above shows the transformation of a normal cell to a primary tumor mass. Below highlight metastasis of the primary tumor mass into the local lymphatic and circulatory systems. (Reprinted with permission from [4-5]. Copyright Cancer Council Victoria)

Due to the many stages of cancer progression, cancer diagnosis has been divided into several different stages, ranging from stage 0 to IV.[6] These different stages are determined using the TNM system, which encompasses (T) or the extent and size of the primary tumor (T1, T2, T3, T4), (N) or the extent of lymphatic invasion (N1, N2, N3), and (M) or the detection of distant metastasis. However, criteria for each stage are strongly depended on the type of cancer being diagnosed.

Among the various cancer treatment options include surgery, radiation therapy, chemotherapy, and immunotherapy. Typically, treatment will depend on the type and stage of cancer progression; however, most regiments include a combination of two or more of the above

treatment options. Recently, the field of chemotherapy has made significant progress by both increasing potency and specificity of drugs employed.

Chemotherapy is defined as the treatment of cancer by use of antineoplastic drugs, or more explicitly, the inhibition of the development or growth of malignant cells. In order to effect the development and growth of malignant cells specifically, chemotherapy relies on the inherent differences between malignant and normal systemic cells. Due to the fast growth rate of cancer cells, the rate of cellular uptake is enhanced making them susceptible to these antineoplastic drugs. Unfortunately, other non-malignant cells that replicate quite frequently such as bone marrow cells, epithelial cells, and hair follicle cells also fall victim to antineoplastic drugs. Due to this unfortunate fact, chemotherapy has also been known for its various side effects which include hair loss, nausea and vomiting, diarrhea or constipation, anemia, and depression of the immune system. Recently, research has shown promising results in targeting drug delivery, reducing the side effects associated with chemotherapeutics.

Chemotherapy often leads to semi-effective treatment, typically resulting in episodes of remission and reoccurrence rather than complete recovery. Therefore, continued use of chemotherapeutics often lead to cases of (MDR) multi-drug resistance. Commonly, malignant cells begin to react to the structure and activity of a drug, desensitizing the cell and reducing overall drug efficacy. Thus, chemotherapeutic drugs that can overcome MDR have been researched quite extensively.

The choice of chemotherapeutic drugs can vary greatly on the cancer type. Cocktails of several drugs are commonly used to benefit from synergistic effects. Thus, the market has warranted the investigation and discovery of several different types of chemotherapeutic agents. Among these include DNA alkylating agents (*e.g.* cisplatin), antimatabolites (*e.g.* mercaptopurine), anthracyclines (*e.g.* doxorubicin), plant alkaloids (*e.g.* vinca alkaloids, taxanes), topoisomerase inhibitors (*e.g.* camptothecin, teniposide), antitumor antibiotics (*e.g.* dactinomycin), and kinase inhibitors (*e.g.* erlotinib). In particular, paclitaxel and the second generation taxoid SB-T-1214 will be discussed.

§1.0.2 Taxol® Discovery and the Development of New Generation Taxoids:

Taxol® (paclitaxel) was one of the first chemotherapeutic drugs marketed commercially for the treatment of cancer and still remains as a relevant choice for chemotherapy today. This taxoids origins can be traced back to the 1950's, when the U.S. National Cancer Institute (NCI) initiated a program to find anticancer plants in 35,000 species.[7] In 1963-64, extracts of the bark from the Pacific Yew tree, *Taxus brevifolia*, were shown to possess significant cytotoxicity towards leukemic cells.[8] It was later discovered that the active chemical responsible for this cytotoxic property was the diterpenoid Taxol® shown in **Figure 1-2**. In 1992, Bristol-Myers-Squibb (BMS) commercialized Taxol® as an injectable drug formulation. The names Taxol® and paclitaxel thereafter have been used interchangeably in literature. Following commercialization, paclitaxel was approved by the U.S. Food and Drug Administration (FDA) for breast cancer (1994), Kaposi's sarcoma (1997), and lung cancer (1998). Ongoing clinical trials are still in progress for additional cancer treatments.

Prior to commercialization, supply of paclitaxel provided to be severely problematic. The bark of the Pacific Yew tree continued to be the only source of this molecule and extraction yielded only small quantities, not relevant for cancer treatment.[8] Specifically, paclitaxel could only be isolated at 1 kg per 9100 kg of bark. Additionally, this cultivation process killed the tree. Thus a significant supply issue emerged and scientists looked towards fully synthetic means. Unfortunately synthetic routes provided to be just as challenging, requiring complex synthesis of paclitaxel's stereoselective β-phenylisoserine side chain and unique oxetane ring. Ultimately, total synthesis did not provide to be cost effective for practical application. Thus, a desire to develop semi-synthetic approaches emerged, which will be discussed later in this chapter.

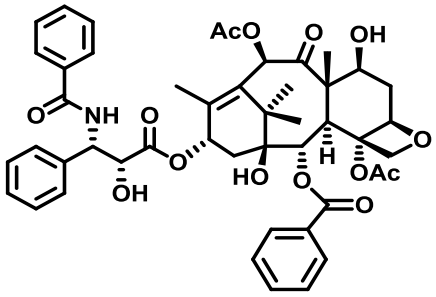

Figure 1-2. The structure of Taxol® (paclitaxel)

§1.0.2.1 Taxol® Mechanism of Action:

In 1979, Horwitz and co-workers reported that paclitaxel acted on tubulin, disrupting mitotic cell division.[9] Specifically, paclitaxel blocked cell division in the G_2 / M phase of the cell cycle (Anaphase) as shown in **Figure 1-3**. This effect was a result of the promotion and over-stabilization of protofilaments by paclitaxel. Ultimately, this resulted in more compact and stabilized microtubules. At the time, this unique mechanism of action was quite revolutionary as previously known spindle toxins such as vinca alkaloids and podophyllotoxins were known to inhibit tubulin polymerization rather than stabilize it.

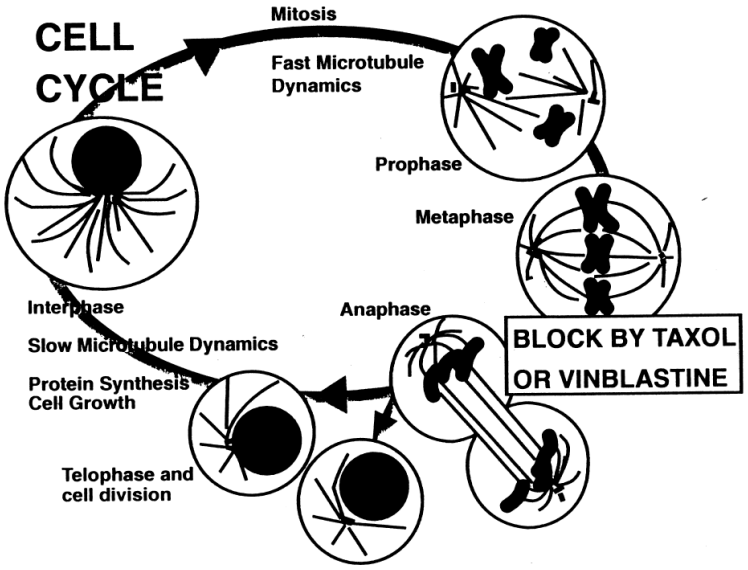

Figure 1-3: The effects of paclitaxel on the cell cycle (Reprinted with permission from [7]. Copyright (1995) American Chemical Society.)

In 1996, it was discovered that the asynchronous cell cycle induced by altered microtubule dynamics could induce apoptosis.[10] Traditionally, it was thought that cancer cells could recover from exposure to small concentrations of paclitaxel, due to its reversible binding. On the contrary, it was evident from experiments that small concentrations of paclitaxel induced cellular changes that were not initially considered. Specifically, it was observed that paclitaxel treated cells reverted to interphase precluding anaphase or cytokinesis. Furthermore, the nuclear membranes of these cells were observed to reform, producing multinucleated cells. Research by Wang and co-workers has recently suggested a signaling pathway responsible for this asynchronous cell cycle effect, triggered by p53 shown in **Figure 1-4**.[11]

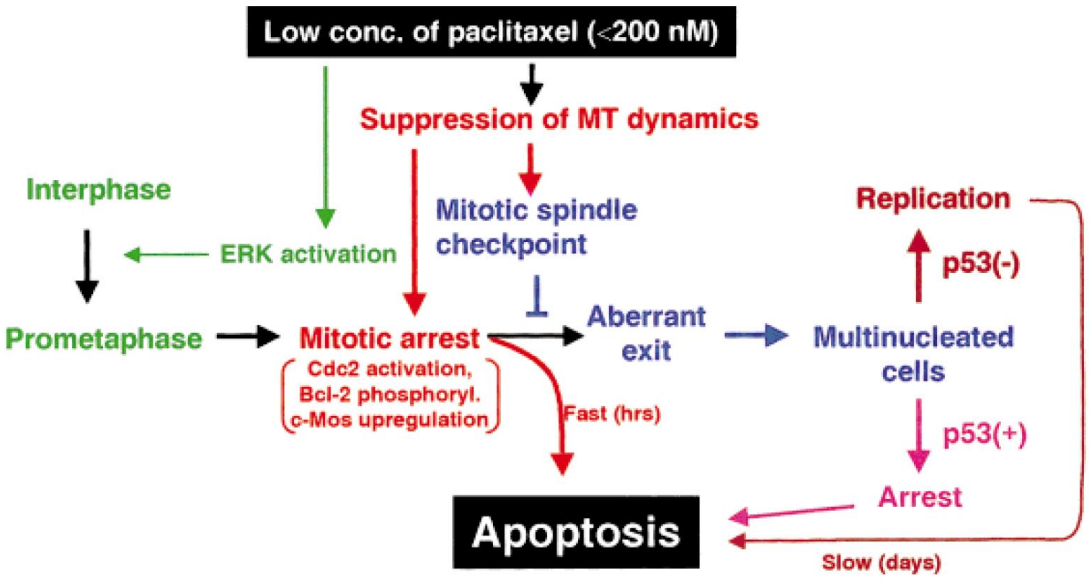

Figure 1-4: Proposed mechanism describing the connection of apoptosis and asynchronous cell cycle (Reprinted with permission from reference [11])

Recent elucidation of the p53 and p21 pathways associated in paclitaxel induced apoptosis have been conducted.[12] Paclitaxel has been shown to activate the Fas-associated death domain protein (FADD). FADD in turn has been shown to activate the signaling cascade of caspase-10, producing caspase-6, which in turn can cleave several regulatory proteins. Upon cleavage of these proteins, activation of p53 and p21 proteins has been shown to initiate apoptosis.

§1.0.2.2 Microtubule Dynamics:

To acquire a deeper understanding of how paclitaxel interacted with microtubules, specifically binding of paclitaxel to tubulin, extensive efforts were expended to understand the dynamics of microtubules. In 1977, it was reported that microtubules were composed of smaller protein building blocks α-tubulin and β-tubulin containing the hydrolysable nucleotide Guanosine Tri-phosphate (GTP).[13] It was found that α and β monomers of tubulin formed hetero-dimer complexes which were confirmed by cross-linking experiments. After hetero-dimer formation, (α/β) hetero-dimers could associate by hydrolyzing GTP mediated by Mg^{2+} and microtubule-associated proteins (MAPs) forming macromolecular protofilament structures. Protofilaments could then associate to form even larger microtubule structures. Specifically, each microtubule structure was composed of 13 protofilament structures, shown in **Figure 1-5**.

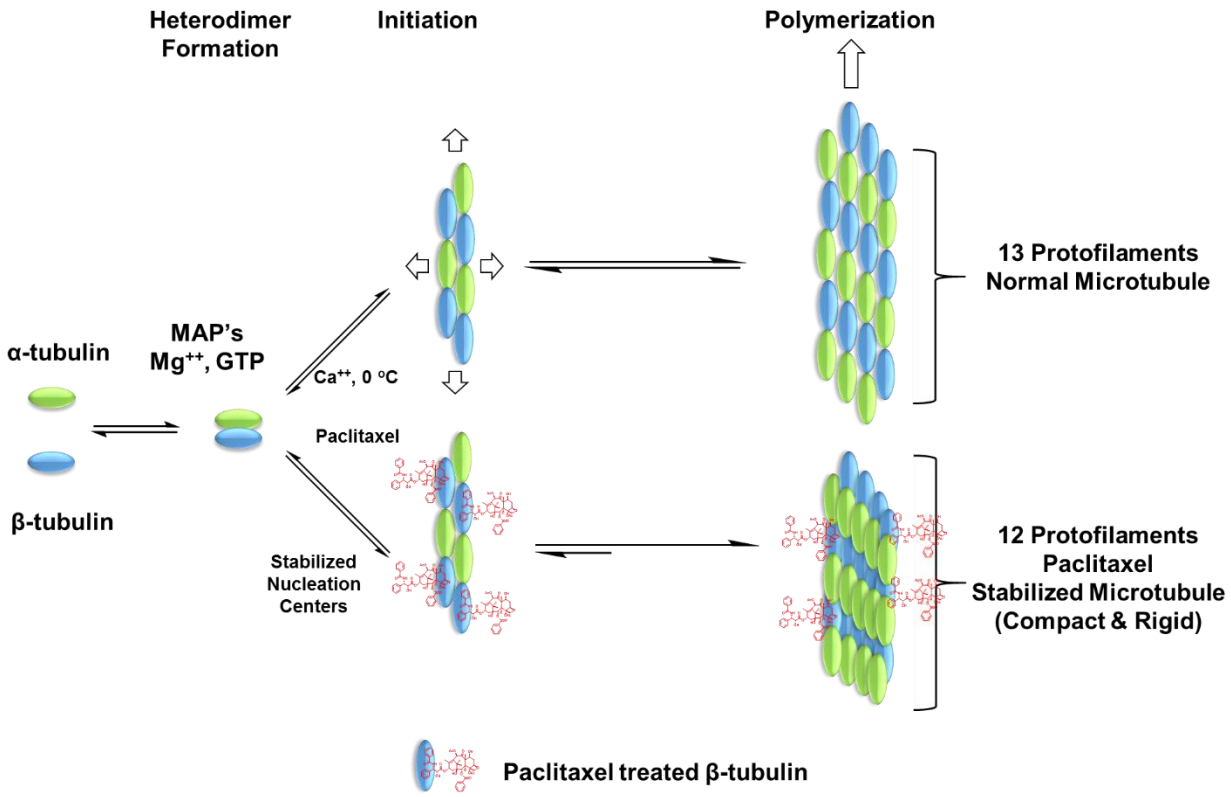

Figure 1-5: Microtubule dynamics with and without paclitaxel (Adapted from reference [14])

Further investigation in 1984 revealed the mechanistic nature of these biological structures.[14] Microtubules were found to be dynamic in nature and were shown to grow and shrink rapidly, termed "Dynamic Instability". Specifically, this process was found to be concentration dependent, as it was found that the cell could manipulate the length of its microtubules based on the rate of GTP hydrolysis.

Horwitz and co-workers recognized paclitaxel's role in promoting and stabilizing tubulin polymerization and microtubule assembly.[15, 16] Unlike typical microtubule formation, in the presence of paclitaxel, protofilaments would form much faster and promote more stable structures. Ultimately, this translated to promoting more tightly packed microtubules consisting of 12 protofilaments. Even in depolymerization conditions (4 ^{o}C or 4 mM $CaCl_2$ solution), microtubules formed in the presence of paclitaxel remained intact.

§1.0.2.3 Taxol® Binding and Effects on Microtubules:

Although the association of microtubules and paclitaxel has been known since Horwitz's first experiments in 1979, the binding site of paclitaxel had remained unclear until 1995.[17]

Utilizing electron diffraction, crude images of paclitaxel bound to tubulin were constructed. From these images, it was proposed that paclitaxel bound preferentially to β-tubulin. However, the coarseness of these electron diffraction images could not yield definitive binding information. Thus, the specific binding mode of paclitaxel has still remained a debate even in current literature.

In 1998, a more detailed 3.7Å electron diffraction image of tubulin was produced with paclitaxel bound.[18] From this structure several things were deduced. First, paclitaxel indeed was definitively bound to β-tubulin as seen in **Figure 1-6**. Secondly, the GTP-cap held the GDP-hydrolyzed hetero-dimers locked into a GTP-like conformation. Third, upon hydrolysis of the cap, strain contained within the GDP-matrix was relieved driving rapid depolymerization as seen in **Figure 1-7**.[19] Conversely, when treated with paclitaxel, protofilament stabilization of the GDP-bound hetero-dimer led to overall stability regardless of the status of the GTP-cap. Thus, this unnatural stabilization by paclitaxel provided the driving force behind microtubule stability ultimately leading to altered "Dynamic Instability".

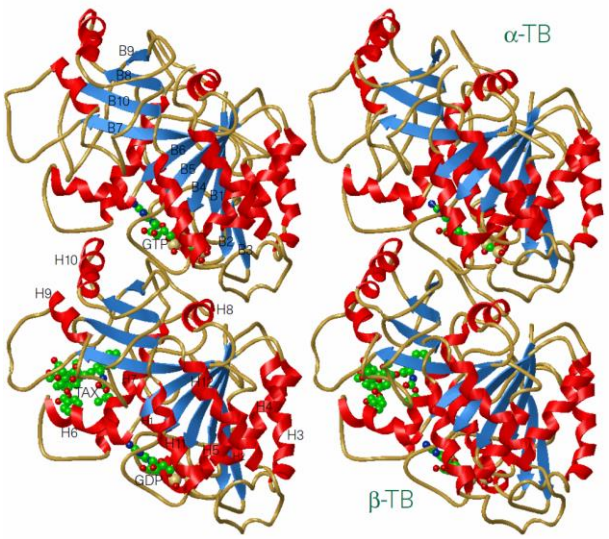

Figure 1-6: First electron diffraction image of paclitaxel bound to β-tubulin (Reprinted with permission from reference [19])

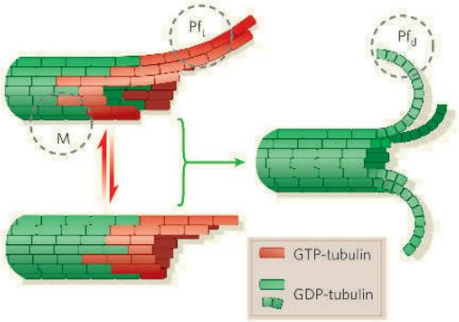

Figure 1-7: Strained microtubule model (Reprinted with permission from reference [20])

§1.0.2.4 Development of Semi-Synthetic Approaches to Taxol® and Taxotere®:

As previously stated, before 1988, paclitaxel could only be isolated naturally from the non-renewable bark of the *T. brevifolia* at 1 kg per 9100 kg of bark. Thus, the commercial application of paclitaxel appeared infeasible. As a response to this problem, various total synthesis were published including Holton,[20] Nicolaou,[21-24] Danishefsky,[25] Wender,[26, 27] Kuwajima,[28] Makaiyama,[29] and a recent racemic version by Takahashi.[30]. However, none of these fully synthetic routes could produce sufficient quantities to make total synthesis of paclitaxel a viable option. Fortunately, nature provided chemists with an important building block, 10-deacetylbacctin III, which subsequently led to several efficient semi-synthetic methodologies.

In 1981, 10-deacetylbaccatin III (10-DAB III) shown in **Figure 1-8** was isolated as a natural product from the leaves of the European yew (*Taxus baccata*) in modest quantities (1 g / 1 kg of leaves).[31] Furthermore, cultivation of the leaves did not result in the death of the tree and thus provided a renewable source of 10-DAB III. Thus with the ability to isolate large and renewable quantities of the 10-deacetylbaccatin III, extensive research efforts by several research laboratories were expended for the efficient semi-synthetic of paclitaxel from 10-DAB III.

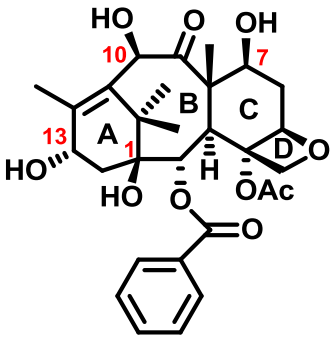

Figure 1-8: Structure of de-acetyl-baccatin III (10-DAB III)

In 1988, the first semi-synthetic route was published by Greene and Potier shown in **Scheme 1-1**.[32] Greene and Potier's approach to semi-synthesis was focused on the use of a direct carboxylic acid/alcohol esterification at the C-13 position of 7-TES-baccatin III with (2R,3S)-N-benzoyl-3-phenylisoserine. Their research revealed that the four hydroxyl groups of 10-DAB III had significantly different reactivities. Upon acetylation, 10-DAB III yielded exclusively the C-7 acetylated product. Therefore, protection of the C-7 was explored. Under certain conditions, triethylsilyation of the C-7 was selective with yields ranging from 84 to 86 %. After protection of the C-7 alcohol, selective acetylation at the C-10 position was accomplished with yields around

86 %. These initial steps are still used today in the semi-synthesis of paclitaxel and other analogues; however, the sterically hindered C-13 alcohol still provides quite cumbersome to esterification.

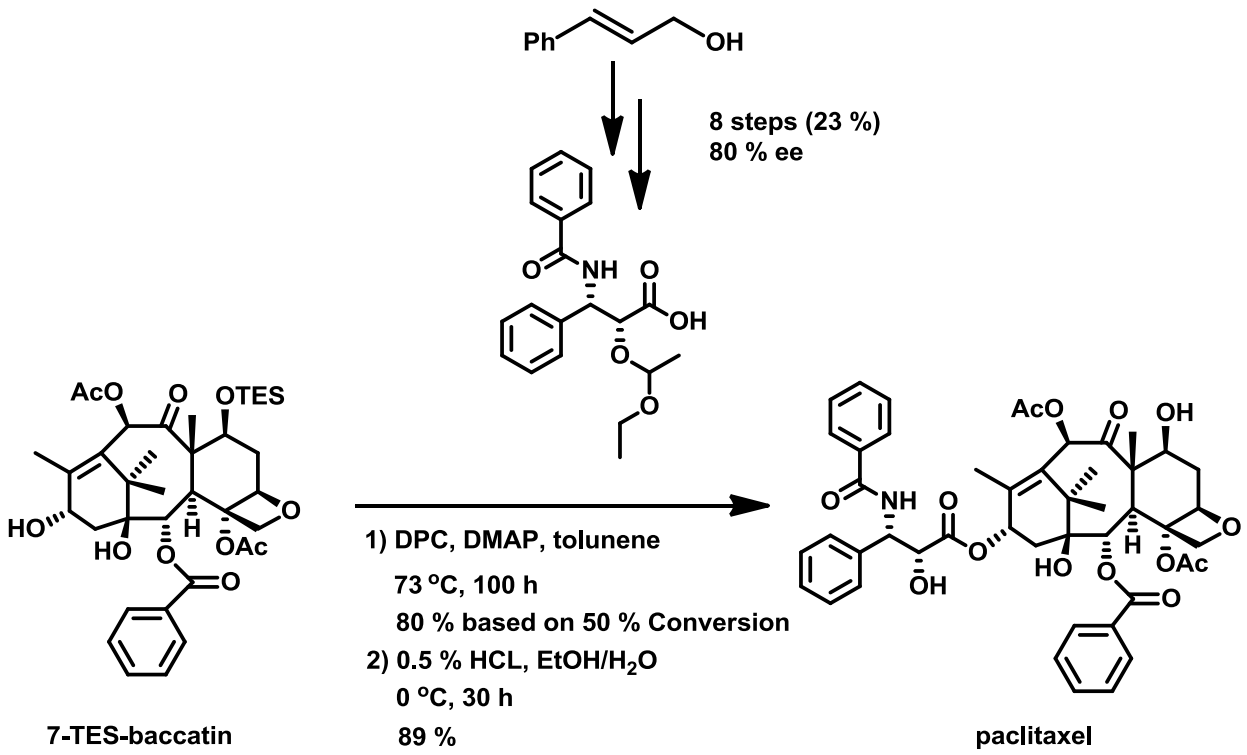

Scheme 1-1: First semi-synthesis protocol design by Potier and Greene[32]

Due to the inverted cup-shape structural geometry of the baccatin core, coupling to the C-13 alcohol provided to be quite challenging. The resulting steric hindrance encountered by the electrophile at C-13 severely limited this reaction, providing paclitaxel in only 80 % yield based on a 50 % conversion after 100 hours. Unfortunately, epimerization at C-2' was also found to be significant due to the long and harsh conditions used.

In addition to significant epimerization during esterification, the synthesis of enantiopure (2R,3S)-N-benzoyl-3-phenylisoserine was also quite challenging. In fact, Greene and Potier could only afford this critical component of paclitaxel semi-synthesis in 23 % yield after 8 steps with only a modest 80 % enantiomeric excess. In the early 1990's, Greene was able to improve this enantiomeric excess to 98 % using Sharpless dihydroxylation. The initial product itself formed after the dihydroxylation did not possess high enantiomeric purity, but enrichment by

recrystallization from hexanes and DCM could afford the side chains of Taxol® and Taxotre® in moderate yields and excellent enantiopurity.[33]

Following Greene and Potier's synthetic coupling scheme, much effort was focused on the asymmetric synthesis of the critical component of paclitaxel semi-synthesis, the (2R,3S)-N-benzoyl-3-phenylisoserine side chain. These include ligand directed Sharpless dihydroxylation,[34] Sharpless and Jocobsen asymmetric epoxidation,[35, 36] Chen's enzymatic trans-esterification,[37] the Hanaoka aldol reaction,[38] Sharpless asymmetric aminohydroxylation,[39] and the Kobayashi's chiral Lewis acid catalyzed Mannich-type reaction.[40] Unfortunately, epimerization forced groups to search for alternative routes to replace the C-13 coupling *via* carboxylic acid/alcohol direct esterification.

An alternative to carboxylic acid coupling, the strained β-lactam four member ring provided to be a critically important structure for paclitaxel synthesis. In 1990, Holton and co-workers reported that (*3R,4S*)-*N*-benzol-3-*O*-(1'-ethoxylethoxyl)-4-phenylazetidin-2-one could be coupled to 7-TES-baccatin III in the presence of pyridine and DMAP catalyst in 92 % in 12 hours as shown in **Scheme 1-2**.[41] This novel coupling provided the C-13 side chain with proper stereochemistry and no epimerization. However, this new strategy had its own advantages and disadvantages. Although this β-lactam coupling strategy provided a solution to epimerization, the slow reaction rate and large excess of β-lactam required limited its practicality.

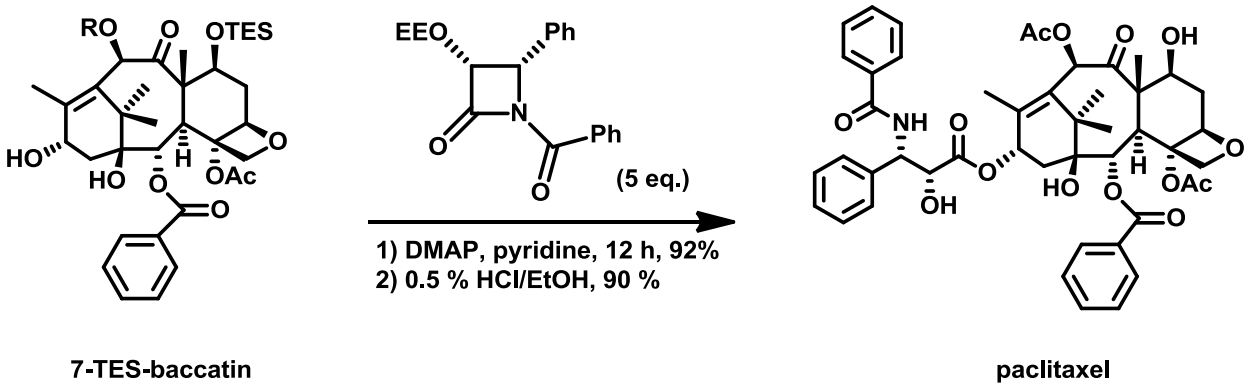

Scheme 1-2: First approach to β-lactam coupling by the Holton laboratory[41]

In 1992, Ojima and co-workers reported a more efficient approached to coupling highly enantiopure β-lactam to the C-13 side chain 7-TES-baccatin III termed the "*β-lactam Synthon Method* (β-LSM)" shown in **Scheme 1-3**.[42-44] Using a strong base at low temperatures it was discovered that the coupling of β-lactam could be accomplished in 85 to 93 % yield with only a slight excess of β-lactam in 30 minutes. This discovery was determined by screening a number of

strong bases such as NaH, *n*-BuLi, LDA, LiHMDS, NaHMDS, providing NaHMDS as the best at - 30 ^{o}C. In addition, an additional benefit to the β-LSM over Holton coupling was its capacity to accommodate more sterically hindered protection groups at the C-3' alcohol, such as TIPS. Furthermore, TIPS was found to be critical for the formation of highly enantioselective β-lactams' *via* chiral enolate – imine cyclocondensation. It was through this method of β-lactam synthesis and coupling that enabled paclitaxel to be explored by SAR to yield potentially more efficient new generation taxoids discussed later in this chapter.

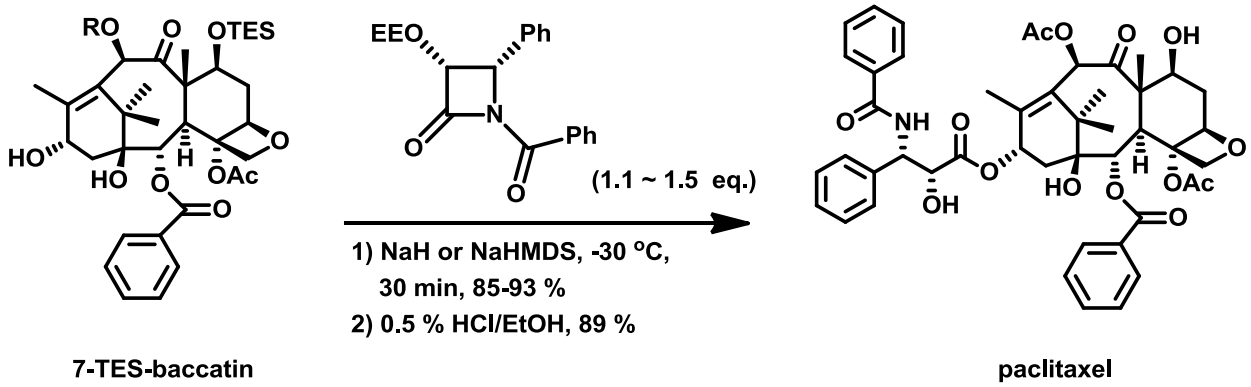

Scheme 1-3: Improved β-lactam coupling by the Ojima laboratory[42-44]

§1.0.2.5 Structure Activity Relationship (SAR) Studies and the Discovery of 2nd Generation Taxoid SB-T-1214:

In the early 1990's, with a reliable method to produce both Taxol® and Taxotere® shown in **Figure 1-9** in hand, the exploration of chemical space became a new frontier for paclitaxel research and development.[45] This new direction in paclitaxel research was indeed important due to the emergence of MDR to both Taxol® and Taxotere®. Specifically the varying degree of MDR seen between these two known taxanes.[46]

In response to MDR seen in various cancer cell lines, Ojima and co-workers design new synthetic taxoids. One of the first modifications made was to C3' position.[47] It was found that BOC replacement of phenyl moiety protecting the C3' amine as well as C3' isobutenyl replacement significantly increased the efficacy of taxoids especially in MDR breast cancer cell lines. In particular, Stony Brook taxoid 1212 (SB-T-1212) shown in **Figure 1-10** was found to exhibit sub-nanomolar activity against drug sensitive cancer cell lines A121 (ovarian), A549 (NSCLC), HT-29 (colon) and MCF7 (breast). Additionally, SB-T-1212 had substantial activity against drug resistant cell line MCF7R, a significant improvement over Taxol® and Taxotere® shown in **Table 1-1**.

Due to the success of the C3' modification of taxoid SB-T-1212 in both drug sensitive and resistant cell lines, exploration of the C-10 position of 10-DAB III was explored as shown in **Figure 1-10**. In 1996, it was reported that by replacing the acetyl moiety with cyclopropanecarbonyl, potency of taxanes could be even further increased as shown in **Table 1-1**.[48] Specifically, SB-T-1214 showed 6 times more potency against the MDR MCF7 cell line due to its ability to evade efflux most notably by p-glycoprotein (Pgp).[48, 49]

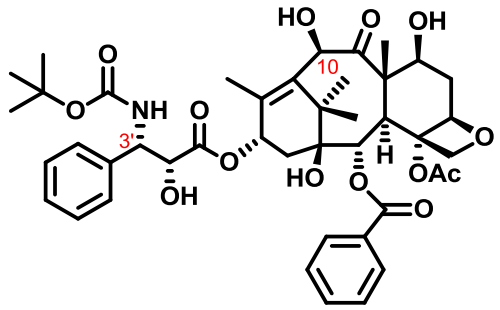

Taxotere®

Figure 1-9: The structure of Taxotere®

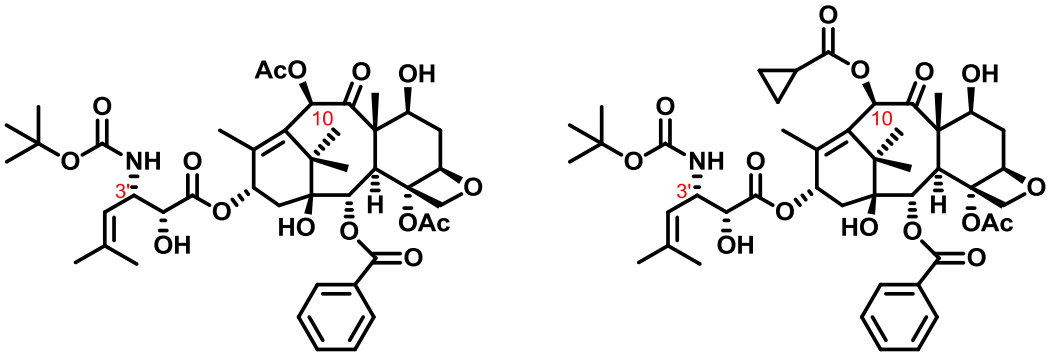

SB-T-1212 SB-T-1214

Figure 1-10: 2nd generation taxoids designed in Ojima laboratory

Table 1-1: Cytotoxicity results of 2nd generation taxoids versus market taxoids Taxol® and Taxotere®[48]					
Taxoid	A121 (ovarian)	A549 (NSCLC)	HT-29 (colon)	MCF7 (breast)	MCF7-R
Paclitaxel	6.1 nM	3.6 nM	3.2 nM	1.7 nM	300 nM
Docetaxel	1.2 nM	1.0 nM	1.2 nM	1.0 nM	235 nM
SB-T-1212	0.46 nM	0.27 nM	0.63 nM	0.55 nM	12 nM
SB-T-1214	0.26 nM	0.57 nM	0.36 nM	0.20 nM	2.1 nM

§1.1 New-Generation Taxoid SB-T-1214:

§1.1.1 Introduction:

Stony Brook Taxoid 1214 (SB-T-1214) has become a drug of choice within the Ojima laboratory. First reported in 1996, SB-T-1214 was found to possess superior activity (2.1 nM) against drug-resistant cell line MCF7-R[50] (mammalian carcinoma 180-fold resistant to doxorubicin) when compared with other 2nd generation taxoids. Due to its exception activity against both sensitive and MDR cancer cell lines, it has also been the drug of choice when developing drug delivery systems such as DHA-SB-T-1214,[51] Vitamin-Disulfide-Linker-SB-T-1214,[52] and Vitamin-SWCNT-Disulfide-Linker-SB-T-1214 as seen in **Figure 1-11**.[53] In addition, SB-T-1214 has been shown recently to down-regulate stem cell-related genes in $CD133^{high}/CD44^{high}$ cells derived from HCT116, HT29 and DLD-1 cell lines.[54]

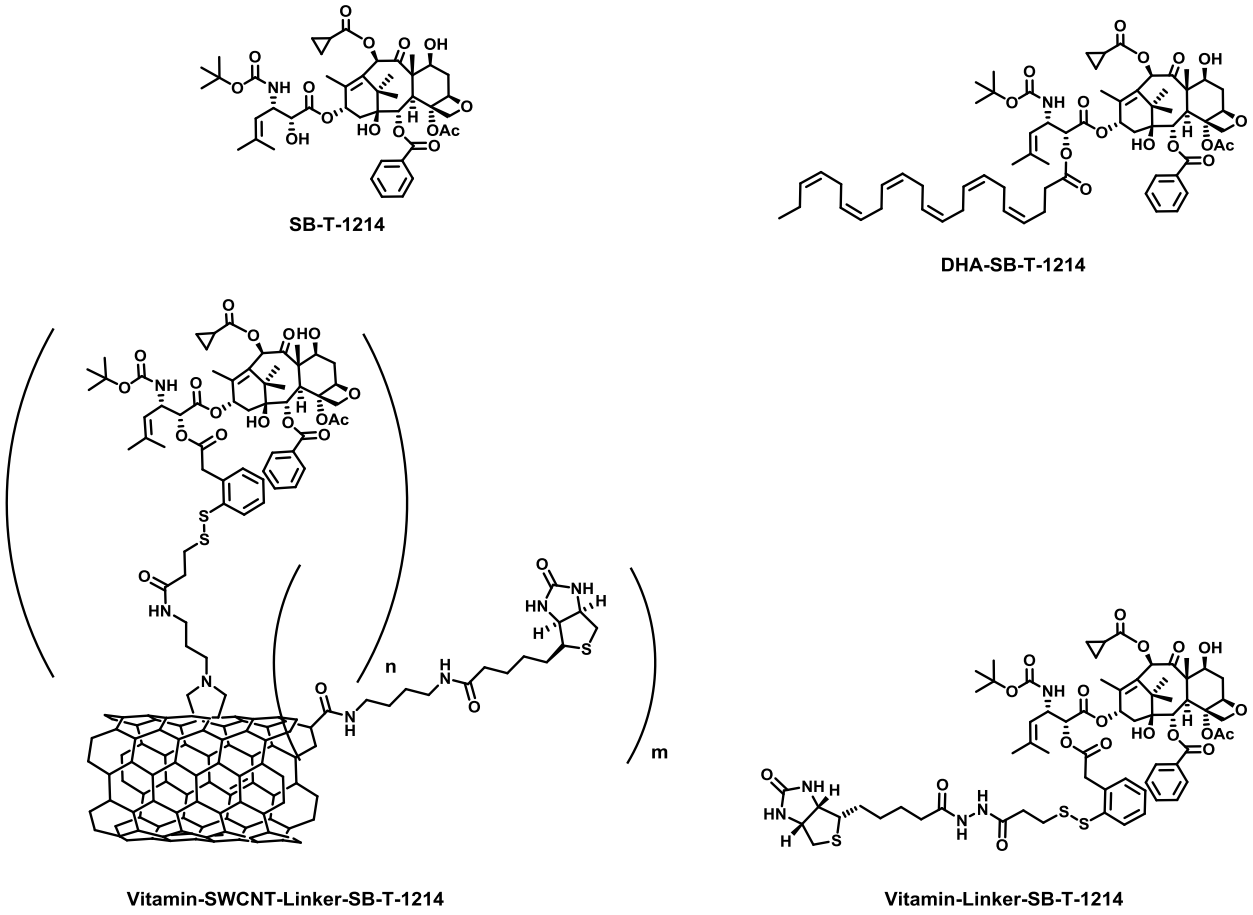

Figure 1-11: SB-T-1214 and three SB-T-1214 conjugates developed in the Ojima laboratory.

The synthesis of SB-T-1214 through the *β*-LSM has provided to be a very effective route for procurement of this highly used 2nd generation taxoid. The *β*-LSM utilizes the Ojima-Holton coupling to couple *β*-lactams' with high enantioselectivity to functionalized baccatin. In the particular case of SB-T-1214, the *β*-lactam used was ((*3R,4S*)-4-*iso*butenyl-1-(*tert*-butoxycarbonyl)-3-(tri*iso*propylsilyloxy)-azetidin-2-one) synthesized previously, which can then be coupled via Ojima-Holton coupling to 7-TES-10-cyclopropanecarbonyl-DAB III as shown in **Scheme 1-4**.

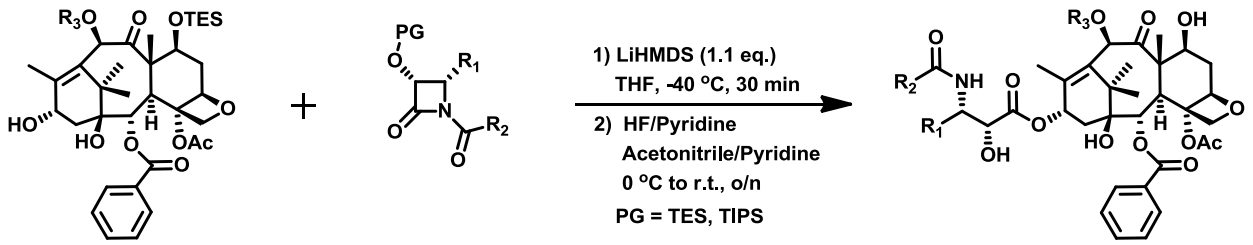

Scheme 1-4: Ojima-Holton coupling

§1.1.2 Results and Discussion:

§1.1.2.1 C7 Protection and C10 Modification of 10-DAB III:

Synthesis of SB-T-1214 began with functionalization of the DAB III shown in **Scheme 1-5**. A selective Corey silyl protection protocol was employed that could afford selective C-7 TES protected DAB III **1-1** at 0 ^{o}C with the use of excess TESCl and imidazole in high yield. After C-7 protection, selective C-10 functionalization was performed using cyclopropanecarbonyl chloride in the presence of LiHMDS at -40 ^{o}C to yield the 7-TES-10-cyclopropanecarbonyl-DAB III **1-2** in high yield.

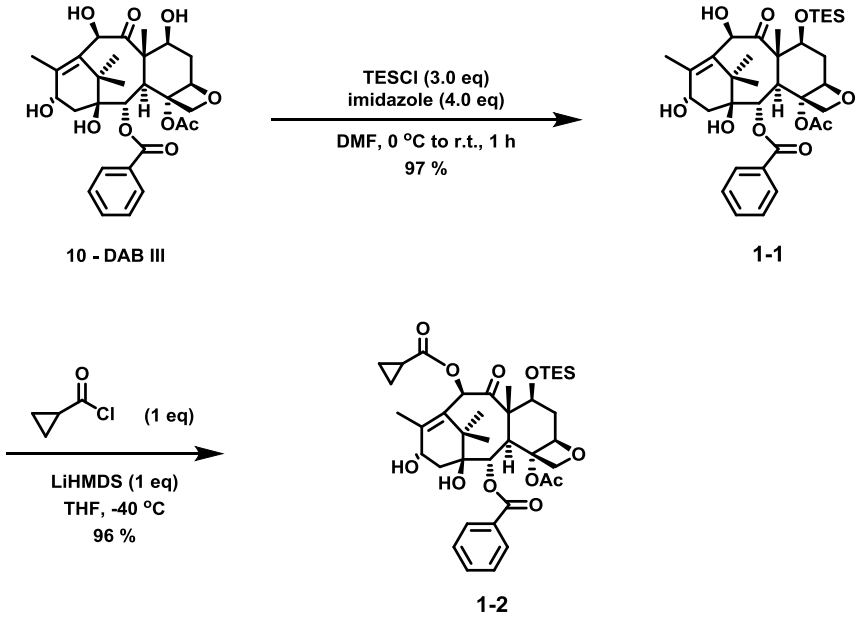

Scheme 1-5. Synthesis of 7-TES-10-cyclopropanecarbonyl-DAB III

§1.1.2.2 Ojima-Holton Coupling and Deprotection:

Following the synthesis of 7-TES-10-cyclopropanecarbonyl-DAB III, synthesis of SB-T-1214 via the Ojima-Holton coupling was accomplished and followed by silyl deprotection shown in **Scheme 1-6**. To 7-TES-10-cyclopropanecarbonyl-DAB III in THF at -40 ^{o}C was added 1.2 equivalents of LiHMDS followed by 1.2 equivalents of ((*3R,4S*)-4-*iso*butenyl-1-(*tert*-butoxycarbonyl)-3-(tri*iso*propylsilyloxy)-azetidin-2-one). This reaction proceeded for 30 minutes the yield the 2'-*O*-TIPS-7-*O*-TES-SB-T-1214 **1-3** in good yield. This compound was then dissolved in 50/50 acetonitrile/pyridine and 0.1 mL of 70 % HF/Pyridine was added for every 10 mg of 2'-*O*-TIPS-7-*O*-TES-SB-T-1214 to yield SB-T-1214 **1-4** after recrystallization from DCM/hexanes in high yield and high purity.

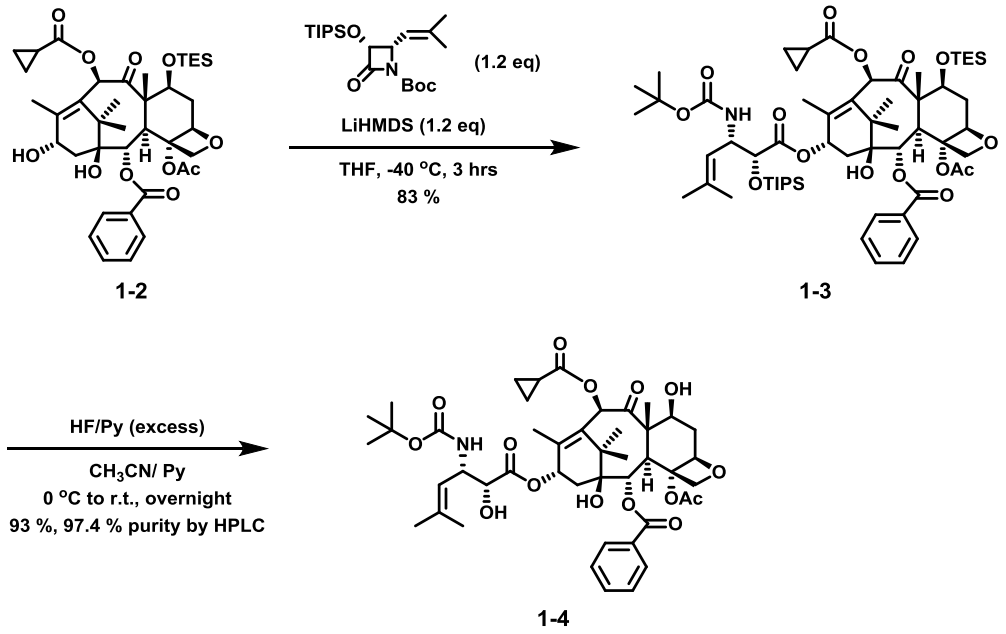

Scheme 1-6. Synthesis of SB-T-1214 via Ojima-Holton coupling and HF deprotection

§1.2 β-Lactams and Their Application towards Taxoid Semi-Synthesis:

§1.2.1 Introduction:

The *β*-lactam structure is defined as a 4-membered heterocyclic amide containing two sp^3 carbons. This well-known structure in medicine serves as both the core functional group in penicillin, and additionally, as critical building block in the semi-synthesis of Taxol® and taxoid analogues. Interestingly, the first recorded synthesis of the *β*-lactam structure dates back to 1907 when Hermann Staudinger reacted a Schiff base comprised of aniline and benzaldehyde with dephenylketene via a [2+2] cycloaddition reaction.[55]

The importance of the *β*-lactam structure was discovered in 1928 when Nobel laureate Alexander Fleming revealed the medicinal properties of penicillin. This work was pioneered by Nobel laureate Howard Walter Florey, Nobel laureate Ernst Chain, and the English biochemist Norman Heatley. Interestingly, it was not until 1945 when Nobel laureate Dorothy Crowfoot Hodgkin produced the first x-ray crystallographic image of penicillin providing the β-lactam structure. A decade later in 1957, John C. Sheehan developed the first total synthesis of Penicillin V.[56] Since then, many new analogues have emerged such as amoxicillin, ampicillin, and cephalosporins such as cephalexin as shown in **Figure 1-12** all containing the same β-lactam core (red).

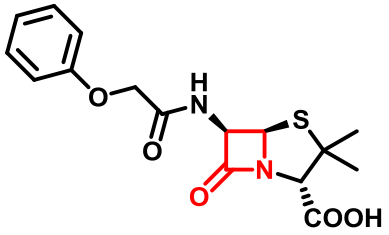

penicillin V

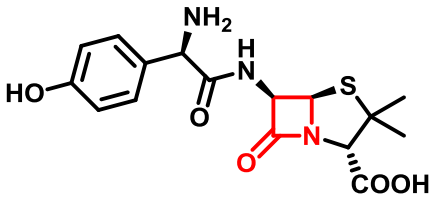

amoxicillin

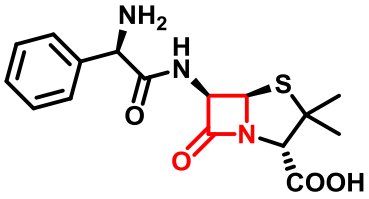

ampicillin

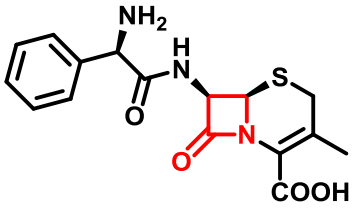

cephalexin

Figure 1-12: Various β-lactam antibiotics used clinically

Although seemingly coincidental, the β-lactam structure has become a privileged structure[57], due not only to its role in antibiotics, but also as a key intermediate in the semi-synthesis of paclitaxel, docetaxel, and many other new generation taxoids. Due to this demand, numerous synthetic methodologies towards the synthesis of enantiopure β-lactams' have been documented in literature. Among these included hydroxamate cyclization,[58] ester enolate-imine cyclocondensation,[59-62] ketene-imine cycloaddition,[55, 63] chromium carbene-imine reaction,[64] and isocyanate-alkene cycloaddition.[65]

In the Ojima group, two synthetic routes have been extensively used for the synthesis of chiral β-lactams', chiral ester-imine cyclocondensation[43] and ketene-imine cycloaddition followed by enzymatic resolution[66]. Each method has had advantages and disadvantages which will be described in the following sections.

§1.2.1.1 β-lactam Formation via 2+2 Cycloaddition:

Traditionally, chiral β-lactam for paclitaxel semi-synthesis has been accessed through chiral ester-imine cyclocondensation; however, due to the length and difficulty of this synthetic route, [2 + 2] cycloaddition and direct β-lactam enzymatic resolution has been recently adopted as a standard protocol in the Ojima laboratory. In particular, several lipases have been investigated for catalyzed hydrolysis of acetylated *β*-lactam.[66]

[2 + 2] cycloaddition (Staudinger reaction) is believed to proceed through *in situ* generated ketene formation, followed by nucleophilic attack of an imine, and finally cyclization through electrocyclic conrotatory ring closure **Scheme 1-7**. This heat and light sensitive reaction can produce to up to four different diastereoisomers and two sets of enantiomers depending on the conditions used Scheme 1-8. Typically, it has been shown that (E)-imines lead predominantly to *cis*-β-lactams while (Z)-mines lead predominantly to *trans*-β-lactams.[67] However, the exact ratio of *cis/trans* relies largely on the transition state equilibrium. Electronic torquoselectivity has been shown to play a contributing role in transition state equilibrium.[68-71]

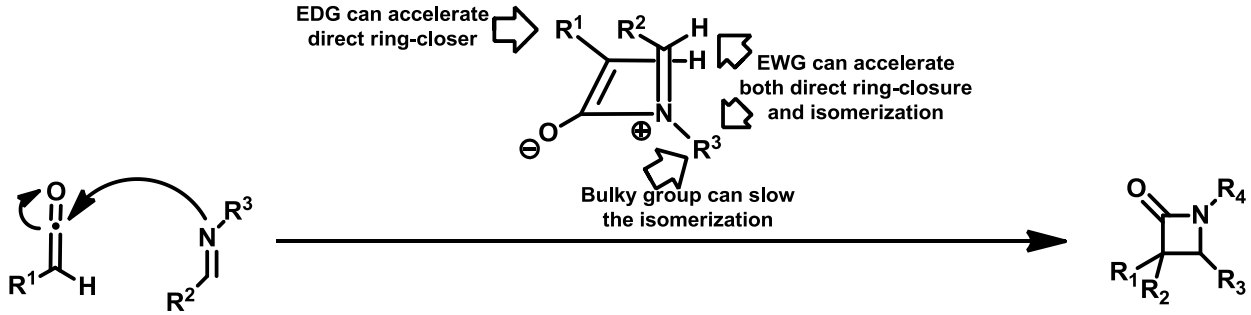

Scheme 1-7: [2 + 2] cycloaddition[67]

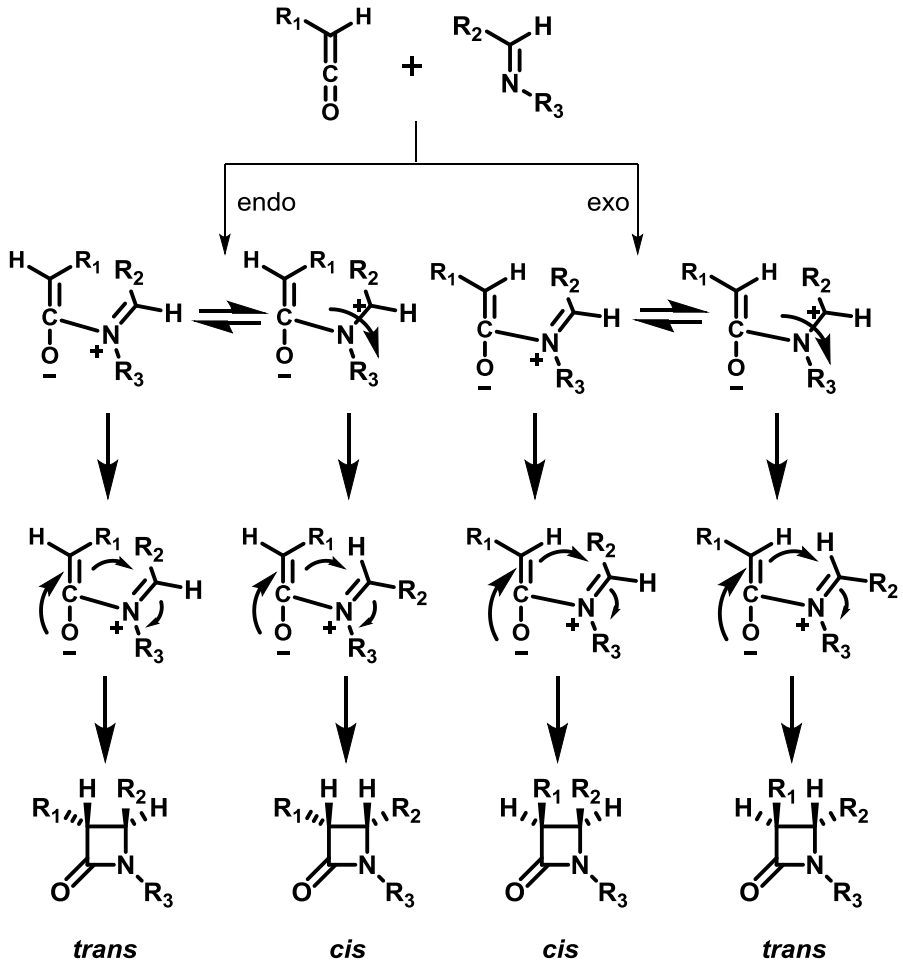

Scheme 1-8: Chiral selectivity of the 2 + 2 cycloaddition reaction (Adapted with permission from [75]. Copyright (2008) American Chemical Society.)[72-75]

§1.2.1.2 Chiral β-Lactam via Ester-Imine Cyclocondensation:

As the original synthetic route to optically pure β-lactams, ester-imine cyclocondensation efficiently provided chiral β-lactam building blocks utilized for the semi-synthesis of paclitaxel, docetaxel, and new generation taxoids. Chiral ester-imine cyclocondensation arose from careful and exhaustive trial and error. After extensive research, the Ojima laboratory reported a chiral ester-imine cyclocondensation that could afford (*3R,4S*) β-lactams with excellent (98 -99 % ee) (**Scheme 1-4**).[43, 76] In particular, (-)-*trans*-2-phenylcyclohexanol (Whitesell's chiral auxiliary (WCA)) chiral ester was required for high enantioselectivity to be achieved utilizing the ester-imine cyclocondensation as seen in **Scheme 1-9**[77, 78] Furthermore, an additional benefit from the chiral ester-imine cyclocondensation was the recovery of WCA which could be reused in subsequent reactions.

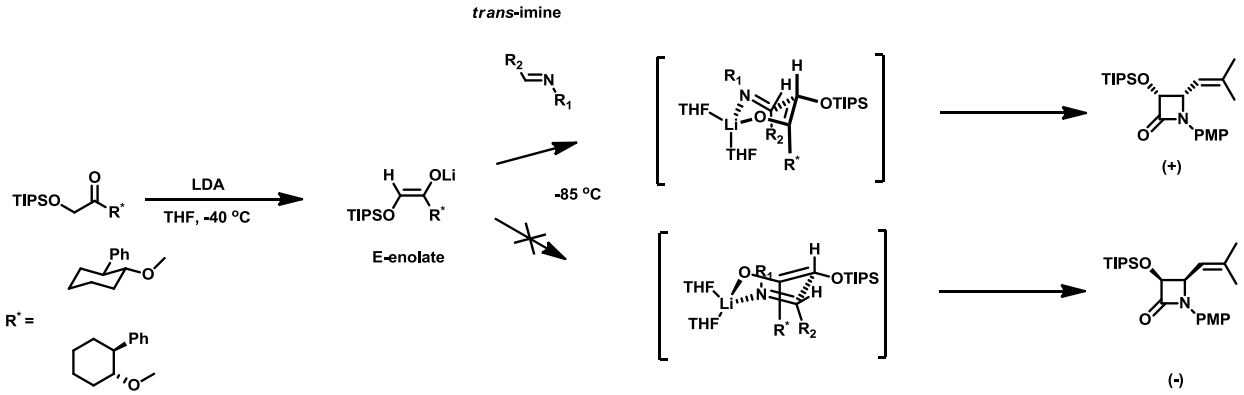

Scheme 1-9: Chiral ester-imine cyclocondensation[43]

The selectivity of the chiral ester-imine cyclocondensation reaction was found to be substantially substrate dependent.[43] Considerable effort was afforded to determine which substituents on the chiral ester would energetically favor the E-enolate 6-member-ring transition state with the chiral auxiliary in the endo position as seen in **Figure 1-13**. Using *N*-(TMS)-benzaldimine several cyclocondensation reactions were carried out. From these many exhaustive experiments, it was concluded that the chiral ester bearing both (-)-*trans*-2-phenylcyclohexanol and *O*-protected TIPS produced the best enantioselectivity (96 % ee). Furthermore, MM2 calculations of both the E-enolate and Z-enolate isomers was conducted and revealed a 2.5 kcal / mol difference. This result suggesting that the E-enolate was more thermodynamically favorable. Thus, temperature was found to be critical factor influencing enantioselectivity.

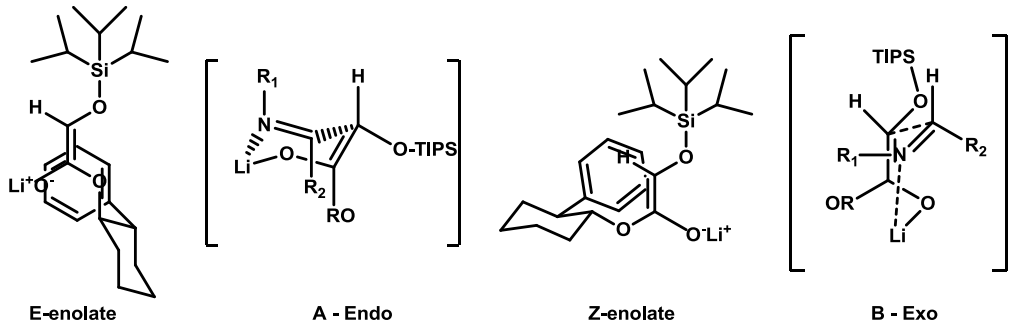

Figure 1-13: Thermodynamically favored E-enolate leads to the endo chair like transition state

In addition to varying substituents on the chiral ester, imine functionality was also explored. Protection of the imine with *para*-methoxyphenyl (PMP) instead of TMS was found to give similar enantioselectivity and provided more stability. PMP protection also provided a chromophore by which the reaction could be monitored by UV. Generally, it was found that bulky and rigid groups provided the best enantioselectivity.

β-lactam formation, through imine-enolate cyclocondensation, has also been extended to afford β-lactam intermediates for the synthesis of docetaxel and other second generation taxoids. In particular, the isobutenyl-PMP-imine was examined and found to afford the C4-isobutenyl β-lactam with high enantioselectivity.[47]

As a component of many of the new generation taxoids, including SB-T-1214, (*3R,4S*)-4-*iso*butenyl-1-(*tert*-butoxycarbonyl)-3-(tri*iso*propylsilyloxy)azetidin-2-one has become a key intermediate, shown in **Figure 1-14**. Thus, efficient methods for the procurement of this key intermediate have become vital to research in the Ojima laboratory and ongoing pre-clinical trials currently being conducted at the Stony Brook DLAR by Jean Rooney and Dr. Tom Zimmerman.

Traditionally, chiral ester-imine cyclocondensation had been used to produce this β-lactam intermediate; however, recently this procedure has been predominantly replaced by Staudinger [2 + 2] cycloaddition followed by enzymatic resolution. Despite advantages to using this synthetic route, revisiting this chiral controlled reaction has recently provided an efficient and reliable new strategy for β-lactam intermediate synthesis. Specific aims of this work were to provide a new more efficient route for the procurement of β-lactam intermediates for future projects.

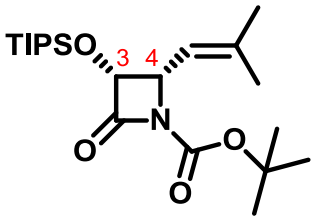

Figure 1-14: (*3R,4S*)-4-*iso*butenyl-1-(*tert*-butoxycarbonyl)-3-(tri*iso*propylsilyloxy)azetidin-2-one

§1.2.2 Results and Discussion:

§1.2.2.1 Synthesis of β-Lactams via 2+2 Cycloaddition and Enzymatic Resolution:

Traditional synthesis of enantiopure β-lactams for semi-synthesis of paclitaxel and taxol derivatives proceeds through 7 steps. These steps consist of both synthetic and biosynthetic transformations as seen in **Scheme 1-10**. Problematic of this synthetic route is the first three steps. Foremost, the first two of these reactions (cycloaddition) can only be carried out with moderate yields (65 – 70 %). More specifically, the cycloaddition produces a substantial (20 to 30 %) uncyclized byproduct **(Figure 1-15)** and furthermore produces at best a 50/50 enantiomeric mixture of the desired cis-β-lactam. This 50/50 mixture of cis-β-lactam is thus resolved by a long enzymatic process producing only one suitable enantiomer while the (-) optical enantiomer remains unusable in the synthesis of taxoids. Thus during these three critical steps only 29 % of highly enantioenriched material can be obtained. This has remained a bottle neck for large quantities of optically pure β-lactams for taxoid research.

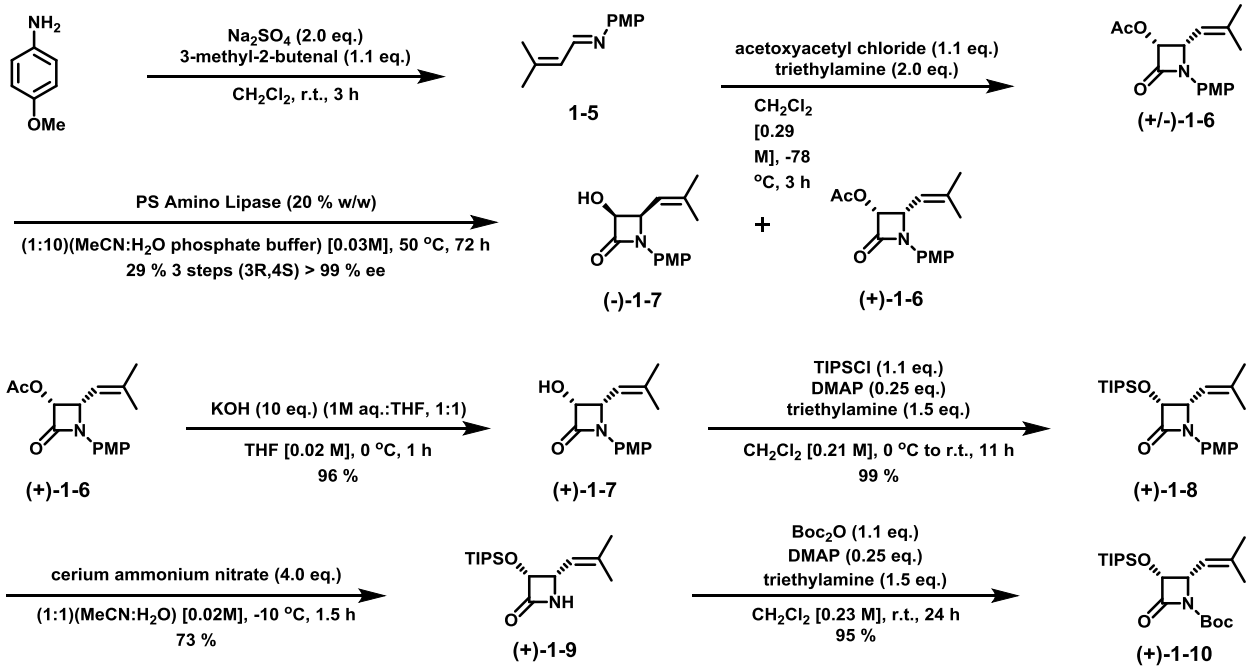

Scheme 1-10: 7 step synthetic route to (*3R,4S*) β-lactams through cycloaddition followed by enzymatic resolution.

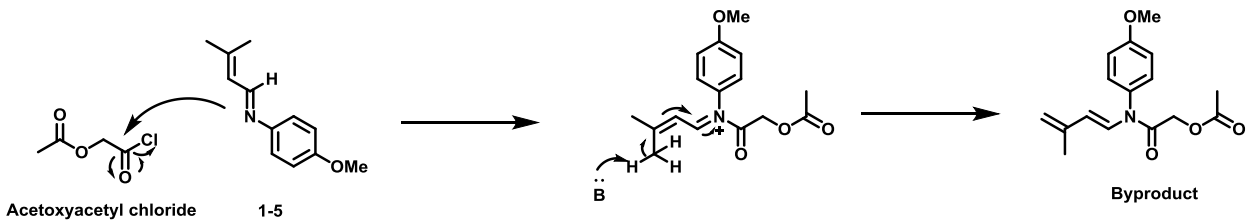

Figure 1-15: Byproduct of the 2+2 cycloaddition of Acetoxyacetyl chloride and imine **1-5**.[79]

§1.2.3 Traditional Synthesis of β-lactam via Ester-Imine Cyclocondensation:

Traditional synthesis of (*3R,4S*)-4-*iso*butenyl-1-(*tert*-butoxycarbonyl)-3-(tri*iso*propylsilyloxy)azetidin-2-one began with the synthesis of the chiral ester intermediate **1-14** as seen in **Scheme 1-11**. First, substitution of bromoacetic acid was carried out in the presence of sodium and benzyl alcohol by heating a mixture of benzyl alcohol and sodium to 150 ^{o}C for 3 hours. After cooling to room temperature, slow addition of bromoacetic acid afforded the benzyl protected glycolic acid **1-11** overnight in good yield.[80] Next, coupling of the acid with the secondary alcohol of (-)-*trans*-2-phenylcyclohexanol (which is traditionally produced enzymatically see section 1.3.4) was performed with catalytic *p*-tolunenesulfonic acid to produce the corresponding benzyl-protected chiral ester **1-12** in excellent yield. This step was then followed by benzyl deprotection, employing Pd/C and hydrogen. It was later discovered the lack of column purification in previous steps left minute traces of acid. Ultimately this led to some acid catalyzed methanol transesterification, reducing the yield of chiral ester glycolic acid **1-13**. Lastly, overlap between free WCA and compound **1-12** on TLC and column provided an overestimation of the yield for compound **1-13.** Thus after TIPS protection and separation via column chromatography, an even lower yield was obtained. Mainly this was due to selective protection of compound 1-13 whereas the WCA mixed in the last reaction could be now separated.

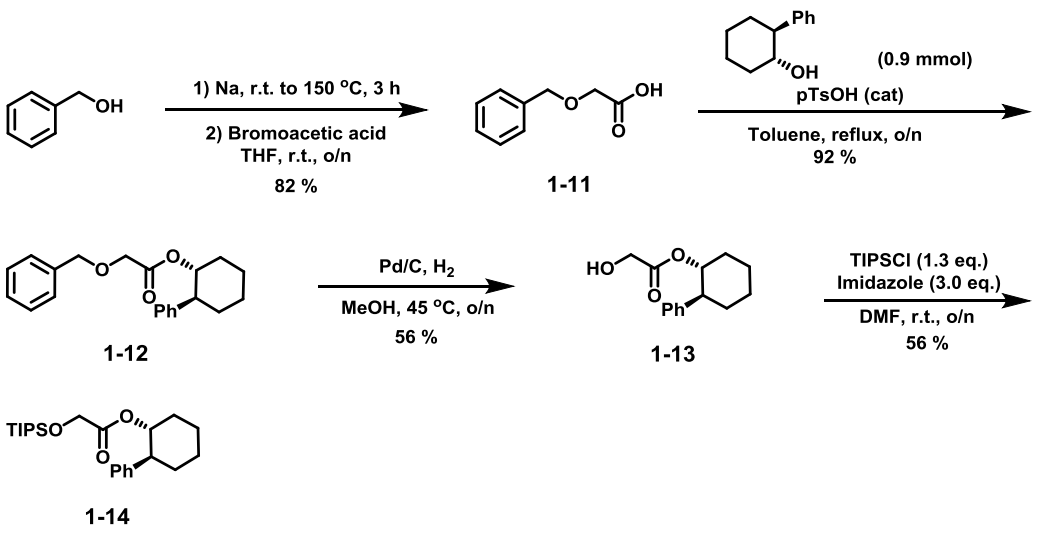

Scheme 1-11. Synthesis of *O*-TIPS protected chiral ester **1-14**

Following the synthesis of the chiral ester, chiral ester-imine cyclocondensation was performed followed by PMP deprotection and subsequent BOC protection shown in Scheme **1-12**. The chiral ester was cooled to -80 °C in the presence of LDA and *trans*-(E)-imine **1-5** was added dropwise to yield the chiral (*3R,4S*)-TIPS-PMP-β-lactam **(+)-1-8** in moderate yield and excellent enantioselectivity. The PMP protection group was then removed with CAN to give the amide **(+)-1-9** in good yield followed by protection with BOC anhydride to give the final (*3R,4S*)-TIPS-BOC-β-lactam **(+)-1-10** in excellent yield.

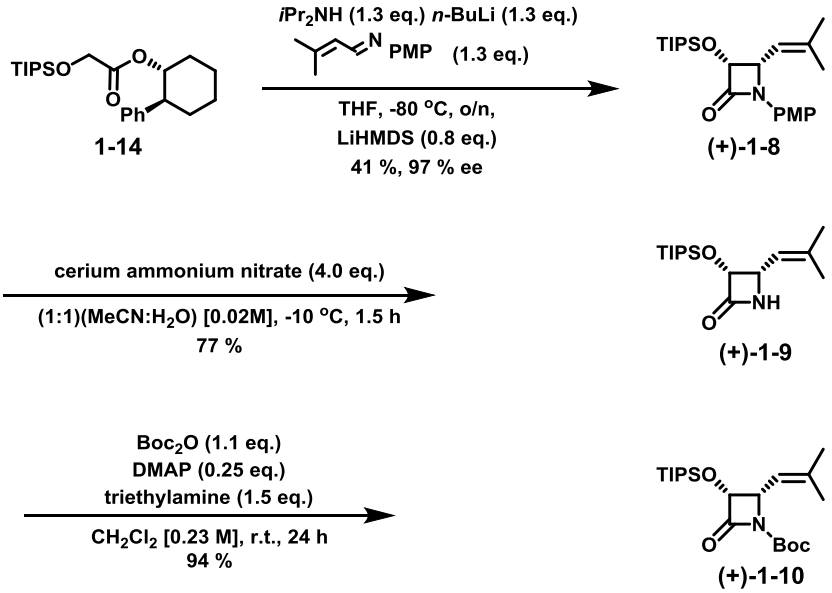

Scheme 1-12: Cyclocondensation followed by PMP deprotection then BOC protection

§1.3 Cyclocondensation Process Improvement via Asymmetric Synthesis of WCA:

§1.3.1 Introduction:

Traditionally, the primary method by which chiral β-lactams via enolate-imine cyclocondensation proceeded was through induction by enzymatically resolved (-)-*trans*-2-phenylcyclohexanol. Additionally, this particular enzymatic resolution was accomplished using pig liver acetone powder (PLAP) as shown in **Scheme 1-13**. Overall, the enzymatic resolution process suffered from poor yield (~35 %) and long reaction times (~1 week). Interestingly, these two critical problems could be overcome by adapting asymmetric synthetic methods shown in **Scheme 1-14**.

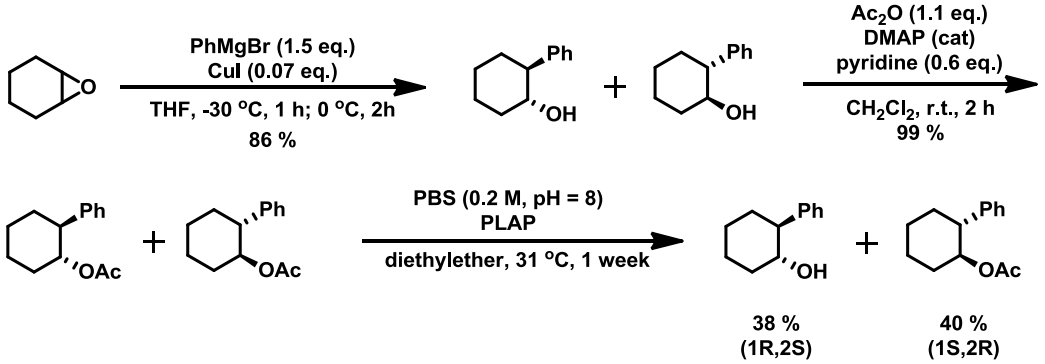

Scheme 1-13: Synthesis of Whitesell's chiral auxiliary through enzymatic resolution with PLAP

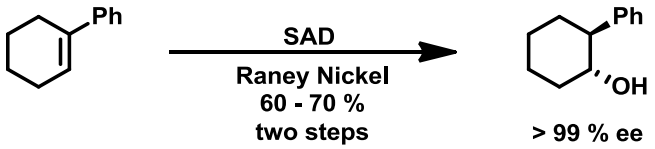

Scheme 1-14. Asymmetric synthesis of Whitesell's chiral auxiliary

In 1994, Sharpless and co-workers published a procedure by which (-)-*trans*-2-phenylcyclohexanol could be obtained through asymmetric synthesis.[81] This procedure was later scaled up by Truesdale and co-workers in 2002.[82] Specifically, asymmetric synthesis was accomplished through asymmetric dihydroxylation as a key step in chiral induction, followed by a selective dehydroxylation step.

Sharpless asymmetric dihydroxylation as developed by Sharpless and coworkers makes use of chiral amine ligands derived from the natural product qunine ($DHQD_2$-PHAL and DHQ_2-PHAL), shown in **Figure 1-16**, to induce stereoselectivity in the normal [3 + 2] syn addition of osmium (VIII) to the double bond of alkenes as shown in **Scheme 1-15**.[83] Specifically, the use of $DHQD_2$PHAL as a chiral ligand in the dihydroxylation of 1-phenylcyclohexene was found to give

exclusively (+)-(1R,2S)-1-phenylcyclohexane-cis-1,2-diol in > 99 % enantiomeric excess. Dihydroxylation of alkenes is typically catalyzed by the metal osmium (osmium (VIII) tetroxide) and normally requires no addition of ligand. However, the asymmetric version which makes use of the inductive effect of the ligand-metal complex requires formation of this $DHQD_2PHAL$-osmium (VIII) tetraoxide complex first, by the addition of excess ligand. Upon coordination and formation of the osmium-ligand complex, subsequent addition of the alkene is quickly followed by [3 + 2]-cycloaddition to the olefin to give a 5-membered metallacycle. Under basic conditions (potassium carbonate), hydrolysis of this metallacycle quickly leads to liberation of the desired diol generating reduced osmium (VI) oxide. Regeneration of the catalyst is accomplished by reoxidiation by potassium ferricyanide or NMO, thus completing the catalytic cycle.

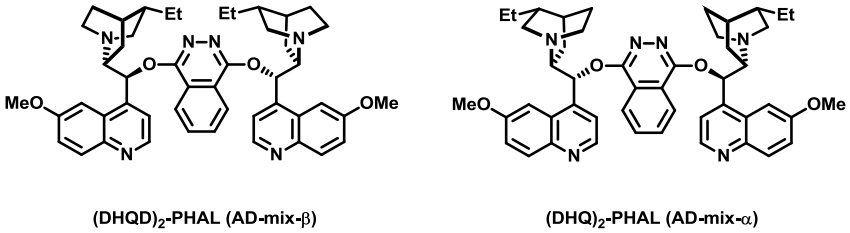

Figure 1-16: Ligands utilized by Sharpless asymmetric dihydroxlyation

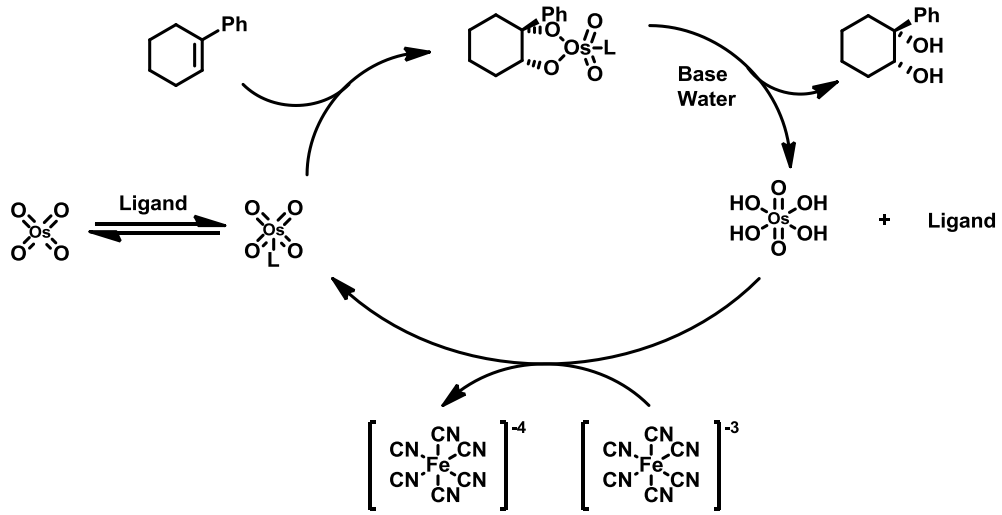

Scheme 1-15: Catalytic cycle of Sharpless asymmetric dihydroxylation

To selectively remove the alcohol at the benzylic position while providing no reactivity at the secondary alcohol, a concerted same face reductive hydrogenation was employed using Raney nickel shown in **Scheme 1-16**[81] This reaction proceeds via nickel insertion into the C-O bond at

the benzylic position followed by elimination to afford (-)-*trans*-2-phenylcyclohexanol with complete retention of stereochemistry. Utilizing these steps, Sharpless was able to yield (-)-*trans*-2-phenylcyclohexanol with enantiomeric excess greater than 99.5 %.

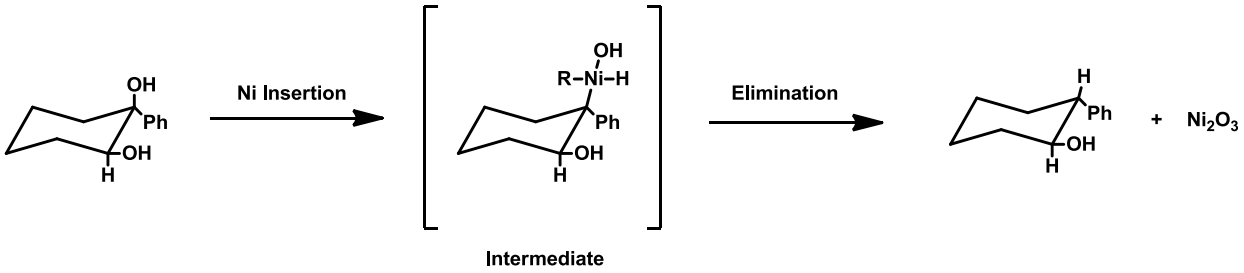

Scheme 1-16. Selective dehydroxylation by Raney nickel

§1.3.2 Results and Discussion:

§1.3.2.1 Process Improvement to WCA Synthesis:

The asymmetric synthesis of (-)-*trans*-2-Phenylcyclohexanol can be accomplished from cyclohexanone in 4 steps seen in **Scheme 1-17**. Starting with cyclohexanone, nucleophilic attack by phenylmagnesium bromide provides a benzylic tertiary alcohol. Subsequently dehydration is quickly accomplished in the presence of *p*-toluenesulfonic acid yielding 1-phenylcyclohexene **1-15** in good yield. After synthesis of compound **1-15**, asymmetric dihydroxylation to the alkene provided the chiral diol **1-16** in quite good yield and decent purity as shown in **Figure 1-17**. Thus, the diol **1-16** is used crude in the following reaction with excess Raney nickel to afford the final (-)-*trans*-2-phenylcyclohexanol **1-17** in good yield and greater than 99.5 % ee after enrichment by recrystallization shown in **Figure 1-17**.

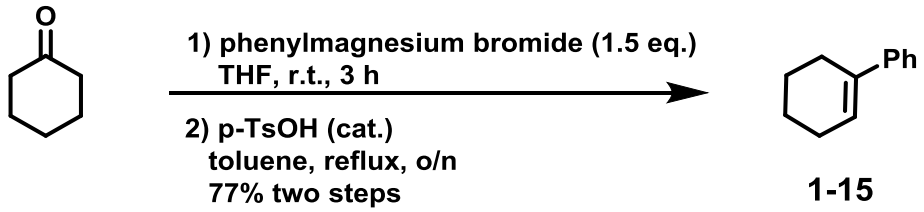

Scheme 1-17: Synthesis of 1-Phenylcyclohexene

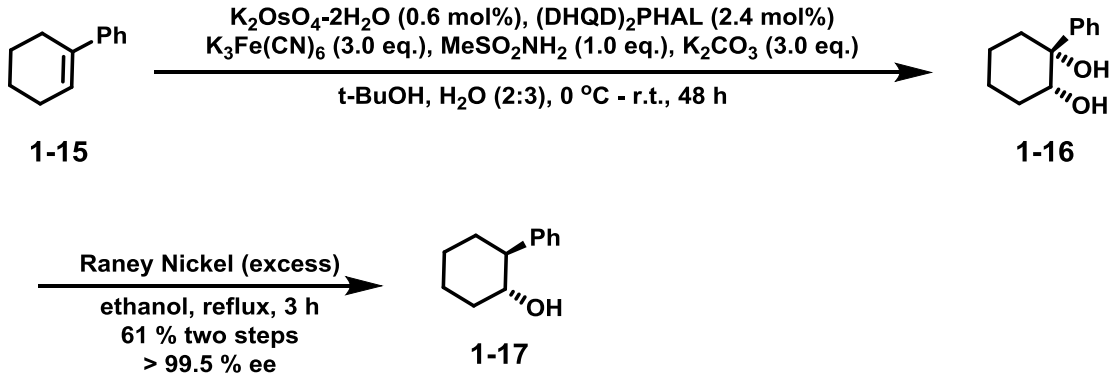

Scheme 1-18: Asymmetric synthesis of (-)-*trans*-2-phenylcyclohexanol

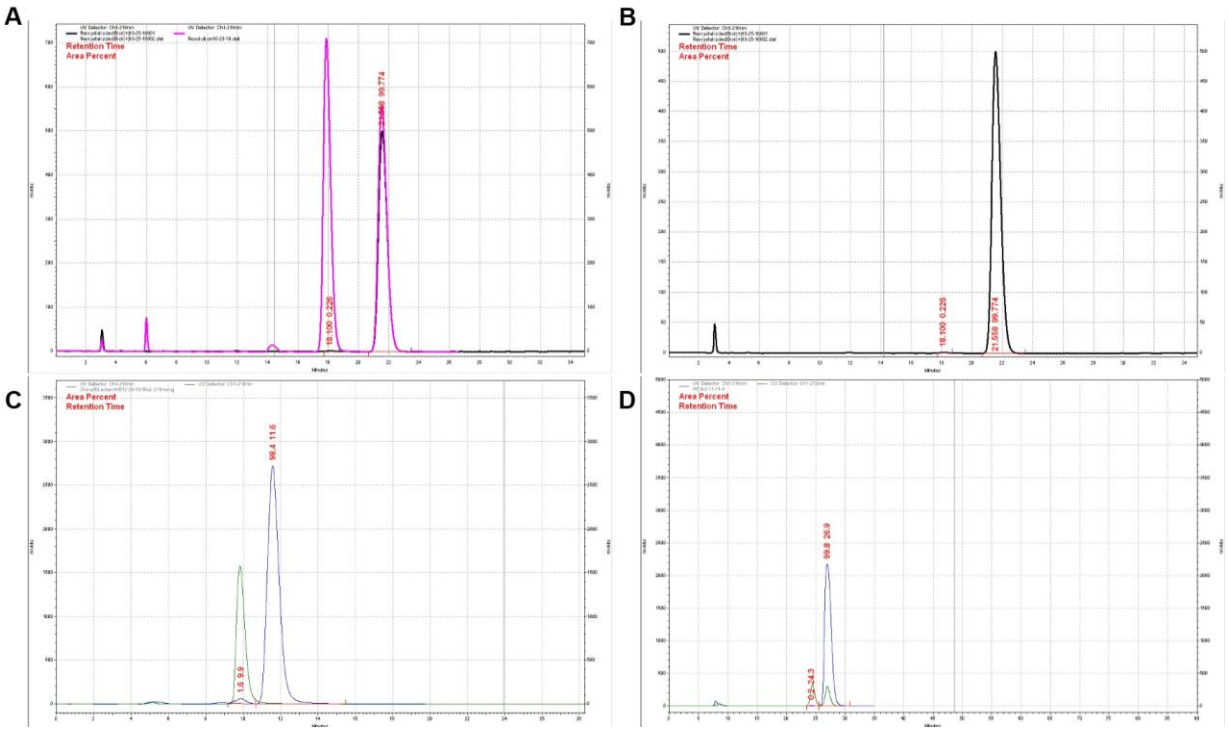

Figure 1-17: Chiral HPLC analysis of WCA and intermediates (absorbance vs. retention time). **A)** Resolution of cis-diols (SS/RR) 1-13 RT_{SS} = 18.1 min, RT_{RR} = 21.6 min (see methods section for HPLC conditions). **B)** RR-cis diol **1-16** asymmetrically derived using Sharpless asymmetric dihydroxylation (see methods section for HPLC conditions). **C)** Separate injections of (+)-*trans*-2-phenylcyclohexanol and (-)-*trans*-2-phenylcyclohexanol, RT_{+trans} = 9.9 min, RT_{-trans} = 11.6 min (see methods section for HPLC conditions). **D)** Separate injections of resolution (1:1) (+/-)-*trans*-2-phenylcyclohexanol (green) and compound **1-17** after recrystallization (blue), 99.8 % ee shown (see methods section for HPLC conditions).

§1.4 Cyclocondensation Process Improvement via a Modified Synthetic Route:

§1.4.1 Introduction:

Owing to the improved asymmetric synthesis of (-)-*trans*-2-phenylcyclohexanol, a desire emerged to explore more practical and efficient synthetic routes to the chiral ester **1-14**, a critical bottleneck in the asymmetric cyclocondensation of chiral β-lactams. Previously in **Scheme 1-11** above, synthesis of benzyl protected glycolic acid provided a suitable intermediate for subsequent TIPS protection, while blocking a potential intramolecular side reaction during the WCA coupling. Although providing moderate yields of the final chiral ester, this scheme led to unnecessary protection and deprotection steps, and furthermore, the use of Pd/C in sizeable quantities. Additionally, low yields following the coupling step to WCA resulted in significant losses and reduction in WCA recovery after chiral ester-imine cyclocondensation. Thus to improve upon the original cyclocondensation methodology, a new approach was developed using the novel compound (triisopropylsilyl)-oxyacetyl chloride as shown in **Scheme 1-18**.

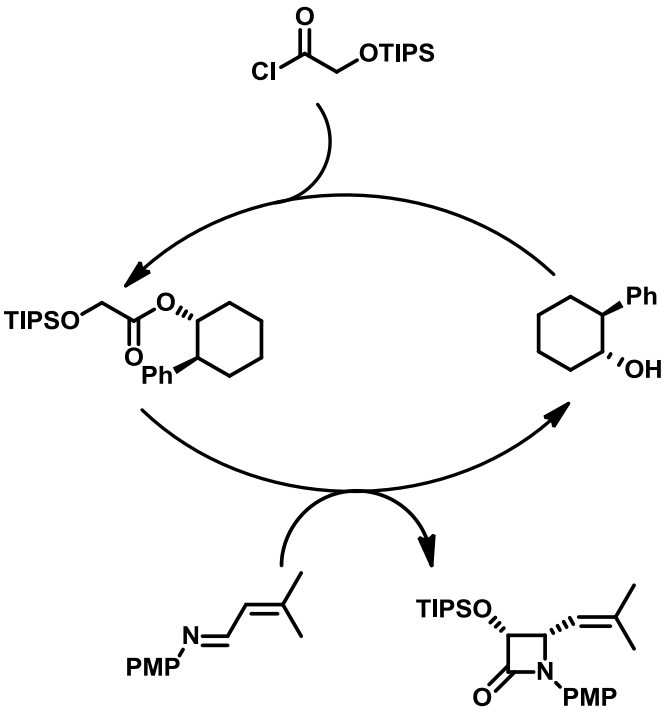

Scheme 1-19: Revised asymmetric enolate-imine cyclocondensation.

§1.4.2 Results and Discussion:

§1.4.2.1 Synthesis of β-lactams through Novel Intermediates:

Synthesis of the novel compound (triisopropylsilyl)-oxyacetyl chloride **1-20** could be accomplished in high yield in 3 steps without column purification as seen in **Scheme 1-19**. The

standard Corey protocol was used to TIPS protect methylglycolate to yield **1-18** in excellent yield. Selective hydrolysis of the methyl ester could be accomplished in the presence of TIPS-ether with 1.5 equivalents of lithium hydroxide monohydrate to yield the *O*-TIPS glycolic acid **1-19**. Acyl chloride formation proceeded smoothly in the presence of the acid sensitive TIPS-ether using oxalyl chloride with catalytic DMF to give the desired (triisopropylsilyl)-oxyacetyl chloride **1-20** in excellent yield.

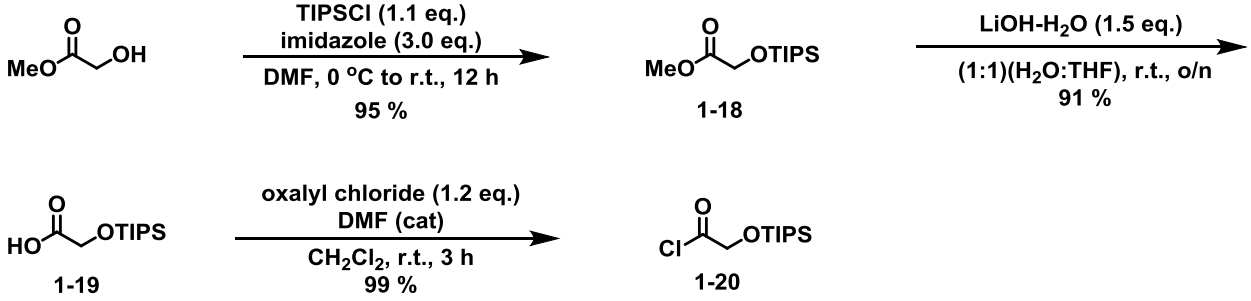

Scheme 1-20: Synthesis of (TIPS)-oxyacetyl chloride **1-20**

Synthesis of the chiral ester was then accomplished by addition of (triisopropylsilyl)-oxyacetyl chloride to (-)-*trans*-2-phenylcyclohexanol in the presence of 1.5 equivalents of pyridine and 1.1 equivalents of DMAP as seen in **Scheme 1-20**. This reaction provided the chiral ester **1-21** in excellent yield effectively trapping the generated HCl as the pyridine salt.

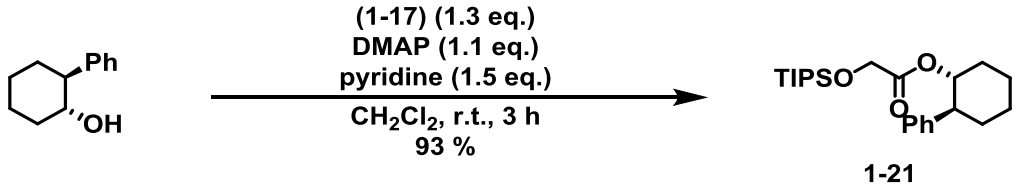

Scheme 1-21: Synthesis of chiral ester **1-21**

Following the synthesis of the chiral ester through the acyl chloride intermediate, cyclocondensation was performed as shown in **Scheme 1-21**. Synthesis of (*3R,4S*)-TIPS-PMP-β-lactam **(+)-1-8** was accomplished in good yield and excellent enantioselectivity. The enantiomeric excess was determined following the standard β-lactam HPLC method (see methods section) after removal of the TIPS by HF/pyridine. In addition, 60 % of the chiral auxiliary used was recovered and was found to have greater than 99.5 % ee. Following recovery of the chiral auxiliary the process of chiral ester formation through the acyl chloride intermediate could be performed

followed by cyclocondensation to provide quick access to the (*3R,4S*)-TIPS-PMP-β-lactam intermediate.

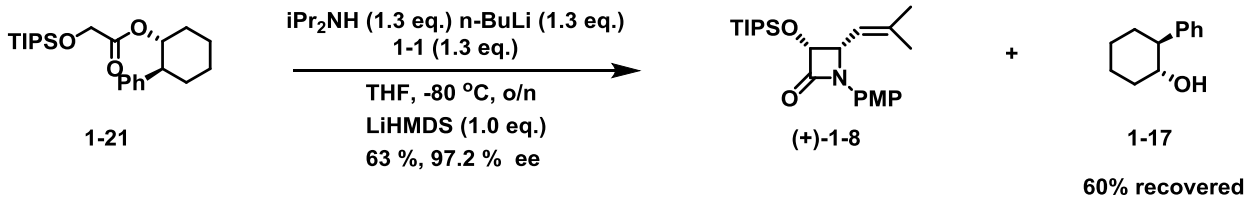

Scheme 1-22: Cyclocondensation and recovery of WCA

§1.5 Conclusions:

The synthesis of SB-T-1214 **1-4** from 10-DAB II was accomplished in 4 steps using the *β*-LSM. Currently, SB-T-1214 is also being pursued in clinical trials for its applications in DHA-SB-T-1214 and LNA-SB-T-1214.

The synthesis of (*3R,4S*)-TIPS-PMP-β-lactam **(+)-1-8** was accomplished utilizing a newly developed route towards chiral ester-imine cyclocondensation. Significant improvement in the synthetic precursors leading up to cyclocondensation has provided **(+)-1-8** in about 50 % yield (starting from methylglycolate, 5 steps) and 97.2 % enantiomeric excess. This synthetic strategy nearly doubles the yield obtained via the [2 + 2] cycloaddition route (28 %, 5 steps up to PMP deprotection). Furthermore, 60 % of the chiral auxiliary used in the reaction was recovered and found to retain stereochemistry. Thus, cyclocondensation with recovered chiral auxiliary via the (triisopropylsilyl)-oxyacetyl chloride intermediate can provide quick and easy access to large quantities of (*3R,4S*)-4-*iso*butenyl-1-(*tert*-butoxycarbonyl)-3-(tri*iso*propylsilyloxy)azetidin-2-one in a relatively short time frame.

§1.6 Experimental Section:

General Methods: ^{1}H NMR was measured on a Varian 300 or 500 MHz NMR spectrometer. The melting points were measured on a "Uni-melt" capillary melting point apparatus from Arthur H. Thomas Company, Inc. TLC analyses were performed on Merck DC-alufolien with Kieselgel 60F-254 and were visualized with UV light and stained with sulfuric acid-EtOH, 10 % PMA-EtOH or 10 % Vanillin-EtOH with 1% sulfuric acid. Column chromatography was carried out on silica gel 60 (Merck; 230-400 mesh ASTM). Chiral purity of diol **1-16** was determined using a Shimazu HPLC with a DAICEL-CHIRACEL OJ chiral column (25 x 0.46 cm) employing a (94.5 % / 5.5

%) hexane/2-propanol mobile phase with a flow rate of 1.0 mL / min and detection at 210 nm (S,S) = 18.1 min (R,R) = 21.6 min. Chiral purity of (-)-*trans*-2-phenylcyclohexanol **1-17** was determined using a Shimazu HPLC with a DAICEL-CHIRACEL OD-H chiral column (25 x 0.46 cm) employing a (98 % / 2 %) hexane/2-propanol mobile phase with a flow rate of 0.4 mL / min and detection at 210 nm (S,R) = 24.3 min (R,S) = 26.9 min. Chiral purity of (*3R,4S*)-TIPS-PMP-β-lactam **(+)-1-8** was determined using a Shimazu HPLC with a DAICEL-CHIRACEL OD-H chiral column (25 x 0.46 cm) employing a (96 % / 4 %) hexane/2-propanol mobile phase with a flow rate of 1.0 mL / min and detection at 210 nm (S,R) = 5.4 min (R,S) =13.0 min. Chiral purity of (*3R,4S*)-OH-PMP-β-lactam **(+)-1-7** was determined using a Shimazu HPLC with a DAICEL-CHIRACEL OD-H chiral column (25 x 0.46 cm) employing a (80 % / 20 %) hexane/2-propanol mobile phase with a flow rate of 0.6 mL / min and detection at 210 nm (S,R) = 9.9 min (R,S) = 11.6 min. Purity of SB-T-1214 **1-4** was determined using a Shimazu HPLC with a Phenomenex Kintex 2.6 µ PFP column (10 x 0.46 cm) employing a (50 % / 50 %) to (90 % / 10 %) methanol/water gradient mobile phase with a flow rate of 0.6 mL / min and detection at 254 nm, retention time = 21 min.

Materials: The chemicals were purchased from Sigma-Aldrich Company, Fischer Company or VWR Company. 10-Deacetyl baccatin III (DAB) was donated by Indena, SpA, Italy. DCM and methanol were dried before use by distillation over calcium hydride under nitrogen. Ether and THF were dried before use by distillation over sodium-benzophenone kept under nitrogen. Dry DMF was purchased from Sigma-Aldrich chemical company, and used without further purification. Reaction flasks were dried in a 100 ^{o}C oven and allowed to cool to room temperature in a desiccator over "*Drierite*" (calcium sulfate) and assembled under an inert nitrogen gas atmosphere.

7-Triethylsilyl-10-deacetylbaccatin III (1-1):[84]

10-Deacetyl baccatin III (105 mg, 0.20 mmol) and (58 mg, 0.80 mmol) of imidazole were dissolved in 1.75 mL of DMF and cooled to 0 °C. Then (0.1 mL, 0.6 mmol) of TESCl was added dropwise. The mixture was stirred and monitored via TLC. The starting material was monitored for conversion to the di-TES product. The reaction mixture was immediately quenched upon conversion with (10 mL) saturated ammonium chloride. The resulting solution was then extracted with (3 x 20 mL) ethyl acetate. The combined organic layers were dried over anhydrous $MgSO_4$,

and concentrated *in vacuo*. Purification of **(1-1)** was performed using normal phase column chromatography with hexanes and ethyl acetate to yield the desired product (120 mg, 91%) as a white solid: mp: 193 – 195 ^{o}C; ^{1}H NMR (500 MHz, $CDCl_3$) δ 0.56 (m, 6 H,), 0.94 (t, *J* = 8.0 Hz, 9 H), 1.09 (s, 6 H), 1.74 (s, 3 H), 1.90 (dt,1 H, H6a), 2.00 (d, *J* = 5.0 Hz, 1 H), 2.08 (s, 3 H), 2.26 (s, 1 H), 2.29 (s, 3 H), 2.48 (m, 1 H, H6b), 3.95 (d, *J* = 7.0 Hz, 1 H, H3), 4.16 (d, *J* = 9.0 Hz, 1 H, H20a), 4.25 (s, 1 H), 4.31 (d, *J* = 8.5 Hz, 1 H, H20b), 4.41 (dd, *J* = 7.0 Hz, 11.0 Hz, 1 H, H7), 4.88 (q, 1H, H13), 4.95 (d, *J* = 9.0 Hz, 1 H), 5.17, (s, 1 H, H10), 5.60, (d, *J* = 7.0 Hz, 1 H, H2), 7.47, (t, *J* = 7.5 Hz, 2 H), 7.60, (t, *J* = 8.0 Hz, 1 H), 8.10 (d, *J* = 7.5, 2 H). All data are in agreement with literature values.[84]

7-Triethylsilyl-10-cyclopropanecarbonyl-10-deacetylbaccatin III (1-2):[84]

7-Triethylsilyl-10-deacetylbaccatin III **(1-1)** (106 mg, 0.16 mmol) was dissolved in 2.74 mL of THF and cooled to -40 °C with a Cryo-Cool apparatus. After 10 minutes at -40 °C, (0.23 mL, 0.23 mmol) of 1.0 M LiHMDS in THF was added and the resulting solution was stirred for an additional 10 minutes. (0.02 mL, 0.19 mmol) of cyclopropanecarboxylic acid chloride was then added dropwise to the mixture. The reaction was monitored via TLC until the starting material was completely consumed. After 1.25 hours, the reaction was quenched with (30 mL) of saturated ammonium chloride. The resulting solution was then extracted with (3 x 30 mL) CH_2Cl_2. The combined organic layers were dried over anhydrous $MgSO_4$, and concentrated *in vacuo*. Purification of **1-2** was performed using normal phase column chromatography with hexanes and ethyl acetate to yield the desired product (77.3 mg, 69 %) as a white solid: ^{1}H NMR (300 MHz, $CDCl_3$) δ 0.57 (m, 6 H,), 0.91 (t, *J* = 8.4 Hz, 9 H), 1.05 (s, 3 H), 1.20 (s, 3 H), 1.68 (s, 3 H), 1.76 (m,1 H), 1.87 (m, 1 H, H6a), 2.19 (d, 3 H), 2.26 (m, 2 H), 2.28 (s, 3 H, OAc), 2.52 (m, 1 H, H6b), 3.88 (d, *J* = 8.7 Hz, 1 H, H3), 4.14 (d, *J* = 8.4 Hz, 1 H, H20a), 4.29 (s, 1 H), 4.32 (d, *J* = 8.4 Hz, 1 H, H20b), 4.48 (dd, *J* = 6.6 Hz, 10.2 Hz, 1 H, H5), 4.83 (m, 1H, H13), 4.96 (d, *J* = 7.8 Hz, 1 H), 5.63 (d, *J* = 6.9 Hz, 1 H, H2), 6.46 (s, 1 H, H 10), 7.47 (t, *J* = 7.8 Hz, 2 H), 7.60 (t, *J* = 7.2 Hz, 1 H), 8.11 (d, *J* = 6.9, 2 H). All data are in agreement with literature values.[84]

3'-Dephenyl-3'-(2-methyl-1-propenyl)-7-triethylsilyl-10-cyclopropanecarbonyl-10-deacetyldocetaxel (1-3):[84]

7-TES-10-cyclopropanecarbonyl-10-deacetylbaccatin III **(1-2) (**72 mg, 0.10 mmol) and (98 mg, 0.25 mmol) of **(+)** β-lactam **(+)-1-10** were dissolved in 3 mL of THF and cooled to -40 °C with a

Cryo-Cool apparatus. After 10 minutes, (0.15 mL, 0.15 mmol) of 1.0 M LiHMDS in THF was added dropwise to the mixture and stirred. The reaction was then monitored via TLC. After 30 minutes, the reaction was complete and was subsequently quenched with (20 mL) saturated ammonium chloride. The resulting solution was extracted using (3 x 20 mL) CH_2Cl_2. The combined organic layers were then dried over $MgSO_4$, and concentrated *in vacuo*. Purification of **(1-3)** was performed using normal phase column chromatography with hexanes and ethyl acetate to yield the desired product (92.3 mg 83%) as a white solid: ^{1}H NMR (500 MHz, $CDCl_3$) δ 0.56 (m, 6 H,), 0.94 (t, *J* = 8.0 Hz, 9 H), 1.09 (s, 6 H), 1.74 (s, 3 H), 1.90 (dt,1 H, H6a), 2.00 (d, *J* = 5.0 Hz, 1 H), 2.08 (s, 3 H), 2.26 (s, 1 H), 2.29 (s, 3 H), 2.48 (m, 1 H, H6b), 3.95 (d, *J* = 7.0 Hz, 1 H, H3), 4.16 (d, *J* = 9.0 Hz, 1 H, H20a), 4.25 (s, 1 H), 4.31 (d, *J* = 8.5 Hz, 1 H, H20b), 4.41 (dd, *J* = 7.0 Hz, 11.0 Hz, 1 H, H7), 4.88 (q, 1H, H13), 4.95 (d, *J* = 9.0 Hz, 1 H), 5.17 (s, 1 H, H10), 5.60 (d, *J* = 7.0 Hz, 1 H, H2), 7.47 (t, *J* = 7.5 Hz, 2 H), 7.60 (t, *J* = 8.0 Hz, 1 H), 8.10 (d, *J* = 7.5, 2 H). All data are in agreement with literature values.[84]

3'-Dephenyl-3'-(2-methyl-1-propenyl)-10-(cyclopropanecarbonyl)docetaxel (1-4):[84]

3'-Dephenyl-3'-(2-methyl-1-propenyl)-7-triethylsilyl-10-cyclopropanecarbonyl-10-deacetyldocetaxel **(1-3)** was dissolved in a suitable amount of (1:1) acetonitrile/pyridine and cooled to 0 °C under inert conditions. Then an excess amount of HF/pyridine was added dropwise and stirred at room temperature overnight. The reaction was monitored via TLC. After completion, the reaction was quenched with saturated (30 mL) $NaHCO_3$. The resulting solution was then diluted with ethyl acetate (2 x 30 mL). After dilution, the organic layer was washed with saturated cupric sulfate solution (3 x 30 mL), H_2O (2 x 30 mL) and then brine (3 x 30 mL). The organic layer was then dried over $MgSO_4$, and concentrated *in vacuo*. Purification of **(1-4)** was performed using normal phase column chromatography. Purity was determined by HPLC (97%): ^{1}H NMR (300 MHz, $CDCl_3$) δ 0.98 – 1.02 (m, 2 H,), 1.15 (m, 2 H), 1.34 (s, 9 H), 1.42 (m, 1 H), 1.66 (s, 3 H), 1.75-1.79 (m, 10 H), 1.89 (s, 3 H), 2.03 (s, 3 H), 2.35 (s, 4 H), 2.53 (m, 1 H), 2.61 (d, *J* = 3.9, 1 H), 3.44 (d, *J* = 6.6 Hz, 1 H), 3.80 (d, *J* = 7.2 Hz, 1 H), 4.21 (m, 2 H), 4.29 (d, *J* = 8.4 Hz, 1 H), 4.40 (m, 1 H), 4.74 (t, *J* = 8.4 Hz, 1 H), 4.83 (d, *J* = 8.7 Hz, 1 H), 4.95 (d, *J* = 7.8 Hz), 5.31 (d, *J* = 9.6 Hz, 1 H), 5.66 (d, *J* = 6.9 Hz, 1 H), 6.17 (t, *J* = 8.1 Hz, 1 H), 6.30 (s, 1 H), 7.46 (t, *J* = 7.8 Hz, 2 H), 7.60 (t, *J* = 7.2 Hz, 1 H), 8.09 (d, *J* = 6.8, 2 H). All data are in agreement with literature values.[84]

***N*-(4-Methoxyphenyl)-3-methyl-2-butenaldimine (1-5):[85]**

Preparation of **1-1** was performed by the addition of (10.9 mL, 110.23 mmol) of 3-Methylbut-2-enal, added dropwise, to a solution of *p*-anisidine (11.3 g, 91.86 mmol; decanted from hexanes) and (52.2 g, 367.44 mmol) anhydrous $MgSO_4$ dissolved in CH_2Cl_2. The reaction mixture was stirred at room temperature for 1 hour and monitored via TLC. After completion the solvent was evaporated to yield N-(4-Methoxyphenyl)-3-methyl-2-butenaldimine (**1-1**), which was then used immediately in the subsequent step without further purification: ^{1}H NMR (300 MHz, $CDCl_3$) δ1.96 (s, 3 H), 2.01 (s, 3 H), 3.81 (s, 3 H), 6.20 (d, *J* = 6.6 Hz, 1 H), 6.89 (d, *J* = 6.9 Hz, 2 H), 7.11 (d, *J* = 6.9 Hz, 2 H), 8.39 (d, *J* = 9.6 Hz, 1 H). All data are in agreement with literature values.[85]

(±)-1-(4-Methoxyphenyl)-3-acetoxyl-4-(2-methylprop-1-enyl)azetidin-2-one ((+/-)-1-6):[86]

N-(4-Methoxyphenyl)-3-methyl-2-butenaldimine (**1-5)** previously made and (25.6 mL, 183.72 mmol) of TEA was added to 480 mL of CH_2Cl_2. The solution was then cooled to -78 ˚C *via* a Cryo-Cool apparatus and maintained at that temperature for 30 minutes. Then (14.8 mL, 137.79 mmol) of acetoxyacetyl chloride was added dropwise. The resulting solution was stirred vigorously at -78 ºC for 3 hours and then allowed to warm to room temperature overnight. After completion, the reaction was quenched with (100 mL) saturated ammonium chloride and extracted (3 x 100 mL) CH_2Cl_2. The organic layers were combined and washed with saturated ammonium chloride, water and then brine. The resulting organic layer was dried over anhydrous $MgSO_4$, and concentrated *in vacuo*. Purification of **(+/-)-1-6** was performed using normal phase column chromatography with hexanes and ethyl acetate to yield the desired product (18.5 g, 70%) as a white solid: mp: 105-108 ºC [lit[86] 107-109 ºC]; ^{1}H NMR (300 MHz, $CDCl_3$) δ 1.81 (dd, *J* = 8.4 Hz, 1.5 Hz, 6 H), 2.12 (s, 3 H), 3.79 (s, 3 H), 4.97 (dd, *J* = 9.6 Hz, 4.8 Hz, 1 H), 5.14 (m, *J* = 9.6 Hz, 1 H), 5.81 (d, *J* = 5.7 Hz, 1 H), 6.87 (d, *J* = 6.9, 2 H), 7.20 (d, *J* = 7.2 Hz, 2 H). All data are in agreement with literature values.[86]

(+)-1-(4-Methoxyphenyl)-3-acetoxyl-4-(2-methylprop-1-enyl)azetidin-2-one ((+)-1-6):[72]

Racemic **(±)**-1-(4-Methoxyphenyl)-3-acetoxyl-4-(2-methylprop-1-enyl)azetidin-2-one **(+/-)-1-6** (7.0 g, 24.19 mmol) was dissolved in a suitable amount of (88 mL : 877 mL) acetonitrile : 0.2 M sodium phosphate buffer (pH = 7.5). This solution was mixed vigorously at 50 °C while (1.4 g, 20 % w/w) of PS-amino lipase was added. The reaction was allowed to stir for 72 hours while monitoring ^{1}H NMR for 50/50 conversion of its C3 and C4 hydrogens. After the reaction had

reached 50% conversion, it was quenched with ethyl acetate (400 mL). The resulting solution was extracted with ethyl acetate (3 x 200 mL). The combined organic layers were dried with anhydrous $MgSO_4$, and concentrated *in vacuo*. Purification of **(+)-1-6** was performed using normal phase column chromatography with hexanes and ethyl acetate to yield the desired product (2.9 g, 41%) as a white solid: ^{1}H NMR (300 MHz, $CDCl_3$) δ 1.81 (dd, *J* = 8.4 Hz, 1.5 Hz, 6 H), 2.12 (s, 3H), 2.12 (s, 3 H), 3.79 (s, 3 H), 4.97 (m, 1 H), 5.14 (m, 1 H), 5.81 (d, *J* = 4.8 Hz, 1 H), 6.86 (d, *J* = 6.9, 2 H), 7.31 (d, *J* = 7.8 Hz, 2 H). All data are in agreement with literature values.[86]

(*3R,4S*)-1-(4-Methoxyphenyl)-3-hydroxy-4-(2-methylprop-1-enyl)azetidin-2-one ((+)-1-7):
To a suitable solution of (96 mL : 96 mL) THF : 1M aqueous KOH maintained at 0 °C, acetate compound (2.8 g, 9.57 mmol) **(+)-1-6** in 191 mL of THF was added. This solution was stirred for 1 hour. After completion, it was quenched with (100 mL) saturated ammonium chloride and extracted with (3 x 75 mL) ethyl acetate. The combined organic layers were dried over $MgSO_4$, and concentrated *in vacuo*. After completion the solvent was evaporated to yield **(+)-1-7** as a white solid (2.3 g, 96%, >99% ee by chiral HPLC), which was then used immediately in the subsequent step without further purification: mp: 164-165 °C; ^{1}H NMR (300 MHz, $CDCl_3$) δ 1.86 (d, *J* = 1.2 Hz, 6 H), 3.78 (s, 3 H), 4.89 (dd, *J* = 9.0 Hz, 5.1 Hz, 1 H), 5.02 (d, *J* = 5.4 Hz, 1 H), 5.25-5.29 (m,1 H,), 6.84 (d, *J* = 9.0, 2 H), 7.31 (d, *J* = 9.0 Hz, 2 H).

Enzymatically derived (*3R,4S*)-1-*p*-Methoxyphenyl-3-triisopropylsiloxy-4-(2-methylpropen-2-yl)azetidin-2-one ((+)-1-8):[85]
(*3R,4S*)-1-(4-Methoxyphenyl)-3-hydroxy-4-(2-methylprop-1-enyl)azetidin-2-one **(+)-1-7** (2.3 g, 9.22 mmol) and 225 mg of DMAP were dissolved in 43 mL of CH_2Cl_2. The solution was then cooled to 0 °C. 1.9 mL of TEA was then added dropwise and the solution was allowed to stir 10 minutes. Next, 2.7 mL of TIPSCl was added dropwise. The mixture was then stirred for 11 hours while allowed to warm to room temperature. After completion, the resulting solution was quenched with (40 mL) saturated ammonium chloride. The aqueous layer was extracted with (3 x 40 mL) ethyl acetate and the combined organic layers will be washed with (2 x 40 mL) brine. The organic layer was then dried over $MgSO_4$, and concentrated *in vacuo*. Purification of **(+)-1-8** was performed using normal phase column chromatography with hexanes and ethyl acetate to yield the desired product (3.7 g, 99%) a white crystalline product with the aroma of sand: mp: 89-91 °C; ^{1}H NMR (300 MHz, $CDCl_3$) δ 1.02 (m, 21 H) 1.78 (dd, *J* = 15.3 Hz, 1.2 Hz, 6 H), 3.79 (s,

3 H), 4.57 (m, 1 H), 5.00 (d, *J* = 4.2 Hz, 1 H), 5.60 (m, 1 H), 6.84 (d, *J* = 9.0, 2 H), 7.31 (d, *J* = 9.0 Hz, 2 H). All data are in agreement with literature values.[85]

(*3R,4S*)-3-Triisopropylsilyloxy-4-(2-methylpropen-2-yl)azetidin-2-one ((+)-1-9):[85]

1-*p*-Methoxyphenyl-3-triisopropylsiloxy-4-(2-methylpropen-2-yl)azetidin-2-one **(+)-1-8** (520 mg, 1.29 mmol) was dissolved in 32 mL of acetonitrile and cooled to -10 °C with a Cryo-Cool machine. After 10 minutes at -10 °C, (2.8 g, 5.16 mmol) cerium ammonium nitrate in 32 mL H_2O was added dropwise and stirred. The reaction was allowed to stir for 1.5 hours. When the starting material was no longer seen by TLC, the resulting solution immediately quenched with 60 mL saturated aqueous sodium sulfate. After quenching the resulting solution was extracted with (3 x 60 mL) aliquots of CH_2Cl_2. The combined organic layers were then washed with (60 mL) H_2O, (2 x 60 mL) sodium bicarbonate, and then (2 x 60 mL) brine. The organic layer was then dried over $MgSO_4$, and concentrated *in vacuo*. Purification of **(+)-1-9** was performed using normal phase column chromatography with hexanes and ethyl acetate to yield the desired product (280 mg, 73%) as a white solid: mp: 85-86 ^oC; ^1H NMR (300 MHz, $CDCl_3$) δ 1.02-1.13 (m, 21 H), 1.69 (d, *J* = 1.2, 3 H), 1.76 (d, *J* = 1.5, 3 H), 4.44 (q, *J* = 4.8 Hz, 1 H), 5.00 (q, *J* = 2.1 Hz, 1 H), 5.32 (m, 1 H), 5.83 (br, 1 H). All data are in agreement with literature values.[85]

(*3R,4S*)-1-(*tert*-Butoxycarbonyl)-3-triisopropylsiloxy-4-(2-methylpropen-2-yl)azetidin-2-one ((+)-1-10):[85]

3-Triisopropylsilyloxy-4-(2-methylpropen-2-yl)azetidin-2-one **(+)-1-9** (533 mg, 1.79 mmol), (57 mg, 0.45 mmol) of DMAP, and (0.37 mL, 2.69 mmol) of TEA was dissolved in a 7.9 mL of CH_2Cl_2. While stirring, (430 mg, 1.97 mmol) of di-*tert*-butyl dicarbonate in 7.9 mL was added dropwise. This mixture was allowed to stir for 24 hours at room temperature. After completion, the resulting solution was quenched with (30 mL) saturated ammonium chloride. The resulting solution was extracted using (3 x 30 mL) ethyl acetate. The combined organic layers were combined and washed with (30 mL) brine, dried over $MgSO_4$, and concentrated *in vacuo*. Purification of **(+)-1-10** was performed using normal phase column chromatography with hexanes and ethyl acetate to yield the desired product (673 mg, 95%) as a slightly yellow oil: ^1H NMR (300 MHz, $CDCl_3$) δ 1.01-1.13 (m, 21 H), 1.48 (s, 9 H), 1.76 (d, *J* = 1.5, 3 H), 1.78 (d, *J* = 1.2, 3 H), 4.75 (q, *J* = 5.4 Hz, 1 H), 4.96 (d, *J* = 5.7 Hz), 5.31 (m, 1 H). All data are in agreement with literature values.[85]

Benzyloxyacetic acid (1-11):[87]

To a 250 mL round bottomed flask was added 24 mL (231.4 mmol) of benzyl alcohol. To this solution was added 4.837 g (210.4 mmol) of sodium, in portions, until hydrogen gas evolution stopped. This solution was then heated to 120 ^{o}C until all of the sodium had dissolved. After completion the solution was then cooled to room temperature and 76.8 mL of THF was added. To this solution was then added dropwise a solution of 5.861 g (42.08 mmol) of bromoacetic acid previously dissolved in 19.2 mL of THF. The combined solution was then allowed to stir for 12 hours. After completion, 100 mL of cold distilled water was added. Then the aqueous layer was washed twice with 200 mL of diethyl ether. 100 mL of diethyl ether was then added and the pH of the solution was adjusted with 6 N HCl to 2 with litmus paper. The organic layer was collected and the remaining aqueous layer was extracted two more times with 100 mL of diethyl ether. The combined organic extracts were then dried over $MgSO_4$, and concentrated *in vacuo* to yield the desired product **1-11** (5.717 g, 82 %) as a clear oil: ^{1}H NMR (300 MHz, $CDCl_3$) δ 4.16 (s, 2 H), 4.65 (s, 2 H), 7.38 (m 5 H), 8.77 (br, 1 H). All data are in agreement with literature values.[87]

(*1R, 2S*)-(-)-2-Phenylcyclohexyl benyloxyacetate (1-12):[87]

To a 25 mL round bottomed flask was added 1.395 g (7.91 mmol) (-)-*trans*-2-phenylcyclohexanol and 11 mL of dry toluene. Then 1.496 g (8.70 mmol) of benzyloxyacetic acid **1-11** was added. While stirring, 10 mg (cat) *p*-toluenesulfonic acid was added and the resulting solution was reflux overnight while collecting molecular water with a Dean-Stark trap. After completion, resulting solution was concentrated *in vacuo* and then re-dissolved in 100 mL of diethyl ether and washed twice with 100 mL of saturated sodium bicarbonate. The organic layer was collected, dried over $MgSO_4$, and concentrated *in vacuo* to yield the desired product **1-12** (2.395g, 93 %) as an off-white solid: ^{1}H NMR (300 MHz, $CDCl_3$) δ 1.32-1.71 (m, 4 H), 1.84-2.06 (m, 3 H), 2.19-2.25 (m, 1 H), 2.76 (dt, *J* = 11.1, 3.9 Hz, 1 H), 3.86 (q, *J* = 18.0 Hz, 2 H), 4.33 (s, 2 H), 5.16-5.24 (m, 1 H), 7.22-7.45 (m, 10 H). All data are in agreement with reported values.[87]

(*1R, 2S*)-(-)-2-Phenylcyclohexyl hydroxyacetate (1-13):[87]

To a 250 mL round bottomed flask was added 2.382 g (7.34 mmol) **1-12** and 24 mL of dry methanol. Then to this solution was added 1.46 g 10% Pd/C. The flask was then sealed purged with H_2 gas and heated to 45 ^{o}C while stirring overnight. After completion, the resulting solution was filtered through a bed of Celite and washed with 100 mL of methanol. The resulting solution

was concentrated *in vacuo* and re-dissolved in 100 mL of ethyl acetate and washed twice with 100 mL of brine. The organic layer was collected, dried over $MgSO_4$, and concentrated *in vacuo* to yield the desired product **1-13** (999 mg, 58 %) as a white solid: ^{1}H NMR (300 MHz, $CDCl_3$) δ 1.32-1.71 (m, 4 H), 1.84-2.06 (m, 3 H), 2.19-2.25 (m, 1 H), 2.75 (dt, *J* = 12.0, 3.9 Hz, 1 H), 3.09 (br, 1 H), 3.73 (d, *J* = 17.1 Hz, 1 H), 3.95 (d, *J* = 16.8 Hz, 1 H), 5.10-5.19 (m, 1 H), 7.20- 7.40 (m, 5 H). All data are in agreement with reported values.[87]

(*1R, 2S*)-(-)-2-Phenylcyclohexyl triisopropylsilyloxyacetate (1-14):[88]

To a 10 mL round bottomed flask was added 864 mg (3.69 mmol) **1-13**, 731 mg imidazole (11.07 mmol), and 1.8 mL of DMF. Then slowly 1.19 mL of TIPSCl (5.54 mmol) was added while stirring. The solution was allowed to stir for 6 hours. After completion, the reaction was quenched with 3 mL of saturate ammonium chloride. To the resulting solution 50 mL of ethyl acetate was added and the resulting organic layer was washed twice with 100 mL of brine. The organic layer was collected, dried over $MgSO_4$, and concentrated *in vacuo*. Purification of **1-14** was performed using silica gel chromatography with 5 % ethyl acetate/hexanes to yield the desired product (805 mg, 56%) as a colourless oil: ^{1}H NMR (600 MHz, $CDCl_3$) δ 0.92-1.07 (m, 21 H), 1.29-1.58 (m, 4 H), 1.78 (d, *J* = 13.2 Hz, 1 H), 1.85 (dt, *J* = 10.8, 2.4 Hz, 1 H), 1.93 (dt, *J* = 13.2, 3.0 Hz, 1 H), 2.13-2.15 (m, 1 H), 2.66 (td, *J* = 10.8, 3.0 Hz, 1 H), 3.91 (d, *J* = 16.2 Hz, 1 H), 4.07 (d, *J* = 16.8 Hz, 1 H), 5.05-5.09 (m, 1 H), 7.14-7.17 (m, 3 H), 7.23-7.26 (m, 2 H). All data are in agreement with reported values.[88]

Asymmetrically derived 1-*p*-Methoxyphenyl-3-triisopropylsiloxy-4-(2-methylpropen-2-yl)azetidin-2-one ((+)-1-8):[72]

To a 50 mL round bottomed flask added 8 mL of THF and 0.34 mL (2.39 mmol) of diisopropylamine. This solution was then cooled down to -15 ^{o}C and 0.96 mL (2.39 mL of *n*-BuLi was added dropwise. This solution was stirred for 1 hour. Then the solution was cooled to -82 ^{o}C for 1 hour. Then 720 mg (1.84 mmol) of (1R,2S)-(-)-2-phenylcyclohexyl TIPS-oxyacetate **1-14** in 8 mL of THF was added over 2 hours with a syringe pump. Then over 2 hours added *trans-N*-PMP-3-methyl-2-butenaldimine **1-5** (2.76 mmol) in 9 mL THF with a syringe pump. The reaction was allowed to stir an addition 2 hours and then 0.74 mL 1M LiHMDS in tert-butyldimethylether was added and the reaction was allowed to warm to 0 ^{o}C. The reaction was quenched with 10 mL of saturated ammonium chloride solution and allowed to warm to room temperature. The reaction

was diluted with 50 mL of ethyl acetate and then washed with 50 mL of saturated ammonium chloride, 50 mL of brine. The organic layer was collected and dried with $MgSO_4$ and concentrated *in vacuo* to give a crude brown oil **(+)-1-8** that was purified by column chromatography (2% - 5 % ethyl acetate to hexanes) to yield a 485 mg (1.20 mmol), 65% of a yellow solid. The solid was then subsequently recrystallized twice from pentane to yield 302 mg (0.75 mol), 41 % of a white crystalline solid 96.8% ee by chiral HPLC: ^{1}H NMR (600 MHz, CDCl3) δ 0.99-1.18 (m, 21 H), 1.79 (d, *J* = 1.2 Hz, 3 H), 1.84 (d, *J* = 1.2 Hz, 3 H), 3.76 (s, 3 H), 4.79 (dd, *J* = 4.8 Hz, *J* = 9.9 Hz, 1 H), 5.04 (d, *J* =5.1 Hz, 1 H), 5.32 (dt, *J* = 1.2 Hz, *J* = 9.9 Hz, 1 H), 6.83 (d, *J* = 9.0 Hz, 2 H), 7.30 (d, *J* = 10.2 Hz, 2 H); ^{13}C NMR (75 MHz, CDCl3) δ 11.8, 17.5, 18.3, 26.1, 55.3, 57.5, 77.5, 114.2, 118.2, 120.1, 131.4, 139.1, 155.9, 165.5. All data are in agreement with reported values.[72]

1-Phenyl-1-cyclohexene (1-15):[89]

To a 250 mL three-neck round bottomed flask equipped with a condenser was added 3.715 g (152.83 mmol) of previously dried magnesium turnings. Then to the same flask was added 100 mL of THF. While stirring a catalytic amount of I_2 was added. To this dark solution was added 19.3 mL (183.39 mmol) of bromobenzene dropwise at room temperature (caution extremely exothermic) over 2 hours using a syringe pump which became clear after the first mL of addition. After complete addition of bromobenzene, the reaction was heated to 65 ^oC for 1 hour until all of the magnesium turnings reacted. Next, the reaction was cooled down to room temperature and 10.101 g (102.90 mmol) of previously distilled cyclohexanone was added dropwise (caution extremely exothermic) over 3 hours using a syringe pump. The reaction was then allowed to stir overnight (12 hours). After completion the reaction was quenched very slowly with 100 mL of aqueous saturated ammonium chloride solution (caution extremely exothermic) and then extracted with diethyl ether 100 mL. The organic layer was then washed with 100 mL of brine and the resulting organic layer was dried over anhydrous sodium sulfate and concentrated *in vacuo* to yield a yellow crude oil: ^{1}H NMR (400 MHz, CDCl3) δ 1.23-1.34 (m, 1 H), 1.57-1.87 (m, 10 H), 7.22 (t, *J* = 5.6 Hz, 1 H), 7.33 (t, *J* = 8.0 Hz, 2 H), 7.49 (t, *J* = 7.2 Hz, 2 H); ^{13}C NMR (100 MHz, CDCl3) δ 22.2, 25.5, 38.8, 73.1, 124.5, 126.7, 128.2, 149.4. All data are in agreement with reported values.[89] This oil was then re-suspended in 100 mL of toluene in a 250 mL round bottomed flask quipped with a Dean-Stark trap with 50 mL of toluene previously charged in the 60 mL solvent trap. A catalytic amount of p-toluenesulfonic acid was then added and the solution was refluxed for 3 hours. The resulting solution was cooled and then concentrated *in vacuo* to yield

a brown crude oil **1-15**. This crude oil was then transferred to a 25 mL round bottomed flask and distilled at 90 °C under reduced pressure 0.1 mmHg to yield a clear liquid: ^{1}H NMR (300 MHz, CDCl3) δ 1.61-1.70 (m, 2 H), 1.74-1.82 (m, 2 H), 2.17-2.24 (m, 2H), 2.38-2.43 (m, 2H), 6.10-6.13 (m, 1H), 7.19 (tt, *J* = 2.4, *J* = 7.8 Hz, 1 H), 7.29 (tt, *J* =2.1 , *J* = 8.1 Hz, 2 H), 7.38 (dd, *J* = 1.5, *J* = 7.8 Hz, 2 H); ^{13}C NMR (75 MHz, CDCl3) δ 22.1, 23.0, 25.8, 27.3, 124.7, 124.9, 126.4, 128.1, 136.5, 142.6. All data are in agreement with reported values.[89]

(+)-(*1R,2R*)-1-Phenylcyclohexane-cis-1,2-diol (1-16):[82, 90]

To a 500 mL round bottomed flask added 74.1 g (225 mmol) potassium ferricyanide, 31.1 g (225 mmol) potassium carbonate, and 7.1 g (75 mmol) methanesulfonamide. Then added 72 mL of *tert*-butnaol and 112 mL of distilled water. While stirring with a magnetic stir bar vigorously cooled down to 0 ºC in an ice bath. To this stirring solution added 183 mg (0.50 mmol) of potassium osmate dehydrate and 1.37 g (1.73 mmol) of $DHQD_2PHAL$ ligand. Stirred an additional 20 minutes. Then to this solution added dropwise 11.47 g (72.48 mmol) of 1-Phenylcyclohexene **1-15**. This solution was allowed to warm to room temperature and stir for 48 hours. The reaction mixture visibly changed from a dark orange color to a light yellow color as the potassium ferricyanide was reduced by the catalyst. After 48 hours 50 mL of ethyl acetate was added to the solution while stirring and this was allowed to stir for 15 minutes. The entire solution was then filtered to remove solid potassium ferrocyanide and then the resulting liquid was diluted with an additional 100 mL of ethyl acetate. The aqueous layer was discarded and the resulting organic layer was washed 3 times with 100 mL of 2N potassium hydroxide solution. This organic layer was then dried with $NaSO_4$ and concentrated *in vacuo* to yield a slightly yellow solid **1-16** 13.9g (72.30 mmol), quant. This solid was pure enough by ^{1}H NMR for the next synthetic step without further purification: ^{1}H NMR (400 MHz, CDCl3) δ 1.36-1.47 (m, 1 H), 1.52-1.57 (m, 2 H), 1.64-1.78 (m, 3H), 1.81-1.91 (m, 3H), 2.59 (d, *J* = 1.6 Hz, 1H) 4.00 (dd, *J* = 4.0, *J* = 10.8 Hz, 1H), 7.27 (tt, *J* = 1.2, *J* = 7.6 Hz, 1 H), 7.38 (td, *J* =2.0 , *J* = 7.6 Hz, 2 H), 7.38 (dt, *J* = 1.6, *J* = 8.0 Hz, 2 H); ^{13}C NMR (100 MHz, CDCl3) δ 22.1, 24.4, 29.2, 38.5, 74.5, 75.8, 125.1, 127.0, 128.5, 146.3. All data are in agreement with reported values.[82, 90]

(-)-*Trans*-2-phenyl-cyclohexanol (1-17):[82, 90]

To a 1000 mL round bottomed flask containing 13.9 g of crude diol **1-16** was added 143 mL of ethanol. This solution was stirred to dissolve the solid. The reaction flask was purged with N_2.

Then to this solution was added 230 mL of Raney®-Nickel 2800 catalyst in water while stirring. The reaction flask was then equipped with a reflux condenser and heated to 100 °C for 3 hours. The reaction was monitored by TLC (20 % ethyl acetate/hexanes) with the diol disappearing at an R_f of 0.2 and the dehydroxylated product appearing at an R_f of 0.4. After completion, the reaction was cooled to room temperature and then filtered through a 3 mm bed of celite while taking care not to dry the solution. (dry Raney nickel is pyrogenic and will ignite) The resulting black Ni solid was washed copiously with ethanol (300 mL) and then diluted with water and disposed of in a proper waste container containing water. The resulting filtrate was then concentrated *in vacuo* and then dissolved in 100 mL of ethyl acetate. The organic layer was then washed two times with 100 mL of brine. The resulting organic layer was dried with $NaSO_4$ and concentrated *in vacuo* to yield 8.28 g of a white solid **1-17**. This solid was then dissolved in hexanes and purified by flash chromatography (1% to 10 % ethyl acetate / hexanes). After column purification 6.38 g (36.20 mmol) of the desired product was obtained. This solid was determined by Chiral HPLC to have an enantiomeric excess of 90 % for the (*1R,2S*) enantiomer. Enantiomeric enrichment by recrystallization was then performed by dissolving 6.38 g of the product in 50 mL of pentane by heating in a water bath with a boiling stick and allowing this solution to slowly recrystallize at room temperature overnight. After initial crystal formation the solution was allowed to cool at 0 °C for one hour and then the resulting solid was filtered and washed with chilled pentane to yield long white needle crystals 4.32 g (24.51 mmol) with an enantiomeric excess of > 99.5 %. The mother liquor was then roto-evaporated down and the recrystallization was then re-performed to produce long white needle crystals 1.60 g (9.08 mmol) with an enantiomeric excess of 98.0 %. Total yield is 5.92 g (33.59 mmol), 46 % two steps: ^{1}H NMR (300 MHz, $CDCl_3$) δ 1.33 – 1.73 (m, 5 H), 1.79 – 1.86 (m, 1 H), 1.89 – 1.98 (m, 2H), 2.16 – 2.21 (m, 1H), 2.46 – 2.54 (m, 1H) 3.69 – 3.77 (m, 1H), 7.28 – 7.34 (m, 3 H), 7.39 – 7.44 (m, 2 H); ^{13}C NMR (75 MHz, $CDCl_3$) δ 25.0, 26.0, 34.3, 53.1, 74.4, 126.8, 127.9, 128.7, 143.2. All data are in agreement with reported values.[82, 90]

Methyl-3-(triisopropyl-silanyloxy)-propionic acid (1-18):[91]

To a 25 mL round bottomed flask added 1.015 g (9.26 mmol) methyl glycolate and 1.836 g (27.79 mmol) imidazole. Then added 4.5 mL of dry DMF and stirred this solution. The solution was cooled down to 0 °C with an ice bath and 2.18 mL (10.19 mmol) of TIPSCl was added dropwise. This solution was allowed to stir for 18 hours and then quenched with saturate ammonium chloride

(10 mL). The resulting solution was dissolved in 50 mL of ethyl acetate and washed two times with 50 mL of saturated ammonium chloride and once with 50 mL of brine. The resulting organic layer was dried with $MgSO_4$ and concentrated *in vacuo* to yield **1-18** a slightly yellow oil 2.41 g (9.25 mmol), quant. This oil was pure enough by ^1H NMR for the next synthetic step without further purification: ^1H NMR (300 MHz, CDCl3) δ 1.02-1.16 (m, 21 H), 1.27 (t, *J* = 7.2 Hz, 3 H), 4.21 (q, *J* = 6.9 Hz, 2 H), 4.30 (s, 2H); ^{13}C NMR (75 MHz, CDCl3) δ 11.9, 14.1, 17.8, 60.7, 62.0, 171.6.

3-(triisopropyl-silanyloxy)-propionic acid (1-19):

To a 250 mL round bottomed flask added 1.003 g (3.85 mmol) of **1-18** and 50 mL of THF. This solution was cooled down to 0 ^oC in an ice bath and then 19 mL (41.96 mmol) of aqueous 2M LiOH solution was added dropwise over 15 minutes. The ice bath was removed and the resulting solution was allowed to stir at room temperature for 2 hours. The reaction was diluted with 50 mL of water and the THF was removed by roto-evaporation. The resulting aqueous solution was then extracted with 50 mL of diethyl ether twice. Then 50 mL of diethyl ether was added and the pH of the aqueous layer was adjusted to pH 2.0 with 1N HCl. The aqueous solution was extracted with 50 mL of diethyl ether twice and the resulting organic layer was dried with $MgSO_4$ and concentrated *in vacuo* to give **1-19** a clear oil 705 mg (3.03 mmol), 79 % two steps: ^1H NMR (400 MHz, CDCl3) δ 1.03-1.13 (m, 18 H), 1.15-1.18 (m, 3 H), 4.30 (s, 2 H), 9.36 (b, 1H); ^{13}C NMR (100 MHz, CDCl3) δ 11.7, 17.7, 61.7, 173.3.

3-(triisopropyl-silanyloxy)-propionic chloride (1-20):[92]

To a 100 mL round bottomed flask was added 1.004 g (4.32 mmol) of **1-19** and 43 mL of DCM. Then added 0.48 mL (5.62 mmol) oxalyl chloride dropwise followed by 3 drops of DMF. The reaction was allowed to stir with constant nitrogen flow for 24 hours. After completion, the reaction was concentrated *in vacuo* to yield **1-20** a slightly yellow oil (1.028 g, 95 %). This oil was pure enough by ^1H NMR for the next synthetic step without further purification: ^1H NMR (500 MHz, CDCl3) δ 1.05-1.22 (m, 21 H), 4.61 (s, 2 H); ^{13}C NMR (125 MHz, CDCl3) δ 11.8, 17.6, 70.1, 172.6.

(*1R, 2S*)-(-)-2-Phenylcyclohexyl triisopropylsilyloxyacetate (1-21):[88]

To a 10 mL round bottomed flask was added 122 mg (0.69 mmol) of Whitesell's chiral auxiliary **1-17** and 76 mg (0.62 mmol) of DMAP. Then 1 mL of dry DCM and 0.05 mL (0.84 mmol) of dry pyridine was added and allowed to stir. To this solution was added 210 mg (0.84 mmol) of **1-20** and the resulting solution was allowed to stir for 24 hours. After completion the reaction was quenched with 5 mL of saturated sodium bicarbonate. The resulting solution was then extracted with ethyl acetate 50 mL and washed with 100 mL of saturated sodium bicarbonate, 100 mL of aqueous cupric sulfate, and 100 mL of brine. The organic layer was dried with $MgSO_4$ and concentrated *in vacuo* to give a crude oil **1-21**. The resulting mixture of product and starting material was then purified by flash chromatography (1% EtAC/Hexanes to 2% EtAc/Hexanes) to yield a clear oil 261 mg (0.67 mmol), 97 %: ^{1}H NMR (600 MHz, CDCl3) δ 0.93-1.08 (m, 21 H), 1.33-1.55 (m, 4 H), 1.76-1.94 (m, 3H), 2.13 (d, *J* = 11.4 Hz, 1H), 2.64 (t, *J* = 10.8 Hz, 1H) 3.91 (d, *J* = 16.5 Hz, 1H), 4.07 (d, *J* = 16.5 Hz, 1H), 5.07 (t, *J* = 9.6 Hz, 1H), 7.16 (d, *J* = 6.6 Hz, 3 H), 7.25 (t, *J* = 7.8Hz, 2 H); ^{13}C NMR (100 MHz, CDCl3) δ 11.8, 17.7, 24.7, 25.8, 32.3, 34.0, 49.7, 61.7, 76.1, 126.4, 127.4, 128.3, 142.9, 170.8.[88]

§1.7 References:

1. Jemal, A.; Seigel, R.; Ward, E.; Hao, Y.; Xu, J.; Murray, T.; Thun, M. J., Cancer Statistics, 2008. *CA Cancer J Clin* **2008,** *58*, 71 - 96.
2. American Cancer Society: Cancer facts & figures 2008. **2008**.
3. Hanahan, D.; Weinberg, R. A., The Hallmarks of Cancer. *Cell* **2000,** *100*, 57 - 70.
4. http://www.cancervic.org.au/images/CISS/cancer-types/cancer-spreading.gif (accessed, 12/08/13),
5. http://www.cancervic.org.au/images/CISS/cancer-types/cancer-beginning.gif (accessed, 12/08/13),
6. http://www.cancer.gov/cancertopics/factsheet/detection/staging (accessed, 11/09/13),
7. Jordon, M. A.; Wilson, L., Microtubule Polymerization Dynamics, Mitotic Block, and Cell Death by Paclitaxel at Low Concentrations. In *Taxane anticancer agents: Basic science and current status*, Georg, G. I.; Chen, T. T.; Ojima, I.; Vyas, D. M., Eds. American Chemical Society, Washington D.C.1994; pp 138 - 153.
8. Kingston, D. G. I., Recent Advances in the Chemistry of Taxol. *J. Nat. Prod.* **2000,** *63*, 726 - 734.
9. Schiff, P. B.; Fant, J.; Horwitz, S. B., Promotion of microtubule assembly in vitro by taxol. *Nature* **1979,** *277*, 665 - 667.

10. Jordan, M. A.; Wendell, K.; Gardiner, S.; Brent Derry, W.; Copp, H.; Wilson, L., Mitotic Block Induced in HeLa Cells by Low Concentrations of Paclitaxel (Taxol) Results in Abnormal Mitotic Exit and Apoptotic Cell Death. *Cancer Res.* **1996,** *56*, 816 - 825.
11. Wang, T. H.; Wang, H. S.; Soong, Y. K., Paclitaxel-induced cell death: where the cell cycle and apoptosis come together. *Cancer* **2000,** *88*, 2619 - 2628.
12. Park, S. J.; Wu, C. H.; Gordon, J. D.; Zhong, X.; Emami, A.; Safa, A. R., Taxol induces caspase-10-dependent apoptosis. *J. Biol. Chem.* **2004,** *279*, 51057 - 51067.
13. Luduena, R. F.; Shooter, E. M.; Wilson, L., Structure of the tubulin dimer. *J. Biol. Chem.* **1977,** *252*, 7006 - 7014.
14. Mitchison, T.; Kirschner, M., Dynamic instability of microtubule growth. *Nature* **1984,** *312*, 237 - 242.
15. Schiff, P. B.; Horwitz, S. B., Taxol stabilizes microtubules in mouse fibroblast cells. *Proc. Natl. Acad. Sci* **1980,** *77*, 1561 - 1565.
16. Schiff, P. B.; Horwitz, S. B., Taxol assembles tubulin in the absence of exogenous Guanosine 5'-Triphosphate or Microtubule-Associated Proteins. *Biochemistry* **1981,** *20*, 3247 - 3252.
17. Nogales, E.; Wolf, S. G.; Khan, I. A.; Luduena, R. F.; H., D. K., Structure of tubulin at 6.5 angstrom and location of the taxol-binding site. *Nature* **1995,** *375*, 424 - 427.
18. Nogales, E.; Wolf, S. G.; Downing, K. H., Structure of the [alpha][beta] tubulin dimer by electron crystallography. *Nature* **1998,** *391*, 199 - 203.
19. Mahadevan, L.; Mitchison, T. J., Cell biology: Powerful curves. *Nature* **2005,** *435*, 895 - 897.
20. Holton, R. A.; Kim, H. B.; Somoza, C.; Liang, F.; Biediger, R. J.; Boatman, P. D.; Shindo, M.; Smith, C. C.; Kim, S.; Nadizadeh, H.; Suzuki, Y.; Tao, C.; Vu, P.; Tang, S.; Zhang, P.; Murthi, K. K.; Gentile, L. N.; Liu, J. H., First total synthesis of Taxol. 2. Completion of the C and D rings. *J. Am. Chem. Soc.* **1994,** *116*, 1599 - 1600.
21. Nicolaou, K. C.; Yang, Z.; Liu, J. J.; Ueno, H.; Nantermet, P. G.; Guy, R. K.; Claiborne, C. F.; Renaud, J.; Couladouros, E. A.; Paulvannan, K.; Sorensen, E. J., Total Synthesis of Taxol. *Nature* **1994,** *367*, 630 - 634.
22. Nicolaou, K. C.; Liu, J. J.; Yang, Z.; Ueno, H.; Sorensen, E. J.; Claiborne, C. F.; Guy, R. K.; Hwang, C. K.; Nakada, M.; Nantermet, P. G., Total synthesis of Taxol. 2. Construction of A and C ring intermediates and intial attempts to construct the ABC ring system. *J. Am. Chem. Soc.* **1995,** *117*, 634 - 644.
23. Nicolaou, K. C.; Yang, Z.; Liu, J. J.; Nantermet, P. G.; Claiborne, C. F.; Renaud, J.; Guy, R. K.; Shibayama, K., Total synthesis of Taxol. 3. Formation of Taxol's ABC ring skeleton. *J. Am. Chem. Soc.* **1995,** *117*, 645 - 652.
24. Nicolaou, K. C.; Ueno, H.; Liu, J. J.; Nantermet, P. G.; Yang, Z.; Renaud, J.; Paulvannan, K.; Chadha, R., Total synthesis of Taxol. 4. The final stages and completion of the synthesis of Taxol. 4. The final stages and completion of the synthesis. *J. Am. Chem. Soc.* **1995,** *117*, 653 - 659.

25. Danishefsky, S. J.; Masters, J. J.; Young, W. B.; Link, J. T.; Snyder, L. B.; Jung, D. K.; Isaccs, R. C.; Bornmann, W. G.; Alaimo, C. A.; Coburn, C. A.; Di Grandi, M. J., Total Synthesis of Baccatin III and Taxol. *J. Am. Chem. Soc.* **1996,** *118*, 2843 - 2859.
26. Wender, P. A.; Mucciaro, T. P., A new and practical approach to the synthesis of Taxol and Taxol analogues: The pinene path. *J. Am. Chem. Soc.* **1992,** *114*, 5878 - 5879.
27. Wender, P. A.; Badham, N. F.; Conway, S. P.; Florencig, P. E.; Glass, T. E.; Houze, J. B.; Krauss, N. E.; Lee, D.; Marquess, D. G.; McGrane, P. L.; Meng, W.; Natchus, M. G.; Shuker, A. J.; Sutton, J. C.; Taylor, R. E., The pinene path to taxenes. 6. A concise sterocontrolled synthesis of Taxol. *J. Am. Chem. Soc.* **1997,** *119*, 2757 - 2758.
28. Morihira, K.; Hara, R.; Kawahara, S.; Nishimori, T.; Nakamura, N.; Kusama, H.; Kuwajima, I., Enantioselective total synthesis of taxol. *J. Am. Chem. Soc.* **1998,** *120*, 12980 - 12981.
29. Mukaiyama, T.; Shiina, I.; Iwadare, H.; Saitoh, M.; Nishimura, T.; Ohkawa, N.; Sakoh, H.; Nishimura, K.; Tani, Y.-I.; Hasegawa, M.; Yamada, K.; Saitoh, K., Asymmetric total synthesis of taxol. *Eur. J. Chem.* **1999,** *5*, 121 - 161.
30. Doi, T.; Fuse, S.; Miyamoto, S.; Nakai, K.; Sasuga, D.; Takahashi, T., A Formal Total Synthesis of Taxol Aided by an Automated Synthesizer. *Chemistry – An Asian Journal* **2006,** *1*, 370-383.
31. Gueitte-Voegelein, F.; Senilh, V.; David, B.; Gueard, D.; Potier, P., Chemical studies of 10-deacetyl baccatin III. Semisynthesis of taxol derivatives. *Tetrahedron* **1986,** *42*, 4451 - 4460.
32. Denis, J. N.; Greene, A. E.; Gueard, D.; Gueitte-Voegelein, F.; Mangatal, L.; Potier, P., A highly efficent, practical approach to natural taxol. *J. Am. Chem. Soc.* **1988,** *110*, 5917 - 5919.
33. Denis, J. N.; Correa, A.; Greene, A. E., An improved synthesis of the taxol side chain and of RP 56976. *J. Org. Chem.* **1990,** *55*, 1957 - 1959.
34. Wang, Z.-M.; Kolb, H. C.; Sharpelss, K. B., Large-scale and highly enantioselective synthesis of the Taxol C-13 side chain through asymmetric dihydroxylation. *J. Org. Chem.* **1994,** *59*, 5104 - 5105.
35. Denis, J. N.; Greene, A. E.; Serra, A. A.; Luche, M. J., An efficient, enantioselective synthesis of the taxol side chain. *J. Org. Chem.* **1986,** *51*, 46 - 50.
36. Deng, L.; Jacobsen, E. N., A practical, highly enantioselective synthesis of taxol side chain *via* asymmetric catalysis. *J. Org. Chem.* **1992,** *57*, 4320 - 4323.
37. Gou, D.-M.; Liu, Y.-C.; Chen, C.-S., A practical chemoenzymatic synthesis of the Taxol C-13 side chain *N*-benzoyl-(2R,3S)-3-phenylisoserine. *J. Org. Chem.* **1993,** *58*, 1287 - 1289.
38. Mukai, C.; Kim, I. J.; Furu, E.; Hanaoka, M., Highly stereocontrolled asymmetric synthesis of taxol and taxotere C-13 side chain analouges. *Tetrahedron* **1993,** *49*, 8323 - 8336.
39. Li, G.; Sharpless, K. B., Catalytic asymmetric aminonohydroxylation provides a short Taxol side-chain synthesis. *Acta. Chem. Scand.* **1996,** *50*, 649 - 651.

40. Kobayashi, S.; Ishitani, H.; Ueno, M., Catalytic asymmetric synthesis of both *syn*- and *anti*-B-amono alcohols. *J. Am. Chem. Soc.* **1998,** *120*, 431 - 432.
41. Holton, R. A. Vol. Eur. Pat. Appl. 1990.
42. Ojima, I.; M.;, S. C.; Zucco, M.; Park, Y. H.; Duclos, O.; Kuduk, S., A highly efficient route to taxotere by the B-lactam synthon method. *Tetrahedron Lett.* **1993,** *34*, 4149 - 4152.
43. Ojima, I.; Habus, I.; Zhao, M.; Zucco, M.; Park, Y. H.; Sun, C. M.; Brigaud, T., New and efficient approches to the semisynthesis of taxol and its C-13 side chain analogs by means of B-lactam synthon method. *Tetrahedron* **1992,** *48*, 6985 - 7012.
44. Ojima, I., Recent Advances in the B-Lactam Synthon Method. *Acc. Chem. Res.* **1995,** *28*, 383 - 389.
45. Guenard, D.; Gueitte-Voegelein, F.; Potier, P., Taxol and Taxotere: Discovery, Chemistry, and Structure-Activity Relationships. *Acc. Chem. Res.* **1992,** *26*, 160 - 167.
46. Verweij, J.; Clavel, M.; Chevalier, B., Paclitaxel (Taxol) and docetaxel (Taxotere): Not simply two of a kind. *Annals of Oncology* **1994,** *5*, 495 - 505.
47. Ojima, I.; Duclos, O.; Kuduk, S. D.; Sun, C. M.; Slater, J. C.; Lavelle, F.; Veith, J. M.; Bernacki, R. J., Synthesis and Biological Activity of 3'-alkyl- and 3'-alkenyl-3'-dephenyldocetaxel. *Bioorg. Med. Chem. Lett.* **1994,** *4*, 2631 - 2634.
48. Ojima, I.; Slater, J. C.; Michaud, E.; Kuduk, S.; Bounaud, P.-Y.; Vrignaud, P.; Bissery, M.-C.; Veith, J. M.; Pera, P.; Bernacki, R. J., Synthesis and Structure-Activity Relationships of the Second-Generation Antitumor Taxoids: Exceptional Activity against Drug-Resistant Cancer Cells. *J. Med. Chem.* **1996,** *39*, 3889 - 3896.
49. Gottesman, M.; Pastan, I., Biochemistry of multidrug ressitance mediated by the multidrug transporter. *Ann. Rev. Biochem.* **1993,** *62*, 385 - 427.
50. Skehan, P.; Streng, R.; Scudierok, D.; Monks, A.; McMahon, J.; Vistica, D.; Warren, J. T.; Bokesch, H.; Kenny, S.; Boyd, M. R., New Colorimetric Cytotoxicity Assay for Anticancer-Drug Screening. *J. Natl. Cancer. Int.* **1990,** *82*, 1107 - 1112.
51. Kuznetsova, L.; Chen, J.; Sun, L.; Wu, X.; Pepe, A.; Veith, J. M.; Pera, P.; Bernacki, R. J.; Ojima, I., Syntheses and evaluation of novel fatty acid-second-generation taxoid conjugates as promising anticancer agents. *Bioorg. Med. Chem. Lett.* **2006,** *16*, 974 - 977.
52. Chen, S.; Zhao, X.; Chen, J.; Chen, J.; Kuznetsova, L.; Wong, S. S.; Ojima, I., Mechanism-Based Tumor-Targeting Drug Delivery System. Validation of Efficient Vitamin Receptor-Mediated Endocytosis and Drug Release. *Bioconjugate Chem.* **2010,** *21*, 979 - 987.
53. J.;, C.; Chen, S.; Zhao, X.; Kuznetsova, L. V.; Wong, S. S.; Ojima, I., Functionalized Single-Walled Carbon Nanotubes as Rationally Designed Vehicles for Tumor-Targeted Drug Delivery. *J. Am. Chem. Soc.* **2008,** *130*, 16778 - 16785.
54. Botchkina, G. I.; Zuniga, E. S.; Manisha, D.; Wang, Y.; Wang, H.; Zhu, S.; Savitt, A. G.; Rowehl, R. A.; Leyfmann, Y.; Ju, J.; Shroyer, K.; Ojima, I., New-generation taxoid SB-T-1214 inhibits stem cell-related gene expression in 3D cancer spheroids induced by purified colon tumor-initiating cells. *Molecular Cancer* **2010,** *9*, 192.
55. Staudinger, H., *Justus Liebigs Annalen der Chemie* **1907,** *356*, 51 - 123.

56. Sheehan, J. C.; Henery-Logan, K. R., The Total Synthesis of Penicillin V. *J. Am. Chem. Soc.* **1958,** *81*, 3089 - 3094.
57. Evans, B. E.; Rittle, K. E.; Bock, M. G.; DiPardo, R. M.; Freidinger, R. M.; Whitter, W. L.; Lundell, G. F.; Veber, D. F.; Anderson, P. S.; Chang, R. S. L.; Lotti, V. J.; Cerino, D. J.; B.;, C. T.; Kling, P. J.; Kunkel, K. A.; Springer, J. P.; Hirshfield, J., Methods for Drug Discovery: Development of Potent, Selective, Orally Effective Cholecystokinin Antagonists *J. Med. Chem.* **1988,** *31*, 2235 - 2246.
58. Miller, M. J., Hydroxamate Approach to the Synthesis of B-Lactam Antibiotics. *Acc. Chem. Res.* **1986,** *19*, 49 - 56.
59. Hart, D. J.; Ha, D. C., The ester enolate-imine condesation route to beta-lactams. *Chem. Rev.* **1989,** *89*, 1447 - 1465.
60. Brown, M. J., Literature review of the ester enolate imine condensation. *Heterocycles* **1989,** *29*, 2225 - 2244.
61. Cainelli, G.; Panunzio, M.; Andreoli, P.; Martelli, G.; Spunta, G.; Giacomini, D.; Bandini, E., Metallo-imines: useful reagents in organic synthesis. *Pure Appl. Chem.* **1990,** *62*, 605 - 612.
62. Fujisawa, T.; Shimizu, M., Switching of stereochemistry using different metal enolate species for construction of B-lactam skeletons. *Rev. Heteroatom Chem.* **1996,** *15*, 203 - 225.
63. Xu, J., Steroselectivity in the synthesis of 2-azetidinones from ketenes and imines via the Staudinger reaction. *ARKIVOC* **2009**, 21 - 44.
64. Hegedus, L. S., Synthesis of Amino Acids and Peptides Using Chromium Carbene Complex Photochemistry. *Acc. Chem. Res.* **1995,** *28*, 299 - 305.
65. Chmielewski, M.; Kaluza, Z.; Furman, B., Stereocontrolled synthesis of 1-oxabicyclic B-lactam antibiotics *via* [2 + 2]cycloaddition of isocyanates to sugar vinyl ethers. *Chem. Commun.* **1996**, 2689 - 2696.
66. Brieva, R.; Crich, J. Z.; Sih, C. J., Chemoenzymatic Synthesis of the C-13 Chain of Taxol: Optically-Active 3-Hydroxy-4-phenyl B-Lactam Derivatives. *J. Org. Chem.* **1993,** *58*, 1068 - 1075.
67. Georg, G. I.; Ravikumar, V. T., Stereocontrolled ketene-imine cycloaddition reactions. In Organic Chemistry of *B*-Lactams. Georg, G. I., Ed. VCH: New York1993.
68. Cossio, F. P.; Ugalde, J. M.; Lopez, X.; Lecea, B.; Palomo, C., A semiempierical theoretical study on the formation of B-lactams from ketenes and imines. *J. Am. Chem. Soc.* **1993,** *115*, 995 - 1004.
69. Cossio, F. P.; Arrieta, A.; Lecea, B.; Ugalde, J. M., Chiral Control in the Staudinger Reaction between Ketenes and Imines. A Theoretical SCF-MO Study on Asymmetric Torquoselectivity. *J. Am. Chem. Soc.* **1994,** *116*, 2085 - 2093.
70. Lopez, R.; Sordo, T. L.; Sordo, J. A.; Gonzalez, J., Torquoelectronic effect in the control of the steroselectivity of ketene-imine cycloaddition reactions. *J. Org. Chem.* **1993,** *58*, 7036 - 7037.

71. Jiao, L.; Liang, Y.; Xu, J., Origin of the Relative Stereoselectivity of the B-Lactam Formation in the Staudinger Reaction. *J. Am. Chem. Soc.* **2006,** *128*, 6060 - 6069.
72. Zhao, X. Ph. D. Dissertation: Design, synthesis and biological evaluation of novel taxane-based anticancer agents and their applications to tumor-targeting drug delivery systems. Stony Brook University2009.
73. Palomo, C.; Aizpurua, J. M.; Ganboa, I.; Oiarbide, M., Asymmetric synthesis of β-Lactams by Staudinger ketene-imine cycloaddtion reaction. *Eur. J. Org. Chem.* **1999,** *1999*, 3223 - 3235.
74. Liang, Y.; Jiao, L.; Zhang, S.; Yu, Z.-X.; Xu, J., New insights into the torquoselectivity of the Staudinger Reaction. *J. Am. Chem. Soc.* **2009,** *131*, 1542 - 1549.
75. Cossio, F.; Arrieta, A.; Sierra, M., The mechanism of the ketene-imine (Staundinger) Reaction in its centennial: Still and unsolved problem? *Acc. Chem. Res.* **2008,** *41*, 925 - 936.
76. Ojima, I.; Park, Y. H.; Sun, C. M.; Brigaud, T.; Zhao, M., New and efficient routes to norstatine and its analogs with high enantiomeric purity by B-Lactam Synthon Method. *Tetrahedron Lett.* **1992,** *33*, 5737 - 5740.
77. Whitesell, J. K.; Chen, H. H.; Lawrence, R. M., trans-2-Phenylcyclohexanol. A powerful and redibly available chiral auxilary. *J. Org. Chem.* **1985,** *50*, 4663 - 4664.
78. Schwartz, A.; Madan, P.; Whitesell, J. K.; Lawrence, R. M., Lipase-catalyzed kinetic resolution of alcohols via chloroacetate esters: (-)-(1R,2S)-trans-2-phenylcyclohexanol and (+)-(1S,2R)-trans-2-phenylcyclohexanol. *Org. Syn.* **1990,** *69*, 1 - 9.
79. Seitz, J. Ph.D. Dissertatoin: The design, synthesis and biological evaluation of novel taxoid anticancer agents and their tumor-targeted drug conjugates. Stony Brook University2013.
80. Tietze, L. F.; Gericke, K. M.; Guntner, C., First Total Synthesis of the Bioactive Anthraquinone Kwanzoquinone C and Related Natural Products by a Diels-Alder Approach. *Eur. J. Org. Chem.* **2006,** *2006*, 4910 - 4915.
81. King, S. B.; Sharpelss, K. B., An Efficient Synthesis of Enantiomerically Pure *trans*-2-Phenylcylohexanol. *Tetrahedron Lett.* **1994,** *35*, 5611 - 5612.
82. Gonzalez, J.; Aurigemma, C.; Truesdale, L., Synthesis of (+)-(1S,2R)- and (-)-(1R,2S)-trans-2-phenylcyclohexanol via Sharpless asymmetric dihydroxylation (AD). *Org. Synth.* **2002,** *79*, 93 - 99.
83. Sharpless, K. B.; Amberg, W.; Youssef, B. L.; Crispino, G. A.; Hartung, J.; Jeong, K.-S.; Kwong, H.-L.; Morikawa, K.; Wang, Z.-M.; Xu, D.; Zhang, X.-L., The Oxmium-Catalyzed Asymmetric Dihydroxylation: A New Ligand Class and a Process Improvement. *J. Org. Chem.* **1992,** *57*, 2768 - 2771.
84. Ojima, I.; Sun, L.; Borell, C. P.; Wang, T.; Miller, M. L.; Lin, S.; Geng, X.; Kuznetsova, L.; Qu, C.; Gallager, D.; Zhao, X.; Zanardi, I.; Xia, S.; Horwitz, S. B.; Mallen-St. Clair, J.; Guerriero, J. L.; Bar-Sagi, D.; Veith, J. M.; Pera, P.; Bernacki, R. J., Design, Synthesis, and Biological Evaluation of New-Generation Taxoids. *J. Med. Chem.* **2008,** *51*, 3203 - 3221.

85. Ojima, I.; Slater, J. C.; Kuduk, S. D.; Takeuchi, C. S.; Gimi, R. H.; Sun, C.-M.; Park, Y. H.; Pera, P.; Veith, J. M.; Bernacki, R. J., Synthesis and Structure - Activity Relationships of Taxoids Derived From 14B-Hydroxy-10-deacetylbaccatin III. *J. Med. Chem.* **1997,** *40*, 267 - 278.
86. Lin, S.; Geng, X.; Qu, C.; Tynebor, R.; Gallagher, D. J.; Pollina, E.; Rutter, J.; Ojima, I., Synthesis of Highly Potent Second-Generation Taxoids Through Effective Kinetic Resolution Coupling of Racemic B-Lactams with Baccatins. *Chirality* **2000,** *12*, 431 - 441.
87. Slater, J. C. PhD Dissertation. Stony Brook University1997.
88. Lin, S. Ph.D. Dissertation. Stony Brook University1999.
89. Ceylan, M.; Budak, Y.; Gurdere, M. B.; Ozdemir, I.; Findik, E., Synthesis and Isolation of 1-Cyclohex-1,2-dien-1-ylbenzene from 1-(2-Iodocyclohex-1-en-1-yl)benzene and 1-(2-Iodocyclohex-2-en-1-yl)benzene. *Turk. J. Chem.* **2007,** *31*, 647 - 657.
90. King, S. B.; Sharpelss, B. K., An Efficient Synthesis of Enantiomerically Pure trans-2-Phenylcyclohexanol. *Tetrahedron Lett.* **1994,** *35*, 5611 - 5612.
91. Brenner, S.; Goelet, P.; Stackhouse, J.; Millward, S. W. Drug conjugates and methods of designing the same. WO 01/13958 A2, 01-03-2001, **2001**.
92. Batchelor, M. J.; Bebbington, D.; Bemis, G. W.; Fridman, W. H.; Gillespie, R. J.; Golec, J. M. C.; Gu, Y.; Lauffer, D. J.; Livingston, D. J.; Matharu, S. S.; Mullican, M. D.; Murcko, M. A.; Murdoch, R.; Nyce, P. L.; Robidoux, A. L. C.; Su, M.; Wannamaker, M. W.; Wilson, K. P.; Zelle, R. E. Inhibitors of interleukin-1B converting enzyme. WO 9722619, **1997**.

Chapter 2

Tumor Targeted Chemotherapy

Content

§2.0 Introduction:

§2.0.1 Tumor-targeted Chemotherapeutics:

One of the most common problems in the development of effective chemotherapeutics is their inherent lack of specificity; generally between actively dividing normal tissues and tumor tissues. Current chemotherapy relies on the assumption that cytotoxic agents will be more readily taken up by rapidly dividing cancer cells.[1] In actuality, many other types of rapidly dividing healthy tissues (e.g., bone marrow, hair follicles) can also be affected, leading to off-target systemic toxicity. In addition to concerns of target liability, clinically effective treatment of cancer via chemotherapy requires excessive tumor mass reduction exceeding 99 % to viably reduce tumor growth and suppress metathesis. Thus, despite the many new promising chemotherapeutic therapies currently available clinically, there still remains an ongoing effort to improve upon existing treatments by both increasing potency while reducing side effects.

Extensive efforts by the Ojima laboratory over the past 10 years have focused on developing highly efficacious tumor-targeting drug conjugates to overcome the shortcomings of conventional chemotherapy.[2-6] These conjugates make use of the inherent differences between normal cell types and the expression levels of specific biomarkers on the cancer cell surface. For example, rapidly growing cancer cells often overexpress receptors for the enhanced uptake of nutrients critical for their enhanced proliferation. Furthermore, enhanced receptor levels on the surface of the cancer cells can provide molecular targets for the delivery of cytotoxic drugs through receptor-mediated endocytosis.

A variety of ligands for receptor specific targeting have been exploited to create various targeted chemotherapeutics in the Ojima laboratory **(Figure 2-1)**.[4, 5, 7-9] Among these include monoclonal antibodies (mAbs), polyunsaturated fatty acids (PUFAs), vitamins such as biotin and folic acid, and recently designed ankyrin repeat proteins (DARPin's). These conjugates typically consist of a tumor-targeting molecule (TTM) connected to an anticancer agent via a suitable "smart" linker. Furthermore, these tumor-activated prodrugs (TAPs) remain nontoxic and stable within blood circulation to minimize systemic toxicity, but are effectively release once internalized into targeted tumor cell types.

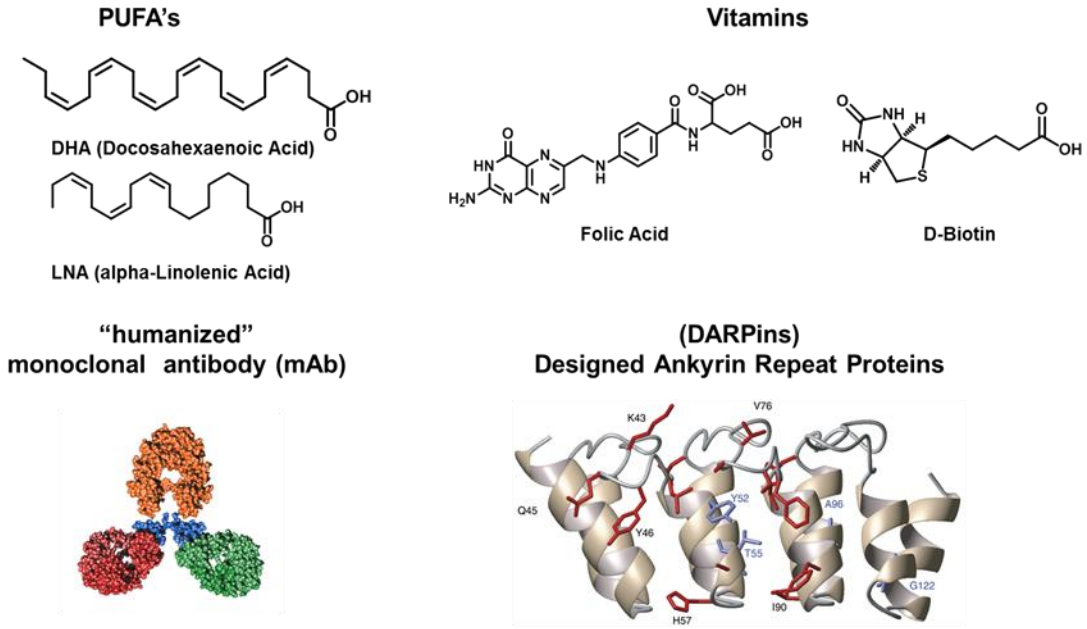

Figure 2-1. Various tumor targeting modules used in the Ojima laboratory (Adapted with permission from reference [8])

§2.0.2 Self Immolative Disulfide "Smart" Linkers:

Originally, 1st generation disulfide linkers were designed for the effective delivery of taxoids via mAb's; linking the mAb to the taxoid at the C-10 position.[10] Nevertheless, functionalization at the C-10 proved problematic, contributing to an 8 fold drop in potency. This loss in potency ultimately resulted in the failure of this conjugate in more advanced clinical trials. Thus, considerable efforts were focused on developing a new linker system by which the taxoid could be released fully without any loss of activity.

2nd generation linkers were designed specifically to reestablish the cytotoxic agent to its original form and potency.[5] Furthermore, these linkers were made somewhat versatile so that they could be coupled, after modifications, to any TTM or cytotoxic agent. The mechanism-based design provided a drug release cascade triggered by intercellular glutathione, thereby cleaving the disulfide linkage. Specifically, this design enabled the TTM and lower section of the linker to be susceptible to attack by the naturally increased levels of reduced glutathione found within tumor tissues, while the upper portion of the linker, still attached to the cytotoxic agent, underwent nucleophilic acyl substitution of the ester moiety forming a 5 member thiolactone ring releasing the taxoid. Thus after cyclization of the thiolactone, the cytotoxic agent is returned to its original form, thereby reactivating its activity as seen in **Figure 2-2**.

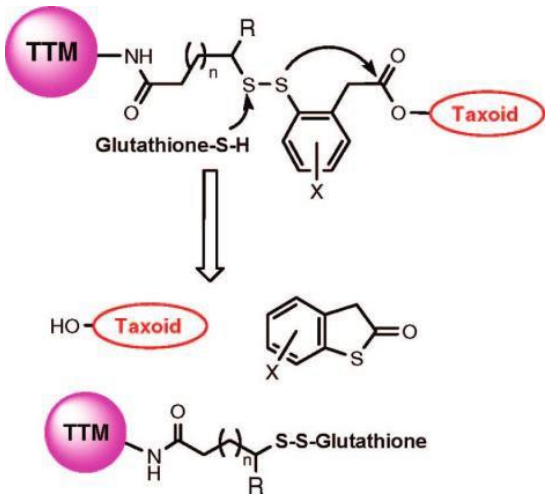

Figure 2-2: Proposed cleavage mechanism for 2nd generation disulfide "smart" linkers. Attack of the disulfide bond by glutathione, intramolecular ring closure proceeds to form a thiolactone ring results in liberation of the ester bond freeing the taxoid. (Reprinted with permission from [5]. Copyright (2005) American Chemical Society.)

To provide a detailed measurement of this thiolactonization based release mechanism, a model reaction of the 2nd generation linker was monitored using ^{19}F NMR. *Para*-fluoro phenol was used to mimic a drug while an additional fluorine tag was incorporated into the aromatic ring of linker. Cysteine was then used to mimic the effect of glutathione in a pH 7.4 buffer solution at 37 ^{o}C with acetonitrile as a co-solvent. Kinetics of the linker cyclization was monitored using a time-dependent ^{19}F NMR technique to show the thiolactone formation and ester bond cleavage as shown in **Figure 2-3**. The time-dependent chemical shift change showed the occurrence of chemical ligation and thiolactone formation. This experiment was then re-performed on SB-T-1213 to show validation of the taxoid-2nd generation linker system.

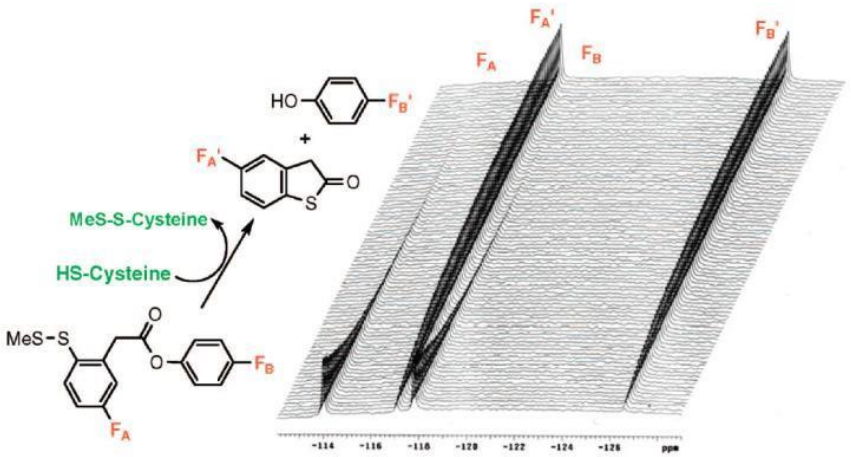

Figure 2-3: ^{19}F NMR experimental based evidence of ester bond ligation following linker disulfide bond cleavage (Reprinted with permission from [5]. Copyright (2005) American Chemical Society.)

Self-immolative disulfide linkers have been validated *in-vitro* and carry and release taxoid's efficiently inside cancer cells primarily by receptor mediated endocytosis (RME).[2d] The process of RME for the biotin-taxoid conjugate is illustrated in **Figure 2-4**. Second generation disulfide linkers have been incorporated into numerous drug delivery systems and have been evaluated against various cancer cell lines.

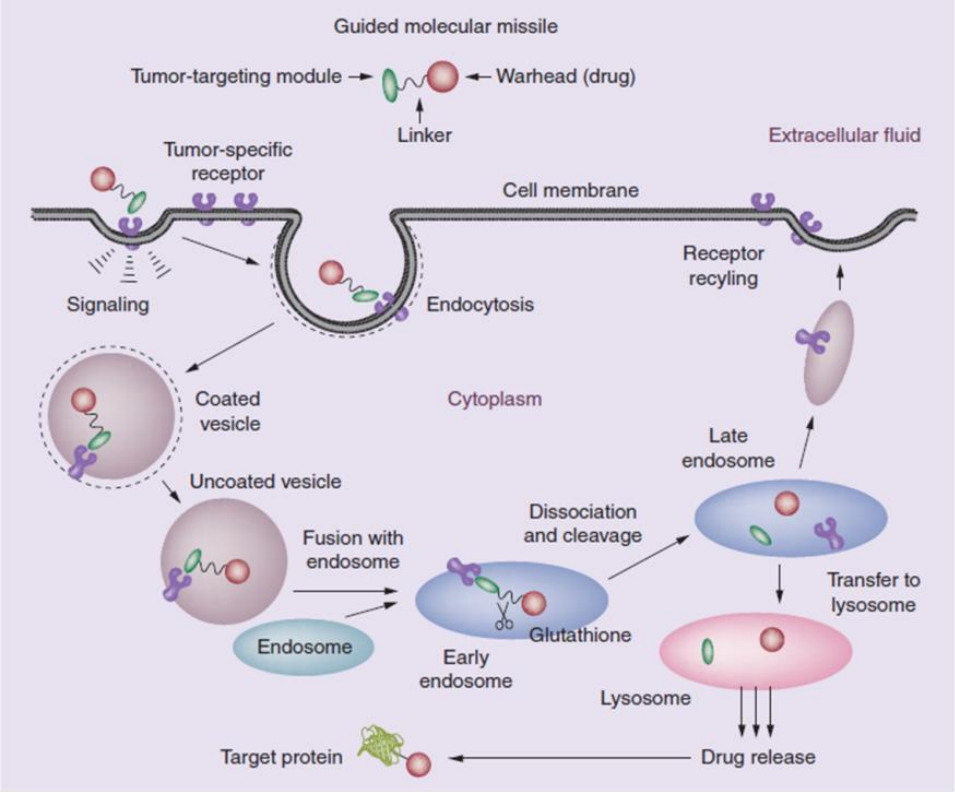

Figure 2-4: RME of a TTM-linker-drug conjugate "guided molecular missile". The tumor activated prodrug (TAP) is composed of a TTM, a linker, and a warhead or drug. First, the TAP binds a tumor specific receptor on the surface of the cell followed by cell signaling. The receptor-conjugate complex is then internalized by clathrin coated vesicles at the surface of the cell membrane. De-polymerization of the clathrin coating is then followed by fusion with an endosome forming an "early endosome". At this step, high intracellular levels of reduced glutathione within the cancer cell cleave the disulfide linker, resulting in the dissociation of the drug into the lysosome and ultimately incorporation into the cytosol where it can act upon its target. The unbound receptor is then recycled to the cell surface within the endosome. (Reproduced from [6], with permission of Future Science Ltd)

§2.0.3 Vitamin Based Taxoid Conjugates:

Typically, a vitamin mediated tumor targeting conjugate consists of 3 essential parts as shown in **Figure 2-5**. Each is crucial to the activity and delivery of the active drug attached. The TTM is responsible in cell discrimination and binding to the cell membrane surface. The TTM is also important in transport of the pro-drug into to cell. The "smart" linker is important in keeping the drug inactive

during transport to the targeted cell, as well as reactivation of the drug by chemical detachment from the TTM. Lastly, the drug is important in the mechanism of action desired. In the case of cancer, the drug released is a cytotoxic agent that regains its potency after chemical ligation.

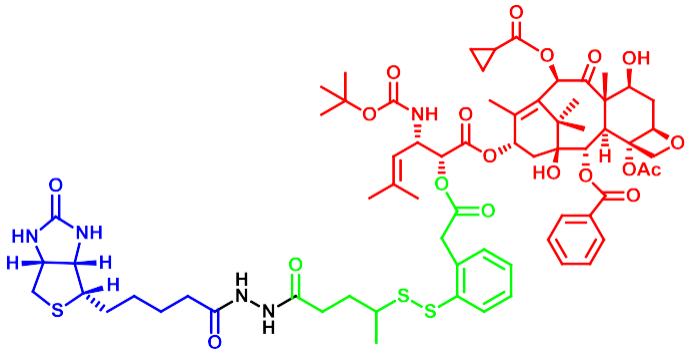

Figure 2-5: A vitamin-linker-drug conjugate. Three distinct parts make up a vitamin-linker-drug conjugate: TTM (blue), "smart" linker (green), and cytotoxic drug (red).

§2.0.3.1 Folic Acid Targeting Taxoid Conjugates:

Folic acid (vitamin B9) is an important cofactor in one-carbon transfer reactions in de novo nucleotide biosynthesis and plays crucial roles in DNA and RNA synthesis, cellular proliferation and survival pathways.[11] Nevertheless, folate is nonindigenous to animals which incorporated this vitamin primarily through their diet.[12, 13] Thus, folic acid has been studied by various research groups involved with tumor-targeting chemotherapies since rapidly dividing cells elevate their folic acid intake to compensate for their rising metabolic needs.[8, 12-17]

The Ojima laboratory has designed a folate-taxoid conjugate bearing second generation taxoid SB-T-1214 which has shown promise in targeted drug delivery shown in **Figure 2-6**.[7] *In-vitro* evaluation of this conjugate has clearly shown that L1210FR, ID8 and L1210 cell lines overexpressing folate receptors exhibit substantial cytotoxicity when compared with cell line A549 (1000 times greater than folate (-) cell line A549) as shown in **Table 2-1**.

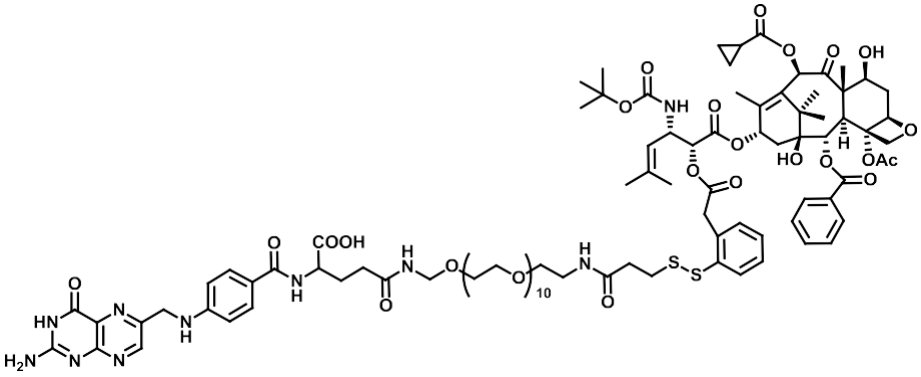

Figure 2-6: Folic acid-SB-T-1214 conjugate

Table 2-1: Folate-SB-T-1214 *in vitro* cytotoxicity results against various cell lines			
Cell Line	Paclitaxel	SB-T-1214	Folate-SB-T-1214
L1210	180 nM	17.0 nM	13 nM
L1210FR	200 nM	11.5 nM	3 nM
A549	7.3 nM	1.4 nM	> 1000 nM
ID8	36.4 nM	7.6 nM	< 1 nM

§2.0.3.2 Biotin Targeting Taxoid Conjugates:

In 2004, various cancer cell types were screened by Russel-Jones et al. versus several vitamin B subtypes (B_6, B_7, B_{12}) seen in **Figure 2-7**.[18] Interestingly, in addition to an increased expression of folate receptors, biotin receptors were also over expressed, and in several particular cases predominantly.

Biotin (vitamin B_7) is essential for cell division, cell growth, fatty acid production, metabolism of fats and amino acids and plays a role in energy production. Thus the use of biotin as a tumor-targeting moiety, a previously unexplored option, seemed quite relevant and promising as a new targeting therapy. These results have subsequently led the Ojima laboratory to investigate biotin-based tumor targeting drug delivery systems shown in **Figure 2-8**.[3] *In vitro* cytotoxicity assays showed clearly that only (L1210FR) overexpressing the biotin receptor showed substantial activity (100 times greater than biotin (-) cell lines L1210 and WI38) shown in **Table 2-2**.

Tumour	Mouse	Type	Folate	Cbl	Biotin
O157	Balb/C	Bcell lymph	+/–	+/–	+/–
BW5147	AKR/J	Lymphoma	+/–	+/–	+/–
B16	C57/Bl	Melanoma	–	–	–
LL-2	C57/Bl	Lung	–	–	–
HCT-116	Balb/C-Nu	Colon	–	–	–
L1210	DBA/2	Leukemia	+/–	+/–	–
L1210FR	DBA/2	Leukemia	++	+	+++
Ov 2008	Balb/C-Nu	Ovarian	+++	–	++
ID8	C57/Bl	Ovarian	+++	–	++
Ovcar-3		Ovarian	+++	–	++
Colo-26	Balb/C	Colon	+/–	++	+++
P815	DBA/2	Mastocytoma	+/–	++	+++
M109	Balb/C	Lung	+	+++	+++
RENCA	Balb/C	Renal cell	+	+++	+++
RD995	C3H/HeJ	Renal cell	+	++	+++
4T1	Balb/C	Breast	+	++	+++
JC	Balb/C	Breast	+	++	+++
MMT060562	Balb/C	Breast	+	++	+++

Figure 2-7: Biotin expression in several tumor cell lines and tissue types. The positive (+) sign represents expression while additional (+) signs represent over expression in that particular cell type versus normal cells. (Reprinted with permission from reference [18])

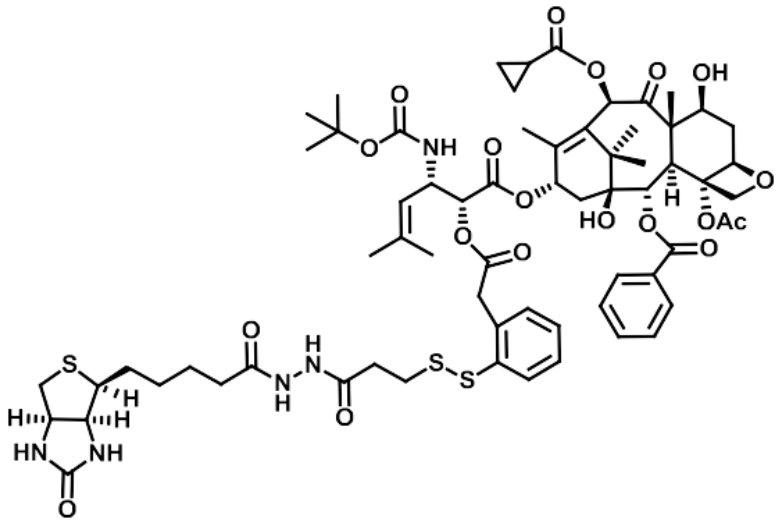

Figure 2-8: Biotin-"smart linker"-SB-T-1214 conjugate.

Table 2-2: (3C)-BLT *in vitro* cytotoxicity results against various cell lines.			
Cell Line	Paclitaxel	SB-T-1214	Biotin-SB-T-1214
L1210	151 nM	9.72 nM	522 nM
L1210FR	121 nM	9.50 nM	8.80 nM
WI38	157 nM	10.7 nM	570 nM

§2.1 Re-synthesis of the (5C)-BLT Conjugate:

§2.1.1 Introduction:

Biotin-Linker-Taxoid (BLT) conjugates make use of the essential vitamin (D)-biotin linked via a disulfide "smart linker" to a cytotoxic drug. Previously, the Ojima group reported the synthesis of both (3C)-BLT and (5C)-BLT conjugates. The (3C)-BLT conjugate was used for the validation of RME via biotin receptors, although this particular conjugate was known to be susceptible to premature drug release in blood plasma due to a reverse Michael addition (beta- elimination) pathway shown in **Figure 2-9**. Thus, two alternatives for *in vivo* applications were the previously synthesized (5C)-BLT and a novel conjugate, the (4C)-BLT shown in **Figure 2-10**. Precise, release times of these conjugates were however unknown, and therefore, synthesis and analysis of both would be optimal to understand their *in vivo* stability.

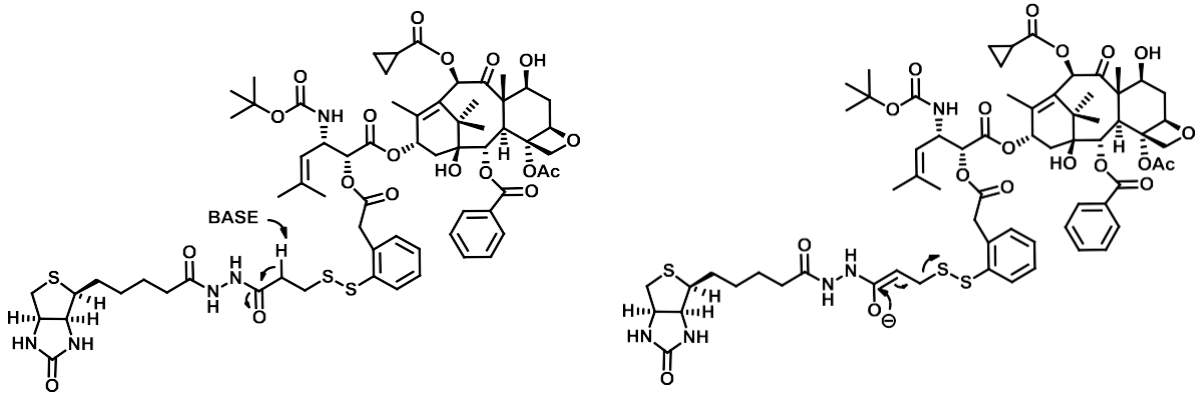

Figure 2-9: Proposed reverse Michael addition pathway for the breakdown of the (3C)-BLT conjugates.

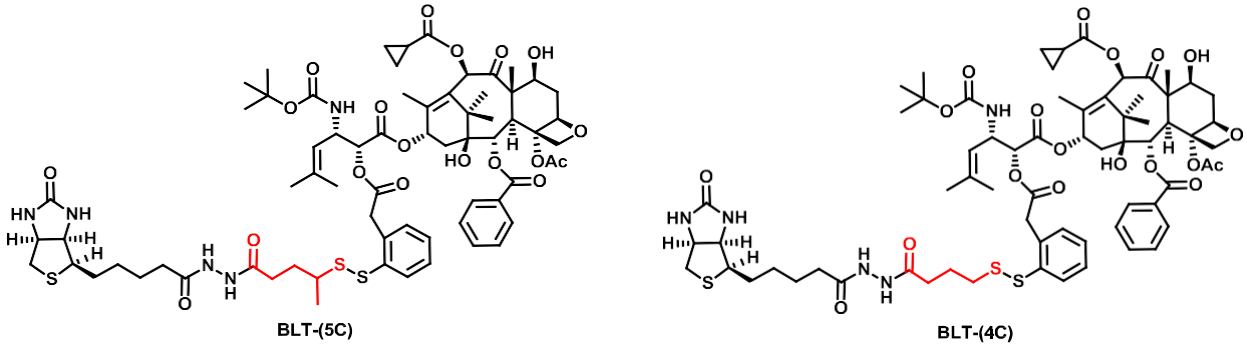

Figure 2-10: Proposed alternative BLT conjugates. Highlighted in red is the alkyl tether substituent modified for each conjugate.

§2.1.2-Results and Discussion:

§2.1.2.1-Mercaptopentanoic Acid Optimization:

Traditional synthesis of 4-mercaptopentanoic acid has provided typically 29 to 38 % yield after 3 steps as shown in **Scheme 2-1**.[19] Synthesis typically began with ring opening of γ-valerolactone with 2 equivalence of boron tribromide to yield crude 4-bromopentanoic acid 2-1 after 48 hours. This reaction was observed to be reversible and therefore could revert back to starting material. Nucleophilic substitution of the bromide group was then subsequently accomplished by refluxing with 1.2 equivalence of thiourea in methanol to form the crude thiouronium bromide salt methoxy ester 2-2 in 48 hours. Thereafter, this salt was subsequently treated with aqueous 8 M KOH at 60 ^{o}C neat to afford the hydrolyzed product 4-mercapto-pentanoic acid 38% 2-3 after 48 hours. This synthetic route provided only low quantities of the desired compound. Long reaction times, poor quality and low yields all provided an impetus for method improvement.

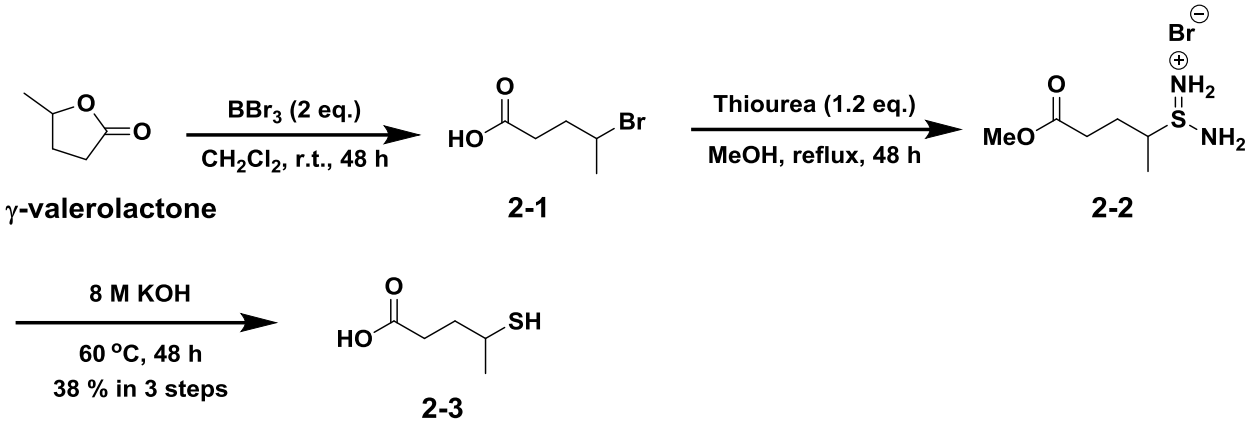

Scheme 2-1: Traditional synthetic route towards 4-mercaptopentanoic acid.[19]

In an attempt to increase yield, initial modifications were focused on accessing the secondary thiol through the thioketal formation of 4-oxo-pentanoic acid and subsequent decomposition in the presence of strong base. However, this route remained unfruitful and yielded only the undesired n-butyl addition to the carboxylic acid.

A new synthetic strategy towards 4-mercaptopentanoic acid was devised. Using methodology developed earlier by Langford et al., 4-mercaptobutanoic acid could be obtained in two steps with 73 % yield shown in **Scheme 2-2**.[20] Following their conditions, γ-valerolactone was reacted with 1.1 equivalent of thiourea in 1.2 equivalent of 48 % hydrobromic acid at reflux condition (135 ^{o}C) and was found to produce the desired isothiouronium bromide salt. This reaction was monitored by FIA Positive Mass for 9.5 hours after which no more starting material was consumed. The solution was then treated with 25 equivalents of 25 M NaOH to produce the desired crude 4-mercapto-pentanoic acid (52 % based on 1H NMR) in 3 hours after an acid workup to pH 2 with 6 M HCl. Surprisingly, this procedure did not produce the desired yield of 73 % as noted by Langford et al. for 4-mercaptobutyric acid. However, it did require less time (12.5 hours total) and less solvent then the previous scheme. The lower yield was most likely caused by the steric crowding of the secondary carbon in the Sn2 like attack of thiourea.

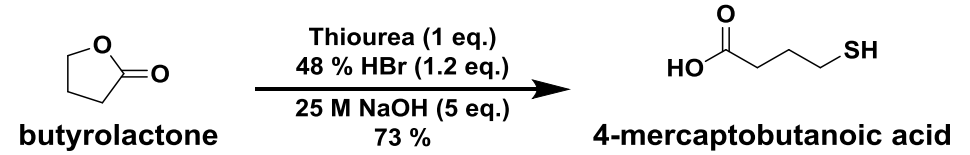

Scheme 2-2: Langford protocol for the synthesis of 4-mercaptobutanoic acid.[20]

Initial success of the Langford synthetic scheme subsequently led to further optimization. At first, it was not clear whether increasing the acid or the nucleophile would be more beneficial. Thus,

the amount of hydrobromic acid used was increased to 5 equivalents, resulted in a surprising decrease in yield to 46 %. Interestingly, the rate of ring opening of the γ-valerolactone was not the issue; rather, the activation energy barrier for nucleophilic attack.

Based upon the idea of a Sn2 type reaction scheme, thiourea was increased from 1.1 equivalents to 2.0 equivalents and the reflux time was increased to 24 hours. Furthermore, the remaining starting material could be extracting in acidic conditions as the isothiouronium bromide salt **2-4** generated was water soluble while the remaining unreacted γ-valerolactone remained in the organic layer. Subsequent hydrolysis with 25 equivalents of 25 M NaOH thereby resulted in 64 % of the desired product **2-3**. This result showed that the quantity of nucleophile influenced the reaction, and so different quantities were evaluated as shown in **Table 2-3**. Plotting the data, an exponential relationship could be extrapolated for the product versus the quantity of thiourea as seen in **Figure 2-11**. Theoretically, one could reach almost quantitative yields; however, the most reasonable amount of thiourea centered on 5 equivalents and about an 80 % yield seen in **Scheme 2-3**. In addition, it was also discovered that longer refluxing times were required for a larger quantity of substrate.

Table 2-3: Optimizations for the synthesis of 4-mercaptopentanoic acid

γ-valerolactone (mM)	Thiourea (equivalents)	Hydrobromic acid (equivalents)	Time (hours)	Yield (%)
5	1.1	1.2	9.5	52
10	1.1	5.0	18	46
10	2.0	5.0	24	64
10	5.0	6.3	24	79
50	5.0	6.3	48	76

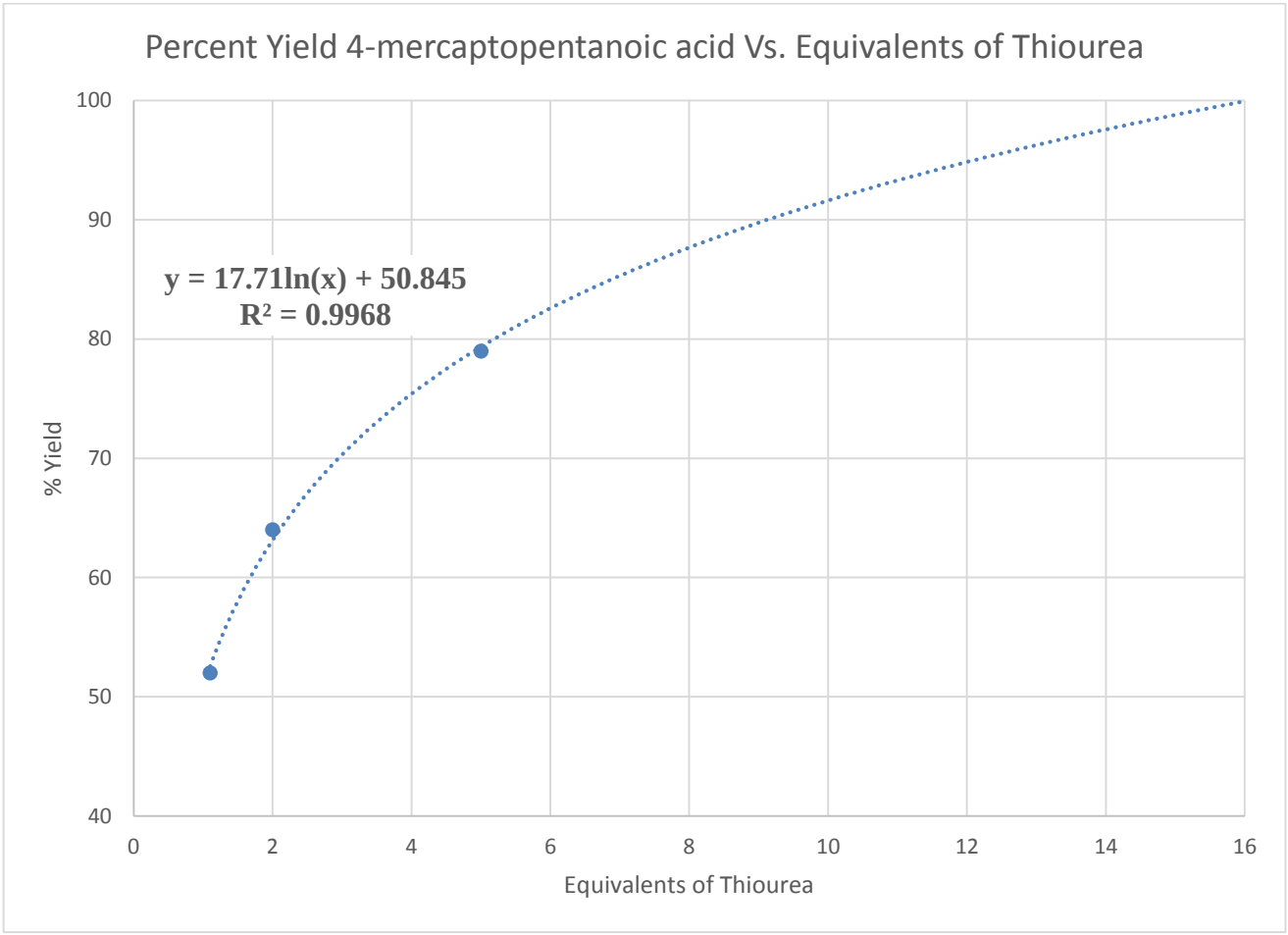

Figure 2-11: Quantity of thiourea versus produced 4-mercaptopentanoic acid

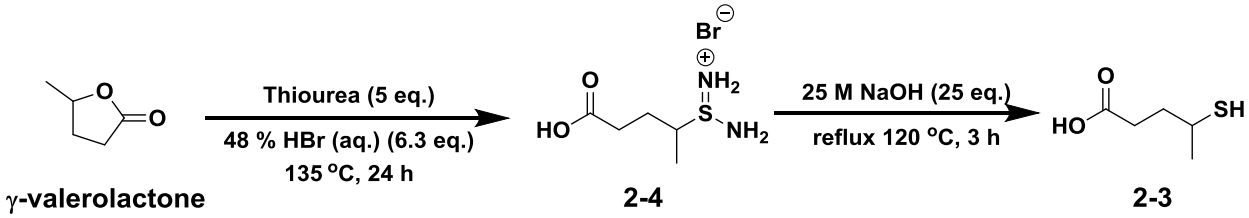

Scheme 2-3: Optimized synthesis of 4-mercaptopentanoic acid.

§2.1.2.2 Synthesis of 2-Mercaptophenylacetic Acid:

Following previous methodology from the Ojima laboratory, synthesis of 2-mercaptophenylacetic acid was accomplished in good yield in two steps shown in **Scheme 2-4**. Starting from benzothiophene-2-boronic acid, treatment with 30 % peroxide in ethanol provided benzothiolactone **2-5** in good yeild after 12 hours. Benzothiolactone **2-5** was then subsequently hydrolyzed with LiOH at 60 °C to afford 2-meracaptophenylacetic acid **2-6** in good yield after 10 hours and HCl workup.

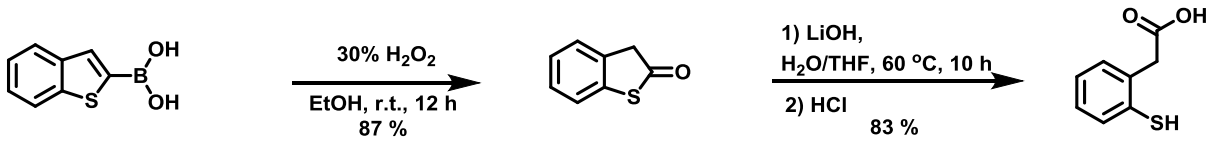

Benzothiophene-2-boronic acid **2-5** **2-6**

Scheme 2-4: Synthesis of upper-linker tether 2-mercaptophenylacetic acid **2-6**.

§2.1.2.3 Synthesis of the (5C)-SB-T-1214 Couple-Ready Construct:

In addition to providing an improved route for (5C)-linker synthesis, re-synthesis of the (5C)-BLT conjugate was performed for the purpose of evaluating linker release rates. Re-synthesis of the completed (5C)-linker was thus required additionally to provided substrate for conjugation with the second-generation taxoid SB-T-1214. Re-synthesis of (5C)-linker for the purpose of BLT-conjugates has remained a bottle-neck as the linker was found to be highly unstable when stored. It has been proposed that the phenylacetic acid moiety promotes the deprotection or transesterification of the TIPS ester. Thus in general, it was discovered that the (5C)-linker could only be stored after drug coupling.

Re-synthesis of the couple-ready SB-T-1214 (5C)-linker construct **2-13** was accomplished in 6 steps **(Scheme 2-5)** from 4-mercaptopentanoic acid **2-3** previously optimized. First, the sulfhydryl group of compound **2-3** was activated using a di-pyridine-di-sulfide (DPDS). This reaction proceeded by means of a slow addition of 6 equivalents DPDS in ethanol to **2-3** in ethanol in reflux conditions to yield the resulting compound **2-7** in good yield. Protection of the carboxylic acid end of compound **2-7** with a TIPS group was accomplished in high yield to afford compound **2-8**. The resulting compound **2-8** with both activated disulfide and protected carboxylic acid was then subsequently exchanged with 2-mercapto phenylacetic acid in THF at 0 ^{o}C for 4 hours to yield compound **2-9** in high yield. As stated previously, protection of the carboxylic acid end of **2-8** provided desymmetrization of the linker, with only one free carboxylic acid end for drug coupling. Thus in the presence of excess drug (1.5 eq.), attachment of the linker to the C2' alcohol of SB-T-1214 was accomplished in high yield utilizing the coupling reagent DIC with a catalytic amount of DMAP at 0 ^{o}C. Lastly, TIPS removal and subsequent activation of the previously protected carboxylic acid end was accomplished in two steps in high yields to afford the couple-ready SB-T-1214 construct **2-12**.

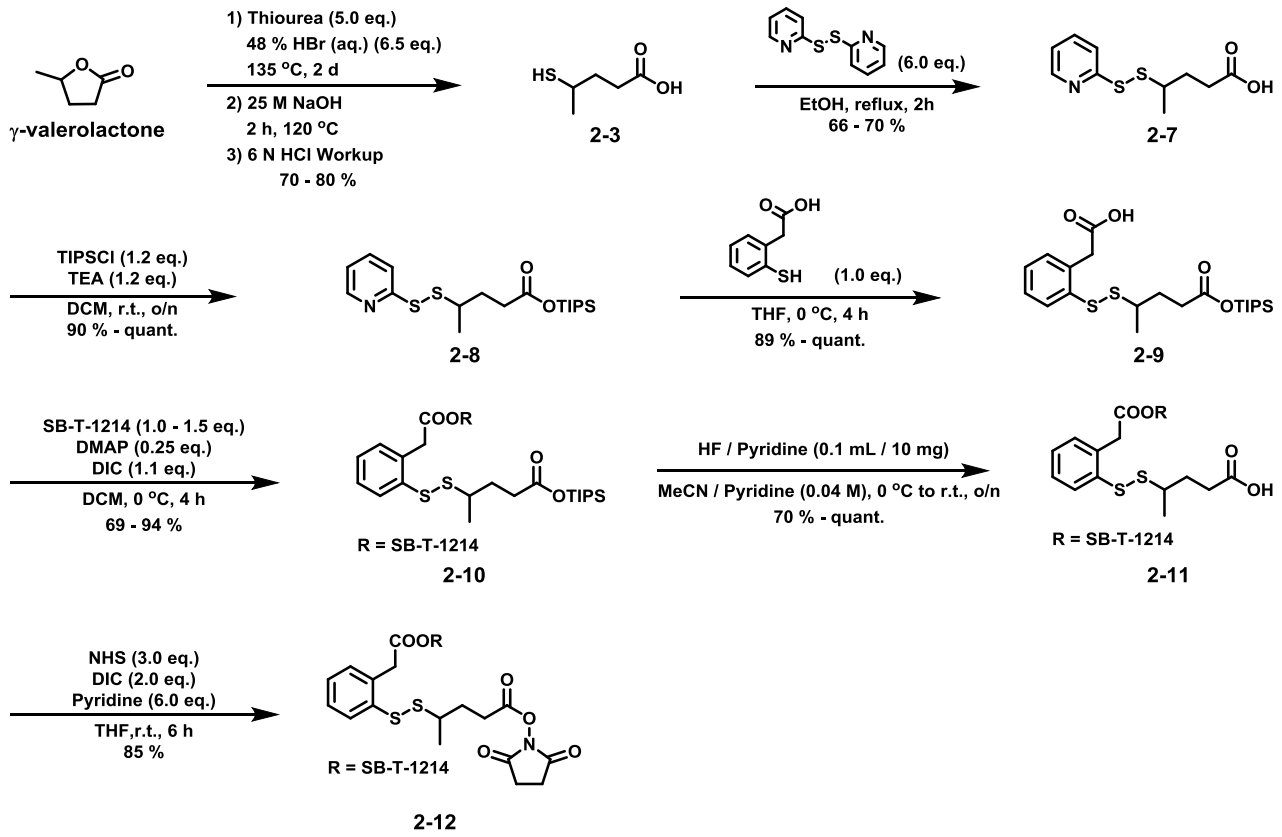

Scheme 2-5: Re-synthesis of Couple-Ready SB-T-1214 construct **2-12**.

§2.1.2.4 Synthesis of Biotin Hydrazide:

In order to provide a hydrazide bond between the linker and TTM resistant to hydrolysis, biotin was first modified with hydrazine. Incorporation of the hydrazine into biotin was accomplished through condensation between (D)-biotin-methyl ester and hydrazine shown in **Scheme 2-6**. D-Biotin was esterified with methanol by the addition of thionyl chloride to afford the compound **2-13** in high yield. This was followed by condensation in the presence of excess (5.0 eq.) hydrazine in methanol at reflux to yield compound **2-14** in high yield.

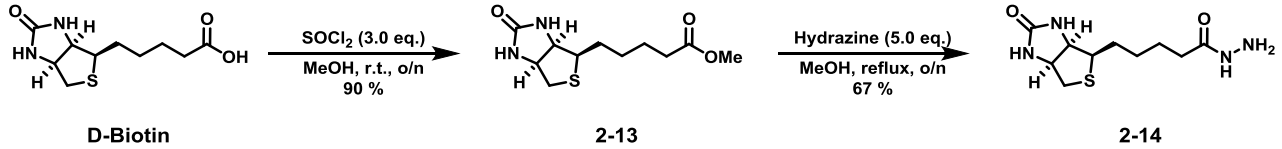

Scheme 2-6: Synthesis of Biotin-hydrazide compound **2-14** from D-Biotin.

§2.1.2.5 Coupling Biotin to the SB-T-1214 Couple-Ready Construct:

With the couple-ready SB-T-1214 construct **2-12** and (D)-biotin-hydrazide **2-14** in hand, the final coupling was attempted to produce the (5C)-BLT conjugate **2-15** as seen in **Scheme 2-7**. First the compound **2-12** was diluted in DMSO to a final concentration of 0.5 M and then 0.5 equivalence

of biotin hydrazide **2-14** was added. The resulting solution was then allowed to react over 2 days at room temperature while monitoring by TLC. After two days the reaction was worked up, and the resulting (5C)-BLT conjugate **2-15** was obtained in moderate yield. The remaining unreacted construct **2-12** was recovered.

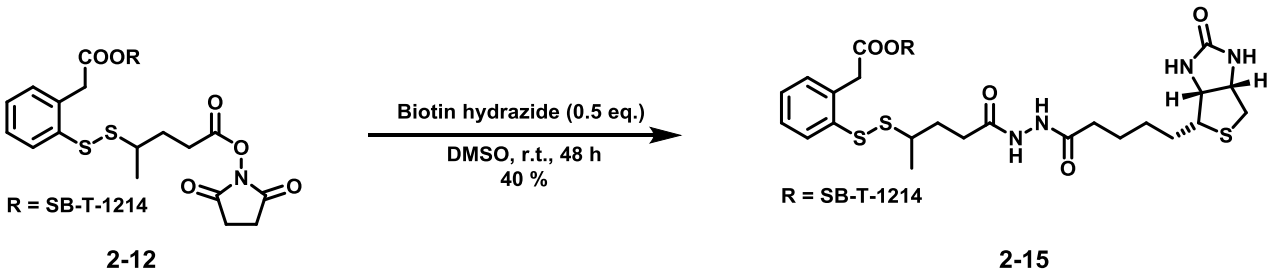

2-12 **2-15**

Scheme 2-7: Final coupling of the couple-ready construct to D-Biotin hydrazide

§2.2 Linker Intermediate:

§2.2.1 Introduction:

Due to the inability to store the linker prior to drug coupling, a new strategy was devised to couple first to the TTM and thus provide a stable intermediate for rapid drug attachment. Strategically this would enable quick access to various drug-conjugates within 1 coupling step as seen in **Scheme 2-8**.

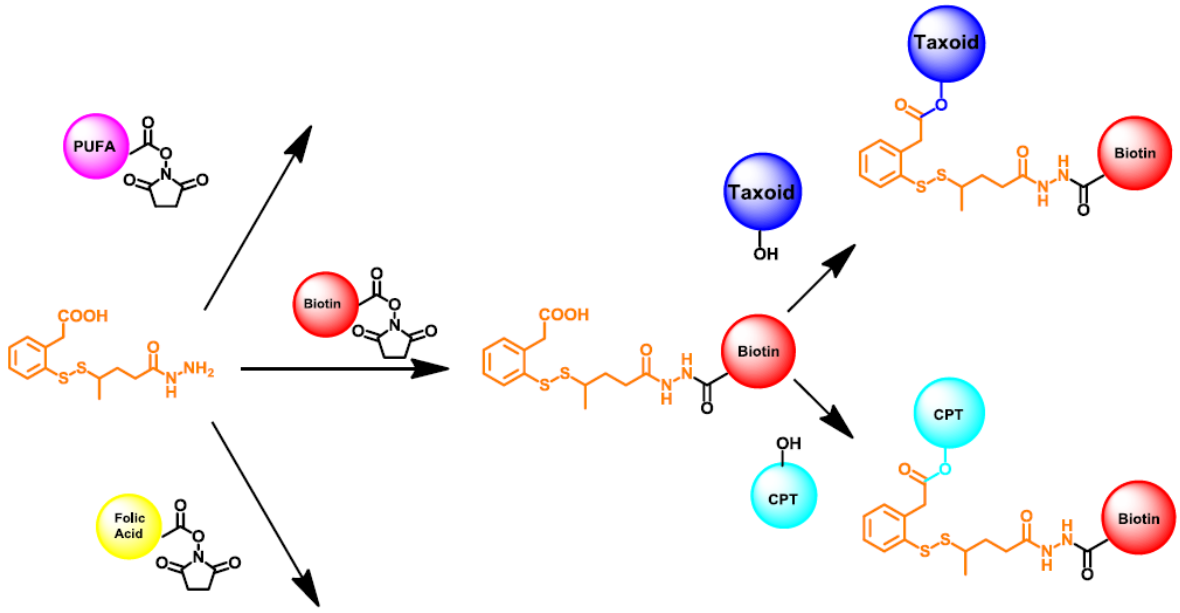

Scheme 2-8: Strategy for the "Linker Intermediate" to access multiple "smart linker" conjugates

§2.2.2 Results and Discussion:

§2.2.2.1 Synthesis of the Linker Intermediate:

To accommodate biotin into the linker before drug coupling, hydrazine was first coupled to 4-

(Pyridin-2-yldisulfanyl) pentanoic acid **2-7** via CDI coupling shown in **Scheme 2-9**. 1.5 equivalence of CDI was added to 4-(Pyridin-2-yldisulfanyl) pentanoic acid in THF and heated for 2 hours at 45 ^{o}C. Then 3.0 equivalence of BOC hydrazide was added and the reaction mixture was heated to 55 ^{o}C for 27 hours. After column purification 91 % of the desired BOC hydrazide **2-16** could be obtained.

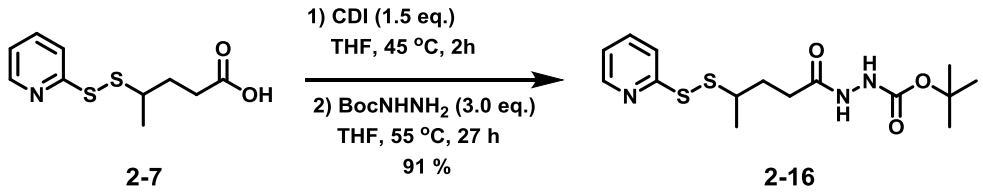

Scheme 2-9: CDI coupling of BOC hydrazide to 4-(Pyridin-2-yldisulfanyl) pentanoic acid

Disulfide exchange of pyridine disulfide with 1.0 equvalence of 2-mercapto phenylacetic acid proceeded well in THF at 60 ^{o}C for 2 hours to yield the BOC protected linker-hydrazide **2-17** in 82 % yield after purification as seen in **Scheme 2-10**. This linker intermediate could then be stored indefinitely until need.

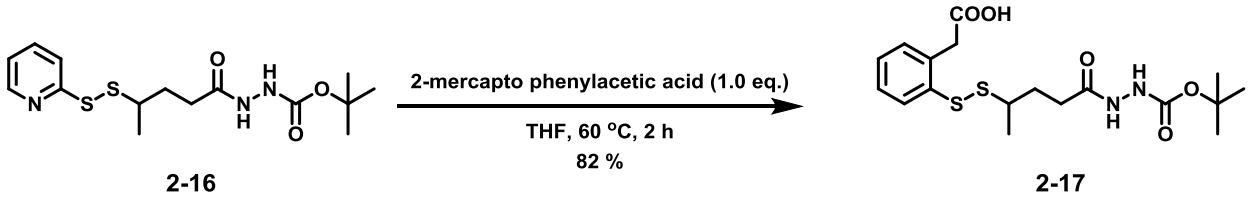

Scheme 2-10: Disulfide exchange of 2-mercaptophenylacetic acid

§2.2.2.2 Activation of Biotin for Coupling:

Based on the strategy detailed above, biotin was prepared as the activated ester shown in **Scheme 2-11**. Following the procedure by Power et. al. D-biotin was dissolved in DMF and 3.0 equivalence of NHS was added. Then 2.0 equivalence of DIC was added dropwise and the solution was stirred 48 hours at 45 ^{o}C. After recrystallization from isopropanol, the NHS ester **2-18** was isolated in 83 % yield.

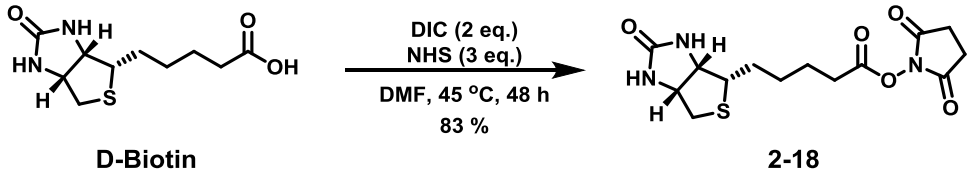

Scheme 2-11: Synthesis of D-Biotin-NHS

§2.2.2.3 Coupling Biotin to the Linker Intermediate:

After obtaining both the BOC protected linker intermediate **2-17** and D-biotin-NHS ester **2-18** a sequential deprotection followed by activated ester coupling was performed, shown in **Scheme 2-12**.

The BOC protected linker intermediate **2-17** was dissolved in 70 % TFA / DCM and stirred at r.t. for 30 minutes. The reaction was monitored by ninhyrin stain on TLC. Once completed, the solvent and excess TFA were removed *in vacuo*. The resulting solid **2-19** was dissolved in DMF and 1.0 equivalents of biotin-NHS ester **2-18** was added. Subsequently, 1.1 equivalence of TEA was added and the solution was stirred at r.t. for 48 hours and monitored by HPLC **(Figure 2-12)** affording the biotin-linker intermediate **2-20**.

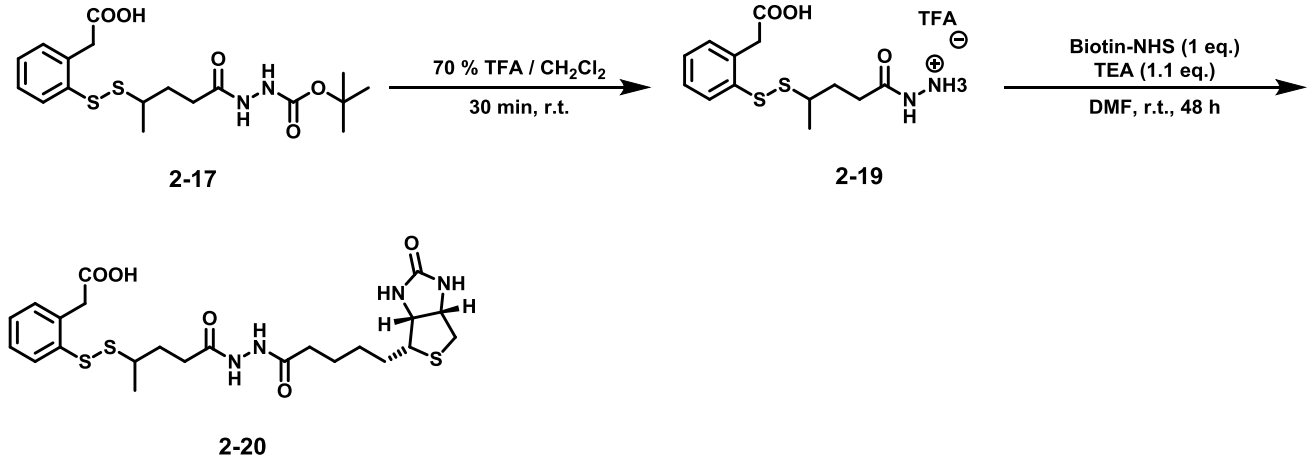

Scheme 2-12: Deprotection of BOC followed by coupling with D-Biotin-NHS

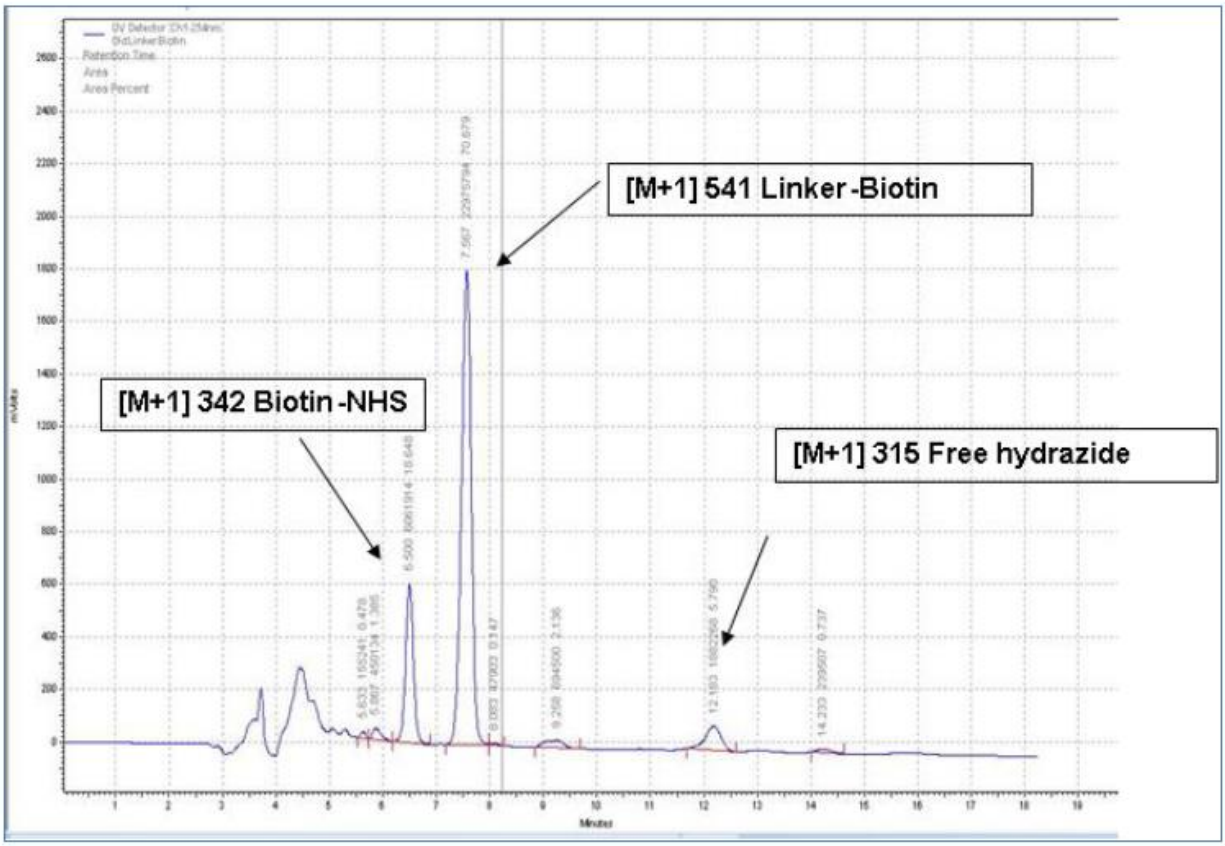

Figure 2-12: HPLC trace of the biotin-linker coupling reaction

§2.2.2.4 Coupling SB-T-1214 to the Linker Intermediate:

Final coupling of the drug SB-T-1214 was attempted with the crude biotin-linker shown in **Scheme 2-13**. To a flask containing the biotin-linker **2-20** was added THF:DMF (50:50). While stirring 1.5 equivalents of SB-T-1214 and 0.25 equivalents of DMAP was added. Then 2.0 equivalents of DIC was added dropwise and the reaction was stirred at r.t. for 48 hours.

Unfortunately, due to the polar nature of the biotin-linker intermediate, DMF was required as a co-solvent with THF to dissolve the starting material which contributed to an N-acyl rearrangement of the DIC complex. In addition, the polar nature of the biotin-linker intermediate in the previous step made purification by flash chromatography infeasible. Due to these two setbacks, mainly the first, a low yield of 25 % was obtained for the final conjugate **2-21** with 88 % purity by HPLC shown in **Figure 2-13**.

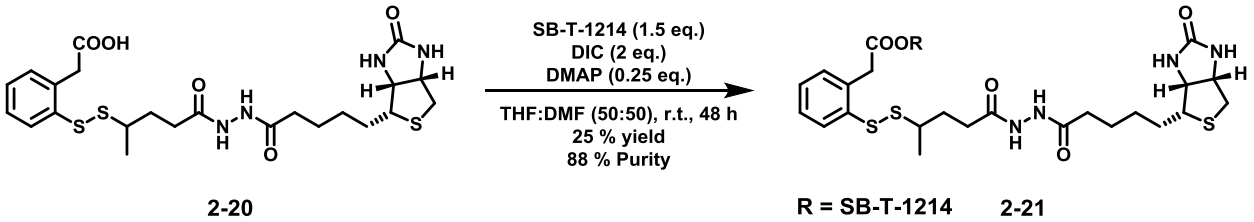

Scheme 2-13: DIC coupling of SB-T-1214 to the Biotin "Linker Intermediate"

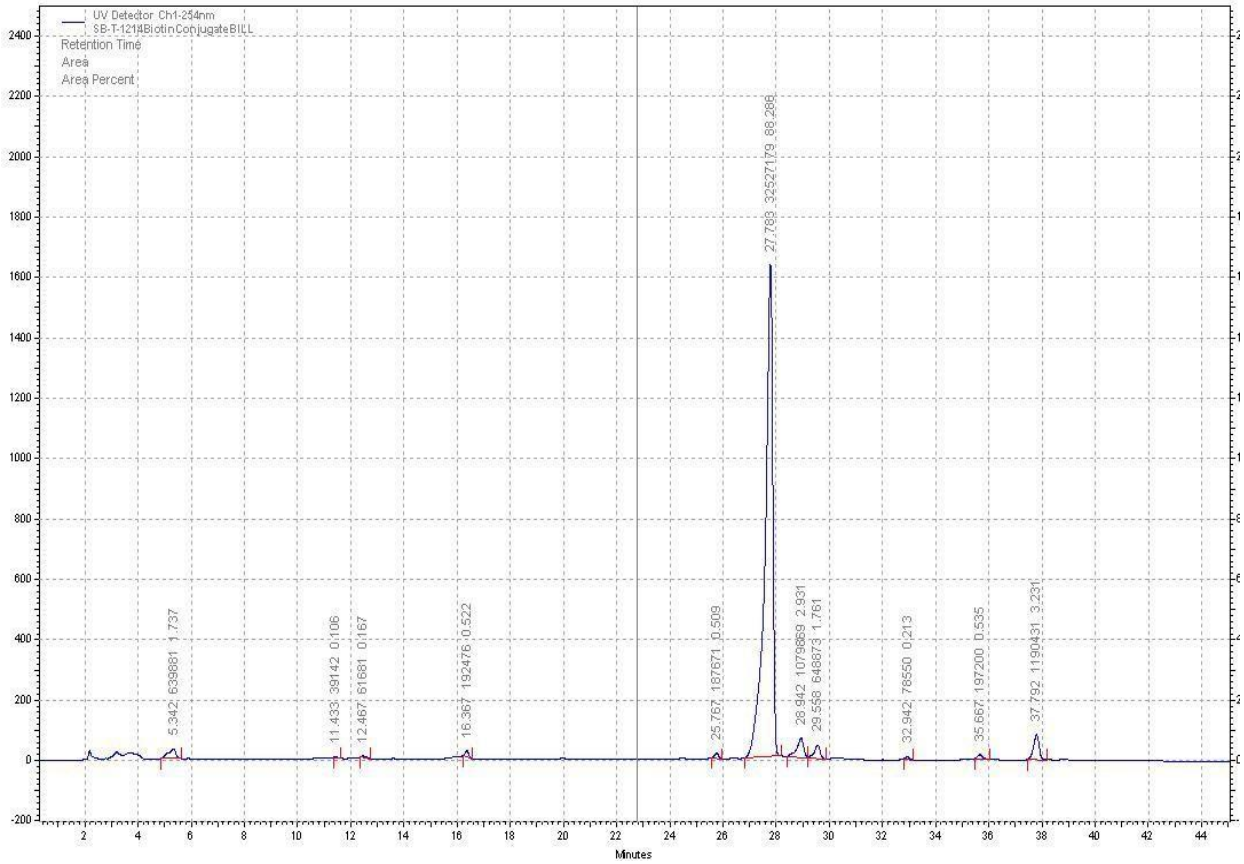

Figure 2-13: HPLC trace of the (5C)-BLT conjugate via the Linker Intermediate

§2.3 Synthesis and Kinetic Release Evaluation of the (4C)-BLT Conjugate:

§2.3.1 Introduction:

Based upon disappointing *in vivo* results obtained from the taxoid-mAb conjugate designed by Ojima et al.[10], Ojima proposed a new generation of disulfide linkers which could be used to create a new generation of conjugates. Upon cyclization these new-generation likers theoretically could completely detach from the cytotoxic drug reestablishing full activity, as seen in **Scheme 2-14**. Among these newer generation of disulfide-based "smart linkers" included both thermodynamically favorable 5 and 6 member ring thiolactonization products shown in **Figure 2-14**. Model experiments of several of linkers utilizing *para*-fluorophenol where carried out to determine the kinetic rates of lactonization

shown in **Scheme 2-15**. Among those tested, the most successful, 2-mercaptophenylacetic acid (**Scheme 2-15A)** when exposed to 100 equivalents of glutathione in pH 7.4 buffer/acetonitrile at 37 ºC, released *para*-fluorophenol with a half-life of 11.4 minutes. Methylene insertion between the disulfide and aromatic substituents was then evaluated. This additional methylene added stability to the disulfide bond, ultimately leading to long and incomplete cleavage of the ester. Interestingly, incorporation of isopropyl to the other side disulfide bond extended linker half-life by blocking glutathione attack. Thus, it was originally envisioned that several BLT conjugates could be synthesized utilizing this linker system an analyzed by HPLC for glutathione triggered taxoid release rates as shown in **Figure 2-15**. Nevertheless, the (4C)-BLT conjugate was never formally synthesized and compared to the (3C) and (5C)-BLT conjugates. Thus, the specific aims of this work were to compare by means of HPLC glutathione triggered release kinetics of the (5C)-BLT conjugate versus the (4C)-BLT conjugate.

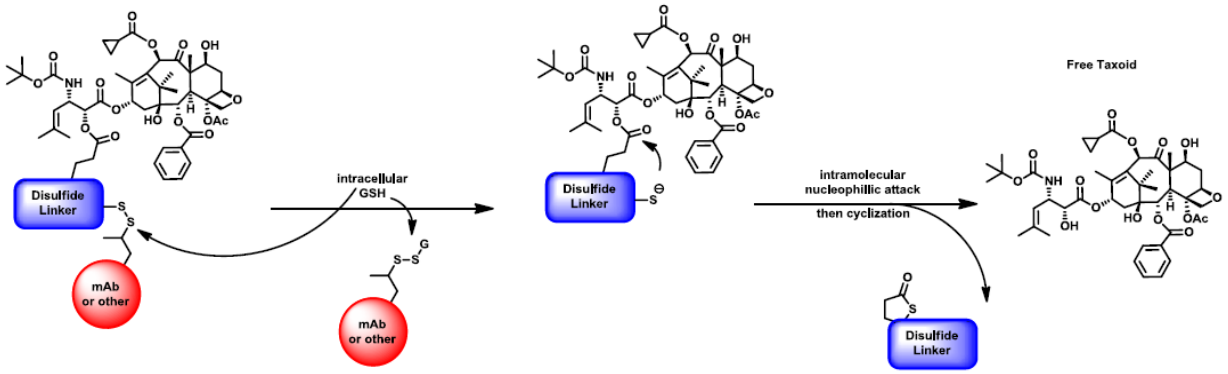

Scheme 2-14: Two step mechanism of disulfide-linker cleavage followed by intramolecular cyclization and drug release. (adapted from Prof. Ojima's Proposal)

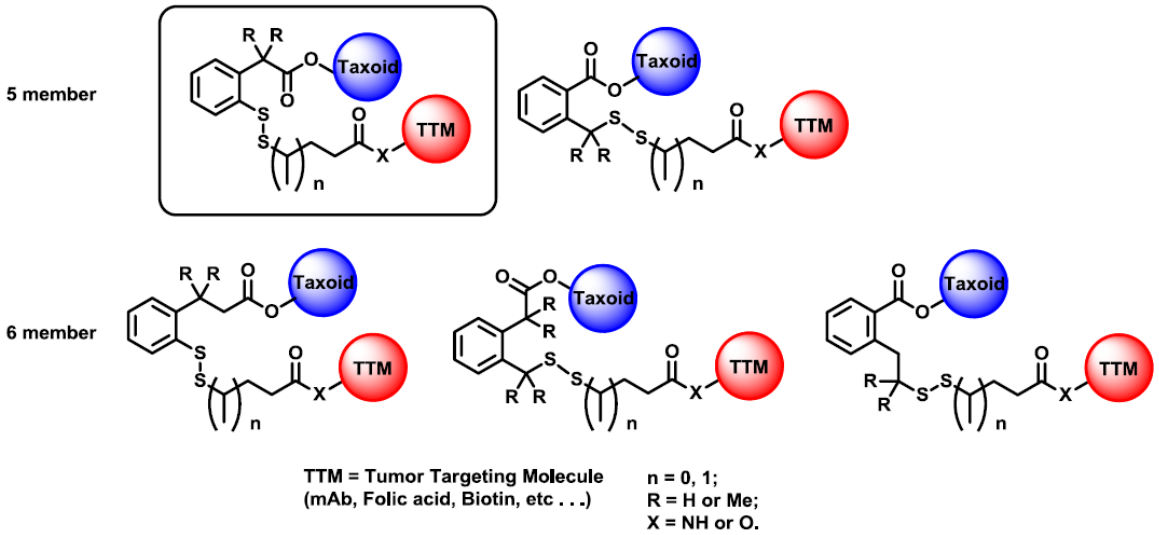

Figure 2-14: New generation linkers proposed by the Ojima laboratory. Thiolactonization products include 5 and 6 member rings. Highlighted is the linker system currently used which has been validated by HPLC to completely release the taxoid. (adapted from Prof. Ojima's Proposal)

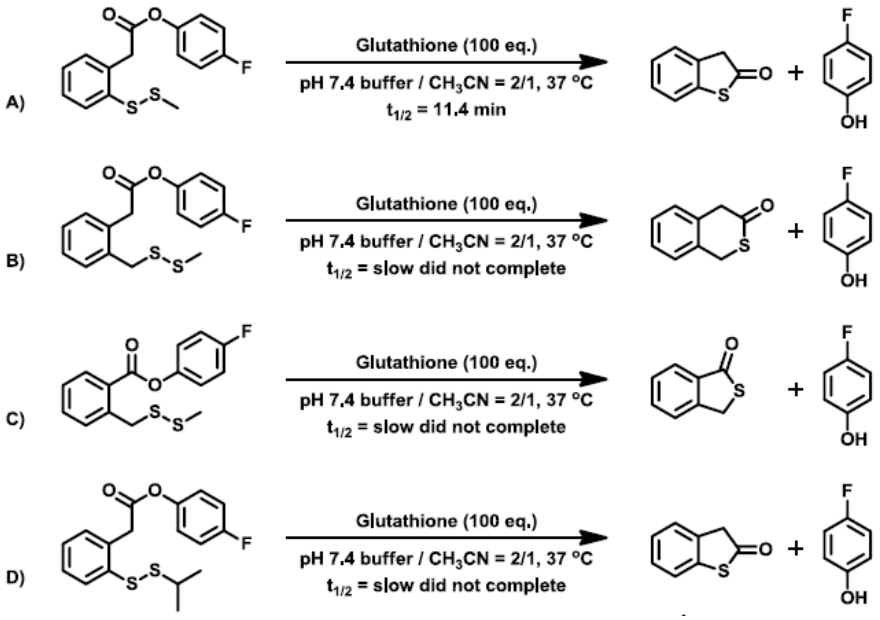

Scheme 2-15: Model kinetic experiments carried out to study the stability of the various 2[nd]-generation self-immolative disulfide linkers. A) 2-mercapto-phenylacetic acid with methyl-disulfide tether showing the best result of complete release of the *para*-fluorophenol. B) 6-membered ring formation showing incomplete conversion due to deactivation of the disulfide by methylene insertion between the aromatic system and the disulfide. C) 5-membered ring formation showing incomplete conversion due to deactivation of the disulfide by methylene insertion between the aromatic system and the disulfide. D) Increased steric bulk of the alkyl disulfide tether provided increased half-life.[21]

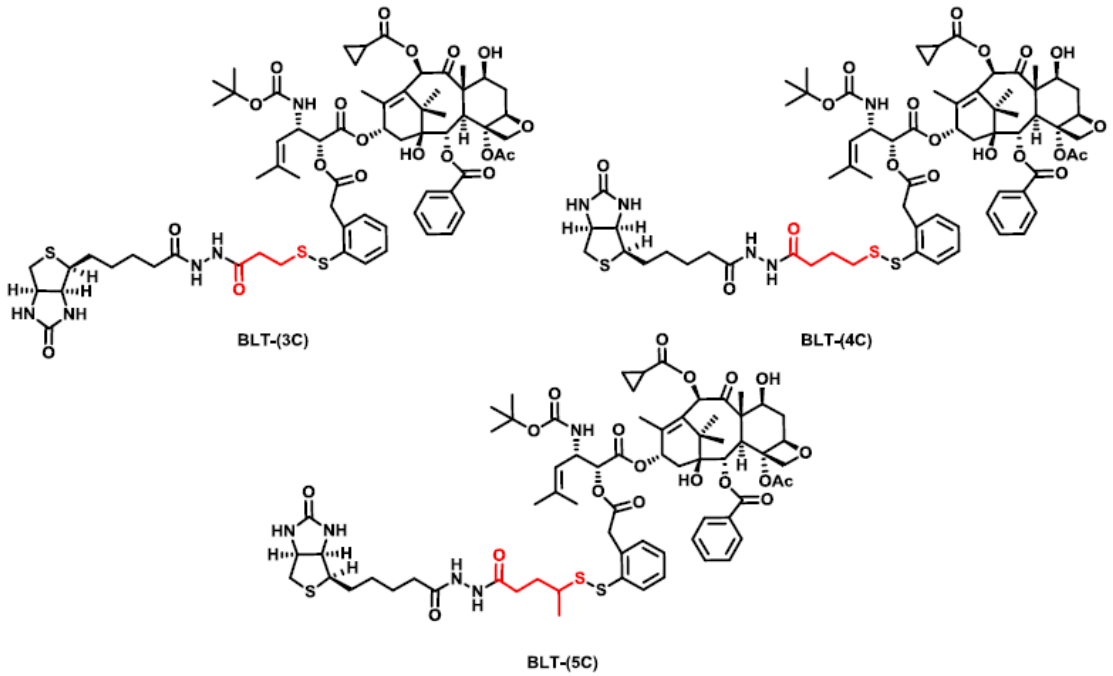

Figure 2-15: BLT conjugates with various sized alkyl disulfide linker substituents. Highlighted in red are the different alkyl disulfide substituents that have been used for stability studies.

§2.3.2 Results and Discussion:

§2.3.2.1 Synthesis of 4-Mercaptobutanoic Acid:

Synthesis of the (4C)-BLT began with synthesis of the alkyl tether 4-mercaptobutanoic acid. Using methodology from Langford et al. described earlier, synthesis started with ring opening of butyrolactone with 5.0 equivalents of thiourea in 6.3 equivalents of 48 % hydrobromic acid under reflux for 24 hours as seen in **Scheme 2-16**. The crude salt 2-22 was then directly subjugated to basic hydrolysis conditions. To the crude salt 2-22 was added 25 equivalents of 25 M aqueous sodium hydroxide, and the resulting solution was refluxed for 3 hours. Despite the previous success of this synthetic route adapted from Langford et al. in the synthesis of 4-mercaptobutanoic acid, the primary isothironium bromide salt obtained was more readily attacked by bromine (primary versus secondary substitution). Thus, mixtures of 4-bromobutyric acid 2-24 and 4-mercaptobutanoic acid 2-23 were obtained after hydrolysis and thereby provided problematic to isolate.

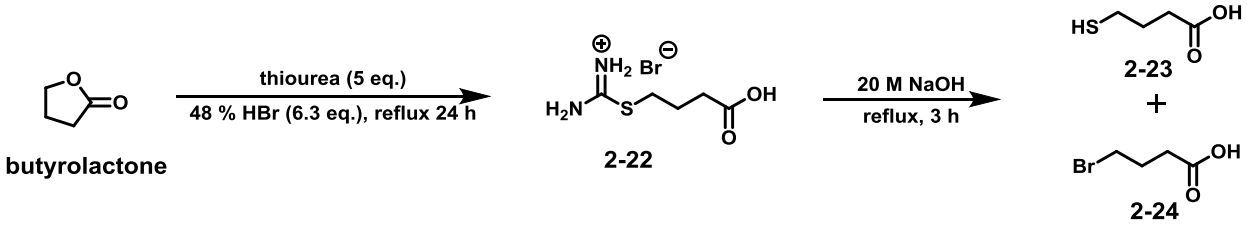

Scheme 2-16: Langford synthetic protocol resulted in inseparable byproduct

To provide a better synthetic route to 4-mercaptobutyric acid, direct substitution of Ethyl-4-bromobutyate with thiourea followed by simultaneous hydrolysis of both the ester and isothironium salt was performed as shown in **Scheme 2-17**. Ethyl-4-bromobutyrate and 2 equivalents of thiourea were reflux in acetone for 24 hours to obtain the crude isothironium bromide salt **2-25** which was washed with ether to remove any starting materials. Then the salt was hydrolyzed in 20 M sodium hydroxide under reflux for 24 hours to give 4-mercaptobutanoic acid **2-23** in 82 % isolated yield after two steps.

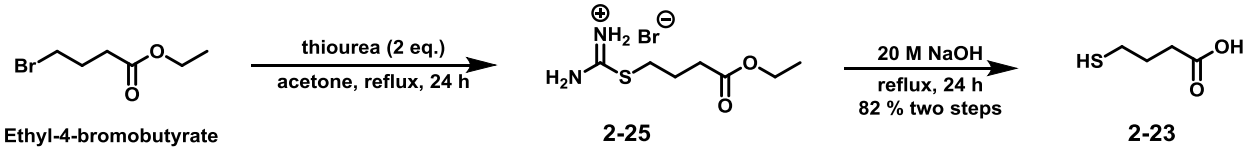

Scheme 2-17: New synthetic strategy from ethyl-4-bromobutyrate

§2.3.2.2 Synthesis of the (4C)-Disulfide Linker:

After obtaining 4-mercaptobutyric acid in sufficient quantities, disulfide activation followed by TIPS protection and disulfide exchange was performed as seen in **Scheme 2-18**. To DPDS in ethanol

at reflux was added 4-mercaptobutanoic acid **2-23** dropwise over 2 hours which gave the desired compound **2-26** in 87 % isolated yield. Compound **2-26** was then protected at the carboxylic acid end by the addition of 1.2 equivalents of TIPSCl and 1.2 equivalents of TEA in DCM overnight at room temperature to give the desired compound **2-27** in quantitative yield. After protection, disulfide exchange of compound **2-27** with 2-mercapto phenylacetic acid in THF at 0 ^{o}C for 2 hours provided compound **2-28** in 82 % isolated yield.

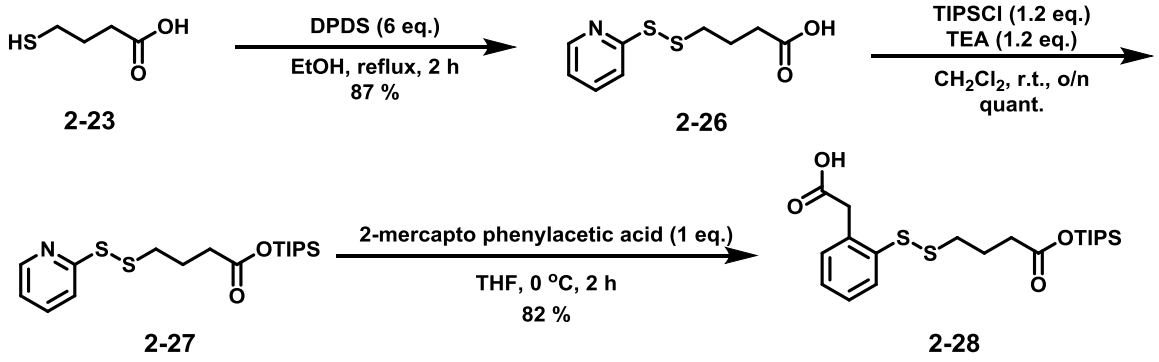

Scheme 2-18: Synthesis of the new (4C) butanoic acid based linker

§2.3.2.3 Final Synthesis of the (4C)-BLT Conjugate:

After obtaining a suitable quantity of (4C)-linker, subsequent couplings of the drug SB-T-1214 and D-biotin were performed shown in **Scheme 2-19**. SB-T-1214 was coupled to the 4C-disulfide linker with 1.5 equivalents of SB-T-1214, 0.25 equivalents of DMAP catalyst, and 1.1 equivalents of DIC to the linker **2-28** in DCM at 0 ^{o}C for 2 hours to give compound **2-29** in 92 % isolated yield. After coupling the drug, compound **2-29** was then deprotected in the presence of HF/pyridine in acetonitrile/pyridine at 0 ^{o}C to room temperature overnight to give compound **2-30** in 94 % isolated yield. After deprotection, the free carboxylic acid was then activated using NHS. To compound **2-30** was added 5.0 equivalents of NHS and 2.0 equivalents of DIC in THF/pyridine at room temperature for 24 hours to give compound **2-31** in 92 % isolated yield. After activation of compound **2-31**, 1.2 equivalents of D-biotin hydrazide was added in DMSO to give compound **2-32** the final (4C)-BLT conjugate in 74 % isolated yield.

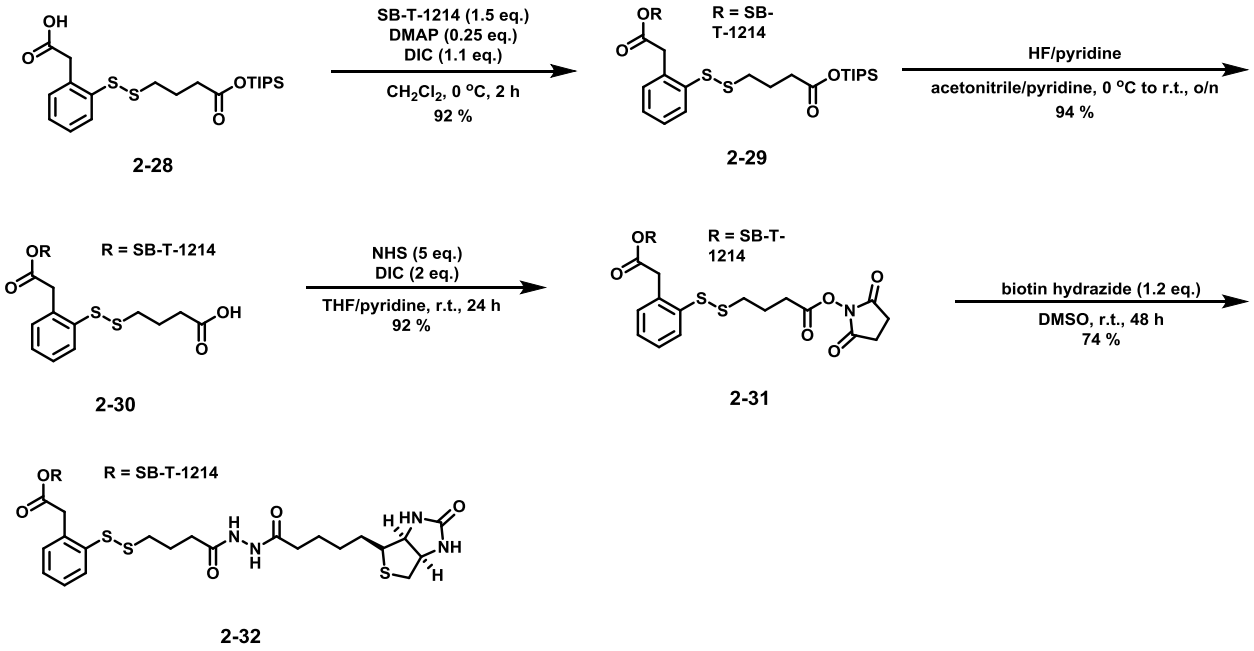

Scheme 2-19: Synthesis of the (4C)-BLT conjugate

§2.3.2.4 Calculation of the Relative Molar Extinction Coefficient of BLT Conjugates Versus Free Taxoid:

In order to properly calculate the release of the SB-T-1214 from various BLT conjugates, the approximate molar extinction coefficient ratio between the BLT conjugates and SB-T-1214 was calculated. Since 235 nm was the most optimal wavelength to perform the HPLC release experiments, the molar extinction coefficients for both SB-T-1214 and (4C)-BLT were determined at this wavelength. Approximately 1 mg of each compound was diluted with 1 mL of acetonitrile and analyzed by HPLC as shown in **Figure 2-16**. Using Beer's law (**Equation 2-1**) as seen in **Table 2-4** the molar extinction coefficients for each compound were calculated and compared with each other to determine the relative response factor. Accordingly, it was calculated that the (4C)-BLT conjugate absorbed 1.46 times as much as SB-T-1214. The BLT conjugates used were assumed to have similar relative response factors to SB-T-1214 since the BLT-conjugates only varied by 1 alkyl carbon.

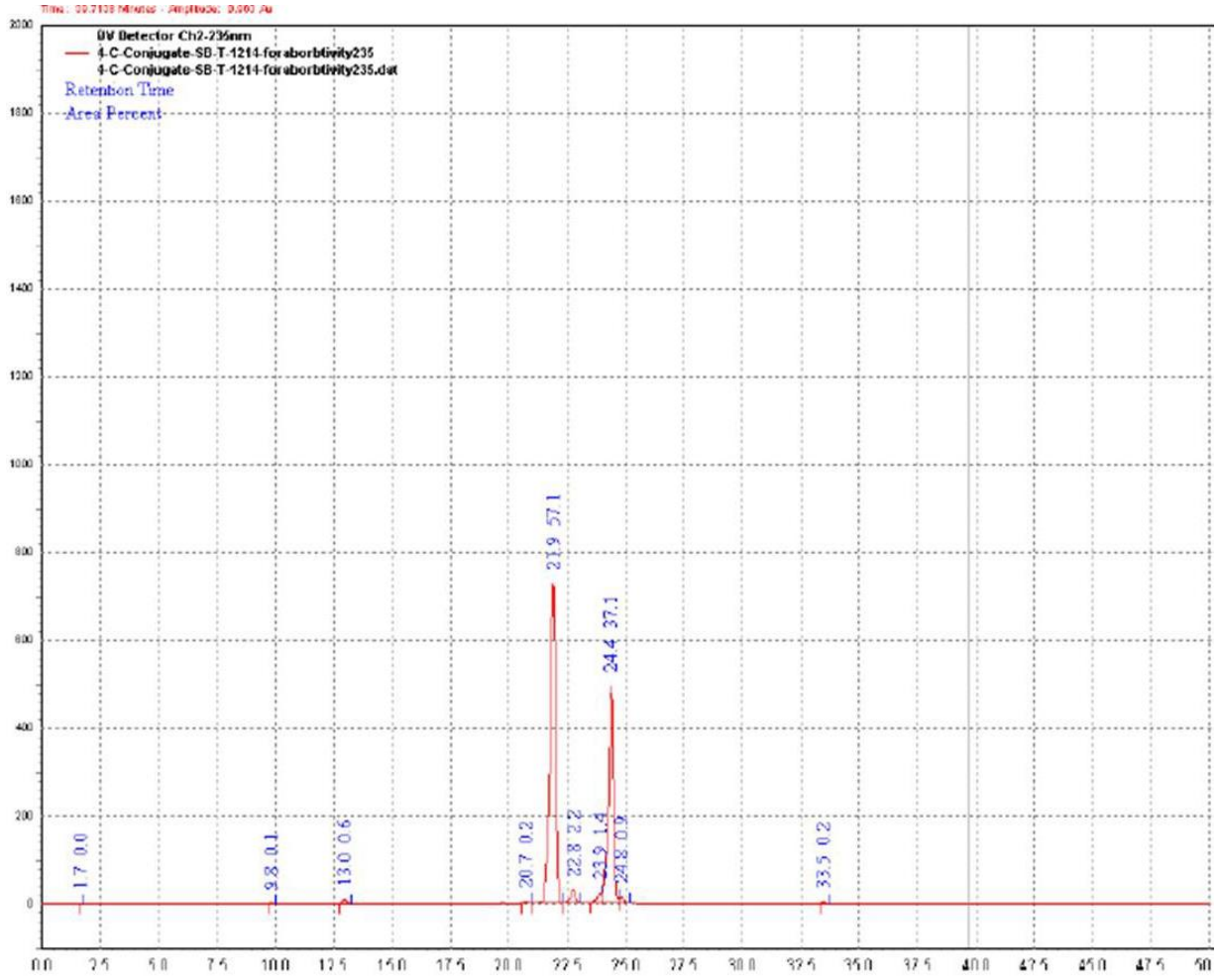

Figure 2-16: HPLC trace of the co-injection of SB-T-1214 and (4C)-BLT conjugate. Legends absorbance versus retention time.

$$A = \varepsilon c l$$

$$\text{Where is: } A = \text{absorbance}, \varepsilon = \text{molar extinciton coefficient},$$

$$c = \text{concentration } \frac{\text{mg}}{\text{mL}} \text{ x purity}, \qquad l = \text{pathlength (1 cm)}$$

Equation 2-1: Beer's law

Table 2-4: Molar extinction coefficient and factor between SB-T-1214 and the (4C)-BLT conjugate at 235 nm.

Name	Weight (mg)	M.W. (amu)	mmol	Purity	Area λ235	ε(Aλ235/mmol)	F λ235
SB-T-1214	1.6	835.95	1.9×10^{-3}	97.0	11633307	6312157895	x
(4C)-BLT	1.2	1362.62	8.8×10^{-4}	93.3	7569259	9219111127	1.46

§2.3.2.5 HPLC Release Analysis of SB-T-1214 from (4C)-BLT and (5C)-BLT Conjugates:

In an attempt to measure the stability of the BLT conjugates versus intracellular thiol an experiment was performed using phosphate buffer solution (pH ~ 7.4) and 10 equivalence of glutathione. Utilizing high performance liquid chromatography to separate the drug SB-T-1214 and the BLT conjugate, the areas of each peak were quantified in **Table 2-5** and **Table 2-6**. In addition, the area of the BLT conjugate was divided by 1.46, the response factor, determined to normalize the areas of both compounds.

Table 2-5: Calculation of the ratio of (4C)-BLT to SB-T-1214 released over time

Time	Area BLT	Area BLT Adjusted	Area SB-T-1214	Total Area	Ratio
15	474089	324719	17366	342085	0.949235
30	871694	597051	35738	632789	0.943523
150	478908	328019	128728	456747	0.718164
240	258095	176777	93198	269975	0.654791
300	272160	186411	136958	323369	0.576465
360	326493	223625	183968	407593	0.548648

Table 2-6: Calculation of the ratio of (5C)-BLT to SB-T-1214 released over time

Time	Area BLT	Area BLT Adjusted	Area SB-T-	Total Area	Ratio (BLT/Taxoid)
15	338678	231971	12283	244254	0.949712
60	278004	190413	45973	236387	0.805518
120	249666	171004	68273	239277	0.71467
180	225631	154541	79804	234346	0.65946
240	190967	130799	91907	222706	0.587317
300	172817	118368	98475	216842	0.545869
360	142872	97858	105047	202906	0.482284

Subsequently, the rate constant for release of SB-T-1214 from the (4C)-BLT conjugate with 10 eq. glutathione in PBS was calculated according to rate law, rate = -d[A]/dt = k[A][B]. When [B] is in large excess, rate = -d[A]/dt = q[A], wherein q = k[B]. As shown in **Figure 2-17**, ln(A) exhibited a linear relationship with time course ($R^2 = 0.9843$), which indicated that this reaction was considered a pseudo-first order reaction. Consequently, ln(At) = ln(A0)-qt, q = - 1.31×10^{-1} min^{-1} , half time $t^{1/2}$ = 634 min, 10.6 hr.

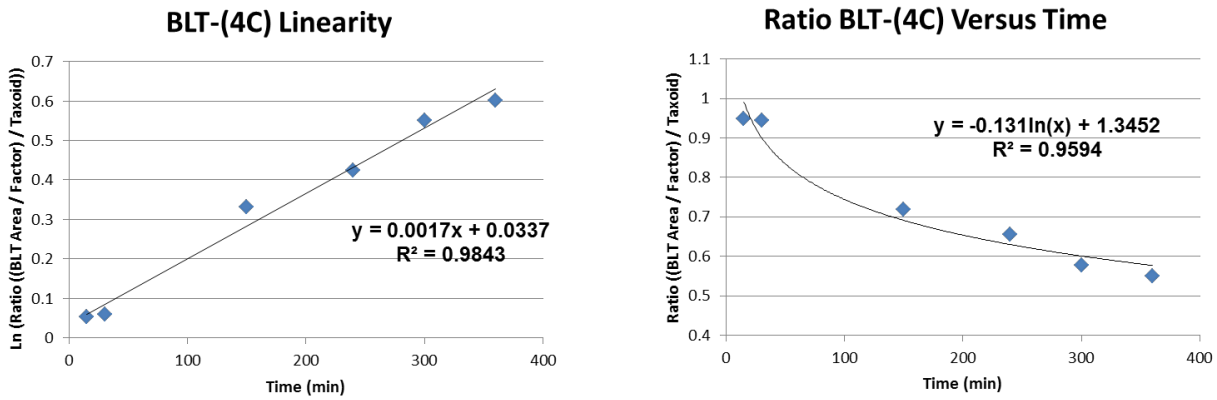

Figure 2-17: SB-T-1214 release kinetics determined for the (4C)-BLT. The graph shows linearity of (ln(ratio)/time) revealing that the release reaction proceeded by a pseudo-first order mechanism. The half-life was then determined by plotting the ratio versus time.

In a similar fashion, the rate constant for release of SB-T-1214 from the (5C)-BLT conjugate with 10 eq. glutathione in PBS was calculated according to rate law, rate = -d[A]/dt = k[A][B]. When B is in large excess, rate = -d[A]/dt = q[A], wherein q = k[B]. As shown in **Figure 2-18**, ln(A) exhibited a linear relationship with time course (R^2 = 0.9816), which indicated that this reaction was considered a pseudo-first order reaction. Consequently, ln(At) = ln(A0)-qt, q = - 1.42×10^{-1} min^{-1}, half time $t^{1/2}$ = 436 min, 7.3 hr.

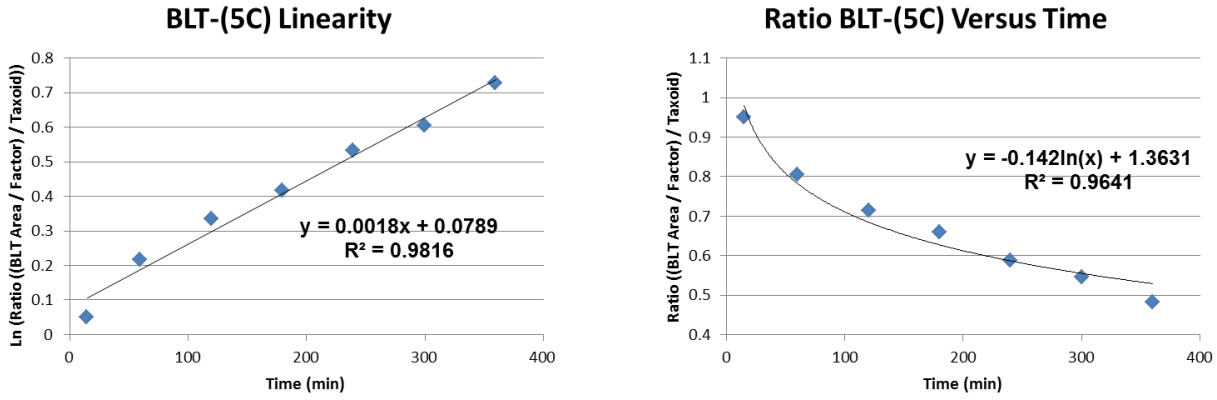

Figure 2-18: SB-T-1214 release kinetics determined for the (5C)-BLT conjugate. The graph shows linearity of (ln(ratio)/time) revealing that the reaction proceeded by a pseudo-first order mechanism. The half-life was then determined by plotting the ratio versus time.

§2.4 Conclusion:

The (5C)-BLT conjugate was successfully synthesized using methodology previously discovered in the Ojima laboratory. Subsequent improvements were made the synthesis of the (5C)-linker by optimizing of the synthesis of 4-mercaptopentanoic acid.

Although promising, the "linker-intermediate" strategy while providing a linker which could be stored and subsequently coupled to different cytotoxic agents via a 1-step coupling provided to be cumbersome. This was ultimately due to the vast differences in solubility between the cytotoxic agent SB-T-1214 and biotin resulting in the need for more polar solvents in the final DIC coupling. Ultimately the final coupling reaction with DIC, which is susceptible to rearrangements in polar solvents, proved unfruitful as the yield and purity were drastically reduced. Thus, in order to reduce byproducts further work would need to be performed (eg. HATU coupling).

Lastly, a new (4C)-BLT conjugate was synthesized utilizing a butanoic acid (4C) -alkyl tether an evaluated by HPLC for glutathione triggered release to establish the relative stability compared with the BLT- (5C). Accordingly, the kinetic experiment showed that the release of SB-T-1214 from the BLT- (5C) was roughly 1.45 times the rate observed for the (4C)-BLT.

§2.5 Experimental:

General Methods: ^{1}H NMR and ^{13}C NMR was measured on a Varian 300, 400, 500, or 600 MHz NMR spectrometer. Melting points were measured on a "Uni-melt" capillary melting point apparatus from Arthur H. Thomas Company, Inc. TLC analyses were performed on Merck DC-alufolien with Kieselgel 60F-254 and were visualized with UV light and stained with sulfuric acid-EtOH, 10 % PMA-EtOH or 10 % Vanillin-EtOH with 1% sulfuric acid. Column chromatography was carried out on silica gel 60 (Merck; 230-400 mesh ASTM). HPLC Purity was determined by Shamazu HPLC employing a Phenomenex Proteo® column (CH3CN/H2O = 20/80 gradient to 95/5 over 45 min, flow rate at 1 mL/min).

Materials: The chemicals were purchased from Sigma-Aldrich Company, Fischer Company or VWR Company. 10-Deacetyl baccatin III (DAB) was donated by Indena, SpA, Italy. DCM and methanol were dried before use by distillation over calcium hydride under nitrogen. Ether and THF were dried before use by distillation over sodium-benzophenone kept under nitrogen. Dry DMF and DMSO were purchased from Sigma-Aldrich chemical company, and used without further purification. Reaction flasks were dried in a 100 ^{o}C oven and allowed to cool to room temperature in a desiccator over "*Drierite*" (calcium sulfate) and assembled under an inert nitrogen gas

atmosphere.

4-Mercaptopentanoic acid (2-3):[19, 20]

Method A: To a round bottomed flask was added (2.0 mL, 20.98 mmol) of γ-valerolactone and 20 mL of CH_2Cl_2. The reaction was cooled to 0 °C and (4.0 mL, 41.51 mmol) of BBr_3 in 10 mL of CH_2Cl_2 was added dropwise. The solution was stirred for 48 hours. After completion, the resulting solution was quenched with chilled H_2O. The reaction was placed in an ice bath and the pH was adjusted to 2 with 1N HCl. The resulting solution was extracted with CH_2Cl_2 and the combined organic layers were washed with brine (2 x 50 mL), dried with MgSO4 and concentrated *in vacuo* to obtain a brownish oil **2-1** (3.7 g, 75 % by 1H NMR). ^{1}H NMR (300 MHz, $CDCl_3$) δ 1.74 (dd, *J* = 6.6 Hz, 2.7 Hz, 3 H), 2.11 (m, 2 H), 2.60 (m, 2 H), 4.18 (m, 1 H). The brownish oil **2-1** was then placed into a round bottomed flask and 128 mL of methanol was added. To this solution 2.0 g of thiourea was added and the solution was refluxed at 75 °C and monitored via FIA. After 48 hours, the solvent was evaporated and the subsequent salt was washed with CH_2Cl_2 to obtain an off white solid **2-2** (3.4 g, 12.39 mmol). [M+1] = 191.1. To the white solid **2-2** obtained was added 42.5 mL of 8.0 M KOH and the resulting solution was stirred at 60 °C for 48 hours. After completion the resulting solution was allowed to cool to room temperature and then placed in an ice bath. The pH was adjusted to 2 with 1 N HCl and extracted with ether. The combined organic layers were subsequently washed with (20 mL) of brine (20 mL) of H_2O, and then dried with $MgSO_4$ and concentrated *in vacuo* to obtain a yellow oil **2-3** with a strong sulfur smell (646 mg, 38 % for 3 steps): ^{1}H NMR (300 MHz, $CDCl_3$) δ 1.33 (d, 3 H), 1.93 (m, 2 H), 2.51 (m, 2 H), 2.85 (m, 1 H). All data are in agreement with literature values.[19]

Method B: To a 25 mL round bottomed flask was added 1.002 g of γ-valerolactone, 3.738 g of thiourea, and 7 mL of aqueous hydrobromic acid (48 %). This solution was refluxed at 135 °C for 24 hours and monitored via positive FIA Mass to form the 4-isothiouronium bromide pentanoic acid **2-4** [M+1] = 171.1. After completion, the aqueous layer was extracted with (3 x 20 mL) of DCM. Then the combined aqueous layer was added to a 100 mL round bottomed flask and 7 mL of 25 M NaOH was added. This solution was stirred and refluxed at 120 °C for 4 hours. After completion, the solution was then extracted again with (2 x 50 mL) DCM. Then 50 mL of DCM was added and the pH of the aqueous layer was adjusted to 2 with 6N HCl. The organic layer was collected and the aqueous layer was subsequently extracted 3 more times with 50 mL of DCM each time. The combined organic layers were dried with $MgSO_4$ and concentrated *in vacuo* to yield (1.042 g, 7.76

mmol), 79 % of the desired 4-mercapto pentanoic acid **2-3**: Negative FIA Mass [M-1] = 133.0; ^{1}H NMR (500 MHz, $CDCl_3$) δ 1.34 (d, 3 H), 1.75 (m, 1 H), 1.94 (m, 1 H) 2.51 (m, 2 H), 2.93 (m, 1 H). All data are in agreement with literature values.[19, 20]

Benzothiolactone (2-5):[19]

To a 100 mL round bottomed flask was added (5.354 g, 29.47 mmol) of benzothiophene-2-boronic acid and 50 mL of ethanol. Then 10 mL of 30 % H_2O_2 was added and the resulting solution was allowed to stir for 48 hours. The reaction was monitored by TLC. After completion, the reaction mixture was extracted with CH_2Cl_2 and washed (2 x 50 mL) with brine. The combined organic layers were dried with $MgSO_4$ and concentrated *in vacuo.* The resulting solid was purified by flash chromatography using (Ethyl Acetate / Hexanes) to yield 3.653 g (24.32 mmol), 83 % of the desired pure benzothiolactone **2-5** as a yellow solid: ^{1}H NMR (500 MHz, $CDCl_3$) δ 3.95 (s, 2 H), 7.21 (m, 1 H), 7.29 (m, 2 H) 7.34 (m, 1 H). All data are in agreement with literature values.[19]

2-Mercaptophenylacetic Acid (2-6):[19]

To a 50 mL round bottomed flask was added (3.653 g, 24.32 mmol) of benzothiolactone **2-5** and 25 mL of THF. Then 25 mL of 3M LiOH (aq) was added and the resulting solution was allowed to stir for 10 hours at 60 ^{o}C. The reaction was monitored by TLC. After completion, the reaction mixture was extracted with CH_2Cl_2 (3 x 50 mL). The resulting solution was adjusted with 6N HCl to a pH of 2. The reaction mixture was then extracted again with CH_2Cl_2 (3 x 50 mL). The combined organic layers were dried with $MgSO_4$ and concentrated *in vacuo.* The resulting solid was purified by flash chromatography using (Ethyl Acetate / Hexanes) to yield 3.400 g (20.21 mmol), 83 % of the desired 2-mercaptophenylacetic acid **2-6** as a yellow solid: ^{1}H NMR (600 MHz, $CDCl_3$) δ 3.49 (s, 1 H), 3.82 (s, 2 H), 7.17-7.21 (m, 2 H), 7.24-7.25 (m, 1 H), 7.40-7.42 (m, 1 H); ^{13}C NMR (100 MHz, $CDCl_3$) δ 39.9, 126.9, 128.2, 130.7, 131.0, 132.4, 133.3, 176.9. All data are in agreement with literature values.[19]

4-(Pyridin-2-yldisulfanyl)pentanoic acid (2-7):[19]

To a 500 mL round bottomed flask was added (9.800 g, 44.48 mmol) of di-pyridine-di-sulfide and 200 mL of ethanol. The reaction mixture was then heated to reflux. To this solution was added (1.007 g, 7.50 mmol) of 4-mercapto pentanoic acid previously dissolved in 20 mL of ethanol and the reaction was allowed to stir and additional 2 hours. The reaction was monitored by TLC. After completion, the reaction mixture was dried with $MgSO_4$ and concentrated *in vacuo.* The resulting

solid was purified by flash chromatography using (Ethyl Acetate / Hexanes) to yield 1.253 g (5.93 mmol), 79 % of the desired compound **2-7** as a white solid: ^{1}H NMR (300 MHz, $CDCl_3$) δ 1.32 (d, *J* = 6.6 Hz, 3 H), 1.87-2.03 (m, 2 H), 2.50-2.55 (m, 2 H), 2.98-3.04 (m, 1 H), 7.06-7.11 (m, 1 H), 7.61-7.67 (m, 1 H), 7.72-7.75 (m, 1 H), 8.43-8.46 (m, 1 H). All data are in agreement with literature values.[19]

Triisopropylsilyl 4-(Pyridin-2-yldisulfanyl)pentanoate (2-8):[19]

To a 10 mL round bottomed flask was added (227 mg, 0.93 mmol) of **2-7** and 4 mL of CH_2Cl_2. The reaction mixture was then cooled to 0 ^oC. To this solution was added (0.16 mL, 1.12 mmol) of TEA and then (0.24 mL, 1.12 mmol) of triisopropylsilyl chloride dropwise. The reaction was monitored by TLC for 19 hours. After completion, the reaction mixture was quenched with saturated ammonium chloride (5 mL) and extracted with CH_2Cl_2 (3 x 50 mL). The combined organic layers were dried with $MgSO_4$ and concentrated *in vacuo.* The resulting solid was purified by flash chromatography using (Ethyl Acetate / Hexanes) to yield 337 mg (0.84 mmol), 91 % of the desired compound **2-8** as a white solid: ^{1}H NMR (600 MHz, $CDCl_3$) δ 1.01-1.05 (m, 18 H), 1.21-1.26 (m, 3 H), 1.30 (d, *J* = 7.2 Hz, 3 H), 1.82-1.88 (m, 1 H), 1.93-2.00 (m, 1 H), 2.44-2.53 (m, 2 H), 2.97-3.00 (m, 1 H), 7.01-7.03 (m, 1 H), 7.58 (td, *J* = 2.4 Hz, *J* = 7.8 Hz, 1 H), 7.69 (d, *J* = 8.4 Hz, 1 H), 8.39 (d, *J* = 4.8 Hz, 1 H). All data are in agreement with literature values.[19]

Triisopropylsilyl 4-(2-hydroxycarbonylmethyl-phenyldisulfanyl)pentanoate (2-9):[19]

To a 10 mL round bottomed flask was added (337 mg, 0.84 mmol) of **2-8** and 2.5 mL of THF. The reaction mixture was then cooled to 0 ^oC. To this solution was added (142 mg, 0.84 mmol) of compound **2-6** in 1 mL of THF dropwise. The reaction was monitored by TLC for 4 hours. After completion, the combined organic layers were concentrated *in vacuo.* The resulting solid was purified by flash chromatography using (Ethyl Acetate / Hexanes) to yield 352 mg (0.77 mmol), 92 % of the desired compound **2-9** as a white solid: ^{1}H NMR (600 MHz, $CDCl_3$) δ 1.05-1.08 (m, 18 H), 1.24-1.30 (m, 6 H), 1.79-1.85 (m, 1 H), 1.92-1.98 (m, 1 H), 2.38-2.44 (m, 2 H), 2.91 (q, *J* = 7.2 Hz, 1 H), 3.89 (s, 2 H), 7.20 (d, *J* = 4.2 Hz, 2 H), 7.27-7.30 (m, 1 H), 7.79 (d, *J* = 7.8 Hz, 1 H). All data are in agreement with literature values.[19]

SB-T-1214-(5C)-linker-TIPS (2-10):[19]

To a 25 mL round bottomed flask added (60 mg, 0.13 mmol) of compound **2-9**, 146 mg (0.17 mmol) of SB-T-1214 and 0.3 mg (0.03 mmol) of DMAP was added and then diluted with 6.5 mL of DCM.

This solution was cooled to 0 ^{o}C. Then (20 μL, 0.13 mmol) of DIC was added and allowed to stir for 5 minutes. This solution was allowed to stir and warm to r.t. for 5 hours. After completion, the reaction solution was added directly onto a normal phase column and purified using (Ethyl Acetate / Hexanes) to yield 98 mg (0.08 mmol), 62 % of the desired compound **2-10** as a white solid: ^{1}H NMR (500 MHz, $CDCl_3$) δ 0.92 – 0.97 (m, 2 H), 0.99 -1.02 (m, 12 H), 1.06 (d, 4 H), 1.10 (s, 2 H), 1.61 (s, 2 H), 1.65 (s, 2 H), 1.68 (s, 2 H), 1.91 – 1.78 (m, 5 H), 1.98 (s, 1 H), 2.31 (s, 3 H), 2.38 (m, 2 H), 2.47 (m, 1 H), 2.64 (t, 1 H), 2.90 (m, 1 H), 3.75 – 3.79 (m , 1 H), 3.89 - 3.93 (m, 1 H), 4.02 – 4.07 (m, 1 H), 4.13 (d, 1 h), 4.24 – 4.29 (m, 1 H), 4.36 – 4.39 (m, 1 H), 4.83 (s, 1 H), 4.88 – 4.92 (m, 2 H), 5.04 (d, 1 H), 5.62 (d, 1 H), 6.14 – 6.16 (m, 1 H), 6.24 (s, 1 H), 7.17 – 7.27 (m, 3 H), 7.41 (t, 2 H), 7.54 (t, 1 H), 7.76 (d, 1 H), 8.05 (d, 2 H); ^{13}C NMR (126 MHz, $CDCl_3$) δ 8.97, 9.16, 9.43, 11.75, 12.89, 14.65, 17.65, 18.34, 20.36, 20.42, 22.12, 22.27, 23.33, 25.56, 26.57, 28.09, 30.85, 32.84, 32.88, 35.33, 35.45, 38.65, 41.87, 43.06, 45.51, 45.88, 58.32, 71.70, 71.99, 74.84, 75.17, 75.34, 76.25, 79.08, 79.65, 80.83, 84.38, 119.92, 127.57, 128.18, 128.48, 129.24, 130.03, 130.73, 132.39, 133.04, 133.43, 137.27, 137.50, 143.28, 154.82, 156.98, 166.79, 167.96, 169.50, 170.00, 172.86, 174.90, 203.96. All data were in agreement with literature values.[19]

SB-T-1214-(5C)-linker-carboxylic acid (2-11):[19]

To a 50 mL round bottomed flask was added (258 mg, 0.20 mmol) of compound **2-10** and diluted with 5 mL of pyridine and 5 mL of acetonitrile. Then the solution was cooled to 0 ^{o}C in an ice bath and 1.92 mL of HF/Pyridine solution was added dropwise. The reaction was monitored via TLC and upon completion (24 hours) quenched with 10 % citric acid. The resulting solution was then diluted with 100 mL ethyl acetate and extracted (3 x 100 mL) with saturated aqueous cupric sulfate solution and 100 mL of brine. The organic layer was collected dried with $MgSO_4$ and concentrated *in vacuo*. The resulting solid was dissolved in DCM and normal phase column purification was performed eluting with 45 % (Ethyl Acetate / Hexanes). After collecting and concentrating *in vacuo* the desired fractions, (188 mg, 0.17 mmol), 86 % of the desired compound **2-11** was obtained as a white solid: ^{1}H NMR (300 MHz, $CDCl_3$) δ 0.92 – 0.97 (m, 2 H), 1.13 - 1.16 (m, 8 H), 1.23 – 1.28 (m, 9 H), 1.35 (s, 9 H), 1.66 (s, 3 H), 1.71 – 1.72 (m, 6 H), 1.90 (s, 3 H), 2.04 (s, 2 H), 2.37 – 2.40 (m, 4 H), 2.52 (m, 1 H), 2.98 (m, 1 H), 3.75 – 3.79 (m , 2 H), 3.89 (s, 1 H), 3.96 (s, 1 H), 4.04 – 4.18 (m, 5 H), 4.30 (d, 1 H), 4.38 – 4.40 (m, 1 H), 4.90 – 5.00 (m, 3 H), 5.10 – 5.14 (m, 1 H), 5.66 (d, 1 H), 6.17 – 6.24 (m, 1 H), 6.28 (d, 1 H), 7.44 – 7.50 (m, 2 H), 7.57 – 7.62 (m, 1 H), 7.80 (t, 1 H), 8.10 (d, 2 H). All data were in agreement with literature values.[19]

SB-T-1214-(5C)-linker-OSu (2-12):[19]

To a 10 mL round bottomed flask added (188 mg, 0.17 mmol) of compound **2-11** and (98 mg, 0.85 mmol) of NHS and diluted with 5 mL of pyridine and 5 mL of THF. While stirring 0.05 mL of DIC was added dropwise and stirred and additional 5 minutes. The resulting solution was allowed to warm to room temperature overnight. This reaction was monitored via TLC until completion (24 hours) and was then quenched with 10 % citric acid solution. This solution was then diluted with distilled water and extract (3 x 50 mL) with ethyl acetate. The organic layers were collected and dried with $MgSO_4$ and concentrated *in vacuo*. The solid obtained was then dissolved in DCM and purified via normal phase chromatography using 50 % (Ethyl Acetate / Hexanes). After collecting and concentrating *in vacuo* the desired fractions, (198 mg, 0.16 mmol), 94 % of the desired compound **2-12** was obtained as a white solid: ^{1}H NMR (600 MHz, $CDCl_3$) δ 0.92 – 0.98 (m, 3 H), 1.11 - 1.13 (m, 12 H), 1.35 (s, 6 H), 1.30 – 1.33 (m, 14 H), 1.64 (s, 4 H), 1.70 – 1.75 (m, 8 H), 1.81 - 1.89 (m, 6 H), 1.95 (m, 1 H), 2.02 (s, 3 H), 2.30 – 2.34 (m, 6 H), 2.48 – 2.52 (m, 1 H), 2.63 – 66 (m, 3 H), 2.80 (s, 4 H), 2.98 (m, 1 H), 3.79 (d , 2 H), 3.96 (d, 2 H), 4.05 – 4.11 (m, 2 H), 4.16 (d, 1 H), 4.27 (d, 2 H), 4.40 (m, 1 H), 4.83 (d, 1 H), 4.91 – 4.96 (m, 3 H), 5.08 (d, 1 H), 5.65 (d, 1 H), 6.16 – 6.18 (m, 1 H), 6.27 (s, 1 H), 7.22 – 7.32 (m, 3 H), 7.45 (t, 2 H), 7.58 (t, 1 H), 7.78 (d, 1 H), 8.09 (d, 2 H); ^{13}C NMR (126 MHz, $CDCl_3$) δ 9.02, 9.20, 9.48, 12,93, 14.10, 14.70, 18.39, 20.30, 20.94, 22.12, 22.32, 23.36, 25.50, 25.62, 26.60, 28.14, 28.19, 30.21, 35.40, 35.47, 38.67, 42.03, 43.10, 45.52, 45.59, 58.36, 60.31, 71.74, 72.00, 74.90, 75.16, 75.39, 76.30, 79.01, 79.13, 80.88, 84.41, 119.91, 127.92, 128.36, 128.54, 129.26, 130.08, 130.55, 130.60, 130.89, 132.40, 133.36, 133.49, 137.11, 137.65, 143.30, 154.89, 157.05, 166.85, 168.01, 168.06, 169.02, 169.55, 170.09, 171.09, 174.92, 204.03. All data were in agreement with literature values.[19]

(D)-biotin-methyl ester (2-13):[19]

To a 10 mL round bottomed flask added (298 mg, 1.22 mmol) of (D)-biotin purchased from sigma-aldrich and diluted with 3 mL of methanol. Then added dropwise 0.29 mL of previously distilled thionyl chloride and stirred overnight at room temperature. After completion, the reaction was concentrated *in vacuo* to produce the desired compound **2-13** (285 mg, 1.10 mmol), 90% without further purification: ^{1}H NMR (300 MHz, $CDCl_3$) δ 1.25 – 1.81 (m, 6 H), 2.32 (t, J = 7.1 Hz, 2 H), 2.71 (d, J = 12.0 Hz, 1 H), 2.94 (dd, J = 12.8, 4.2 Hz, 1 H), 3.22 (m, 1 H), 3.63 (s, 3 H), 4.33 (m, 1 H), 4.49 (m, 1 H). All data were in agreement with literature values.[19]

(D)-biotin-hydrazide (2-14):[19]

To a 5 mL round bottomed flask added (77 mg, 0.30 mmol) of compound **2-13** and diluted with 0.65 mL of methanol. Then added (0.03 mL, 0.89 mmol) of anhydrous hydrazine dropwise and heated to 80 ^{o}C. This solution was stirred overnight and then concentrated *in- vacuo* to yield (51 mg, 0.20 mmol), 67 % of the desired compound **2-14** without further purification: Positive FIA [M+1] = 259.1; ^{1}H NMR (300 MHz, DMSO-d_6) δ 1.27 – 1.61 (m, 6 H), 1.99 (t, *J* = 7.5 Hz, 2 H), 2.56 (d, *J* = 12.6 Hz, 1 H), 2.81 (dd, *J* = 12.3, 3.9 Hz, 1 H), 3.08 (m, 1 H), 4.11 (m, 1 H), 4.29 (m, 1 H). All data were in agreement with literature values.[19]

(5C)-BLT Conjugate (2-15):[19]

To a 5 mL round bottomed flask added (119 mg, 0.10 mmol) of compound **2-12** and diluted with 0.36 mL of DMSO. To a separate 5 mL round bottomed flask added (20 mg, 0.05 mmol) of compound **2-14** and diluted with 0.3 mL of DMSO. Then compound **2-14** in DMSO was added dropwise to the compound **2-12** and allowed to stir at room temperature for 48 hours. The reaction was monitored via TLC and after completion was quenched with distilled water. The precipitate that formed was then filtered and dissolved in DCM. Column purification was carried out with 5 % (methanol / DCM) to produce the desired conjugate **2-15 (**24 mg, 0.02 mmol), 40 % yield as a white solid. Purity was determined to be 88 % by HPLC: ^{1}H NMR (500 MHz, CD_3OD) δ 0.85 – 0.88 (m, 2 H), 0.95 – 0.10 (m, 4 H), 1.04 – 1.07 (m, 2 H), 1.14 (s, 6 H), 1.25 (d, *J* = 6.5 Hz, 7 H), 1.39 (s, 9 H), 1.44 – 1.45 (m, 2 H), 1.53 – 1.58 (m, 2 H), 1.63 (s, 3 H), 1.67 (t, *J* = 7.0 Hz, 2 H), 1.72 (d, *J* = 11.0 Hz, 9 H), 1.89 (s, 3 H), 1.92 – 1.97 (m, 1 H), 2.23 (dt, *J* = 7.0, 2.0 Hz, 3 H), 2.29 (t, *J* = 6.0 Hz, 2 H), 2.35 (s, 3 H), 2.39 – 2.44 (m, 2 H), 2.63 (m, 2 H), 2.89 (dd, *J* = 13.0, 5.0 Hz, 1 H), 2.92 – 2.95 (m, 1 H), 3.13 – 3.19 (m, 1 H), 3.82 (d, *J* = 7.0 Hz, 1 H), 3.98 (dd, *J* = 16.5, 3.5 Hz, 1 H), 4.08 (m, 1 H), 4.17 (q, *J* = 8.5 Hz, 2 H), 4.25 – 4.31 (m, 2 H), 4.43 – 4.46 (m, 1 H), 4.89 (s, 2 H), 4.97 (d, *J* = 9.0 Hz, 1 H), 5.23 (m, 1 H), 5.64 (d, *J* = 4.5 Hz, 1 H), 6.10 (m, 1 H), 6.43 (s, 1 H), 7.22 – 7.32 (m, 3 H), 7.48 (t, *J* = 7.5 Hz, 2 H), 7.61 (t, *J* = 7.0 Hz, 1 H), 7.79 (d, *J* = 8.0 Hz, 1 H), 8.09 (d, *J* = 7.5 Hz, 2 H). All data were in agreement with literature values.[19]

***N*-4-(Pyridin-2-yldisulfanyl)pentanoyl N'-BOC hydrazide (2-16):**

To a 10 mL round bottomed flask added (300 mg, 1.23 mmol) of compound **2-7** and 3 mL of THF and heated to 45 ^{o}C. While stirring (299 mg, 1.85 mmol) of CDI was added and allowed to stir an additional 2 hours. After 2 hours, (488 mg, 3.69 mmol) of BOC-carbazate was added and the

temperature was increased to 55 ^{o}C and stirred an additional 3 hours. After completion the reaction was cooled to room temperature and quenched with saturated ammonium chloride. The resulting solution was extracted with DCM (100 mL) and washed with saturated ammonium chloride (2 x 100 mL) and brine (1 x 100 mL). The organic layers were collected and dried with $MgSO_4$ and concentrated *in vacuo*. The solid obtained was then dissolved in DCM and purified via normal phase chromatography using 50 % (Ethyl Acetate / Hexanes). After collecting and concentrating *in vacuo* the desired fractions, 399 mg (1.12 mmol), 91 % of the desired compound **2-16** was obtained pure: ^{1}H NMR (300 MHz, $CDCl_3$) δ 1.25 (dd, *J* = 2.4 Hz, *J* = 6.9 Hz, 3 H), 1.38 – 1.42 (m, 9 H), 1.83 – 1.98 (m, 2 H), 2.33 – 2.44 (m, 1 H), 2.94 – 3.00 (m, 1 H), 6.91 – 7.03 (m, 1 H), 7.54 – 7.69 (m, 2 H), 8.38 – 8.52 (m, 1 H), 9.89 (b, 1 H); ^{13}C NMR (75 MHz, $CDCl_3$) δ 20.6, 28.0, 29.6, 31.0, 46.0, 81.3, 119.8, 120.0, 120.6, 136.9, 149.2, 155.6, 160.3, 172.0.

_N_-4-(2-hydroxycarbonylmethyl-phenyldisulfanyl)pentanoyl N'-BOC hydrazide (2-17):

To a 25 mL round bottomed flask added (390 mg, 1.09 mmol) compound **2-16** and 4 mL of THF. Then the solution was heated to 60 ^{o}C. To an addition funnel was added (184 mg, 1.09 mmol) of 2-mercapto-phenylacetic acid and 6 mL of THF. The 2-mercapto-phenylacetic acid solution was added dropwise over 2 hours. After completion the reaction was cooled and concentrated *in vacuo*. The resulting oil was purified by flash chromatography using 25 – 30 % ethyl acetate in hexanes. The resulting pure fraction were collected and concentrated *in vacuo* to give 370 mg (0.89 mmol), 82 % of the desired compound **2-17**: mp: 35 – 37 ^{o}C; ^{1}H NMR (500 MHz, $CDCl_3$) δ 1.26 (d, *J* = 7.0 Hz, 3 H), 1.45 – 1.48 (m, 9 H), 1.78 – 1.81 (m, 1 H), 2.03 –2.13 (m, 2 H), 2.15 – 2.19 (m, 1 H), 2.73 – 2.74 (m, 1 H), 3.73 – 3.92 (dd, *J* = 17 Hz, *J* = 79 Hz, 2 H), 7.19 – 7.23(m, 2 H), 7.29 – 7.33 (m, 1 H), 7.82 (d, *J* = 7.5 Hz, 1 H), 8.54 – 8.70 (b, 1 H); ^{13}C NMR (100 MHz, $CDCl_3$) δ 20.6, 28.3, 31.5, 32.0, 39.5, 44.8, 82.9, 127.7, 128.4, 129.7, 131.7, 134.2, 137.1, 156.3, 172.2, 175.2.

D-Biotin-NHS ester (2-18):[22]

To a 5 mL round bottomed flask was added (100 mg, 0.40 mmol) of D-biotin and (114 mg, 0.99 mmol) of NHS. Then 2 mL of DMF was added and the solution was heated to 45 ^{o}C. To this solution was added (0.10 mL, 0.66 mmol) of DIC dropwise and the resulting solution was allowed to stir for 48 hours. After completion, the solution was cooled and isopropanol was added which immediately formed a white precipitate. This precipitate was then filtered and washed with isopropanol. The resulting white precipitate was then heated in isopropanol until dissolved and then

allowed to cool to room temperature until crystals formed. After completion, the resulting crystals were filtered and washed with room temperature isopropanol to yield compound **2-18** (114 mg, 0.33 mmol), 83 % as a white solid: mp: 212 – 213 ^{o}C [lit 212 – 214 ^{o}C]; ^{1}H NMR (300 MHz, DMSO-d_6) δ 1.30 – 1.70 (m, 6 H), 2.57 (m, 1 H), 2.65 (m, 2 H), 2.81 (s, 4 H), 2.84 (m, 1 H), 3.11 (m, 1 H), 4.15 (m, 1 H), 4.30 (m, 1 H), 6.38 (s, 1 H), 6.44 (s, 1 H). All data are in agreement with literature values.[22]

***N*-4-(2-hydroxycarbonylmethyl-phenyldisulfanyl)pentanoyl N'-biotin hydrazide (2-20):**

To a 10 mL round bottomed flask was added (102 mg, 0.25 mmol compound **2-17** and 0.8 mL of DCM. Then added 1.8 mL of TFA was added dropwise and allowed to stir for 30 minutes at room temperature. The reaction was monitored by TLC and when completed the reaction was concentrated *in vacuo* to yield the compound **2-19**. In the same flask (44 mg, 014 mmol) of compound **2-18** and 1 mL of DMF was added. While stirring 0.03 mL of TEA was added and the reaction was allowed to stir an additional 48 hours at room temperature. After completion, acetonitrile was added and a white precipitate immediately formed. This precipitate was collected and washed with acetonitrile to yield (65 mg, 0.12 mmol) of a white solid which was crude by HPLC: FIA [M+1] = 541, [M-1] = 539. Continued to the next step without further purification.

(5C)-BLT Conjugate (2-21):[19]

To a 10 mL round bottomed flask was added (20.3 mg, 0.04 mmol) of compound **2-20**, (51 mg, 0.07 mmol) of SB-T-1214, and (1 mg, 0.01 mmol) of DMAP. Then 0.5 mL of THF was added. The starting material did not dissolve. Then 0.5 mL of DMF was added and the solution became clear. To this solution at room temperature was added 12 uL of DIC and the solution was allowed to stir at room temperature for 48 hours. After completion the reaction was concentrated *in vacuo* and directly subjugated to flash chromatography using (5 % methanol in DCM) to yield (16 mg, 0.01 mmol), 25 % of the desired conjugate **2-21** as a white solid. Purity by HPLC was determined to be 88 %: ^{1}H NMR (500 MHz, CD_3OD) δ 0.85 – 0.88 (m, 2 H), 0.95 – 0.10 (m, 4 H), 1.04 – 1.07 (m, 2 H), 1.14 (s, 6 H), 1.25 (d, *J* = 6.5 Hz, 7 H), 1.39 (s, 9 H), 1.44 – 1.45 (m, 2 H), 1.53 – 1.58 (m, 2 H), 1.63 (s, 3 H), 1.67 (t, *J* = 7.0 Hz, 2 H), 1.72 (d, *J* = 11.0 Hz, 9 H), 1.89 (s, 3 H), 1.92 – 1.97 (m, 1 H), 2.23 (dt, *J* = 7.0, 2.0 Hz, 3 H), 2.29 (t, *J* = 6.0 Hz, 2 H), 2.35 (s, 3 H), 2.39 – 2.44 (m, 2 H), 2.63 (m, 2 H), 2.89 (dd, *J* = 13.0, 5.0 Hz, 1 H), 2.92 – 2.95 (m, 1 H), 3.13 – 3.19 (m, 1 H), 3.82 (d, *J* = 7.0 Hz, 1 H), 3.98 (dd, *J* = 16.5, 3.5 Hz, 1 H), 4.08 (m, 1 H), 4.17 (q, *J* = 8.5 Hz, 2 H), 4.25 – 4.31

(m, 2 H), 4.43 – 4.46 (m, 1 H), 4.89 (s, 2 H), 4.97 (d, *J* = 9.0 Hz, 1 H), 5.23 (m, 1 H), 5.64 (d, *J* = 4.5 Hz, 1 H), 6.10 (m, 1 H), 6.43 (s, 1 H), 7.22 – 7.32 (m, 3 H), 7.48 (t, *J* = 7.5 Hz, 2 H), 7.61 (t, *J* = 7.0 Hz, 1 H), 7.79 (d, *J* = 8.0 Hz, 1 H), 8.09 (d, *J* = 7.5 Hz, 2 H). All data were in agreement with literature values.[19]

4-Mercaptobutanoic acid (2-23):[23]

Method A: To a 50 mL round bottomed flask added (1.017 g, 11.81 mmol) of γ-butyrolactone and (4.501 g, 59.13 mmol) of thiourea. Then to this same flask added 8.5 mL of 48 % aqueous hydrobromic acid and the resulting solution was stirred and refluxed at 135 ^{o}C for 48 hours. After completion, the solution was cooled down and washed with (3 x 50 mL) DCM to remove excess starting materials. The aqueous layer was then added to a 100 mL round bottomed flask and 10.0 mL of 20 M NaOH was added slowly. The resulting solution was then stirred and refluxed at 120 ^{o}C for 4 hours. After completion the resulting solution was cooled and then washed with (3 x 50 mL) of DCM. The aqueous layer was then acidified with 6 N HCl to a pH of 2 and extracted (3 x 100 mL) with DCN. The combined organic layers were collected, dried with $MgSO_4$ and concentrated *in vacuo* to yield 789 mg of a (50/50) mixture of compound **2-24** and compound **2-23** determined by crude ^{1}H NMR.

Method B: To a 25 mL round bottomed flask added (2.051 g, 9.99 mmol) of ethyl-4- bromobutyrate and (1.521 g, 19.98 mmol) of thiourea. Then to the same flask added 10 mL of acetone and stirred and refluxed at 60 ^{o}C for 20 hours. A white solid formed which was washed with diethyl ether (2 x 50 mL). To a 100 mL round bottomed flask was added the crude salt previously obtained and 2 mL of 20 M NaOH and the resulting solution was stirred and refluxed at 120 ^{o}C for 24 hours. After completion the resulting solution was cooled and then washed with (3 x 50 mL) of DCM. The aqueous layer was then acidified with 6 N HCl to a pH of 2 and extracted (3 x 100 mL) with DCM. The combined organic layers were collected, dried with $MgSO_4$ and concentrated *in vacuo* to yield the desired compound **2-23** (990 mg, 8.24 mmol), 82 % as a smelly clear slightly yellow oil: ^{1}H NMR (500 MHz, $CDCl_3$) δ 1.33 (t, *J* = 8.5 Hz, 1 H), 1.85 (m, 2 H), 2.43 (t, *J* = 7.5 Hz, 2 H), 2.51 (m, 2 H), 11.19 (b, 1 H); ^{13}C NMR (126 MHz, CDCl3) δ 23.6, 28.4, 32.2, 179.2. All data are in agreement with literature values.[23]

4-(Pyridin-2-yldisulfanyl) butanoic acid (2-26):[24]

To a 250 mL two neck round bottomed flask was added (7.100 g, 32.22 mmol) of di-pyridine-di-

sulfide and 161 mL of anhydrous ethanol. This solution was heated to reflux and stirred. Then with the aid of an addition funnel (645 mg, 5.37 mmol) of 4-mercapto-butanoic **2-23** in 26 mL of anhydrous ethanol was added dropwise to the refluxing solution. After 2 hours the resulting yellow solution was cooled and then concentrated *in vacuo*. The crude yellow oil obtained was purified via normal phase chromatography using 20 % (Ethyl Acetate / Hexanes). After collecting and concentrating *in vacuo* the desired fractions, (1.075 g, 4.69 mmol), 87 % isolated yield of the desired compound **2-26** was obtained as a clear oil: ^{1}H NMR (300 MHz, $CDCl_3$) δ 2.00 (m, 2 H), 2.46 (t, *J* = 6.9 Hz, 2 H), 2.82 (t, *J* = 6.9 Hz, 2 H), 7.05 – 7.09 (m, 1 H), 7.60 – 7.66 (m, 1 H), 7.69 – 7.72 (m, 1 H), 8.43 – 8.46 (m, 1 H), 11.00 (b, 1 H). All data are in agreement with literature values.[24]

Triisopropylsilyl 4-(Pyridin-2-yldisulfanyl) butanoate (2-27):

To a 25 mL round bottomed flask added (61 mg, 0.27 mmol) of compound **2-26** and 2 mL of DCM. While stirring, added (0.05 mL, 0.32 mmol) of TEA and (0.07 mL, 0.32 mmol) of triisopropylsilylchloride dropwise. The resulting solution was stirred at room temperature overnight and then quenched with 10 mL of saturated ammonium chloride. The resulting solution was then extracted (3 x 50 mL) with DCM and the combined organic layers were collected, dried with $MgSO_4$ and concentrated *in vacuo*. The crude oil obtained was purified via normal phase chromatography using 5 % (Ethyl Acetate / Hexanes). After collecting and concentrating *in vacuo* the desired fractions, (105 mg, 0.27mmol), quantitative yield of the desired compound **2-27** was obtained as a clear oil: ^{1}H NMR (600 MHz, $CDCl_3$) δ 0.99 – 1.06 (m, 18 H), 1.24 – 1.27 (m, 3 H), 2.01 (t, *J* = 7.2 Hz, 2 H), 2.47 (t, *J* = 7.2 Hz, 2 H), 2.84 (t, *J* = 7.2 Hz, 2 H), 7.05 – 7.07 (m, 1 H), 7.60 – 7.62 (m, 1 H), 7.67 – 7.69 (m, 1 H), 8.43 (d, *J* = 4.2 Hz, 1 H).

Triisopropylsilyl 4-(2-hydroxycarbonylmethyl-phenyldisulfanyl) butanoate (2-28):

To a 25 mL round bottomed flask was added (105 mg, 0.27 mmol) of compound **2-27** and 1 mL of THF. The solution was then cooled to 0 ^{o}C and stirred. To an addition funnel was added (45 mg, 0.27 mmol) of 2-mercapto phenylacetic acid **2-6** in 1 mL of THF. This solution was then added dropwise over 2 hours to the stirring solution of compound **2-27**. The resulting yellow solution was then concentrated *in vacuo.* The crude yellow oil obtained was purified via normal phase chromatography using 15 % (Ethyl Acetate / Hexanes). After collecting and concentrating *in vacuo* the desired fractions, (98 mg, 0.22 mmol), 82 % isolated yield of the desired compound **2-28** was obtained as a clear oil: ^{1}H NMR (500 MHz, $CDCl_3$) δ 1.05 – 1.08 (m, 18 H), 1.25 – 1.31 (m, 3

H), 1.99 (p, *J* = 7.0 Hz, 2 H), 2.44 (t, *J* = 7.0 Hz, 2 H), 2.74 (t, *J* = 7.0 Hz, 2 H), 3.88 (s, 2 H) 7.23 - 24 (m, 2 H), 7.28 – 7.31 (m, 1 H), 7.77 (d, *J* = 8.0 Hz, 1 H); ^{13}C NMR (126 MHz, $CDCl_3$) δ 11.8, 17.7, 24.1, 34.1, 37.5, 38.9, 127.8, 128.3, 130.5, 130.9, 133.6, 137.0, 173.1, 176.4.

SB-T-1214-(4C)-linker-TIPS (2-29):

To a 10 mL round bottomed flask added (20 mg, 0.0452 mmol) of linker **2-29**, (2 mg, 0.0113 mmol) of DMAP and (58 mg, 0.0677 mmol) of SB-T-1214 and then diluted with 1.0 mL of DCM. This solution was cooled to 0 ^{o}C. Then (0.01 mL, 0.0497 mmol) of DIC was added and allowed to stir for 2 hours. After completion, the reaction solution was added directly onto a normal phase column and purified using (30 to 50 % Ethyl Acetate / Hexanes) to yield (48 mg, 0.0375 mmol), 83 % isolated yield of the desired compound **2-29** as a white solid: FIA [M+1] = 1279.4; ^{1}H NMR (500 MHz, $CDCl_3$) δ 1.13 - 1.20 (m, 18 H), 1.21 – 1.29 (m, 10 H), 1.33 (m, 9 H), 1.69 – 1.78 (m, 8 H), 1.82 – 1.90 (m, 5 H), 1.99 (m, 3 H), 2.34 (m, 5 H), 2.44 (t, *J* = 6.6 Hz, 2 H), 2.52 (m, 1 H), 2.64 (m, 1 H), 2.77 (t, *J* = 6.6 Hz, 2 H), 3.68 – 3.72 (m , 1 H), 3.89 - 3.93 (m, 1 H), 3.94 (d, *J* = 16.2 Hz, 1 H), 4.08 (d, *J* = 16.2 Hz, 1 H), 4.29 (d, *J* = 8.4 Hz, 1 H), 4.40 – 4.42 (m, 1 H), 4.80 (m, 1 H), 4.92 – 4.97 (m, 3 h), 5.06, (d, *J* = 8.4 Hz, 1 H), 5.29 (s, 1 H), 5.66 (d, *J* = 7.2 Hz, 1 H), 6.18 (t, *J* = 8.4 Hz, 1 H), 6.28 (s, 1 H), 7.24 – 7.32 (m, 3 H), 7.46 (t, *J* = 7.8 Hz, 2 H), 7.59 (t, *J* = 6.6 Hz, 1 H), 7.77 (d, *J* = 7.8 Hz, 1 H), 8.10 (d, *J* = 8.4 Hz, 2 H); ^{13}C NMR (126 MHz, $CDCl_3$) δ 9.1, 9.3, 9.5, 11.9, 13.0, 14.8, 17.7, 18.4, 22.2, 22.3, 23.5, 24.1, 25.7, 26.7, 28.2, 34.0, 35.5, 37.6, 38.8, 42.0, 42.1, 43.2, 43.8, 45.6, 58.5, 71.8, 72.1, 74.9, 75.2, 75.4, 76.4, 79.2, 81.0, 84.5, 120.0, 128.0, 128.3, 128.6, 129.3, 130.1, 130.5, 131.0, 133.6, 136.6, 157.0, 167.0, 168.0, 169.6, 170.1, 172.8, 175.1, 204.1.

SB-T-1214-(4C)-linker-carboxylic acid (2-30):

To a 100 mL round bottomed flask added (67 mg, 0.0524 mmol) of compound **2-29** and diluted with 2.6 mL of pyridine and 2.6 mL of acetonitrile. Then the solution was cooled to 0 ^{o}C in an ice bath and 0.67 mL of HF/Pyridine solution was added dropwise. The reaction was monitored via TLC and upon completion (24 hours) quenched with 10 % citric acid. The resulting solution was then diluted with 100 mL ethyl acetate and extracted 3 x 100 mL with saturated aqueous cupric sulfate solution and 100 mL of brine. The organic layer was collected dried with $MgSO_4$ and concentrated *in vacuo*. The resulting solid was purified by flask chromatography eluting with 45 % (Ethyl Acetate / Hexanes). After collecting and concentrating *in vacuo* the desired fractions, (55 mg, 0.0490 mmol), 94 % of the desired compound **2-30** was obtained as a white solid: FIA [M+1]

= 1123.3; ^{1}H NMR (400 MHz, $CDCl_3$) δ 0.95 – 1.00 (m, 3 H), 1.12 – 1.13 (m, 5 H), 1.25 (s, 5 H), 1.33 (m, 10 H), 1.66 (s, 4 H), 1.72 – 1.80 (m, 8 H), 1.82 – 1.90 (m, 5 H), 1.99 (m, 3 H), 2.34 (m, 7 H), 2.52 (m, 1 H), 2.77 (t, *J* = 6.6 Hz, 2 H), 3.78 (d , *J* = 6.8 Hz, 1 H), 3.89 - 3.93 (m, 1 H), 4.06 (m, 1 H), 4.17 (d, *J* = 8.8 Hz, 1 H), 4.30 (d, *J* = 8.4 Hz, 1 H), 4.38 – 4.43 (m, 1 H), 4.96 – 4.99 (m, 3 h), 5.04, (m, 1 H), 5.10, (m, 1H), 5.30 (s, 1 H), 5.67 (d, *J* = 7.2 Hz, 1 H), 6.21 (t, *J* = 8.8 Hz, 1 H), 6.29 (s, 1 H), 7.30 – 7.35 (m, 1 H), 7.47 (t, *J* = 7.6 Hz, 2 H), 7.60 (t, *J* = 7.6 Hz, 1 H), 7.79 (d, *J* = 8.0 Hz, 1 H), 8.10 (d, *J* = 7.6 Hz, 2 H).

SB-T-1214-(4C)-linker-OSu (2-31):

To a 10 mL round bottomed flask added (30 mg, 0.0267 mmol) of compound **2-30** and diluted it with 0.2 mL of THF and 0.2 mL of pyridine. Then added to this solution (17 mg, 0.1470 mmol) of NHS. While stirring (0.01 mL, 0.0497 mmol) of DIC was added and allowed to stir for 24 hours. After completion, the reaction solution was added directly onto a normal phase column and purified using (40 to 70 % Ethyl Acetate / Hexanes) to yield (30 mg, 0.0246 mmol), 92 % isolated yield of the desired compound **2-31** as a white solid: FIA [M+1] = 1220.3; ^{1}H NMR (500 MHz, $CDCl_3$) δ 0.95 – 1.00 (m, 3 H), 1.12 – 1.13 (m, 5 H), 1.25 (s, 5 H), 1.33 (m, 10 H), 1.65 (s, 3 H), 1.71 – 1.75 (m, 8 H), 1.82 – 1.90 (m, 5 H), 2.03 (s, 4 H), 2.10 (m, 2 H), 2.34 (m, 5 H), 2.52 (m, 1 H), 2.64 (s, 4 H), 2.70 (t, *J* = 7.5 Hz, 3 H), 2.79 – 2.85 (m, 9 H), 2.91 (t, *J* = 6.0 Hz, 1 H), 3.65 (m, 1 H), 3.74 – 3.79 (m , 3 H), 4.04 – 4.07 (m, 1 H), 4.09 – 4.13 (m, 1 H), 4.17 (d, *J* = 8.5 Hz, 1 H), 4.28 (d, *J* = 8.0 Hz, 1 H), 4.40 (dd, *J* = 10.0 Hz, *J* = 6.5 Hz, 2 H), 4.87 – 4.97 (m, 4 h), 5.08, (d, *J* = 8.5 Hz, 1 H), 5.66 (d, *J* = 7.5 Hz, 1 H), 6.18 (t, *J* = 9.0 Hz, 1 H), 6.28 (s, 1 H), 7.24 – 7.32 (m, 4 H), 7.45 (t, *J* = 7.5 Hz, 2 H), 7.58 (t, *J* = 7.5 Hz, 1 H), 7.76 (d, *J* = 8.0 Hz, 1 H), 8.10 (d, *J* = 8.0 Hz, 2 H); ^{13}C NMR (126 MHz, $CDCl_3$) δ 9.08, 9.26, 9.52, 11.9, 12.98, 13.65, 14.14, 14.74, 17.23, 18.45, 19.07, 20.99, 22.16, 22.36, 23.28, 23.57, 24.64, 25.33, 25.42, 25.55, 25.68, 26.63, 28.16, 28.41, 29.28, 29.65, 30.60, 31.51, 35.44, 35.55, 36.61, 36.87, 37.36, 38.72, 42.38, 43.14, 45.64, 49.05, 58.40, 60.39, 64.36, 71.82, 72.02, 74.94, 75.23, 75.44, 76.38, 79.06, 80.01, 80.95, 84.50, 119.81, 128.24, 128.46, 128.55, 129.36, 130.15, 130.97, 131.05, 132.51, 133.47, 133.86, 136.45, 137.90, 143.25, 155.05, 166.81, 167.98, 169.12, 169.61, 170.16, 172.04, 175.01, 204.07.

(4C)-BLT Conjugate (2-32):

To a solution of **2-31** (30 mg, 0.0246 mmol) in DMSO (0.1 mL) was added compound **2-14** (8.9 mg, 0.0344 mmol) at room temperature. After stirring the mixture for 48 h, the reaction mixture

was directly loaded onto a silica gel column. Column chromatography of the residue (eluent: 5% MeOH in DCM) afforded conjugate **2-32** (25 mg, 0.0183 mmol), 81% yield as white powder: FIA [M+1] = 1363.5; ^{1}H NMR (500 MHz, CD_3OD) δ 0.82 – 0.88 (m, 5 H), 0.95 – 1.00 (m, 3 H), 1.00 (m, 1 H), 1.06 (m, 2 H), 1.15 (s, 6 H), 1.30 - 1.39 (m, 6 H), 1.43 – 1.49 (m, 10 H), 1.63 (s, 3 H), 1.71 – 1.75 (m, 8 H), 1.82 – 1.90 (m, 3 H), 1.99 (m, 2 H), 2.24 (m, 3 H), 2.31 (t, *J* = 7.5 Hz, 2 H), 2.36 (s, 3 H), 2.42 (m, 2 H), 2.65 (d, *J* = 12.5 Hz, 1 H), 2.76 (t, *J* = 8.0 Hz, 2 H), 2.88 (dd, *J* = 5.0 Hz, *J* = 13.0 Hz, 1 H), 3.16 (m, 1 H), 3.82 (d, *J* = 6.5 Hz, 1 H), 3.96 (d, *J* = 17.5 Hz, 1 H), 4.06 (d, *J* = 17.5 Hz, 1 H), 4.17 (q, *J* = 8.0 Hz, 2 H), 4.25 – 4.31 (m, 2 H), 4.44 (dd, *J* = 4.5 Hz, *J* = 7.0 Hz, 1 H), 4.89 (s, 2 H), 4.97 (d, *J* = 9.5 Hz, 1 H), 5.22 (d, *J* = 6.5 Hz, 1 H), 5.64 (d, *J* = 7.0 Hz, 1 H), 6.11 (t, *J* = 8.0 Hz, 1 H), 6.43 (s, 1 H), 7.24 – 7.32 (m, 3 H), 7.48 (t, *J* = 7.5 Hz, 2 H), 7.60 (t, *J* = 7.5 Hz, 1 H), 7.77 (d, *J* = 8.0 Hz, 1 H), 8.09 (d, *J* = 7.5 Hz, 2 H); ^{13}C NMR (126 MHz, CD_3OD) 9.32, 9.35, 10.61, 11.93, 13.97, 14.60, 15.16, 18.83, 21.19, 22.36, 23.43, 23.87, 25.26, 26.26, 26.39, 26.53, 27.17, 28.98, 29.53, 29.69, 30.34, 32.92, 33.20, 34.54, 35.86, 35.92, 36.96, 37.71, 38.66, 39.73, 41.22, 44.78, 48.25, 49.81, 57.08, 59.48, 61.85, 63.43, 72.50, 73.20, 76.54, 76.70, 76.93, 77.65, 79.30, 82.54, 86.08, 121.43, 129.39, 129.66, 129.86, 131.32, 131.62, 132.18, 132.62, 134.73, 135.00, 135.67, 138.33, 138.87, 142.81, 157.46, 166.13, 167.62, 170.29, 171.51, 172.23, 173.99, 174.86, 175.13, 205.31; HRMS (ESI) *m/e* calcd for $C_{67}H_{88}N_5O_{19}S_3H^+$:1362.5236. Found: 1362.5256 (Δ = 1.5 ppm).

§2.6 References:

1. Chari, R. V. J., Targeted delivery of chemotheraputics: tumor-activated prodrug therapy. *Advanced Drug Delivery Reviews* **1998,** *31*, 89 - 104.
2. Chen, J.; Stanislav, J.; Zhao, X.; Chen, S.; Ojima, I., Antibody-cytotoxic agent conjugates for cancer therapy. *Expert Opinion on Drug Delivery* **2005,** *2*, 873 - 890.
3. Chen, S.; Zhao, X.; Chen, J.; Chen, J.; Kuznetsova, L. V.; Wong, S. S.; Ojima, I., Mechanism-Based Tumor-Targeting Drug Delivery System. Validation of Efficent Vitamin Receptor-Mediated Endocytosis and Drug Release. *Bioconjugate Chemistry* **2010,** *21*, 979 - 987.
4. Jaracz, S.; Chen, J.; Kuznetsova, L. V.; Ojima, I., Recent advances in tumor-targeting anticancer drug conjugates. *Bioorg. Med. Chem.* **2005,** *13*, 5043 - 5054.
5. Ojima, I., Guided Molecular Missiles for Tumor-Targeting Chemotherapy-Case Studies Using the Second-Generation Taxoids as Warheads. *Accounts of Chemical Research* **2008,** *41*, 108 - 119.
6. Ojima, I.; Zuniga, E. S.; Berger, W. T.; Seitz, J. D., Tumor-targeting drug delivery of new-generation taxoids. *Future Med. Chem.* **2012,** *4*, 33 - 50.
7. Das, M. Ph.D. Dissertaiton: Design, Synthesis and Biological Evaluation of Novel Tumor-

targeting Taxane-based Drug Delivery Systems. Stony Brook University, Stony Brook, NY, **2010**.

8. Reddy, J. A.; Westrick, E.; Vlahov, I. R.; Howard, S. J.; Santhapuram, H. K.; Leamon, C. P., Folate receptor specific anti-tumor activity of folate-mitomycin conjugates. *Cancer Chemother. Parmacol.* **2006,** *58*, 229 - 236.
9. Zahnd, C.; Wyler, E.; Schwenk, J. M.; Steiner, D.; Lawrence, M. C.; McKern, N. M.; Pecoran, F.; Ward, C. W.; Joos, T. O.; Pluckthun, A., A Designed Ankyrin Repeat Protein Evolved to Picomolar Affinity to Her2. *J. Mol. Biol.* **2007,** *269*, 1015 - 1028.
10. Ojima, I.; Genhelm, X.; Wu, X.; Qu, C.; Borella, C. P.; Xie, H.; Wilhelm, S. D.; Leece, B. A.; Bartle, L. M.; Goldmacher, V. S.; Chari, R. V. J., Tumor-Specific Novel Taxoid-Monoclonal Antibody Conjugates. *J. Med. Chem.* **2002,** *45*, 5620 - 5623.
11. Weinstein, S. J.; Hartman, T. J.; Stolzenberg-Soloman, R.; Pietinen, P.; Barrett, M. J.; Taylor, P. R.; Virtamo, J.; Albanes, D., Null association between prostate cancer and serum folate, vitamin B6, vitamin B12 and homocysteine. *Cancer Epdemiol. Biomarkers Prev.* **2003,** *12*, 1271 - 1272.
12. Reddy, J. A.; Leamon, C. P., *Folate receptor targeted cancer chemotherapy*. Springer Science & Business Media LLC2011.
13. Xia, W.; Low, P. S., Folate-targeted therapies for cancer. *J. Med. Chem.* **2010,** *53*, 6811 - 6824.
14. Leamon, C. P.; Reddy, J. A., Folate-targeted chemotherapy. *Adv. Drug Deliv. Rev.* **2004,** *56*, 1127 - 1141.
15. Leamon, C. P.; Reddy, J. A.; Vlahov, I. R.; Vetzel, M.; Parker, N.; Nicoson, J. S.; Xu, L.-C.; Westrick, E., Synthesis and biological evaluation of EC72: a new folate-targeted chemotherapeutic. *Bioconjugate Chemistry* **2005,** *16*, 803 - 811.
16. Lu, Y.; Leamon, C. P.; Low, P. S., Folate receptor-targeted immunotherapy of cancer: mechanism and theraputic potential. *Adv. Drug Deliv. Rev.* **2004,** *56*, 1161 - 1176.
17. Lu, Y.; Low, P. S., Folate-mediated delivery of macromolecular anticancer therapeutic agents. *Adv. Drug Deliv. Rev.* **2002,** *54*, 675 - 693.
18. Russell-Jones, G.; McTavish, K.; McEwan, J.; Rice, J.; Nowotnik, D., Vitamin-mediated targeting as a potential mechanism to increase drug uptake by tumors. *J. Inorg. Biochemistry* **2004,** *98*, 1625 - 1633.
19. Zhao, X. Ph.D. Dissertation: Design, synthesis and biological evaluation of novel taxane-based anticancer agents and their applications to tumor-targeting drug delivery systems. Stony Brook University, Stony Brook, NY, **2009**.
20. Kharasch, N.; Langford, R. B., Derivatives of Sulfenic Acids. XLII. 3-Chloroformylpropanesulfenyl Chloride and 1,2-Thiazan-3-one. *J. Org. Chem.* **1963,** *28*, 1901 - 1903.
21. Chen, J. Ph.D. Dissertation: Tumor-targeting Drug Delivery System of Anticancer Agent. Ph.D., Stony Brook University, **2008**.
22. Kai, L.; Chen, Y.; Siqi, L.; Nguyen, H. G.; Niu, Z.; You, S.; Mello, C. M.; Lu, X.; Wang, Q., Chemical Modification of M13 Bacteriophage and Its Application in Cancer Cell

Imaging. *Bioconjugate Chemistry* **2010,** *21*, 1369 - 1377.

23. Li, M.; Yamato, K.; Ferguson, J. S.; Gong, B., Sequence-Specific Association in Aqueous Media by Integrating Hydrogen Bonding and Dynamic Covalent Interactions. *J. Am. Chem. Soc.* **2006,** *128*, 12628 - 12629.
24. Lin, R.; Cheetham, A. G.; Zhang, P.; Lin, Y.-A.; Cui, H., Supramolecular filaments containing a fixed 41% paclitaxel loading. *Chem. Commun.* **2013,** *49*, 4968 - 4970.

Chapter 3

Polyunsaturated Fatty Acids in Targeted Cancer Chemotherapy

Content

§3.0 Introduction:

§3.0.1 The Role of PUFAs in Targeted Cancer Chemotherapy:

Polyunsaturated fatty acids (PUFAs) are naturally occurring compounds commonly found in vegetable oils, cold-water fish, and meat products. Among the many PUFAs found naturally, omega-3 PUFAs (DHA, LNA) have been shown particularly to be essential for human health and development.[1] In addition, PUFAs have also been shown to be taken up more rapidly by tumor tissues than normal tissues.[2] Furthermore, some omega-3 PUFAs have sown anticancer and drug-sensitizing ability against various cancers in both clinical and preclinical trials.[3, 4] In particular, drug-sensitization has been attributed to by the rapid incorporation of PUFAs into the lipid bilayers of growing tumor cells, which in-turn disrupts the morphology of the cell presumably influencing the susceptibility of the tumor cells to anticancer drug permeability.[5, 6]

The conjugation of PUFAs to cytotoxic agents has been found to substantially alter their pharmacokinetic properties, enhancing both tumor specificity and efficacy.[7] In particular, tumor-specific accumulation of paclitaxel has been verified when DHA is conjugated at the C2' position. This selective accumulation of paclitaxel in tumor tissues has been attributed to by the ability of PUFA-taxoid conjugates to readily bind human serum albumin (HSA), vastly improving the solubility and half-life of the taxoid within blood plasma.[8] There has also been evidence that suggests gp60 and secreted proteins play a crucial role in the transport of HSA-bound conjugates from blood vessels to the tumor interstitium, leading to the observed accumulation of conjugates within the tumor tissues shown in **Figure 3-1**.[9-11] Once internalized, certain PUFAs and their metabolites may result in synergism with the cytotoxic drug due to their ability to modulate several key intracellular processes.[12] Thus, the conjugation of cytotoxic agents to PUFAs has been studied intensely in recent years.

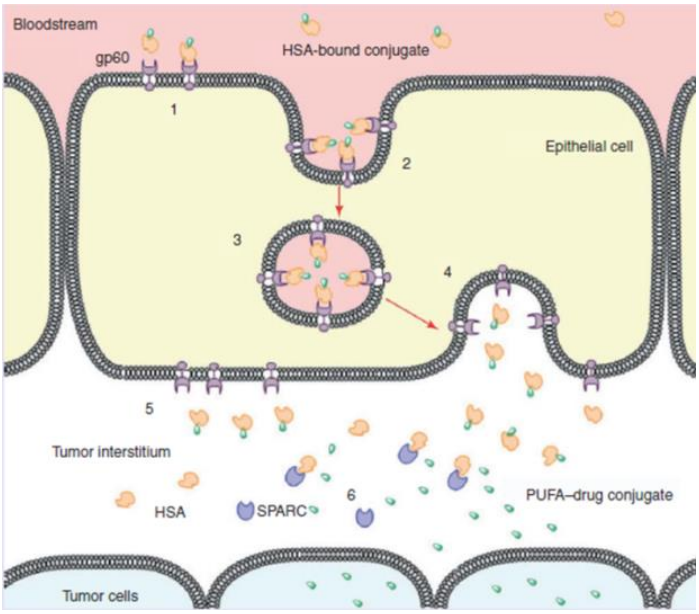

Figure 3-1: gp60-mediated transcytosis. (1) HSA (orange) bound to drug conjugate (green) travels through blood stream and binds to gp60 (purple) on the tumor epithelial cell surface. (2) Ligand binding initiates transcytosis. (3) Vesicles containing drug conjugate–protein complex are transported across the cell. (4) Fusion of the vesicle to the interstitial cell wall occurs. (5) Drug conjugate–HSA complex is released into the tumor interstitium. (6) Binding of SPARC to HSA causes release of a free drug conjugate, which permeates into tumor cells. HSA: Human serum albumin; PUFA: Polyunsaturated fatty acid; SPARC: Secreted protein acidic and rich in cysteine. (Reprinted with permission from reference [11])

§3.0.2 DHA-SB-T-1214 Conjugate *In Vivo* Selectivity:

As stated above, the conjugation of DHA to paclitaxel (Taxoprexin®) has shown great success clinically; increasing both the efficacy and specificity of paclitaxel by reducing systemic toxicity *in vivo*.[7, 13] Specifically, DHA-paclitaxel exhibits less systemic toxicity than the parent compound by one to two orders of magnitude. Furthermore, high conjugate-HSA binding significantly reduces the clearance rate and volume of distribution, resulting in lower concentrations systemically and higher tumor localization.[14] DHA-paclitaxel has since advanced to Phase III clinical trials against several cancer types.[13] Despite the prominence of DHA-paclitaxel as breakthrough chemotherapeutic drug; use of the cytotoxic agent paclitaxel, a known substrate for Pgp, would most likely confer resistance against MDR tumors. Thus, the Ojima laboratory has added to this design by incorporating highly effective second-generation taxoids that exhibit orders of magnitude more potency against MDR tumors.[15-17]

Based upon the promising results of DHA-paclitaxel, the Ojima laboratory sought to broaden and improve upon this existing drug delivery strategy. Thus, several PUFA-second generation taxoid conjugates were synthesized and tested *in vivo* against different drug-resistant and drug-sensitive human tumor xenografts in SCID mice.[18] Interestingly, several of these conjugates led to complete remission in surviving mice with minimal systemic toxicity. In particular, DHA-SB-T-1214 led to complete regression in the growth of the highly drug-resistant colorectal adenocarcinoma DLD as a xenograft in 5 out of 5 mice. Quite extraordinary, reoccurrence was not seen for more than 190 days after treatment as shown in **Figure 3-2**. As this biological results for DHA-SB-T-1214 highlighted the exceptional selectivity of this particular conjugate for DLD tumors *in vivo*, it also raised the question if other PUFA-second-generation taxoid conjugates not tested would provide different selectivities. Furthermore, as there was no formal receptor for DHA, the question arose as to what was producing the selectivity seen. The hypothesis developed was that cellular transport and selective release was major contributor, but additionally, some cellular level selectivity not fully understood could be occurring.

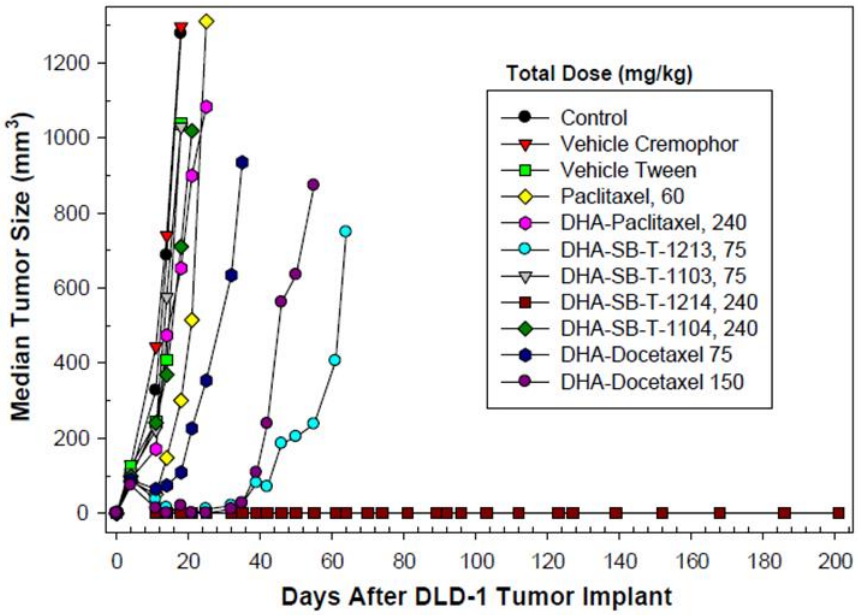

Figure 3-2: Effect of DHA–Taxoid conjugates on human colon tumor xenograft DLD-1 *in vivo* (Reprinted with permission from reference [18])

§3.1 *In Vitro* Analysis of PUFA and PUFA-Second-Generation Taxoids:

§3.1.1 Introduction:

To further understand the selectivity of different PUFA and PUFA-taxoid conjugates seen in the *in vivo* evaluation models, PUFA-fluorescein and PUFA-taxoid-fluorescein molecular probes were designed and synthesized to evaluate cell level selectivity. Primarily, the major focus of the experiment was placed on the cell level selectivity of PUFAs LNA and DHA. Furthermore, evaluation of these PUFAs attached to second-generation taxoid SB-T-1214 was conducted to study how the taxoid influenced the cellular intake of the PUFAs while conjugated to taxoids. Thus the specific aims of this project were to create PUFA and PUFA-SB-T-1214 fluorescein probes and utilize them to gain insight into cell level selectivity.

§3.1.2 Results and Discussion:

§3.1.2.1 Synthesis of a DHA-FITC Molecular Probe:

Synthesis of the DHA-FITC probe was accomplished in 3 steps from commercially obtained DHA as shown in **Scheme 3-1**. Due to the unstable nature of DHA, especially to higher temperatures, a neutral coupling protocol using (1.5 equivalents) EDC and (1.2 equivalents) BOC carbazate was used to form the protected hydrazide **3-1** in 55 % isolated yield. Subsequent deprotection of the hydrazide **3-1** was accomplished in the presence of TFA to afford the crude TFA-hydrazide salt **3-2**, which was used directly to couple to (1.2 equivalents) 6-FITC in the presence of (1.5 equivalents) of TEA to yield the final DHA-FITC probe **3-3** in 48 % isolated yield after two steps.

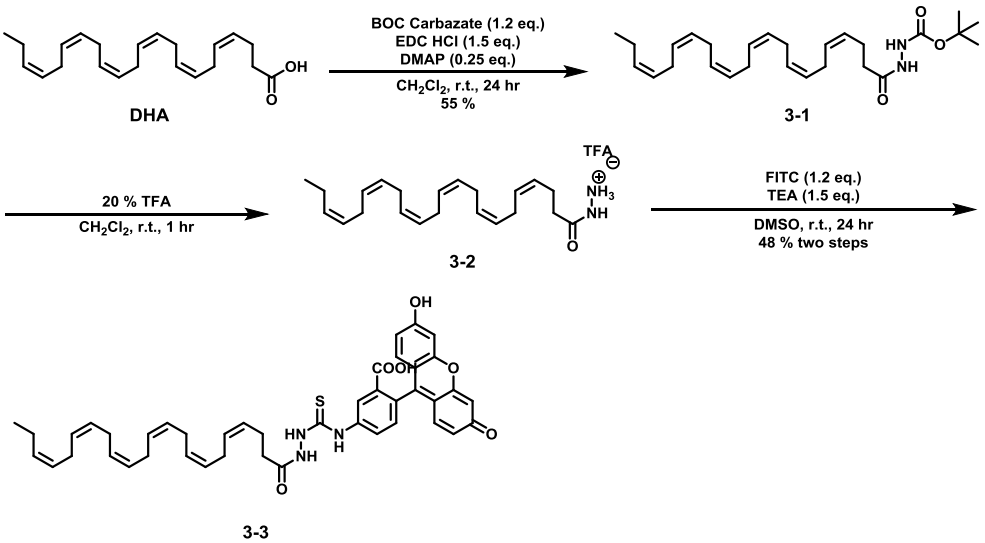

Scheme 3-1: Synthesis of a DHA-FITC molecular probe for FACS and CFM analysis

§3.1.2.2 Synthesis of a LNA-FITC Molecular Probe:

Synthesis of the LNA-FITC probe was accomplished in 2 steps from commercially obtained alpha-linoleic acid (LNA) methyl ester as shown in **Scheme 3-2**. Directly heating LNA-methyl ester and hydrazine monohydrate (3.0 equivalents) in methanol at 60 ^{o}C for 22 hours afforded the hydrazide **3-4** which was then subsequently reacted with (1.0 equivalents) 6-FITC to yield the final LNA-FITC probe **3-5** in 26 % after two steps.

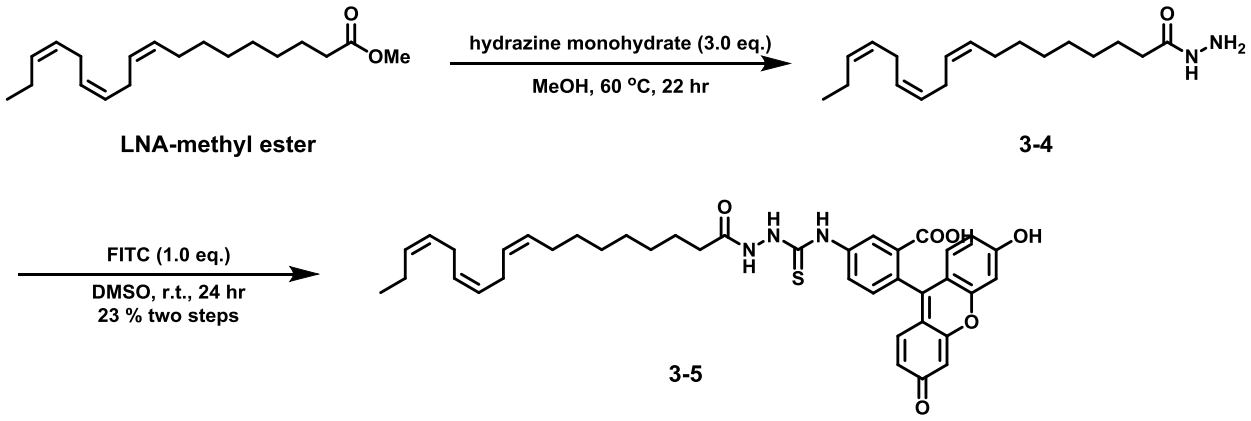

Scheme 3-2: Synthesis of a LNA-FITC molecular probe for FACS and CFM analysis

§3.1.2.3 Biological Evaluation of PUFA-FITC and PUFA-Taxoid-Fluorescein Probes by FACS and CFM Imaging:

Biological evaluation of the PUFA probes was conducted on five different cell lines, including human ovarian carcinoma (A-2780), human colon carcinomas (HT-29, DLD-1), human breast ductal carcinoma (MCF-7), normal cell lines human foreskin fibroblast (HS27) and human lung fibroblast (WI-38). To each cell line 1 uM and 10 uM of PUFA-FITC and PUFA-taxoid-fluorescein probe (PUFA-taxoid-fluorescein probes were synthesized by Dr. Larisa Kuznetsova) was added respectively and incubated at 37 ^{o}C for 3 hours. The resulting cells were washed with PBS following incubation and then measured by fluorescence activated cell sorting (FACS) shown in **Figure 3-3**. These experiments were then repeated under the same exact conditions and photographed using confocal fluorescence microscopy (CFM). The resulting FACS data was open in WinMDI and the geometric mean was calculated for each of the corresponding peaks in the histograms.

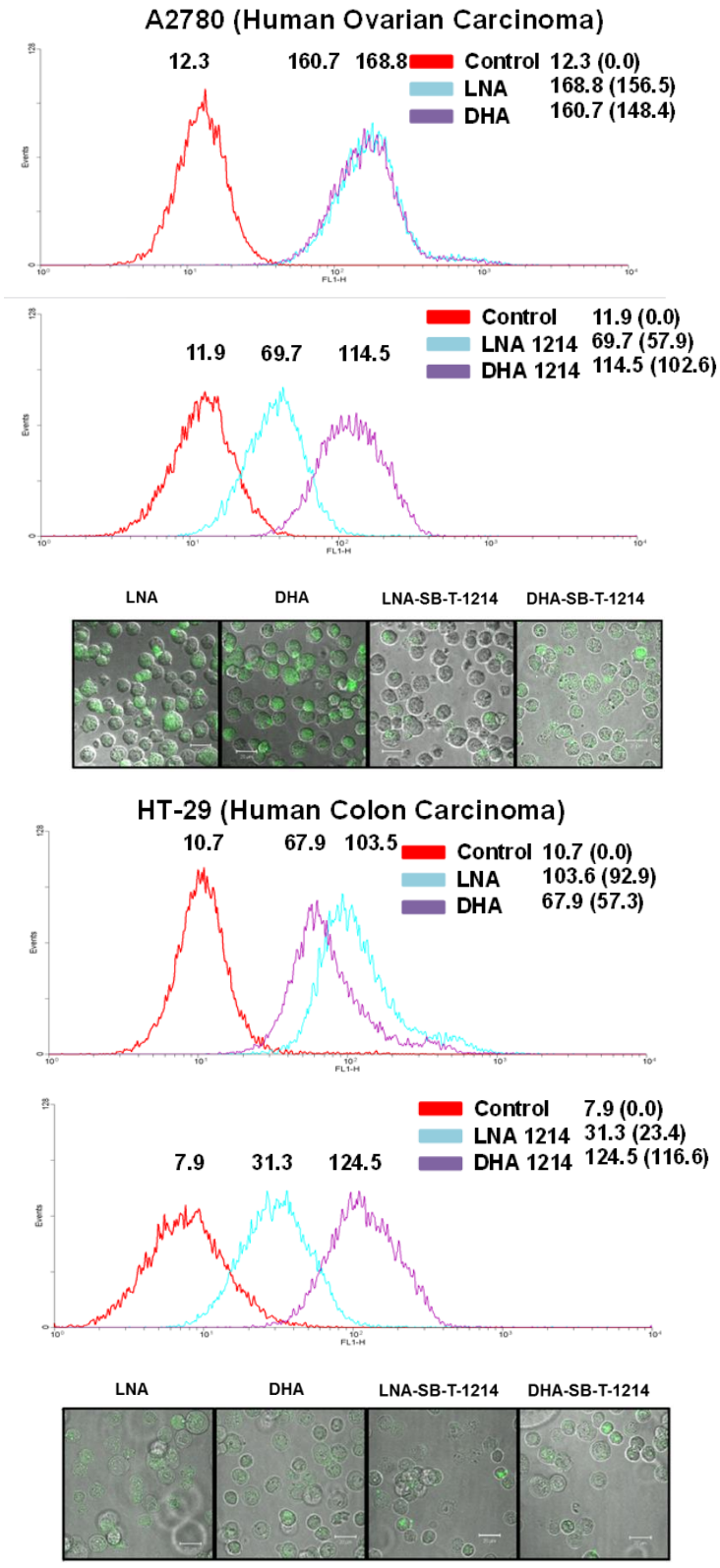
A2780 (Human Ovarian Carcinoma)
12.3
160.7
168.8
Control 12.3 (0.0)
LNA 168.8 (156.5)
DHA 160.7 (148.4)
Events
FL1-H
11.9
69.7
114.5
Control 11.9 (0.0)
LNA 1214 69.7 (57.9)
DHA 1214 114.5 (102.6)
LNA
DHA
LNA-SB-T-1214
DHA-SB-T-1214
HT-29 (Human Colon Carcinoma)
10.7
67.9
103.5
Control 10.7 (0.0)
LNA 103.6 (92.9)
DHA 67.9 (57.3)
7.9
31.3
124.5
Control 7.9 (0.0)
LNA 1214 31.3 (23.4)
DHA 1214 124.5 (116.6)
LNA
DHA
LNA-SB-T-1214
DHA-SB-T-1214

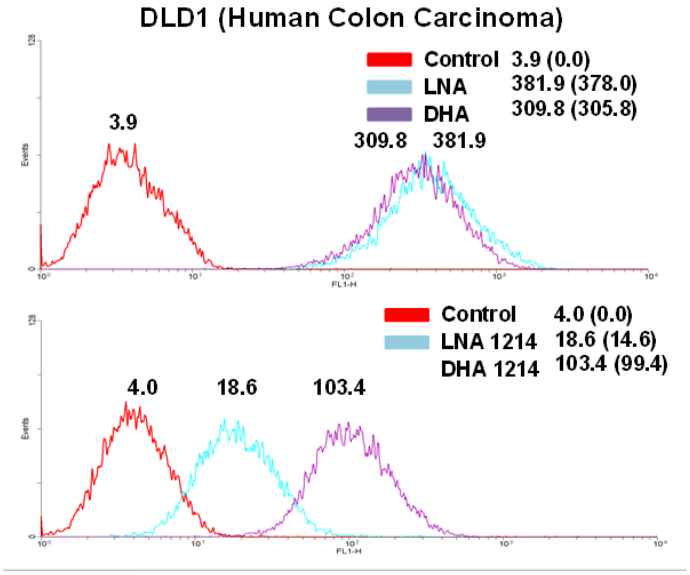
DLD1 (Human Colon Carcinoma)
Control 3.9 (0.0)
LNA 381.9 (378.0)
DHA 309.8 (305.8)
3.9
309.8 381.9
Events
FL1-H
Control 4.0 (0.0)
LNA 1214 18.6 (14.6)
DHA 1214 103.4 (99.4)
4.0 18.6 103.4
Events
FL1-H

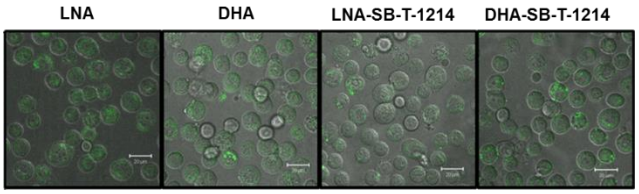
LNA
DHA
LNA-SB-T-1214
DHA-SB-T-1214

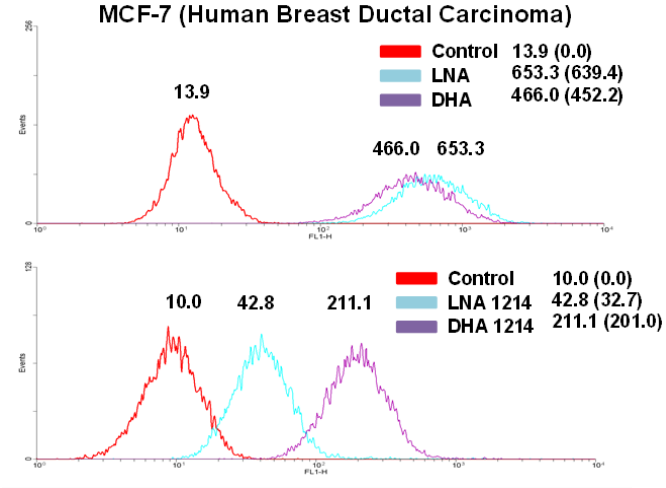
MCF-7 (Human Breast Ductal Carcinoma)
Control 13.9 (0.0)
LNA 653.3 (639.4)
DHA 466.0 (452.2)
13.9
466.0 653.3
Events
FL1-H
Control 10.0 (0.0)
LNA 1214 42.8 (32.7)
DHA 1214 211.1 (201.0)
10.0 42.8 211.1
Events
FL1-H

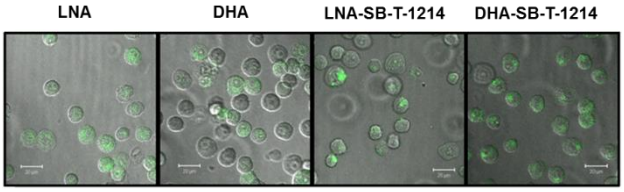
LNA
DHA
LNA-SB-T-1214
DHA-SB-T-1214

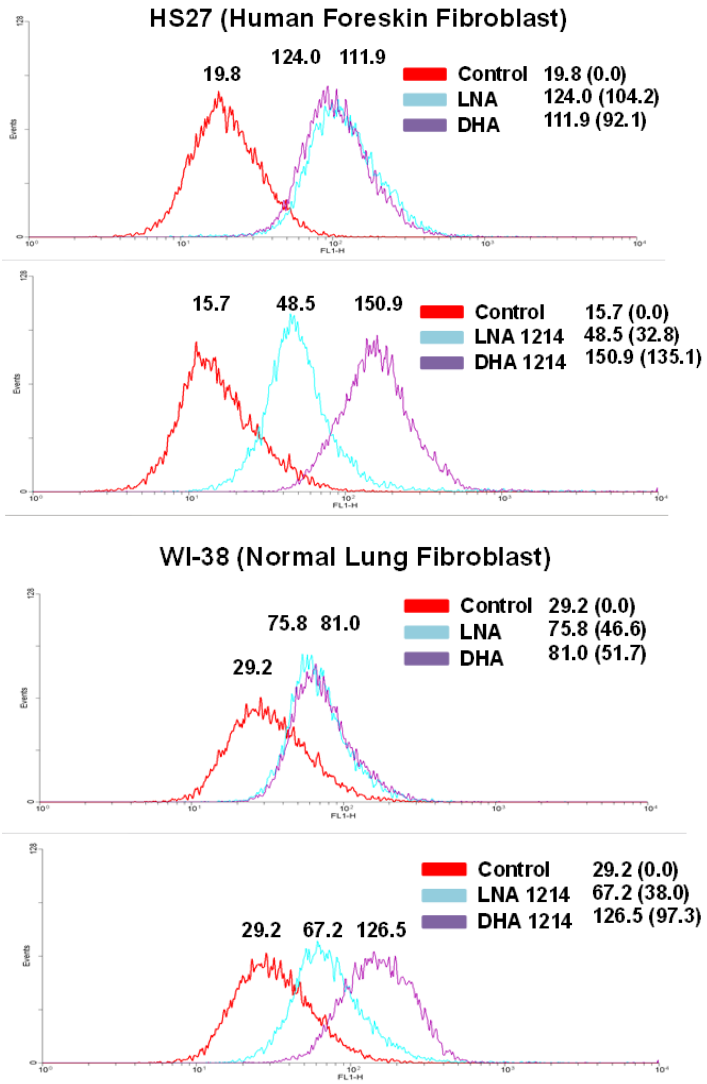

Figure 3-3: FACS and CFM data for A2780, DLD-1, HT-29, MCF-7, HS27, and WI-38 cell lines versus LNA-FITC, DHA-FITC, LNA-SB-T-1214-Fluoroscein, and DHA-SB-T-1214-Fluoroscein molecular probes

After obtaining the geometric mean values of the various probes versus each of the six cell lines, a comparison between each of the cell lines for each individual probe was evaluated. Since each of the probes themselves could have varying amounts of fluorescence intensity, only the same probe was used in this comparison. First auto-fluorescence of the cell line was removed by subtracting the control fluorescence which gave the corresponding number shown in parenthesis (e.g., 0.0 for the control). Then, each of the cancer cell lines was divided by the values obtained from the normal cell line (WI-38) to obtain an order of magnitude of enhanced uptake shown in **Table 3-1**.

Table 3-1: The internalization of 4 molecular fluorescent probes into various cell lines compared with noncancerous cell line (WI-38). In the first two columns, the enhanced uptake of LNA and DHA without SB-T-1214 attached remains fairly consistent for each of the cell lines tested with preference for LNA (yellow). In red, the A2780 cell line shows enhanced uptake of LNA-SB-T-1214 while the MCF7 cell line shows enhanced uptake of DHA-SB-T-1214.

Cell Line	LNA	DHA	LNA-SB-T-1214	DHA-SB-T-1214
WI-38	1.0	1.0	1.0	1.0
HS27	2.2	1.8	0.9	1.4
A2780	3.4	2.9	1.5	1.1
DLD-1	8.1	5.9	0.4	1.0
HT-29	2.0	1.1	0.6	1.2
MCF-7	13.7	8.7	0.9	2.1

Based on the cell level evaluation of PUFA-FITC and PUFA-SB-T-1214-fluoroscein probes, selectivity of PUFA's, particularly when conjugated to SB-T-1214 appears to be occurring on the cell level. Furthermore, the enhanced uptake of DHA-SB-T-1214-fluoroscein in the MCF-7 cell line is fairly consistent with the clinical use of Taxoprexen® for the treatment of breast cancer. Interestingly, conjugation of SB-T-1214 to LNA provided a different selectivity profile with enhanced uptake in the ovarian cancer cell line A2780. Additionally, while most cell lines favored incorporation of LNA over DHA, attachment of SB-T-1214 to PUFAs produced graded selectivity as seen in **Table 3-2**. Thus, higher DHA to LNA internalization rates were somewhat concurrent with lower DHA-SB-T-1214 to LNA-SB-T-1214 ratios. Overall, it is evident that at the cellular level, some cell selectivity for PUFA-taxoid conjugates is occurring. Ultimately, this contribution to *in vivo* results seen, is not exclusively per cell type as the DLD-1 cells did not show enhanced selectivity for the DHA-SB-T-1214 conjugate over normal cell lines. Thus, cellular selectivity is most likely dependent of HAS-transport. For example, if the transportation of PUFA-SB-T-1214 conjugates is similar (considering HSA transport is non-specific to the PUFA) to all tumors, then DLD-1 tumors would prefer DHA-SB-T-1214 nearly 7 times more than LNA-SB-T-1214.

Table 3-2: The internalization geometric means of each molecular probes in various cell line tested. the DHA/LNA internalization ratio and the DHA-SB-T-1214/LNA-SB-T1214 ratio is calculated.

Cell Line	LNA	DHA	Ratio (DHA/LNA)	LNA-SB-T-1214	DHA-SB-T-1214	Ratio (DHA/LNA)
WI-38	46.58	51.74	1.11	37.99	97.28	2.56
HS27	104.24	91.12	0.87	32.77	135.13	4.12
A2780	156.54	148.42	0.95	57.88	102.63	1.77
DLD1	377.95	305.84	0.81	14.55	99.38	6.83
HT-29	92.85	57.26	0.62	23.35	116.61	4.99
MCF-7	639.41	452.19	0.71	32.72	201.02	6.14

§3.1.3 Conclusion:

In conclusion, several molecular probes were used to evaluate PUFA and PUFA conjugates *in vitro* against several known cancer cell lines. In particular, DHA-SB-T-1214 showed some enhancement in the MCF7 cell line (2 times that of WI-38). Additionally, LNA-SB-T-1214 showed some enhancement in the A2780 cell line (1.5 times that of WI-38). Lastly, the *in vivo* results for DHA-SB-T-1214 obtained showed no correlation to the DLD-1 results by themselves. However, when compared with LNA-SB-T-1214, DHA-SB-T-1214 exhibited 7 times more selectivity against DLD-1 cells. Overall, two mechanism, HSA-transport and cell selectivity, may both be contributing to the vivo results seen. Thus, direct cellular comparison between cancerous and non-cancerous cells for PUFA-taxoid conjugates may not be a true gage of *in vivo* effectiveness.

§3.2 LNA-SB-T-1214:

§3.2.1 Introduction:

LNA-taxoid conjugates have been synthesized and tested *in vivo* previously in the Ojima laboratory, although LNA-SB-T-1214 was not among them. Furthermore, LNA-SB-T-1214 showed reduced intake into the DLD-1 cell line *in vitro* when compared to DHA-SB-T-1214 as seen in **Table 3-1**. Despite the *in vitro* results for PUFA-SB-T-1214 conjugates showing selectivity of DHA-SB-T-1214 over LNA-SB-T-1214 nearly 7 times in DLD-1 tumor xenografts, LNA-SB-T-1213 has shown great efficacy in DLD-11 xenografts, even exceeding that of DHA-SB-T-1213 as seen in **Figure 3-4**. Thus, it was evident that the taxoid in the PUFA-taxoid

conjugate could also influencing *in vivo* selectivity. The specific aim in synthesizing LNA-SB-T-1214 was to evaluate the conjugate both *in vitro* in cell based MTT assay and *in vivo* against mice bearing xenografts.

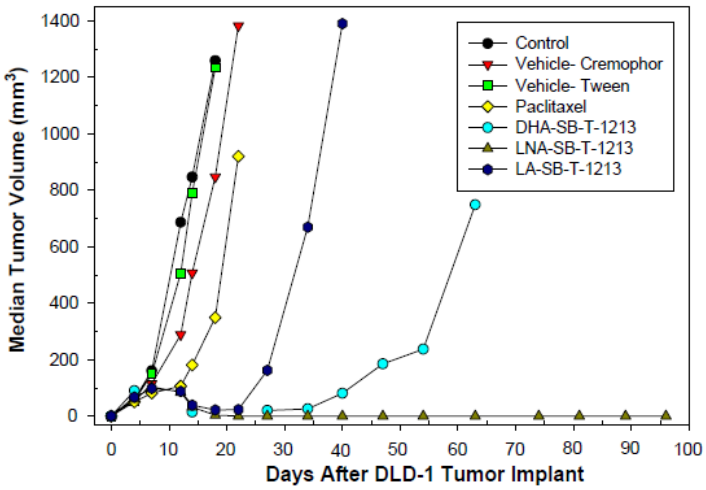

Figure 3-4: Efficacy of different PUFAs-SB-T-1213 conjugates against human colon tumor xenograft DLD-1 *in vivo* (Reprinted with permission from reference [18])

§3.2.2 Results and Discussion:

§3.2.2.1 Synthesis of LNA-SB-T-1214:

The synthesis of LNA-SB-T-1214 was accomplished in 1 step from SB-T-1214 yielding a highly pure PUFA-taxoid conjugate as shown in **Scheme 3-3**. SB-T-1214 was coupled to LNA (1.0 equivalents) assisted by DMAP (0.25 equivalents) in DCM by DIC (1.1 equivalents) at 0 ^{o}C which was allowed to warm to room temperature over 1.5 hours to yield the LNA-SB-T-1214 conjugate **3-6** in 68 % isolated yield and 97.1 % purity by HPLC at 220 nm. Additionally, further reaction time lead to some functionalization of LNA at the C7 position, thus 68 percent conversion was optimal and the unreacted SB-T-1214 was recovered.

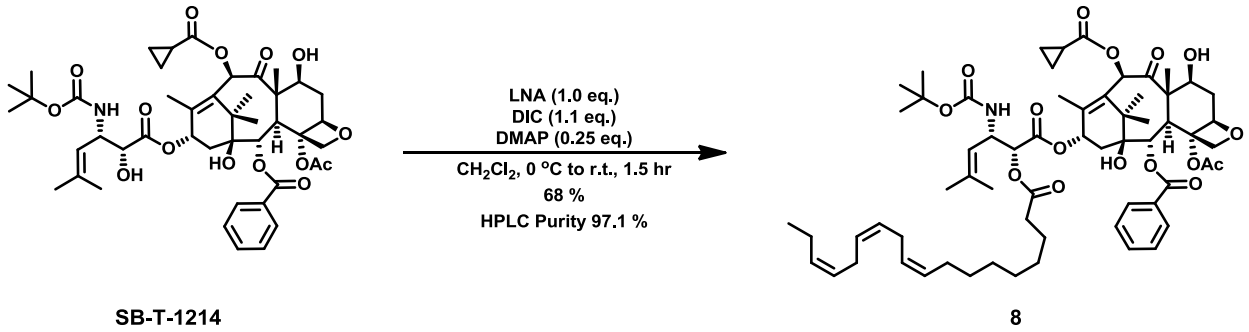

Scheme 3-3: Synthesis of LNA-SB-T-1214

§3.2.3 Conclusion:

In conclusion, an LNA-SB-T-1214 conjugated was synthesized in high purity for further *in vitro* and *in vivo* evaluations. Recently, the LNA-SB-T-1214 has been evaluated *in vivo* again MX-1 breast cancer xenografts in animal models by Jean Rooney and Dr. Tom Zimmerman at the Division of Laboratory Animal Resources (DLAR) at Stony Brook University.[19] LNA-SB-T-1214 showed similar activity towards tumor reduction as DHA-SB-T-1214. Additionally, it was noted that LNA-SB-T-1214 was faster at reducing tumor mass.

§3.3 Experimental Section:

§3.3.1 Chemical Synthesis:

General Methods: ^{1}H NMR and ^{13}C NMR was measured on a Varian 300, 400, 500, or 600 MHz NMR spectrometer. Melting points were measured on a "Uni-melt" capillary melting point apparatus from Arthur H. Thomas Company, Inc. TLC analyses were performed on Merck DC-alufolien with Kieselgel 60F-254 and were visualized with UV light and stained with sulfuric acid-EtOH, 10 % PMA-EtOH or 10 % Vanillin-EtOH with 1% sulfuric acid. Column chromatography was carried out on silica gel 60 (Merck; 230-400 mesh ASTM). HPLC Purity of was determined by Shamazu HPLC employing a Phenomenex Proteo® column (CH3CN/H2O = 20/80 gradient to 95/5 over 45 min, flow rate at 1 mL/min, UV 254 nm).

Materials: The chemicals were purchased from Sigma-Aldrich Company, Fischer Company or VWR Company. 10-Deacetyl baccatin III (DAB) was donated by Indena, SpA, Italy. DCM and methanol were dried before use by distillation over calcium hydride under nitrogen. Ether and THF were dried before use by distillation over sodium-benzophenone kept under nitrogen. Dry DMF and DMSO were purchased from Sigma-Aldrich chemical company, and used without further purification. Reaction flasks were dried in a 100 ^{o}C oven and allowed to cool to room temperature in a desiccator over "*Drierite*" (calcium sulfate) and assembled under an inert nitrogen gas atmosphere.

tert-Butyl DHA-carbazate (3-1):[20]

To a 5 mL round bottomed flask added (94 mg, 029 mmol) of DHA and 1.5 mL of DCM. To this solution was added (77 mg, 0.40 mmol) of EDC while stirring and the solution was allowed to stir an additional 2 minutes at room temperature. Then to this stirring solution was added (53 mg, 0.40 mmol) of *tert*-butyl carbazate portion-wise and the resulting solution was stirred at room

temperature an additional 24 hours. After completion 3 mL of saturated ammonium chloride was added and the resulting solution was extracted with (3 x 10 mL) of DCM. The resulting combined organic layers were collected, dried with $MgSO_4$ and concentrated *in vacuo*. The crude oil obtained was purified via flash chromatography using 5 % to 20 % (Ethyl Acetate / Hexanes). After collecting and concentrating *in vacuo* the desired fractions, (70 mg, 0.16 mmol), 55 % isolated yield of the desired compound **(3-1)** was obtained as a sticky solid: ^{1}H NMR (500 MHz, $CDCl_3$) δ 0.96 (t, *J* = 8.0 Hz, 3 H), 1.46 (s, 9 H), 2.06 (p, *J* = 7.0 Hz, 2 H), 2.27 (t, *J* = 7.5 Hz, 2 H), 2.42 (p, *J* = 7.0 Hz, 2 H), 2.83 (m, 10 H), 5.28 – 5.43 (m, 12 H), 6.71 (b, 1 H), 7.79 (b, 1 H); ^{13}C NMR (126 MHz, $CDCl_3$) δ 14.44, 20.73, 23.13, 25.72, 25.77, 25.82, 28.32, 34.01, 81.99, 127.21, 127.98, 128.07, 128.22, 128.28, 128.44, 128.50, 128.75, 129.76, 155.88, 172.10. All data are in agreement with reported values.[20]

DHA-hydrazide (3-2):

To a 25 mL round bottomed flask added (30 mg, 0.06 mmol) of compound **(3-1)** and 0.68 mL of DCM. While stirring added 0.17 mL of TFA and stirred at room temperature for one hour to yield compound **3-2** as a crude brown oil that was used in the next reaction without further purification.

DHA-FITC (3-3):[21]

To a 10 mL round bottomed flask added the 0.06 mmol of crude compound **3-2** and 0.35 mL of DMSO. While stirring added (32 mg, 0.0814 mmol) of 6-FITC and continued an additional 24 hours at room temperature. After completion, the crude compound was subjected to direct column purification by flash chromatography using 4 % (methanol / DCM) to yield compound **3-3** in (20 mg, 0.03 mmol), 48 % isolated yield as an orange solid: ^{1}H NMR (500 MHz, $CDCl_3$) δ 0.86 (t, *J* = 7.2 Hz, 3 H), 1.18 (m, 3 H), 1.97 (p, *J* = 7.2 Hz, 2 H), 2.29 (t, *J* = 7.5 Hz, 2 H), 2.37 (q, *J* = 7.2 Hz, 2 H), 2.83 (m, 10 H), 5.16 – 5.25 (m, 9 H), 5.30 – 5.38 (m, 3 H), 6.43 (dd, *J* = 2.4 Hz, *J* = 8.4 Hz, 2 H), 6.55 – 6.58 (m, 4 H), 7.05 (d, *J* = 8.4 Hz, 1 H), 7.77 (dd, *J* = 1.8 Hz, *J* = 8.4 Hz, 1 H), 8.08 (s, 1 H); ^{13}C NMR (126 MHz, $CDCl_3$) δ 14.81, 21.65, 24.17, 26.59, 26.69, 26.71, 26.73, 30.87, 34.93, 103.70, 111.57, 113.76, 125.50, 128.34, 129.08, 129.26, 129.32, 129.37, 129.44, 129.61, 130.42, 130.59, 132.95, 142.32, 154.33, 161.49, 171.18, 175.20, 184.24. All values are in agreement with reported values.[21]

LNA-hydrazide (3-4):[20]

To a 5 mL round bottomed flask added (80 mg, 0.27 mmol) of methyl-linolenate and 1.6 mL of methanol. This solution was stirred and heated to 60 ^{o}C. Then while stirring added (0.04 mL, 1.15 mmol) of hydrazine monohydrate and stirred and additional 22 hours at 60 ^{o}C to give compound **(3-4)** (80 mg) which was concentrated *in vacuo* and subsequently used in the next step without purification: ^{1}H NMR (600 MHz, $CDCl_3$) δ 0.93 (t, *J* = 7.2 Hz, 3 H), 1.22 – 1.30 (m, 8 H), 1.59 (m, 2 H), 1.99 - 2.06 (m, 4 H), 2.11 (t, *J* = 7.2 Hz, 2 H), 2.76 (s, 4 H), 3.62 (s, 1 H), 3.81 (b, 2 H), 5.25 – 5.37 (m, 6 H), 7.42 (b, 1 H); ^{13}C NMR (126 MHz, $CDCl_3$) δ 14.14, 20.42, 25.40, 25.49, 27.07, 28.99, 29.01, 29.09, 29.13, 29.45, 34.40, 127.00, 127.64, 128.11, 128.17, 130.08, 130.12, 131.82, 173.98. All data are in agreement with reported values.[20]

LNA-FITC (3-5):

To a 5 mL round bottomed flask added 80 mg crude LNA-hydrazide **3-4** and (105 mg, 0.27 mmol) of 6-FITC (isomer 1) and then added 1 mL of DMSO and stirred overnight at room temperature. After completion the crude compound was subjected to direct column purification by flash chromatography using 2 % (methanol / DCM) to yield compound **3-5** in (46 mg, 0.07 mmol), 26 % isolated yield in two steps as an orange solid: ^{1}H NMR (600 MHz, $CDCl_3$) δ 0.96 (m, 3 H), 1.34 (m, 8 H), 1.59 – 1.69 (m, 2 H), 2.06 (m, 4 H), 2.24 (t, *J* = 7.8 Hz, 1 H), 2.33 (t, *J* = 7.8 Hz, 1 H), 2.80 (m, 4 H), 5.28 – 5.39 (m, 6 H), 6.53 (dd, *J* = 1.8 Hz, *J* = 9.0 Hz, 2 H), 6.63 – 6.68 (m, 4 H), 7.15 (d, *J* = 8.4 Hz, 1 H), 7.86 (dd, *J* = 1.8 Hz, *J* = 8.4 Hz, 1 H), 8.01 (d, *J* = 8.4 Hz, 1 H), 8.18 (s, 1 H); ^{13}C NMR (126 MHz, $CDCl_3$) δ 14.81, 21.63, 26.38, 26.44, 26.55, 26.66, 28.32, 30.39, 30.50, 30.86, 34.97, 35.05, 103.70, 111.58, 113.79, 125.50, 128.38, 129.00, 129.35, 130.42, 131.02, 131.23, 132.88, 142.36, 154.33, 161.56, 171.21, 176.02, 184.30. HRMS (ESI) *m/e* calcd for $C_{39}H_{44}N_3O_6SH^+$:682.2951. Found: 682.2950 (Δ = 0.1 ppm)

LNA-SB-T-1214 (3-6):

To a 5 mL round bottomed flask added (250 mg, 0.29 mmol) SB-T-1214 and (81 mg, 0.29 mmol) of LNA and 1.5 mL of DCM. While stirring added (9 mg, 0.07 mmol) of DMAP and cooled this solution to 0 ^{o}C. While stirring added (0.03 mL, 0.32 mmol) of DIC and allowed to stir an additional 1.5 hours. After completion the crude compound was subjected to direct column purification by flash chromatography using 30 % (ethyl acetate / hexanes) to yield compound **3-6**

in (220 mg, 0.20 mmol), 69 % isolated yield as a white solid: ^{1}H NMR (400 MHz, $CDCl_3$) δ 0.94 – 1.03 (m, 5 H), 1.08 – 1.14 (m, 5 H), 1.19 (d, *J* = 5.6 Hz, 1 H), 1.25 (s, 3 H), 1.26 – 1.38 (m, 17 H), 1.60 – 1.68 (m, 7 H), 1.73 – 1.80 (m, 7 H), 1.92 (s, 3 H), 2.03 – 2.11 (m, 4 H), 2.37 (m, 4 H), 2.45 (td, *J* = 3.2 Hz, *J* = 11.6 Hz, 2 H), 2.52 (m, 1 H), 2.62 (d, *J* = 4.0 Hz, 1 H), 2.80 (t, *J* = 6.4 Hz, 4 H), 3.81 (d, *J* = 6.8 Hz, 1 H), 4.18 (d, *J* = 8.8 Hz, 1 H), 4.30 (d, *J* = 8.4 Hz, 1 H), 4.43 (m, 1 H), 4.77 (d, *J* = 8.8 Hz, 1 H), 4.92 – 4.98 (m, 2 H), 5.18 (d, *J* = 8.4 Hz, 1 H), 5.30 – 5.41 (m, 6 H), 5.67 (d, *J* = 6.8 Hz, 1 H), 6.18 (t, *J* = 8.8 Hz, 1 H), 6.30 (s, 1 H), 7.47 (t, *J* = 8.0 Hz, 2 H), 7.60 (t, *J* = 7.6 Hz, 1 H), 8.11 (d, *J* = 7.2 Hz, 2 H); ^{13}C NMR (100 MHz, $CDCl_3$) δ 9.33, 9.54, 9.75, 13.20, 14.47, 14.98, 18.72, 20.76, 22.45, 22.60, 24.95, 25.51, 25.74, 25.83, 26.90, 28.41, 29.24, 29.31, 29.38, 29.80, 33.98, 35.65, 43.39, 45.82, 49.15, 58.69, 71.90, 72.27, 72.36, 74.60, 75.46, 75.67, 76.62, 79.40, 79.51, 80.09, 81.21, 84.72, 120.24, 127.32, 127.99, 128.44, 128.52, 128.84, 129.52, 130.38, 130.42, 132.18, 132.70, 133.81, 138.14, 143.71, 155.11, 167.22, 168.61, 169.87, 173.17, 175.34, 204.32; HRMS (ESI) *m/e* calcd for $C_{63}H_{88}NO_{16}H^{+}$: 1114.6103. Found: 1114.6116 (Δ = 1.2 ppm)

§3.3.2 FACS and CFM Protocols:

Cell culture: The A2780, MCF-7, HT-29, DLD-1, WI-38 and HS27 cell lines were obtained from Dr. Rebecca A. Rowehl at the cell culture center at Stony Brook University. HT-29 cells were incubated in DMEM media with 5 % fetal bovine serum (FBS) 5 % NuSerum and 1 % Penicillin/Streptomycin. A2780, MCF-7, DLD-1, WI-38 and HS27 cells lines were incubated in RPMI media with 5 % fetal bovine serum (FBS) 5 % NuSerum and 1 % Penicillin /Streptomycin. Prior to incubation, the cells were collected by centrifugation at 1000 rpm for 5 min and resuspended in medium at a cell density of 10 × 10 cells / mL.

Incubation of DHA-FITC (3-3) / LNA-FITC (3-5) probes:

The cells were harvested, collected, and resuspended in 500 μL of the appropriate media at a concentration of 100 x 10_4 cells per well in 6-well plates. For the adhesive cell type, the cells were allowed to reseed to the bottom of the plates overnight and upon about 80 % confluence was added DHA-FITC (3-3) / LNA-FITC (3-5) probes to make a final concentration of probe (1 uM). The 6-well plate was incubated for 3 hours at 37 ^{o}C and then aspirated and washed 2 times with 1000 uL of PBS.

Incubation of DHA-SB-T-1214-Fluoroscein and LNA-SB-T-1214-Fluoroscein probes:

The cells were harvested, collected, and resuspended in 500 μL of the appropriate media at a concentration of 100 x 10_4 cells per well in 6-well plates. For the adhesive cell type, the cells were allowed to reseed to the bottom of the plates overnight and upon about 80 % confluence was added DHA-SB-T-1214-Fluoroscein and LNA-SB-T-1214-Fluoroscein probes to make a final concentration of probe (10 uM). The 6-well plate was incubated for 3 hours at 37 ^{o}C and then aspirated and washed 2 times with 1000 uL of PBS.

Flow cytometry fluorescent measurements of the cells:

Flow cytometry analysis was performed immediately after the incubation and washing steps. Cells were resuspended in 1.0 mL of PBS and analyzed using a flow cytometer, FACSCalibur, operating at a 488 nm excitation wavelength and detecting emission wavelengths with a 530/30 nm bandpass filter. At least 10,000 cells were counted for each experiment using CellQuest 3.3 software (Becton Dickinson) and the distribution of FITC fluorescence was analyzed using WinMDI 2.8 freeware (Joseph Trotter, Scripps Research Institute).

Confocal microscopy imaging of the cells:

All of the confocal images were taken immediately after the incubation and washing steps. 100 uL of the cell suspension was transferred to the bottom-glass dish using a micropipette. Confocal fluorescence microscopy (CFM) was performed using a Zeiss LSM 510 META NLO two-photon laser scanning confocal microscope system, operating at a 488 nm excitation wavelength and detecting emission wavelengths using a 505-550 nm bandpass filter. Images were captured with a C-Apochromat 63×/1.2 Water (corr.) objective and a Plan-Apochromat 100×/1.45 oil objective. Data were analyzed using LSM 510 META software.

§3.4 References:

1. Holman, R. T., The Slow Discovery of the Importance of omega-3 Essential Fatty Acids in Human Health. *Nutr.* **1998,** *128*, 427S - 433S.
2. Sauer, L. A.; Dauchy, R. T.; Blask, D. E., Mechanism for the antitumor and anticachectic effects of omega-3 faty acids. *Cancer Res.* **2000,** *60*, 5289 - 5295.
3. Wigmore, S. J.; Ross, J. A.; Falconer, J. S.; Plester, C. E.; Tisdale, M. J.; Carter, D. C.; Fearon, K. C., The effect of polyunsaturated fatty acids on the progress of cachexia in patients with pancreatic cancer. *Nutrition* **1996,** *12*, S27 - S30.

4. Hawkins, R. A.; Sangster, K.; Arends, M. J., Apoptotic death of pancreatic cancer cells induced by polyunsaturated fatty acids varies with double bond number and involves an oxidative mechanism. *J. Pathol.* **1998,** *185*, 61 - 70.
5. Grammatikos, S. I.; Subbaiah, P. V.; Victor, T. A.; Miller, W. M., omega-3 and omega-6 fatty acid processing and growth effects in neoplastic and noncancerous human mammary epithelial cell lines. *Br. J. Cancer* **1994,** *70*, 219 - 227.
6. Diomede, I.; Colotta, F.; Piovani, B.; Re, F.; Modest, E. J.; Salmona, M., Induction of apoptosis in human leukemic cells by the ether lipid 1-octadecyl-2-methyl-racglycero-3-phosphocholine. A possible basis for its selective action. *Int. J. Cancer Res.* **1993,** *53*, 124 - 130.
7. Bradley, M. O.; Webb, N. L.; Anthony, F. H.; Devanesan, P.; Witman, P. A.; Hemamalini, W. S.; Chander, M. C.; Baker, S. D.; He, L.; Horwitz, S. B.; Swindell, C. S., Tumor Targeting by Covalent Conjugation of a Natural Fatty Acid to Paclitaxel. *Clin. Cancer. Res.* **2001,** *7*, 3229 - 3238.
8. Sparreboom, A.; Wolff, A. C.; Verweij, J.; Zabelina, Y.; van Zomeren, D. M.; McIntire, G. L.; Swindell, C. S.; Donehower, R. C.; Baker, S. D., Disposition of docosahexaenoic acid-paclitaxel, a novel taxane, in blood: in vitro and clinical pharmacokinetic studies. *Clin. Cancer. Res.* **2003,** *9*, 151 - 159.
9. Ibrahim, N. K.; Desai, N.; Legha, S.; Soon-Shiong, P.; Theriault, R. L.; Rivera, E.; Esmaeli, B.; Ring, S. E.; Bedikian, A.; Hortobagyi, G. N.; Ellerhorst, J. A., Phase I and Pharmacokinetic Study of ABI-007, a Cremophor-free, Protein-stabilized, Nanoparticle Formulation of Paclitaxel. *Clin. Cancer. Res.* **2002,** *8*, 1038 - 1044.
10. Desai, N.; Trieu, V.; Yao, Z.; Louie, L.; Ci, S.; Yang, A.; Tao, C.; De, T.; Beals, B.; Dykes, D.; Noker, P.; Yao, R.; Labao, E.; Hawkins, M.; Soon-Shiong, P., Increased antitumor activity, intratumor paclitaxel concentrations, and endothelial cell transport of cremophor-free, albumin-bound paclitaxel, ABI-007, compared with cremophor-based pacllitaxel. *Clin. Cancer. Res.* **2006,** *12*, 1317 - 1324.
11. Seitz, J. D.; Ojima, I., Drug conjugates with polyunsaturated fatty acids. In *Drug Delivery in Oncology: From Basic Research to Cancer Therapy*, Kratz, F.; Senter, P.; Steinhagen, H., Eds. Wiley-VCH, Weinheim, Germany: Drug Delivery in Oncology: From Basic Research to Cancer Therapy, **2011**; pp 1323 - 1360.
12. Rose, D. P.; Connolly, J. M., Omega-3 fatty acids as cancer chemopreventitive agents. *Pharmacol. Ther.* **1999,** *83*, 217 - 244.
13. Guegan, C.; Vila, M.; Rosoklija, G.; Hays, A. P.; Przedborski, S., Recruitment of the Mitochondrial-Dependent Apoptotic Pathway in Amyotrophic Lateral Sclerosis. *J. Neurosci.* **2001,** *21*, 6569 - 6576.
14. Whelan, J., Targeted taxane therapy for cancer. *Drug. Discov. Today* **2002,** *7*, 90 - 92.
15. Ojima, I.; Slater, J. C.; Michaud, E.; Kuduk, S. D.; Bounaud, P. Y.; Vrignaud, P.; Bissery, M. C.; Veith, J. M.; Pera, P.; Bernacki, R. J., Syntheses and structure-activity relationships

of the second-generation antitumor taxoids: exceptional activity against drug-resistant cancer cells. *J. Med. Chem.* **1996,** *39*, 3889 - 3896.

16. Ojima, I.; Slater, J. C.; Kuduk, S. D.; Takeuchi, C. S.; Gimi, R. H.; Sun, C. M.; Park, Y. H.; Pera, P.; Veith, J. M.; Bernacki, R. J., Syntheses and structure-activity relationships of taxoids derived from 14 beta-hydroxy-10-deacetylbaccatin III. *J. Med. Chem.* **1997,** *40*, 267 - 278.
17. Ojima, I.; Chen, J.; Sun, L.; Borella, C. P.; Wang, T.; Miller, M. L.; Lin, S.; Geng, X.; Kuznetsova, L.; Qu, C.; Gallager, D.; Zhao, X.; Zanardi, I.; Xia, S.; Horwitz, S. B.; Mallen-St. Clair, J.; Guerriero, J. L.; Bar-Sagi, D.; Veith, J. M.; Pera, P.; Bernacki, R. J., Design, Synthesis, and Biological Evaluation of New-Generation Taxoids. *J. Med. Chem.* **2008,** *51*, 3203 - 3221.
18. Kuznetsova, L.; Chen, J.; Sun, L.; Wu, X.; Pepe, A.; Veith, J. M.; Pera, P.; Bernacki, R. J.; Ojima, I., Syntheses and evaluation of novel fatty acid-second-generation taxoid conjugates as promising anticancer agents. *Bio. Org. Med. Chem. Letters* **2006,** *16*, 974 - 977.
19. Seitz, J. D. Ph.D. Dissertation: The design, synthesis and biological evaluation of novel taxoid anticancer agents and their tumor-targeted drug conjugates. Stony Brook University, **2013**.
20. Breyer, S.; Effenberger, K.; Schobert, R., Effects of Thymoquinone-Fatty Acid Conjugates on Cancer Cells. *ChemMedChem* **2009,** *4*, 761 - 768.
21. Chen, J., Ph.D. Dissertation., Stony Brook University, **2006**.

Chapter 4

Development of DARPin Based SB-T-1214 Conjugates

Content

§4.0 Introduction:

§4.0.1 DARPins and the Development of Taxoid-DARPin Conjugates:

Designed Ankyrin Repeat Proteins (DARPins) are small nonimmunoglobulin binding proteins specific to the modularity of their ankyrins units as seen in **Figure 4-1**.[1-4] By advantageous design, DARPins are highly soluble facilitating high yield-expression in *Escherichia coli* (*E.coli*) allowing engineering procedures less tolerated by antibodies. In particular, cysteine residues which are nonnative to DARPins can be incorporated through molecular cloning and provide excellent molecular handles for specific chemical modifications.[5] Thus, DARPins provide a new and novel platform by which a new class of targeted conjugate therapies can be explored.[6]

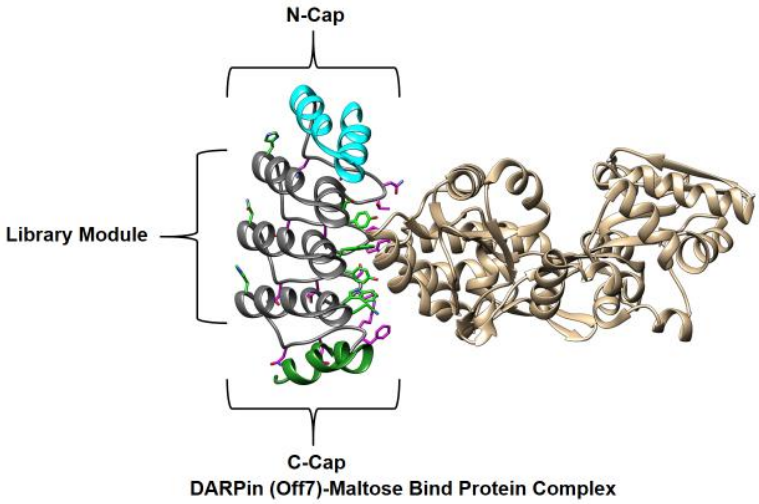

Figure 4-1: The DARPin Off7 bound to its molecular target MBP (PDB 1SVX, 2.24 Å). DARPins are composed of two terminal caps, an N-Cap (cyan) and C-Cap (dark green), and a varying number of Library Modules (grey). Characteristic of the Library Modules are repeats of 33 amino acids (Off7: 21 alpha helix, 12 loop) which contain 7 variable amino acid sequence locations, 3 alpha helix (green) and 4 loop (magenta). (Adapted with permission from reference [1])

In the past decade, immunoconjugates have progressively become common as cancer therapies; both directly influencing cell regulation and also as carriers of cytotoxic payloads.[7, 8] In particular, Ojima et al. have provided taxoid-antibody immunoconjugates showing remarkable target-specific antitumor activity in vivo.[9] Advantageous to the use of antibodies in targeting therapies, immunoconjugates uniquely provide high specificity and long serum half-lives. Nevertheless, the larger size of antibodies restricts their ability to move through solid tumor mass. Furthermore, despite an increase in permeability and retention (EPR), higher interstitial pressure and lower migration from capillaries into the solid tumors substantially reduces the penetration of these macromolecular structures.[10-12]

DARPins provide an alternative approach to targeted antibody chemotherapy; providing antibody like specificity without the structural and immunological restrains. Structurally, DARPins are 1/10th the size of an antibody and 1/3rd the size of an fab fragment (around 18 kDa) and have no adverse immunological effects.[2, 13] Additionally, DARPins are stable at physiological temperatures having a robust serum half-life of 60 days. In vivo, circulation studies have shown that unlike antibodies, DARPins generally have short circulation half-lives (<3 minutes).[13] Nevertheless, DARPins have shown remarkable tumor to blood ratios in mice 48 hours after injection (12.67 ± 3.34 % injection dose per gram of tissue (ID/g) in 1 hour, 71.78 ± 26.62 % ID/g in 48 hours).

In 2009, Winkler et al. developed and reported first Epithelial cell adhesion molecule (EpCAM) specific DARPin-conjugate that was shown to successful deliver small interfering RNA (siRNA) complementary to mRNA encoding for Bcl-2.[14] Previous interest in EpCAM specific targeting in the Plückthun laboratory had started in 2006 following the delivery cytotoxic-payloads via an EpCAM specific humanized single-chain Fv antibody fragment 4D5MOCB.[15] Following these designs, Martin-Killias et al. in 2011 showed the successful delivery of fused EpCAM specific DARPin-*Pseudomonas aeruginosa* exotoxin A (Ec4-ETA") with high specificity and antitumor activity in vivo.[16] Internalization of Ec4 was verified by CFM, providing conclusive evidence that the DARPin Ec4 entered the cell by means of receptor-mediated endocytosis.

The EpCAM receptor-complex is responsible for modulating E-cadherin and has ties to cell aggression and growth. Furthermore, EpCAM receptors are over-expressed in numerous cancer tissues.[17] As seen in **Table 4-1**, over 85 % of colon, gastric, prostrate and ovarian cancer tissues have been found to express high levels of EpCAM receptors. Additionally, the levels of EpCAM receptors expressed in breast cancers have been found to be highly correlated with overall patient survival rates as shown in **Figure 4-2**.[18] Interestingly, studies have shown that cells that are EpCAM^{+} often display cancer stem cell (CSC)-like properties, which is often associated with regression.[19-21]

Table 4-1: Relative levels of EpCAM receptors expressed in isolated tissue samples[17]				
Tissue Type	Quant.	Neg. (%)	Mod. (%)	High (%)
Breast	1715	10.0	48.0	42.0
Prostrate	414	1.9	10.9	87.2
Colon	1186	0.3	1.9	97.7
Gastric	473	2.5	6.8	90.7
Lung	1287	13.5	22.5	63.9
Ovarian	272	2.6	12.1	85.3

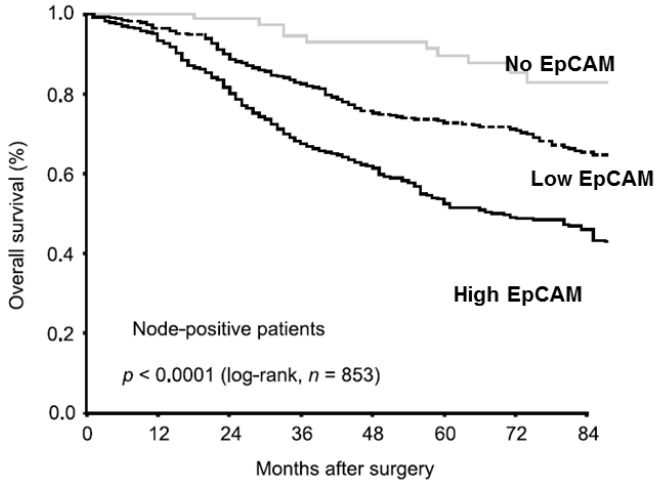

Figure 4-2: Kaplan-Meier analysis of 853 node-positive breast cancer patients after surgery level of EpCAM receptor expression versus overall survival. Specifically expression levels of EpCAM (No EpCAM n = 75, Low EpCAM n = 395, High EpCAM n = 383) are highly correlated to overall survival. (Reprinted with permission from reference [18])

In addition to being highly over-expressed in several cancers types, EpCAM also serves important functionality within non-cancerous cells as seen in **Figure 4-3**.[22] Typically, EpCAM receptors are localized within the intracellular junctions and thus are insulated within the cellular matrix. In tumor tissues however, receptors play an intricate role in cell proliferation; modulating E-cadherin, a major component of the cellular matrix.

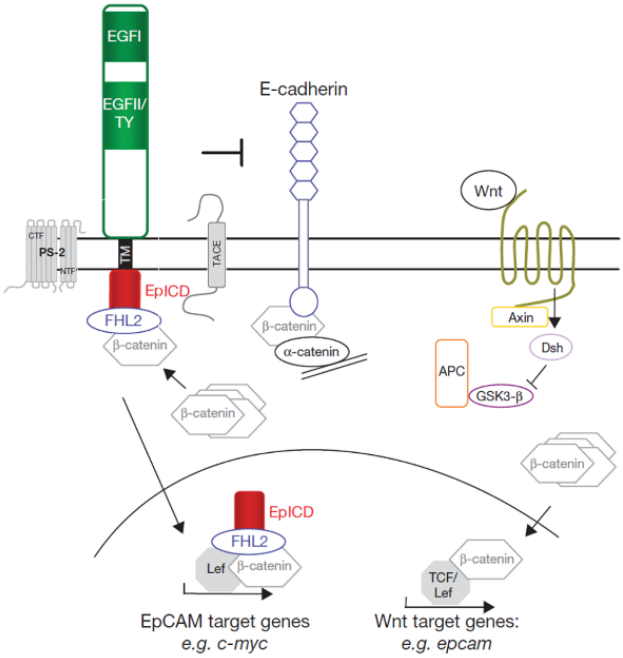

Figure 4-3: Cell signaling in the EpCAM pathway. Binding to EpCAM leads to cleavage of the extracellular domain (EpEX) and intracellular domain (EpICD) through regulated intramembrane proteolysis (RIP) via tumor-necrosis-factor alpha converting enzyme (TACE) and gamma-secretase complex containing presenilin 2 (PS2). Release of the EpICD complex from the membrane is accomplished with associated four and one-half LIM domains protein 2 (FHL2) and β-catenin which interacts with lymphoid enhancer-binding factor 1 (LEF-1) and contacts the DNA. Increasing the interaction of β-catenin with the EpICD complex leads to interference with E-cadherin. Additionally, cross talk with the Wnt pathway is accomplished at the level of the EpICD by influencing its interactions of β-catenin and LEF-1 and is known for the induction of the promoter *epcam* by Tcf4. Upregulation of Cyclins and *c-myc* are responsible for cancer aggressiveness. (Reprinted with permission from reference [22])

Despite the expression of EpCAM receptors in both cancerous and non-cancerous cells alike, EpCAM still remains a highly attractive targeted for its highly selective tumor-targeted delivery. This is primarily due to expression levels, localization, and accessibility of these receptors on the cancer cell surface. Unlike in normal cell morphology, cancer cells overexpressing EpCAM typically degrade their cellular matrix. Furthermore, signaling through the Wnt pathway by EpCAM leads to up-regulation of transcription factors such as *c-myc* leading to cell proliferation. Ultimately, cancerous cells up-regulate and expose their EpCAM receptors in order to stimulate growth and mobility, and as a consequence, provide excellent molecular targets for tumor-targeted chemotherapeutics.[23] In particular, the delivery of SB-T-1214 into $EpCAM^{+}$ cells may be beneficial as SB-T-1214 has shown a specific propensity to down regulate stem cell-related genes.[24] Thus, the conjugation of a DARPin targeting EpCAM to a highly potent

and multi-drug resistant "new-generation" taxoid such as SB-T-1214, provides a very promising approaching to targeted chemotherapy.

§4.1 Design, Synthesis and Biological Evaluation of an Ec4-disulfide-SB-T-1214 Conjugate:

§4.1.1 Introduction:

The general strategy developed at the onset of the collaboration between the Ojima laboratory and the Plückthun laboratory was for the delivery of "second-generation" taxoid via a "smart linker" and designed ankyrin repeat protein (DARPin) by means of: 1) incorporation of a cysteine at the C-terminus of an EpCAM specific DARPin Ec4; 2) modification of the existing "couple-ready" SB-T-1214 construct to incorporate a maleimide for bioconjugation; 3) to find suitable conditions to couple both drug construct and the DARPin together as seen in **Scheme 4-1**.

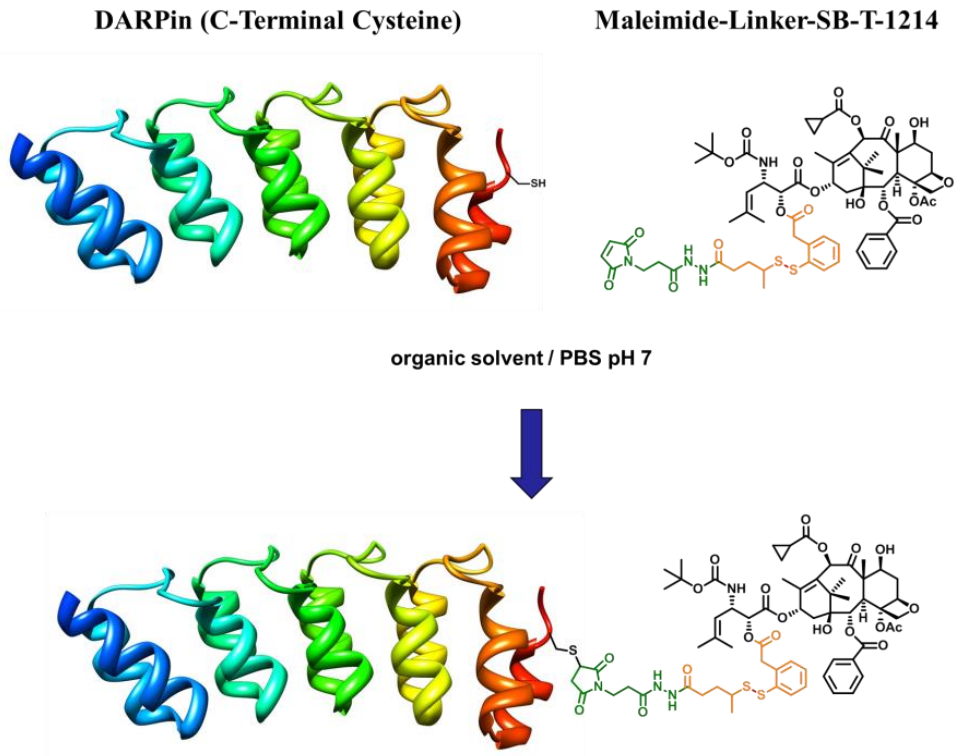

Scheme 4-1: Strategy for the synthesis of DARPin-taxoid conjugates. First obtain a DARPin with a free cysteine strategically placed at the C-terminus. Synthetic incorporation of a maleimide group into the SB-T-1214-(5C)-linker construct. Bioconjugation of the SB-T-1214-(5C)-linker-maleimide construct to the DARPin.

§4.1.2 Results and Discussion:
§4.1.2.1 Initial Experiments Towards DARPin Conjugate Synthesis:

The first criteria were met by graduate student Manuel Simon in Professor Plückthun's laboratory at the University of Zurich, and the resulting DARPins were shipped on dry ice to Stony Brook University. Incorporation of the terminal cysteine was performed on several DARPin constructs including Ec4, Off7, Ac2, 3E_5. These proteins were then designated with the addition of the letter "c" (e.g., Ec4c, Off7c …) as seen in **Table 4-2**.

Table 4-2: Mass and concentrations of various DARPin C-terminal cysteine constructs sent from the Plückthun laboratory.

DARPin	m/z (Zürich)	Conc (mM) (PBS)
Ec4c	18674.2	0.835
Ac2c	18773.5	0.580
Off7c	18501.4	0.700
E3_5c	18285.7	0.675

While awaiting the shipment of DARPins, synthesis of the SB-T-1214-(5C-disulfide-linker)-maleimide construct was performed shown in **Scheme 4-2**. 3-maleimide-propanoic-hydrazide-trifluoroacetic acid salt (1.2 equivalents) commercially purchased (Thermo Fisher) was coupled to the activated acid of compound **2-12 (Chapter 2)** in the presence of DIPEA base (1.0 equivalents). After 72 hours and column chromatography 62 % isolated yield of compound **4-1** was obtained. The HPLC purity was 94 %.

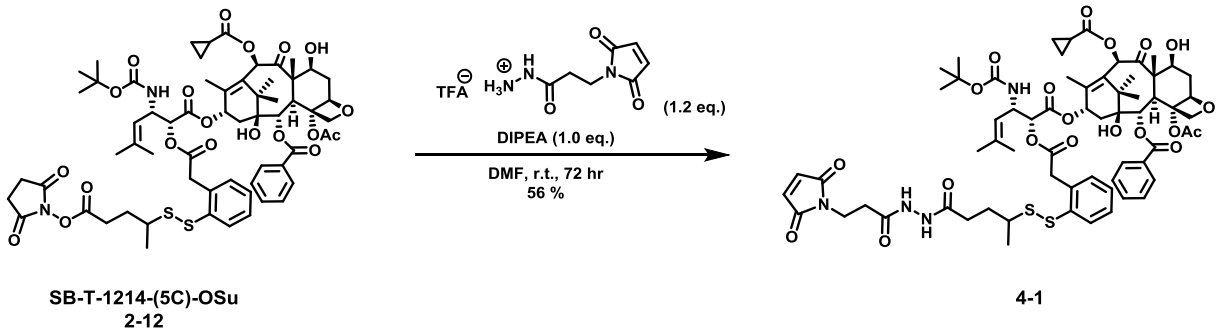

Scheme 4-2: Synthesis of the SB-T-1214-disulfide-maleimide construct

After obtaining the desired SB-T-1214-(5C-disulfide-linker)-maleimide construct **4-1**, coupling to the DARPin (Ec4c) was attempted as shown in **Scheme 4-3**. To 0.0835 µmol of Ec4c in PBS pH 7 was added 1.5 equivalents of SB-T-1214-(5C-disulfide-linker)-maleimide construct **4-1** and the resulting solution was stirred overnight at room temperature and analyzed by MALDI,

shown in **Figure 4-4**. Analysis of the MALDI spectrum revealed that the reaction did proceed but with low yield, with a peak at 19984.6. A majority of the protein had dimerized at the terminal cysteine and thus it was discovered that reduction prior to coupling was required.

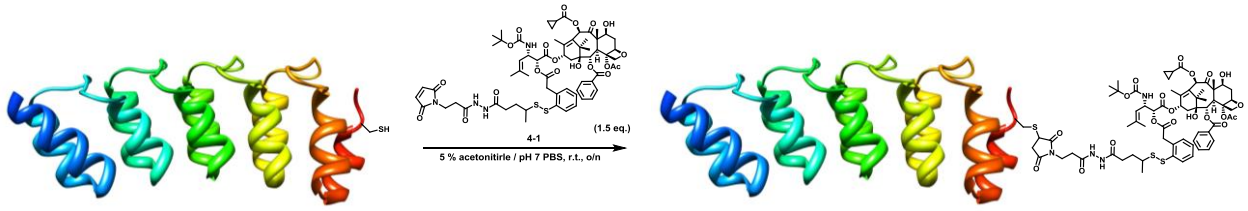

Ec4c **4-2**

Scheme 4-3: Conjugation of the SB-T-1214-disulfide-maleimide construct to DARPin Ec4c

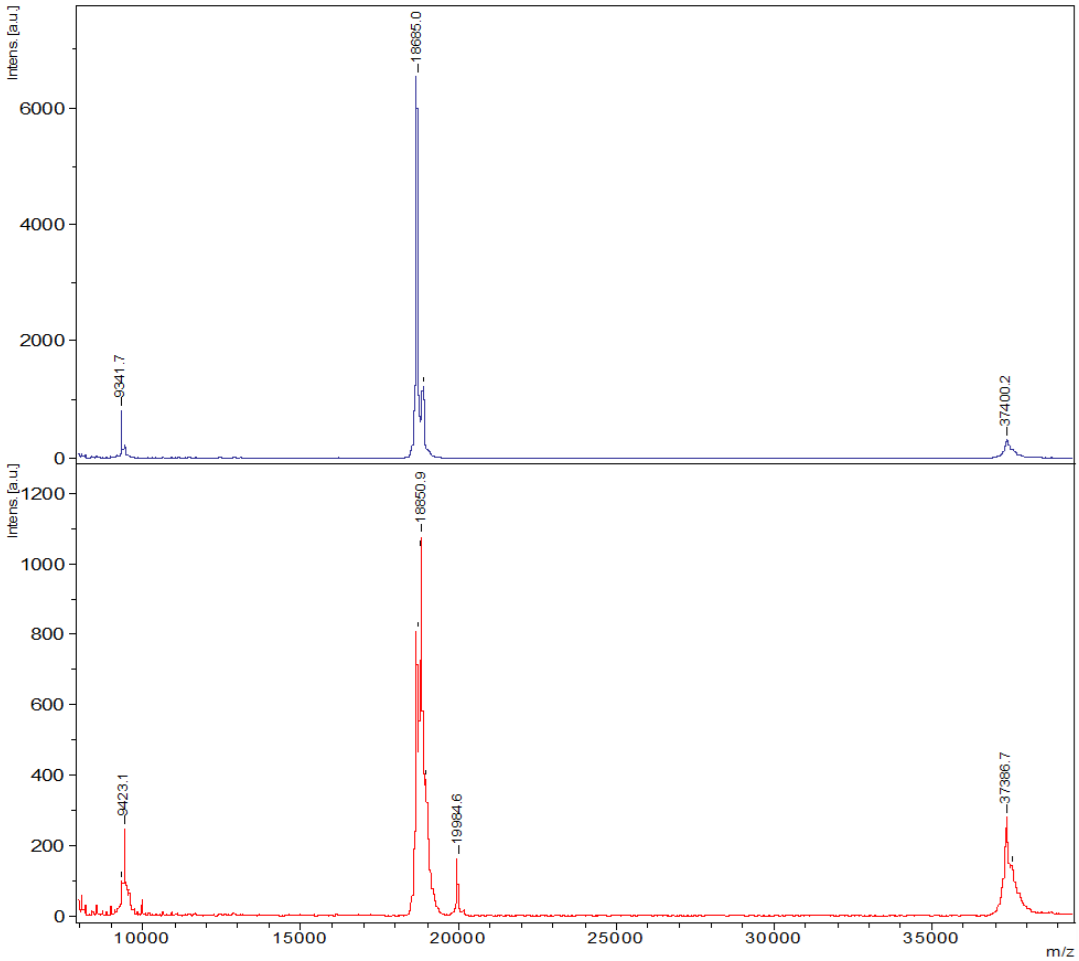

Figure 4-4: MALDI mass result of DARPin maleimide conjugation. The reaction did not progress to completion but some of the conjugate was formed with a mass of 19984.6. The top spectrum is of the Ec4c (before) and the bottom spectrum is of the reaction mixture (after).

§4.1.2.2 Optimization of Maleimide-DARPin Coupling:

Evident from the MALDI, covalent dimers of the cysteine appeared to be impairing the maleimide coupling. Thus, a protocol for reducing the disulfide formation using tris(2-carboxyethyl)phosphine (TCEP) was employed shown in **Scheme 4-4**. After the reduction, protein could be purified from the TCEP by use of a 3 kDa MWCO filter.

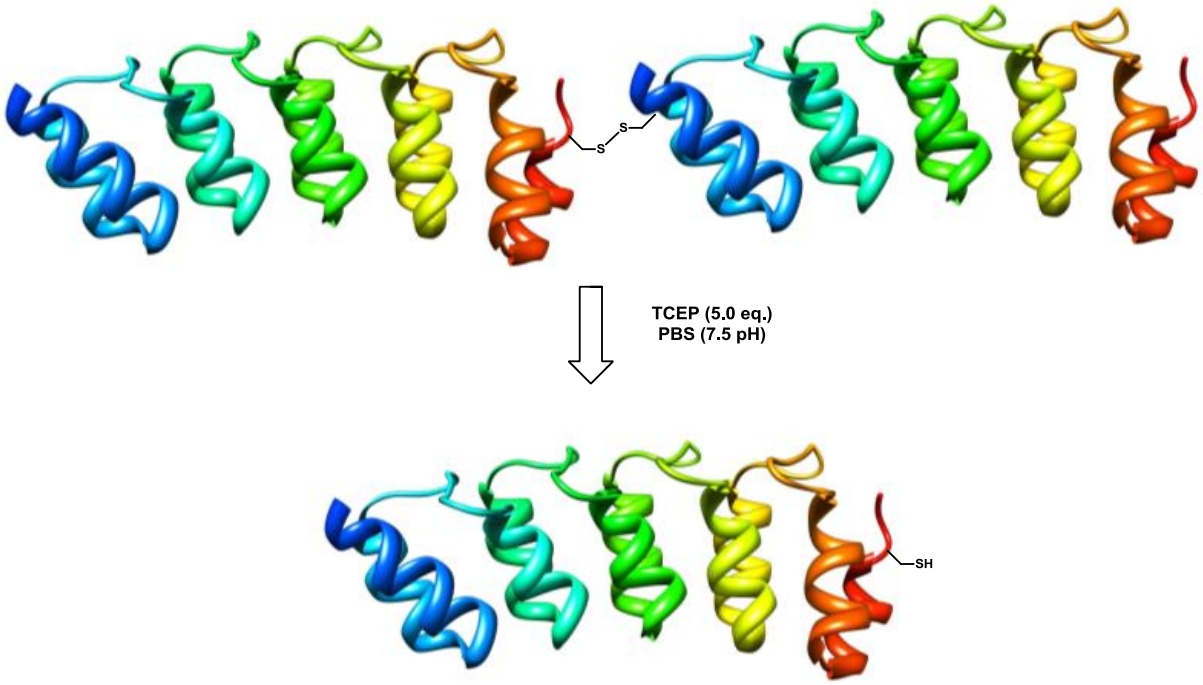

Scheme 4-4: Reduction protocol for DARPins prior to conjugation

After reduction, further optimization to the coupling was made by modification to the coupling solvent system. Previous experiments in the Plückthun laboratory have shown that DARPins show great structural stability. Based on this observation, a 30 % ethanol/PBS solvent system was chosen to be more accommodating to the hydrophobic nature of the SB-T-1214-maleimide construct as seen in **Scheme 4-5**. As a result of this modification, complete conversion of free protein to conjugate resulted in a single molecular entity in MALDI. The MALDI showed clearly that the conjugate **4-2** was form [M+1] = 19975.7 plus [M+2] = 9979.8 shown in **Figure 4-5**. The peak at 18940.2 was believe to be a result of cleavage of the disulfide bond rather than free protein. Thus, the coupling in 30 % ethanol/PBS after disulfide reduction in TCEP proceeded

to completion. To note, precipitation was seen during the reaction and the resulting lyophilized powder (~20 mg) was purified by reverse phase HPLC.

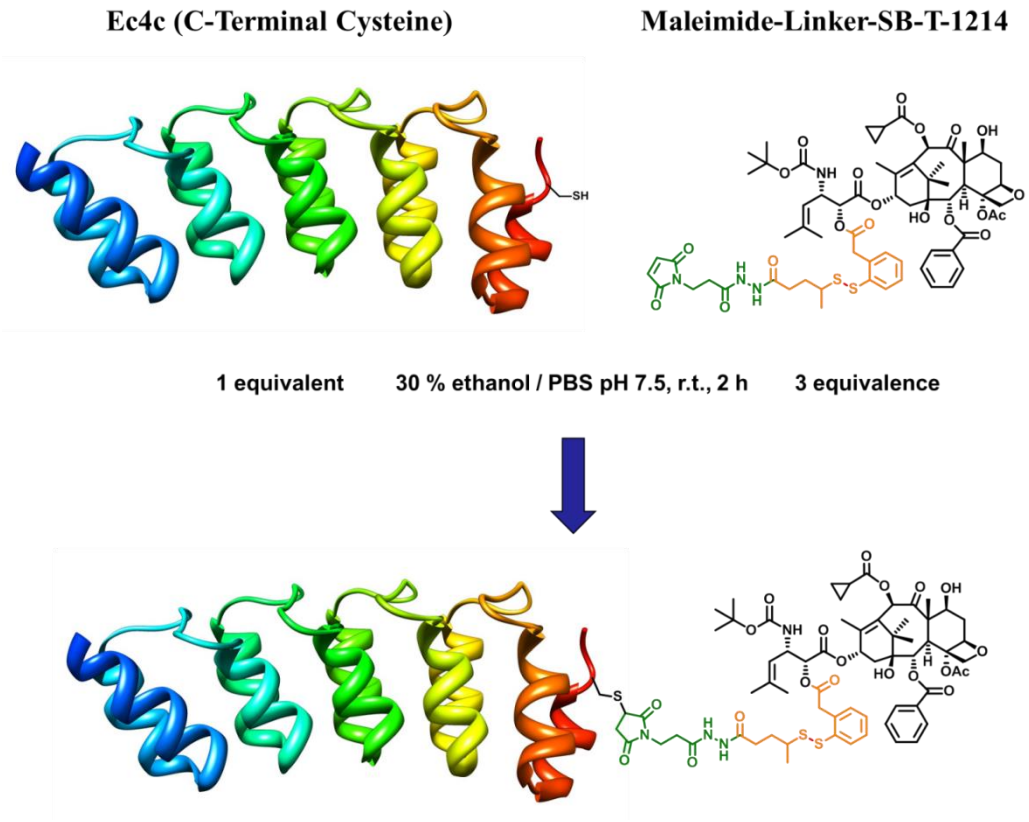

Scheme 4-5: Revised coupling conditions SB-T-1214-disulfide-maleimide to DARPin Ec4c in 30% ethanol

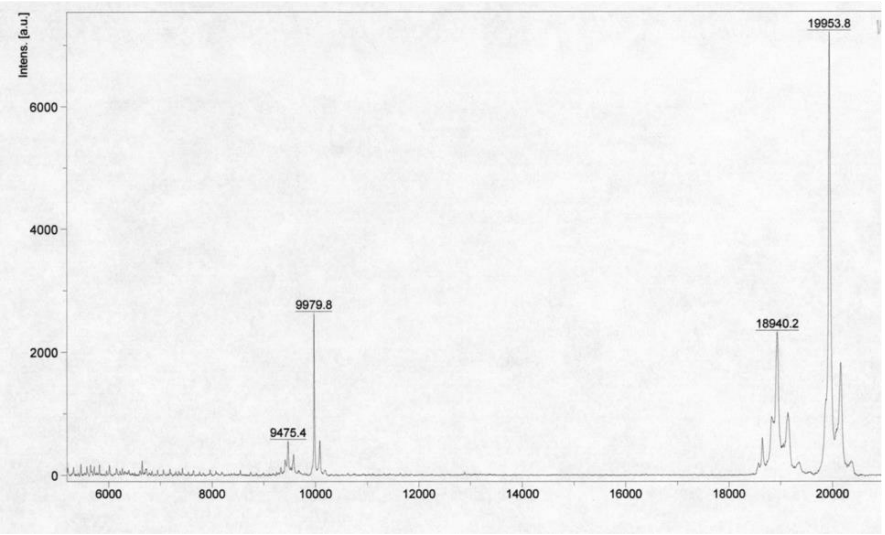

Figure 4-5: MALDI results of the Ec4-disulfide-SB-T-1214 conjugate **4-2**

§4.1.2.3 Biological Evaluation of the Ec4-disulfide-SB-T-1214 Conjugate:

To evaluate the synthesized conjugate for selectivity and cytotoxicity, some of the SB-T-1214-disulfide-maleimide construct was sent to Manuel Simon in the Plückthun laboratory while biological testing started at Stony Brook. Using the construct sent, Manuel reproduced the experiment to couple the SB-T-1214-maleimide construct to Ec4c and Off7c and then evaluated these conjugates using several biochemical techniques.

To verify that the conjugate was formed, characterization by SDS-PAGE and MALDI were performed by Manuel in Pluckthuns laboratory. First, an SDS-PAGE gel analysis in reducing and non-reducing conditions to highlight the formation and cleavage of the conjugate at the disulfide bond as seen in **Figure 4-6**. The gel clearly showed that Ec4c was nearly all converted to conjugate during the maleimide-cysteine reaction. Further verification of the mass by MALDI was conducted and gave the corresponding mass of 19979.9 which was consistent with the conjugate **4-2** shown in **Figure 4-7**.

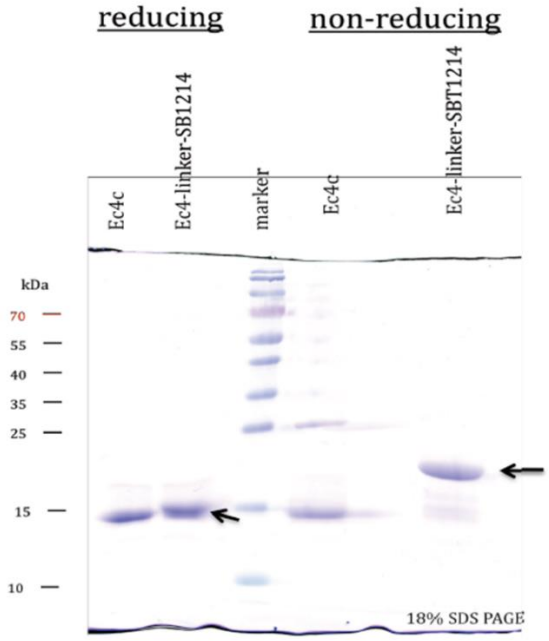

Figure 4-6: 18 % SDS-PAGE gel of the SB-T-1214-Ec4c conjugate linker release study.

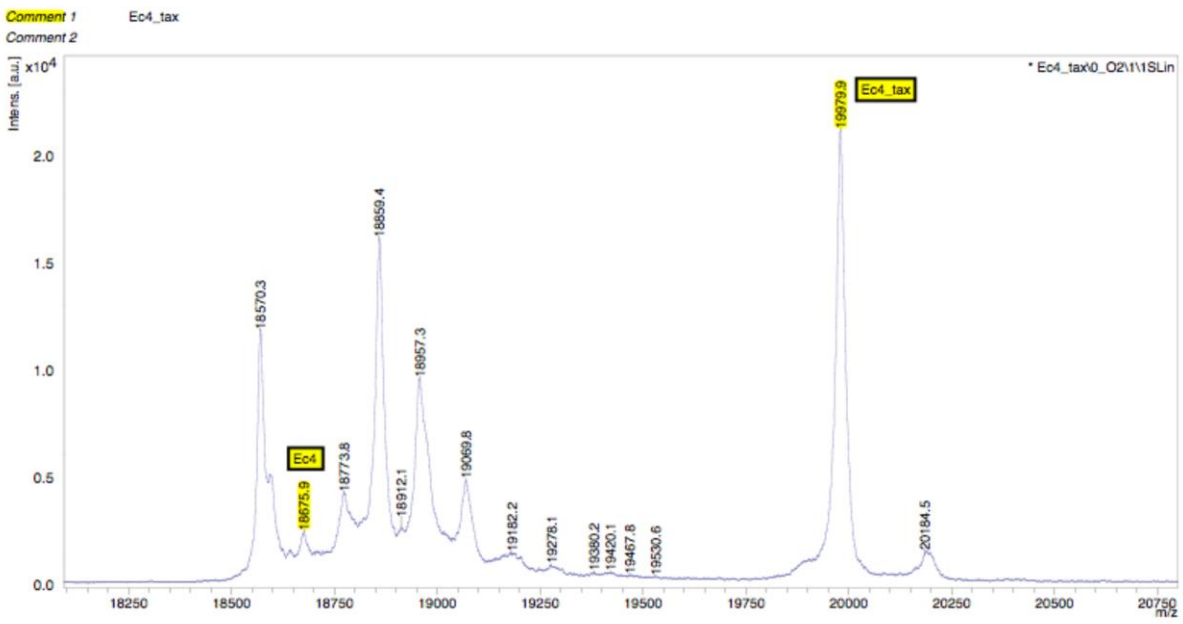

Figure 4-7. MALDI results of the Ec4-disulfide-SB-T-1214 conjugate created in the Plückthun laboratory

To show that the conjugate could bind its molecular target, a phage enzyme-linked immunosorbent assay (ELISA) was performed shown in **Figure 4-8**. The results from the ELISA showed clearly that the DARPin-SB-T-1214 conjugates (off7-disulfide-SB-T-1214 and Ec4-disulfide-SB-T-1214) could bind their respective molecular target with similar affinity as unmodified DARPin's. In addition, these respective SB-T-1214-disulfide-DARPin conjugates were run against non-specific targets and showed no binding. Thus, the ELISA assay gave definitive proof that DARPin-disulfide-SB-T-1214 conjugates did indeed specifically bind their respective molecular targets.

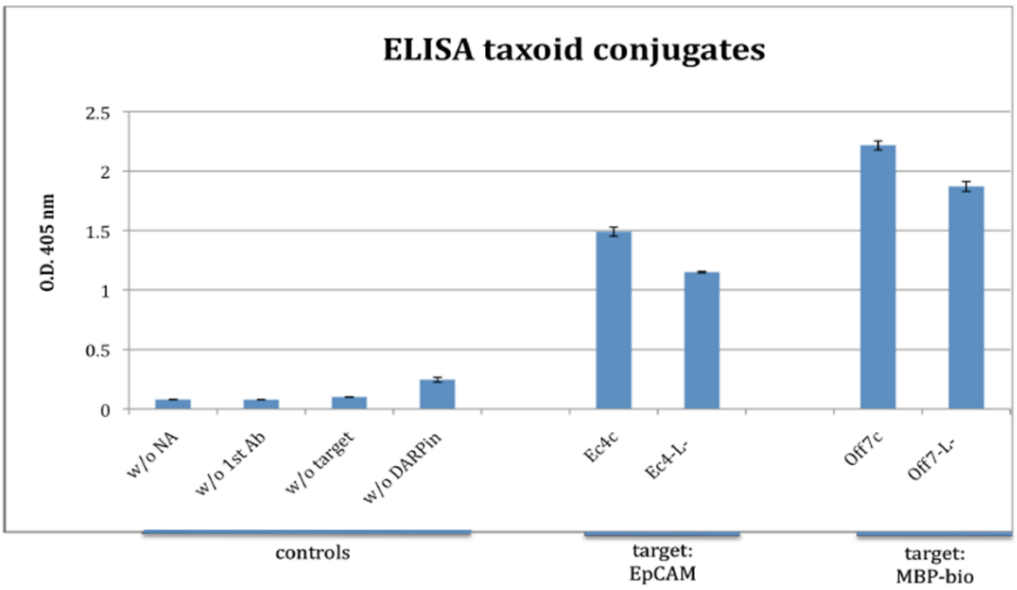

Figure 4-8: Phage ELISA performed by the Plückthun laboratory. The above chart shows the ability of the Ec4-disulfide-SB-T-1214 and Off7-disulfide-SB-T-1214 to bind their respective molecular targets on a similar scale to the original unmodified DARPins. In addition several controls were run to show the validity of the assay, which included the test without neutravidin, anti-M13 antibody horseradish peroxidase conjugate tag, biotinylated-EpEx receptor, and the respective DARPin.

To assess the ability of the conjugate to specifically target and kill cancer cells, HT-29 colon carcinoma cells known to overexpress EpCAM were used against EpCAM specific Ec4-disulfide-SB-T-1214 conjugate and EpCAM non-specific Off7c-disulfide-SB-T-1214 conjugate in-vitro shown in **Figure 4-9**. 6000 HT-29 cells were plated per well in a 96 well plate and serial dilutions with media of: 1) Ec4-disulfide-SB-T-1214; 2) Ec4-disulfide-SB-T-1214 with 20 times excess Ec4; 3) Off7-disulfide-SB-T-1214; 4) and free taxoid (SB-T-1214-disulfide-maleimide) were added and incubated for 96 hours at 37 ^{o}C. Unfortunately the results of the cytotoxicity assay showed no difference between the EpCAM specific and EpCAM nonspecific conjugates as all the constructs produced cytotoxicity. This was very surprising result since the ELISA assay showed definitively that the Ec4-disulfide-SB-T-1214 conjugate bound EpCAM while the Off7-disulfide-SB-T-1214 did not. Thus, attention shifted to the stability of the conjugate in media, since media did contain thiol proteins which could possibly cleave the disulfide linker liberating the drug prematurely and allowing it to penetrate into the cell without specificity.

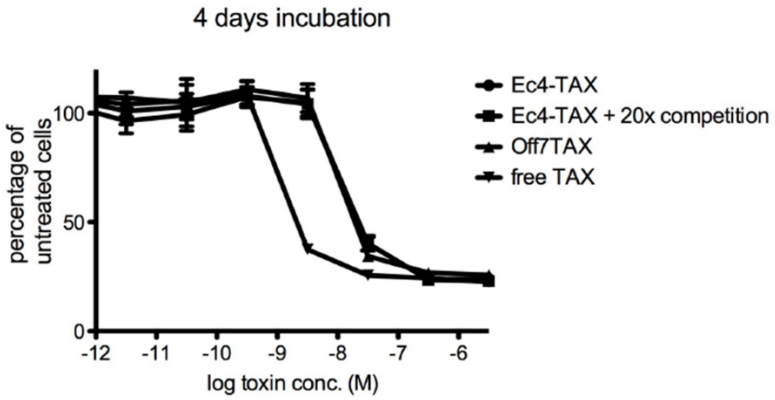

Figure 4-9: XTT cytotoxicity assay of Ec4-disulfide-SB-T-1214 conjugate by the Plückthun laboratory. The above graph plots the effect of the Ec4-disulfide-SB-T-1214 and Off7-disulfide-SB-T-1214 conjugates on the HT-29 cancer carcinoma cell line. Free TAX noted in the table is the SB-T-1214-maleimide construct and not the free taxoid, enhanced cellular uptake may be attributed by chemical ligation to media proteins.

Using a SDS-PAGE gel, the Ec4c-disulfide-SB-T-1214 conjugate was evaluated in media (DMEM/10% FCS) over 24 hours shown in **Figure 4-10**. Analysis of the time dependent gel showed that **4-2** was indeed cleaving in the media with a half-life around 3-4 hours. With this in mind, this gel provided evidence that internalization may be a slow process (> 3-4 hours) and thus the drug cleaved before RME providing reduced specificity. Thus, to test this hypothesis incubation times were reduce to 30 minutes and the cytotoxicity assay was rerun.

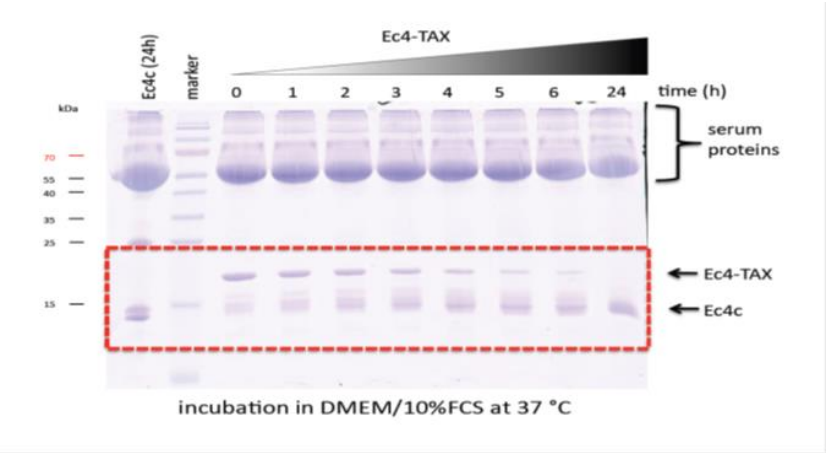

Figure 4-10: SDS-PAGE gel performed at the Plückthun laboratory highlighting linker stability of the Ec4-disulfide-SB-T-1214 conjugate

The Ec4-disulfide-SB-T-1214 conjugate **4-2** was thus reevaluated under the new conditions of 30 minute treatment, followed by two washing with PBS and then addition of media

followed by incubation for 96 hours shown in **Figure 4-11**. Surprisingly, the modifications to the assay made absolutely no difference in the results previously obtained in the first assay.

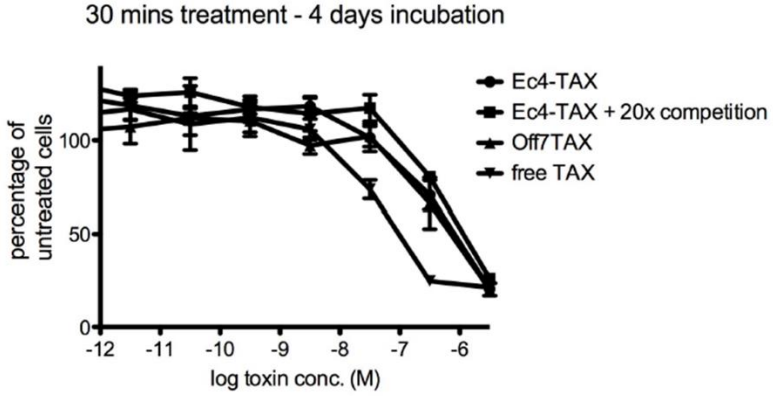

Figure 4-11: Modified XTT cytotoxicity assay of the SB-T-1214-disulfide-Ec4 conjugate by the Plückthun laboratory. The above graph plots the effect of the Ec4-disulfide-SB-T-1214 and Off7-disulfide-SB-T-1214 conjugates on the HT-29 cancer carcinoma cell line with only 30 minute treatment followed by 2 x washing with PBS and incubation 4 days.

Since the results of the cytotoxicity XTT assay were not consistent with the ELISA assay, in-vitro cytotoxicity was re-performed in the lab at Stony Brook shown in **Table 4-3**. Ec4c-SB-T-1214 conjugate **4-2** was evaluated against HT-29 colon carcinoma, MCF-7 breast ductal carcinoma, and HS-27 a normal human foreskin fibroblast cell lines. 6000 cells were plated in 96 well plates and serial dilutions in DMEM for HT-29 and RPMI for MCF-7 and HS29 with 5 % FBS and 5 % NuSerum of SB-T-1214 and Ec4-disulfide-SB-T-1214 conjugate were evaluated. To stay consistent with the media stability data, exposure time was set at 3 hours and followed by washing with PBS 3 times. After washing the cells, fresh media was added and the resulting plates were incubated for 48 hours (cancer cell lines) and 72 hours (normal cell line). An addition 24 hours was required for the normal cell line since the normal cells were greatly affected by the PBS washing. Overall, it was seen that the free SB-T-1214 was more toxic than the conjugate in all cases; however, in the case of the normal cell line HS27 there was more than 150 times difference between cancerous cell types indicative of the ability of the conjugate to specifically target these cancer cell types. Thus, despite contradictory results seen in Zurich by Plückthun laboratory, data collected at Stony Brook by the Ojima laboratory showed definitive evidence of selective targeting.

Table 4-3: MTT cytotoxicity assay of the Ec4-disulfide-SB-T-1214 conjugate performed in the Ojima laboratory. This table reflects the effect of the Ec4-disulfide-SB-T-1214 conjugate and SB-T-1214 on HT-29 (colon carcinoma), MCF-7 (breast ductal carcinoma), HS-27 (normal human fibroblast) cell lines. EC_{50} values were calculated using the SigmaPlot version 10.0 program. These values were determined from three individual experiments. DMEM was used (HT-29) RPMI (MCF-7, HS-27).

Cell Line	Drug	Exposure Time	Incubation Time	EC_{50} (nM)
HT-29	SB-T-1214	3 h	48 h	6.28, 4.92, 6.85 Avg. 6.02 ± 0.99
	Conjugate **4-2**	3 h	48 h	30.20, 31.69, 29.77 Avg. 30.55 ± 1.01
MCF-7	SB-T-1214	3 h	48 h	0.69, 0.67, 1.13 Avg. 0.83 ± 0.26
	Conjugate **4-2**	3 h	48 h	8.34, 9.11, 10.31 Avg. 9.25 ± 0.25
HS27	SB-T-1214	3 h	72 h	2.05, 1.55, 3.02 Avg. 2.21 ± 0.74
	Conjugate **4-2**	3 h	72 h	483.97, 60.45, 381.61 Avg. 308.68 ± 220.98

§4.1.3 Conclusion:

An Ec4-disulfide-SB-T-1214 conjugate **4-2** was synthesized with high efficiency based on MALDI. The resulting conditions were then transferred to Dr. Plückthun's lab and the University of Zurich where further testing by graduate student Manuel Simon confirmed that the conjugate was created with high efficiency.

Further assay by ELISA confirmed that the Ec4-disulfide-SB-T-1214 conjugate **4-2** did bind its molecular target EpCAM. Furthermore, Off7c-SB-T-1214 was tested against EpCAM and showed no binding. Thus, based on this very promising data, XTT cytotoxicity testing began against the EpCAM positive cell line HT-29.

Surprisingly, there was no selectivity seen in the XTT assay performed by Pluckthuns laboratory, instead there was cytotoxicity seen for all the conditions. Further analysis by SDS-PAGE of the Ec4-disulfide-SB-T-1214 conjugate **4-2** in DMEM media containing 10 % FCS revealed that the disulfide bond of the linker could be cleaved with a half-life around 3 to 4 hours. Thus, the XTT cytotoxicity assay was performed again with 30 minute incubation time followed by washing with PBS and subsequent incubation 4 days. Even more surprising, reducing the exposure time to far less than the linker half-life had little or no effect on the specificity.

At Stony Brook, an MTT cytotoxicity assay was performed on the Ec4-disulfide-SB-T-1214 conjugate **4-2** synthesized at Stony Brook against several cell lines including EpCAM

positive HT-29, MCF-7 and EpCAM negative HS-27. The results thus obtained from the MTT assay supported cell selectivity for the conjugate **4-2** for HT-29 and MCF-7 cell lines versus HS27 cells.

In conclusion, the results of the Ec4-disulfide-SB-T-1214 conjugate **4-2** were not as conclusive as previously theorized. Possible concerns were differences in testing conditions. In Zurich, one cell line HT-29 was evaluated against two different conjugates (Ec4-conjugate and Off7-conjugate) while at Stony Brook, Ec4-disulfide-SB-T-1214 conjugate was evaluated exclusively against normal and cancer cell lines. Lastly, of possible concern; during the coupling reaction with 30 % ethanol / PBS conditions a significant quantity of precipitate was formed at Stony Brook was purified by reverse phase chromatography.

§4.2 Design, Synthesis and Biological Evaluation of DARPin Ester-Based conjugates:

§4.2.1 Introduction:

Previously it was realized that the disulfide "smart-linker" could potential complicate the results of the in-vitro MTT and XTT assays due to the possibility of pre-mature cleavage in media. Pre-mature cleavage may result due to slower internalization and receptor turnover seen in larger macromolecules. In fact, disulfide linkers were devised originally to combat vitamin-conjugate efflux.[25] Efflux of vitamin-conjugates was found to occur because these conjugates preferentially trafficked to neutral lysosomes thus the ester linker could not be efficiently cleaved. Multi-valiant species such as proteins are typically found to traffic to acid lysosomes, thus favoring the cleavage of esters. Based on this information and previous experience with ester based linkers, such as the linker functionality seen in PUFA-based conjugates, ester based maleimide constructs were synthesized and tested for *in-vitro* activity and selectivity.

§4.2.2 Results and Discussion:

§4.2.2.1 Synthesis of the Maleimido-HL-SB-T-1214 Construct:

To mimic a PUFA as a functional maleimide linker, aminocaproic acid was used to make a 6-maleimido-aminocaproic acid linker. Starting from commercially available aminocaproic acid, 1 equivalent of maleic anhydride was stirred in acetic acid at room temperature for 24 hours to afford compound **4-3** crude, which was then diluted with acetic acid and refluxed overnight to afford compound **4-4** in 71 % isolated yield after two steps as shown in **Scheme 4-6**.

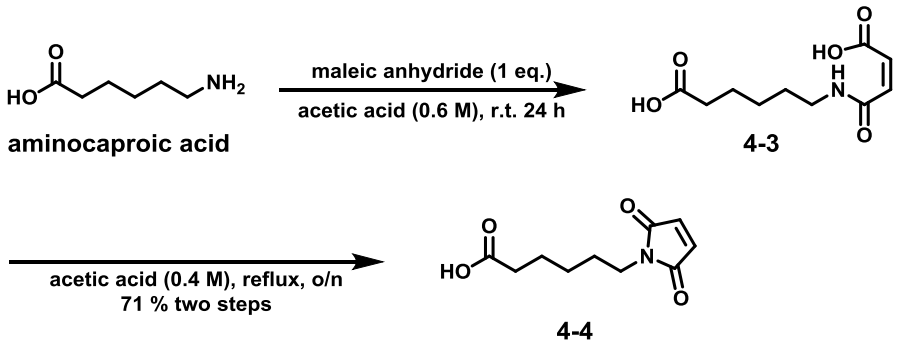

Scheme 4-6: The stepwise synthesis of 6-maleimido-aminocaproic acid

Following the synthesis of maleimide **4-4** subsequent coupling to SB-T-1214 was accomplished via EDC coupling to yield compound **4-5** in 8 % yield after purification shown in **Scheme 4-7**. The low yield was attributed to the difficulty in separating the starting material from the product.

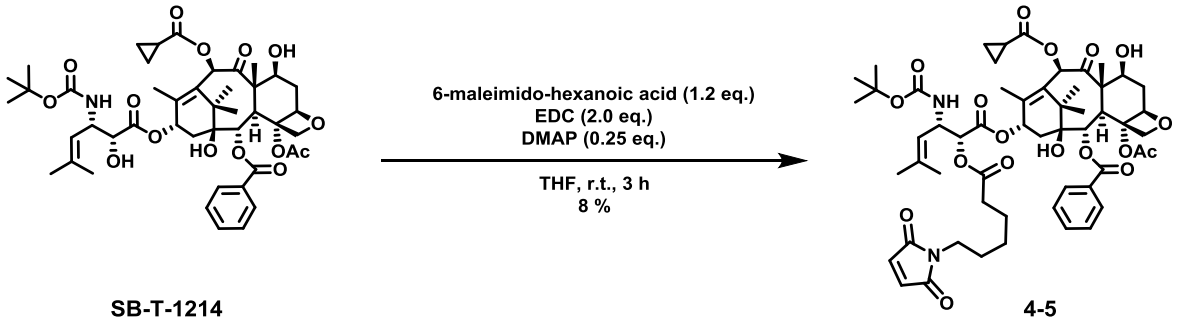

Scheme 4-7: Synthesis of the SB-T-1214-HL-maleimide construct

§4.2.2.2 Coupling of the Maleimido-HL-SB-T-1214 to the DARPin Ec4c:

Following the synthesis of the maleimide construct compound **4-5**, subsequent coupling proceeded with no complications as seen in **Scheme 4-8**. Consistent with previous coupling, Ec4c was reduced prior to coupling with TCEP. In contrast, the concentration of protein during the reaction was changed from 0.2 mM to ~ 4-5 µM. Furthermore, the ethanol content of the coupling solvent system was reduced for 30 % to 20 % to further reduce possible aggregation. After the reaction, the conjugate **4-6** was concentrated using a 20 mL 10 kDa MWCO filter and analyzed by MALDI with a final ethanol content of 2.5 % in PBS. The MALDI showed definitively that the conjugate **4-6** was formed with a mass of 19694.3 with an expected molecular weight of 19721.7 as shown in **Figure 4-12**.

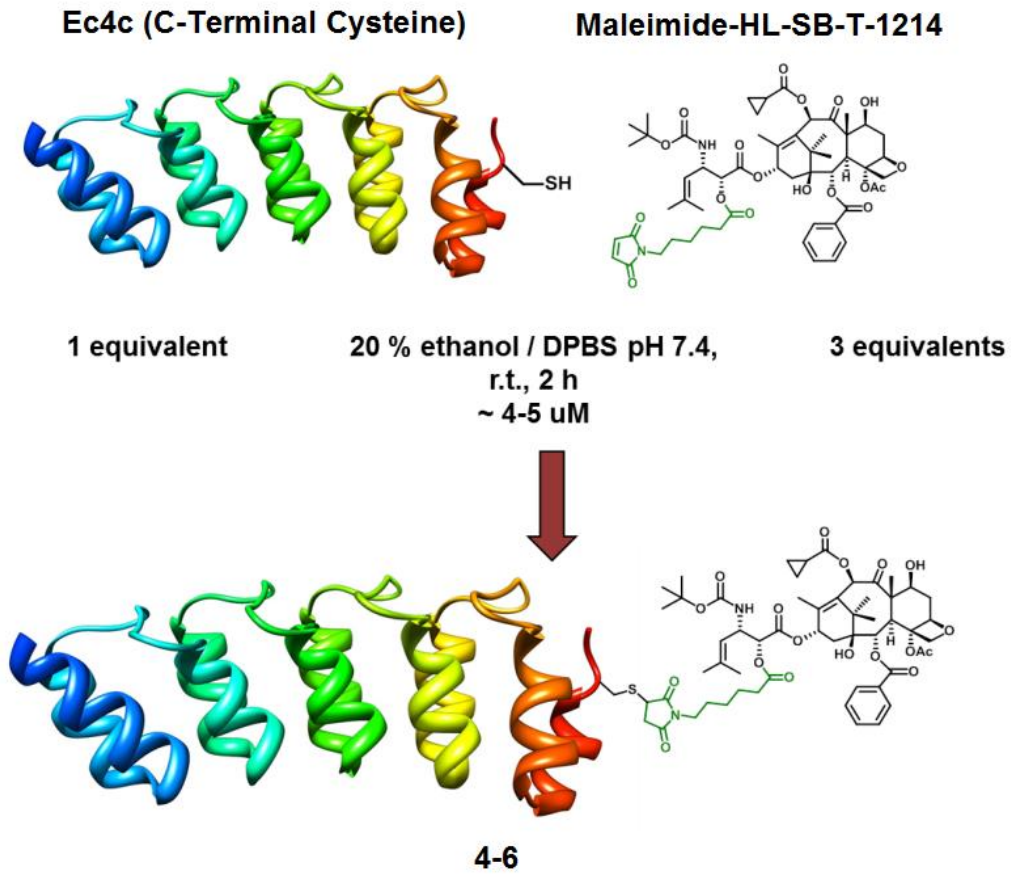

Scheme 4-8: Coupling of the SB-T-1214-HL-maleimide construct to DARPin Ec4c

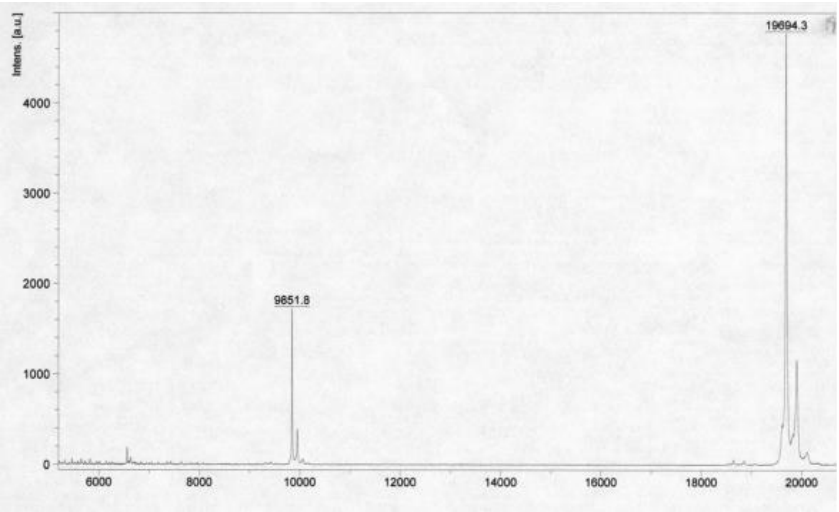

Expected MW : 19721.7
Actual : 19694.3
Determined by MALDI-TOF

Figure 4-12: MALDI spectrum of the Ec4-HL-SB-T-1214 conjugate **4-6**

§4.2.2.3 Solubility of the Ec4-HL-SB-T-1214 Conjugate:

Despite the successful coupling, more effort was expended to understand any possible aggregation of the conjugate **4-6**. A bicinchoninic acid (BCA) assay was used to assess the

available conjugate in solution. Indeed, bicinchoninic acid assay showed that no conjugate was in solution suggesting that during the reaction that the protein aggregated and thus became insoluble. Furthermore upon centrifugation, the insoluble conjugate would fall out of solution.

The results of the BCA assay brought new insight into why previously synthesized DARPin conjugates, targeting and non-targeting alike, appeared to be toxic. The most likely explanation appeared to be aggregation of the protein during the coupling reaction which resulted in a suspension of insoluble conjugate which after time could concentrate on the bottom of the assay plates. Thus an investigation into a possible reversal of the aggregation was carried out.

Based on the conception that the DARPin Ec4 would partially unfold during the coupling reaction, especially at 20 – 30 % ethanol, it was hypothesized that the hydrophobic taxoid could be interfering with protein refolding, resulting in the observed aggregation. In order to combat this effect, and test this hypothesis, tween80 was used to reverse the aggregation by creating a hydrophobic environment around the taxoid through micelle formation. At 5 % tween80/PBS this indeed was the case with an increase in solubility from 0 to 9.273 μg per mL determined by BCA acid assay after centrifugation.

§4.2.2.4 Biological Evaluation of the Ec4-HL-SB-T-1214 Conjugate:

Ec4-HL-SB-T-1214 **4-6** was evaluated against HT-29 a human colon carcinoma cell line and HS27 a normal human foreskin fibroblast cell line shown in **Table 4-4**. 6000 HT-29 and HS-27 cells were plated in 96 well plates and serial dilutions of SB-T-1214 and Ec4-HL-SB-T-1214 conjugate **4-6** were made in DMEM for HT-29 and RPMI for HS-27 with 5 % FBS, 5 % NuSerum and 1 % streptomycin/penicillin. As anticipated the ester based conjugate showed activity, although one order of magnitude less than the free drug. Furthermore, the conjugate showed specificity, up to 6 times more activity against HT-29 colon carcinoma than the normal cell line HS-27. Unfortunately, all standard dilutions at and above 47 nM in concentration caused cytotoxicity due to the toxicity of tween80 itself at high concentration (0.5 % v/v). This observation ultimately led to the decision to use polyethylene glycol directly incorporated into the linker.

Table 4-4: MTT cytotoxicity assay of the Ec4-HL-SB-T-1214 conjugate. This table reflects the effects of the Ec4-HL-SB-T-1214 and SB-T-1214 on HT-29 (human colon carcinoma) and HS-27 (normal human fibroblast) cell lines. EC_{50} values were calculated using the SigmaPlot version 10.0 program. These values were determined from three individual experiments. DMEM was used for the HT-29 cell line and RPMI used for HS-27 cell line.

Cell Line	Drug	Incubation Time	EC_{50} (nM)
HT-29	SB-T-1214	72 h	0.48, 1.37, 0.43 Avg. 0.76 ± 0.53
	Conjugate **4-6**	72 h	7.21, 7.03, 5.81 Avg. 6.68 ± 0.76
HS27	SB-T-1214	72 h	2.10, 0.68, 0.93 Avg. 1.24 ± 0.76
	Conjugate **4-6**	72 h	Inconclusive as the highest standard 47 nM was cytotoxic due to tween80

§4.2.2.5 Synthesis of the Maleimido-PEG_3-SB-T-1214 Construct:

Previous observations of the Ec4c-HL-SB-T-1214 conjugate **4-6** in the BCA assay highlighted that the hydrophobicity of the taxoid was most likely interfering with the coupling reaction causing aggregation. Thus it was decided to incorporate a polyethylene glycol (PEG) unit into the linker. Utilizing this approach, the solubility of the maleimide construct in water could be increased thus requiring less ethanol during the coupling. In turn, the DARPin would not be subjugated to such harsh denaturing conditions and forgo unfolding altogether.

Maleimido-PEG linkers had been known previously to solubilize hydrophobic drugs for similar protein couplings, thus this methodology was adapted to DARPin/Taxoid conjugation shown in **Scheme 4-9**.[26] Starting from commercially available triethylene glycol, conjugate addition to *tert*-butyl acrylate in the presence of catalytic potassium *tert*-butoxide afforded the mono-functionalized compound **4-7** in 58 % isolated yield. Subsequently, the maleimide functionality was added to the hydroxyl end using a Mitsunobu reaction with commercially available maleimide to give compound **4-8** in 55 % isolated yield. Last, deprotection of the *tert*-butylester with TFA provided the free carboxylic acid compound **4-9** which was further purified using an Amberlyst A-21 resin (weakly basic) to scavenge any remaining TFA in quantitative yield.

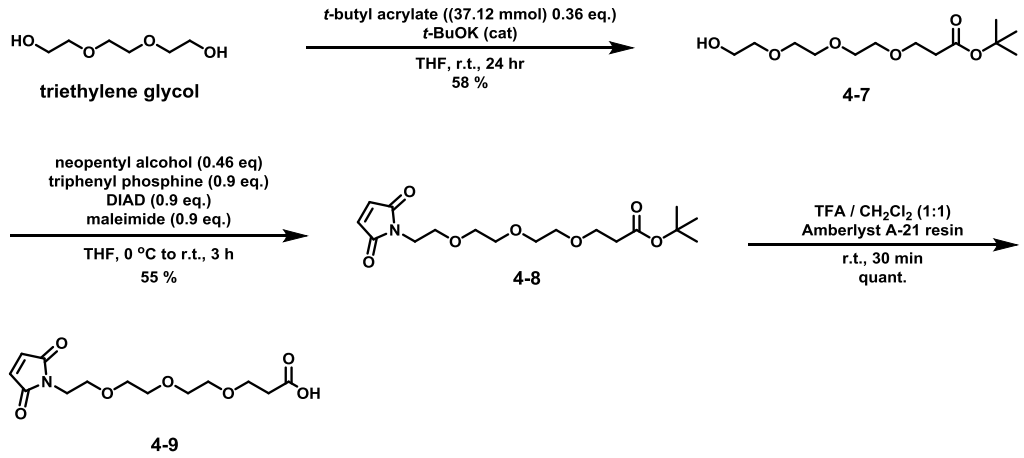

Scheme 4-9: The stepwise synthesis of 12-maleimido-4,7,10-trioxadodecanoic acid

Following the synthesis of the maleimido-PEG_3 linker compound **4-9** subsequent EDC coupling provided the maleimide-PEG_3-SB-T-1214 construct **4-10** shown in **Scheme 4-10**. Using a slight excess of compound **4-9** and excess EDC maleimide-PEG_3-SB-T-1214 compound **4-10** was afforded in 50 % isolated yield. Unlike the maleimide-HL-SB-T-1214 construct **4-5** made earlier, the starting material and product could be separated using traditional flash chromatography greatly increasing the yield. Nevertheless, the catalyst DMAP lead to side reaction thus reducing the overall yield of the reaction. Additionally, DMAP was found to be critical for the coupling to proceed.

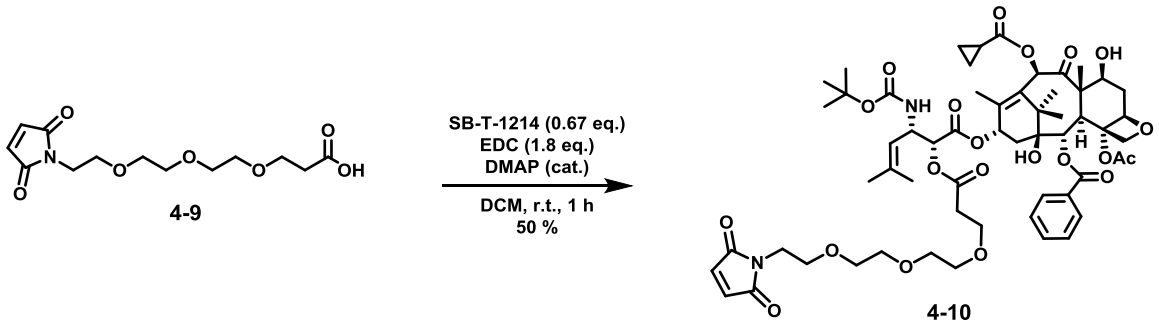

Scheme 4-10: Synthesis of the Maleimido-PEG_3-SB-T-1214 construct **4-10**

§4.2.2.6 Coupling of the Maleimido-PEG_3-Ester-SB-T-1214 to the DARPin Ec1c:

Following the synthesis of the maleimide construct compound **4-10**, subsequent coupling proceeded without complications as seen in **Scheme 4-11**. Consistent with the previous coupling of conjugate **4-6**, Ec1c a more potent DARPin was reduced prior to coupling with TCEP. Coupling conditions were modified to 9.8 % Ethanol/PBS at a concentration of 4–5 μM Ec1c. Due to the increase in the water solubility of compound **4-10**, the coupling reaction proceeded well to afford

the Ec1-PEG$_3$-SB-T-1214 conjugate **4-11**. After completion, the conjugate was concentrated using a 10 kDa MWCO filter and analyzed by MALDI in 100 % PBS shown in **Figure 4-13**. The MALDI showed definitively that the conjugate **4-11** was formed with a mass of 19651.9 and an expected molecular weight of 19651.17. A BCA assay was performed to evaluate soluble conjugate and it was determined that 249 µg / mL of Ec1-PEG$_3$-SB-T-1214 conjugate **4-11** was freely soluble in PBS.

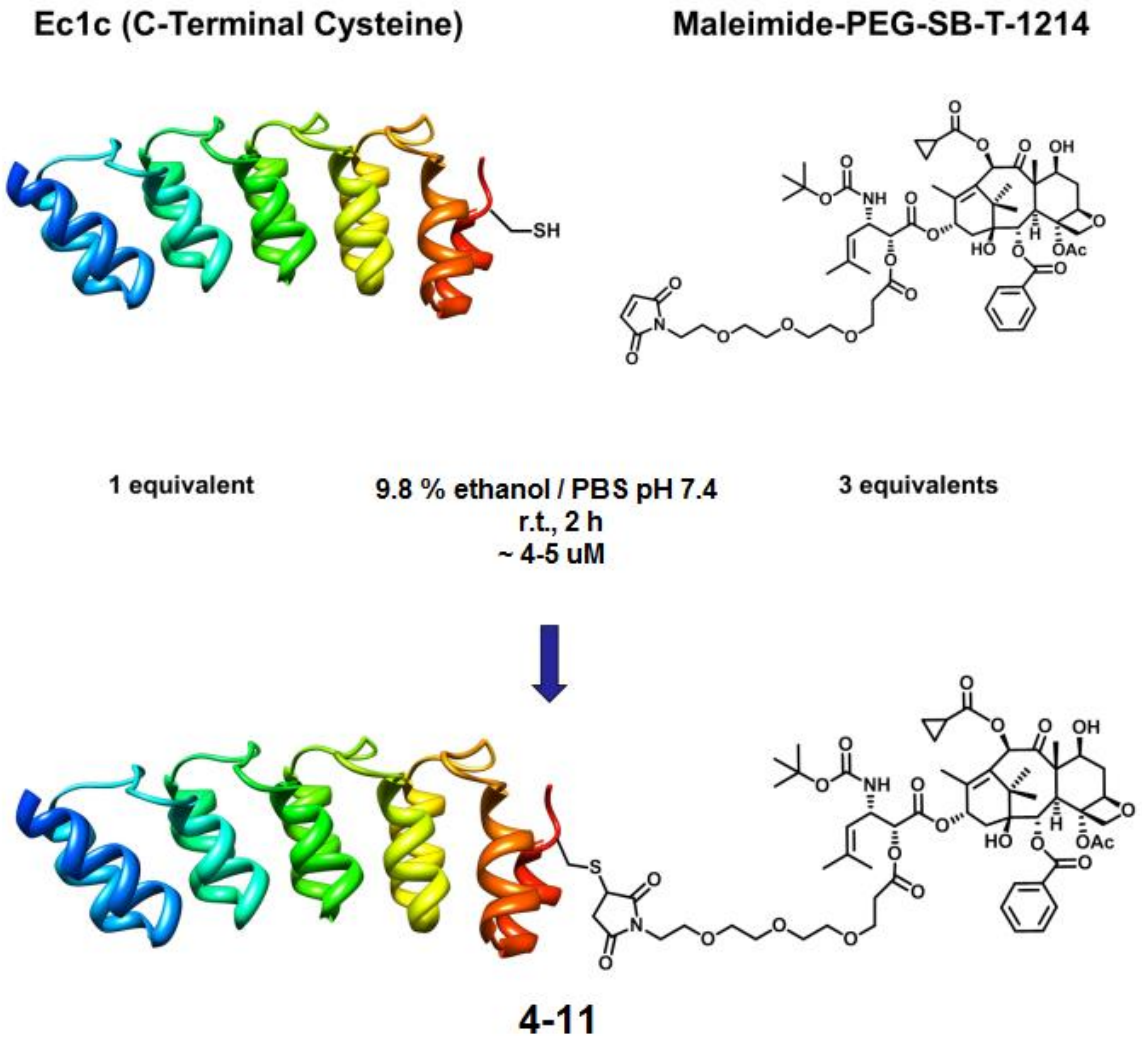

Scheme 4-11: Coupling of the SB-T-1214-PEG3-SB-T-1214 construct to DARPin Ec1c

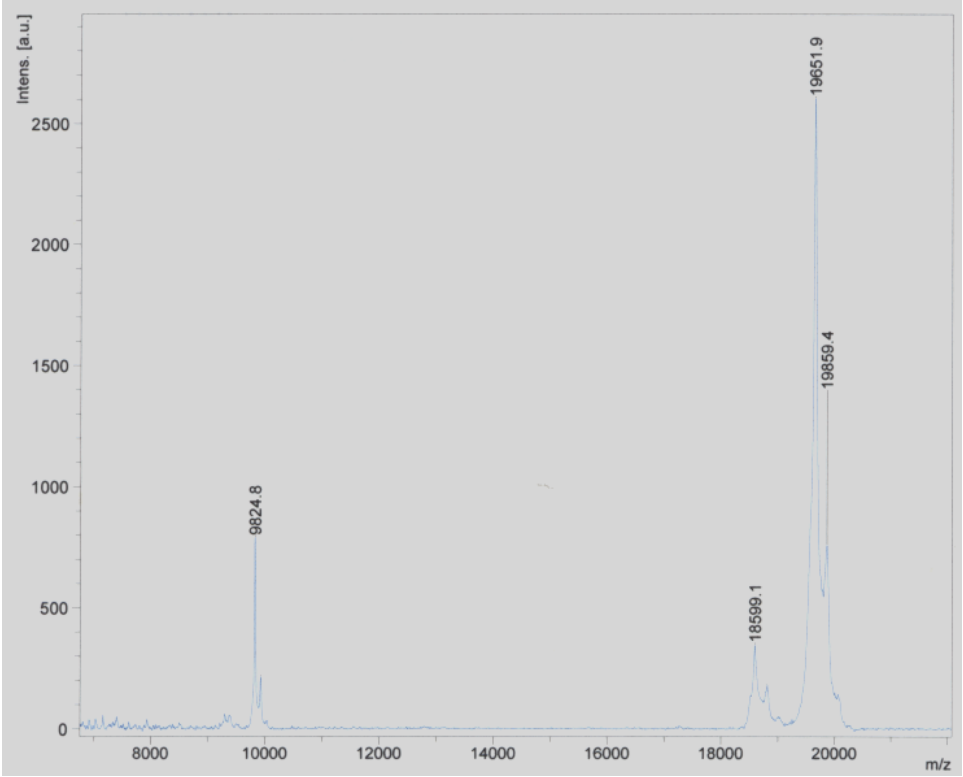

Figure 4-13: MALDI spectrum of the Ec1-PEG$_3$-SB-T-1214 Conjugate **4-11**

§4.2.2.7 Biological Evaluation of the Ec1-PEG$_3$-SB-T-1214 Conjugate:

The Ec1-PEG$_3$-SB-T-1214 conjugate **4-11** was evaluated against HT-29 colon carcinoma and HS-27 normal human foreskin fibroblast cell lines shown in **Table 4-5**. 6000 HT-29 and HS-27 cells were plated in 96 well plates and inoculated with serial dilutions of SB-T-1214 and Ec1-PEG$_3$-SB-T-1214 **4-11** respectively in DMEM/RPMI with 5 % FBS and 5 % NuSerum and 1 % streptomycin/penicillin. As anticipated the PEG$_3$ ester based conjugate did have activity with an EC$_{50}$ of approximately 14 nM at 72 hour exposure. Consistent with previous biological evaluations of the Ec4-HL-SB-T-1214 **4-6,** the Ec1-PEG$_3$-SB-T-1214 conjugate **4-11** showed preference in toxicity towards the cancer cell line HT-29. However, this preference was only approximately 4 times. This value for specificity was slightly less than the Ec4-HL-SB-T-1214 conjugate **4-6**, approximately 6 times. These values were quite surprising since the DARPin Ec1 has a K_{on} of 3.6 x 10^5 $M^{-1}s^{-1}$ and a K_d of 6.8 x 10^{-11} M suggesting that specificity for the HT-29 cell line should be quite high (orders of magnitude) over HS27. Thus Ec1 molecular probes were designed and synthesized to analyze internalization trends in these same cell lines.

Table 4-5: MTT cytotoxicity assay of the Ec1-PEG_3-SB-T-1214 conjugate. This table reflects the effects of the Ec1-PEG_3-SB-T-1214 conjugate **4-11** and SB-T-1214 on HT-29 (human colon carcinoma) and HS-27 (normal human fibroblast) cell lines. EC_{50} values were calculated using the SigmaPlot version 10.0 program. These values were determined from three individual experiments. DMEM was used for the HT-29 cell line and RPMI used for HS-27 cell line.

Cell Line	Drug	Incubation Time	EC_{50} (nM)
HT-29	SB-T-1214	72 h	0.92, 1.48, 0.50 Avg. 1.30 ± 0.33
	Conjugate **4-11**	72 h	11.95, 14.94, 13.69 Avg. 13.53 ± 1.50
HS27	SB-T-1214	72 h	0.66, 0.31, 1.19 Avg. 0.72 ± 0.44
	Conjugate **4-11**	72 h	44.12, 45.82, 46.85 Avg. 45.60 ± 1.38

§4.2.2.8 Synthesis and Evaluation of an Ec1-Flourocsein Probe by FACS:

Synthesis of the Ec1-Flouroscien molecular probe was carried out in a one-step coupling reaction with commercially available Fluorescein-Maleimide (Vector Labs) shown in **Scheme 4-12**. Coupling was performed in PBS as the fluorescein-maleimide regent was water soluble. Ec1c was reduced using TCEP at (0.2 mM) and then diluted to 4 to 5 μM with PBS. Then 3 equivalents of fluorescein-maleimide regent was added and the solution was allowed to react at room temperature for 3 hours to afford the Ec1-Fluoroscene probe **4-12**. The resulting solution was then concentrated with a 10 kDa MWCO filter and was then analyzed with 15 % SDS-PAGE shown in **Figure 4-14**. The gel revealed the probe **4-12** at approximately 18 kDa which additionally showed fluorescence at 365 nm.

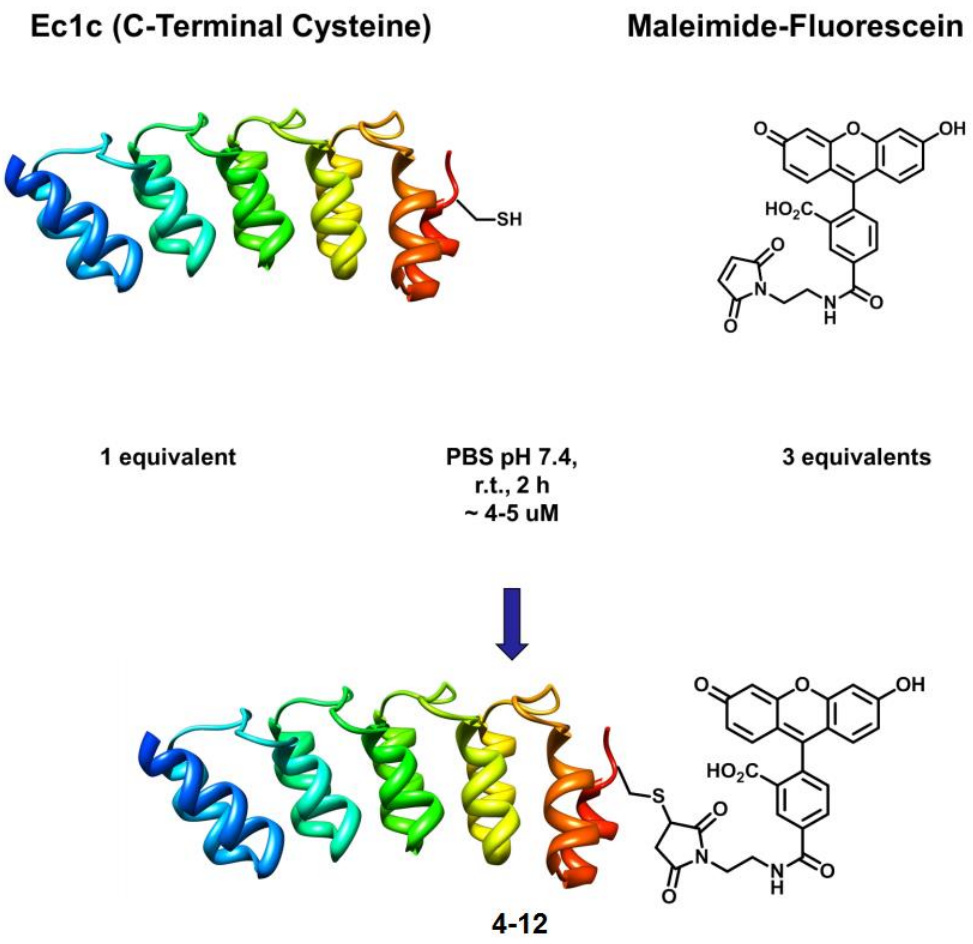

Scheme 4-12: Coupling of maleimido-fluorescein to DARPin Ec1c

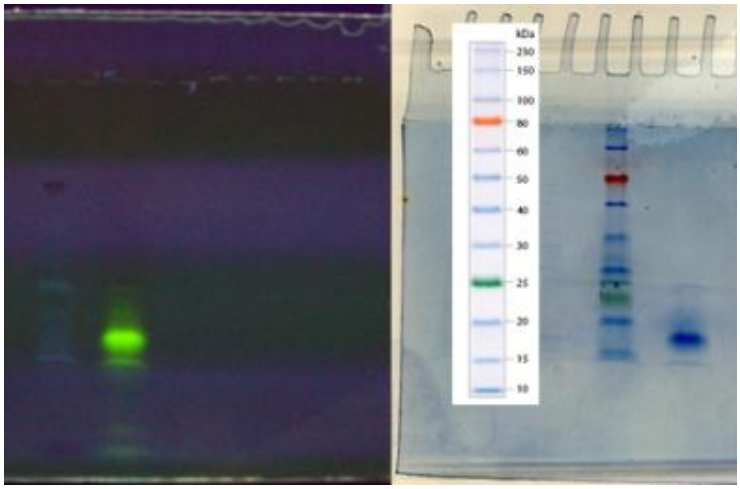

Figure 4-14: 15 % SDS Page gel of the Ec1-Fluorescein probe **4-12**. On the left is the gel exposed to 365 nm light highlighting a concentration of tagged protein that corresponds to the major protein stained on the gel to the right. The stained protein's molecular weight based on the ladder is between 15 to 20 kDa which is consistent with the expected molecular weight of the probe.

Biological evaluation of the Ec1-Fluorescein probe **4-12** was conducted on two different cell lines: 1) human colon carcinoma (HT-29); 2) human foreskin fibroblast (HS27). To each cell line 500 nM of Ec1-Fluorescein probe **4-12** was added and incubated at 37 ^{o}C for varying time periods (24 h, 1 h, 45 min, 30 min, 15 min). The resulting cells were washed with PBS following incubation and then measured by fluorescence activated cell sorting (FACS) shown in **Figure 4-15**.

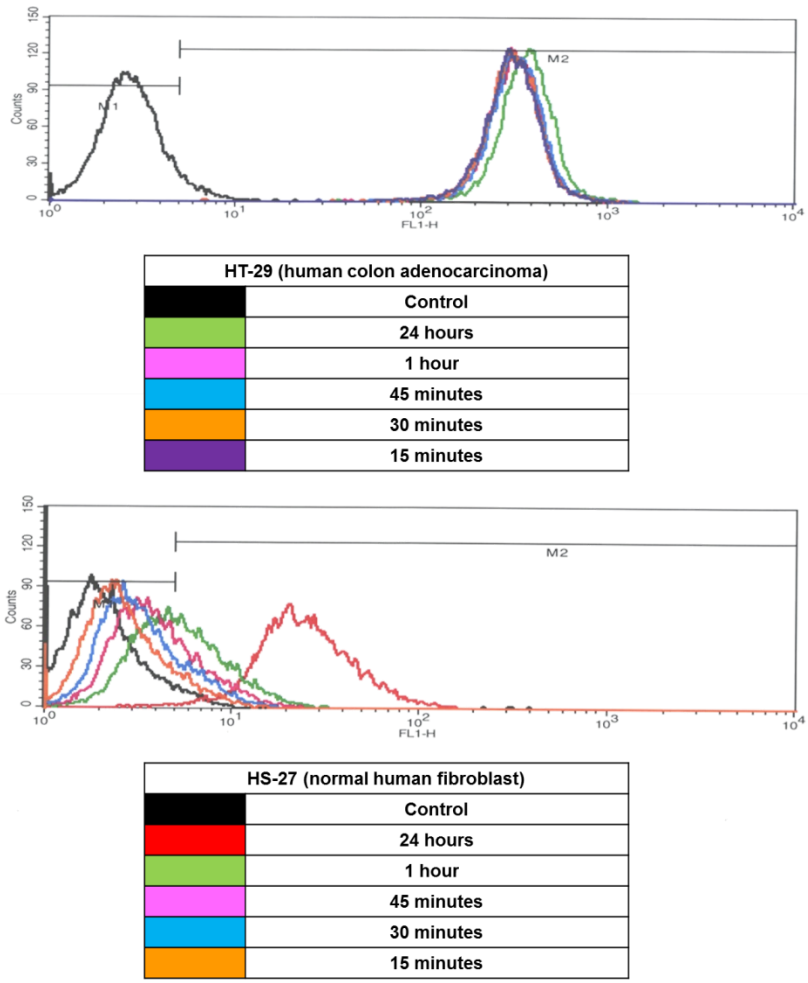

Figure 4-15: FACS analysis of the Ec1c-Fluorescein into HT-29 (top) and HS-27 (bottom) cell lines. Interestingly depicted is the internalization of Ec1 into HS-27 cells following exposure time exceeding 1 hour. The legend below the histogram color coordinates the time of exposure to each of the graphed histograms.

Immediately it was quite evident from the FACS data that Ec1 internalized into HT-29 cells readily (within 15 minutes) while there appeared to be no signification internalization into HS-27 cells within 1 hour. Furthermore, no additional internalization into HT-29 cells was seen

within 1 hours of exposure. Interestingly, after 24 hours of Ec1 exposure to the HS-27 cell line, some non-specific internalization began to emerge. This data suggested an underlying internalization mechanism separate from RME, while not prevalent, over time could contribute to a drop in specificity. Coupled with the artificially long exposure times inherent to MTT cytotoxicity testing, it made good sense that the MTT was artificially showing a decline in specificity over time due to this less prevalent internalization mechanism becoming more prevalent. In contrast, circulation half-lives of DARPins and DARPin conjugates in-vivo are within minutes of injection (typically 3 – 15 mintues).[23] Thus the poorer than expected specificity seen in the MTT assay can be attributed to the artificially long and stagnant exposure to the cells in the 96 well plates.

§4.2.2.9 Modified MTT Evaluation of the Ec1-PEG$_3$-SB-T-1214 Conjugate:

In an attempt to more accurately reflect the specificity seen in an in-vivo model, additional MTT cytotoxicity assays were carried out on the Ec1-PEG$_3$-SB-T-1214 conjugate **4-11** at 30 min and 3 hour exposure times shown in **Table 4-6**. Due to the required 72 hour incubation time needed for SB-T-1214 to exert its cellular effects and trigger apoptosis, exposing the cells for shorter periods provided to be quite elaborate. This was achieved by first incubating serial dilutions of the Ec1-PEG$_3$-SB-T-1214 conjugate **4-11** in media for specified exposure times followed by aspiration of the media and then 2 washings with PBS. After the cells were effectively washed of conjugate, fresh media was then added to the wells and the 96 well plate was then allowed to incubate 72 hours at which the plate was prepared with MTT reagent, read and calculated. Interestingly, a trend emerged consistent with the FACS. Shorter exposure times corresponded with more specificity towards HT-29, with 30 minute and 3 hour exposures showing greater than 1 order of magnitude specificity as shown in **Figure 4-16**.

Table 4-6: Modified MTT cytotoxicity assay of the Ec1-PEG$_3$-SB-T-1214 on HT-29 (colon carcinoma) and HS-27 (normal human fibroblast) cell lines. EC_{50} values were calculated using the SigmaPlot version 10.0 program. These values were determined from three individual experiments. DMEM was used for the HT-29 cell line and RPMI used for HS-27 cell line.

Cell Line	Drug	Exposure Time	Incubation Time	EC_{50} (nM)
HT-29	SB-T-1214	30 min	72 h	3.01, 4.60, 5.66 Avg. 4.42 ± 1.09
	SB-T-1214	3 h	72 h	4.24, 4.02, 3.67 Avg. 3.98 ± 0.23
	Conjugate **4-11**	30 min	72 h	154.54, 142.05, 138.65 Avg. 145.08 ± 6.83
	Conjugate **4-11**	3 h	72 h	59.18, 69.87, 64.66 Avg.64.57 ± 4.36
HS27	SB-T-1214	30 min	72 h	3.14, 4.81, 3.10 Avg. 3.68 ± 0.80
	SB-T-1214	3 h	72 h	3.94, 3.79, 3.29 Avg. 3.67 ± 0.28
	Conjugate **4-11**	30 min	72 h	> 1000
	Conjugate **4-11**	3 h	72 h	646.70, 588.10, 632.30 Avg. 622.37 ± 24.93

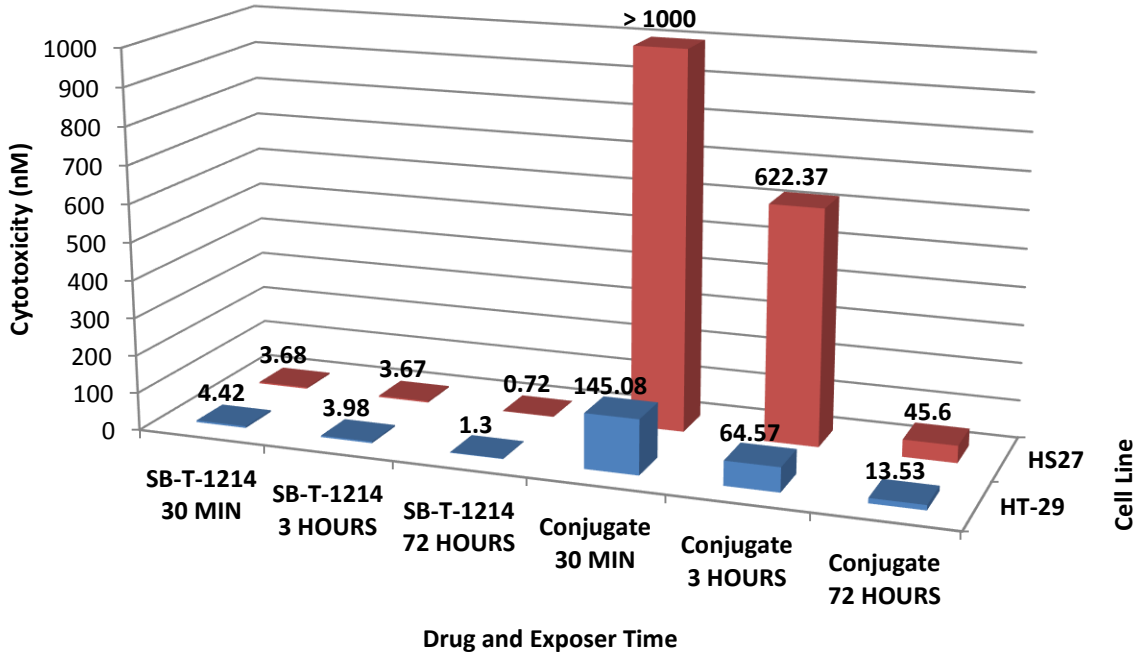

Figure 4-16: Comparison between cytotoxicity and exposure time of free SB-T-1214 and Ec1-PEG$_3$-SB-T-1214 conjugate **4-11**

§4.2.2.10 Evaluation of the Ec1-PEG$_3$-SB-T-1214 Conjugate against MCF7:

In addition to testing of Ec1-PEG$_3$-SB-T-1214 conjugate **4-11** against human colon carcinoma cell line (HT-29), conjugate **4-11** was also evaluate against the breast ductal adenocarcinoma cell line (MCF7) as seen in **Table 4-7**. The rational for testing this particular cell line was the high correlation between node-positive breast cancer patients expressing high levels of EpCAM and overall survival rate. Following the established protocol, 6000 MCF7 cells were plated in 96 well plates and inoculated with serial dilutions of SB-T-1214 and Ec1-PEG$_3$-SB-T-1214 **4-11** respectively in RPMI with 5 % FBS and 5 % NuSerum and 1 % streptomycin/penicillin. Interestingly, the Ec1-PEG$_3$-SB-T-1214 conjugate **4-11** provided to be almost 2 hours of magnitude more cytotoxic towards the MCF7 cell line compared with the control HS27 a noncancerous fibroblast shown in **Table 4-8**. Thus in our hands, the Ec1-PEG$_3$-SB-T-1214 conjugate **4-11** showed remarkable specificity and cytotoxicity against the MCF7 cell line, human breast adenocarcinoma.

Table 4-7: MTT cytotoxicity assay of the Ec1-PEG$_3$-SB-T-1214 conjugate against the MCF7 cell line (human ductal breast adenocarcinoma). EC_{50} values were calculated using the SigmaPlot version 10.0 program. These values were determined from three individual experiments.

Cell Line	Drug	Exposure Time	Incubation Time	EC_{50} (nM)
MCF7	SB-T-1214	30 min	72 h	0.20, 0.22, 0.61 Avg. 0.34 ± 0.19
	Conjugate **4-11**	30 min	72 h	29.07, 31.90, 29.32 Avg. 30.10 ± 1.28

Table 4-8: Cytotoxicity profile comparison between HS27 (control), HT-29 (human colon carcinoma) and MCF7 (human ductal breast adenocarcinoma) cell lines after 30 minute exposures.

Drug	HS27 (Control)	HT-29	MCF7
SB-T-1214	3.68 nM ± 0.80 nM	4.42 nM ± 1.09 nM	0.34 nM ± 0.19 nM
Conjugate **4-11**	> 1000 nM	145.08 nM ± 6.83 nM	30.10 nM ± 1.28 nM

§4.2.3 Conclusion:

In conclusion, a Ec4c-HL-SB-T-1214 conjugate **4-6**, a Ec1c-PEG$_3$-SB-T-1214 conjugate **4-11** and an Ec1-Flouroscein probe **4-12** were synthesized with in high efficiency based on MALDI and SDS-PAGE gel. These constructs where then analyzed using cell based measurements.

Specifically the Ec4c-HL-SB-T-1214 conjugate **4-6** was found to suffer from poor solubility due to aggregation during the DARPin coupling procedure. The main caused of this aggregation was due to harsh denaturing conditions required to solubilize the corresponding maleimide construct. The resulting aggregated conjugate suffered from a loss in specificity, but when treated with tween80, resulted in de-aggregation and increased solubility. Unfortunately, tween80 provided to be toxic at higher concentrations and was incompatable with the MTT in-vitro assay. Thus, PEG was incorporated directly into the maleimde linker.

The Ec1-PEG_3- SB-T-1214 conjugate **4-11** provided to be a better conjugate due to the better water solubility of its corresponding maleimide construct. Indeed, coupling required only 9.8 % ethanol and thus did not expose the Ec1c DARPin to harsh denaturing conditions. The solubility thus increased from 9.273 µg / mL (Conjugate **4-6** in 5% tween80/PBS) to 249 µg / mL (Conjugate **4-11** in PBS). Additionally, Ec1-PEG_3- SB-T-1214 conjugate **4-11** provided to be almost equally cytotoxicity to the Ec4-HL-SB-T-1214 conjugate **4-6** against the HT-29 cell line with 72 hour exposure. The Ec1-Flouroscein probe **4-12** was then synthesized an evaluated by FACS to better understand the specificity of HT-29 and HS-27 cell lines towards the DARPin Ec1.

FACS analysis of the Ec1-Flouroscein probe **4-12** verified that the HT-29 cancer cell line did indeed show preference to Ec1 over HS-27. Surprisingly over the course of 24 hours, HS-27 cells eventually began to internalize the Ec1-Flouroscein probe **4-12** signifying a possible secondary mechanism of internalization. Furthermore, mice models have shown that DARPins *in-vitro* have short serum clearance half-lives (approximately 3-11 minutes) and thus an exposure time of 72 hours in an MTT assay did not properly reflect the in-vivo model. Thus exposure times were reduced.

Finally, the Ec1-PEG_3-SB-T-1214 conjugate **4-11** was evaluated at 30 min and 3 hour exposure times and both provided specificity towards $EpCAM^+$ cell lines versus the noncancerous cell line HS27. Specifically, the Ec1-PEG_3-SB-T-1214 conjugate **4-11** has shown substantial specificity towards cancer $EpCAM^+$ cell lines HT-29 and MCF7. Furthermore, the Ec1-PEG_3-SB-T-1214 conjugate **4-11** has sown great promise against human breast adenocarcinoma MCF7 with almost a 2 fold selectivity over the control HS27. Combined with a good solubility profile of 259 µg / mL in PBS for the Ec1-PEG_3-SB-T-1214 conjugate **4-11**, formulations required for taxoid compatibility are no longer required as the DARPin Ec1 inherently provides the solubilization of

SB-T-1214. Thus, these results strongly suggest that the Ec1-PEG_3-SB-T-1214 conjugate **4-11** offers a highly promising and tunable drug platform for future study.

§4.3 Experimental Procedure:

§4.3.1 Synthesis and Chemical Biology:

General Methods: ^{1}H NMR and ^{13}C NMR spectra were measured on a Varian 300, 400, 500, or 600 MHz NMR spectrometer. High-resolution mass spectrometric analyses were conducted at the Mass Spectrometry Laboratory, University of Illinois at Urbana-Champaign, IL. TLC analyses were performed on Merck DC-alufolien with Kieselgel 60F-254 and were visualized with UV light and stained with sulfuric acid-EtOH, 10 % PMA-EtOH or 10 % Vanillin-EtOH with 1% sulfuric acid. Column chromatography was carried out on silica gel 60 (Merck; 230-400 mesh ASTM). MALDI analysis was performed on the Bruker AutoFlex II. UV-vis spectra were recorded on a UV spectrometer (Honda Group). HPLC Purity was determined by Shamazu HPLC employing a Phenomenex Kinetex™ 2.6 μm PFP 100 Å, LC Column 30 x 4.6 mm (CH3CN/H2O = 60/40 gradient to 95/5 over 45 min, flow rate at 1 mL/min, UV 254 nm). Fluorescence Active Cell Sorting (FACS) was performed at the Research Flow Cytometry Core facility using a Becton Dickinson FACScalibur Flow Cytometer at 530 nanometers.

Materials: The chemicals were purchased from Sigma-Aldrich Company, Fischer Company or VWR Company. 10-Deacetyl baccatin III (DAB) was donated by Indena, SpA, Italy. Designed Ankyrin Repeat Proteins (DARPin's) were obtained from Prof. Adreas Plückthun at the Universitat Zurich, Zurich, Switzerland. 3-maleimido-propanoic-hydrazide-trifluoroacetic acid salt was obtained from Thermo-Peirce Corporation (Item number 22297). Fluorescein maleimide was obtained from Vector Labs (Item number SP-1502). DCM and methanol were dried before use by distillation over calcium hydride under nitrogen. Ether and THF were dried before use by distillation over sodium-benzophenone kept under nitrogen. Dry DMF and DMSO were purchased from Sigma-Aldrich chemical company, and used without further purification. Reaction flasks were dried in a 100 ^{o}C oven and allowed to cool to room temperature in a desiccator over "*Drierite*" (calcium sulfate) and assembled under an inert nitrogen gas atmosphere.

SB-T-1214-(5C)-linker-maleimide (4-1):

To a 5 mL round bottom flask containing (27 mg, 0.0219 mmol) of SB-T-1214-(5C)-linker-OSu **2-12** added (7.8 mg, 0.0263 mmol) of 3-maleimido-propanoic-hydrazide-trifluoroacetic acid salt

(BMPH, Thermo Scientific) and diluted with 0.1 mL of DMF. While stirring added 3.8 µL of DIPEA and allowed to stir an addition 72 hours at room temperature. After completion the resulting solution was added directly to the column and purified using a gradient of 2 % (MeOH/DCM) to 4 % (MeOH/DCM) to yield (16 mg, 0.0123 mmol), 56 % isolate yield of the desired SB-T-1214-(5C)-linker-maleimide 4-1 as a white solid. HPLC purity = 94 % at 220 nm: FIA [M-1] = 1300.4; ^{1}H NMR (500 MHz, CD_3OD) δ 0.94 – 1.06 (m, 4 H), 1.15 (s, 6 H), 1.25 (m, 6 H), 1.30 (m, 2 H), 1.38 (s, 7 H), 1.63 (s, 4 H), 1.71 – 1.79 (m, 8 H), 1.82 – 1.90 (m, 4 H), 2.27 (m, 3 H), 2.35 (s, 3 H), 2.42 (m, 3 H), 2.52 (t, *J* = 6.5 Hz, 1 H), 2.91 (m, 1 H), 3.50 (t, *J* = 7.0 Hz, 1 H), 3.76 (t, *J* = 7.5 Hz, 1 H), 3.82 (d, *J* = 6.5 Hz, 1 H), 3.98 (d, *J* = 16.5 Hz, 1 H), 4.08 (d, *J* = 16.5 Hz, 1 H), 4.17 (q, *J* = 8.0 Hz, 2 H), 4.30 (q, *J* = 7.0 Hz, 1 H), 4.90 (s, 2 H), 4.98 (d, *J* = 9.0 Hz, 1 H), 5.23 (b, 1 H), 5.64 (d, *J* = 7.0 Hz, 1 H), 6.12 (m, 1 H), 6.43 (s, 1 H), 6.77 (s, 2 H), 7.24 – 7.32 (m, 3 H), 7.48 (t, *J* = 7.5 Hz, 2 H), 7.60 (t, *J* = 7.5 Hz, 1 H), 7.78 (d, *J* = 8.0 Hz, 1 H), 8.09 (d, *J* = 7.5 Hz, 2 H); ^{13}C NMR (126 MHz, CD_3OD) δ 9.21, 9.31, 10.57, 13.93, 15.13, 18.79, 21.06, 22.54, 23.39, 26.23, 27.13, 28.93, 32.01, 32.12, 32.44, 33.37, 34.38, 35.04, 36.70, 36.94, 37.65, 39.68, 44.74, 48.21, 59.43, 72.46, 73.13, 76.51, 76.69, 76.88, 77.61, 79.28, 80.65, 82.49, 86.04, 121.40, 127.81, 129.07, 129.57, 129.82, 131.08, 131.58, 131.67, 131.73, 132.54, 134.69, 134.94, 135.11, 135.63, 138.83, 138.93, 142.82, 157.59, 167.78, 170.42, 171.62, 171.77, 172.26, 172.38, 172.77, 174.06, 174.30, 175.27, 205.30; HRMS (ESI) *m/e* calcd for $C_{65}H_{81}N_4O_{20}S_2H^+$:1301.4886. Found: 1301.4883 (Δ = 0.2 ppm).

SB-T-1214-(5C)-disulfidelinker-Ec4 (4-2):

To a 1 mL aliquot of Ec4c in PBS (1.0925 mM) was added 10 µL of 0.5 M TCEP (TCEP, Pierce, Thermo Fisher Scientific, Lausanne, Switzerland). The resulting solution was allowed to shake for 1 hour at room temperature and filtered with a 3 kDa MWCO filter (Pall Nanosep®) by centrifugation at 14000 rpm. The resulting solution was diluted to 7 mL with PBS (DPBS, Lonza, Walkersville, MD) in a 15 mL eppendorf tube. 3 mLs of ethanol were added to the solution and the resulting solution was mixed. To a 5 mL vial was added 21.8 mg (16.75 µmol) of compound **4-1** and this was diluted with 1 mL of ethanol (16.75 mM). 200 µL of this solution containing compound **4-1** (3.35 µmol) was added to the solution of Ec4c (1.0925 µmol, 30 % ethanol in PBS) and the solution was shaken and allow to sit at r.t. for 3 hours. After completion the crude reaction was analyzed by MALDI: 19953.8 actual, 19953.8 expected. Using a 3 kDa MWCO filter (Pall

Nanosep®) the conjugate reaction mixture was filtered using PBS (2 x 15 mL). The resulting conjugate **4-2** was then diluted in PBS (5 mL). HPLC was used to purify the conjugate on the Agilent 1100 LC-MSD (Flow rate: 0.9 mL / min, Column: 250 x 4.6 mm Jupiter C_4, 300 Å, 5 µM, Mobile Phase: (A: H_2O, 0.2 % Acetic Acid, 0.05% TFA; B: acetonitrile, 0.2 % Acetic Acid, 0.02 % TFA), UV = 228 nm, Eluded at 30 minutes. Fractions were collected and lyophilized.

6-Maleimido hexanoic acid (4-4):[27]

To a 100 mL round bottom flask was added 1.230 g (9.38 mmol) of 6-aminocaproic acid and 4 mL of glacial acetic acid. To an Erlenmeyer flask was added 920 mg (9.38 mmol) of maleic anhydride and 11 mL of glacial acetic acid. The Erlenmeyer flask was shaken until all of the maleic anhydride was dissolved. Then this solution was added dropwise to the 100 mL round bottom flask while stirring. The resulting solution was stirred an addition 1 hour at room temperature. Then 7 mL of glacial acetic acid was added and the resulting solution was reflux at 150 ^oC overnight (11 hours). The resulting solution was evaporated under reduced pressure and was purified using silica gel chromatography 2% - 4% methanol in DCM to afford the desired product **4-4** (1.400 g, 71 %) as a white solid: ^1H NMR (400 MHz, $CDCl_3$) δ 1.30-1.37 (m, 2 H), 1.57-1.69 (m, 4 H), 2.34 (t, *J* = 7.2 Hz, 2 H), 3.51 (t, *J* = 7.2 Hz, 2 H), 6.69 (s, 2 H); ^{13}C NMR (100 MHz, CDCl3) δ 24.1, 26.1, 28.1, 33.6, 37.6, 134.1, 170.8.[27]

SB-T-1214-2' 6-maleimido hexanoic acid ester (4-5):

To a 10 mL round bottom flask added 209 mg (0.25 mmol) of SB-T-1214 and 61 mg (0.29 mmol) of 6-maleimido hexanoic acid **4-4** then added 7 mg (0.06 mmol) of DMAP followed by 1 mL of THF. To this solution while stirring was added 96 mg (0.50 mmol) of EDC-HCL. The reaction was monitored by HPLC (22 % conversion). The solvent was removed and the resulting solid was purified using Prep-MPLC. Fractions containing the desired product were lyophilized to afford the desired product **4-5** (20 mg, 8 %) as a white flaky solid: ^1H NMR (500 MHz, $CDCl_3$) δ 0.97-0.99 (m, 2 H), 1.12-1.15 (m, 4 H), 1.25 (s, 4 H), 1.34-1.43 (m, 12 H), 1.66 (m, 9 H), 1.76 (m, 9 H), 1.92 (m, 3 H), 2.38 (m, 4 H), 2.42-2.56 (m, 3 H), 3.52 (t, *J* = 7.0 Hz, 2 H), 3.81 (d, *J* = 7.0 Hz, 1 H), 4.18 (d, *J* = 8.5 Hz, 1 H), 4.30 (d, *J* = 8.0 Hz, 1 H), 4.44 (dd, *J* = 3.9 Hz, *J* = 10.5 Hz, 1 H), 4.88-4.98 (m, 4 H), 5.19 (d, *J* = 7.5 Hz, 1 H), 6.18 (t, *J* = 9.0 Hz, 1 H), 6.30 (s, 1 H), 6.67 (s, 2 H), 7.47 (t, *J* = 8.0 Hz, 2 H), 7.60 (t, *J* = 7.0 Hz, 1 H), 8.11 (d, *J* = 7.0 Hz, 1 H); ^{13}C NMR (125 MHz,

CDCl3) δ 9.1, 9.3, 9.5, 13.0, 14.8, 18.5, 22.2, 22.4, 24.1, 25.7, 26.0, 26.7, 28.2, 33.5, 35.4, 35.5, 37.5, 43.2, 45.6, 49.0, 58.5, 71.7, 72.1, 74.5, 75.2, 75.5, 76.4, 79.3, 79.8, 81.0, 84.5, 120.0, 128.6, 129.3, 130.2, 132.5, 133.6, 134.0, 138.0, 143.5, 154.9, 167.0, 168.3, 169.7, 170.8, 172.6, 175.1, 204.1.

SB-T-1214-HL-Ec4 (4-6):

To a 200 µL aliquot of Ec4 in PBS was added 10 µL of 0.5 M TCEP (TCEP, Pierce, Thermo Fisher Scientific, Lausanne, Switzerland). The resulting solution was allowed to shake for 1 hour at room temperature. After completion, the resulting solution was diluted to 20 mL with PBS (DPBS, Lonza, Walkersville, MD). Then using a 10 kD MWCO filter (GE Healthcare, VectaSpin™ 3) the resulting solution was filtered by centrifugation at 5000 rpm while maintaining the temperature of 4 ^{o}C. After the solution had been reduced to 1 mL an additional 19 mL of PBS was added and the solution was filtered again. This process was followed by another washing in a similar manner. The resulting solution was diluted to 50 mL with PBS. Then 10 mL of this solution (0.0520 µmol) was placed into a 15 mL tube and 2.5 mL of ethanol was added (20 % Ethanol in PBS). To a 5 mL vial was added 4.1 mg (3.915 µmol) of compound **4-5** and this was diluted with 1.9 mL of ethanol (2.0607 mM). 78 µL of this solution containing compound **4-5** (0.156 µmol) was added to the solution of Ec4 (0.0520 µmol, 20 % ethanol in PBS) and the solution was shaken and allow to sit at 4 ^{o}C for 3 hours. After completion the crude reaction was analyzed by MALDI: 19694.3 actual, 19721.7 expected. A bicinchoninic acid (BCA) (BCA Kit, Thermo Scientific) assay was then used to determine the amount of protein conjugate present considering 100 % conversion to the conjugate. The crude suspension had a protein concentration of 65.556 µg per mL. Then a 200 µL aliquot was removed and centrifuged at 13000 rpm for 5 minutes to remove insoluble suspended protein. BCA was performed and gave a concentration of soluble protein at 45.072 µg per mL (20 % ethanol in PBS). Using a 10 kDa MWCO filter the crude suspension was filtered reducing the final concentration of ethanol to 2.5 %. A BCA assay was performed and showed no solubility. The addition of Tween 80 (final concentration 5 %) followed by vigorous shaking was then evaluated by BCA and showed a solubility of 9.273 µg per mL after a 5 minute centrifugation at 13000 rpm.

***tert*-Butyl 12-hydroxy-4,7,10-trioxadodecanoate (4-7):[28]**

To a 100 mL round bottom flask added 15.607 g (103.93 mmol) of triethylene glycol and 52 mL of THF. Then added to this solution 100 mg of potassium *tert*-butoxide and let this solution stir for 5 minutes. After the solid had dissolved then added dropwise 5.5 mL of *tert*-buylacrylate and allowed this solution to stir overnight (24 hours). After completion the solution was neutralized with 1 M HCl. The solvent was removed under reduced pressure. To the resulting oil was added 100 mL of ethyl acetate. The resulting organic layer was washed with 3 x 200 mL aliquots of brine. The resulting organic layer was dried over $MgSO_4$. The solvent was then removed under reduced pressure to afford the desired product **4-7**, (6.001 g, 58 %) as a colorless oil: ^{1}H NMR (600 MHz, $CDCl_3$) δ 1.40 (s, 9 H), 2.46 (t, *J* = 6.6 Hz, 2 H), 2.80 (br, 1 H), 3.55-3.66 (m, 14 H). All data are in agreement with reported values.[28]

***tert*-Butyl 12-maleimido-4,7,10-trioxadodecanoate (4-8):[28]**

To a 250 mL round bottom flask added 1.000 g (10.10 mmol) of maleimide, 3.123 g (11.22 mmol) of compound **4-7**, 2.649 g (10.10 mmol) of triphenyl phosphine, and 455 mg (5.16 mmol) of neopentyl alcohol. Then added 69 mL of THF. While stirring cooled to 0 ^{o}C with an ice bath. Then added 2 mL of DIAD dropwise. The reaction was allowed to stir overnight (14 hr). The solvent was removed under reduced pressure and the resulting crude material was purified using silica gel chromatography employing a 3 to 1 mixture of ether to hexanes to afford the desired product **4-8**, (1.989 g, 55 %) as a white solid: ^{1}H NMR (300 MHz, $CDCl_3$) δ 1.43 (s, 9 H), 2.48 (t, *J* = 6.6 Hz, 2 H), 3.58-3.71 (m, 14 H), 6.69 (s, 2 H); ^{13}C NMR (75 MHz, CDCl3) δ 21.9, 28.0, 36.2, 37.0, 66.8, 67.8, 70.0, 70.3, 70.5, 80.5, 134.1, 170.6, 170.9. All data are in agreement with reported values.[28]

12-Maleimido-4,7,10-trioxadodecanoic Acid (4-9):[28]

To a 25 mL round bottom flask added 1.641 g (4.59 mmol) of compound **4-8** and 7.3 mL of DCM. To this solution 7.3 mL of trifluoroacetic acid was added and the resulting solution was allowed to stir for 2 hours. After completion, 2 g of Amberst 12 resin was added and the resulting solution was allowed to stir for 30 minutes. The resulting solution was filtered to remove the resin and the resulting organic layer was concentrated under reduced pressure to afford the desired product **4-9**, (1.395 g, quant.) clear oil: ^{1}H NMR (300 MHz, $CDCl_3$) δ 2.60 (t, *J* = 6.3 Hz, 2 H), 3.57-3.75 (m,

14 H), 6.69 (s, 2 H)); ^{13}C NMR (100 MHz, CDCl3) δ 34.7, 37.0, 66.2, 67.7, 69.9, 70.3, 70.4, 134.2, 170.7, 176.0. All data are in agreement with reported values.[28]

SB-T-1214-2' 12-maleimido-4,7,10-trioxadodecanoate (4-10):

To a 10 mL round bottom flask was added 89 mg (0.10 mmol) of SB-T-1214 and 75 mg (0.25 mmol) of compound **4-9**. To this mixture was added 1 mL of DCM. Then to this mixture will stirring was added 88 mg (0.46 mmol) of EDC-HCl. To resulting solution was mixed for 2 hours. No conversion was seen on TLC. Thus, 4 mg of DMAP (catalytic) was added and this reaction was monitored by TLC additional 1 hour until conversion no longer proceeded. The solvent was removed under reduced pressure and the resulting crude solid was purified using silica gel chromatography employing 50 % to 70 % ethyl acetate in hexanes to afford the desired product **4-10**, (55 mg, 50 %) as a white solid: ^{1}H NMR (500 MHz, $CDCl_3$) δ 0.93-1.02 (m, 2 H), 1.09-1.12 (m, 4 H), 1.25 (s, 4 H), 1.34 (m, 9 H), 1.66 (s, 3 H), 1.72 (s, 2 H), 1.75 (s, 7 H), 1.83-1.89 (m, 1 H), 1.92 (s, 3 H), 2.36 (s, 4 H), 2.50-2.56 (m, 1 H), 2.61 (d, *J* = 4.0 Hz, 1 H), 2.74 (t, *J* = 6.5 Hz, 2 H), 3.58-3.64 (m, 9 H), 3.71-3.81 (m, 5 H), 4.18 (d, *J* = 8.5 Hz, 1 H), 4.30 (d, *J* = 8.5 Hz, 1 H), 4.43 (m,1 H), 4.92-4.98 (m, 4 H), 5.20 (d, *J* = 7.5 Hz, 1 H), 5.67 (d, *J* = 7.0 Hz, 1 H), 6.17 (t, *J* = 8.5 Hz, 1 H), 6.29 (s, 1 H), 6.70 (s, 2 H), 7.47 (t, *J* = 8.0 Hz, 2 H), 7.60 (t, *J* = 8.0 Hz, 1 H), 8.11 (d, *J* = 7.5 Hz, 1 H); ^{13}C NMR (125 MHz, CDCl3) δ 9.1, 9.3, 9.5, 13.0, 14.8, 18.5, 22.2, 22.4, 24.1, 25.7, 26.7, 28.2, 29.7, 34.6, 35.5, 37.1, 43.2, 45.6, 48.9, 58.5, 66.1, 67.8, 70.0, 70.4, 70.5, 71.8, 72.1, 74.6, 75.2, 75.4, 76.2, 79.8, 81.0, 84.5, 120.0, 128.6, 129.3, 130.2, 132.5, 133.6, 134.1, 137.9, 143.4, 154.9, 166.9, 168.3, 169.6, 170.6, 170.8, 175.1, 204.1.

SB-T-1214-PEG$_3$-Ec1 (4-11):

To a 200 µL aliquot of Ec1c in PBS was added 10 µL of 0.5 M TCEP (TCEP, Pierce, Thermo Fisher Scientific, Lausanne, Switzerland). The resulting solution was allowed to shake for 1 hour at room temperature. After completion, the resulting solution was diluted to 20 mL with PBS (DPBS, Lonza, Walkersville, MD). Then using a 10 kD MWCO filter (GE Healthcare, VectaSpin™ 3) the resulting solution was filtered by centrifugation at 5000 rpm while maintaining the temperature of 4 ^{o}C. After the solution had been reduced to 1 mL an additional 19 mL of PBS was added and the solution was filtered again. This process was followed by another washing in a similar manner. The resulting solution was diluted to 50 mL with PBS. Then 30 mL of this

solution (0.156 µmol) was placed into a 50 mL tube and 3 mL of ethanol was added (20 % Ethanol in PBS). To a 5 mL vial was added 2.0 mg (1.7587 µmol) of compound **4-10** and this was diluted with 1.0 mL of ethanol (1.7587 mM). 267 µL of this solution containing compound **4-10** (0.4696 µmol) was added to the solution of Ec1c (0.156 µmol, 9 % ethanol in PBS) and the solution was shaken and allow to sit at 4 ^{o}C for 3 hours. After completion the crude reaction was purified by molecular weight by a 10 kDa MWCO filter. The 30 mL crude mixture in 9.8 % ethanol was spun down to 1 mL with at 5000 rpm at 4 ^{o}C. This was followed by two washings with 30 mL of PBS (ethanol content less than 0.01 %). The 1 mL of conjugate in PBS was then spun at 13000 rpm for 5 minutes to remove aggregates. A bicinchoninic acid (BCA) acid assay (BCA Kit, Thermo Scientific) was then used to determine the amount of protein conjugate present considering 100 % conversion to the conjugate. The crude suspension had a protein concentration of 258.7188 µg per mL. MALDI was used to characterize the conjugate: actual [M+1] 19651.9 (19650.9), expected 19651.17.

Ec1-Fluroscein probe (4-12):

To a 200 µL aliquot of Ec1c (1.3 mM) in PBS was added 10 µL of 0.5 M TCEP (TCEP, Pierce, Thermo Fisher Scientific, Lausanne, Switzerland). The resulting solution was allowed to shake for 1 hour at room temperature. After completion, the resulting solution was diluted to 20 mL with PBS (DPBS, Lonza, Walkersville, MD). Then using a 10 kD MWCO filter (GE Healthcare, VectaSpin™ 3) the resulting solution was filtered by centrifugation at 5000 rpm while maintaining the temperature of 4 ^{o}C. After the solution had been reduced to 1 mL an additional 19 mL of PBS was added and the solution was filtered again. This process was followed by another washing in a similar manner. This solution was diluted to 40 mL with PBS (0.26 µmol Ec1c). To a separate 5 mL vial added 0.3 mg (0.6019 µmol) and 1 mL of DMSO. Added the 1 mL of FITC-MAL (FITC-MAL, Vector Laboratories, Burlingame, CA, USA) to the 40 mL of Ec1c in PBS and shook for 1 hour in the dark. The resulting solution was then purified by molecular weight 10 kDa MWCO filter 3 x 20 mL of PBS and reduced to 1 mL. A 15 % SDS-PAGE gel was run revealing the tagged protein between 15 to 20 kDa. Additionally, a bicinchoninic acid (BCA) acid assay was then used to determine the amount of protein conjugate present considering 100 % conversion to the conjugate. The 10 x 1 mL suspension first was centrifuged at 13000 rpm for 5 minutes and then the protein concentration was determined to be 312.7691 µg per mL.

§4.3.2 FACS and MTT Assays:

Fluorescence activated cell sorting analysis of the Ec1-Flouroscein probe (4-12):

A cell suspension of human colon adenocarcinoma cell line HT-29 and normal human fibroblast HS-27 were cultured and incubated at 37 ^{o}C for (24 h) at a concentration of ~ 100 × 10^4 (1000 µL) in each well of a 6-well plate. After 24 hours, the old media was aspirated and replaced with freshly prepared media. To these wells was added a 500 nM of Ec1-Flouroscein probe **4-12** previously dissolved in PBS (concentration: 312.7691 µg per mL) at predefined time points so that the final exposure times were 15 minutes, 30 mintues, 45 minutes, 1 hour, and 24 hours respectively. After the specified exposure times, the media was aspirated and the cells were detached from the 6-well plate and centrifuged at 1000 rpm in a 15 mL ependorff tube. The cells were then washed with PBS (2 x 1000 µL) repeating the centrifugation and aspiration steps after each wash. To the 15 mL ependorff tube containing the resulting cells, 1000 µL of fresh PBS was added. Flow cytometry analysis was performed immediately after the incubation and washing steps. Cells resuspended in 1 mL of PBS were analyzed using a flow cytometer, FACSCalibur, operating at a 488 nm excitation wavelength and detected emission wavelength with a 530/30 nm bandpass filter. At least 10,000 cells were counted for each experiment using CellQuest 3.3 software (Becton Dickinson) and the distribution of FITC fluorescence was analyzed using WinMDI 2.9 freeware (Joseph Trotter, Scripps Research Institute).

In vitro cytotoxicity assay (48/72 hr with washing) SB-T-1214-disulfide-Ec4 (4-2):

The cytotoxicity of SB-T-1214-disulfide-Ec4 conjugate **4-2** was quantitatively evaluated in vitro the on human colon adenocarcinoma cell line HT-29 and normal human fibroblast HS-27 and measurements were performed with the well-established MTT (3-(4,5-dimethylthiazolyl)-2,5-diphenyl-2H-tetrazolium bromide) cell proliferation assay using DMEM/RPI media with 5 % FBS, 5 % NuSerum, and 1 % streptomycin/penicillin. The 2nd-generation taxoid, SB-T-1214 (free cytotoxic agent) was also assayed as a control. The cell suspension was cultured and incubated at 37 ^{o}C for (24 h) at a concentration of ~ 6 × 10^4 (200 µL) in each well of a 96-well plate. The old media was aspirated and cells were subsequently treated at 37 ^{o}C with SB-T-1214-disulfide-Ec4 conjugate **4-2** dissolved in PBS and free SB-T-1214 dissolved in DMSO and dispersed in medium at five (5) different final concentrations ranging from 0.05 to 500 nM (100

μL) for 2 or 3 days (48/72 hours). After a given time period (3 hours) the media was aspirated and washed with PBS 2 x (100 μL). Then 100 μL of fresh media was added and the 96-well plate was incubated for a total of 72 hours. After removal of the old medium, the fresh PBS containing MTT (*e.g.* 40 μL of 0.5 mg/mL) was added and incubated at 37 ^{o}C for 3 h. The resulting PBS/MTT solution was then removed and the as-produced insoluble violet formazan crystals, which were the product of the mitochondrial reduction of MTT by succinic dehydrogenase, were further dissolved using 0.1 N HCl in isopropanol with 10 % Triton X-100 to give a violet solution. The spectrophotometrical absorbance measurement of each well in the 96-well plate was performed at 570 nm and gave a direct estimate of cell viability and activity. The viability of the cells were plotted as a function of concentration and the cytotoxicity of SB-T-1214-disulfide-Ec4 conjugate **4-2** and free SB-T-1214 to calculated each respective EC_{50} value, which was defined as the drug concentration inducing 50 % of the cells death. The EC_{50} value from the viability-concentration curve was calculated with the software Sigma Plot 10.

In vitro cytotoxicity assay SB-T-1214-HL-Ec4 (4-6):

The cytotoxicity of the SB-T-1214-HL-Ec4 conjugate **4-6** was quantitatively evaluated in vitro on human colon adenocarcinoma cell line HT-29 and normal human fibroblast HS-27 and the measurement was performed with the well-established MTT (3-(4,5-dimethylthiazolyl)-2,5-diphenyl-2H-tetrazolium bromide) cell proliferation assay using DMEM/RPI media with 5 % FBS, 5 % NuSerum, and 1 % streptomycin/penicillin. The 2nd-generation taxoid, SB-T-1214 (free cytotoxic agent) was also assayed as a control. The cell suspension was cultured and incubated at 37 ^{o}C for (24 h) at a concentration of ~ 6 × 10^{4} (200 μL) in each well of a 96-well plate. The old media was aspirated and cells were subsequently treated at 37 ^{o}C with SB-T-1214-HL-Ec4 conjugate **4-6** previously dissolved in (5 % Tween80 / PBS) and free SB-T-1214 dissolved in DMSO dispersed in medium at five (5) different final concentrations ranging from 0.005 to 47 nM (100 μL) for 3 days (72 hours). After removal of the old medium, the fresh PBS containing MTT (*e.g.* 40 μL of 0.5 mg/mL) was added and incubated at 37 ^{o}C for 3 h. The resulting PBS/MTT solution was then removed and the as-produced insoluble violet formazan crystals, which were the product of the mitochondrial reduction of MTT by succinic dehydrogenase, were further dissolved using 0.1 N HCl in isopropanol with 10 % Triton X-100 to give a violet solution. The spectrophotometrical absorbance measurement of each well in the

96-well plate was performed at 570 nm and gave a direct estimate of cell viability and activity. The viability of the cells were plotted as a function of concentration and the cytotoxicity of the SB-T-1214-HL-Ec4c conjugate **4-6** and free SB-T-1214 to calculated each respective EC_{50} value, which was defined as the drug concentration inducing 50 % of the cells death. The EC_{50} value from the viability-concentration curve was calculated with the software Sigma Plot 10. All blanks died as the highest concentration of Tween80 killed the cells. Thus the lowest concentration standard 0.05 nM was used as the blank.

In vitro cytotoxicity assay (72 hr) SB-T-1214-PEG_3-Ec1 (4-11):

The cytotoxicity of SB-T-1214-PEG_3-Ec1c conjugate **4-11** was quantitatively evaluated in vitro on human colon adenocarcinoma cell line HT-29 and normal human fibroblast HS-27 and the measurement was performed with the well-established MTT (3-(4,5-dimethylthiazolyl)-2,5-diphenyl-2H-tetrazolium bromide) cell proliferation assay using DMEM/RPI media with 5 % FBS, 5 % NuSerum, and 1 % streptomycin/penicillin. The 2^{nd}-generation taxoid, SB-T-1214 (free cytotoxic agent) was also assayed as a control. The cell suspension was cultured and incubated at 37 ^{o}C for (24 h) at a concentration of ~ 6×10^4 (200 µL) in each well of a 96-well plate. The old media was aspirated and cells were subsequently treated at 37 ^{o}C with SB-T-1214-PEG_3-Ec1c conjugate **4-11** dissolved in PBS and free SB-T-1214 dissolved in DMSO and dispersed in medium at five (5) different final concentrations ranging from 0.05 to 500 nM (100 µL) for 3 days (72 hours). After removal of the old medium, the fresh PBS containing MTT (*e.g.* 40 µL of 0.5 mg/mL) was added and incubated at 37 ^{o}C for 3 h. The resulting PBS/MTT solution was then removed and the as-produced insoluble violet formazan crystals, which were the product of the mitochondrial reduction of MTT by succinic dehydrogenase, were further dissolved using 0.1 N HCl in isopropanol with 10 % Triton X-100 to give a violet solution. The spectrophotometrical absorbance measurement of each well in the 96-well plate was performed at 570 nm and gave a direct estimate of cell viability and activity. The viability of the cells were plotted as a function of concentration and the cytotoxicity of SB-T-1214-PEG_3-Ec1c conjugate **4-11** and free SB-T-1214 to calculated each respective EC_{50} value, which was defined as the drug concentration inducing 50 % of the cells death. The EC_{50} value from the viability-concentration curve was calculated with the software Sigma Plot 10.

In vitro cytotoxicity assay (72 hr with washing) SB-T-1214-PEG$_3$-Ec1 (4-11):

The cytotoxicity of SB-T-1214-PEG$_3$-Ec1c conjugate **4-11** was quantitatively evaluated in vitro the on human colon adenocarcinoma cell line HT-29, human ductal breast adenocarcinoma cell line, and normal human fibroblast HS-27 and measurements were performed with the well-established MTT (3-(4,5-dimethylthiazolyl)-2,5-diphenyl-2H-tetrazolium bromide) cell proliferation assay using DMEM/RPI media with 5 % FBS, 5 % NuSerum, and 1 % streptomycin/penicillin. The 2nd-generation taxoid, SB-T-1214 (free cytotoxic agent) was also assayed as a control. The cell suspension was cultured and incubated at 37 ^{o}C for (24 h) at a concentration of ~ 6 × 10^4 (200 µL) in each well of a 96-well plate. The old media was aspirated and cells were subsequently treated at 37 ^{o}C with SB-T-1214-PEG$_3$-Ec1c conjugate **4-11** dissolved in PBS and free SB-T-1214 dissolved in DMSO and dispersed in medium at six (6) different final concentrations ranging from 0.01 to 1000 nM (100 µL) for 3 days (72 hours). After a given time period (30 min or 3 hours) the media was aspirated and washed with PBS 2 x (100 µL). Then 100 µL of fresh media was added and the 96-well plate was incubated for a total of 72 hours. After removal of the old medium, the fresh PBS containing MTT (*e.g.* 40 µL of 0.5 mg/mL) was added and incubated at 37 ^{o}C for 3 h. The resulting PBS/MTT solution was then removed and the as-produced insoluble violet formazan crystals, which were the product of the mitochondrial reduction of MTT by succinic dehydrogenase, were further dissolved using 0.1 N HCl in isopropanol with 10 % Triton X-100 to give a violet solution. The spectrophotometrical absorbance measurement of each well in the 96-well plate was performed at 570 nm and gave a direct estimate of cell viability and activity. The viability of the cells were plotted as a function of concentration and the cytotoxicity of SB-T-1214-PEG$_3$-Ec1c conjugate **4-11** and free SB-T-1214 to calculated each respective EC_{50} value, which was defined as the drug concentration inducing 50 % of the cells death. The EC_{50} value from the viability-concentration curve was calculated with the software Sigma Plot 10.

§4.4 References:

1. Binz, K. H.; Amstutz, P.; Kohl, A.; Stumpp, M. T.; Briand, C.; Forrer, P.; Grutter, M. G.; Plückthun, A., High-affinity binders selected from designed ankyrin repeat proteins libraries. *Nat. Biotech.* **2004,** *22*, 575 - 582.

2. Binz, K. H.; Stumpp, M. T.; Forrer, P.; Amstutz, P.; Plückthun, A., Designing Repeat Proteins: Well-expressed, Soluble and Stable Proteins from Combinatorial Libraries of Consensus Ankyrin Repeat Proteins. *J. Mol. Biol.* **2003,** *332*, 489 - 503.
3. Zahnd, C.; Pecorari, F.; Straumann, N.; Wyler, E.; Plückthun, A., Selection and characterization of Her2 binding-designed ankyrin repeat proteins. *J. Biol. Chem.* **2006,** *281*, 167 - 175.
4. Zahnd, C.; Wyler, E.; Schwenk, J. M.; Steiner, D.; Lawrence, M. C.; McKen, N. M.; Pecorari, F.; Ward, C. W.; Joos, T. O.; Plückthun, A., A designed ankyrin repeat protein evolved to picomolar affinity to Her2. *J. Mol. Biol.* **2007,** *369*, 1015 - 1028.
5. Simon, M.; Zangemeister-Wittke, U.; Plückthun, A., Facile double-functionalization of designed ankyrin repeat proteins using click and thiol chemistries. *Bioconjugate Chem.* **2012,** *23*, 279 - 286.
6. Stumpp, M. T.; Binz, K. H.; Amstutz, P., DARPins: A new generation of protein therapeutics. *Drug Discov. Today* **2008,** *13*, 695 - 701.
7. Ojima, I.; Zuniga, E. S.; Berger, W. T.; Seitz, J. D., Tumor-targeting drug delivery of new-generation taxoids. *Future Med. Chem.* **2012,** *4*, 33 - 50.
8. Sharkey, R. M.; Goldenberg, D. M., Targeted Therapy of Cancer: New Prospects for Antibodies and Immunoconjugates. *CA: A Cancer Journal for Clinicians* **2006,** *56*, 226-243.
9. Ojima, I.; Geng, X.; Wu, X.; Qu, C.; Borella, C. P.; Xie, H.; Wilhelm, S. D.; Leece, B. A.; Bartle, L. M.; Goldmacher, V. S.; Chari, R. V. J., Tumor-specific novel taxoid-monoclonal antibody conjugates. *J. Med. Chem.* **2002,** *45*, 5620 - 5623.
10. Fujimora, K.; Covell, D. G.; Fletcher, J. E.; Weinstein, J. N., A modeling analysis of monoclonal antibody percolation through tumors: a binding-site barrier. *J. Nuc. Chem.* **1990,** *31*, 1191 - 1198.
11. Heldin, C.-H.; Rubin, K.; Pietras, K.; Ostman, A., High interstitial fluid pressure - an obstacle in cancer therapy. *Nat. Rev. Cancer* **2004,** *4*, 806 - 813.
12. Jain, R. K., Transport of molecules, particles, and cells in solid tumors. *Annu. Rev. Biomed. Eng.* **1999,** *1*, 241 - 263.
13. Zahnd, C.; Kawe, M.; Stumpp, M. T.; Pasquale, C. d.; Tamaskovic, R.; Nagy-Davidescu, G.; Dreier, B.; Schibli, R.; Binz, H. K.; Waibel, R.; Plückthun, A., Efficient tumor targeting with high-affinity designed ankyrin repeat proteins: effects of affinity and molecular size. *Cancer Res.* **2010,** *70*, 1595 - 1605.
14. Winkler, J.; Martin-Killas, P.; Plückthun, A.; Zangemeister-Wittke, U., EpCAM-targeted delivery of nanocomplexed si RNA to tumor cells with designed ankyrin repeat proteins. *Mol Cancer Ther* **2009,** *8*, 2674 - 2683.
15. Hussain, S.; Plückthun, A.; Allen, T. M.; Zangemeister-Wittke, U., Chemosensitization of carcinoma cells using epithelial cell adhesion molecule-targeted liposomal antisense against bcl-2/bcl-xL. *Mol. Cancer Ther.* **2006,** *5*, 3170 - 3180.

16. Martin-Killas, P.; Stefan, N.; Rothschild, S.; Plückthun, A.; Zangemeister-Wittke, U., A novel fusion toxin derived from an EpCAM-sepcific designed ankyrin repeat protein has potent antitumor activity. *Clin. Cancer Res.* **2011,** *17*, 100 - 110.
17. Went, P.; Vasei, M.; Bubendorf, L.; Terracciano, L.; Tornillo, L.; Riede, U.; Kononen, J.; Simon, R.; Sauter, G.; Baeuerle, P. A., Frequent high-level expression of the immunotherapeutic target Ep-CAM in colon, stomach, prostate and lung cancers. *Br. J. Cancer* **2006,** *94*, 128 - 135.
18. Spizzo, G.; Went, P.; Dirnhofer, S.; Obrist, P.; Simon, R.; Spichtin, H.; Maurer, R.; Metzger, U.; Von Castelberger, B.; Bart, R.; Stopatschinskaya, S.; Kochli, O. R.; Haas, P.; Mross, F.; Zuber, M.; Dietrich, H.; Bischoff, S.; Mirlacher, M.; Sauter, G.; Gastl, G., High Ep-CAM Expression is Associated with Poor Prognosis in Node-positive Breast Cancer. *Breast Cancer Res. And Treatment* **2004,** *86*, 207 - 213.
19. Schmelzer, E.; Zhang, L.; Bruce, A.; Wauthier, E.; Ludlow, J.; Yao, H.-I.; Moss, N.; Melhem, A.; McClelland, R.; Turner, W.; Kulik, M.; Sherwood, S.; Tallheden, T.; Cheng, N.; Furth, M. E.; Reid, L. M., Human hepatic stem cells from fetal and postnatal donors. *J. Exp. Med.* **2007,** *204*, 1973 - 1987.
20. Tanaka, M.; Okabe, M.; Suzuki, K.; Kamiya, Y.; Tsukahara, Y.; Saito, S.; Miyajima, A., Mouse hepatoblasts at distinct developmental stages are characterized by expression of EpCAM and DLK1: drastic change of EpCAM expression during liver development. *Mech. Dev.* **2009,** *126*, 665 - 676.
21. Terris, B.; Cavard, C.; Perret, C., EpCAM, a new marker for cancer stem cells in hepatocellular carcinoma. *Journal of hepatology* **2010,** *52*, 280-281.
22. Maetzel, D.; Denzel, S.; Mack, B.; Canis, M.; Went, P.; Benk, M.; Kieu, C.; Papior, P.; Baeuerle, P. A.; Munz, M.; Gires, O., Nuclear signalling by tumour-associated antigen EpCAM. *Nat. Cell Biol.* **2009,** *11*, 162 - 171.
23. Martin-Killas, P.; Stefan, N.; Rothschild, S.; Plückthun, A.; Zangemeister-Wittke, U., A Novel Fusion Toxin Derived from an EpCAM-Specific Designed Ankyrin Repeat Protein Has Potent Antitumor Activity. *Clin. Cancer. Res.* **2011,** *17*, 100 - 110.
24. Botchkina, G. I.; Zuniga, E. S.; M.;, D.; Wang, Y.; Wang, H.; Zhu, S.; Savitt, A. G.; Rowehl, R. A.; Leyfman, Y.; Ju, J.; Shroyer, K.; Ojima, I., New-generation taxoid SB-T-1214 inhibits stem cell-related gene expression in 3D cancer spheroids induced by purified colon tumor-initiating cells. *Mol. Cancer* **2010,** *9*, 192.
25. Xia, W.; Low, P. S., Folate-Targeted Therapies for Cancer. *J. Med. Chem.* **2010,** *53*, 6811 - 6824.
26. Warnecke, A.; Kratz, F., Maleimide-oligo(ethylene glycol) Derivatives of Camptothecin as Albumin-Binding Prodrugs: Synthesis and Antitumor Efficacy. *Bioconjugate Chem.* **2003,** *14*, 377 - 387.
27. Willner, D.; Trail, P. A.; Hofstead, S. J.; King, H. D.; Lasch, S. J.; Braslawsky, G. R.; Greenfield, R. S.; Kaneko, T.; Firestone, R. A., (6-Maleimidocaproyl)hydrazone of

Doxorubicin-A New Derivative for the Preparation of Immunoconjugates of Doxorubicin. *Bioconjugate Chem.* **1993,** *4*, 521-527.

28. Warnecke, A.; Kratz, F., Maleimide-oligo(ethylene glycol) Derivatives of Camptothecin as Albumin-Binding Prodrugs: Synthesis and Antitumor Efficacy. *Bioconjugate Chem.* **2003,** *14*, 377 - 387.

Chapter 5

Development of Novel Small Molecule Inhibitors of Botulinum Neurotoxin A

Content

§5.0 Introduction:
§5.0.1 Botulism:

Botulinum neurotoxins (BotNTs) are among the most potent neurotoxins known to exist, with LD_{50} values in the range of 0.1 to 1 ng per kg.[1] BotNTs consist of seven serotypes (A-G); however, primarily serotypes A, B, E, and F have been implicated as the main cause of botulism in humans. Exposure to BotNTs coincides with co-infection with *Clostridium botulinum* shown in **Figure 5-1**, a gram-positive obligate anaerobic bacterium commonly found in soil. Typically, *Clostridium botulinum* enters the body either through an open wound or more commonly through ingestion. Once inside the host, BotNTs are secreted into the blood stream where they are taken up by motor neurons.[2, 3] In turn, the loss of acetylcholine release from the motor neurons results in flaccid paralysis and eventual respiratory failure. Recently, BotNTs have been weaponized and consequently have been categorized by the Center for Disease Control as a Category A bio-threat.[4]

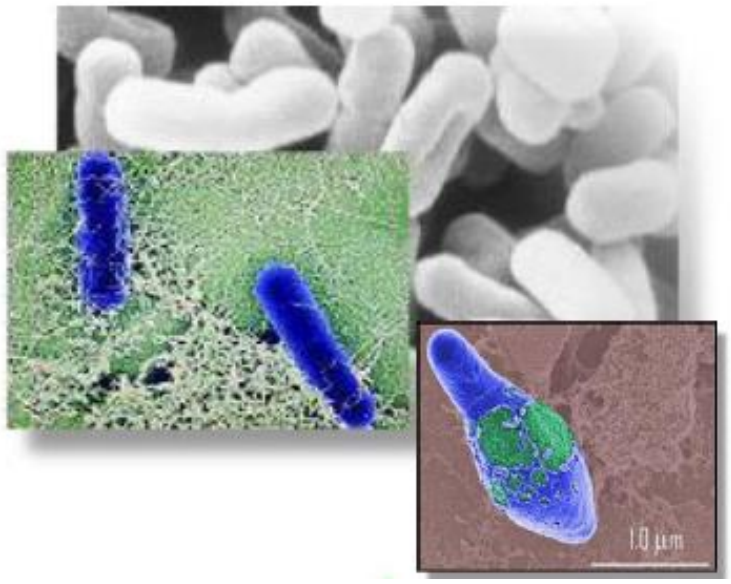

Figure 5-1: Electron micrograph image of *Clostridium botulinum* (Adapted from reference [5])[5]

Clostridium botulinum releases BotNTs into the blood stream of the infected host as a single 150 kDa inactive polypeptide. This dimer is specifically composed of a 100 kDa (heavy chain) translocation domain and 50 kDa (light chain) catalytic domain connected via a single disulfide bond. Circulating within the blood stream, the inactive polypeptide binds to the presynaptic membrane of motor neurons and internalizes through vesicles shown in **Figure 5-2**. After internalization, the disulfide bond connecting the translocation domain and catalytic domains

is cleaved and the catalytic domain is ejected into the cytosol of the motor neuron. Here, the catalytic domain actively catalyzes proteolysis of polypeptides of the SNARE complex.

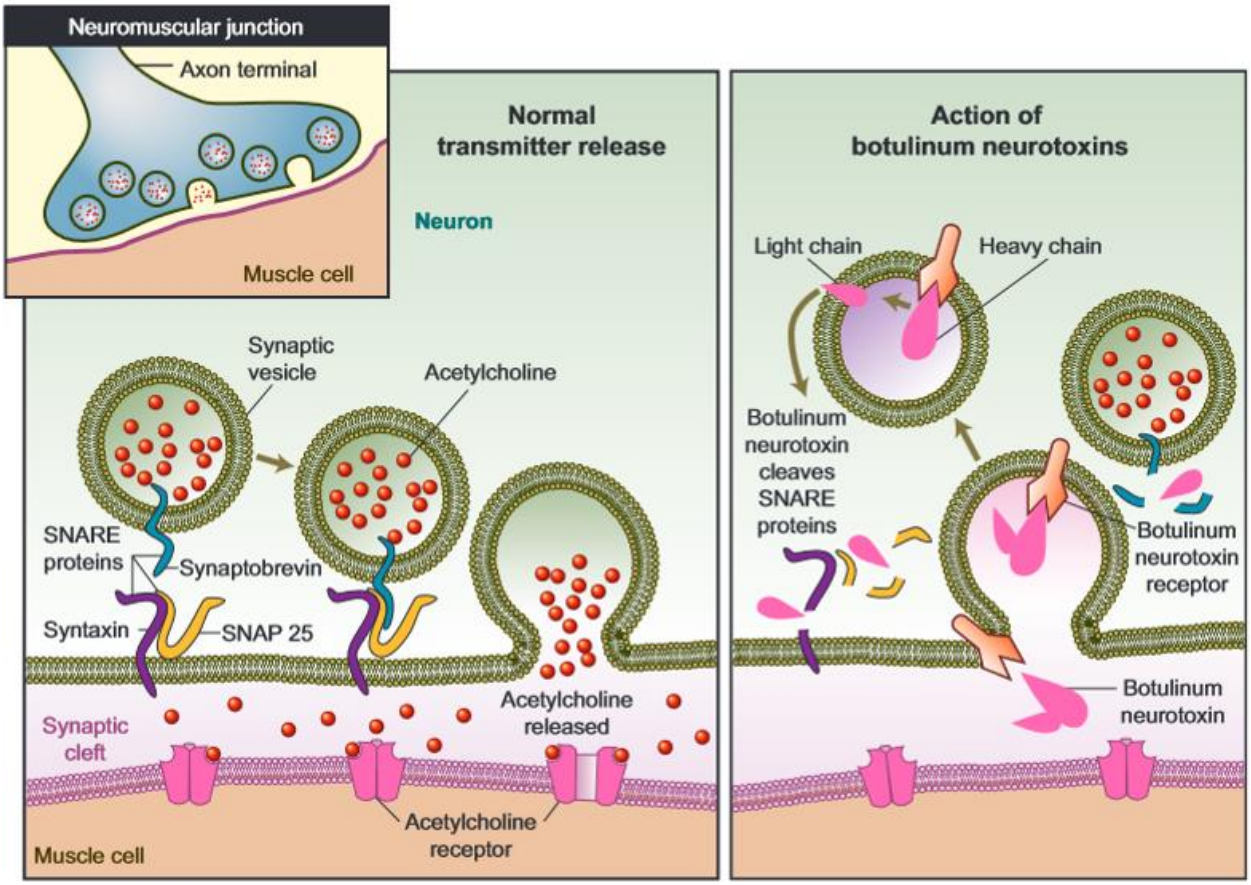

Figure 5-2: Normal acetylcholine release versus the disease model of infection with Botulism neurotoxin. Typically SNARE proteins (Synaptobervin, Syntaxin, SNAP-25) promote the fusion of vesicles carrying acetylcholine into the synaptic cleft. Acetylcholine acts to chemically transmit signals between neuronal cells and the muscle cells. In the disease model, botulism neurotoxin (heavy chain and light chain) binds to and infiltrates the neuronal cell. Once inside the light chain cleaves from the heavy chain via a disulfide bond connection and is ejected into the cytosol where it cleaves SNARE proteins. In the case of BotNT/LC-A, the SNAP-25 protein is the primary substrate. Ultimately the vesicles carrying acetylcholine to the snaptic cleft are inhibited from fusing and releasing this signal transmission between the neuron and muscle cell resulting in flaccid paralysis. (Reproduced with permission from [6], Copyright Massachusetts Medical Society)[6]

Through experimental evidence, BotNT-LC serotypes were known to vary in structure quite substantially, and as such, their substrates also varied substantially.[7] Currently there are no inhibitors providing broad-spectrum inhibition against BotNT-LCs. Thus, most of the literature

exploring inhibition of the Botulism Neurotoxins has focused on the most commonly serotype, BotNT/LC-A.

§5.0.2 Development of Peptidomimetic Inhibitors of BotNT/LC-A:

Initial attempts at designing catalytic inhibitors of BotNT/LC-A were based upon competitive inhibition. Thus the initial design was focused around peptidomimetics providing SAR data through x-ray co-crystal structures.[8, 9] This is the case with substrate inhibitor I1 [K_i = 41 nM] which was used to better understand the biochemical mechanism shown in **Scheme 5-1**. Ultimately, four highly potent tetrapeptides RRGC [K_i = 157 nM], RRGM [K_i = 845 nM], RRGL [K_i = 660 nM], RRGI [K_i = 786 nM] were derived and were found to be highly active based on three essential binding pockets S1, S1`, and S3` shown in **Figure 5-3**.

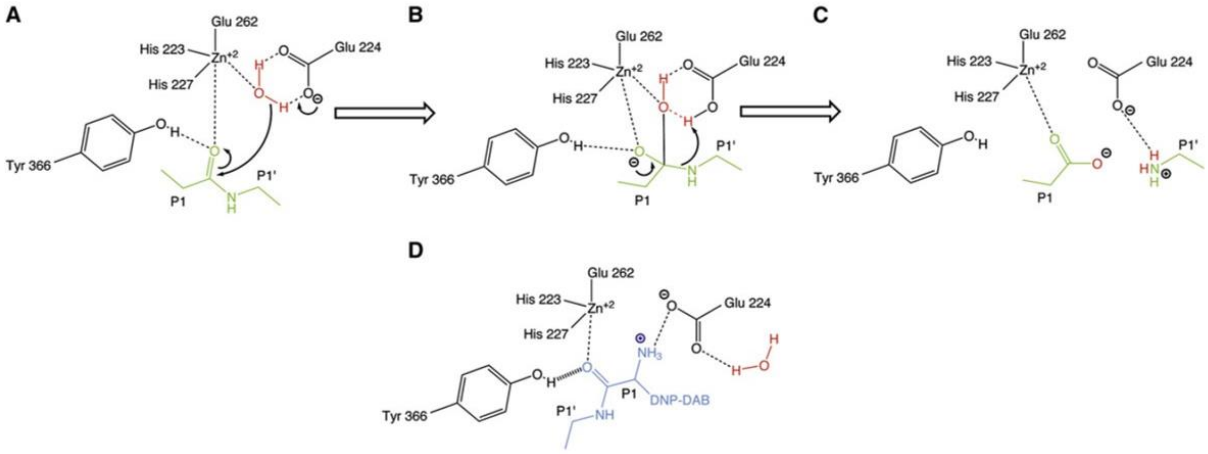

Scheme 5-1. Biological mechanism of the Zinc-dependent proteolysis of SNAP-25 substrate by BotNT/LC-A. A) Coordination of P1/P1' amino acid back bone to Zinc with the nearby tyrosine transferring electron density through hydrogen bonding towards the carbonyl oxygen. B) Driven by the partial positive carbonyl carbon, the nearby coordinated water molecule can attack thus forming a tetrahedral intermediate. The basicity of the amino group facilitates proton transfer from the water. C) After two proton transfers from the nucleophilic water, the stable amino group and carboxyl group prevent reverse reactions, thus proteolysis is complete. D) Alpha-carbon amino groups provide a stable-uncleavable substrate that poisons catalytic activity. (Reprinted with permission from reference [9])

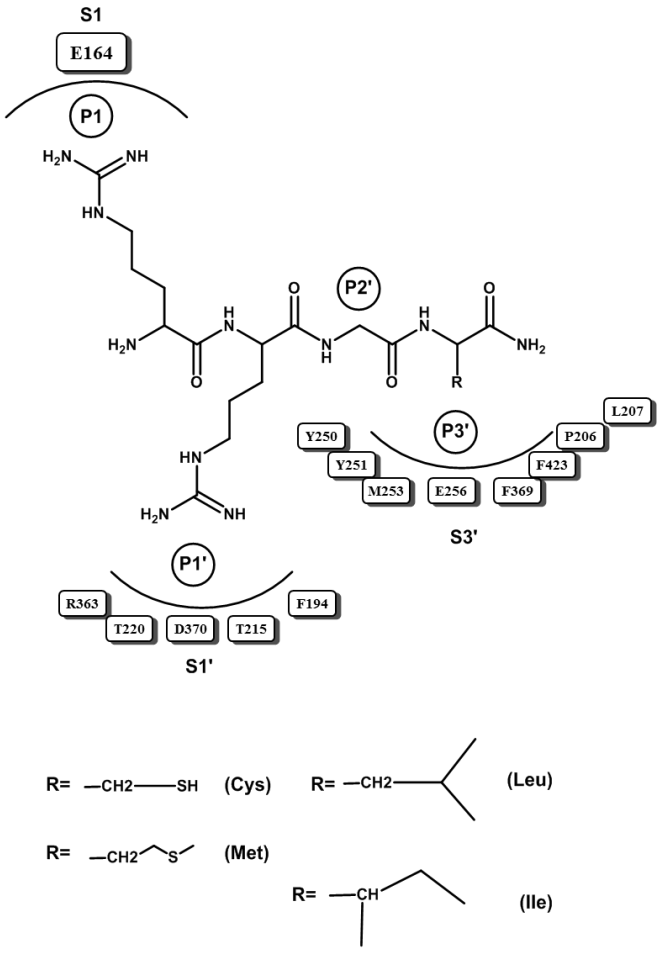

Figure 5-3: Binding pocket of BotNT/LC-A with critical binding pockets S1, S1', and S3' highlighted. Each of the peptides varies only in the last amino acid as such RRG(X) which corresponds to the S3' site. (Adapted with permission form reference [8])

§5.0.3 Molecular Foot-Print Based Rescoring Methodology:

In an attempt to identify new BotNT/LC-A inhibitors, a large-scale virtual screening of over one million commercially available compounds was performed and resulted in the purchase of compounds for subsequent experimental evaluation. Overall, high-throughput virtual screening provided a powerful and practical approach for the virtual screening of ligand libraries to identify new drug-like leads for BotNT/LC-A.

Traditionally, many screening programs such as DOCK[10], employ a simple two-term scoring function (score) consisting of intermolecular van der Waals and electrostatic terms to rank-order compatibility of ligands with a target. Complementary, a relatively new scoring function developed by the Rizzo laboratory, termed molecular footprint similarity (FPS) score[11], utilizes the standard DOCK energy score as a decomposition of the energy by per-residue contributions.

The FPS method was recently employed in the successful discovery of novel HIVgp41 inhibitors and FABP5 inhibitors.[12] As illustrated in **Figure 4-4**, the procedure can be used to identify which compounds are most energetically similar to a known reference. In this example, the van der Waals interaction pattern made by the natural substrate (red line) is compared with that of a candidate ligand (green line). The hypothesis is molecular footprints will enrich for active compounds (positives) by facilitating identification of compound making interaction signatures similar to known binders.

Specific goals of this research included: (1) Screen ca. one million compounds using a subset of the ZINC[13] database (ChemDiv vendor) of commercially available compounds to BotNT/LC-A to prioritize compounds for purchase. (2) Experimentally evaluate purchased compounds for *in vitro* analysis by means of a fluorescence SNAPtide assay to determine binding activity. (3) Determine the most promising compounds for further development.

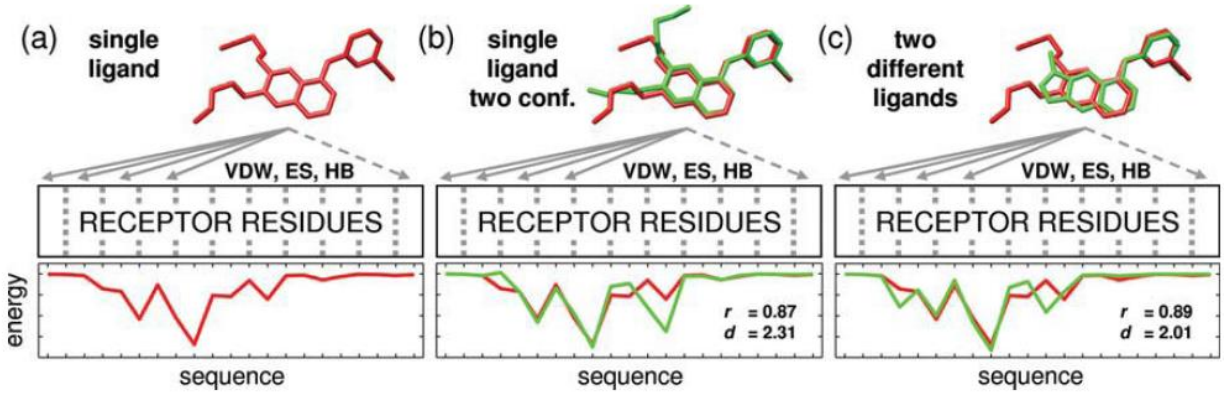

Figure 5-4: Use of a footprint similarity (FPS_{VDW}, FPS_{ES}) score to identify compounds in virtual screening. (a) Reference ligand (red). (b) Comparison between the reference (red) and candidate molecule (green) from the virtual screen. (Reprinted with permission for reference [11])

§5.1 Discovery of Novel BotNT/LC-A Inhibitors by High-Throughput Virtual Screening Utilizing FPS:

§5.1.1 Introduction:

Since the first crystallographic image of BotNT/LC-A, there has been several published co-crystal structures of BotNT/LC-A with various inhibitors shown in **Figure 5-5**.[8, 9, 14, 15] Thus eight (8) of the known crystal structures listed were structurally aligned (**Figure 5-6)** and a heat map matrix of favorable vs unfavorable interaction energies was calculated for each inhibitor by minimization in each receptor shown in **Figure 5-7**. Evident from this cross-minimization heat

maps, larger inhibitors sterically clashed with smaller receptor sites due to induced fit thus producing unfavorable VDW interactions (eg. inhibitor I1 from PDB 3DS9 in receptor from PDB 2ILP). Overall, the sum matrix (ES + VDW) for the ligand RRGC produced the best overall fit (7 out of 8 crystal structures), only producing unfavorable interactions in the receptor from PDB 3DS9. Thus, RRGC was selected as the reference ligand in our virtual screen.

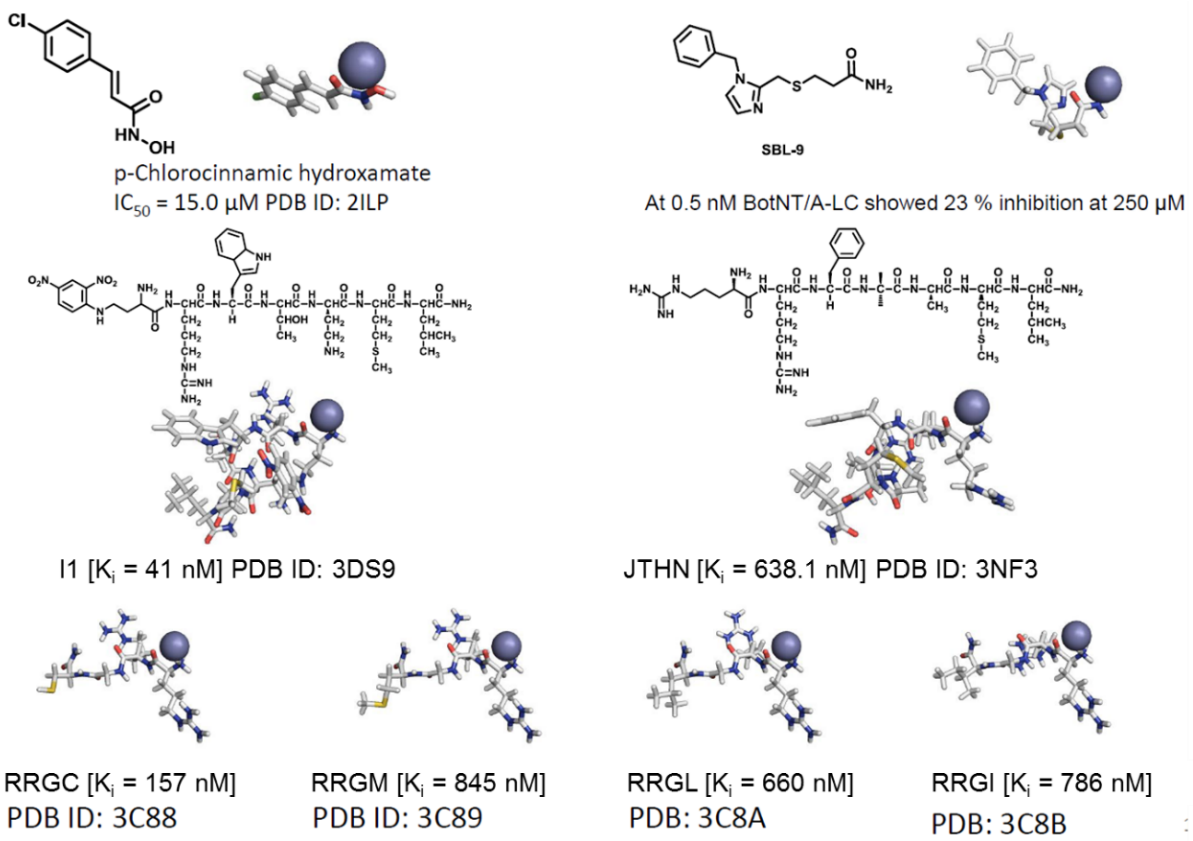

Figure 5-5: Various availible co-crystal structures of inhibitors in the binding pocket of BotNT/LC-A. Listed are the K_i values as well as PDB codes for each crystal structure.

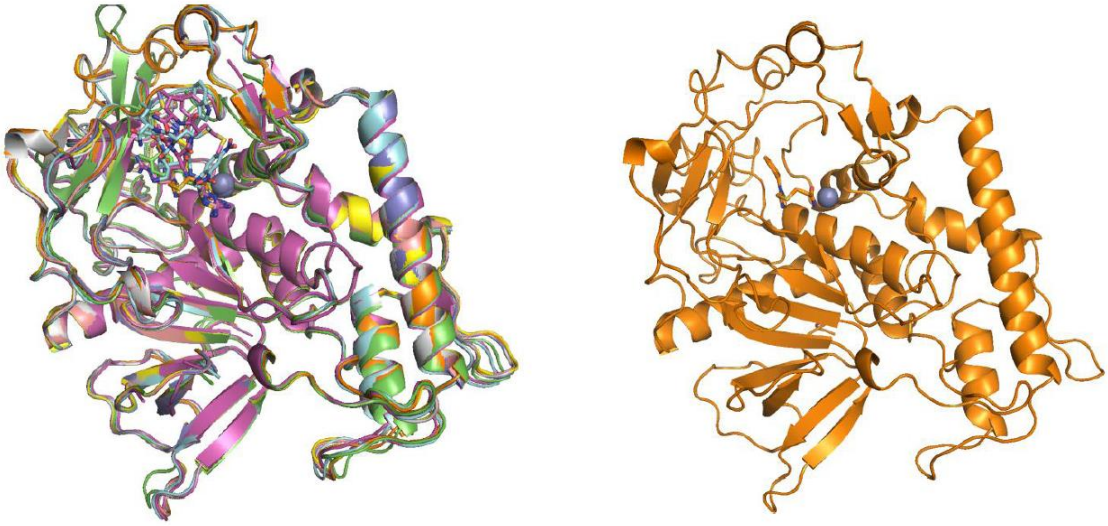

Figure 5-6: Overlay of the eight (8) availible co-crystal structures of BotNT/LC-A using the matchmaker program in Chimera (PDB: 2ILP, 1.90 Å)[14], BotNT/LC-A complexed with SBL-9, (PDB: 3D29, 1.76 Å)[16], (PDB: 3NF3, 2.40 Å)[15], (PDB: 3C88, 1.60 Å)[8], (PDB: 3C89, 1.58 Å)[8], (PDB: 3C8A, 1.52 Å)[8], (PDB: 3C8B, 1.47 Å)[8]. Visual conformation of the crystal structure overlays revealed a binding pocket with vastly different induced fits based on the size of the ligand.

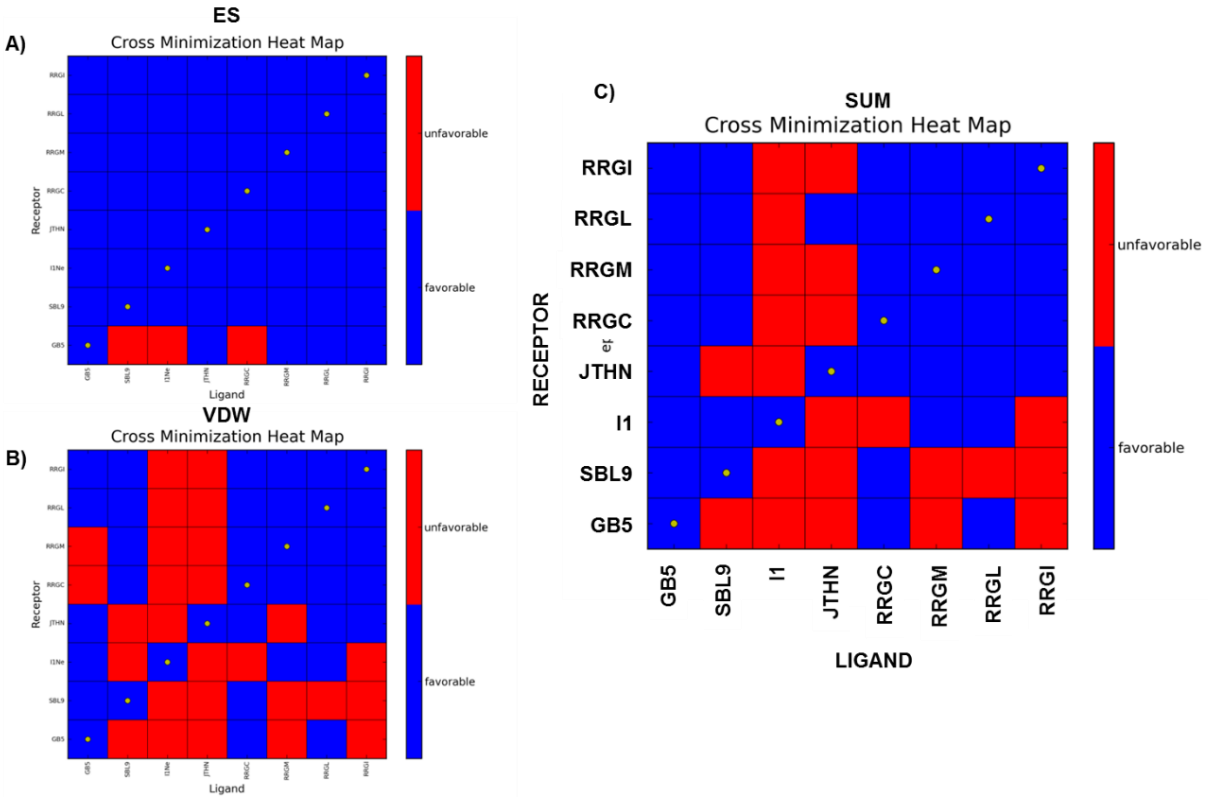

Figure 5-7: Cross minimization heat map matrixes of the eight (8) BotNT/LC-A structurally aligned co-crystal structures. Each of the eight (8) co-crystallized ligands was minimized in each of the eight (8) co-crystallized receptors. The diagonal squares dotted in yellow represents the native ligand/receptor complex which produced favorable interaction for each of the eight (8) complexes. A) ES Matrix showing that only the smaller GB5 (*p*-chlorocinnamic acid hydroxamate) receptor did not produce favorable interaction (red). B) VDW Matrix showing that small inhibitors like GB5, SBL9, RRGC, RRGM, RRGL, RRGI produced mostly favorable (blue) interactions in 5 or more of the receptors. Large inhibitors such as I1 and JTHN produced mostly unfavorable VDW interaction with all but there native receptors. C) The SUM (ES + VDW) matrix showing overall that RRGC produce the most favorable interactions with 7 out of 8 crystal structures used.

High-throughput virtual screening utilizing molecular footprints was conducted on BotNT/LC-A (PDB: 3C88, 1.60 Å resolution)[8] using tetrapeptide RRGC [K_i = 157 nM] as the reference molecule. This entailed: 1) grid setup and docking 2) minimization of each docked molecule and reference molecule on the receptor Cartesian coordinates, 3) calculating the molecular footprints of all docked molecules and reference, 4) calculation of a footprint similarity score (FPS) for each of the docked molecules versus the reference tetrapeptide RRGC, 5) MACCS fingerprint clustering, 6) rank-ordering based on each scoring criteria, 7) analysis and selection of compounds from each of the 250 cluster heads generated for each of the scoring criteria using visual inspection of binding poses and footprints. **Figure 5-8** summarizes the overall work flow.

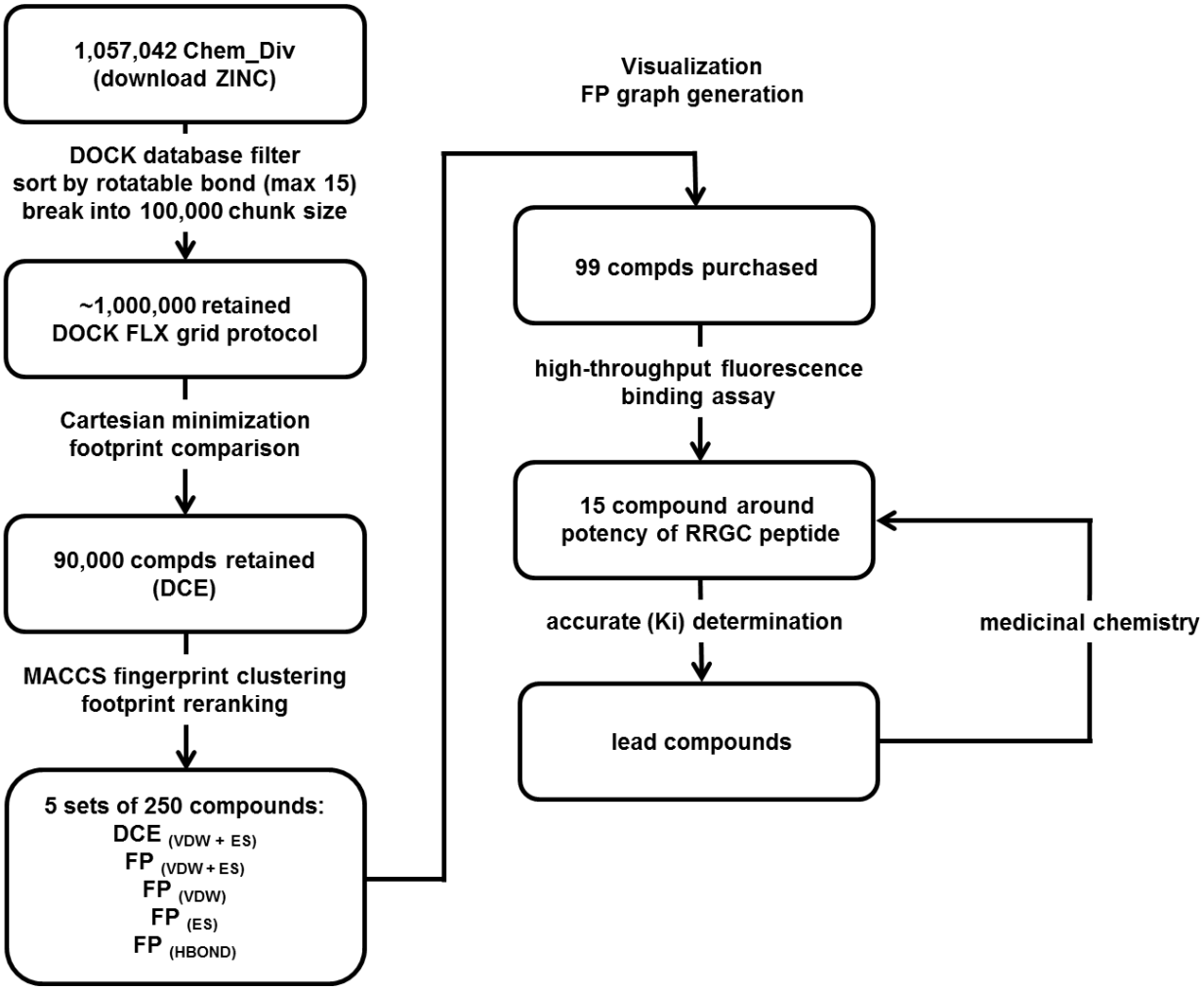

Figure 5-8: Flow chart describing the discovery of ligands through virtual screening, biological assay, and medicinal chemistry.

§5.1.2 Results and Discussion:

§5.1.2.1 Biological and Computational Evaluation of Selected Compounds:

As a result of the virtual screen of BotNT/LC-A, 99 compounds were ultimately selected, purchased, and assayed *in vitro* as shown in **Figure 5-9**.[17] Notably, out of 99 compounds tested 15 compounds exhibited inhibition greater than 10 μM, less than twice the IC_{50} value of RRGC (5.01 ±2.98 nM) shown in **Table 5-1**. Interestingly, there appeared to be no strong correlation between the biological data and the FPS score for the sixteen (16) hit compounds. This could be attributed to sensitivity of the assay since the selected compounds were all very similar in biological assay. Furthermore, six (6) compounds had activity within 1 nM from RRGC and one of these compounds (A8) based on the location in the 96 well plate was found to have better activity (4.67 ±3.50 nM) than RRGC shown in **Figure 5-10**. In the ES and VDW footprints shown in

Figure 5-11 of A8 (ZINC04095444) it can be seen that the VDW profile seems quite similar to RRGC while still maintain strong ES interaction with the Zinc ion and Asp370. This was a very promising result at the time and thus synthesis of A8 (ZINC04095444 or ChemDiv ID 4708-0019) later termed "SBL-11" was undertaken.

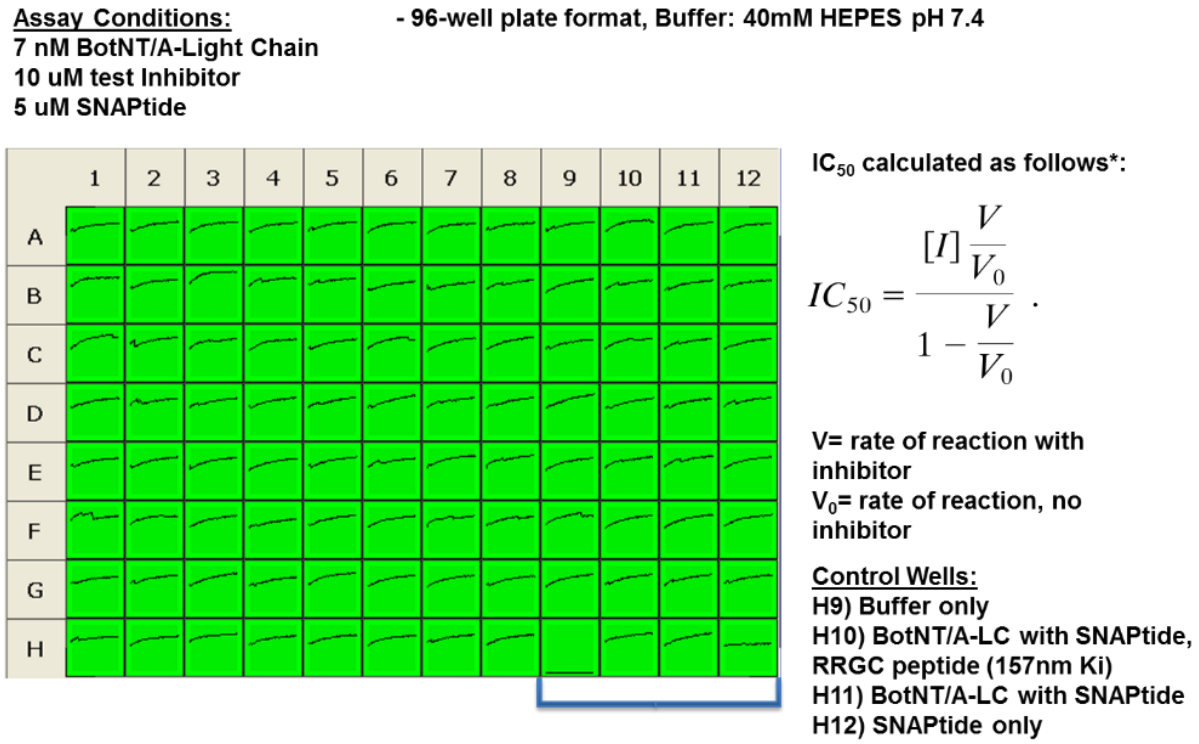

Figure 5-9: High throughput SNAPtide fluorescence assay. Performed by Dr. Eduard Melief. IC_{50} is calculated by the inhibition of catalytic activity of BotNT/LC-A on SNAPtide a substrate which is natively quenched by FRET. Upon cleavage of the substrate fluorescence increases. Thus inhibitors such as RRGC reduce the increase in fluorescence versus time (shown by a flatter line in each well shown above, such as the SNAPtide without BotNT/LC-A, H12). This was carried out at a fixed concentration of BotNT/LC-A (7 nM) a fixed amount of inhibitor (10 µM) and a fixed amount of SNAPtide (5 µM).

Table 5-1. Hit compounds discovered in the high-throughput SNAPtide fluorescence assay with their corresponding DOCK energy and FPS scores

Cell	ChemDiv[a]	ZINC[b]	DCE[c]	FPS[d] VDW+ ES	FPS[d] VDW	FPS[d] ES	N[e]	IC_{50} µM[f]
RRGC	N/A	N/A	N/A	N/A	N/A	N/A	5	5.01 ± 2.98
A8	4708-0019	ZINC04095444	-58.6	0.88	0.48	0.4	3	4.67 ± 3.50
C9	C667-0148	ZINC35349193	-71.2	0.82	0.33	0.49	3	5.05 ± 2.69
A12	5762-1843	ZINC20036308	-72.3	0.93	0.56	0.37	3	5.26 ± 4.57
B10	C087-0800	ZINC04193641	-68.2	0.97	0.41	0.56	3	5.35 ± 1.64
F12	F036-1267	ZINC32943222	-85.3	1.31	0.63	0.68	3	5.37 ± 2.40
G2	F460-1509	ZINC32985892	-61.4	0.88	0.47	0.41	3	5.68 ± 4.11
A6	3716-0255	ZINC27532878	-59.4	0.89	0.54	0.35	3	6.65 ± 3.88
F6	E616-1016	ZINC20531895	-74.2	0.83	0.33	0.5	3	7.00 ± 1.57
E12	E155-0261	ZINC16973392	-73.7	0.92	0.45	0.47	3	7.55 ± 2.98
F7	E645-0285	ZINC15679967	-62.9	0.89	0.42	0.47	3	7.64 ± 1.43
G10	G876-0612	ZINC17041570	-71.3	0.86	0.43	0.43	3	7.64 ± 5.25
D12	D154-0425	ZINC20058781	-60.7	0.9	0.45	0.45	3	8.17 ± 3.51
D11	D128-0108	ZINC17028115	-61.8	0.98	0.47	0.51	3	8.39 ± 5.67
B4	C083-0953	ZINC20107523	-89.8	1.08	0.61	0.47	3	8.68 ± 1.44
C12	C748-0300	ZINC49699099	-74.9	0.93	0.40	0.53	3	9.79 ± 11.49

[a]ChemDiv ID number. [b]ZINC database ID number. [c]DCE scores in kcal / mol. [d]FPS scores in unites of normalized Euclidian distance where 0 represents the best overlap. FPS_{VDW} and FP_{ES} scores range from (0,2] and FPS_{VDW+ES} range from (0,4]. [e]Number of times the assay was run. [f]IC_{50} based on the equation in **Figure 5-9**.

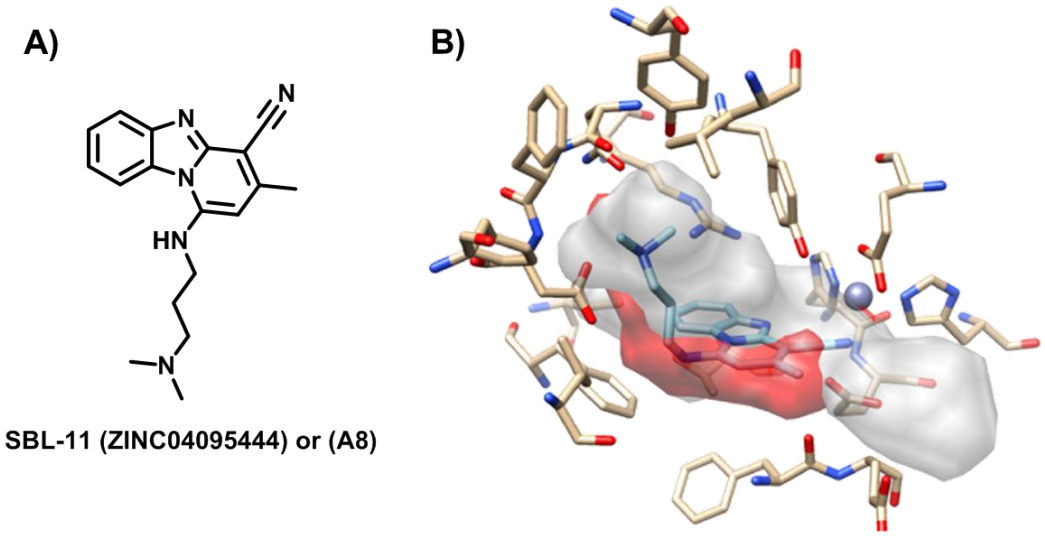

Figure 5-10: Hit compound SBL-11. A) 2D structure of SBL-11. B) Docked 3D structure of SBL-11 bound in the binding pocket of BotNT/LC-A. In gray, is the surface area occupied by the inhibitor RRGC. In red, is the surface area occupied by SBL-11. The cyano-group plays a role in interacting with the Zinc ion while the dimethyl-amino group, most likely protonated at physiological pH is shown interacting with a nearby Asp 370.

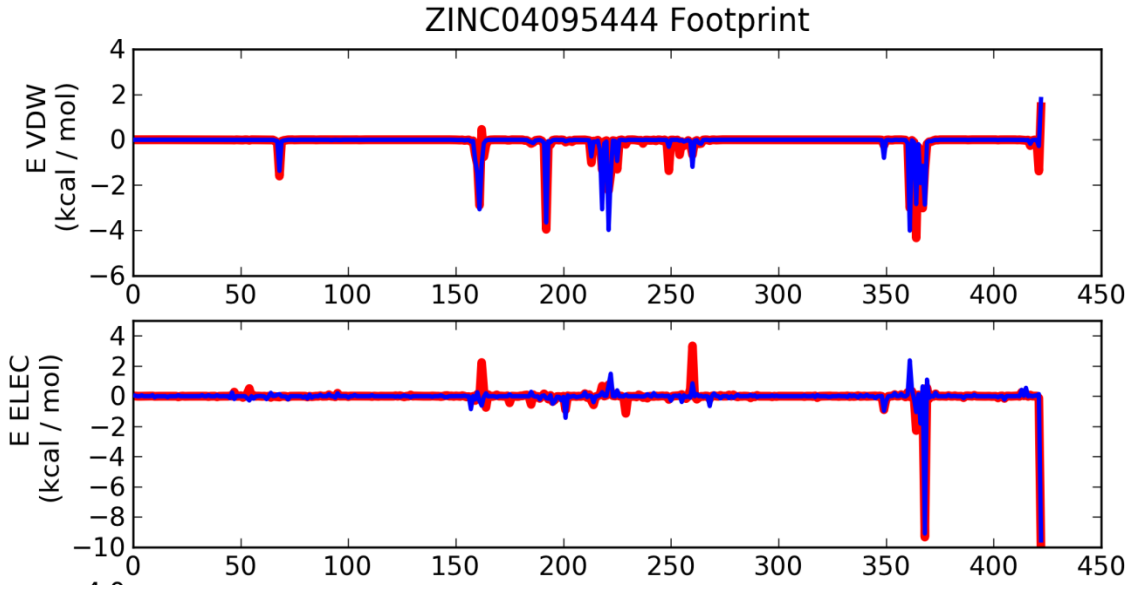

Figure 5-11: The VDW and ES footprint overlay of RRGC (red) and SBL-11 (blue) of the hit compound SBL-11. A significant VDW clash between the reference RRGC and Zinc ion can be seen in the VDW footprint. This steric clash is seen to be offset by the strong ES interactions at Zinc ion and nearby Asp370 in the ES footprint. Energetically DOCK selects ligands from the ChemDiv library that did not have unfavorable interaction, both VDW and ES. Intrinsically FPS selects inhibitors with good ES footprints while mitigating VDW clashing at the Zinc ion, the strongest ES interaction.

§5.1.2.2 Synthesis of SBL-11:

Based on both the virtual screening results and biological results from the high-throughput assay, it was decided that synthesis of SBL-11 **5-4** would be useful to provide further analysis (**Scheme 5-2**).[18, 19] Thus 2-Cyanobenzimidazole was subjugated to (1.1 equivalents) of ethylacetoacetate in the presence of (2.2 equivalents) ammonium acetate to perform a tandem amide condensation and Mannich type reaction to afford compound **5-1** in high yield. The amide was then converted to the aryl chloride using a Vilsmeier-Haack reaction with $POCl_3$ to afford compound **5-2** in high yield. Aryl substitution of the chlorine with 1,3-propanediamine,N,N'dimetyl (2 equivalents) proceeded well in the presence of TEA (4 equivalents) to afford the base for of SBL11 compound **5-3** in moderate yield. Lastly, the compound **5-3** was converted to the salt to improve water solubility with HCL in methanol to afford the SBL11 and an HCl salt **5-4**. After synthesis, compound **5-1**, **5-2**, **5-3**, and **5-4** were all subjugated to biological screening against BotNT/LC-A.

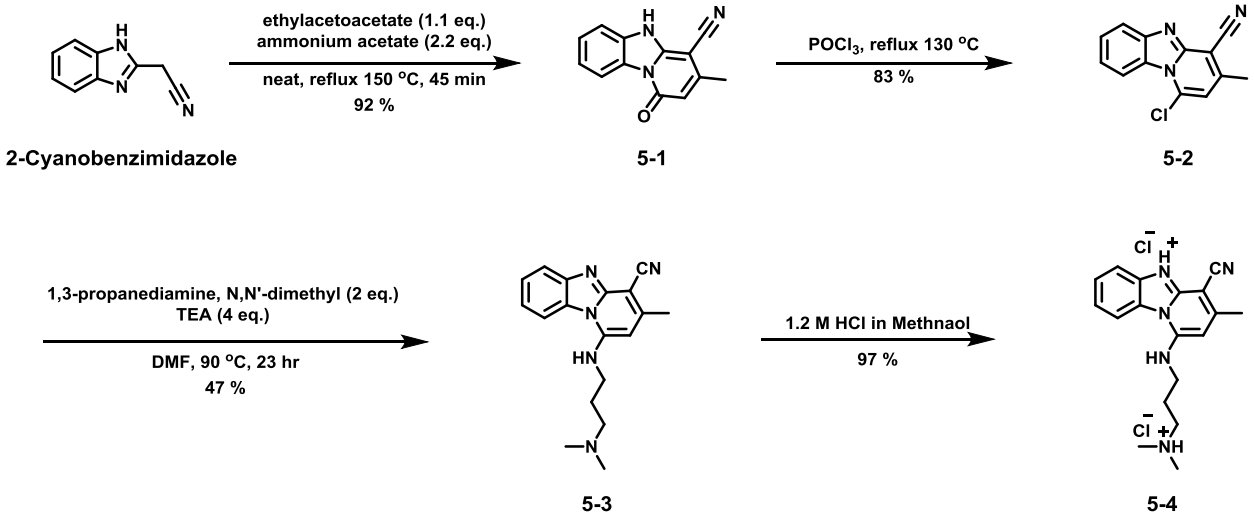

Scheme 5-2: Stepwise synthesis of SBL-11 **5-3** and corresponding HCL salt **5-4**

§5.1.2.3 Rescreening of Synthesized SBL11 and Various Intermediates:

Following the synthesis of SBL-11 **5-3** and the corresponding salt **5-4**, SBL-11 and various intermediates were retested to confirm validity of the assay and inhibitor. Unfortunately, reproducibility of the assay highly fluctuated, thus conformation of the first screening remained problematic even for the control RRGC. Due to assay issues, a modified version of the assay was evaluated which included the addition of zinc chloride, DTT, and increased quantity of BotNT/LC-A. This modified version of the assay reestablished consistency in the results. Unfortunately, the

assay values then shifted; in particular, the IC_{50} value for SBL-11 increased from 4.67 ± 3.50 to greater than 200 µM. This may have been due to the lack of Zinc added or could be due to the higher concentration of BotNT/LC-A used. In any case, the activity of SBL-11 vastly diminished. In hindsight, it is highly probable that SBL11 directly bound Zinc and did not possess good affinity to the binding pocket of BotNT/LC-A. Thus, the low concentration of Zinc in the initial assay screening better than expected results for some compounds. The full 99 compounds were then screening using modified assay conditions.

§5.1.2.4 Synthesis of 2,4-Dichlorocinnamic hydroxamate:

To evaluate our new improved *in vivo* assay conditions for screening compounds, a known compound 2,4-Dichlorocinnamic hydroxamate which has been shown to provide good inhibition of BotNT/LC-A (0.41 ± 0.03 µM) was synthesized for use as a control (**Scheme 5-3**). Starting from commercially available 2,4-Dichlorocinnamic acid, CDI coupling with hydroxylamine HCL afforded 2,4-Dichlorocinnamic hydroxamate acid **5-5** in moderate yield in one step.

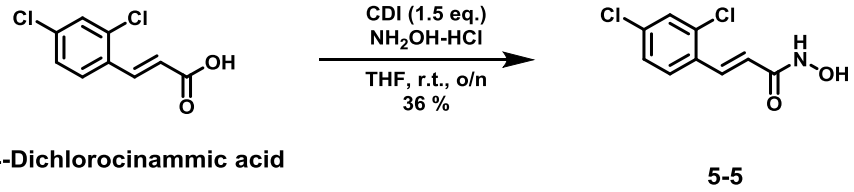

2,4-Dichlorocinammic acid **5-5**

Scheme 5-3: Synthesis of 2,4-Dichlorocinnamic hydroxamate **5-5**

§5.1.2.5 High-Throughput Biological Rescreening:

Following the synthesis of control **5-5** a high-throughput SNAPtide assay was used to rescreen to original library of 99 selected compounds for the virtual screening. This screening was carried out with a substantial increase in protein concentration (100 nM), the addition of 0.15 mM $ZnCl_2$, and the addition of 1.25 mM DTT. The quantity of SNAPtide remained the same at 5µM. As shown in **Table 5-2**, the compound that were found to have the best activity did not match the original screening except for one compound ChemDiv 5762-1843. Previously this compound had activity similar to RRGC and that was reflected in the rescreen. An addition to the new biological ranking, FPS data now trends based on the FPS_{ES}. Based on the IC_{50} values thus obtained from the modified biological screening compounds with an FPS_{ES} scores of less than 0.40 appear to have better activity shown in **Figure 5-12**. Compounds with FPS_{ES} scores greater than 0.40 appear to be more correlated with FPS_{VDW+ES} indicative that the poorer ES comparison makes the VDW effects more substantial.

Table 5-2. Hit compounds rescreened with a modified high-throughput SNAPtide fluorescence assay with their corresponding DOCK energy and FPS scores							
ChemDiv[a]	**Zinc ID[b] / ID**	**DCE[c]**	**FPS[d] VDW+ES**	**FPS[d] VDW**	**FPS[d] ES**	**N[e]**	**IC_{50} µM[f]**
N/A	RRGC	N/A	N/A	N/A	N/A	3	31 ± 14
N/A	5-5	N/A	N/A	N/A	N/A	3	4 ± 0.5
5762-1843	ZINC20036308	-72.3	0.93	0.56	0.37	3	22 ± 2
E843-1064	ZINC21873993	-61.9	1.01	0.71	0.30	3	24 ± 3
3260-0301	ZINC00305216	-61.4	0.92	0.52	0.40	3	55 ± 5
C087-0323	ZINC03662371	-70.0	0.93	0.56	0.37	3	92 ± 5
K786-5716	ZINC20687251	-72.0	0.88	0.45	0.43	3	154 ± 7
C257-0105	ZINC04894271	-62.5	0.86	0.39	0.47	3	157 ± 57
D406-0398	ZINC12112516	-69.0	0.92	0.41	0.51	3	159 ±16
[a]ChemDiv ID number. [b]ZINC database ID number. [c]DCE scores in kcal / mol. [d]FPS scores in unites of normalized Euclidian distance where 0 represents the best overlap. FPS_{VDW} and FP_{ES} scores range from (0,2] and FPS_{VDW+ES} range from (0,4]. [e]Number of times the assay was run. [f]IC_{50} based on the equation in **Figure 5-9**.							

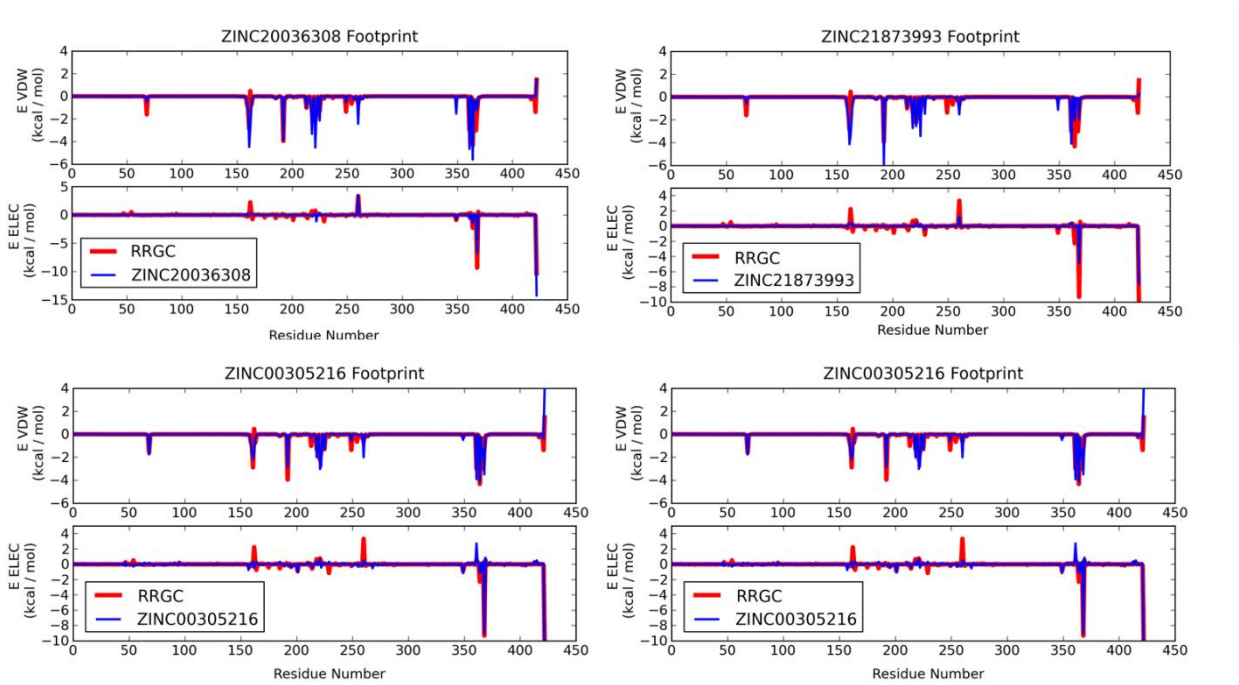

Figure 5-12: The VDW and ES footprint overlay of RRGC (red) and the four (4) best hit compounds from the rescreening (blue).

§5.1.2.6 Cell-Based Assay with Hit Compounds:

Based on the new rescreening, two of the best library compounds ChemDiv E843-1064 and ChemDiv 5762-1843 **(Figure 5-13)** and compound 2,4-dichlorocinnamic hydroxamic acid **5-5** were screened in Neuro-2a cells inoculated with BotNT/LC-A shown in **Figure 5-14** and **Figure**

5-15.[17] Compounds ChemDiv 5762-1843 and ChemDiv E843-1064 were screened and shown to have graded inhibition at 10 µM *in vivo*. Specifically, 10 µM of each of these compounds inhibited the quantity of cleaved SNAP25 *in vivo* after BotNT/LC-A was transfected into the cells. Both of these compounds were not cytotoxic at the concentrations used. *In vivo* testing is ongoing. Additionally, similar to results obtained by Eubanks et al., in our hands 2,4-dichlorocinnamic hydroxamic acid **5-5** was cytotoxic to Neuro-2a cells at concentrations ≥ 5 µM. Thus despite the good *in vitro* activity of 2,4-dichlorocinnamic hydroxamic acid **5-5**, hydroxamates provided to be poor inhibitors *in vivo* due to their inherent cytotoxicity.

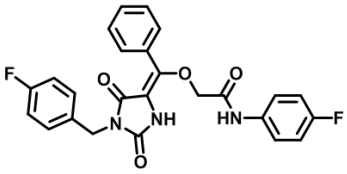

ChemDiv ID 5762-1843

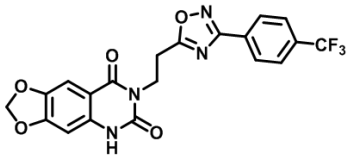

ChemDiv ID E843-1064

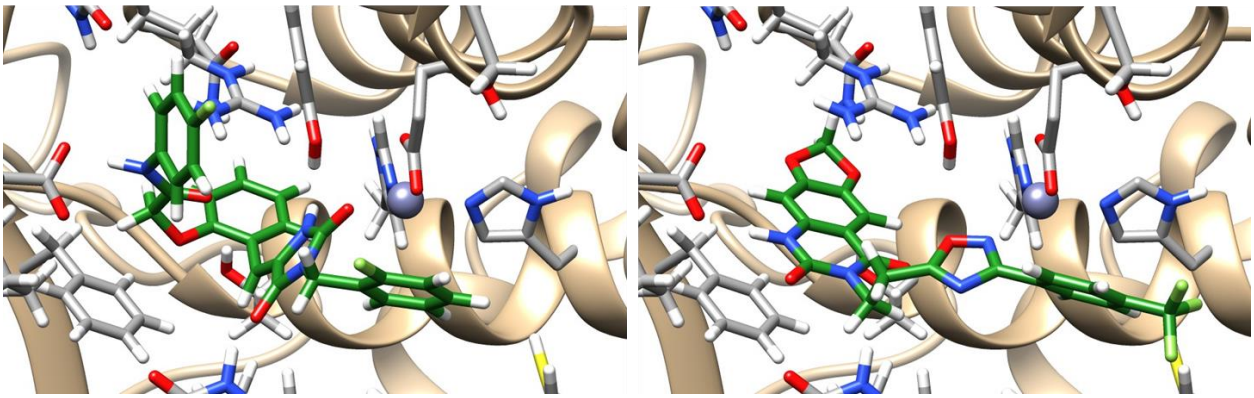

Figure 5-13: 2D chemical structure and 3D docked structures of hit compounds ChemDiv ID 3762-1843 and ChemDiv ID E843-1064. Each of these hit compounds shows interaction with the Zinc ion and also Asp 370. In the case of ChemDiv ID 3762-1843, the coordination group is the urea. In the case of ChemDiv ID E843-1064, the coordination group is the 1,2,4-oxadiazole.

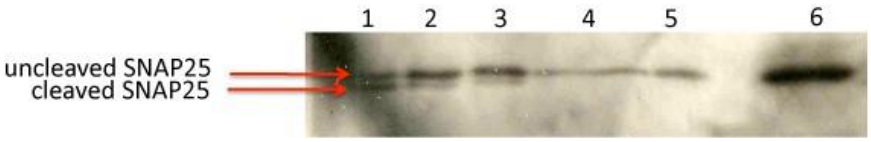

Figure 5-14: Western blot analysis of the inhibition of SNAP-25 cleavage by BotNT/LC-A *in vivo* in Neuro-2a cells by inhibitor ChemDiv E843-1064. 1) no inhibitor; 2) 10 µM E843-1064; 3) 20 µM E843-1064; 4) 50 µM E843-1064; 5) 100 µM E843-1064; 6) SNAP25 marker. Assay Performed by Dr. Natasha Nesbitt.

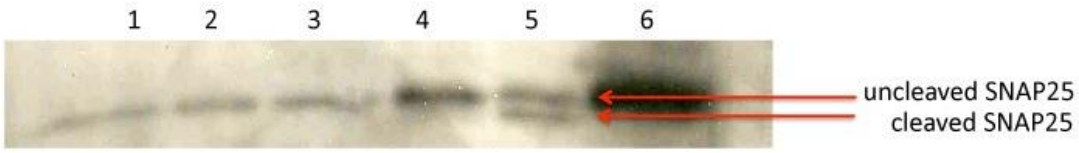

Figure 5-15: Western blot analysis of the inhibition of SNAP-25 cleavage by BotNT/LC-A *in vivo* in Neuro-2a cells by inhibitor ChemDiv 5762-1943. 1) 10 µM 5762-1943; 2) 20 µM 5762-1943; 3) 50 µM 5762-1943; 4) 100 µM 5762-1943; 5) no inhibitor; 6) SNAP25 marker. Assay Performed by Dr. Natasha Nesbitt.

§5.2 Conclusion:

In conclusion, two promising lead compounds ChemDiv 5762-1943 and E843-1064 from a high-throughput virtual screening implementing FPS were selected, purchased, and screened against BotNT/LC-A providing IC_{50} values better than the reference molecule RRGC. Although the high-throughput SNAPtide assay remained problematic, newer modification to the assay have led to the discovery of the two inhibitors ChemDiv 5762-1943 and E843-1064. Satisfyingly, after struggling with *in vitro* work for quite some time, the two library compounds ChemDiv 5762-1943 and E843-1064 originally selected as part of a list of 99 selected by virtual screening have yielded to be active *in vivo* in Neuro-2a cells against BotNT/LC-A at concentrations as low as (10 µM). Ultimately, this result is of significance as other highly potent inhibitors currently used such as 2,4-dichlorocinnamic hydroxamic acid, are cytotoxic to cells, and would provide poor *in vivo* candidates.

§5.3 Experimental Procedures:

§5.3.1 Computation Virtual Screening Utilizing FPS:

High-Throughput Virtual Screening:

A high-throughput virtual screening of over one million molecules from the ChemDiv subset of the ZINC database (http://zinc.docking.org) was conducted on New York Blue, an 18 rack IBM Blue Gene/L massively parallel supercomputer located at Brookhaven National Laboratory using DOCK version 6.5.[20] Prior to docking, the most updated ChemDiv database was downloaded and presorted by rotatable bonds and split into 10 subsets of ~100,000 molecules using the DOCK database filter. Subsequently, an energy grid for BotNT/LC-A (PDB : 3C88) was generated using the grid program.[21] Then, each molecule was flexibly docked to the BotNT/CL-A grid (DOCK FLX protocol)[22] and the single lowest-energy pose was retained.

Footprint-Based Rescoring:

Following high-throughput virtual screening, the footprint-based rescoring methodology reported by Balius et al[23] was implemented to enrich the library of docked molecules. First, the co-crystalized ligand RRGC (reference) was minimized on the BotNT/LC-A Cartesian coordinates within the binding pocket. This was implemented using both a hydrogen optimization followed by a weak restrained minimization (restraint of 10 kcal / mol). Following reference minimization, each molecule of the docked library was subsequently minimized in Cartesian space using the restrained minimization protocol. Last, electrostatic, van der Waals, and hydrogen bond footprint similarity scores were computed using normalized Euclidian distance for each molecule docked versus the reference using DOCK 6.5.

Database Clustering and Compound Selection:

First, subsets 1 through 5 and subset 6 through 10 containing ~ 500,000 molecules were rank-ordered by the DOCK Cartesian energy (DCE) score. The top 45,000 of each combined subset of 500,000 molecules (~ 10% total 90,000 molecules) were then clustered using MACCS fingerprints, as implemented in the program MOE[24] with the Tanimoto coefficient of 0.75. The resulting cluster heads obtained were then further rank-ordered by: (i) standard DOCK score (DCE $_{VDW + ES}$), (ii) van der Waals footprint similarity score (FPS $_{VDW}$), (iii) electrostatic footprint similarity score (FPS $_{ES}$), (iv) H-bond footprint similarity score (FPS $_{HB}$), (v) the sum of van der Waals and electrostatic footprint similarity score (FPS $_{VDW + ES}$). The top 250 molecules rank-ordered by each criteria were then plotted in MathPlotLib[25] and examined by visual inspection and consistency to the reference footprint. This method of analysis allowed us to both visually see key interactions within the binding pocket while simultaneously observing the magnitudes of those key interactions within the footprints for each molecule. Based on this approach, 99 compounds were selected a purchased for biological testing against BotNT/LC-A.

§5.3.2 Chemical Synthesis:

General Methods: ^{1}H NMR and ^{13}C NMR spectra were measured on a Varian 300, 400, 500, or 600 MHz NMR spectrometer. High-resolution mass spectrometric analyses were conducted at the Mass Spectrometry Laboratory, University of Illinois at Urbana-Champaign, IL. TLC analyses were performed on Merck DC-alufolien with Kieselgel 60F-254 and were visualized with UV light

and stained with sulfuric acid-EtOH, 10 % PMA-EtOH or 10 % Vanillin-EtOH with 1% sulfuric acid. Column chromatography was carried out on silica gel 60 (Merck; 230-400 mesh ASTM). HPLC Purity was determined by Shamazu HPLC employing a Phenomenex Kinetex™ 2.6 μm PFP 100 Å, LC Column 30 x 4.6 mm (CH_3CN/H_2O = 60/40 gradient to 95/5 over 45 min, flow rate at 1 mL/min, UV 254 nm.

Materials: The chemicals were purchased from Sigma-Aldrich Company, Fischer Company or VWR Company. DCM and methanol were dried before use by distillation over calcium hydride under nitrogen. Ether and THF were dried before use by distillation over sodium-benzophenone kept under nitrogen. Dry DMF and DMSO were purchased from Sigma-Aldrich chemical company, and used without further purification. Reaction flasks were dried in a 100 ^oC oven and allowed to cool to room temperature in a desiccator over "*Drierite*" (calcium sulfate) and assembled under an inert nitrogen gas atmosphere.

3-Methyl-1-oxo-1,5-dihydropyrido[1,2-a]benzimidazole-4-carbonitrile (5-1):[19]

To a 5 mL round bottomed flask was added (1.000 g, 6.36 mmol) of 1H-benzimidazole-2-acetonitrile, (1 mL, 7.00 mmol) of ethylacetoacetate, and (1.079 g, 14.00 mmol) of ammonium acetate. The resulting solution was heated to 140 ^oC for 45 minutes until the solution became dry. The resulting solid was cooled to room temperature. Then to this solid was added 20 mL of (50:50) diethyl ether / ethanol and the resulting slurry was filtered without further purification to afford **5-1** (1.312 g, 92 %) a white solid: ^1H NMR (500 MHz, DMSO-d_6) δ 2.33 (s, 3 H), 5.90 (s, 1 H), 7.32 (t, J = 7.5 Hz, 1H), 7.50 (t, J = 7.5 Hz, 2 H), 8.52 (t, J = 7.5 Hz, 1H); HRMS (ESI) *m/e* calculated for $C_{13}H_{10}N_3OH^+$: 224.0824. Found: 224.0824 (Δ = 0.0 ppm). Data are consistent with the literature values.[19]

1-Chloro-3-methyl-benzo[4,5]imidazole[1,2-a]pyridine-4-carbonitrile (5-2):[19]

To a 25 mL round bottomed flask added (500 mg, 2.24 mmol) of compound **5-1** and 6.7 mL of $POCl_3$. To resulting solution was refluxed for 2 hours. After completion the solution was cooled to room temperature. The remaining $POCl_3$ was carefully distilled under vacuum. Then the resulting slurry was quenched with 20 mL of $NaHCO_3$. The resulting yellow solid was collected and filtered with 100 mL distilled water without further purification to afford **5-2** (450 mg, 83 %) a yellow solid: HRMS (ESI) *m/e* calculated for $C_{13}H_9N_3ClH^+$: 242.0497. Found: 242.0485 (Δ = 5.0 ppm). Data are consistent with the literature values.[19]

1-(3-Dimethylaminopropylamino)-3-methyl benzol[4,5]imidazole[1,2-a]pyridine-4-carbonitrile (5-3):[26]

To a 10 mL round bottomed flask added (200 mg, 0.83 mmol) of compound **5-2** and 2.5 mL of DMF. Then added (0.46 mL, 3.32 mmol) and (0.21 mL, 1.66 mmol) of 1,3-propaneodiamine,NN'dimethyl and heated the reaction to 90 ºC for 23 hours. The resulting off white solid was collected and filtered hot and washed with 100 mL DMF then 100 mL ethyl acetate and collected without further purification to afford **5-3** (120 mg, 47 %), of an off white solid: ^{1}H NMR (300 MHz, $CDCl_3$) δ 1.73 (s, 3 H), 1.98-2.05 (m, 2 H), 2.38 (s, 6 H), 2.52 (s, 3 H), 2.65-2.68 (m, 2 H), 3.47-3.52 (m, 2 H), 5.62 (s, 1 H), 7.24 (t, *J* = 7.2 Hz, 1H), 7.49 (t, *J* = 8.1 Hz, 1 H), 7.94 (d, *J* = 7.8 Hz, 1H), 8.10 (d, *J* = 8.1 Hz, 1H), 8.71 (br, 1 H); HRMS (ESI) *m/e* calculated for $C_{18}H_{22}N_5H^+$: 308.1884. Found: 308.1875 (Δ = 0.9 ppm). Data are consistent with the literature values.[26]

1-(3-Dimethylaminopropylamino)-3-methyl benzol[4,5]imidazole[1,2-a]pyridine-4-carbonitrile HCl Salt (5-4):[26]

To a 25 mL round bottomed flask added (50 mg, 0.1627 mmol) of compound **5-3** and 9 mL of methanol. To this solution was added 0.5 mL of 1.2 M HCl in methanol. The solution was allowed to stir for 1 hour and then was concentrated *in vacuo* to afford **5-4** as a white solid: ^{1}H NMR (300 MHz, DMSO-d_6) δ 1.42 (t, *J* = 7.2 Hz, 3 H), 1.78 (s, 6 H), 1.90 (s, 3 H), 2.02 (d, *J* = 4.5 Hz, 6 H), 6.08 (s, 1 H), 6.79 (t, *J* = 7.8 Hz, 1H), 6.97 (t, *J* = 7.5 Hz, 2 H), 7.08 (d, *J* = 8.7 Hz, 1H), 7.53 (s, 1 H), 8.11 (d, *J* = 8.1 Hz, 1 H), 10.18 (br, 1 H).[26]

2,4-Dichlorocinammic hydroxamate (5-5):[27]

To a 50 mL round bottomed flask added (1.000 g, 4.61 mmol) of 2,4-dichlorocinammic acid and 8 mL of THF. While stirring added (1.121 g, 6.92 mmol) CDI. Stirred this reaction mixture for 1 hour then added (640 mg, 9.22 mmol) of hydroxylamine HCL salt and stirred overnight. After completion 50 mL of potassium hydrogen carbonate was added and the resulting mixture was extracted (2 x 100 mL) with ethyl acetate. The organic layers were collected and dried with $MgSO_4$ and concentrated *in vacuo* to afford (400 mg, 36 %) **5-5**, as a white solid: ^{1}H NMR (300 MHz, DMSO-d_6) δ 6.52 (d, *J* = 15.9, 1 H), 7.48 (d, *J* = 8.1, 1 H), 7.70-7.73 (m, 3 H), 9.18 (br, 1 H), 10.90 (br, 1 H). Data are consistent with the literature values.[27]

§5.3.3 Biological Assays:

Materials: BotNT/LC-A truncated 1-425 was provided by Dr. Swaminathan at Brookhaven National Laboratory, Upton, NY. RRGC was provided by Dr. Swaminathan at Brookhaven National Laboratory, Upton, NY. Microtest 96-well Assay Plates, Optilux (BD Biosciences, Franklin Lakes, NJ). FLUOstar OPTIMA spectrofluorometer at 460 excitation and 544 nm emission. SNAPtide (list, Biological Laboratories, Inc., Campbell, CA). Primary antibody, anti-SNAP-25 mouse monoclonal IgG1 (200 µg/ml; Santa Cruz Biotechnology, Santa Cruz, CA). Secondary antibody, goat anti-mouse HRP conjugated (10 µg/ml; Pierce, Rockford, IL)

Initial high-thoughput assay conditions:[17]

The activity of BotNT/LC-A was measured in 96 well plates by the use of a Spex Fluorolog 3-21 spectrofluorometer at 460 excitation and 544 nm emission performed by Dr. Eduard Melief. Stock solutions of inhibitors were prepared at 10 mM with DMSO. Assays contained 40 mM Hepes (pH 7.4) buffer, 7 nM of enzyme, and varying concentrations of inhibitor in a final volume of 100 µL. Assay mixtures were preincubated for 5 minutes at 23 ^{o}C and were initiated by the addition of 5 µM SNAPtide. Initial rates were measured from the linear region of each assay, 100 to 300 s. IC_{50} values were determined by the equation in **Figure 5-9**, where [I] is the concentration of inhibitor V_o is the initial rate in the absence of inhibitor, and V is the initial rate in the presence of inhibitor.

Modified high-thoughput assay conditions:

The activity of BotNT/LC-A was measured in 96 well plates by the use of a Spex Fluorolog 3-21 spectrofluorometer at 460 excitation and 544 nm emission performed by Dr. Natasha Nesbitt. Stock solutions of inhibitors were prepared at 10 mM with DMSO. Assays contained 40 mM Hepes (pH 7.4) buffer, 100 nM of enzyme, 0.15 mM $ZnCl_2$, 1.25 mM DTT, and varying concentrations of inhibitor in a final volume of 100 µL. Assay mixtures were preincubated for 5 minutes at 27.3 ^{o}C and were initiated by the addition of 5 µM SNAPtide. Initial rates were measured from the linear region of each assay, 100 to 300 s. IC_{50} values were determined by the equation in **Figure 5-9**, where [I] is the concentration of inhibitor V_o is the initial rate in the absence of inhibitor, and V is the intial rate in the presence of inhibitor.

Cell-Based Assay in Neuro-2a Cells:[17]

Protection of SNAP-25 by ChemDiv compounds performed by Dr. Natasha Nesbitt. Neuro-2a cells (~5 x 10^5) were incubated with 1 μg of full length BoNT/A and various concentrations of inhibitors for 48 hours in Eagle's minimum essential medium with salt containing 2 mM L-glutamine, 1.5 g / L sodium bicarbonate, 0.1 mM nonessential amino acids, 1.0 mM sodium pyruvate, without FBS at 37 ^oC in an atmosphere of 5 % CO_2 and 95 % air. Cells were harvested and proteins were separated by SDS-PAGE using a 12.5% gel. Proteins were transferred onto a nitrocellulose membrane that was blocked with milk followed by treatment with 1:1000 dilution of SNAP-25 mouse monoclonal antibody and subsequent treatment with 1:2000 dilution of goat anti-mouse HRP. The membrane was treated with West Dura Chemiluminescent Substrate (Pierce) and exposed to x-ray film.

§5.4 References:

1. Schiavo, G.; Rossetto, O.; Montecucco, C., Clostridial neurtoxins as tools to investigate the molecular events of neurotransmitter release. *Semin. Cell Biol.* **1994,** *5*, 221 - 229.
2. Dasgupta, B. R.; Rasmussen, S., Purification and amino acid composition of type E botulinum neurotoxin. *Toxicon* **1983,** *21*, 535 - 545.
3. Sathyamurthy, V.; Dasgupta, B. R., Seperation, purification, partial characterizaiton and comparison of the heavy and light chains of botulinum neurtoxin types A, B and E. *J. Biol. Chem.* **1985,** *260*, 10461 - 10466.
4. Franz, D. R.; Jahrling, P. B.; Friedlander, D. J.; McClain, D. L.; Hoover, W. R.; Byrne, J. A.; Pavlin, G. W.; Christopher, G. W.; Eitzen, E. M. J., Clinical recongnition and management of patients exposed to biological warfare agents. *JAMA* **1997,** *278*, 399 - 411.
5. http://www.kennislink.nl/publicaties/werking-botox-ontrafeld (accessed, 11-18-13),
6. Rowland, L. P., Stroke, spasticiity, and botulinum toxin. *N. Engl. J. Med.* **2002,** *347*, 382 - 383.
7. Swaminathan, S.; Eswaramoorthy, S., Structural analysis of the catalytic and binding sites of Clostridium botulinum neurotoxin B. *Nat. Struc. Biol.* **2000,** *7*, 639 - 699.
8. Kumaran, D.; Rawat, R.; Ludivico, M. L.; Ahmed, S. A.; Swaminathan, S., Structure- and Substrate-based Inhibitor Design for *Clostridium botulinum* Neurotoxin Serotype A. *J. Biol. Chem.* **2008,** *283*, 18883 - 18891.
9. Zuniga, J. E.; Schmidt, J. J.; Fenn, T.; Burnett, J. C.; Arac, D.; Gussio, R.; Stafford, R. G.; Badie, S. S.; Bavari, S.; Brunger, A. T., A Potent Peptidomimetic Inhibitor of Botulinum Neurotoxin Serotype A Has a Very Different Conformation than SNAP-25 Substrate. *Structure* **2008,** *16*, 1588 - 1597.
10. *DOCK 6.5*, University of California at San Francisco: San Francisco, CA, 2011.

11. Balius, T. E.; Mukherjee, S.; Rizzo, R. C., Implementation and evaluation of a docking-rescoring method using molecular footprint comparisons. *J Comput Chem* **2011**, 32, 2273 - 2289.
12. Holden, P. M.; Kaur, H.; Gochin, M.; Rizzo, R. C., Footprint-based identification of HIVgp41 inhibitors. *Bioorg. Med. Chem. Lett.* **2012,** *ss*, 3011 - 3016.
13. Irwin, J. J.; Shoichet, B. K., ZINC - A Free Database of Commercially Available Compounds for Virtual Screening. *J. Chem. Inf. Model.* **2005,** *45*, 177 - 182.
14. Silvaggi, N. R.; Boldt, G. E.; Hixon, M. S.; Kennedy, J. P.; Tzipori, S.; Janda, K. D.; Allen, K. N., Structures of Clostridium botulinum neurotoxin serotype A light chain complexed with small-molecule inhibitors highlight active-sit flexibility. *Chem. Biol.* **2007,** *14*, 533 - 542.
15. Zuniga, J. E.; Hammill, J. T.; Drory, O.; Nuss, J. E.; Burnett, J. C.; Gussio, R.; Wipf, P.; Bavari, S.; Brunger, A. T., Iterative structure-based peptide-like inhibitor design against the botulinum neurotoxin serotype A. *Plos One* **2010,** *5*, e11378 - e11378.
16. Hines, J.; Groll, M.; Fahnestock, M.; Crews, C. M., Proteasome Inhibition by Fellutamide B Induces Nerve Growth Factor Synthesis. *Chemistry & biology* **2008,** *15*, 501-512.
17. Eubanks, L. M.; Hixon, M. S.; W.;, J.; Hong, S.; Clancy, C. M.; Tepp, W. H.; Baldwin, M. R.; Malizio, C. J.; Goodnough, M. C.; Barbieri, J. T.; Johnson, E. A.; Boger, D. L.; Dickerson, T. J.; Janda, K. D., An in vitro and in vivo disconnect uncovered through high-thoughput identification of botulinum nerotoxin A antagonists. *PNAS* **2007,** *104*, 2602 - 2607.
18. Ndakala, A. J.; Gressner, R. K.; Gitari, P. W.; October, N.; White, K. L.; Hudson, A.; Fakorede, F.; Shackleford, D. M.; Kaiser, M.; Yeates, C.; Charman, S. A.; Chibale, K., Antimalarial Pyrido[1,2-a]benzimidazoles. *J. Med. Chem* **2011,** *54*, 4581 - 4589.
19. Rida, S. M.; Soliman, F. S. G.; Badawey, E. S.-A. M.; Kappe, T., Benzimidazole condensed ring systems. 1. Synthesis and biological investigations of some substituted pyrido[1,2-a]benzimidazoles. *J. Heterocycl. Chem* **1988,** *25*.
20. DOCK6.5, University of California at San Francisco: San Francisco, CA, 2011.
21. Kuntz, I. D.; Blaney, J. M.; Oatley, S. J.; Langridge, R.; Femin, T. E., A geometric approach to macromolecule-ligand interactions. *Journal of Molecular Biology* **1982,** *161*, 269 - 288.
22. Mukherjee, S.; Balius, T. E.; Rizzo, R. C., Docking Validation Resources: Protein Family and LIgand Flexibility Experiments. *Journal of Chemical Information and Modeling* **2010,** *50*, 1986 - 2000.
23. Balius, T. E.; Mukherjee, S.; Rizzo, R. C., Implementation and evaluation of a docking-rescoring method using molecular footprint comparisons. *Journal of computational chemistry* **2011,** *32*, 2273 - 2289.
24. *Molecular Operating Environment (MOE)*, Chemical Computing Group Inc.: 1010 Sherbooke St. West, Suite #910, Montreal, QC, Canada, H3A 2R7, 2011.

25. Hunter, J. D., Matplotlib: A 2D Graphics Environment. *Computing in Science & Engineering* **2007,** *9*, 90 - 95.
26. ChemDiv Screening Collection. In *ChemDiv Catalog* ChemDiv2012.
27. Boldt, G. E.; Kennedy, J. P.; Janda, K. D., Identificaiton of a Potent Botulinum Neurotoxin A Protease Inhibitor Using in Situ Lead Identificaiton Chemistry. *Org. Lett.* **2006,** *8*, 1729 - 1732.

Chapter 6

Targeting Fatty Acid Binding Protein (FABP) Anandamide Transport – A Novel Therapy for the Management of Pain and Inflammation

This chapter has been published as **Berger, W. T.**; Ralph, B. P.; Kaczocha, M.; Sun, J.; Balius, T. E.; Rizzo, R .C.; Haj-Dahmane, S.; Ojima, I.; Deutsch, D. G. Targeting Fatty Acid Binding Protein (FABP) Anandamide Transporters – A Novel Strategy for Development of Anti-Inflammatory and Anti-Nociceptive Drugs. *PLoS ONE*, **2012,** 7 (12): e50968. doi:10.1371/journal.pone.0050968 PMCID: PMC3517626

Content

§6.0 Introduction:

§6.0.1 The Role of FABs in Endocannabinoid Transport:

Lipids, owing much to their water insolubility, require a variety of chaperones or transporters such as fatty acid binding proteins (FABPs) to carry them throughout cells.[1, 2] Recently, it has been shown that endogenous cannabinoids such as anandamide (an endocannabinoid) utilize FABPs, such as FABP5 (E-FABP) and FABP7 (B-FABP), as intracellular transporters.[2] Thus, FABPs have been recently found to serve a critical part in the pathway for anandamide inactivation by fatty acid amide hydrolase (FAAH), an enzyme localized inside the cell on the endoplasmic reticulum shown in **Figure 6-1**.

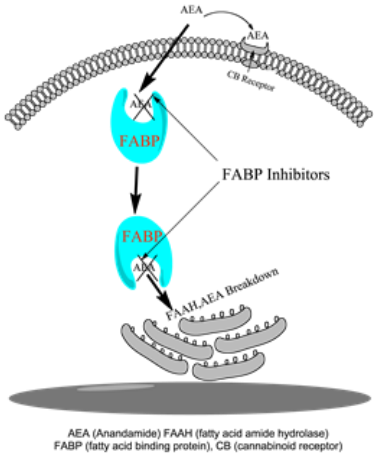

Figure 6-1: Proposed model for anandamide inactivation by FABP inhibition. Anandamide crosses the membrane by diffusion but requires FABPs for transport through the cytoplasm to the endoplasmic reticulum for breakdown by FAAH. FABP inhibitors prevent AEA from being delivered to FAAH for breakdown resulting in increased AEA levels at the receptor.

Owing to their role upstream from FAAH, FABPs are drug targets similar to FAAH. FABP inhibition decreases hydrolysis of anandamide and its uptake into cells, raising levels of extracellular anandamide, a ligand that targets cannabinoid (CB) receptors.[3-5] However, unlike FAAH that is distributed throughout the body, there are approximately ten human FABPs with appreciable tissue specificity. For example, FABP3 (heart FABP), FABP5 (epidermal FABP), FABP7 (brain FABP) and FABP8 (myelin FABP) are all expressed in nervous and other tissues. FABP1 (liver FABP) and FABP4 (adipose FABP), as their names imply, are abundantly expressed in the liver and adipose tissues.[6]

Few specific FABP inhibitors have been described. There are those specifically designed for FABP4 (adipocyte FABP), such as BMS309403, important for the protective effects that they exert in several metabolic syndromes and atherosclerosis.[7, 8] Furthermore, it has been shown that

BMS309403 also binds FABPs, such as FABP5 and FABP7 that carry anandamide as do other inhibitors, originally designed to inhibit a putative anandamide transmembrane transporter.[4] In an attempt to identify new FABP inhibitors, a large-scale virtual screen of over one million commercially available compounds was performed and resulted in the purchase of a subset for subsequent experimental evaluation. Overall, high-throughput virtual screening provided a powerful and practical approach for the virtual screening of ligand libraries to identify new drug-like leads for FABPs.

§6.0.2 Molecular Foot-Print Based Rescoring Methodology:

Traditionally, many screening programs such as DOCK[9], employ a simple two-term scoring function (score) consisting of intermolecular van der Waals and electrostatic terms to rank-order compatibility of ligands with a target. Complementary, a relatively new scoring function developed by the Rizzo laboratory, termed the molecular footprint similarity (FPS) score[10], utilizes the standard DOCK energy score as a decomposition of the energy by per-residue contributions. This FPS method was recently employed in the successful discovery of novel HIVgp41 inhibitors.[11] As illustrated in **Figure 6-2**, the procedure can be used to identify which compounds are most energetically similar to a known reference. In this example, the van der Waals interaction pattern made by the natural FAPB substrate oleic acid (red lines) is compared with that of a candidate ligand (blue line). The hypothesis is molecular footprints will enrich for active compounds (positives) by facilitating identification of compound making interaction signatures similar to known binders.

Specific goals of this research included: (1) Screen ca. one million compounds using a subset of the ZINC[12] database (ChemDiv vendor) of commercially available compounds to FABP7 to prioritize compounds for purchase. (2) Experimentally evaluate purchased compounds in a fluorescence displacement assay to determine binding activity. (3) Determine which hits are most promising for further development. Given the potential beneficial effects on stress, pain, and inflammation continued identification and development of new inhibitors of FAPBs is important.

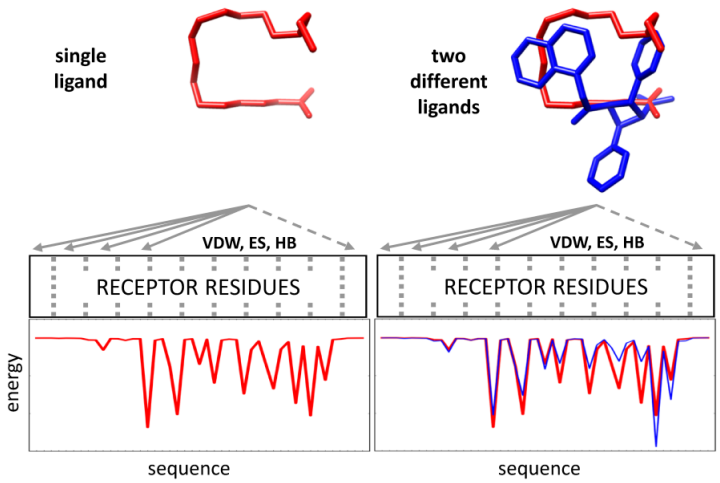

Figure 6-2.: Use of a van der Waals footprint similarity (FPS_{VDW}) score to identify compounds in virtual screening. (a) Oleic acid reference ligand (red). (b) Comparison between the reference (red) and candidate molecule (blue) from the virtual screen.

§6.1 Discovery and Biological Evaluations of Novel FABP Inhibitors by High-throughput Virtual Screening Utilizing FPS:

§6.1.1 Introduction:

The CB-1 receptor is predominately expressed in the brain and thus both FABP5 and FABP7 were considered relevant targets for our virtual screening. FABP5 or epidermal fatty acid binding protein (E-FABP) is typical dispersed throughout the body (tongue, adipose tissue, dendritic cell, mammary gland, brain neurons, kidney, liver, lung and testis) and found abundantly in the epidermal cells of the skin. FABP7 or brain fatty acid binding protein (B-FABP) is typically expressed in high levels during mid-term embryonic development but not present in neurons. Structural alignment (0.93 Å RMSD) of FABP7 (PDB: 1FE3, 2.8 Å resolution) and FABP5 (PDB: 1B56, 2.05 Å resolution) revealed a 47% sequence identity and 66% similarity shown in **Figure 6-3**. Furthermore, both FABP7 and FABP5 bind fatty acid substrates with high affinity; although FABP7 typically shows higher binding affinity *in vitro*. Thus, FABP7 was selected as our initial target for virtual screening.

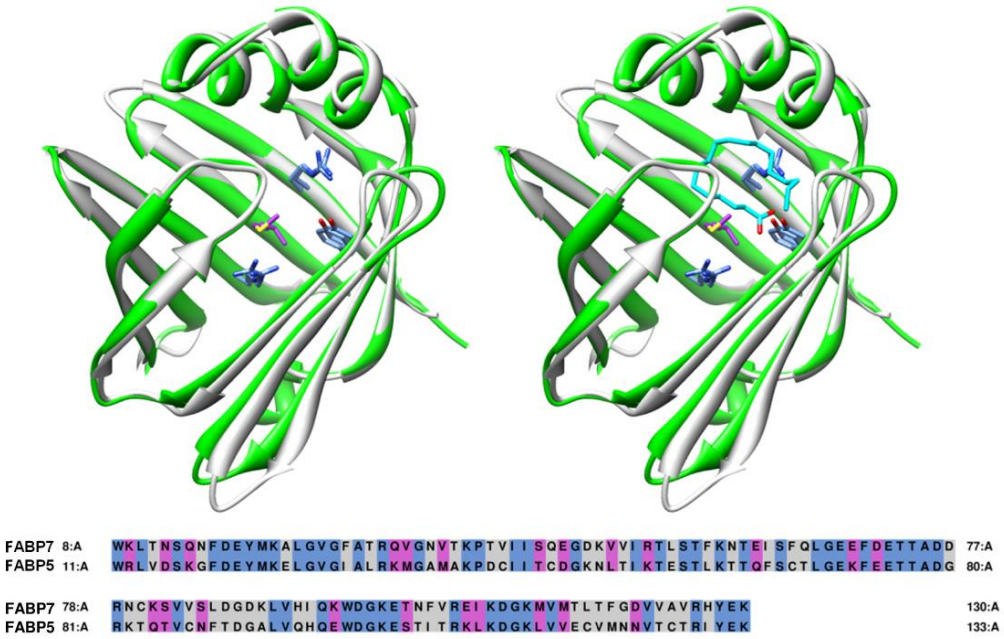

Figure 6-3: Sequence alignment of FABP7 (grey) and FABP5 (green). Binding motif ARG106, ARG126, TYR128 is identical between FABP7 and FABP5 (blue). MET115 in FABP7 is similar but not identical to VAL115 in FABP5 (purple). Oleic acid (cyan) is encapsulated by the FABP.

High-throughput virtual screening utilizing molecular footprints was conducted on FABP7 using oleic acid as the reference molecule. This entailed: 1) grid setup and docking 2) minimization of each docked molecule and reference molecule on the receptor Cartesian coordinates, 3) calculating the molecular footprints of all docked molecules and reference, 4) calculation of a footprint similarity score (FPS) for each of the docked molecules versus the reference oleic acid, 5) MACCS fingerprint clustering, 6) rank-ordering based on each scoring criteria, 7) analysis and selection of compounds from each of the 250 cluster heads generated for each of the scoring criteria using visual inspection of binding poses and footprints. **Figure 6-4** summarizes the overall work flow.

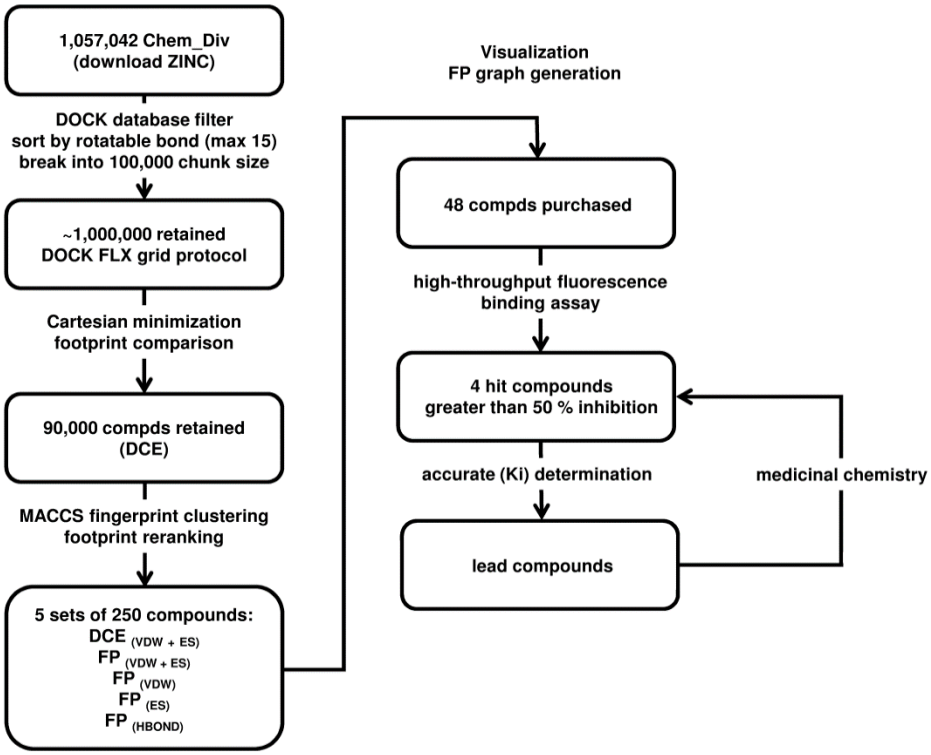

Figure 6-4: Flow chart describing the discovery of ligands through virtual screening, biological assay, and medicinal chemistry

§6.1.2 Results and Discussion:

§6.1.2.1 In Silico Results Identification of Lead Compounds:

As a result of the virtual screening of FABP7, 48 compounds were purchased and subsequently assayed *in vitro* against FABP5. The FABP5 homolog was chosen for the initial experimental testing due ease of experimental expression compared to FAPB7. Notably, out of the 48 compounds tested, 23 showed at least 25% inhibition and 4 compounds, having the following ChemDiv ID (Stony Brook ID) numbers 5511-0235 (SB-FI-19), 8009-2334 (SB-FI-26a or SB-FI-26g), 8009-7646 (SB-FI-27), and C075-0064 (SB-FI-31) showed approximately 50% inhibition or greater (see next section). It is important to note that the isomer provided by the vendor for ChemDiv ID 8009-7646 was the gamma form which is in contrast to alpha isomer downloaded from the ZINC database which was docked into FABP7. The alpha form however was synthesized latter (see Methods) and experimentally evaluated but not in the initial fluorescence displacement assays. To avoid confusion and throughout this chapter, the actual isomer that was used in any given computational or experimental test is indicated as either SB-FI-26 (α-isomer) or SB-FI-49 (γ-isomer). **Figure 6-5** shows the predicted DOCK binding pose for

the four active compounds in relationship to the reference oleic acid. **Figure 6-6** shows the accompanying van der Waals and electrostatic footprint overlaps. **Table 6-1** shows numerical values for the DOCK and FPS scores.

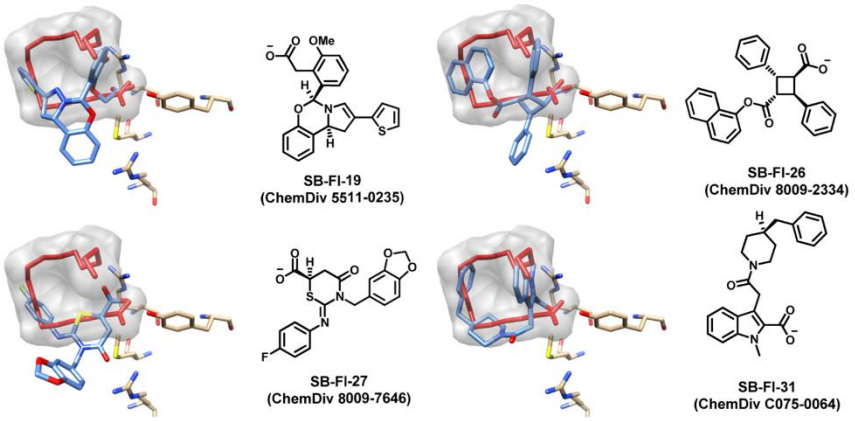

Figure 6-5: Four hit compounds from the virtual screen which show experimental activity in an FABP5 fluorescence displacement assay. The predicted binding pose for each ligand (blue stick) is shown in relationship to the reference oleic acid (red stick, gray surface).

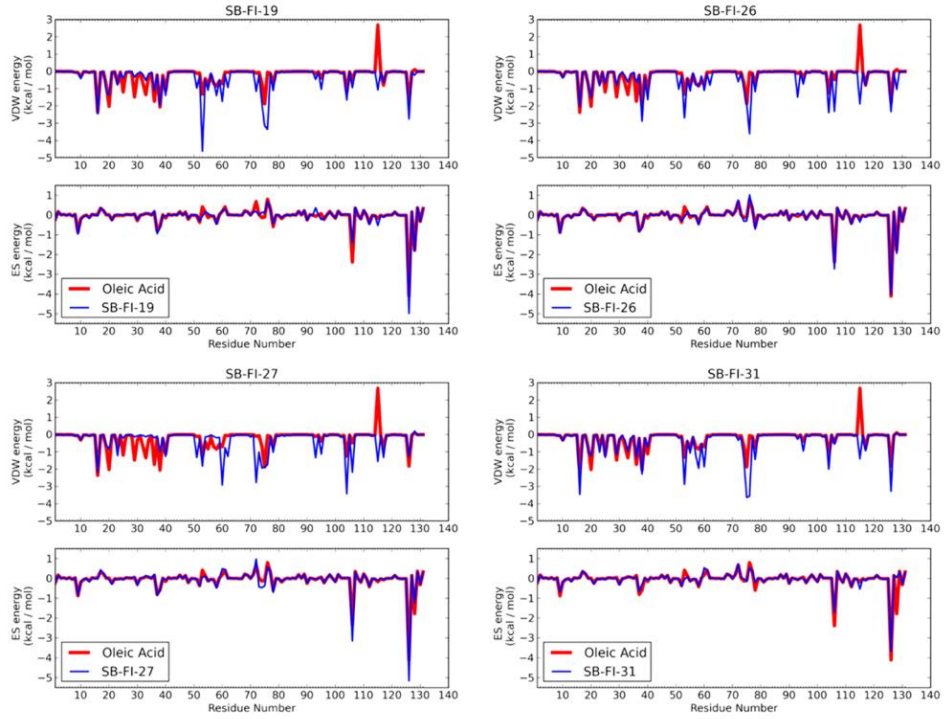

Figure 6-6: The VDW and ES footprint overlay of oleic acid (red) and SB-FI-26 (blue). A significant VDW clash between the reference oleic acid and MET115 can be seen in the VDW footprint. This steric clash is seen to be offset by the strong ES interactions at ARG 106, ARG126, and TYR 128 seen in the ES footprint. Energetically DOCK selected ligands from the ChemDiv library that did not have unfavorable interaction, both VDW and ES, intrinsically selecting inhibitors with a good ES footprint match while mitigating the VDW clash at MET115.

Table 6-1: Dock energy and footprint similarity (FPS) scores for compounds docked to FABP7					
Compound ID[a]	Method[b]	DCE_{VDW+ES}[c]	FPS_{VDW+ES}[d]	FPS_{VDW}[d]	FPS_{ES}[d]
SB-FI-19 5511-0235	FPS_{VDW+ES}	-56.56	1.09	0.81	0.28
SB-FI-26 8009-7646	FPS_{VDW+ES}	-56.76	1.01	0.87	0.14
SB-FI-27 8009-7646	FPS_{ES}	-53.34	1.21	1.00	0.21
SB-FI-31 C075-0064	FPS_{VDW+ES}	-53.77	1.12	0.73	0.39
[a]Stony Brook ID with corresponding ChemDiv number. [b]Footprint scoring function used for compound selection. [c]DCE scores in kcal / mol. [d]FPS scores in unites of normalized Euclidian distance where 0 represents the best overlap. FPS_{VDW} and FP_{ES} scores range from (0,2] and FPS_{VDW+ES} range from (0,4].					

The determining factor in compound selection was the use of the FPS scoring function thus it was expected that the four hit compounds would have overlap with the oleic acid reference. As shown in **Figure 6-6**, and quantified numerically in **Table 6-1**, all actives have substantial overlap in ES footprints (FPS_{ES} scores from 0.14 to 0.39) and to a lesser extent VDW footprints (FPS_{VDW} scores from 0.73 to 1.00). Interestingly the overlays shown in **Figure 6-5** show that three inhibitors (SB-FI-19, SB-FI-26, and SB-FI-27) spatially deviate from the surface defined by the reference which likely accounts for their poorer FPS_{VDW} scores (0.81 to 1.00) compared to SB-FI-31 (0.73). However, SB-FI-31 also has the poorest ES overlap (0.39) among the four thus it is not the most favorably scored compound overall. Importantly, all four actives contain a charged carboxylate moiety, analogous to that in the reference oleic acid **Figure 6-5**, which predicted to occupy the same position in the FABP binding site. All make strong ES interactions with ARG106, ARG126, and in particular at position TYR128 shown in **Figure 6-6**. The footprints indicate that SB-FI-19 and SB-FI-26 interact somewhat more strongly with TYR128 compared with SB-FI-27 and SB-FI-31 which could play a role in these compounds being the two most potent inhibitors among the four identified (see experimental results). Interestingly, SB-FI-19 and SB-FI-26 also have the most favorable DCE_{VDW+ES} scores among the group.

Overall, based on potency and taken into consideration its scaffold, SB-FI-26 was selected for further exploration and development. The core of SB-FI-26 is a prominent structural component of the natural product incarvillateine which is known to produce graded inhibition of pain and inflammation in formalin-induced mouse models, although the mechanism of action was

not fully understood shown in **Figure 6-7**.[13] Furthermore, structural exploration of α-truxillic analogues and various α-truxillic acid di-esters derivatives of the natural product were investigated, producing similar effects in mouse models.[14, 15] Thus, SB-FI-26 provided a means to probe mechanisms underlining the viability of using α-truxillic acid base mono-esters and in particular the 1-napthyl ester derivative to treat pain and inflammation.

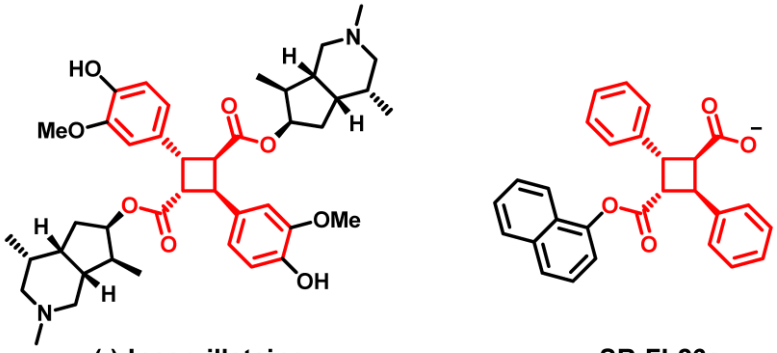

Figure 6-7: The common α-truxillic acid core structure (highlighted in red) of both (-)-Incarvillateine and FABP5 inhibitor SB-FI-26

§6.1.2.2 Identification of Active Compounds - Fluorescence Displacement Assay:

The initial experimental binding evaluation of the 48 compounds purchased from the virtual screen utilized an established fluorescence displacement assay. The degree to which the 48 compounds (10 μM) displaced NBD-stearate (1 μM) from FABP5 is shown in **Figure 6-8**. The first two samples, the buffer and NBD-stearate do not give appreciable fluorescence while the NBD-stearate plus purified FABP5 gives an appreciable fluorescence signal (blue bar). The forth sample is the positive control where arachidonic acid (1 μM), a fatty acid that binds strongly to FABP5 (Ki, 0.13 μM) decreases the signal. Each sample in this screen was measured in duplicate and approximately 1/3 of the test compounds appeared to cause displacement of NBD-stearate with a concomitant decrease in fluorescence. Four of the most potent (red bars) were selected for further evaluation and statistical analysis.

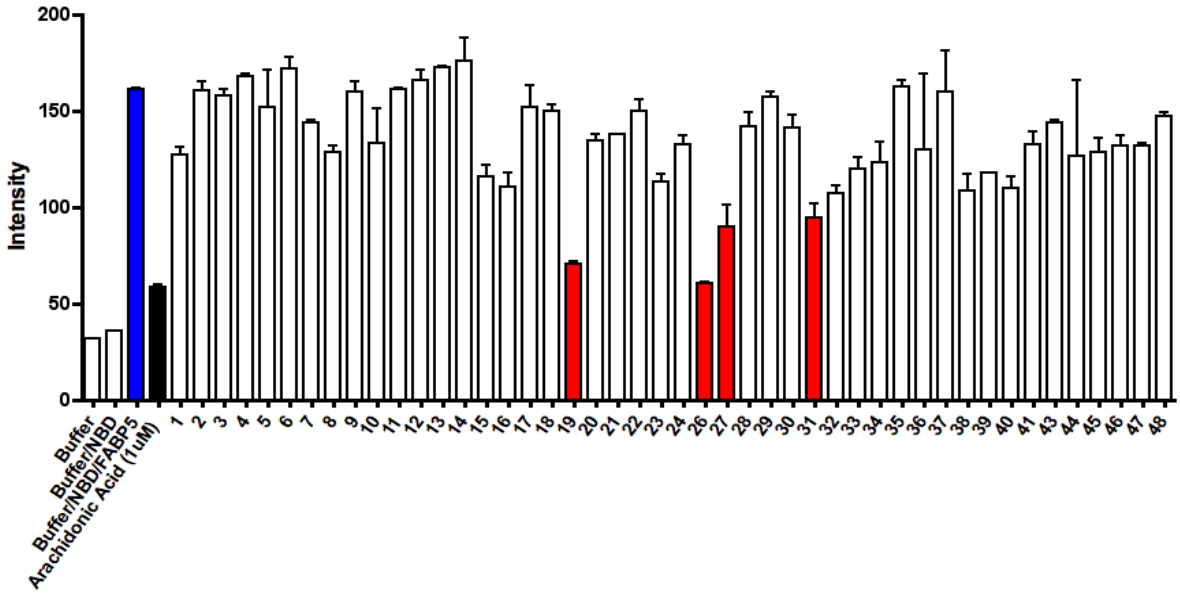

Figure 6-8: High-throughput fluorescence displacement assay with NBD-stearate. Shown in blue is the NBD-stearate FABP5 complex with no inhibitor, in black is arachidonic acid a potent inhibitor of FABP5, and in red are the four lead compounds. Assay performed by Brian P. Ralph.

Of all chemical compounds screened virtually shown in **Figure 6-8**, compounds 5511-0235 (19), 8009-2334 (26), 8009-7646 (27), and C075-0064 (31) proved to have the strongest interactions with FABP binding site in both virtual and biological screening. These compounds were then rerun in the NBD-fluorescent assay with replicate measurements at 10 µM. As shown in **Figure 6-9A,** inhibition of NBD-stearate binding to FABP5 by these compounds was highly significant with ChemDiv 8009-2334 (26) the most potent. In control experiments, it was observed that the four lead compounds did not fluoresce under the assay conditions at 10 µM, nor did 10 µM of these compounds quench the fluorescence of 16 µM NBD-stearate, that is 16 times the fluorophore concentration used in the routine assay shown **Figure 6-9B**.

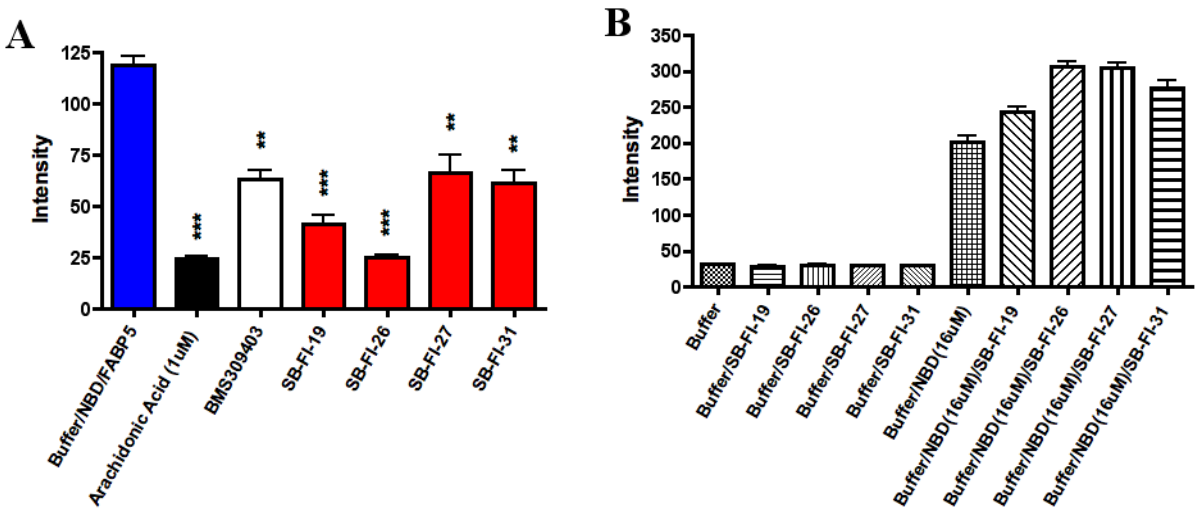

Figure 6-9: Verification of high-throughput fluorescent displacement assay results. (A) Replicate testing of the lead compounds shows that 8009-2334 (SB-FI-49) exhibits the best inhibition of FABP5. One * indicates $p < 0.05$, two ** indicates $p < 0.01$, three *** indicates $p < 0.001$ (n=3). (B) Controls show that all lead compounds exhibited no detectable fluorescence in the assay nor did they add significantly to the fluorescence of the NBD-stearate probe. Assay performed by Brian P. Ralph.

§6.1.2.3 Synthesis of Lead Compounds SB-FI-26 and SB-FI-49:

Since ChemDiv ID 8009-2334 was the best hit compound from the virtual screening and biological assay, it was decided to perform re-synthesis in order to determine the optimal inhibitor concentration as seen in **Scheme 6-1**. Thus, re-synthesis began with the synthesis of α-truxillic acid. Solid trans-cinnamic acid was placed onto a pyrex dish and was subsequently exposed to UV light at 350 nm for 1 week to yield α-truxillic acid **6-1** in good yield. Mono-esterification of the symmetrical compound α-truxillic acid **6-1**, was carried out utilizing a protocol employing oxalyl chloride to afford the di-acylchloride intermediate followed by treatment with a catalytic amount of DMAP, (0.71 equivalents) of TEA, and (0.71 equivalents) of 1-napthol to afford the α-truxillic acid 1-napthol ester as a mixture of enantiomers (SB-FI-26) in good yield after 2 steps. Surprisingly, the ^{1}H NMR spectrum of **6-2** quickly revealed that it was not the same isomer as ChemDiv ID 8009-2334.

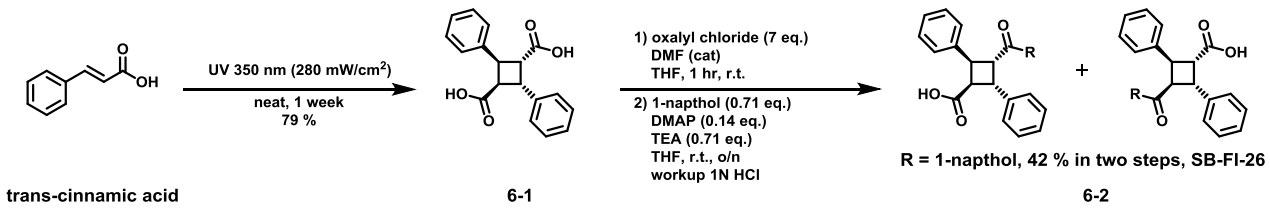

Scheme 6-1: Stepwise synthesis of SB-FI-26

After determining that ChemDiv ID 8009-2334 was not the α-isomer originally proposed in the virtual screening, it was decided to additionally synthesize the γ-isomer as seen in **Scheme 6-2**. Access of γ-truxillic acids could be obtained from α-truxillic acid. Conversion of the α-isomer could be accomplish by refluxing in acetic anhydride to afford the glutaric anhydride **6-3** in good yield. Mono-esterification of the glutaric anhydride **6-3** could be accomplished by the addition of a nucleophile (eg. 1-napthol, 2-naphol) (1.1 equivalents) in the presence of base DIPEA (1.1 equivalents) to afford the γ-truxillic acid 1-napthol **6-4** in good yield. The ^{1}H NMR spectrum of **6-4** then confirmed that ChemDiv ID 8009-2334 was indeed the γ-isomer.

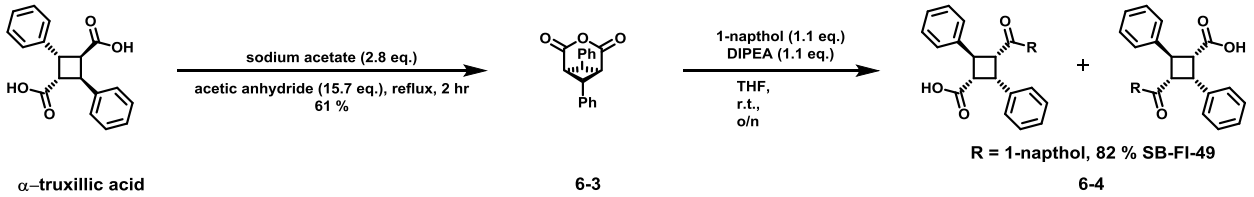

Scheme 6-2: Stepwise synthesis of SB-FI-49

§6.1.2.4 K_i Determination of SB-FI-26 and SB-FI-29:

As noted above, the virtual screening of ChemDiv ID 8009-2334 employed α-truxillic acid 1-naphthyl mono-ester (SB-FI-26) however the form supplied by the vendor and thus experimentally evaluated, was γ-truxillic acid 1-naphthyl mono-ester (SB-FI-49). To reconcile the differences as well as provide additional quantities both α- and γ- forms were chemically synthesized in-house (see Methods). Importantly, the ^{1}H NMR spectrum of the newly synthesized α-form (SB-FI-26) did not match that of the ChemDiv 8009-2334 but the newly synthesized γ-form (SB-FI-49) did, thus confirming the isomeric form which was provided. The inhibitory activity of the newly synthesized alpha form SB-FI-26 was assayed and a K_i value of 0.93 ± 0.08 μM was determined from triplicate analysis shown in **Figure 6-10A**. The inhibitor activity of the newly synthesized gamma form (SB-FI-49) led to an improved Ki value of 0.75 ± 0.07 μM, which was higher than that from the vendor sample (1.19 ± 0.01 μM) presumably due to greater purity.

Overall, SB-FI-49 at a Ki value of 0.75 ± 0.07 µM appears equally as potent as BMS309403 (K_i 0.75 ± 0.16 µM) as shown in Figure 10C. However, although SB-FI-49 appeared to be the most potent inhibitor identified in this study it was substantially less soluble (200 µM in DMSO at 25°C) than either the BMS309403 (1 mM in DMSO at 25°C), or surprisingly, the alpha form SB-FI-26 (1 mM in DMSO at 25°C). Thus, SB-FI-26 provided to be the best lead compound for further evaluation.

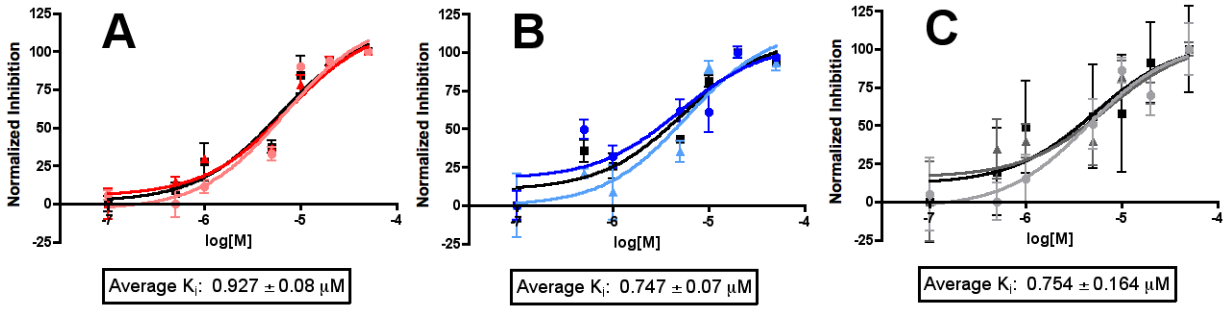

Figure 6-10: Binding analysis of SB-FI-26 (α-truxillic acid 1-naphthyl ester), SB-FI-49 (γ-truxillic acid 1-naphthyl ester), and BMS309403. (A) Assay in triplicate shows that SB-FI-26 derivative attains a K_i within nanoMolar ranges. (B) Analysis of γ-truxillic acid 1-naphthyl ester implies that 8009-2334 is an impure form of the compound and that the pure, synthesized gamma derivative is as potent as BMS309403. (C) BMS309403 was found to be slightly more potent in this study (K_i, 0.75 µM) than published (K_i, 0.89 µM), but still within range of this value. Assay performed by Brian P. Ralph.

§6.2 *In Vitro* and *In Vivo* Validation of SB-FI-26:

§6.2.1 Introduction:

The two most potent compounds, SB-FI-26 and SB-FI-49 (the α-and γ-truxillic acid 1-naphthyl esters), discerned from our *in silico* and biological screening, belong to a class of compounds that have been found to have anti-inflammatory and anti-nociceptive.[14, 15] Heretofore, the mechanism by which these effects were mediated was unknown. Thus it can be speculated that these compounds inhibit the transport of anandamide and other fatty acid ethanolamides, such as palmitoylethanolamide and oleoylethanolamide. These increased NAE levels would lead to greater signaling at the cannabinoid and potentiate NAE-mediated hypoalgesic and anti-inflammatory effects, indicating that modulation of NAE signaling may represent a therapeutic avenue for the treatment of pain.

§6.2.2 Results and Discussion:

§6.2.2.1 Effects of SB-FI-26 on Glutamate-Mediated Synaptic Transmission:

Activation of cannabinoid CB1 receptors inhibits glutamatergic synaptic transmission in numerous brain areas, including the dorsal root ganglion DR.[16] Therefore, to test whether SB-FI-26 exhibits agonist properties at CB1 receptors, its effects were examined on the amplitude of glutamate-mediated excitatory postsynaptic currents (EPSCs) recorded from DR 5-HT neurons. Ultimately it was found that bath application of SB-FI-26 (10 μM) did not inhibit the amplitude of EPSCs (107 ± 6.7% of baseline, n = 8, as shown in **Figure 6-11**. Such a finding suggests that SB-FI-26 is not a CB1 receptor agonist.

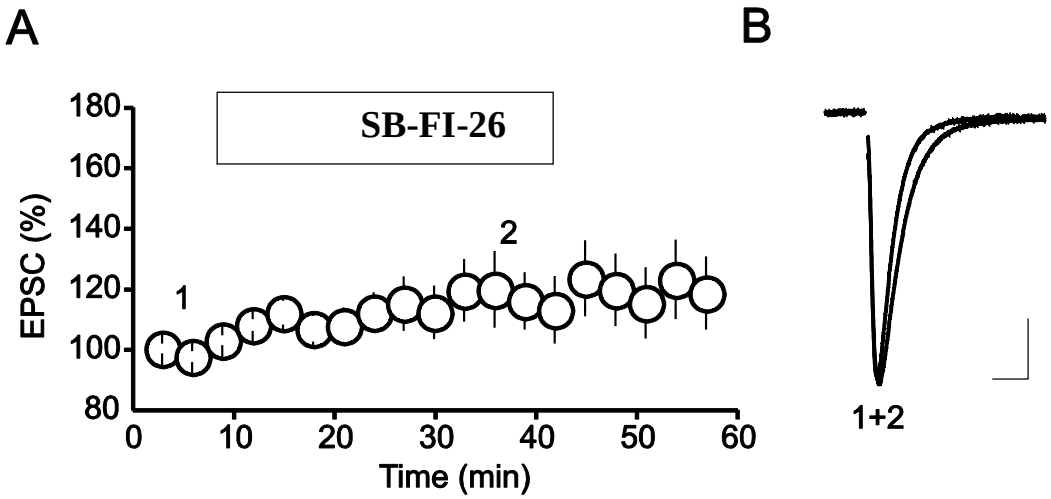

Figure 6-11: FABP inhibitor SB-FI-26 does not reduce amplitude of EPSCs. (A) Summary graph of effect of SB-FI-26 (10 μM) on amplitude of EPSCs. (B) Superimposed average EPSC traces taken at the time point indicated by numbers in panel A. Note that application of α-1-napthol-truxillic acid did not inhibit the amplitude of EPSCs. Assay performed by Dr, Samir Haj-Dahmane.

§6.2.2.2 Effect of SB-FI-26 Upon AEA Uptake In Cells:

It has been previously shown in literature that FABPs are intracellular carriers that shuttle endocannabinoids and related N-acylethanolamines to intracellular sites, such as FAAH for hydrolysis.[2, 4] Pharmacological or genetic inhibition of FABPs reduces AEA catabolism in cells, confirming an essential role for these proteins in endocannabinoid inactivation.[2, 4] Thus, it was examined whether the novel FABP inhibitor SB-FI-26 reduces FABP-mediated AEA uptake in cells. Indeed, SB-FI-26 significantly inhibited cellular AEA accumulation shown in **Figure 6-12A**. Confirming its selectivity for FABPs, SB-FI-26 failed to reduce AEA uptake in cells bearing a knockdown of FABP5 shown in **Figure 6-12A**, the main FABP expressed in HeLa cells [2, 4].

Additionally, SB-FI-26 did not inhibit FAAH shown in **Figure 6-12B**. Collectively, these results indicated that SB-FI-26 was a selective FABP inhibitor.

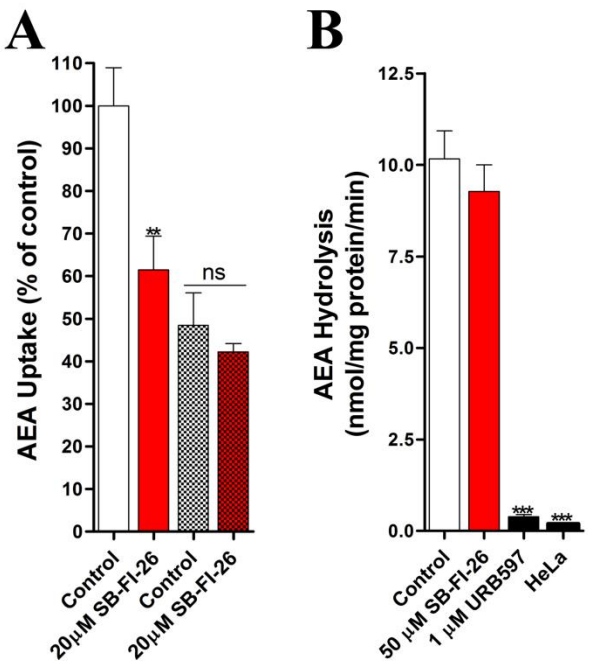

Figure 6-12: SB-FI-26 inhibits the cellular uptake of AEA. (A) AEA uptake in wild-type HeLa (un-shaded) or FABP5 shRNA-expressing HeLa (shaded) cells in the presence or absence of SB-FI-26. (B) AEA hydrolysis in FAAH-transfected HeLa cells in the presence or absence of SB-FI-26 or the FAAH inhibitor URB597. **, $p < 0.01$; ***, $p < 0.001$ ($n = 3$). Assays performed by Professor Martin Kaczocha.

§6.2.2.3 SB-FI-26 Produces Antinociceptive and Anti-Inflammatory Effects in Mice:

Similar to cannabinoid receptor agonists, inhibitors of endocannabinoid inactivation produce anti-inflammatory and antinociceptive effects.[17, 18] Importantly, FAAH inhibitors lack the untoward psychotropic effects of cannabinoid receptor agonists[19], highlighting the therapeutic advantage of pharmacologically targeting endocannabinoid inactivation. Furthermore, inhibition of AEA transport to FAAH reduces AEA inactivation, thus it was hypothesized that FABP inhibitors may likewise possess antinociceptive and anti-inflammatory properties. Thus, the effects of SB-FI-26 was examined using two nociceptive models: the formalin test and carrageenan-induced thermal hyperalgesia. In the formalin test, injection of formalin results in the induction of two temporally distinct phases of pain with the first phase (0-5 min) representing nociceptor activation and the second phase (15-45 min) representing inflammatory pain and central sensitization. As shown in **Figure 6-13A**, SB-FI-26 significantly reduced nocifensive behavior only during the first phase of the formalin test.

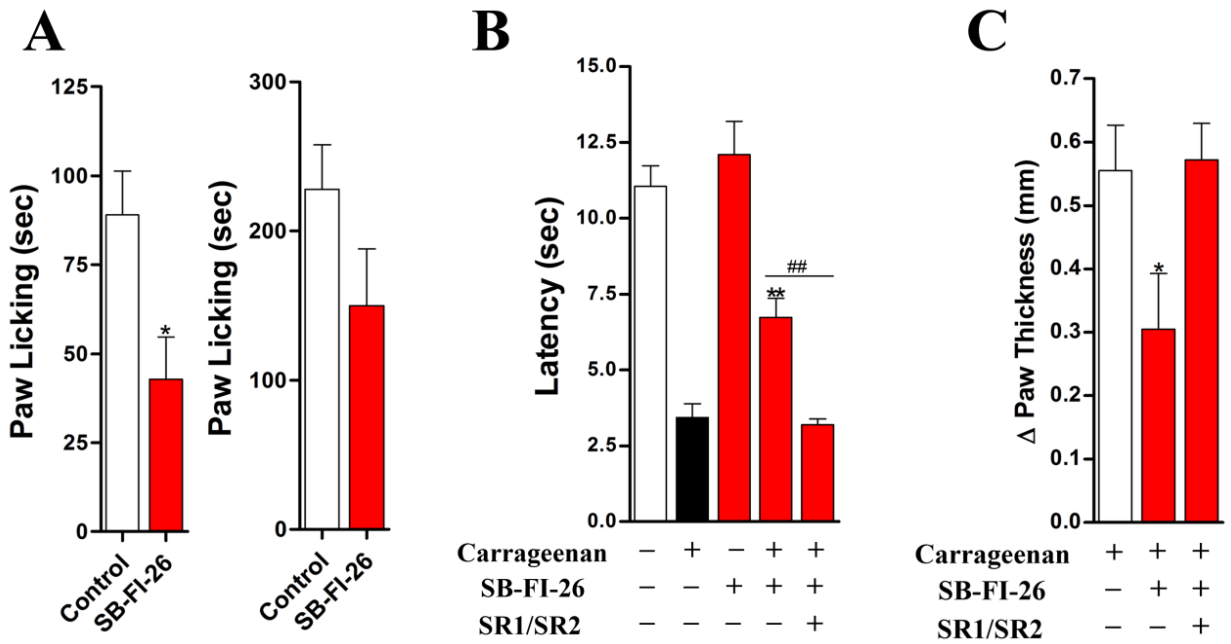

Figure 6-13: Antinociceptive effects of SB-FI-26 in mice. (A) SB-FI-26 (20 mg/kg, i.p.) reduces pain associated with the first phase (left panel) but not the second phase (right panel) of the formalin test. *, $p < 0.05$ (n = 6). (B) SB-FI-26 (20 mg/kg, i.p.) alleviates carrageenan-induced thermal hyperalgesia in mice. Concurrent administration of rimonabant and SR144528 (SR1/SR2) blocked the antinociceptive effects of SB-FI-26. **, $p < 0.01$ versus carrageenan-injected animals; ##, $p < 0.01$ versus SR1/SR2-treated animals (n = 6-9). (C) SB-FI-26 (20 mg/kg, i.p.) reduces carrageenan-induced paw edema. *, $p < 0.05$ (n = 6-9). Assays performed by Professor Martin Kaczocha.

It was then explored whether SB-FI-26 alleviated inflammatory pain induced by intraplantar injection of λ-carrageenan. Indeed, SB-FI-26 (20 mg/kg, i.p.) significantly reduced carrageenan-induced thermal hyperalgesia shown in **Figure 6-13B** and paw edema shown in **Figure 6-13C**. To establish a cannabinoid receptor-mediated mechanism of action, mice were pretreated with a combination of the cannabinoid receptor 1 and 2 antagonists, rimonabant and SR144528, respectively. The antinociceptive and anti-edematous effects of SB-FI-26 were completely reversed by rimonabant and SR144528 shown in **Figure 6-13B** and **Figure 6-13C**. Previous reports indicate that α-truxillic acid derivatives activate peroxisome proliferator-activated receptor γ (PPARγ), which alongside PPARα, modulate nociception.[20-22] In our hands, SB-FI-26 served as a weak agonist at both receptors, displaying ~2-fold activation of PPARα and ~3-fold activation of PPARγ shown in **Figure 6-14**.

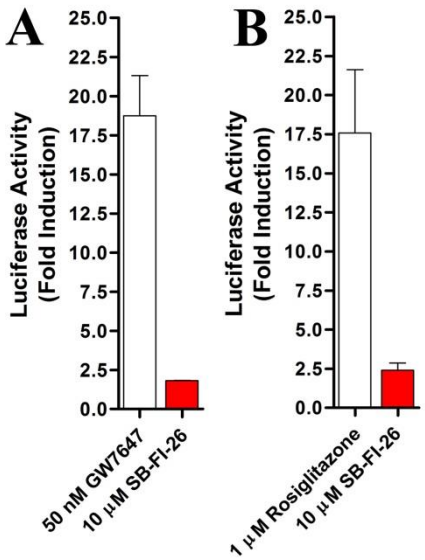

Figure 6-14: SB-FI-26 is a weak agonist at PPARα and PPARγ receptors. (A) PPARα activation by SB-FI-26 and the PPARα agonist GW7647. (B) Activation of PPARγ receptors by SB-FI-26 compared to the PPARγ agonist rosiglitazone (n = 3). Assays performed by Professor Martin Kaczocha.

§6.3 Conclusions:

In conclusion, novel small molecule inhibitors of FABP5 and FABP7 were identified by means of a virtual screening employing DOCK and FPS. Despite having dissimilar distributions within the body, the structural similarity between FABP5 and FABP7 was shown to be as high as 66 % with key binding residues fully conserved. Thus, FABP7 served as a template to identify potential lead compounds using DOCK and FPS. The FPS scoring function was implemented utilizing a normalized Euclidean distance criteria; meticulously matching the VDW and ES footprints the reference substrate Oleic acid with over one million docked small molecules with high speed and accuracy. Forty-eight molecules were identified in the virtual screen and subsequently assayed against FABP5 using a high-throughput fluorescent displacement assay. Overall, four compounds from the ChemDiv compound library were identified as potential competitive inhibitors of FABP5. The most potent compound, ChemDiv 8009-2334, was found to possess a diphenyl-cyclobutane core characteristic of the known natural product (-)-incarvillateine.

A novel α-truxillic acid 1-naphthyl mono-ester, SB-FI-26, was synthesized and the FABP5 NBD-stearate displacement assay of this compound showed a sub-micro molar Ki value. The resynthesized γ-form of truxillic acid 1-naphthyl mono-ester (SB-FI-49) also showed sub-micro

molar efficacy against FABP5, which was considerably more potent than ChemDiv 8009-2334, probably due to an enhanced purity. SB-FI-26 (α-form) and SB-FI-49 (γ-form) were found to be as potent as BMS309403, a well-known FABP inhibitor. Thus with both our virtual and biological screening, truxillic acid mono-esters were identified as a unique class of compounds that target FABPs.

Following biological screening and binding analyses of these inhibitors, the novel FABP inhibitor SB-FI-26 was shown to produce antinociceptive and anti-inflammatory effects in mice. These findings are in agreement with a previous study demonstrating that some α-truxillic acid derivatives exhibited antinociceptive properties, although the mechanism of action was not identified.[15] It was subsequently reported that certain derivatives of α-truxillic acid activate PPARγ.[20] Contrary, our work demonstrates that SB-FI-26 behaves as a weak agonist at PPARα and PPARγ, and the antinociceptive effects of SB-FI-26 were abolished by cannabinoid receptor antagonists. Thus, the antinociceptive effects of SB-FI-26 likely resulted from potentiation of endocannabinoid signaling rather than activation through PPAR receptors. Taken together, these results establish FABPs as novel targets for antinociceptive drug development. In addition to the FABP transporters described here, heat shock protein 70, albumin, and a truncated fatty acid amide hydrolase protein have also been reported as intracellular shuttles for AEA[23-24] and this area has been recently review.[25] These studies show the potential for the design of even more potent inhibitors that will be selective for individual FABPs.

§6.4 Experimental Procedures:

§6.4.1 Computation Virtual Screening Utilizing FPS

High-Throughput Virtual Screening:

A high-throughput virtual screening of over one million molecules from the ChemDiv subset of the ZINC database (http://zinc.docking.org) was conducted on New York Blue, an 18 rack IBM Blue Gene/L massively parallel supercomputer located at Brookhaven National Laboratory using DOCK version 6.5.[26] Prior to docking, the most updated ChemDiv database was downloaded and presorted by rotatable bonds and split into 10 subsets of ~100,000 molecules using the DOCK database filter. Subsequently, an energy grid for FABP7 (PDB : 1FE3) was generated using the grid program.[27] Then, each molecule was flexibly docked to the FABP7 grid (DOCK FLX protocol)[28] and the single lowest-energy pose was retained.

Footprint-Based Rescoring:

Following high-throughput virtual screening, the footprint-based rescoring methodology reported by Balius et al[29] was implemented to enrich the library of docked molecules. First, the co-crystalized ligand oleic acid (reference) was minimized on the FABP Cartesian coordinates within the binding pocket. This was implemented using both a hydrogen optimization followed by a weak restrained minimization (restraint of 10 kcal / mol). Following reference minimization, each molecule of the docked library was subsequently minimized in Cartesian space using the restrained minimization protocol. Last, electrostatic, van der Waals, and hydrogen bond footprint similarity scores were computed using normalized Euclidian distance for each molecule docked versus the reference using DOCK 6.5.

Database Clustering and Compound Selection:

First, subsets 1 through 5 and subset 6 through 10 containing ~ 500,000 molecules were rank-ordered by the DOCK Cartesian energy (DCE) score. The top 45,000 of each combined subset of 500,000 molecules (~ 10% total 90,000 molecules) were then clustered using MACCS fingerprints, as implemented in the program MOE[30] with the tanimoto coefficient of 0.75. The resulting cluster heads obtained were then further rank-ordered by: (i) standard DOCK score (DCE $_{VDW + ES}$), (ii) van der Waals footprint similarity score (FPS $_{VDW}$), (iii) electrostatic footprint similarity score (FPS $_{ES}$), (iv) H-bond footprint similarity score (FPS $_{HB}$), (v) the sum of van der Waals and electrostatic footprint similarity score (FPS $_{VDW + ES}$). The top 250 molecules rank-ordered by each criteria were then plotted in MathPlotLib[31] and examined by visual inspection and consistency to the reference footprint. This method of analysis allowed us to both visually see key interactions within the binding pocket while simultaneously observing the magnitudes of those key interactions within the footprints for each molecule. Based on this approach, 48 compounds were selected a purchased for biological testing against FABP5. Biological screening of these compounds for activity against FABP7 is underway.

§6.4.2 Chemical Synthesis:

General Methods: ^{1}H NMR and ^{13}C NMR spectra were measured on a Varian 300, 400, 500, or 600 MHz NMR spectrometer. High-resolution mass spectrometric analyses were conducted at the Mass Spectrometry Laboratory, University of Illinois at Urbana-Champaign, IL. TLC analyses

were performed on Merck DC-alufolien with Kieselgel 60F-254 and were visualized with UV light and stained with sulfuric acid-EtOH, 10 % PMA-EtOH or 10 % Vanillin-EtOH with 1% sulfuric acid. Column chromatography was carried out on silica gel 60 (Merck; 230-400 mesh ASTM). HPLC Purity was determined by Shamazu HPLC employing a Phenomenex Kinetex™ 2.6 μm PFP 100 Å, LC Column 30 x 4.6 mm (CH_3CN/H_2O = 60/40 gradient to 95/5 over 45 min, flow rate at 1 mL/min, UV 254 nm.

Materials: The chemicals were purchased from Sigma-Aldrich Company, Fischer Company or VWR Company. DCM and methanol were dried before use by distillation over calcium hydride under nitrogen. Ether and THF were dried before use by distillation over sodium-benzophenone kept under nitrogen. Dry DMF and DMSO were purchased from Sigma-Aldrich chemical company, and used without further purification. Reaction flasks were dried in a 100 ^oC oven and allowed to cool to room temperature in a desiccator over "*Drierite*" (calcium sulfate) and assembled under an inert nitrogen gas atmosphere.

α-Truxillic acid (6-1):

E-cinnamic acid (1.272 g , 8.59 mmol) was placed in a pyrex dish and exposed to light at 350 nm and an intensity of 280 mW/cm^2 for 1 week with periodic shaking. This process was performed in the solid state and monitored by ^{1}H NMR. After completion of the photoreaction, the white solid was washed with diethyl ether (200 mL) and allowed to dry. The solid was then recrystallized from pure ethanol to give α-truxillic acid (1.006 g, 79 % yield) as a white solid: mp 276 – 277 ^oC (lit. [32] 274 – 278 ^oC); ^{1}H NMR (300 MHz, DMSO-d_6) δ 12.12 (s, 2H), 7.32 (m, 8H), 7.24 (m, 2H), 4.28 (dd, J = 7.2 Hz, 10.1 Hz, 2H) 3.81 (dd, J = 7.2 Hz, 10.1 Hz, 2H); ^{13}C NMR (75 MHz, DMSO-d_6) δ 173.00, 139.47, 128.19, 127.67, 126.69, 46.17, 41.06. Data are consistent with the literature values.[32]

α-Truxillic acid 1-naphthyl ester (SB-FI-26) (6-2):

To 500 mg of pure α-truxillic acid as added 20 mL of THF was added along with 1.3 mL of oxalyl chloride. Addition of a drop of DMF allowed conversion of α-truxillic acid to the corresponding diacid dichloride, which was used crude in the subsequent reaction. To α-truxillic acid dichloride, thus prepared , 20 mL of THF was added, followed by 0.7 mL of TEA and 100 mg of 4-*N*,*N*-dimethylaminopyridine(DMAP). To this mixture was added dropwise, 170 mg of 1-napthol in 10

mL of THF with stirring. The reaction mixture was allowed to stir overnight and quenched with 1M HCl upon completion of the reaction. The reaction mixture was extracted with 100 mL of DCM and washed with 100 mL of brine. The organic layer was dried over anhydrous $MgSO_4$ and concentrated *in vacuo* to give a brownish oil, which was then purified by flash chromatography on silica gel using 20% ethyl acetate in hexanes followed by 30% ethyl acetate in hexanes as eluents to give α-truxillic acid 1-naphthyl ester (SB-FI-26, 210 mg , 42 % yield) as a white solid: mp 195 ^oC; ^1H NMR (500 MHz, DMSO-d_6) δ 12.24 (s, 1H), 7.88 (d, *J* = 8.5 Hz, 1H), 7.73 (d, *J* = 8.5 Hz, 1H), 7.57 (d, *J* = 7.0 Hz, 2H), 7.52 (d, *J* = 7.5 Hz, 2H), 7.48 – 7.37 (m, 6 H), 7.34 – 7.27 (m, 3 H), 7.06 (d, *J* = 8.0 Hz, 1H), 6.38 (d, *J* = 7.5 Hz, 1H) 4.61 – 4.49 (m, 3H), 3.98 (dd, *J* = 7.0 Hz *J* = 10.0 Hz, 1H); ^{13}C NMR (75 MHz, DMSO-d_6) δ 172.73, 170.93, 146.17, 139.23, 139.03, 133.92, 128.74, 128.25, 128.19, 127.89, 127.67, 127.40, 126.90, 126.47, 126.22, 125.85, 125.45, 121.13, 117.86, 46.17, 41.54, 41.11; HRMS (ESI) *m/e* calculated for $C_{28}H_{23}O_4H^+$: 423.1589. Found: 423.1596 (Δ = 1.7 ppm).

6,7-Diphenyl-3-oxabicyclo[3.1.1]heptane-2,4-dione (γ-truxillic anhydride) (6-3):

A 20 mL round bottomed flask was charged with a mixture of α-truxillic acid (600 mg, 2.02 mmol), anhydrous sodium acetate (775 mg) and 5 mL of acetic anhydride. The mixture was refluxed at 150 ^oC for 24 h. After completion of the reaction (by TLC analysis), the reaction mixture was allowed to cool to room temperature. The resulting white solid was collected on a filter, washed with 100 mL of water, and air dried overnight. The white solid was recrystallized by first dissolving in chloroform (10 mL), followed by the addition of 100 mL of ethanol to give pure γ-truxillic anhydride (398 mg, 71 % yield) as white crystals: mp 187 ^oC (lit. [33] 190 ^oC); ^1H NMR (300 MHz, $CDCl_3$) δ 7.51 -7.39 (m, 4H), 7.37 - 26 (m, 4H), 7.09 – 7.06 (m, 2H), 4.34 (t, *J* = 5.7 Hz, 1H) 4.07 (d, *J* = 5.1 Hz, 2H), 3.99 (s, 1H).

γ-Truxillic acid 1-naphthyl ester (SB-FI-49) (6-4):

To a solution of γ-truxillic anhydride (50 mg, 0.18 mmol) and 1-napthol (29 mg, 0.20 mmol) in 1 mL of THF was added DIPEA (0.03 mL, 0.20 mmol) , and the solution was allowed to stir at room temperature for 15 h. After completion of the reaction (by TLC analysis), the reaction mixture was concentrated *in vacuo* to remove all volatiles. The residue was then extracted with 100 mL of DCM and washed with 100 mL of brine. The organic layer was dried over anhydrous $MgSO_4$ and

concentrated *in vacuo* to give a brownish solid, which was subsequently purified using flash chromatography on silica gel with 20 % ethyl acetate in hexanes followed by 30 % ethyl acetate in hexanes as eluents to give γ-truxillic acid 1-naphthyl ester (SB-FI-49, 61 mg, 80 % yield) as a white solid: ^{1}H NMR (500 MHz, DMSO-d_6) δ 12.27 (b, 1H), 7.87 (d, J = 8.5 Hz, 1H), 7.73 (d, J = 8.0 Hz, 1H), 7.48 – 7.24 (m, 13 H), 6.88 (d, J = 8.0 Hz, 1H), 6.46 (d, J = 7.5 Hz, 1H), 4.59 (t, J = 10.5 Hz, 1H), 4.47 (t, J = 10.0 Hz, 1H), 4.37 (t, J = 10.5 Hz, 1H), 3.85 (t, J = 10.5 Hz, 1H). Data are consistent with the literature values.[34]

§6.4.3 *In Vitro* Fluorescence Assays:

Materials: 12-NBD-stearate [12-*N*-methyl-(7-nitrobenz-2-oxa-1,3-diazo)aminostearic acid] was from Avanti Polar Lipids (Alabaster, AL). BMS309403 was from EMD Chemicals (San Diego, CA). Arachidonic acid was from Cayman Chemical (Ann Arbor, MI). 48 virtually screened test compounds from ChemDiv, Inc. (Moscow, Russia). α-Truxillic acid 1-naphthyl ester (SB-FI-26) and γ-truxillic acid 1-naphthyl ester (SB-FI-49) were synthesized at the Institute of Chemical Biology and Drug Discovery, Stony Brook University.

High-Throughput Fluorescence Displacement Assay with NBD-Stearate:

The high-throughput fluorescence displacement assay was performed by Brian P. Ralph. FABP5 was purified and delipidated as described previously.[4] FABP5 (30 µg), NBD-stearate (1 µM), and a competitor test compound were incubated in 30 mM Tris-HCl, 100mM NaCl buffer (pH 7.6). Competitors included arachidonic acid, BMS309403, 48 test compounds from ChemDiv library, SB-FI-26 and SB-FI-49. The initial assay was run with buffer (30mM Tris-HCl buffer), negative controls (buffer and NBD-stearate), positive controls (buffer, NBD-stearate, FABP5), and experimental wells with a variable test compound added (arachidonic acid or one of the 48 test compounds) at 10 µM. Test compounds that produced high inhibition and proved statistically significant were then added to the fluorescent assay at 10 µM and tested in triplicate to verify their success. The most effective test compound and BMS309403 were measured in increasing concentrations (0.01-50 µM), as were the SB-FI-26 and γ-truxillic acid 1-naphthyl ester, which were discovered following the test. The fluorescent assays were tested in the wells of Microtest 96-well Assay Plates, Optilux (BD Biosciences, Franklin Lakes, NJ) and loss of fluorescence intensity was measured with a FLUOstar OPTIMA spectrofluorometer set to excitation and

emission wavelengths of 460 nm and 544 nm, respectively. For the most effective test compounds, IC_{50} values were calculated with GraphPad Prism. GraphPad Prism was also used to determine the K_i of these select competitors from the equation $K_i = IC_{50}/(1 + ([\text{NBD-stearate}]/K_d))$. The K_d of NBD-stearate for FABP5 had been determined previously through incubating FABP5 with increasing concentrations of NBD-stearate. One site binding analysis in GraphPad Prism indicated that the K_d of NBD-stearate for FABP5 was 0.16 μM.[4]

§6.4.4 Patch-Clamp Electrophysiology in Brain Slices:

The patch-clamp electrophysiological testing was performed by Dr. Samir Haj-Dahmane at the SUNY Buffalo, Buffalo, New York. Whole-cell-voltage clamp recordings of dorsal raphe (DR) serotonin (5-HT) neurons were performed as previously described.[35] Briefly, DR neurons were visualized using an upright microscope (BX 51 WI, Olympus, Tokyo, Japan) equipped with a differential interference contrast and infrared imaging system. Somatic recordings from DR neurons were obtained with path electrodes (3-5 mΩ) back-filled with potassium gluconate based internal solution of the following composition: 120 mM potassium gluconate, 10 mM KCl, 10 mM Na_2-phosphocreatine, 10 mM HEPES, 1 mM $MgCl_2$, 1 mM EGTA, 2 mM Na_2-ATP, 0.25 mM Na-GTP, pH 7.3 (Adjusted with KOH; Osmolarity, 280 to 290 mOsmol/l). All the recordings were conducted in the presence of $GABA_A$ receptor antagonist picrotoxin (100 μM). Excitatory postsynaptic currents (EPSCs) were evoked with a single square stimulus (intensity, 1 to 10 V, duration, 100 to 200 μs) delivered via a glass stimulating electrode. EPSCs were amplified with a Multiclamp 700B (Molecular Devices, Union City, CA, USA) and acquired using pClamp 10 software (Molecular Devices). The amplitude of EPSCs was determined by measuring the average current during a 2-ms period at the peak of each EPSC and subtracted from the baseline current determined during a 5-ms time window before the stimulus. All EPSC amplitudes were normalized to the mean baseline amplitude recorded for at least 10 min before drug application. Results in the text and figures are presented as mean ± SEM. Statistical analysis was conducted using the Student's paired t-test.

§6.4.5 *In Vitro* Cell Based Assays:

All *in vitro* cell based testing was performed by Dr. Martin Kaczocha, Assistant Professor, Department of Anesthesiology, Stony Brook University, Stony Brook, NY.

AEA Uptake Assay:

AEA uptake assays in wild-type and FABP5 knockdown HeLa cells were performed exactly as described.[4]

FAAH Enzyme Assays:

Enzyme assays measuring the hydrolysis of [^{14}C]AEA in the presence of SB-FI-26 or the FAAH inhibitor URB597 were carried out in HeLa homogenates expressing rat FAAH as described.[2]

PPAR Transactivation Assay:

PPARα and PPARγ transactivation assays were performed in HeLa cells exactly as described.[4] Briefly, cells were transfected with the PPAR reporter system, incubated with GW7647, rosiglitazone, or SB-FI-26 for 6 hrs, followed by measurement of luciferase and β-galactosidase activity using a luminometer as described.[4]

§6.4.6 *In Vivo* Studies in Mice:

All *in vivo* experiments in mice were performed by Dr. Martin Kaczocha, Assistant Professor, Department of Anesthesiology, Stony Brook University, Stony Brook, NY.

Animals: Male C57Bl6 mice (22-30g, Taconic Farms) were used for all experiments. The animals were group housed at room temperature and kept on a 12:12 hour light:dark cycle with *ad libitum* access to water and food. The animals were habituated to the experimental room for one week before testing.

Ethics Statement: All experiments were approved by the Stony Brook University Institutional Animal Care and Use Committee (IACUC Permit Number: 2011-1834). The experimenter (Dr. Martin Kaczocha, Assitant Professor, Department of Anesthesiology, Stony Brook Univeristy, Stony Brook, NY was blinded to the treatment conditions of each animal.

Carrageenan-Enduced Paw Edema and Thermal Hyperalgesia:

Paw edema was induced by injecting 1% λ-carrageenan (20 µl, in sterile saline) into the plantar surface of the left hind paw and a control solution of saline into the right hind paw using a 27 gauge needle. Paw diameters were measured before carrageenan injection and 4 hours after injection using digital electronic calipers (Fisher) and expressed to the nearest ± 0.01 mm. SB-FI-

26 (20 mg/kg, i.p.) was dissolved in ethanol:emulphor:saline (1:1:18), requiring sonication and gentle heating for solubilization, and administered 45 min prior to injection of carrageenan. The cannabinoid receptor antagonists, rimonabant and SR144528 (3 mg/kg, i.p.), in ethanol:emulphor:saline (1:1:18), were injected 15 min before the FABP inhibitor. Edema is reported as the change in paw diameter at 4 hr over the baseline. Changes in paw diameter of saline-injected contralateral paws were negligible. Thermal hyperalgesia measured the latency to withdraw the paw from a focused beam of radiant heat applied to the plantar surface of the hind paw using a Hargreaves plantar apparatus (Ugo Basile) set at an intensity of 3.0. For each mouse, the average latencies consisted of three trials spaced at least 5 minutes apart. The mice were habituated to the test chamber for 30 min. The cutoff time was set at 30 sec.

Formalin Test:

Mice were habituated to the observation chamber (Plexiglas box, 25 cm x 25 cm x 25 cm) for 30 min prior to formalin injection. The mice subsequently received an injection of formalin (2.5% in saline, 20 µl) into the plantar surface of the right hind paw using a 27 gauge needle. The animals were immediately placed back into the observation chamber and nocifensive behavior (time spent licking or biting the paw) was recorded for 60 min. The formalin test consists of two phases with the first phase (0-5 min) reflecting nociceptor activation and the second phase (15-45 min) reflecting an inflammatory pain response.

Statistical Analyses:

Behavioral data are presented as means ± S.E.M. for the vehicle and inhibitor-treated groups, each consisting of at least 6 animals. Statistical significance between vehicle and inhibitor groups was determined using unpaired t-tests or one-way ANOVA followed by Dunnett's post hoc analysis. In all cases, differences of $p < 0.05$ were considered significant.

§6.5 References:

1. Furuhashi, M.; Hotamisligil, G. S., Fatty acid-binding proteins: role in metabolic diseases and potential as drug targets. *Nat. Rev. Drug Discov.* **2008,** *7*, 489 - 503.
2. Kaczocha, M.; Glaser, S. T.; Deutsch, D. G., Identification of intracellular carriers for the endocannabinoid anandamide. *Proc Natl Acad Sci U S A* **2009,** *106*, 6375-80.

3. Howlett, A. C.; Reggio, P. H.; Childers, S. R.; Hampson, R. E.; Ulloa, N. M.; Deutsch, D. G., Endocannabinoid tone versus constitutive activity of cannabinoid receptors. *Br J Pharmacol* **2011,** *163*, 1329-43.
4. Kaczocha, M.; Vicieca, S.; Sun, J.; Glaser, S. T.; Deutsch, D. G., Fatty Acid-binding Proteins Transport N-Acylethanolamines to Nuclear Receptors and Are Targets of Endocannabinoid Transport Inhibitors. *J. Biol. Chem.* **2012,** *287*, 3415 - 3424.
5. Ahn, K.; Johnson, D. S.; Cravatt, B. F., Fatty acid amide hydrolase as a potential therapeutic target for the treatment of pain and CNS disorders. *Expert Opin Drug Discov* **2009,** *4*, 763-784.
6. Veerkamp, J. H.; Zimmerman, A. W., Fatty acid-binding proteins of nervous tissue. *J. Mol. Neurosci.* **2001,** *16*, 133 - 142.
7. Barf, T.; Lehmann, F.; Hammer, K.; Haile, S.; Axen, E.; Medina, C.; Uppenberg, J.; Svensson, S.; Rondahl, L.; Lundback, T., N-Benzyl-indolo carboxylic acids:Design and synthesis of potent and selective adipocyte fatty-acid bind protein (A-FABP) inhibitors. *Bioorg. Med. Chem. Lett.* **2009,** *19*, 1745 - 1748.
8. Sulsky, R.; Magnin, D. R.; Huang, Y.; Simpkins, L.; Taunk, P.; Patel, M.; Zhu, Y.; Stouch, T. R.; Bassolino-Klimas, D.; Parker, R.; Harrity, T.; Stoffel, R.; Taylor, D. S.; Lavoie, T. B.; Kish, K.; Jacobson, B. L.; Scheiff, S.; Adam, L. P.; Ewing, W. R.; Robl, J. A., Potent and selective biphenyl azole inhibitors of adipocyte fatty acid binding protein (aFABP). *Bioorg. Med. Chem. Lett.* **2007,** *17*, 3511 - 3515.
9. *DOCK 6.5*, University of California at San Francisco: San Francisco, CA, 2011.
10. Balius, T. E.; Mukherjee, S.; Rizzo, R. C., Implementation and evaluation of a docking-rescoring method using molecular footprint comparisons. *J Comput Chem* **2011**.
11. Holden, P. M.; Kaur, H.; Gochin, M.; Rizzo, R. C., Footprint-based identification of HIVgp41 inhibitors. *Bioorg. Med. Chem. Lett.* **2012,** *ss*, 3011 - 3016.
12. Irwin, J. J.; Shoichet, B. K., ZINC - A Free Database of Commercially Available Compounds for Virtual Screening. *J. Chem. Inf. Model.* **2005,** *45*, 177 - 182.
13. Nakamura, M.; Chi, Y. M.; Yan, W. M.; Nakasugi, Y.; Yoshizawa, T.; Irino, N.; Hashimoto, F.; Kinjo, J.; Nahara, T.; Sakurada, S., Strong Antinociceptive Effect of Incarvillateine, a Novel Monoterpene Alkaloid from *Incarvillea sinensis*. *J. Nat. Prod.* **1999,** *62*, 1293 - 1294.
14. Chi, Y. M.; Nakamura, M.; Yashizawa, T.; Zhao, X. Y.; Yan, W. M.; Hashimoto, F.; Kinjo, J.; Nohara, T.; S., S., Anti-inflammatory activities of alpha-truxillic acid derivatives and there monomer components. *Biol. Pharm. Bull.* **2005,** *28*, 1776 - 1778.
15. Chi, Y. M.; Nakamura, M.; Zhao, X. Y.; Yoshizawa, T.; Yan, W. M.; Hashimoto, F.; Kinjo, J.; Nohara, T.; S., S., Antinociceptive activities of alpha-truxillic acid and beta-truxinic acid derivatives. *Biol. Pharm. Bull.* **2006,** *29*, 580 - 584.
16. Haj-Dahmane, S.; Shen, R. Y., Endocannabinoids suppress excitatory synaptic transmission to dorsal raphe serotonin neurons through the activation of presynaptic CB1 receptors. *J Pharmacol Exp Ther* **2009,** *331*, 186-96.

17. Cravatt, B. F.; Demarest, K.; Patricelli, M. P.; Bracey, M. H.; Giang, D. K.; Martin, B. R.; Lichtman, A. H., Supersensitivity to anandamide and enhanced endogenous cannabinoid signaling in mice lacking fatty acid amide hydrolase. *Proceedings of the National Academy of Sciences of the United States of America* **2001,** *98*, 9371-6.
18. Lichtman, A. H.; Martin, B. R., Spinal action of cannabinoid-induced antinociception. *NIDA Res Monogr* **1990,** *105*, 422-4.
19. Cravatt, B. F.; Lichtman, A. H., The endogenous cannabinoid system and its role in nociceptive behavior. *Journal of neurobiology* **2004,** *61*, 149-60.
20. Steri, R.; Rupp, M.; Proschak, E.; Schroeter, T.; Zettl, H.; Hansen, K.; Schwarz, O.; Muller-Kuhrt, L.; Muller, K. R.; Schneider, G.; Schubert-Zsilavecz, M., Truxillic acid derivatives act as peroxisome proliferator-activated receptor gamma activators. *Bioorg Med Chem Lett* **2010,** *20*, 2920-3.
21. LoVerme, J.; Russo, R.; La Rana, G.; Fu, J.; Farthing, J.; Mattace-Raso, G.; Meli, R.; Hohmann, A.; Calignano, A.; Piomelli, D., Rapid broad-spectrum analgesia through activation of peroxisome proliferator-activated receptor-alpha. *J Pharmacol Exp Ther* **2006,** *319*, 1051-61.
22. Churi, S. B.; Abdel-Aleem, O. S.; Tumber, K. K.; Scuderi-Porter, H.; Taylor, B. K., Intrathecal rosiglitazone acts at peroxisome proliferator-activated receptor-gamma to rapidly inhibit neuropathic pain in rats. *J Pain* **2008,** *9*, 639-49.
23. Fu, J.; Bottegoni, G.; Sasso, O.; Bertorelli, R.; Rocchia, W.; Masetti, M.; Guijarro, A.; Lodola, A.; Armirotti, A.; Garau, G.; Bandiera, T.; Reggiani, A.; Mor, M.; Cavalli, A.; Piomelli, D., A catalytically silent FAAH-1 variant drives anandamide transport in neurons. *Nature neuroscience* **2011,** *15*, 64-9.
24. Maccarrone, M.; Dainese, E.; Oddi, S., Intracellular trafficking of anandamide: new concepts for signaling. *Trends in biochemical sciences* **2010,** *35*, 601-8.
25. Fowler, C. J., Anandamide uptake explained? *Trends in pharmacological sciences* **2012,** *33*, 181-5.
26. DOCK6.5, University of California at San Francisco: San Francisco, CA, 2011.
27. Kuntz, I. D.; Blaney, J. M.; Oatley, S. J.; Langridge, R.; Femin, T. E., A geometric approach to macromolecule-ligand interactions. *Journal of Molecular Biology* **1982,** *161*, 269 - 288.
28. Mukherjee, S.; Balius, T. E.; Rizzo, R. C., Docking Validation Resources: Protein Family and LIgand Flexibility Experiments. *Journal of Chemical Information and Modeling* **2010,** *50*, 1986 - 2000.
29. Balius, T. E.; Mukherjee, S.; Rizzo, R. C., Implementation and evaluation of a docking-rescoring method using molecular footprint comparisons. *Journal of computational chemistry* **2011,** *32*, 2273 - 2289.
30. *Molecular Operating Environment (MOE)*, Chemical Computing Group Inc.: 1010 Sherbooke St. West, Suite #910, Montreal, QC, Canada, H3A 2R7, 2011.

31. Hunter, J. D., Matplotlib: A 2D Graphics Environment. *Computing in Science & Engineering* **2007,** *9*, 90 - 95.
32. Yang H, J. L., Wang Z, Di-Cicco A, Levy D, et al., Novel Photolabile Diblock Copolymers Bearing Truxillic Acid Derivative Junctions. *Macromolecules* **2011**, 159 - 165.
33. Arendaruk AP, S. A., Kharkevich DA, Studies on Cyclobutanedicarboxylic Acids V. Sythesis of Bisquarternary Salts of Alkylamine Esters and Amides of the Stereoisomeric Truxillic Acids. *Khimiko-Farmatsevticheskii Zhurnal* **1967**, 18 - 21.
34. ChemDiv Screening Collection. In. In *ChemDiv, editor.* ChemDive Catalog2012.
35. Haj-Dahmane, S.; Shen, R. Y., The wake-promoting peptide orexin-B inhibits glutamatergic transmission to dorsal raphe nucleus serotonin neurons through retrograde endocannabinoid signaling. *The Journal of neuroscience : the official journal of the Society for Neuroscience* **2005,** *25*, 896-905.

References

References for Chapter 1:

1. Jemal, A.; Seigel, R.; Ward, E.; Hao, Y.; Xu, J.; Murray, T.; Thun, M. J., Cancer Statistics, 2008. *CA Cancer J Clin* **2008,** *58*, 71 - 96.
2. American Cancer Society: Cancer facts & figures 2008. **2008**.
3. Hanahan, D.; Weinberg, R. A., The Hallmarks of Cancer. *Cell* **2000,** *100*, 57 - 70.
4. http://www.cancervic.org.au/images/CISS/cancer-types/cancer-spreading.gif (accessed, 12/08/13),
5. http://www.cancervic.org.au/images/CISS/cancer-types/cancer-beginning.gif (accessed, 12/08/13),
6. http://www.cancer.gov/cancertopics/factsheet/detection/staging (accessed, 11/09/13),
7. Jordon, M. A.; Wilson, L., Microtubule Polymerization Dynamics, Mitotic Block, and Cell Death by Paclitaxel at Low Concentrations. In *Taxane anticancer agents: Basic science and current status*, Georg, G. I.; Chen, T. T.; Ojima, I.; Vyas, D. M., Eds. American Chemical Society, Washington D.C.1994; pp 138 - 153.
8. Kingston, D. G. I., Recent Advances in the Chemistry of Taxol. *J. Nat. Prod.* **2000,** *63*, 726 - 734.
9. Schiff, P. B.; Fant, J.; Horwitz, S. B., Promotion of microtubule assembly in vitro by taxol. *Nature* **1979,** *277*, 665 - 667.
10. Jordan, M. A.; Wendell, K.; Gardiner, S.; Brent Derry, W.; Copp, H.; Wilson, L., Mitotic Block Induced in HeLa Cells by Low Concentrations of Paclitaxel (Taxol) Results in Abnormal Mitotic Exit and Apoptotic Cell Death. *Cancer Res.* **1996,** *56*, 816 - 825.
11. Wang, T. H.; Wang, H. S.; Soong, Y. K., Paclitaxel-induced cell death: where the cell cycle and apoptosis come together. *Cancer* **2000,** *88*, 2619 - 2628.
12. Park, S. J.; Wu, C. H.; Gordon, J. D.; Zhong, X.; Emami, A.; Safa, A. R., Taxol induces caspase-10-dependent apoptosis. *J. Biol. Chem.* **2004,** *279*, 51057 - 51067.
13. Luduena, R. F.; Shooter, E. M.; Wilson, L., Structure of the tubulin dimer. *J. Biol. Chem.* **1977,** *252*, 7006 - 7014.
14. Mitchison, T.; Kirschner, M., Dynamic instability of microtubule growth. *Nature* **1984,** *312*, 237 - 242.
15. Schiff, P. B.; Horwitz, S. B., Taxol stabilizes microtubules in mouse fibroblast cells. *Proc. Natl. Acad. Sci* **1980,** *77*, 1561 - 1565.
16. Schiff, P. B.; Horwitz, S. B., Taxol assembles tubulin in the absence of exogenous Guanosine 5'-Triphosphate or Microtubule-Associated Proteins. *Biochemistry* **1981,** *20*, 3247 - 3252.
17. Nogales, E.; Wolf, S. G.; Khan, I. A.; Luduena, R. F.; H., D. K., Structure of tubulin at 6.5 angstrom and location of the taxol-binding site. *Nature* **1995,** *375*, 424 - 427.

18. Nogales, E.; Wolf, S. G.; Downing, K. H., Structure of the [alpha][beta] tubulin dimer by electron crystallography. *Nature* **1998,** *391*, 199 - 203.
19. Mahadevan, L.; Mitchison, T. J., Cell biology: Powerful curves. *Nature* **2005,** *435*, 895 - 897.
20. Holton, R. A.; Kim, H. B.; Somoza, C.; Liang, F.; Biediger, R. J.; Boatman, P. D.; Shindo, M.; Smith, C. C.; Kim, S.; Nadizadeh, H.; Suzuki, Y.; Tao, C.; Vu, P.; Tang, S.; Zhang, P.; Murthi, K. K.; Gentile, L. N.; Liu, J. H., First total synthesis of Taxol. 2. Completion of the C and D rings. *J. Am. Chem. Soc.* **1994,** *116*, 1599 - 1600.
21. Nicolaou, K. C.; Yang, Z.; Liu, J. J.; Ueno, H.; Nantermet, P. G.; Guy, R. K.; Claiborne, C. F.; Renaud, J.; Couladouros, E. A.; Paulvannan, K.; Sorensen, E. J., Total Synthesis of Taxol. *Nature* **1994,** *367*, 630 - 634.
22. Nicolaou, K. C.; Liu, J. J.; Yang, Z.; Ueno, H.; Sorensen, E. J.; Claiborne, C. F.; Guy, R. K.; Hwang, C. K.; Nakada, M.; Nantermet, P. G., Total synthesis of Taxol. 2. Construction of A and C ring intermediates and intial attempts to construct the ABC ring system. *J. Am. Chem. Soc.* **1995,** *117*, 634 - 644.
23. Nicolaou, K. C.; Yang, Z.; Liu, J. J.; Nantermet, P. G.; Claiborne, C. F.; Renaud, J.; Guy, R. K.; Shibayama, K., Total synthesis of Taxol. 3. Formation of Taxol's ABC ring skeleton. *J. Am. Chem. Soc.* **1995,** *117*, 645 - 652.
24. Nicolaou, K. C.; Ueno, H.; Liu, J. J.; Nantermet, P. G.; Yang, Z.; Renaud, J.; Paulvannan, K.; Chadha, R., Total synthesis of Taxol. 4. The final stages and completion of the synthesis of Taxol. 4. The final stages and completion of the synthesis. *J. Am. Chem. Soc.* **1995,** *117*, 653 - 659.
25. Danishefsky, S. J.; Masters, J. J.; Young, W. B.; Link, J. T.; Snyder, L. B.; Jung, D. K.; Isaccs, R. C.; Bornmann, W. G.; Alaimo, C. A.; Coburn, C. A.; Di Grandi, M. J., Total Synthesis of Baccatin III and Taxol. *J. Am. Chem. Soc.* **1996,** *118*, 2843 - 2859.
26. Wender, P. A.; Mucciaro, T. P., A new and practical approach to the synthesis of Taxol and Taxol analogues: The pinene path. *J. Am. Chem. Soc.* **1992,** *114*, 5878 - 5879.
27. Wender, P. A.; Badham, N. F.; Conway, S. P.; Florencig, P. E.; Glass, T. E.; Houze, J. B.; Krauss, N. E.; Lee, D.; Marquess, D. G.; McGrane, P. L.; Meng, W.; Natchus, M. G.; Shuker, A. J.; Sutton, J. C.; Taylor, R. E., The pinene path to taxenes. 6. A concise sterocontrolled synthesis of Taxol. *J. Am. Chem. Soc.* **1997,** *119*, 2757 - 2758.
28. Morihira, K.; Hara, R.; Kawahara, S.; Nishimori, T.; Nakamura, N.; Kusama, H.; Kuwajima, I., Enantioselective total synthesis of taxol. *J. Am. Chem. Soc.* **1998,** *120*, 12980 - 12981.
29. Mukaiyama, T.; Shiina, I.; Iwadare, H.; Saitoh, M.; Nishimura, T.; Ohkawa, N.; Sakoh, H.; Nishimura, K.; Tani, Y.-I.; Hasegawa, M.; Yamada, K.; Saitoh, K., Asymmetric total synthesis of taxol. *Eur. J. Chem.* **1999,** *5*, 121 - 161.
30. Doi, T.; Fuse, S.; Miyamoto, S.; Nakai, K.; Sasuga, D.; Takahashi, T., A Formal Total Synthesis of Taxol Aided by an Automated Synthesizer. *Chemistry – An Asian Journal* **2006,** *1*, 370-383.

31. Gueitte-Voegelein, F.; Senilh, V.; David, B.; Gueard, D.; Potier, P., Chemical studies of 10-deacetyl baccatin III. Semisynthesis of taxol derivatives. *Tetrahedron* **1986,** *42*, 4451 - 4460.
32. Denis, J. N.; Greene, A. E.; Gueard, D.; Gueitte-Voegelein, F.; Mangatal, L.; Potier, P., A highly efficent, practical approach to natural taxol. *J. Am. Chem. Soc.* **1988,** *110*, 5917 - 5919.
33. Denis, J. N.; Correa, A.; Greene, A. E., An improved synthesis of the taxol side chain and of RP 56976. *J. Org. Chem.* **1990,** *55*, 1957 - 1959.
34. Wang, Z.-M.; Kolb, H. C.; Sharpelss, K. B., Large-scale and highly enantioselective synthesis of the Taxol C-13 side chain through asymmetric dihydroxylation. *J. Org. Chem.* **1994,** *59*, 5104 - 5105.
35. Denis, J. N.; Greene, A. E.; Serra, A. A.; Luche, M. J., An efficient, enantioselective synthesis of the taxol side chain. *J. Org. Chem.* **1986,** *51*, 46 - 50.
36. Deng, L.; Jacobsen, E. N., A practical, highly enantioselective synthesis of taxol side chain *via* asymmetric catalysis. *J. Org. Chem.* **1992,** *57*, 4320 - 4323.
37. Gou, D.-M.; Liu, Y.-C.; Chen, C.-S., A practical chemoenzymatic synthesis of the Taxol C-13 side chain *N*-benzoyl-(2R,3S)-3-phenylisoserine. *J. Org. Chem.* **1993,** *58*, 1287 - 1289.
38. Mukai, C.; Kim, I. J.; Furu, E.; Hanaoka, M., Highly stereocontrolled asymmetric synthesis of taxol and taxotere C-13 side chain analouges. *Tetrahedron* **1993,** *49*, 8323 - 8336.
39. Li, G.; Sharpless, K. B., Catalytic asymmetric aminonohydroxylation provides a short Taxol side-chain synthesis. *Acta. Chem. Scand.* **1996,** *50*, 649 - 651.
40. Kobayashi, S.; Ishitani, H.; Ueno, M., Catalytic asymmetric synthesis of both *syn*- and *anti*-B-amono alcohols. *J. Am. Chem. Soc.* **1998,** *120*, 431 - 432.
41. Holton, R. A. Vol. Eur. Pat. Appl. 1990.
42. Ojima, I.; M.;, S. C.; Zucco, M.; Park, Y. H.; Duclos, O.; Kuduk, S., A highly efficient route to taxotere by the B-lactam synthon method. *Tetrahedron Lett.* **1993,** *34*, 4149 - 4152.
43. Ojima, I.; Habus, I.; Zhao, M.; Zucco, M.; Park, Y. H.; Sun, C. M.; Brigaud, T., New and efficient approches to the semisynthesis of taxol and its C-13 side chain analogs by means of B-lactam synthon method. *Tetrahedron* **1992,** *48*, 6985 - 7012.
44. Ojima, I., Recent Advances in the B-Lactam Synthon Method. *Acc. Chem. Res.* **1995,** *28*, 383 - 389.
45. Guenard, D.; Gueitte-Voegelein, F.; Potier, P., Taxol and Taxotere: Discovery, Chemistry, and Structure-Activity Relationships. *Acc. Chem. Res.* **1992,** *26*, 160 - 167.
46. Verweij, J.; Clavel, M.; Chevalier, B., Paclitaxel (Taxol) and docetaxel (Taxotere): Not simply two of a kind. *Annals of Oncology* **1994,** *5*, 495 - 505.
47. Ojima, I.; Duclos, O.; Kuduk, S. D.; Sun, C. M.; Slater, J. C.; Lavelle, F.; Veith, J. M.; Bernacki, R. J., Synthesis and Biological Activity of 3'-alkyl- and 3'-alkenyl-3'-dephenyldocetaxel. *Bioorg. Med. Chem. Lett.* **1994,** *4*, 2631 - 2634.

48. Ojima, I.; Slater, J. C.; Michaud, E.; Kuduk, S.; Bounaud, P.-Y.; Vrignaud, P.; Bissery, M.-C.; Veith, J. M.; Pera, P.; Bernacki, R. J., Synthesis and Structure-Activity Relationships of the Second-Generation Antitumor Taxoids: Exceptional Activity against Drug-Resistant Cancer Cells. *J. Med. Chem.* **1996,** *39*, 3889 - 3896.
49. Gottesman, M.; Pastan, I., Biochemistry of multidrug ressitance mediated by the multidrug transporter. *Ann. Rev. Biochem.* **1993,** *62*, 385 - 427.
50. Skehan, P.; Streng, R.; Scudierok, D.; Monks, A.; McMahon, J.; Vistica, D.; Warren, J. T.; Bokesch, H.; Kenny, S.; Boyd, M. R., New Colorimetric Cytotoxicity Assay for Anticancer-Drug Screening. *J. Natl. Cancer. Int.* **1990,** *82*, 1107 - 1112.
51. Kuznetsova, L.; Chen, J.; Sun, L.; Wu, X.; Pepe, A.; Veith, J. M.; Pera, P.; Bernacki, R. J.; Ojima, I., Syntheses and evaluation of novel fatty acid-second-generation taxoid conjugates as promising anticancer agents. *Bioorg. Med. Chem. Lett.* **2006,** *16*, 974 - 977.
52. Chen, S.; Zhao, X.; Chen, J.; Chen, J.; Kuznetsova, L.; Wong, S. S.; Ojima, I., Mechanism-Based Tumor-Targeting Drug Delivery System. Validation of Efficient Vitamin Receptor-Mediated Endocytosis and Drug Release. *Bioconjugate Chem.* **2010,** *21*, 979 - 987.
53. J.;, C.; Chen, S.; Zhao, X.; Kuznetsova, L. V.; Wong, S. S.; Ojima, I., Functionalized Single-Walled Carbon Nanotubes as Rationally Designed Vehicles for Tumor-Targeted Drug Delivery. *J. Am. Chem. Soc.* **2008,** *130*, 16778 - 16785.
54. Botchkina, G. I.; Zuniga, E. S.; Manisha, D.; Wang, Y.; Wang, H.; Zhu, S.; Savitt, A. G.; Rowehl, R. A.; Leyfmann, Y.; Ju, J.; Shroyer, K.; Ojima, I., New-generation taxoid SB-T-1214 inhibits stem cell-related gene expression in 3D cancer spheroids induced by purified colon tumor-initiating cells. *Molecular Cancer* **2010,** *9*, 192.
55. Staudinger, H., *Justus Liebigs Annalen der Chemie* **1907,** *356*, 51 - 123.
56. Sheehan, J. C.; Henery-Logan, K. R., The Total Synthesis of Penicillin V. *J. Am. Chem. Soc.* **1958,** *81*, 3089 - 3094.
57. Evans, B. E.; Rittle, K. E.; Bock, M. G.; DiPardo, R. M.; Freidinger, R. M.; Whitter, W. L.; Lundell, G. F.; Veber, D. F.; Anderson, P. S.; Chang, R. S. L.; Lotti, V. J.; Cerino, D. J.; B.;, C. T.; Kling, P. J.; Kunkel, K. A.; Springer, J. P.; Hirshfield, J., Methods for Drug Discovery: Development of Potent, Selective, Orally Effective Cholecystokinin Antagonists *J. Med. Chem.* **1988,** *31*, 2235 - 2246.
58. Miller, M. J., Hydroxamate Approach to the Synthesis of B-Lactam Antibiotics. *Acc. Chem. Res.* **1986,** *19*, 49 - 56.
59. Hart, D. J.; Ha, D. C., The ester enolate-imine condesation route to beta-lactams. *Chem. Rev.* **1989,** *89*, 1447 - 1465.
60. Brown, M. J., Literature review of the ester enolate imine condensation. *Heterocycles* **1989,** *29*, 2225 - 2244.
61. Cainelli, G.; Panunzio, M.; Andreoli, P.; Martelli, G.; Spunta, G.; Giacomini, D.; Bandini, E., Metallo-imines: useful reagents in organic synthesis. *Pure Appl. Chem.* **1990,** *62*, 605 - 612.

62. Fujisawa, T.; Shimizu, M., Switching of stereochemistry using different metal enolate species for construction of B-lactam skeletons. *Rev. Heteroatom Chem.* **1996,** *15*, 203 - 225.
63. Xu, J., Steroselectivity in the synthesis of 2-azetidinones from ketenes and imines via the Staudinger reaction. *ARKIVOC* **2009**, 21 - 44.
64. Hegedus, L. S., Synthesis of Amino Acids and Peptides Using Chromium Carbene Complex Photochemistry. *Acc. Chem. Res.* **1995,** *28*, 299 - 305.
65. Chmielewski, M.; Kaluza, Z.; Furman, B., Stereocontrolled synthesis of 1-oxabicyclic B-lactam antibiotics *via* [2 + 2]cycloaddition of isocyanates to sugar vinyl ethers. *Chem. Commun.* **1996**, 2689 - 2696.
66. Brieva, R.; Crich, J. Z.; Sih, C. J., Chemoenzymatic Synthesis of the C-13 Chain of Taxol: Optically-Active 3-Hydroxy-4-phenyl B-Lactam Derivatives. *J. Org. Chem.* **1993,** *58*, 1068 - 1075.
67. Georg, G. I.; Ravikumar, V. T., Stereocontrolled ketene-imine cycloaddition reactions. In Organic Chemistry of *B*-Lactams. Georg, G. I., Ed. VCH: New York1993.
68. Cossio, F. P.; Ugalde, J. M.; Lopez, X.; Lecea, B.; Palomo, C., A semiempierical theoretical study on the formation of B-lactams from ketenes and imines. *J. Am. Chem. Soc.* **1993,** *115*, 995 - 1004.
69. Cossio, F. P.; Arrieta, A.; Lecea, B.; Ugalde, J. M., Chiral Control in the Staudinger Reaction between Ketenes and Imines. A Theoretical SCF-MO Study on Asymmetric Torquoselectivity. *J. Am. Chem. Soc.* **1994,** *116*, 2085 - 2093.
70. Lopez, R.; Sordo, T. L.; Sordo, J. A.; Gonzalez, J., Torquoelectronic effect in the control of the steroselectivity of ketene-imine cycloaddition reactions. *J. Org. Chem.* **1993,** *58*, 7036 - 7037.
71. Jiao, L.; Liang, Y.; Xu, J., Origin of the Relative Stereoselectivity of the B-Lactam Formation in the Staudinger Reaction. *J. Am. Chem. Soc.* **2006,** *128*, 6060 - 6069.
72. Zhao, X. Ph. D. Dissertation: Design, synthesis and biological evaluation of novel taxane-based anticancer agents and their applications to tumor-targeting drug delivery systems. Stony Brook University2009.
73. Palomo, C.; Aizpurua, J. M.; Ganboa, I.; Oiarbide, M., Asymmetric synthesis of β-Lactams by Staudinger ketene-imine cycloaddtion reaction. *Eur. J. Org. Chem.* **1999,** *1999*, 3223 - 3235.
74. Liang, Y.; Jiao, L.; Zhang, S.; Yu, Z.-X.; Xu, J., New insights into the torquoselectivity of the Staudinger Reaction. *J. Am. Chem. Soc.* **2009,** *131*, 1542 - 1549.
75. Cossio, F.; Arrieta, A.; Sierra, M., The mechanism of the ketene-imine (Staundinger) Reaction in its centennial: Still and unsolved problem? *Acc. Chem. Res.* **2008,** *41*, 925 - 936.
76. Ojima, I.; Park, Y. H.; Sun, C. M.; Brigaud, T.; Zhao, M., New and efficient routes to norstatine and its analogs with high enantiomeric purity by B-Lactam Synthon Method. *Tetrahedron Lett.* **1992,** *33*, 5737 - 5740.

77. Whitesell, J. K.; Chen, H. H.; Lawrence, R. M., trans-2-Phenylcyclohexanol. A powerful and redibly available chiral auxilary. *J. Org. Chem.* **1985,** *50*, 4663 - 4664.
78. Schwartz, A.; Madan, P.; Whitesell, J. K.; Lawrence, R. M., Lipase-catalyzed kinetic resolution of alcohols via chloroacetate esters: (-)-(1R,2S)-trans-2-phenylcyclohexanol and (+)-(1S,2R)-trans-2-phenylcyclohexanol. *Org. Syn.* **1990,** *69*, 1 - 9.
79. Seitz, J. Ph.D. Dissertatoin: The design, synthesis and biological evaluation of novel taxoid anticancer agents and their tumor-targeted drug conjugates. Stony Brook University2013.
80. Tietze, L. F.; Gericke, K. M.; Guntner, C., First Total Synthesis of the Bioactive Anthraquinone Kwanzoquinone C and Related Natural Products by a Diels-Alder Approach. *Eur. J. Org. Chem.* **2006,** *2006*, 4910 - 4915.
81. King, S. B.; Sharpelss, K. B., An Efficient Synthesis of Enantiomerically Pure *trans*-2-Phenylcylohexanol. *Tetrahedron Lett.* **1994,** *35*, 5611 - 5612.
82. Gonzalez, J.; Aurigemma, C.; Truesdale, L., Synthesis of (+)-(1S,2R)- and (-)-(1R,2S)-trans-2-phenylcyclohexanol via Sharpless asymmetric dihydroxylation (AD). *Org. Synth.* **2002,** *79*, 93 - 99.
83. Sharpless, K. B.; Amberg, W.; Youssef, B. L.; Crispino, G. A.; Hartung, J.; Jeong, K.-S.; Kwong, H.-L.; Morikawa, K.; Wang, Z.-M.; Xu, D.; Zhang, X.-L., The Oxmium-Catalyzed Asymmetric Dihydroxylation: A New Ligand Class and a Process Improvement. *J. Org. Chem.* **1992,** *57*, 2768 - 2771.
84. Ojima, I.; Sun, L.; Borell, C. P.; Wang, T.; Miller, M. L.; Lin, S.; Geng, X.; Kuznetsova, L.; Qu, C.; Gallager, D.; Zhao, X.; Zanardi, I.; Xia, S.; Horwitz, S. B.; Mallen-St. Clair, J.; Guerriero, J. L.; Bar-Sagi, D.; Veith, J. M.; Pera, P.; Bernacki, R. J., Design, Synthesis, and Biological Evaluation of New-Generation Taxoids. *J. Med. Chem.* **2008,** *51*, 3203 - 3221.
85. Ojima, I.; Slater, J. C.; Kuduk, S. D.; Takeuchi, C. S.; Gimi, R. H.; Sun, C.-M.; Park, Y. H.; Pera, P.; Veith, J. M.; Bernacki, R. J., Synthesis and Structure - Activity Relationships of Taxoids Derived From 14B-Hydroxy-10-deacetylbaccatin III. *J. Med. Chem.* **1997,** *40*, 267 - 278.
86. Lin, S.; Geng, X.; Qu, C.; Tynebor, R.; Gallagher, D. J.; Pollina, E.; Rutter, J.; Ojima, I., Synthesis of Highly Potent Second-Generation Taxoids Through Effective Kinetic Resolution Coupling of Racemic B-Lactams with Baccatins. *Chirality* **2000,** *12*, 431 - 441.
87. Slater, J. C. PhD Dissertation. Stony Brook University1997.
88. Lin, S. Ph.D. Dissertation. Stony Brook University1999.
89. Ceylan, M.; Budak, Y.; Gurdere, M. B.; Ozdemir, I.; Findik, E., Synthesis and Isolation of 1-Cyclohex-1,2-dien-1-ylbenzene from 1-(2-Iodocyclohex-1-en-1-yl)benzene and 1-(2-Iodocyclohex-2-en-1-yl)benzene. *Turk. J. Chem.* **2007,** *31*, 647 - 657.
90. King, S. B.; Sharpelss, B. K., An Efficient Synthesis of Enantiomerically Pure trans-2-Phenylcyclohexanol. *Tetrahedron Lett.* **1994,** *35*, 5611 - 5612.
91. Brenner, S.; Goelet, P.; Stackhouse, J.; Millward, S. W. Drug conjugates and methods of designing the same. WO 01/13958 A2, 01-03-2001, **2001**.

92. Batchelor, M. J.; Bebbington, D.; Bemis, G. W.; Fridman, W. H.; Gillespie, R. J.; Golec, J. M. C.; Gu, Y.; Lauffer, D. J.; Livingston, D. J.; Matharu, S. S.; Mullican, M. D.; Murcko, M. A.; Murdoch, R.; Nyce, P. L.; Robidoux, A. L. C.; Su, M.; Wannamaker, M. W.; Wilson, K. P.; Zelle, R. E. Inhibitors of interleukin-1B converting enzyme. WO 9722619, **1997**.

References for Chapter 2:

1. Chari, R. V. J., Targeted delivery of chemotheraputics: tumor-activated prodrug therapy. *Advanced Drug Delivery Reviews* **1998,** *31*, 89 - 104.
2. Chen, J.; Stanislav, J.; Zhao, X.; Chen, S.; Ojima, I., Antibody-cytotoxic agent conjugates for cancer therapy. *Expert Opinion on Drug Delivery* **2005,** *2*, 873 - 890.
3. Chen, S.; Zhao, X.; Chen, J.; Chen, J.; Kuznetsova, L. V.; Wong, S. S.; Ojima, I., Mechanism-Based Tumor-Targeting Drug Delivery System. Validation of Efficent Vitamin Receptor-Mediated Endocytosis and Drug Release. *Bioconjugate Chemistry* **2010,** *21*, 979 - 987.
4. Jaracz, S.; Chen, J.; Kuznetsova, L. V.; Ojima, I., Recent advances in tumor-targeting anticancer drug conjugates. *Bioorg. Med. Chem.* **2005,** *13*, 5043 - 5054.
5. Ojima, I., Guided Molecular Missiles for Tumor-Targeting Chemotherapy-Case Studies Using the Second-Generation Taxoids as Warheads. *Accounts of Chemical Research* **2008,** *41*, 108 - 119.
6. Ojima, I.; Zuniga, E. S.; Berger, W. T.; Seitz, J. D., Tumor-targeting drug delivery of new-generation taxoids. *Future Med. Chem.* **2012,** *4*, 33 - 50.
7. Das, M. Ph.D. Dissertaiton: Design, Synthesis and Biological Evaluation of Novel Tumor-targeting Taxane-based Drug Delivery Systems. Stony Brook University, Stony Brook, NY, **2010**.
8. Reddy, J. A.; Westrick, E.; Vlahov, I. R.; Howard, S. J.; Santhapuram, H. K.; Leamon, C. P., Folate receptor specific anti-tumor activity of folate-mitomycin conjugates. *Cancer Chemother. Parmacol.* **2006,** *58*, 229 - 236.
9. Zahnd, C.; Wyler, E.; Schwenk, J. M.; Steiner, D.; Lawrence, M. C.; McKern, N. M.; Pecoran, F.; Ward, C. W.; Joos, T. O.; Pluckthun, A., A Designed Ankyrin Repeat Protein Evolved to Picomolar Affinity to Her2. *J. Mol. Biol.* **2007,** *269*, 1015 - 1028.
10. Ojima, I.; Genhelm, X.; Wu, X.; Qu, C.; Borella, C. P.; Xie, H.; Wilhelm, S. D.; Leece, B. A.; Bartle, L. M.; Goldmacher, V. S.; Chari, R. V. J., Tumor-Specific Novel Taxoid-Monoclonal Antibody Conjugates. *J. Med. Chem.* **2002,** *45*, 5620 - 5623.
11. Weinstein, S. J.; Hartman, T. J.; Stolzenberg-Soloman, R.; Pietinen, P.; Barrett, M. J.; Taylor, P. R.; Virtamo, J.; Albanes, D., Null association between prostate cancer and serum folate, vitamin B6, vitamin B12 and homocysteine. *Cancer Epdemiol. Biomarkers Prev.* **2003,** *12*, 1271 - 1272.

12. Reddy, J. A.; Leamon, C. P., *Folate receptor targeted cancer chemotherapy*. Springer Science & Business Media LLC2011.
13. Xia, W.; Low, P. S., Folate-targeted therapies for cancer. *J. Med. Chem.* **2010,** *53*, 6811 - 6824.
14. Leamon, C. P.; Reddy, J. A., Folate-targeted chemotherapy. *Adv. Drug Deliv. Rev.* **2004,** *56*, 1127 - 1141.
15. Leamon, C. P.; Reddy, J. A.; Vlahov, I. R.; Vetzel, M.; Parker, N.; Nicoson, J. S.; Xu, L.-C.; Westrick, E., Synthesis and biological evaluation of EC72: a new folate-targeted chemotherapeutic. *Bioconjugate Chemistry* **2005,** *16*, 803 - 811.
16. Lu, Y.; Leamon, C. P.; Low, P. S., Folate receptor-targeted immunotherapy of cancer: mechanism and theraputic potential. *Adv. Drug Deliv. Rev.* **2004,** *56*, 1161 - 1176.
17. Lu, Y.; Low, P. S., Folate-mediated delivery of macromolecular anticancer therapeutic agents. *Adv. Drug Deliv. Rev.* **2002,** *54*, 675 - 693.
18. Russell-Jones, G.; McTavish, K.; McEwan, J.; Rice, J.; Nowotnik, D., Vitamin-mediated targeting as a potential mechanism to increase drug uptake by tumors. *J. Inorg. Biochemistry* **2004,** *98*, 1625 - 1633.
19. Zhao, X. Ph.D. Dissertation: Design, synthesis and biological evaluation of novel taxane-based anticancer agents and their applications to tumor-targeting drug delivery systems. Stony Brook University, Stony Brook, NY, **2009**.
20. Kharasch, N.; Langford, R. B., Derivatives of Sulfenic Acids. XLII. 3-Chloroformylpropanesulfenyl Chloride and 1,2-Thiazan-3-one. *J. Org. Chem.* **1963,** *28*, 1901 - 1903.
21. Chen, J. Ph.D. Dissertation: Tumor-targeting Drug Delivery System of Anticancer Agent. Ph.D., Stony Brook University, **2008**.
22. Kai, L.; Chen, Y.; Siqi, L.; Nguyen, H. G.; Niu, Z.; You, S.; Mello, C. M.; Lu, X.; Wang, Q., Chemical Modification of M13 Bacteriophage and Its Application in Cancer Cell Imaging. *Bioconjugate Chemistry* **2010,** *21*, 1369 - 1377.
23. Li, M.; Yamato, K.; Ferguson, J. S.; Gong, B., Sequence-Specific Association in Aqueous Media by Integrating Hydrogen Bonding and Dynamic Covalent Interactions. *J. Am. Chem. Soc.* **2006,** *128*, 12628 - 12629.
24. Lin, R.; Cheetham, A. G.; Zhang, P.; Lin, Y.-A.; Cui, H., Supramolecular filaments containing a fixed 41% paclitaxel loading. *Chem. Commun.* **2013,** *49*, 4968 - 4970.

References for Chapter 3:

1. Holman, R. T., The Slow Discovery of the Importance of omega-3 Essential Fatty Acids in Human Health. *Nutr.* **1998,** *128*, 427S - 433S.
2. Sauer, L. A.; Dauchy, R. T.; Blask, D. E., Mechanism for the antitumor and anticachectic effects of omega-3 faty acids. *Cancer Res.* **2000,** *60*, 5289 - 5295.

3. Wigmore, S. J.; Ross, J. A.; Falconer, J. S.; Plester, C. E.; Tisdale, M. J.; Carter, D. C.; Fearon, K. C., The effect of polyunsaturated fatty acids on the progress of cachexia in patients with pancreatic cancer. *Nutrition* **1996,** *12*, S27 - S30.
4. Hawkins, R. A.; Sangster, K.; Arends, M. J., Apoptotic death of pancreatic cancer cells induced by polyunsaturated fatty acids varies with double bond number and involves an oxidative mechanism. *J. Pathol.* **1998,** *185*, 61 - 70.
5. Grammatikos, S. I.; Subbaiah, P. V.; Victor, T. A.; Miller, W. M., omega-3 and omega-6 fatty acid processing and growth effects in neoplastic and noncancerous human mammary epithelial cell lines. *Br. J. Cancer* **1994,** *70*, 219 - 227.
6. Diomede, I.; Colotta, F.; Piovani, B.; Re, F.; Modest, E. J.; Salmona, M., Induction of apoptosis in human leukemic cells by the ether lipid 1-octadecyl-2-methyl-racglycero-3-phosphocholine. A possible basis for its selective action. *Int. J. Cancer Res.* **1993,** *53*, 124 - 130.
7. Bradley, M. O.; Webb, N. L.; Anthony, F. H.; Devanesan, P.; Witman, P. A.; Hemamalini, W. S.; Chander, M. C.; Baker, S. D.; He, L.; Horwitz, S. B.; Swindell, C. S., Tumor Targeting by Covalent Conjugation of a Natural Fatty Acid to Paclitaxel. *Clin. Cancer. Res.* **2001,** *7*, 3229 - 3238.
8. Sparreboom, A.; Wolff, A. C.; Verweij, J.; Zabelina, Y.; van Zomeren, D. M.; McIntire, G. L.; Swindell, C. S.; Donehower, R. C.; Baker, S. D., Disposition of docosahexaenoic acid-paclitaxel, a novel taxane, in blood: in vitro and clinical pharmacokinetic studies. *Clin. Cancer. Res.* **2003,** *9*, 151 - 159.
9. Ibrahim, N. K.; Desai, N.; Legha, S.; Soon-Shiong, P.; Theriault, R. L.; Rivera, E.; Esmaeli, B.; Ring, S. E.; Bedikian, A.; Hortobagyi, G. N.; Ellerhorst, J. A., Phase I and Pharmacokinetic Study of ABI-007, a Cremophor-free, Protein-stabilized, Nanoparticle Formulation of Paclitaxel. *Clin. Cancer. Res.* **2002,** *8*, 1038 - 1044.
10. Desai, N.; Trieu, V.; Yao, Z.; Louie, L.; Ci, S.; Yang, A.; Tao, C.; De, T.; Beals, B.; Dykes, D.; Noker, P.; Yao, R.; Labao, E.; Hawkins, M.; Soon-Shiong, P., Increased antitumor activity, intratumor paclitaxel concentrations, and endothelial cell transport of cremophor-free, albumin-bound paclitaxel, ABI-007, compared with cremophor-based pacllitaxel. *Clin. Cancer. Res.* **2006,** *12*, 1317 - 1324.
11. Seitz, J. D.; Ojima, I., Drug conjugates with polyunsaturated fatty acids. In *Drug Delivery in Oncology: From Basic Research to Cancer Therapy*, Kratz, F.; Senter, P.; Steinhagen, H., Eds. Wiley-VCH, Weinheim, Germany: Drug Delivery in Oncology: From Basic Research to Cancer Therapy, **2011**; pp 1323 - 1360.
12. Rose, D. P.; Connolly, J. M., Omega-3 fatty acids as cancer chemopreventitive agents. *Pharmacol. Ther.* **1999,** *83*, 217 - 244.
13. Guegan, C.; Vila, M.; Rosoklija, G.; Hays, A. P.; Przedborski, S., Recruitment of the Mitochondrial-Dependent Apoptotic Pathway in Amyotrophic Lateral Sclerosis. *J. Neurosci.* **2001,** *21*, 6569 - 6576.
14. Whelan, J., Targeted taxane therapy for cancer. *Drug. Discov. Today* **2002,** *7*, 90 - 92.

15. Ojima, I.; Slater, J. C.; Michaud, E.; Kuduk, S. D.; Bounaud, P. Y.; Vrignaud, P.; Bissery, M. C.; Veith, J. M.; Pera, P.; Bernacki, R. J., Syntheses and structure-activity relationships of the second-generation antitumor taxoids: exceptional activity against drug-resistant cancer cells. *J. Med. Chem.* **1996,** *39*, 3889 - 3896.
16. Ojima, I.; Slater, J. C.; Kuduk, S. D.; Takeuchi, C. S.; Gimi, R. H.; Sun, C. M.; Park, Y. H.; Pera, P.; Veith, J. M.; Bernacki, R. J., Syntheses and structure-activity relationships of taxoids derived from 14 beta-hydroxy-10-deacetylbaccatin III. *J. Med. Chem.* **1997,** *40*, 267 - 278.
17. Ojima, I.; Chen, J.; Sun, L.; Borella, C. P.; Wang, T.; Miller, M. L.; Lin, S.; Geng, X.; Kuznetsova, L.; Qu, C.; Gallager, D.; Zhao, X.; Zanardi, I.; Xia, S.; Horwitz, S. B.; Mallen-St. Clair, J.; Guerriero, J. L.; Bar-Sagi, D.; Veith, J. M.; Pera, P.; Bernacki, R. J., Design, Synthesis, and Biological Evaluation of New-Generation Taxoids. *J. Med. Chem.* **2008,** *51*, 3203 - 3221.
18. Kuznetsova, L.; Chen, J.; Sun, L.; Wu, X.; Pepe, A.; Veith, J. M.; Pera, P.; Bernacki, R. J.; Ojima, I., Syntheses and evaluation of novel fatty acid-second-generation taxoid conjugates as promising anticancer agents. *Bio. Org. Med. Chem. Letters* **2006,** *16*, 974 - 977.
19. Seitz, J. D. Ph.D. Dissertation: The design, synthesis and biological evaluation of novel taxoid anticancer agents and their tumor-targeted drug conjugates. Stony Brook University, **2013**.
20. Breyer, S.; Effenberger, K.; Schobert, R., Effects of Thymoquinone-Fatty Acid Conjugates on Cancer Cells. *ChemMedChem* **2009,** *4*, 761 - 768.
21. Chen, J., Ph.D. Dissertation., Stony Brook University, **2006**.

References for Chapter 4:

1. Binz, K. H.; Amstutz, P.; Kohl, A.; Stumpp, M. T.; Briand, C.; Forrer, P.; Grutter, M. G.; Plückthun, A., High-affinity binders selected from designed ankyrin repeat proteins libraries. *Nat. Biotech.* **2004,** *22*, 575 - 582.
2. Binz, K. H.; Stumpp, M. T.; Forrer, P.; Amstutz, P.; Plückthun, A., Designing Repeat Proteins: Well-expressed, Soluble and Stable Proteins from Combinatorial Libraries of Consensus Ankyrin Repeat Proteins. *J. Mol. Biol.* **2003,** *332*, 489 - 503.
3. Zahnd, C.; Pecorari, F.; Straumann, N.; Wyler, E.; Plückthun, A., Selection and characterization of Her2 binding-designed ankyrin repeat proteins. *J. Biol. Chem.* **2006,** *281*, 167 - 175.
4. Zahnd, C.; Wyler, E.; Schwenk, J. M.; Steiner, D.; Lawrence, M. C.; McKen, N. M.; Pecorari, F.; Ward, C. W.; Joos, T. O.; Plückthun, A., A designed ankyrin repeat protein evolved to picomolar affinity to Her2. *J. Mol. Biol.* **2007,** *369*, 1015 - 1028.

5. Simon, M.; Zangemeister-Wittke, U.; Plückthun, A., Facile double-functionalization of designed ankyrin repeat proteins using click and thiol chemistries. *Bioconjugate Chem.* **2012,** *23*, 279 - 286.
6. Stumpp, M. T.; Binz, K. H.; Amstutz, P., DARPins: A new generation of protein therapeutics. *Drug Discov. Today* **2008,** *13*, 695 - 701.
7. Ojima, I.; Zuniga, E. S.; Berger, W. T.; Seitz, J. D., Tumor-targeting drug delivery of new-generation taxoids. *Future Med. Chem.* **2012,** *4*, 33 - 50.
8. Sharkey, R. M.; Goldenberg, D. M., Targeted Therapy of Cancer: New Prospects for Antibodies and Immunoconjugates. *CA: A Cancer Journal for Clinicians* **2006,** *56*, 226-243.
9. Ojima, I.; Geng, X.; Wu, X.; Qu, C.; Borella, C. P.; Xie, H.; Wilhelm, S. D.; Leece, B. A.; Bartle, L. M.; Goldmacher, V. S.; Chari, R. V. J., Tumor-specific novel taxoid-monoclonal antibody conjugates. *J. Med. Chem.* **2002,** *45*, 5620 - 5623.
10. Fujimora, K.; Covell, D. G.; Fletcher, J. E.; Weinstein, J. N., A modeling analysis of monoclonal antibody percolation through tumors: a binding-site barrier. *J. Nuc. Chem.* **1990,** *31*, 1191 - 1198.
11. Heldin, C.-H.; Rubin, K.; Pietras, K.; Ostman, A., High interstitial fluid pressure - an obstacle in cancer therapy. *Nat. Rev. Cancer* **2004,** *4*, 806 - 813.
12. Jain, R. K., Transport of molecules, particles, and cells in solid tumors. *Annu. Rev. Biomed. Eng.* **1999,** *1*, 241 - 263.
13. Zahnd, C.; Kawe, M.; Stumpp, M. T.; Pasquale, C. d.; Tamaskovic, R.; Nagy-Davidescu, G.; Dreier, B.; Schibli, R.; Binz, H. K.; Waibel, R.; Plückthun, A., Efficient tumor targeting with high-affinity designed ankyrin repeat proteins: effects of affinity and molecular size. *Cancer Res.* **2010,** *70*, 1595 - 1605.
14. Winkler, J.; Martin-Killas, P.; Plückthun, A.; Zangemeister-Wittke, U., EpCAM-targeted delivery of nanocomplexed si RNA to tumor cells with designed ankyrin repeat proteins. *Mol Cancer Ther* **2009,** *8*, 2674 - 2683.
15. Hussain, S.; Plückthun, A.; Allen, T. M.; Zangemeister-Wittke, U., Chemosensitization of carcinoma cells using epithelial cell adhesion molecule-targeted liposomal antisense against bcl-2/bcl-xL. *Mol. Cancer Ther.* **2006,** *5*, 3170 - 3180.
16. Martin-Killas, P.; Stefan, N.; Rothschild, S.; Plückthun, A.; Zangemeister-Wittke, U., A novel fusion toxin derived from an EpCAM-sepcific designed ankyrin repeat protein has potent antitumor activity. *Clin. Cancer Res.* **2011,** *17*, 100 - 110.
17. Went, P.; Vasei, M.; Bubendorf, L.; Terracciano, L.; Tornillo, L.; Riede, U.; Kononen, J.; Simon, R.; Sauter, G.; Baeuerle, P. A., Frequent high-level expression of the immunotherapeutic target Ep-CAM in colon, stomach, prostate and lung cancers. *Br. J. Cancer* **2006,** *94*, 128 - 135.
18. Spizzo, G.; Went, P.; Dirnhofer, S.; Obrist, P.; Simon, R.; Spichtin, H.; Maurer, R.; Metzger, U.; Von Castelberger, B.; Bart, R.; Stopatschinskaya, S.; Kochli, O. R.; Haas, P.; Mross, F.; Zuber, M.; Dietrich, H.; Bischoff, S.; Mirlacher, M.; Sauter, G.; Gastl, G., High

Ep-CAM Expression is Associated with Poor Prognosis in Node-positive Breast Cancer. *Breast Cancer Res. And Treatment* **2004,** *86*, 207 - 213.

19. Schmelzer, E.; Zhang, L.; Bruce, A.; Wauthier, E.; Ludlow, J.; Yao, H.-I.; Moss, N.; Melhem, A.; McClelland, R.; Turner, W.; Kulik, M.; Sherwood, S.; Tallheden, T.; Cheng, N.; Furth, M. E.; Reid, L. M., Human hepatic stem cells from fetal and postnatal donors. *J. Exp. Med.* **2007,** *204*, 1973 - 1987.
20. Tanaka, M.; Okabe, M.; Suzuki, K.; Kamiya, Y.; Tsukahara, Y.; Saito, S.; Miyajima, A., Mouse hepatoblasts at distinct developmental stages are characterized by expression of EpCAM and DLK1: drastic change of EpCAM expression during liver development. *Mech. Dev.* **2009,** *126*, 665 - 676.
21. Terris, B.; Cavard, C.; Perret, C., EpCAM, a new marker for cancer stem cells in hepatocellular carcinoma. *Journal of hepatology* **2010,** *52*, 280-281.
22. Maetzel, D.; Denzel, S.; Mack, B.; Canis, M.; Went, P.; Benk, M.; Kieu, C.; Papior, P.; Baeuerle, P. A.; Munz, M.; Gires, O., Nuclear signalling by tumour-associated antigen EpCAM. *Nat. Cell Biol.* **2009,** *11*, 162 - 171.
23. Martin-Killas, P.; Stefan, N.; Rothschild, S.; Plückthun, A.; Zangemeister-Wittke, U., A Novel Fusion Toxin Derived from an EpCAM-Specific Designed Ankyrin Repeat Protein Has Potent Antitumor Activity. *Clin. Cancer. Res.* **2011,** *17*, 100 - 110.
24. Botchkina, G. I.; Zuniga, E. S.; M.;, D.; Wang, Y.; Wang, H.; Zhu, S.; Savitt, A. G.; Rowehl, R. A.; Leyfman, Y.; Ju, J.; Shroyer, K.; Ojima, I., New-generation taxoid SB-T-1214 inhibits stem cell-related gene expression in 3D cancer spheroids induced by purified colon tumor-initiating cells. *Mol. Cancer* **2010,** *9*, 192.
25. Xia, W.; Low, P. S., Folate-Targeted Therapies for Cancer. *J. Med. Chem.* **2010,** *53*, 6811 - 6824.
26. Warnecke, A.; Kratz, F., Maleimide-oligo(ethylene glycol) Derivatives of Camptothecin as Albumin-Binding Prodrugs: Synthesis and Antitumor Efficacy. *Bioconjugate Chem.* **2003,** *14*, 377 - 387.
27. Willner, D.; Trail, P. A.; Hofstead, S. J.; King, H. D.; Lasch, S. J.; Braslawsky, G. R.; Greenfield, R. S.; Kaneko, T.; Firestone, R. A., (6-Maleimidocaproyl)hydrazone of Doxorubicin-A New Derivative for the Preparation of Immunoconjugates of Doxorubicin. *Bioconjugate Chem.* **1993,** *4*, 521-527.
28. Warnecke, A.; Kratz, F., Maleimide-oligo(ethylene glycol) Derivatives of Camptothecin as Albumin-Binding Prodrugs: Synthesis and Antitumor Efficacy. *Bioconjugate Chem.* **2003,** *14*, 377 - 387.

References for Chapter 5:

1. Schiavo, G.; Rossetto, O.; Montecucco, C., Clostridial neurtoxins as tools to investigate the molecular events of neurotransmitter release. *Semin. Cell Biol.* **1994,** *5*, 221 - 229.
2. Dasgupta, B. R.; Rasmussen, S., Purification and amino acid composition of type E botulinum neurotoxin. *Toxicon* **1983,** *21*, 535 - 545.
3. Sathyamurthy, V.; Dasgupta, B. R., Seperation, purification, partial characterizaiton and comparison of the heavy and light chains of botulinum neurtoxin types A, B and E. *J. Biol. Chem.* **1985,** *260*, 10461 - 10466.
4. Franz, D. R.; Jahrling, P. B.; Friedlander, D. J.; McClain, D. L.; Hoover, W. R.; Byrne, J. A.; Pavlin, G. W.; Christopher, G. W.; Eitzen, E. M. J., Clinical recongnition and management of patients exposed to biological warfare agents. *JAMA* **1997,** *278*, 399 - 411.
5. http://www.kennislink.nl/publicaties/werking-botox-ontrafeld (11-18-13),
6. Rowland, L. P., Stroke, spasticiity, and botulinum toxin. *N. Engl. J. Med.* **2002,** *347*.
7. Swaminathan, S.; Eswaramoorthy, S., Structural analysis of the catalytic and binding sites of Clostridium botulinum neurotoxin B. *Nat. Struc. Biol.* **2000,** *7*, 639 - 699.
8. Kumaran, D.; Rawat, R.; Ludivico, M. L.; Ahmed, S. A.; Swaminathan, S., Structure- and Substrate-based Inhibitor Design for *Clostridium botulinum* Neurotoxin Serotype A. *J. Biol. Chem.* **2008,** *283*, 18883 - 18891.
9. Zuniga, J. E.; Schmidt, J. J.; Fenn, T.; Burnett, J. C.; Arac, D.; Gussio, R.; Stafford, R. G.; Badie, S. S.; Bavari, S.; Brunger, A. T., A Potent Peptidomimetic Inhibitor of Botulinum Neurotoxin Serotype A Has a Very Different Conformation than SNAP-25 Substrate. *Structure* **2008,** *16*, 1588 - 1597.
10. *DOCK 6.5*, University of California at San Francisco: San Francisco, CA, 2011.
11. Balius, T. E.; Mukherjee, S.; Rizzo, R. C., Implementation and evaluation of a docking-rescoring method using molecular footprint comparisons. *J Comput Chem* **2011**.
12. Holden, P. M.; Kaur, H.; Gochin, M.; Rizzo, R. C., Footprint-based identification of HIVgp41 inhibitors. *Bioorg. Med. Chem. Lett.* **2012,** *ss*, 3011 - 3016.
13. Irwin, J. J.; Shoichet, B. K., ZINC - A Free Database of Commercially Available Compounds for Virtual Screening. *J. Chem. Inf. Model.* **2005,** *45*, 177 - 182.
14. Silvaggi, N. R.; Boldt, G. E.; Hixon, M. S.; Kennedy, J. P.; Tzipori, S.; Janda, K. D.; Allen, K. N., Structures of Clostridium botulinum neurotoxin serotype A light chain complexed with small-molecule inhibitors highlight active-sit flexibility. *Chem. Biol.* **2007,** *14*, 533 - 542.
15. Zuniga, J. E.; Hammill, J. T.; Drory, O.; Nuss, J. E.; Burnett, J. C.; Gussio, R.; Wipf, P.; Bavari, S.; Brunger, A. T., Iterative structure-based peptide-like inhibitor design against the botulinum neurotoxin serotype A. *Plos One* **2010,** *5*, e11378 - e11378.
16. Hines, J.; Groll, M.; Fahnestock, M.; Crews, C. M., Proteasome Inhibition by Fellutamide B Induces Nerve Growth Factor Synthesis. *Chemistry & biology* **2008,** *15*, 501-512.

17. Eubanks, L. M.; Hixon, M. S.; W.;, J.; Hong, S.; Clancy, C. M.; Tepp, W. H.; Baldwin, M. R.; Malizio, C. J.; Goodnough, M. C.; Barbieri, J. T.; Johnson, E. A.; Boger, D. L.; Dickerson, T. J.; Janda, K. D., An in vitro and in vivo disconnect uncovered through high-thoughput identification of botulinum nerotoxin A antagonists. *PNAS* **2007,** *104*, 2602 - 2607.
18. Ndakala, A. J.; Gressner, R. K.; Gitari, P. W.; October, N.; White, K. L.; Hudson, A.; Fakorede, F.; Shackleford, D. M.; Kaiser, M.; Yeates, C.; Charman, S. A.; Chibale, K., Antimalarial Pyrido[1,2-a]benzimidazoles. *J. Med. Chem* **2011,** *54*, 4581 - 4589.
19. Rida, S. M.; Soliman, F. S. G.; Badawey, E. S.-A. M.; Kappe, T., Benzimidazole condensed ring systems. 1. Synthesis and biological investigations of some substituted pyrido[1,2-a]benzimidazoles. *J. Heterocycl. Chem* **1988,** *25*.
20. DOCK6.5, University of California at San Francisco: San Francisco, CA, 2011.
21. Kuntz, I. D.; Blaney, J. M.; Oatley, S. J.; Langridge, R.; Femin, T. E., A geometric approach to macromolecule-ligand interactions. *Journal of Molecular Biology* **1982,** *161*, 269 - 288.
22. Mukherjee, S.; Balius, T. E.; Rizzo, R. C., Docking Validation Resources: Protein Family and LIgand Flexibility Experiments. *Journal of Chemical Information and Modeling* **2010,** *50*, 1986 - 2000.
23. Balius, T. E.; Mukherjee, S.; Rizzo, R. C., Implementation and evaluation of a docking-rescoring method using molecular footprint comparisons. *Journal of computational chemistry* **2011,** *32*, 2273 - 2289.
24. *Molecular Operating Environment (MOE)*, Chemical Computing Group Inc.: 1010 Sherbooke St. West, Suite #910, Montreal, QC, Canada, H3A 2R7, 2011.
25. Hunter, J. D., Matplotlib: A 2D Graphics Environment. *Computing in Science & Engineering* **2007,** *9*, 90 - 95.
26. ChemDiv Screening Collection. In *ChemDiv Catalog* ChemDiv2012.
27. Boldt, G. E.; Kennedy, J. P.; Janda, K. D., Identificaiton of a Potent Botulinum Neurotoxin A Protease Inhibitor Using in Situ Lead Identificaiton Chemistry. *Org. Lett.* **2006,** *8*, 1729 - 1732.

References for Chapter 6:

1. Furuhashi, M.; Hotamisligil, G. S., Fatty acid-binding proteins: role in metabolic diseases and potential as drug targets. *Nat. Rev. Drug Discov.* **2008,** *7*, 489 - 503.
2. Kaczocha, M.; Glaser, S. T.; Deutsch, D. G., Identification of intracellular carriers for the endocannabinoid anandamide. *Proc Natl Acad Sci U S A* **2009,** *106*, 6375-80.
3. Howlett, A. C.; Reggio, P. H.; Childers, S. R.; Hampson, R. E.; Ulloa, N. M.; Deutsch, D. G., Endocannabinoid tone versus constitutive activity of cannabinoid receptors. *Br J Pharmacol* **2011,** *163*, 1329-43.

4. Kaczocha, M.; Vicieca, S.; Sun, J.; Glaser, S. T.; Deutsch, D. G., Fatty Acid-binding Proteins Transport N-Acylethanolamines to Nuclear Receptors and Are Targets of Endocannabinoid Transport Inhibitors. *J. Biol. Chem.* **2012,** *287*, 3415 - 3424.
5. Ahn, K.; Johnson, D. S.; Cravatt, B. F., Fatty acid amide hydrolase as a potential therapeutic target for the treatment of pain and CNS disorders. *Expert Opin Drug Discov* **2009,** *4*, 763-784.
6. Veerkamp, J. H.; Zimmerman, A. W., Fatty acid-binding proteins of nervous tissue. *J. Mol. Neurosci.* **2001,** *16*, 133 - 142.
7. Barf, T.; Lehmann, F.; Hammer, K.; Haile, S.; Axen, E.; Medina, C.; Uppenberg, J.; Svensson, S.; Rondahl, L.; Lundback, T., N-Benzyl-indolo carboxylic acids:Design and synthesis of potent and selective adipocyte fatty-acid bind protein (A-FABP) inhibitors. *Bioorg. Med. Chem. Lett.* **2009,** *19*, 1745 - 1748.
8. Sulsky, R.; Magnin, D. R.; Huang, Y.; Simpkins, L.; Taunk, P.; Patel, M.; Zhu, Y.; Stouch, T. R.; Bassolino-Klimas, D.; Parker, R.; Harrity, T.; Stoffel, R.; Taylor, D. S.; Lavoie, T. B.; Kish, K.; Jacobson, B. L.; Scheiff, S.; Adam, L. P.; Ewing, W. R.; Robl, J. A., Potent and selective biphenyl azole inhibitors of adipocyte fatty acid binding protein (aFABP). *Bioorg. Med. Chem. Lett.* **2007,** *17*, 3511 - 3515.
9. *DOCK 6.5*, University of California at San Francisco: San Francisco, CA, 2011.
10. Balius, T. E.; Mukherjee, S.; Rizzo, R. C., Implementation and evaluation of a docking-rescoring method using molecular footprint comparisons. *J Comput Chem* **2011**.
11. Holden, P. M.; Kaur, H.; Gochin, M.; Rizzo, R. C., Footprint-based identification of HIVgp41 inhibitors. *Bioorg. Med. Chem. Lett.* **2012,** *ss*, 3011 - 3016.
12. Irwin, J. J.; Shoichet, B. K., ZINC - A Free Database of Commercially Available Compounds for Virtual Screening. *J. Chem. Inf. Model.* **2005,** *45*, 177 - 182.
13. Nakamura, M.; Chi, Y. M.; Yan, W. M.; Nakasugi, Y.; Yoshizawa, T.; Irino, N.; Hashimoto, F.; Kinjo, J.; Nahara, T.; Sakurada, S., Strong Antinociceptive Effect of Incarvillateine, a Novel Monoterpene Alkaloid from *Incarvillea sinensis*. *J. Nat. Prod.* **1999,** *62*, 1293 - 1294.
14. Chi, Y. M.; Nakamura, M.; Yashizawa, T.; Zhao, X. Y.; Yan, W. M.; Hashimoto, F.; Kinjo, J.; Nohara, T.; S., S., Anti-inflammatory activities of alpha-truxillic acid derivatives and there monomer components. *Biol. Pharm. Bull.* **2005,** *28*, 1776 - 1778.
15. Chi, Y. M.; Nakamura, M.; Zhao, X. Y.; Yoshizawa, T.; Yan, W. M.; Hashimoto, F.; Kinjo, J.; Nohara, T.; S., S., Antinociceptive activities of alpha-truxillic acid and beta-truxinic acid derivatives. *Biol. Pharm. Bull.* **2006,** *29*, 580 - 584.
16. Haj-Dahmane, S.; Shen, R. Y., Endocannabinoids suppress excitatory synaptic transmission to dorsal raphe serotonin neurons through the activation of presynaptic CB1 receptors. *J Pharmacol Exp Ther* **2009,** *331*, 186-96.
17. Cravatt, B. F.; Demarest, K.; Patricelli, M. P.; Bracey, M. H.; Giang, D. K.; Martin, B. R.; Lichtman, A. H., Supersensitivity to anandamide and enhanced endogenous cannabinoid

signaling in mice lacking fatty acid amide hydrolase. *Proceedings of the National Academy of Sciences of the United States of America* **2001,** *98*, 9371-6.

18. Lichtman, A. H.; Martin, B. R., Spinal action of cannabinoid-induced antinociception. *NIDA Res Monogr* **1990,** *105*, 422-4.
19. Cravatt, B. F.; Lichtman, A. H., The endogenous cannabinoid system and its role in nociceptive behavior. *Journal of neurobiology* **2004,** *61*, 149-60.
20. Steri, R.; Rupp, M.; Proschak, E.; Schroeter, T.; Zettl, H.; Hansen, K.; Schwarz, O.; Muller-Kuhrt, L.; Muller, K. R.; Schneider, G.; Schubert-Zsilavecz, M., Truxillic acid derivatives act as peroxisome proliferator-activated receptor gamma activators. *Bioorg Med Chem Lett* **2010,** *20*, 2920-3.
21. LoVerme, J.; Russo, R.; La Rana, G.; Fu, J.; Farthing, J.; Mattace-Raso, G.; Meli, R.; Hohmann, A.; Calignano, A.; Piomelli, D., Rapid broad-spectrum analgesia through activation of peroxisome proliferator-activated receptor-alpha. *J Pharmacol Exp Ther* **2006,** *319*, 1051-61.
22. Churi, S. B.; Abdel-Aleem, O. S.; Tumber, K. K.; Scuderi-Porter, H.; Taylor, B. K., Intrathecal rosiglitazone acts at peroxisome proliferator-activated receptor-gamma to rapidly inhibit neuropathic pain in rats. *J Pain* **2008,** *9*, 639-49.
23. Fu, J.; Bottegoni, G.; Sasso, O.; Bertorelli, R.; Rocchia, W.; Masetti, M.; Guijarro, A.; Lodola, A.; Armirotti, A.; Garau, G.; Bandiera, T.; Reggiani, A.; Mor, M.; Cavalli, A.; Piomelli, D., A catalytically silent FAAH-1 variant drives anandamide transport in neurons. *Nature neuroscience* **2011,** *15*, 64-9.
24. Maccarrone, M.; Dainese, E.; Oddi, S., Intracellular trafficking of anandamide: new concepts for signaling. *Trends in biochemical sciences* **2010,** *35*, 601-8.
25. Fowler, C. J., Anandamide uptake explained? *Trends in pharmacological sciences* **2012,** *33*, 181-5.
26. DOCK6.5, University of California at San Francisco: San Francisco, CA, 2011.
27. Kuntz, I. D.; Blaney, J. M.; Oatley, S. J.; Langridge, R.; Femin, T. E., A geometric approach to macromolecule-ligand interactions. *Journal of Molecular Biology* **1982,** *161*, 269 - 288.
28. Mukherjee, S.; Balius, T. E.; Rizzo, R. C., Docking Validation Resources: Protein Family and LIgand Flexibility Experiments. *Journal of Chemical Information and Modeling* **2010,** *50*, 1986 - 2000.
29. Balius, T. E.; Mukherjee, S.; Rizzo, R. C., Implementation and evaluation of a docking-rescoring method using molecular footprint comparisons. *Journal of computational chemistry* **2011,** *32*, 2273 - 2289.
30. *Molecular Operating Environment (MOE)*, Chemical Computing Group Inc.: 1010 Sherbooke St. West, Suite #910, Montreal, QC, Canada, H3A 2R7, 2011.
31. Hunter, J. D., Matplotlib: A 2D Graphics Environment. *Computing in Science & Engineering* **2007,** *9*, 90 - 95.

32. Yang H, J. L., Wang Z, Di-Cicco A, Levy D, et al., Novel Photolabile Diblock Copolymers Bearing Truxillic Acid Derivative Junctions. *Macromolecules* **2011**, 159 - 165.
33. Arendaruk AP, S. A., Kharkevich DA, Studies on Cyclobutanedicarboxylic Acids V. Sythesis of Bisquarternary Salts of Alkylamine Esters and Amides of the Stereoisomeric Truxillic Acids. *Khimiko-Farmatsevticheskii Zhurnal* **1967**, 18 - 21.
34. ChemDiv Screening Collection. In. In *ChemDiv, editor.* ChemDive Catalog2012.
35. Haj-Dahmane, S.; Shen, R. Y., The wake-promoting peptide orexin-B inhibits glutamatergic transmission to dorsal raphe nucleus serotonin neurons through retrograde endocannabinoid signaling. *The Journal of neuroscience : the official journal of the Society for Neuroscience* **2005,** *25*, 896-905.

Appendix Chapter 1

7-TES-10-DAB

Pulse Sequence: s2pul
Solvent: CDCl3
Temp. 25.0 C / 298.1 K
User: 1-12-87
INOVA-400 "inv400"

Relax. delay 1.000 sec
Pulse 30.0 degrees
Acq. time 3.273 sec
Width 6000.6 Hz
100 repetitions
OBSERVE H1, 399.8314101 MHz
DATA PROCESSING
FT size 131072
Total time 7 min, 8 sec

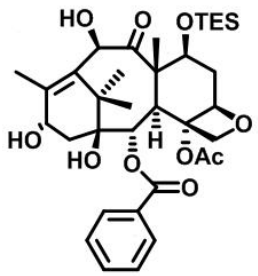

1-1

10-cyclopropanecarbonyl-7-TESbaccatin

Pulse Sequence: s2pul
Solvent: CDCl3
Temp. 25.0 C / 298.1 K
INOVA-600 "inv601"

Relax. delay 1.000 sec
Pulse 61.5 degrees
Acq. time 1.892 sec
Width 8000.0 Hz
16 repetitions
OBSERVE H1, 599.7178142 MHz
DATA PROCESSING
FT size 32768
Total time 0 min, 46 sec

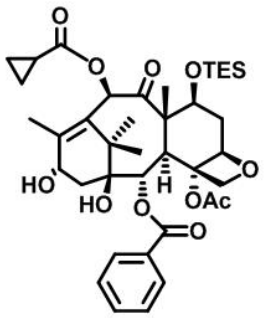

1-2

SB-T-1214TESTIPS

Pulse Sequence: s2pul
Solvent: CDCl3
Temp. 25.0 C / 298.1 K
INOVA-600 "inv601"

Relax. delay 1.000 sec
Pulse 61.5 degrees
Acq. time 1.892 sec
Width 8000.0 Hz
16 repetitions
OBSERVE H1, 599.7178127 MHz
DATA PROCESSING
FT size 32768
Total time 0 min, 46 sec

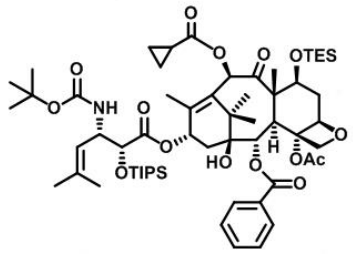

1-3

SB-T-1214

Data Collected on:
inv500-inova500
Archive directory:
/export/home/wberger/vnmrsys/data
Sample directory:

File: PROTON

Pulse Sequence: s2pul
Solvent: CDCl3

Temp. 25.0 C / 298.1 K

Relax. delay 1.000 sec
Pulse 45.0 degrees
Acq. time 1.852 sec
Width 7998.4 Hz
16 repetitions
OBSERVE H1, 499.8948185 MHz
DATA PROCESSING
Line broadening 1.0 Hz
FT size 32768
Total time 1 min

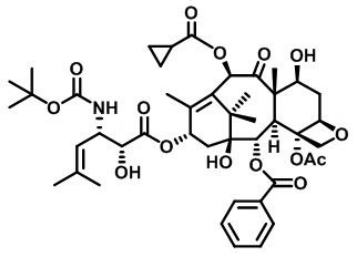

1-4

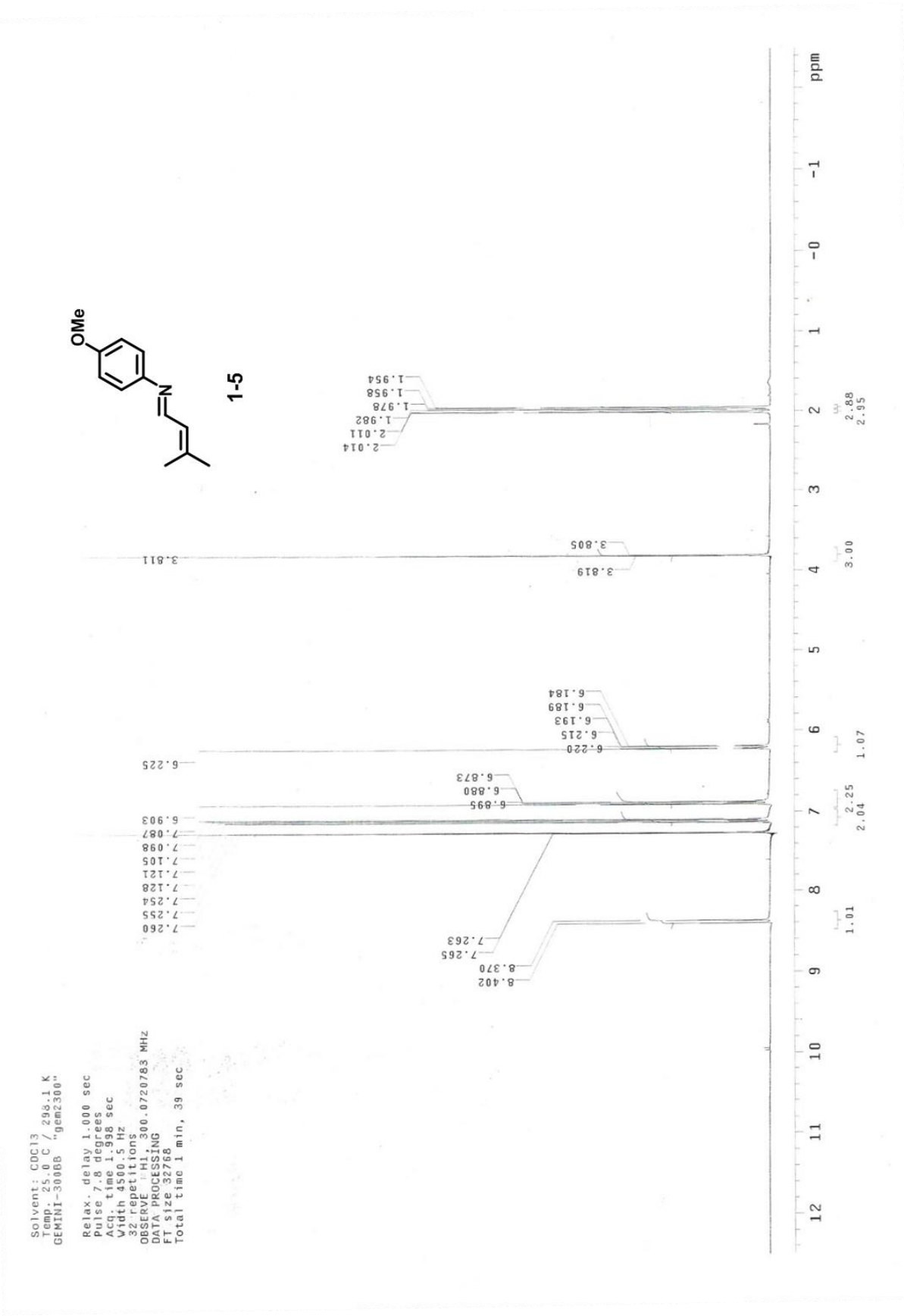
OMe
N
1-5
Solvent: CDCl3
Temp: 25.0 C / 298.1 K
GEMINI-300B "gem2300"
Relax. delay 1.000 sec
Pulse 7.8 degrees
Acq. time 1.998 sec
Width 4500.5 Hz
32 repetitions
OBSERVE H1, 300.0720783 MHz
DATA PROCESSING
FT size 32768
Total time 1 min, 39 sec
ppm

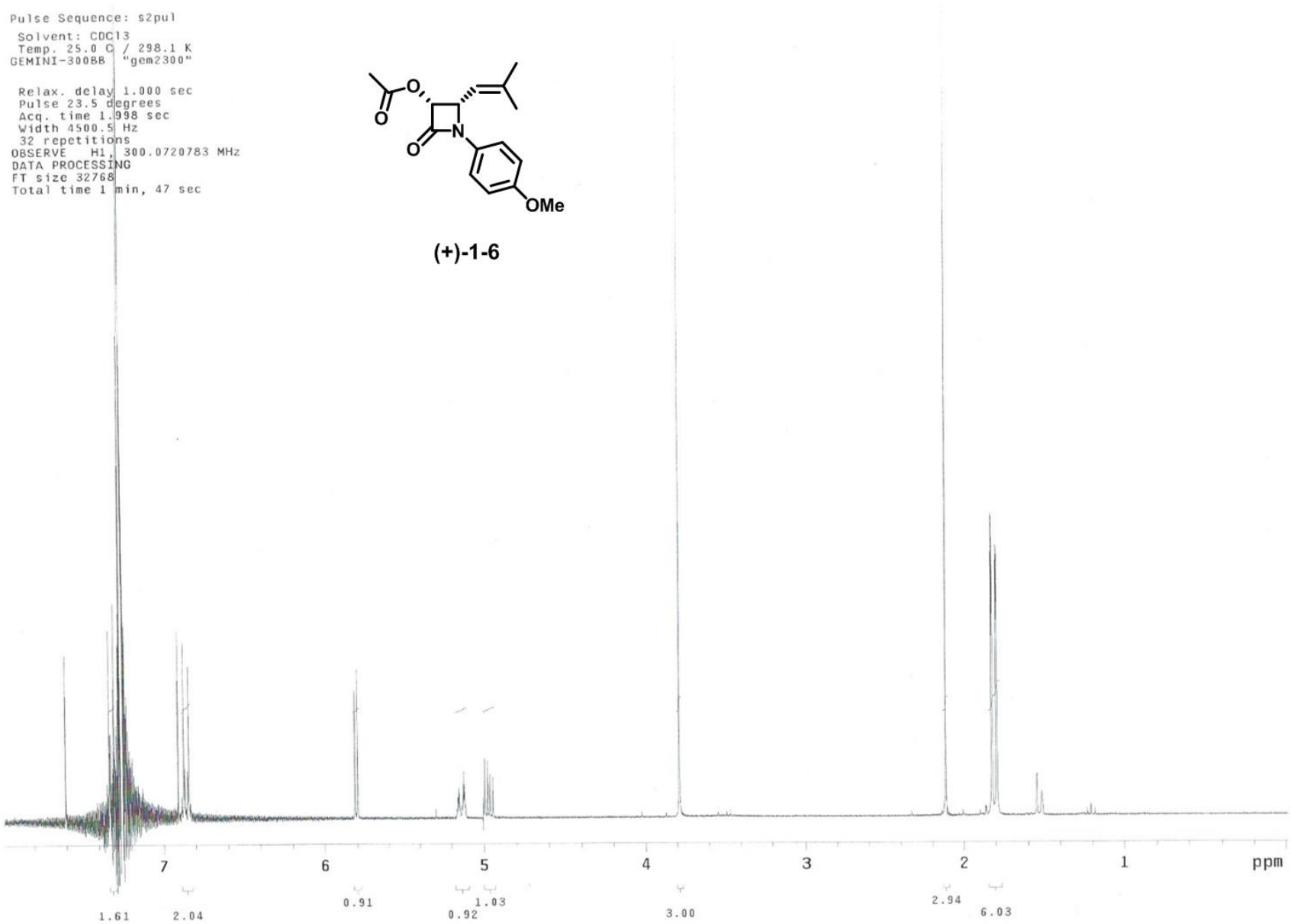
Pulse Sequence: s2pul
Solvent: CDCl3
Temp. 25.0 C / 298.1 K
GEMINI-300BB "gem2300"
Relax. delay 1.000 sec
Pulse 23.5 degrees
Acq. time 1.998 sec
Width 4500.5 Hz
32 repetitions
OBSERVE H1, 300.0720783 MHz
DATA PROCESSING
FT size 32768
Total time 1 min, 47 sec
O
O
O
N
OMe
(+)-1-6
7
6
5
4
3
2
1
ppm
1.61
2.04
0.91
0.92
1.03
3.00
2.94
6.03

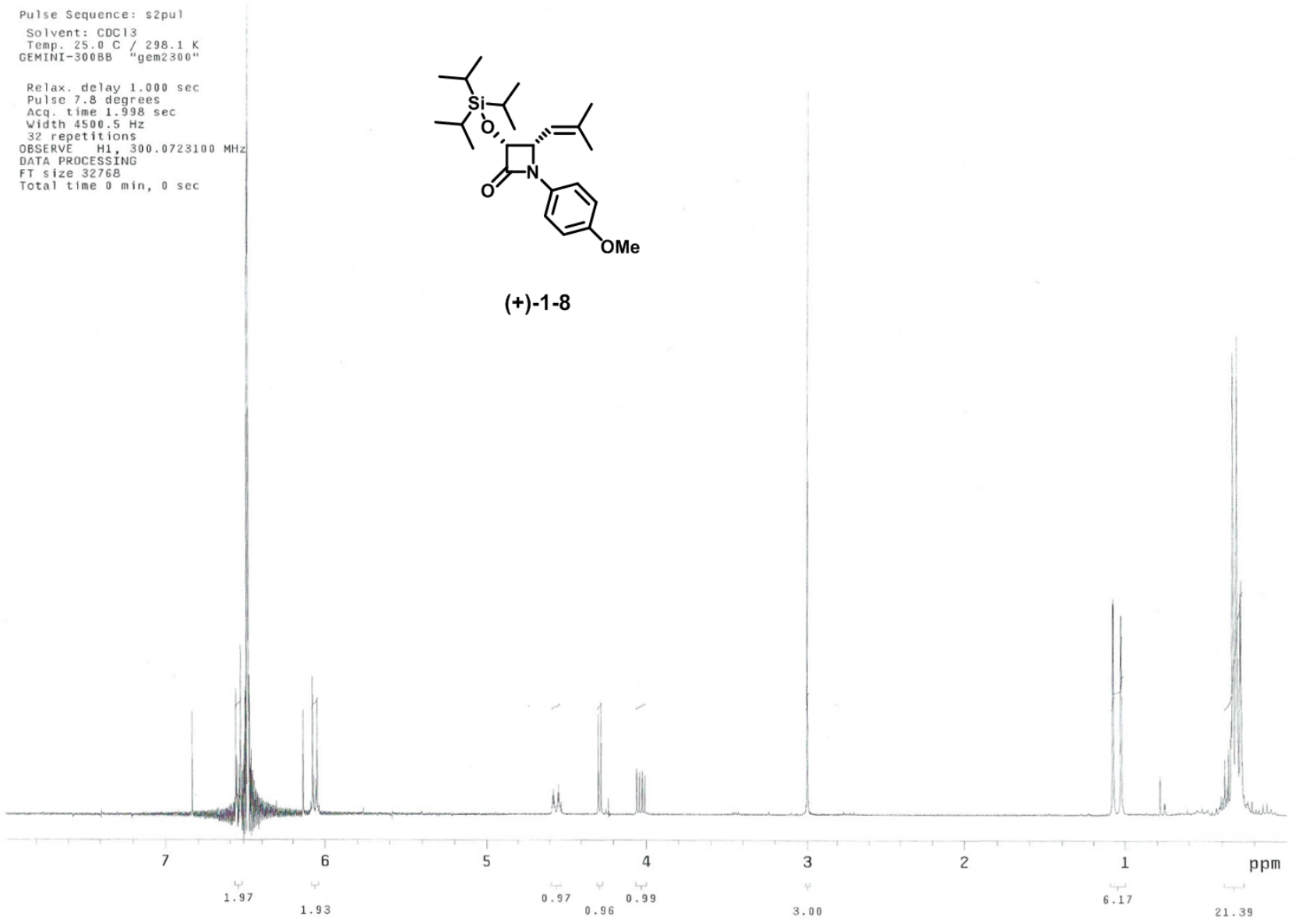
Pulse Sequence: s2pul
Solvent: CDCl3
Temp. 25.0 C / 298.1 K
GEMINI-300BB "gem2300"
Relax. delay 1.000 sec
Pulse 7.8 degrees
Acq. time 1.998 sec
Width 4500.5 Hz
32 repetitions
OBSERVE H1, 300.0723100 MHz
DATA PROCESSING
FT size 32768
Total time 0 min, 0 sec
Si
O
N
O
OMe
7
6
5
4
3
2
1
ppm
1.97
1.93
0.97
0.96
0.99
3.00
6.17
21.39

(+)-1-8

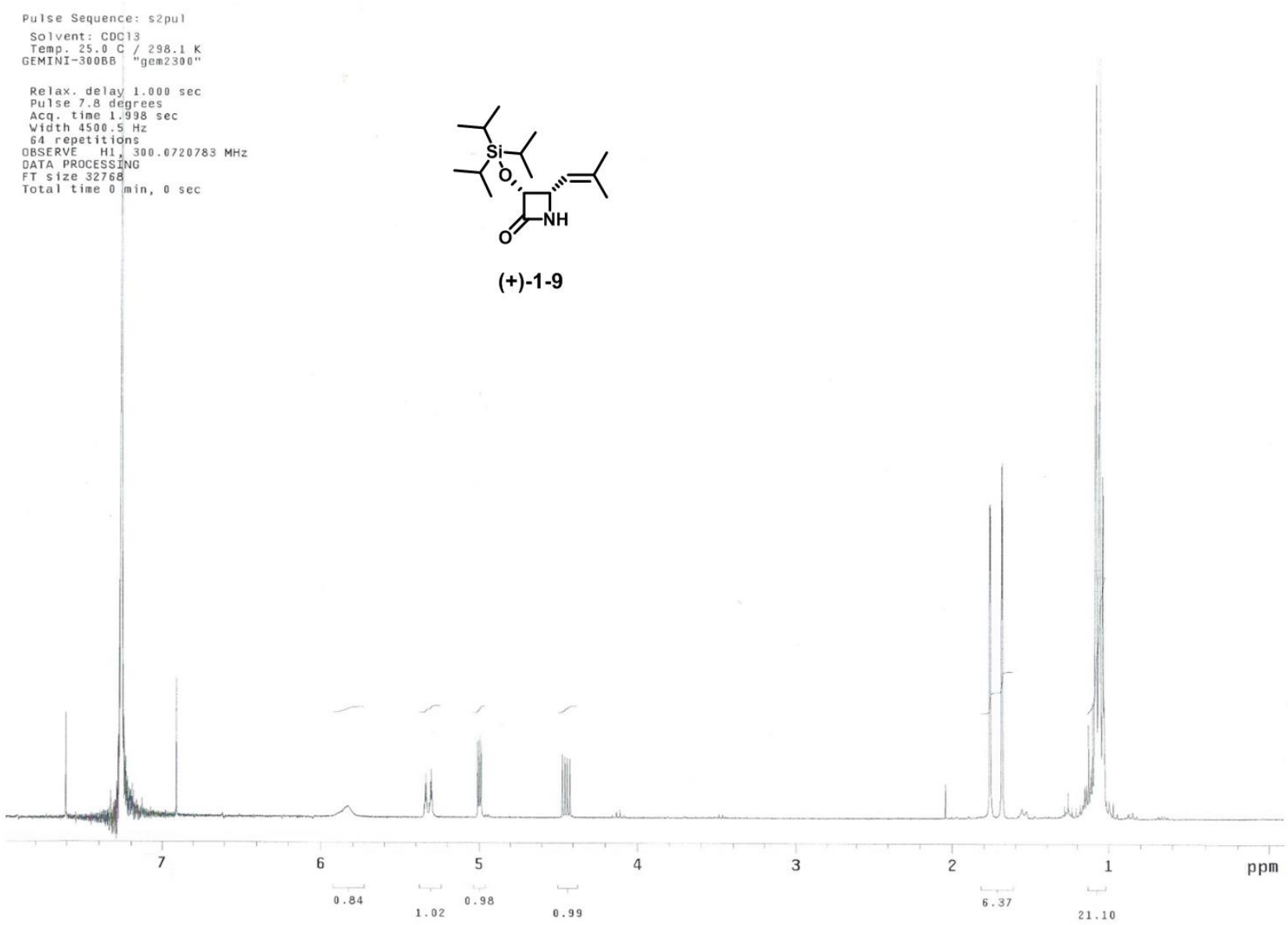
Pulse Sequence: s2pul
Solvent: CDCl3
Temp. 25.0 C / 298.1 K
GEMINI-300BB "gem2300"
Relax. delay 1.000 sec
Pulse 7.8 degrees
Acq. time 1.998 sec
Width 4500.5 Hz
64 repetitions
OBSERVE H1, 300.0720783 MHz
DATA PROCESSING
FT size 32768
Total time 0 min, 0 sec
Si
O
NH
O
(+)-1-9
7
6
5
4
3
2
1
ppm
0.84
1.02
0.98
0.99
6.37
21.10

Pulse Sequence: s2pul
Solvent: CDCl3
Temp. 25.0 C / 298.1 K
GEMINI-300BB "gem2300"

Relax. delay 1.000 sec
Pulse 7.8 degrees
Acq. time 1.998 sec
Width 4500.5 Hz
32 repetitions
OBSERVE H1, 300.0720786 MHz
DATA PROCESSING
FT size 32768
Total time 1 min, 47 sec

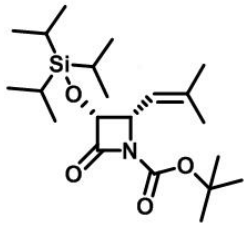

(+)-1-10

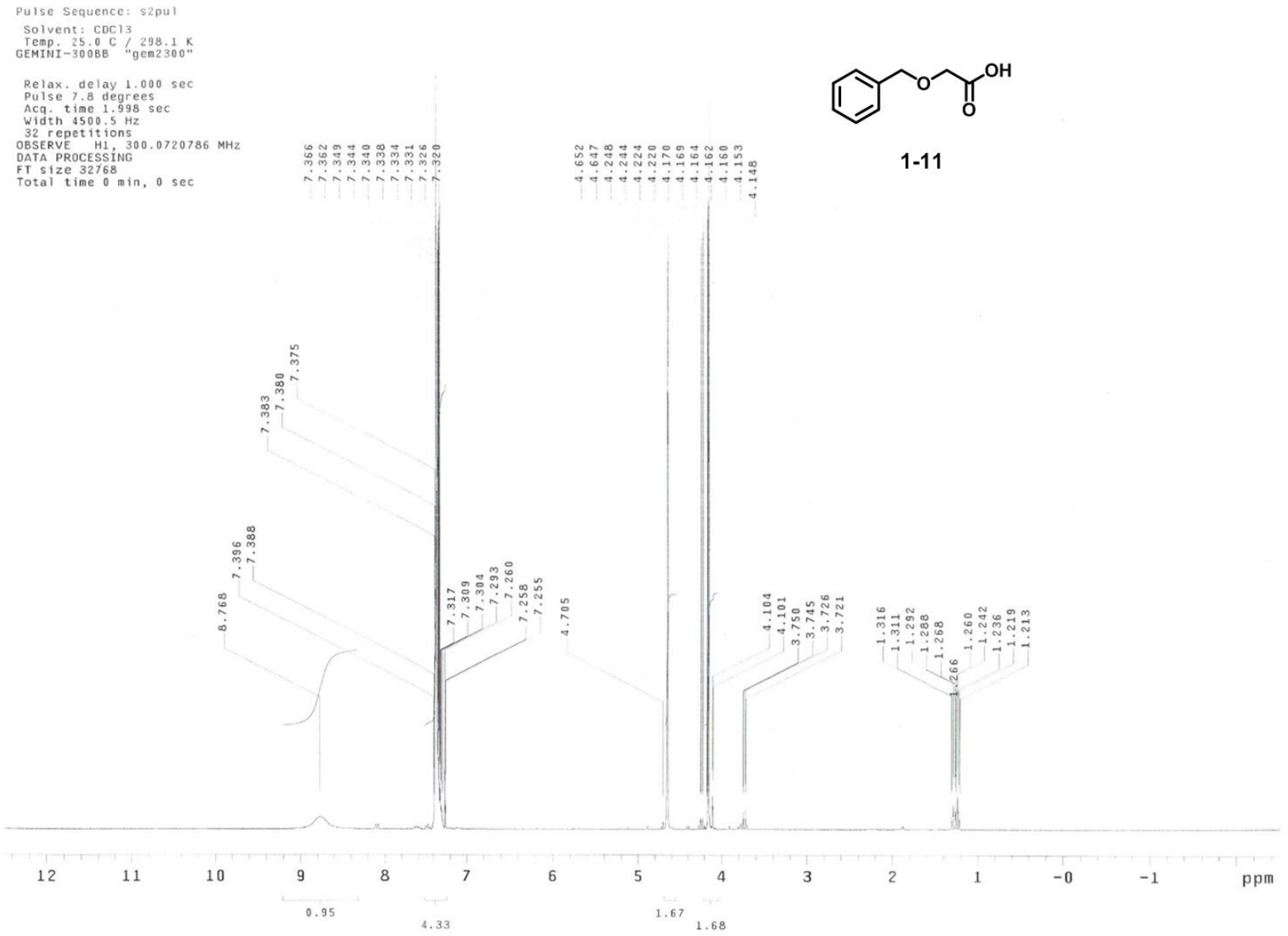
Pulse Sequence: s2pul
Solvent: CDCl3
Temp. 25.0 C / 298.1 K
GEMINI-300BB "gem2300"
Relax. delay 1.000 sec
Pulse 7.8 degrees
Acq. time 1.998 sec
Width 4500.5 Hz
32 repetitions
OBSERVE H1, 300.0720786 MHz
DATA PROCESSING
FT size 32768
Total time 0 min, 0 sec
OH
O
O
1-11
7.366
7.362
7.349
7.344
7.340
7.338
7.334
7.331
7.326
7.320
4.652
4.647
4.248
4.244
4.224
4.220
4.170
4.169
4.164
4.162
4.160
4.153
4.148
7.383
7.380
7.375
7.396
7.388
8.768
7.317
7.309
7.304
7.293
7.260
7.258
7.255
4.705
4.104
4.101
3.750
3.745
3.726
3.721
1.316
1.311
1.292
1.288
1.268
1.266
1.260
1.242
1.236
1.219
1.213
12
11
10
9
8
7
6
5
4
3
2
1
-0
-1
ppm
0.95
4.33
1.67
1.68

Pulse Sequence: s2pul
Solvent: CDCl3
Temp. 25.0 C / 298.1 K
File: chiralauxbenzyloxyaceticesterproton
GEMINI-300BB "gem2300"

Relax. delay 1.000 sec
Pulse 23.5 degrees
Acq. time 1.998 sec
Width 4500.5 Hz
64 repetitions
OBSERVE H1, 300.0720576 MHz
DATA PROCESSING
FT size 32768
Total time 3 min, 35 sec

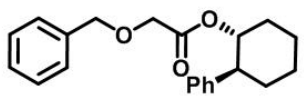

1-12

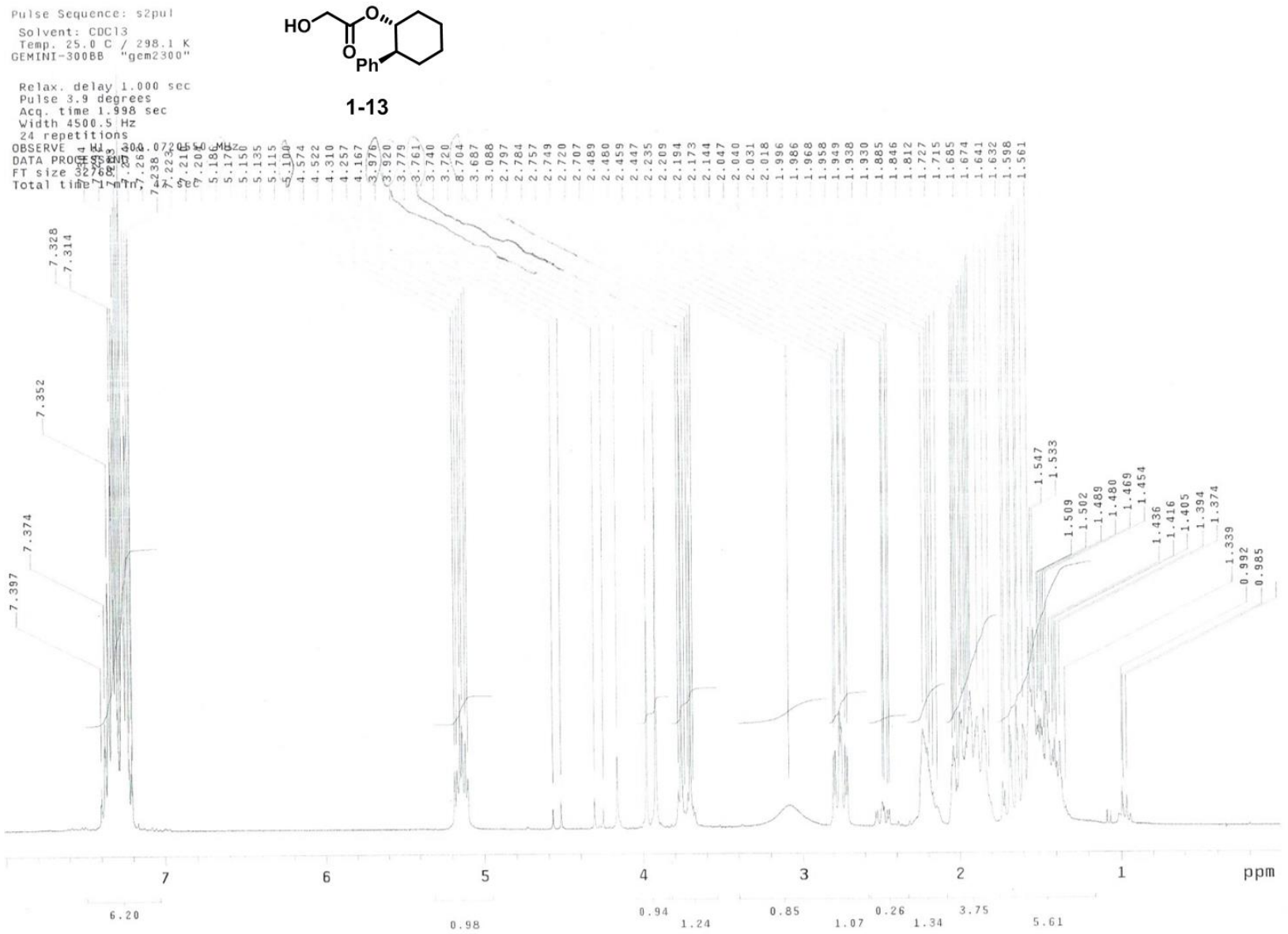
Pulse Sequence: s2pul
Solvent: CDCl3
Temp. 25.0 C / 298.1 K
GEMINI-300BB "gem2300"
Relax. delay 1.000 sec
Pulse 3.9 degrees
Acq. time 1.998 sec
Width 4500.5 Hz
24 repetitions
OBSERVE H1, 300.0720850 MHz
DATA PROCESSING
FT size 32768
Total time 1 min
HO
O
O
Ph
1-13
7.328
7.314
7.352
7.374
7.397
1.547
1.533
1.509
1.502
1.489
1.480
1.469
1.454
1.436
1.416
1.405
1.394
1.374
1.339
0.992
0.985
7
6
5
4
3
2
1
ppm
6.20
0.98
0.94
1.24
0.85
1.07
0.26
1.34
3.75
5.61

Pulse Sequence: s2pul
Solvent: CDCl3
Temp. 25.0 C / 298.1 K
INOVA-600 "inv601"

Relax. delay 1.000 sec
Pulse 61.5 degrees
Acq. time 1.892 sec
Width 8000.0 Hz
32 repetitions
OBSERVE H1, 599.7178159 MHz
DATA PROCESSING
FT size 32768
Total time 1 min, 32 sec

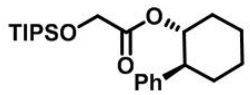

1-14

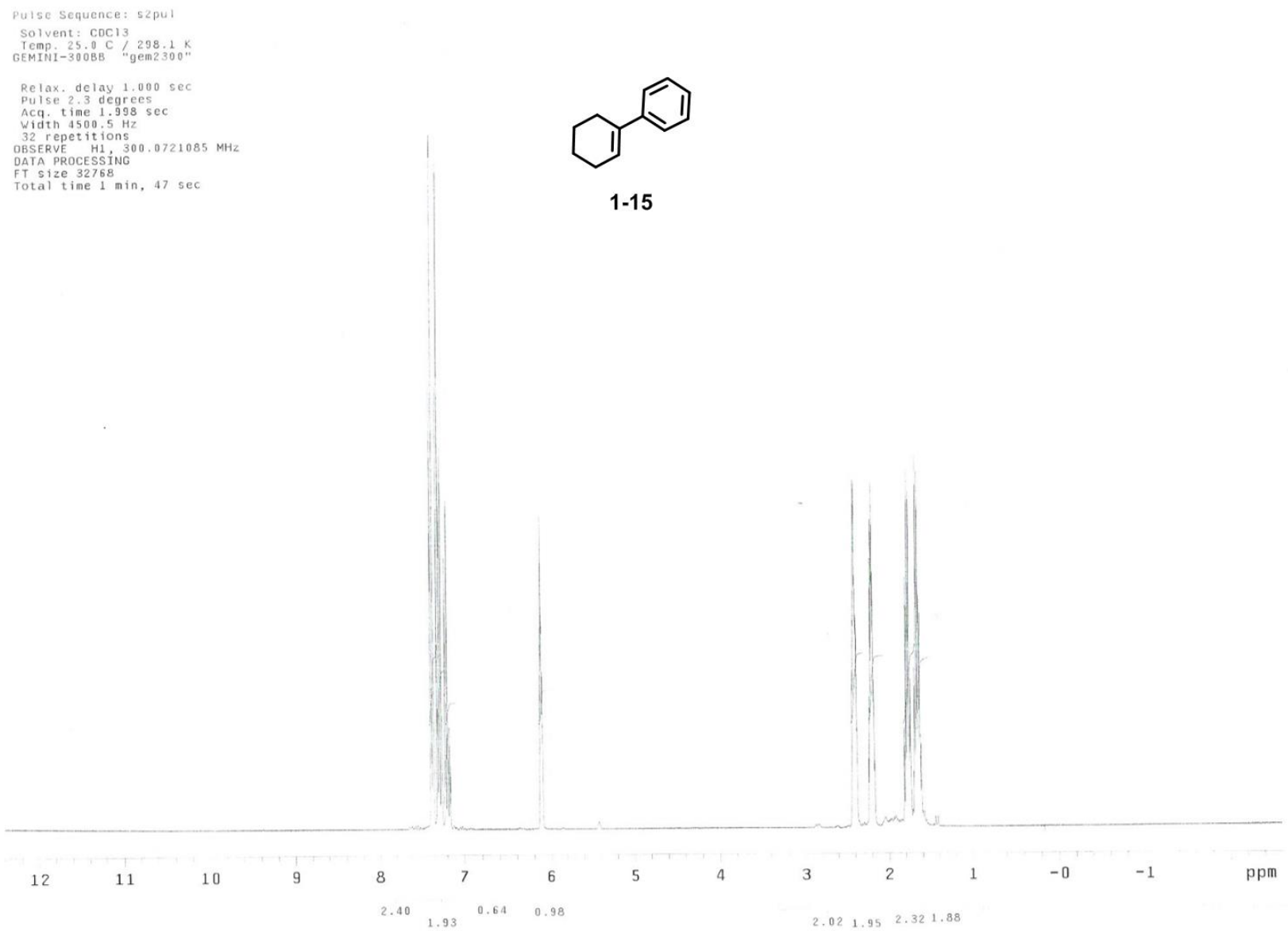
Pulse Sequence: s2pul
Solvent: CDCl3
Temp. 25.0 C / 298.1 K
GEMINI-300BB "gem2300"
Relax. delay 1.000 sec
Pulse 2.3 degrees
Acq. time 1.998 sec
Width 4500.5 Hz
32 repetitions
OBSERVE H1, 300.0721085 MHz
DATA PROCESSING
FT size 32768
Total time 1 min, 47 sec
1-15
12
11
10
9
8
7
6
5
4
3
2
1
-0
-1
ppm
2.40
1.93
0.64
0.98
2.02
1.95
2.32
1.88

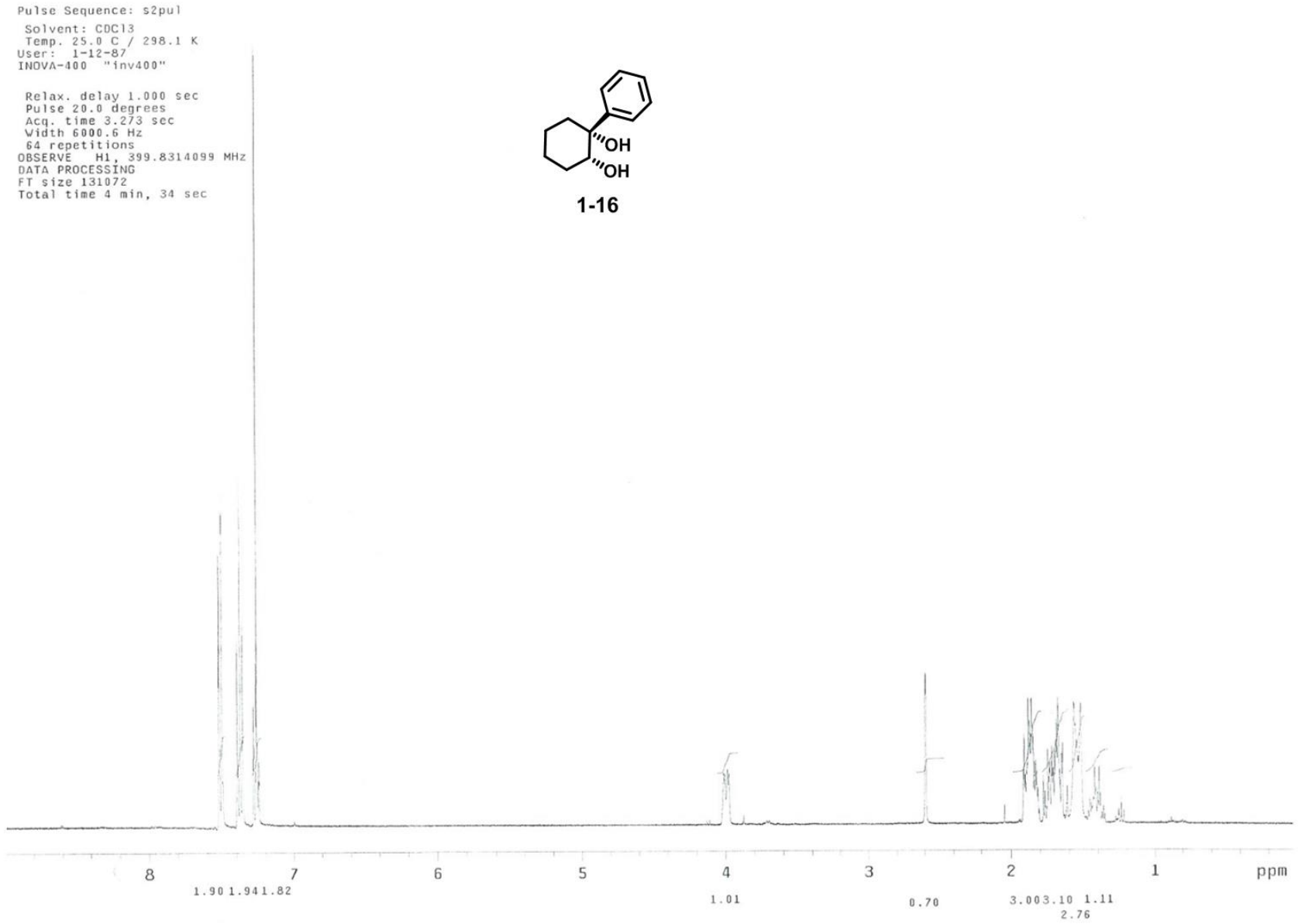
Pulse Sequence: s2pul
Solvent: CDCl3
Temp. 25.0 C / 298.1 K
User: 1-12-87
INOVA-400 "inv400"
Relax. delay 1.000 sec
Pulse 20.0 degrees
Acq. time 3.273 sec
Width 6000.6 Hz
64 repetitions
OBSERVE H1, 399.8314099 MHz
DATA PROCESSING
FT size 131072
Total time 4 min, 34 sec
OH
OH
1-16
8
7
6
5
4
3
2
1
ppm
1.90 1.94 1.82
1.01
0.70
3.00 3.10 1.11
2.76

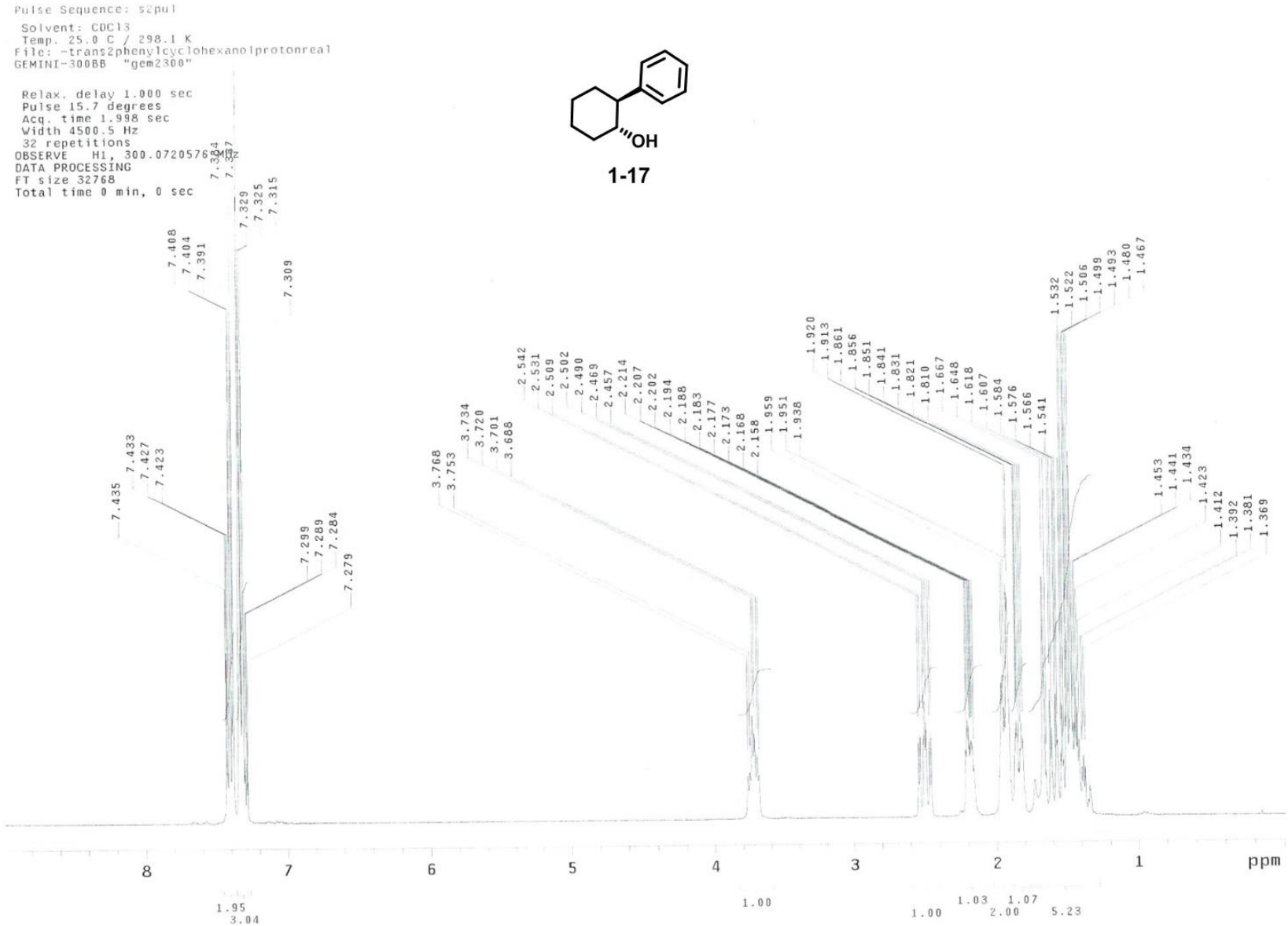
Pulse Sequence: s2pul
Solvent: CDCl3
Temp. 25.0 C / 298.1 K
File: -trans2phenylcyclohexanolprotonreal
GEMINI-300BB "gem2300"
Relax. delay 1.000 sec
Pulse 15.7 degrees
Acq. time 1.998 sec
Width 4500.5 Hz
32 repetitions
OBSERVE H1, 300.0720576 MHz
DATA PROCESSING
FT size 32768
Total time 0 min, 0 sec
OH
1-17
7.435
7.433
7.427
7.423
7.408
7.404
7.391
7.384
7.377
7.329
7.325
7.315
7.309
7.299
7.289
7.284
7.279
3.768
3.753
3.734
3.720
3.701
3.688
2.542
2.531
2.509
2.502
2.490
2.469
2.457
2.214
2.207
2.202
2.194
2.188
2.183
2.177
2.173
2.168
2.158
1.959
1.951
1.938
1.920
1.913
1.861
1.856
1.851
1.841
1.831
1.821
1.810
1.667
1.648
1.618
1.607
1.584
1.576
1.566
1.541
1.532
1.522
1.506
1.499
1.493
1.480
1.467
1.453
1.441
1.434
1.423
1.412
1.392
1.381
1.369
8
7
6
5
4
3
2
1
ppm
1.95
3.04
1.00
1.00
1.03
2.00
1.07
5.23

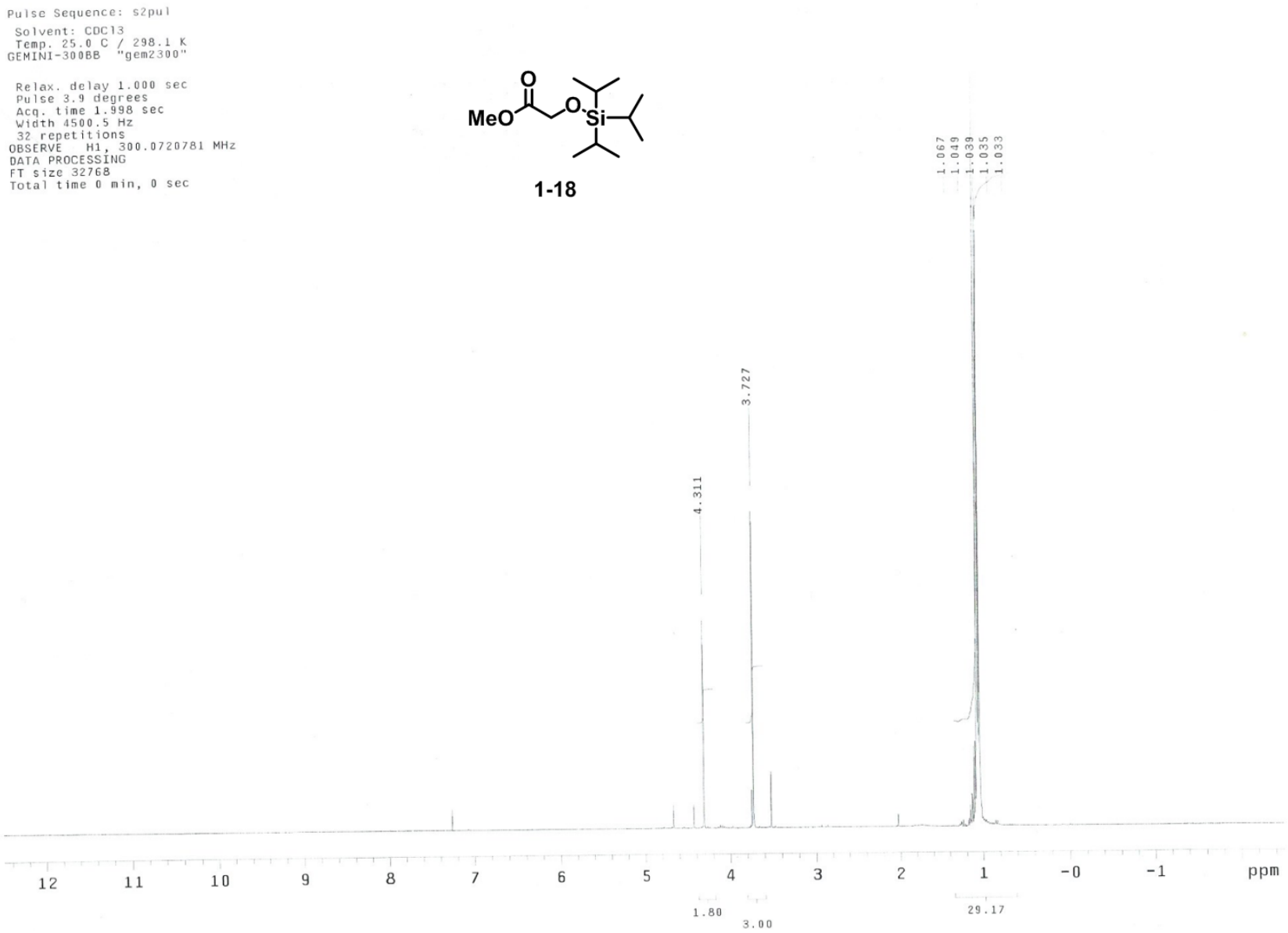
Pulse Sequence: s2pul
Solvent: CDCl3
Temp. 25.0 C / 298.1 K
GEMINI-300BB "gem2300"
Relax. delay 1.000 sec
Pulse 3.9 degrees
Acq. time 1.998 sec
Width 4500.5 Hz
32 repetitions
OBSERVE H1, 300.0720781 MHz
DATA PROCESSING
FT size 32768
Total time 0 min, 0 sec
MeO
O
O
Si
1-18
1.067
1.049
1.039
1.035
1.033
3.727
4.311
12
11
10
9
8
7
6
5
4
3
2
1
-0
-1
ppm
1.80
3.00
29.17

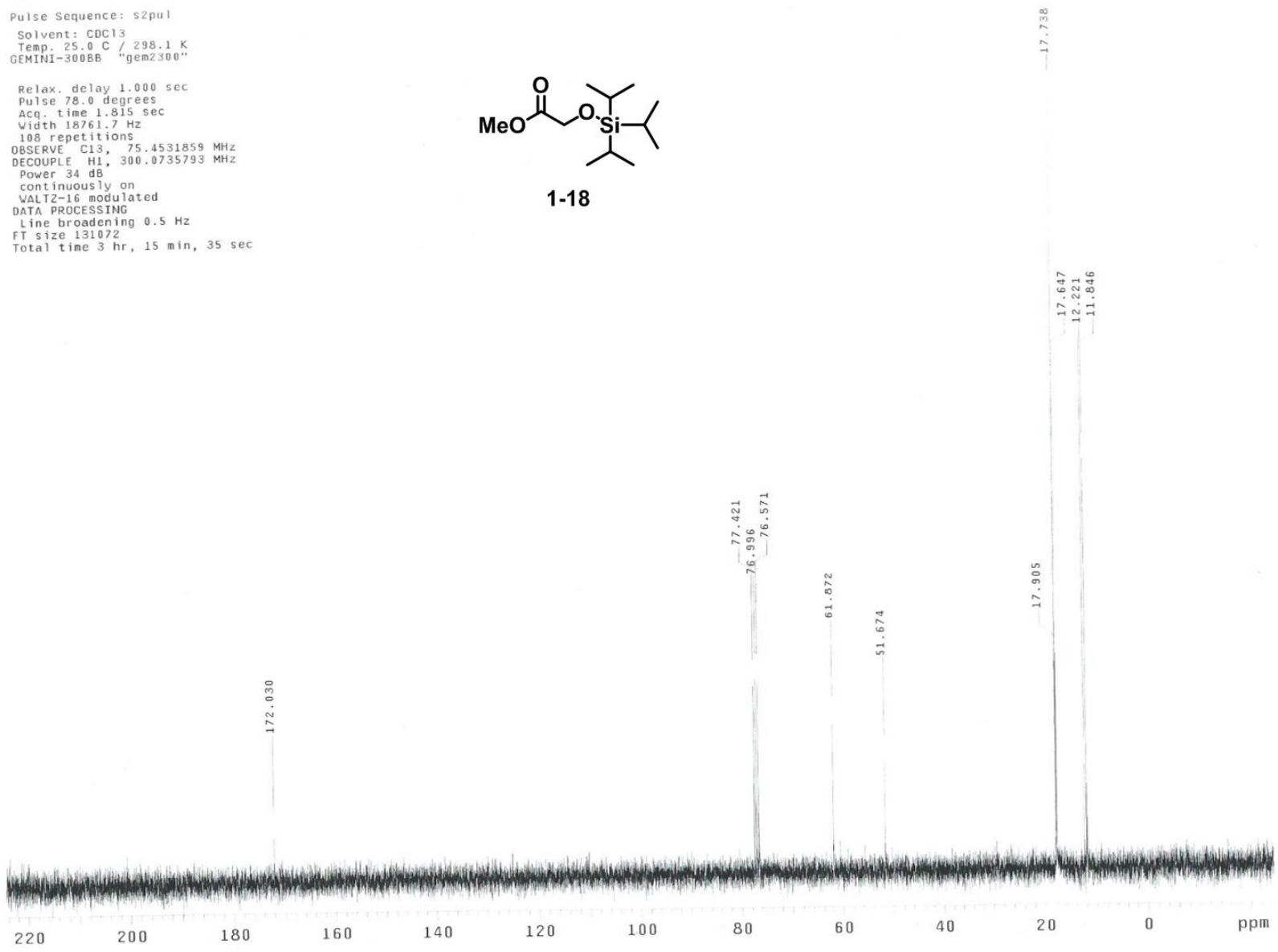
Pulse Sequence: s2pul
Solvent: CDCl3
Temp. 25.0 C / 298.1 K
GEMINI-300BB "gem2300"
Relax. delay 1.000 sec
Pulse 78.0 degrees
Acq. time 1.815 sec
Width 18761.7 Hz
108 repetitions
OBSERVE C13, 75.4531859 MHz
DECOUPLE H1, 300.0735793 MHz
Power 34 dB
continuously on
WALTZ-16 modulated
DATA PROCESSING
Line broadening 0.5 Hz
FT size 131072
Total time 3 hr, 15 min, 35 sec
MeO
O
O
Si
1-18
17.738
17.647
12.221
11.846
77.421
76.996
76.571
61.872
51.674
17.905
172.030
220
200
180
160
140
120
100
80
60
40
20
0
ppm

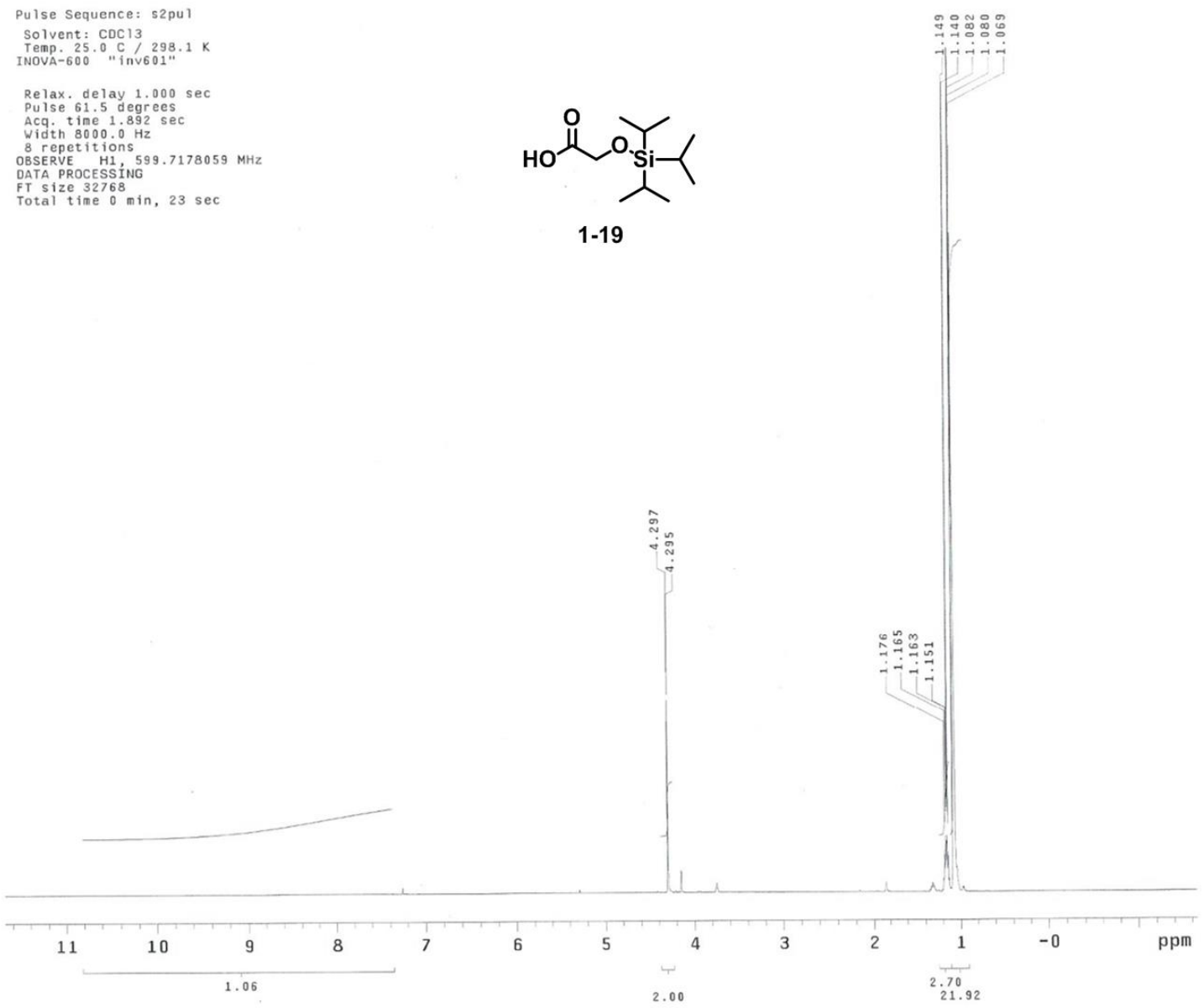
Pulse Sequence: s2pul
Solvent: CDCl3
Temp. 25.0 C / 298.1 K
INOVA-600 "inv601"
Relax. delay 1.000 sec
Pulse 61.5 degrees
Acq. time 1.892 sec
Width 8000.0 Hz
8 repetitions
OBSERVE H1, 599.7178059 MHz
DATA PROCESSING
FT size 32768
Total time 0 min, 23 sec
HO
O
O
Si
1-19
1.149
1.140
1.082
1.080
1.069
4.297
4.295
1.176
1.165
1.163
1.151
11
10
9
8
7
6
5
4
3
2
1
-0
ppm
1.06
2.00
2.70
21.92

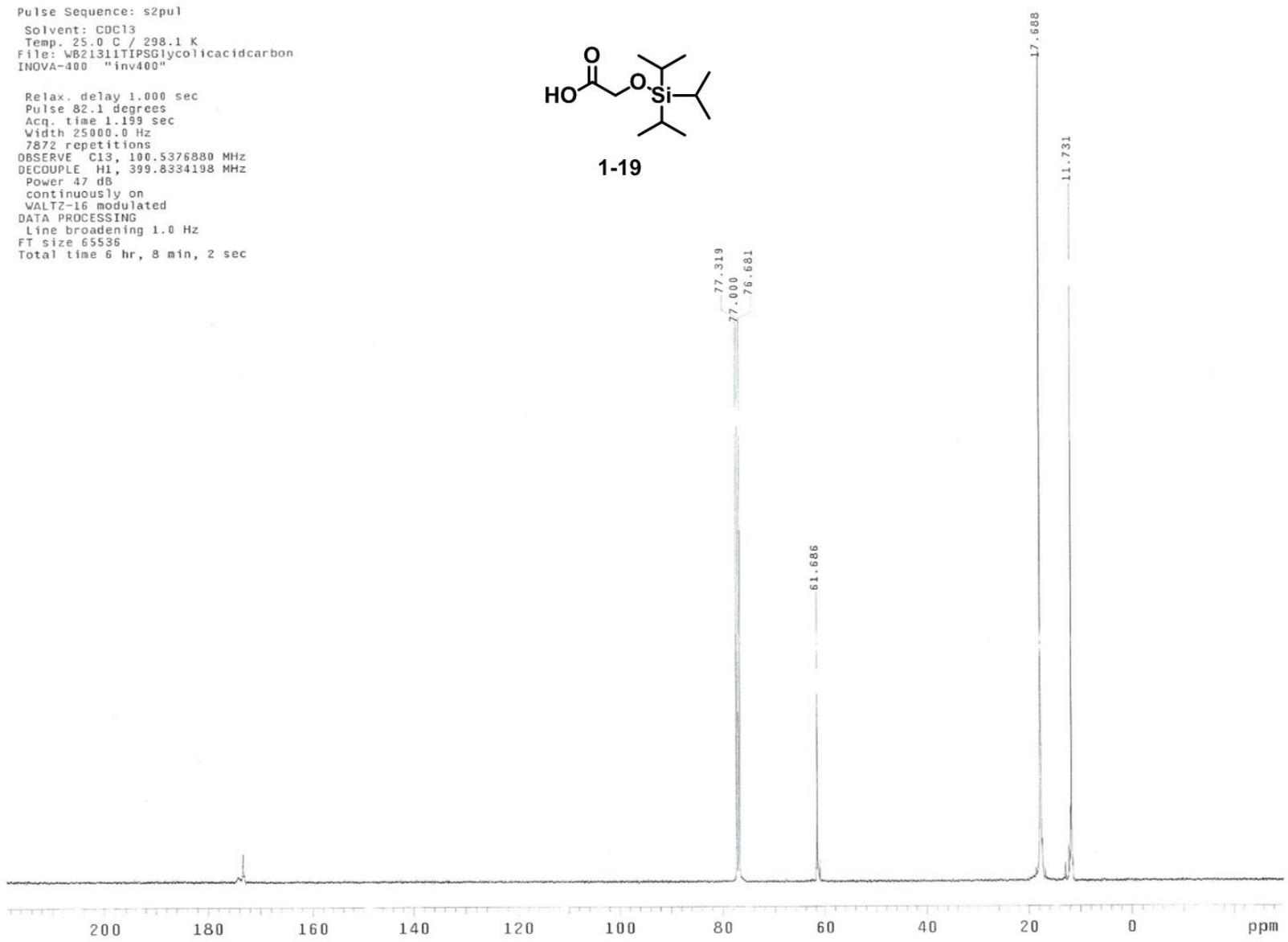
Pulse Sequence: s2pul
Solvent: CDCl3
Temp. 25.0 C / 298.1 K
File: WB21311TIPSGlycolicacidcarbon
INOVA-400 "inv400"
Relax. delay 1.000 sec
Pulse 82.1 degrees
Acq. time 1.199 sec
Width 25000.0 Hz
7872 repetitions
OBSERVE C13, 100.5376880 MHz
DECOUPLE H1, 399.8334198 MHz
Power 47 dB
continuously on
WALTZ-16 modulated
DATA PROCESSING
Line broadening 1.0 Hz
FT size 65536
Total time 6 hr, 8 min, 2 sec
HO
O
O
Si
1-19
17.688
11.731
77.319
77.000
76.681
61.686
200
180
160
140
120
100
80
60
40
20
0
ppm

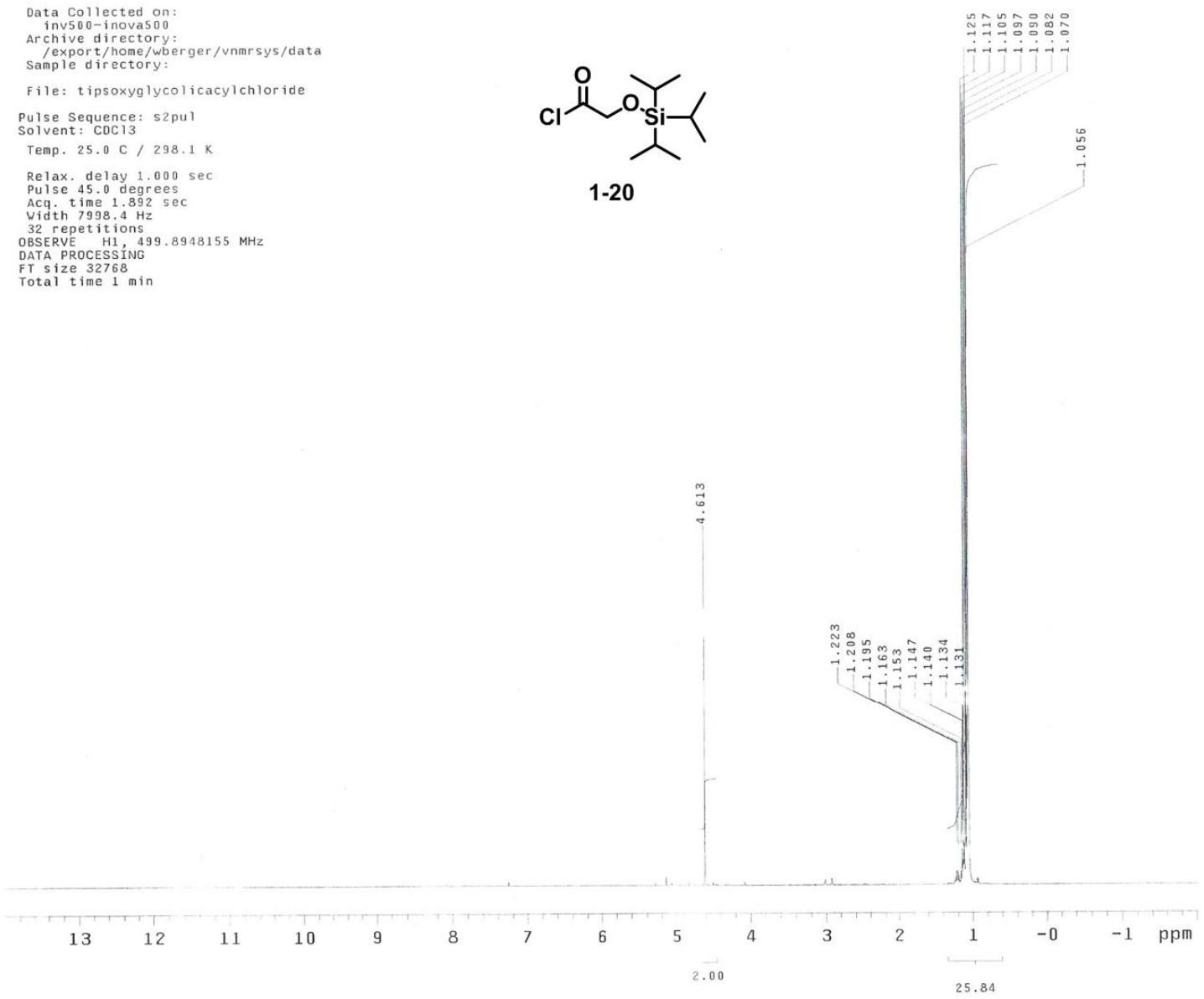
Data Collected on:
inv500-inova500
Archive directory:
/export/home/wberger/vnmrsys/data
Sample directory:
File: tipsoxyglycolicacylchloride
Pulse Sequence: s2pul
Solvent: CDCl3
Temp. 25.0 C / 298.1 K
Relax. delay 1.000 sec
Pulse 45.0 degrees
Acq. time 1.892 sec
Width 7998.4 Hz
32 repetitions
OBSERVE H1, 499.8948155 MHz
DATA PROCESSING
FT size 32768
Total time 1 min
Cl
O
O
Si
1-20
1.125
1.117
1.105
1.097
1.090
1.082
1.070
1.056
4.613
1.223
1.208
1.195
1.163
1.153
1.147
1.140
1.134
1.131
13
12
11
10
9
8
7
6
5
4
3
2
1
-0
-1
ppm
2.00
25.84

Data Collected on:
inv500-inova500
Archive directory:
/export/home/wberger/vnmrsys/data
Sample directory:

File: TIPSoxyglycolicacylchloridecarbon

Pulse Sequence: s2pul
Solvent: CDCl3

Temp. 25.0 C / 298.1 K
User: 1-14-87

Relax. delay 1.000 sec
Pulse 45.0 degrees
Acq. time 1.300 sec
Width 31421.8 Hz
120 repetitions
OBSERVE C13, 125.6986513 MHz
DECOUPLE H1, 499.8973075 MHz
Power 45 dB
continuously on
WALTZ-16 modulated
DATA PROCESSING
Line broadening 2.0 Hz
FT size 131072
Total time 11 min

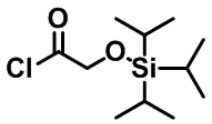

1-20

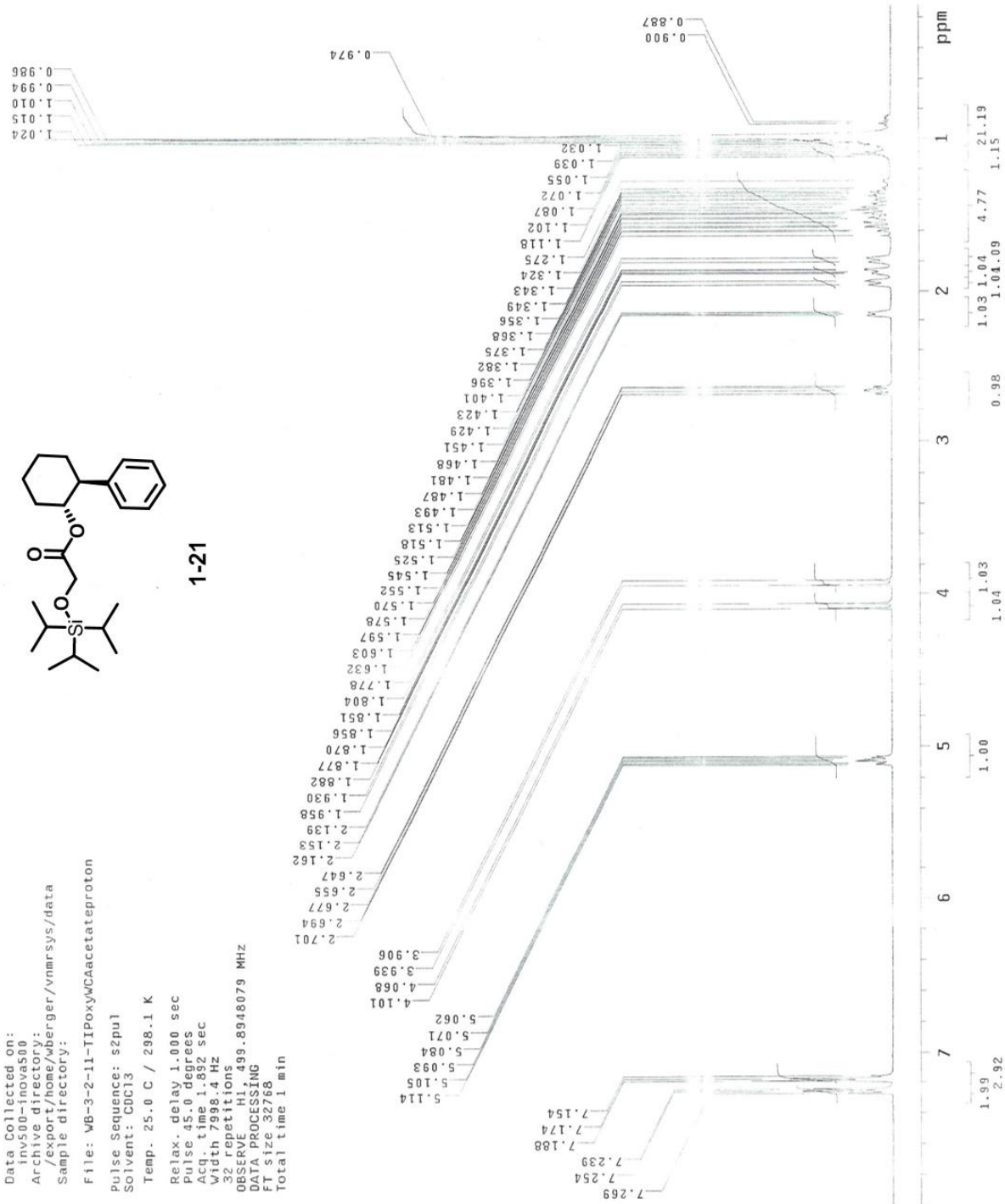
Data Collected on:
inv500-inova500
Archive directory:
/export/home/wberger/vnmrsys/data
Sample directory:
File: WB-3-2-11-TIPoxyWCAacetateproton
Pulse Sequence: s2pul
Solvent: CDCl3
Temp. 25.0 C / 298.1 K
Relax. delay 1.000 sec
Pulse 45.0 degrees
Acq. time 1.892 sec
Width 7998.4 Hz
32 repetitions
OBSERVE H1, 499.8948079 MHz
DATA PROCESSING
FT size 32768
Total time 1 min
1-21
ppm

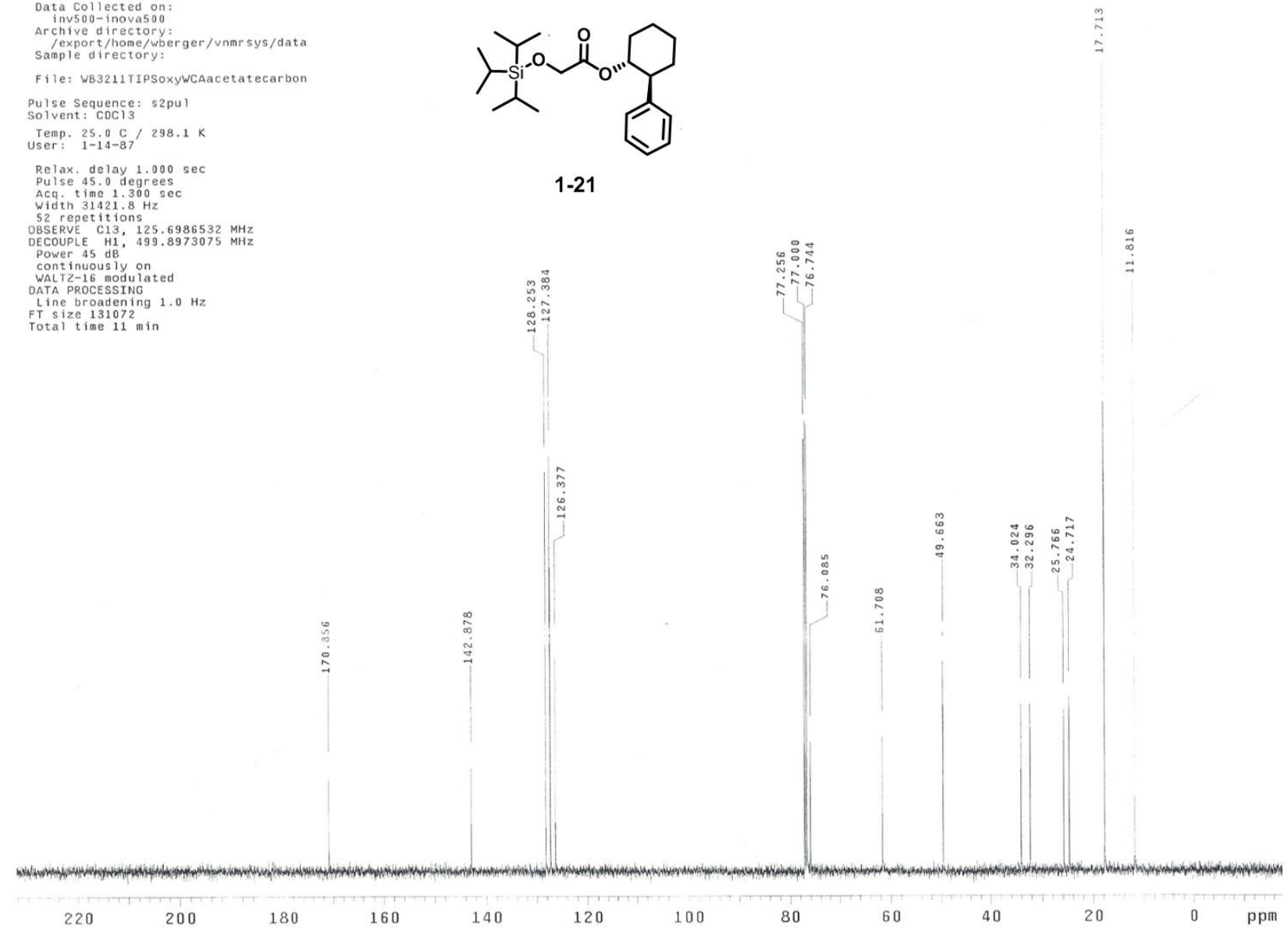
Data Collected on:
inv500-inova500
Archive directory:
/export/home/wberger/vnmrsys/data
Sample directory:
File: WB3211TIPSoxyWCAacetatecarbon
Pulse Sequence: s2pul
Solvent: CDCl3
Temp. 25.0 C / 298.1 K
User: 1-14-87
Relax. delay 1.000 sec
Pulse 45.0 degrees
Acq. time 1.300 sec
Width 31421.8 Hz
52 repetitions
OBSERVE C13, 125.6986532 MHz
DECOUPLE H1, 499.8973075 MHz
Power 45 dB
continuously on
WALTZ-16 modulated
DATA PROCESSING
Line broadening 1.0 Hz
FT size 131072
Total time 11 min
1-21
170.356
142.878
128.253
127.384
126.377
77.256
77.000
76.744
76.085
61.708
49.663
34.024
32.296
25.766
24.717
17.713
11.816
220
200
180
160
140
120
100
80
60
40
20
0
ppm

Appendix Chapter 2

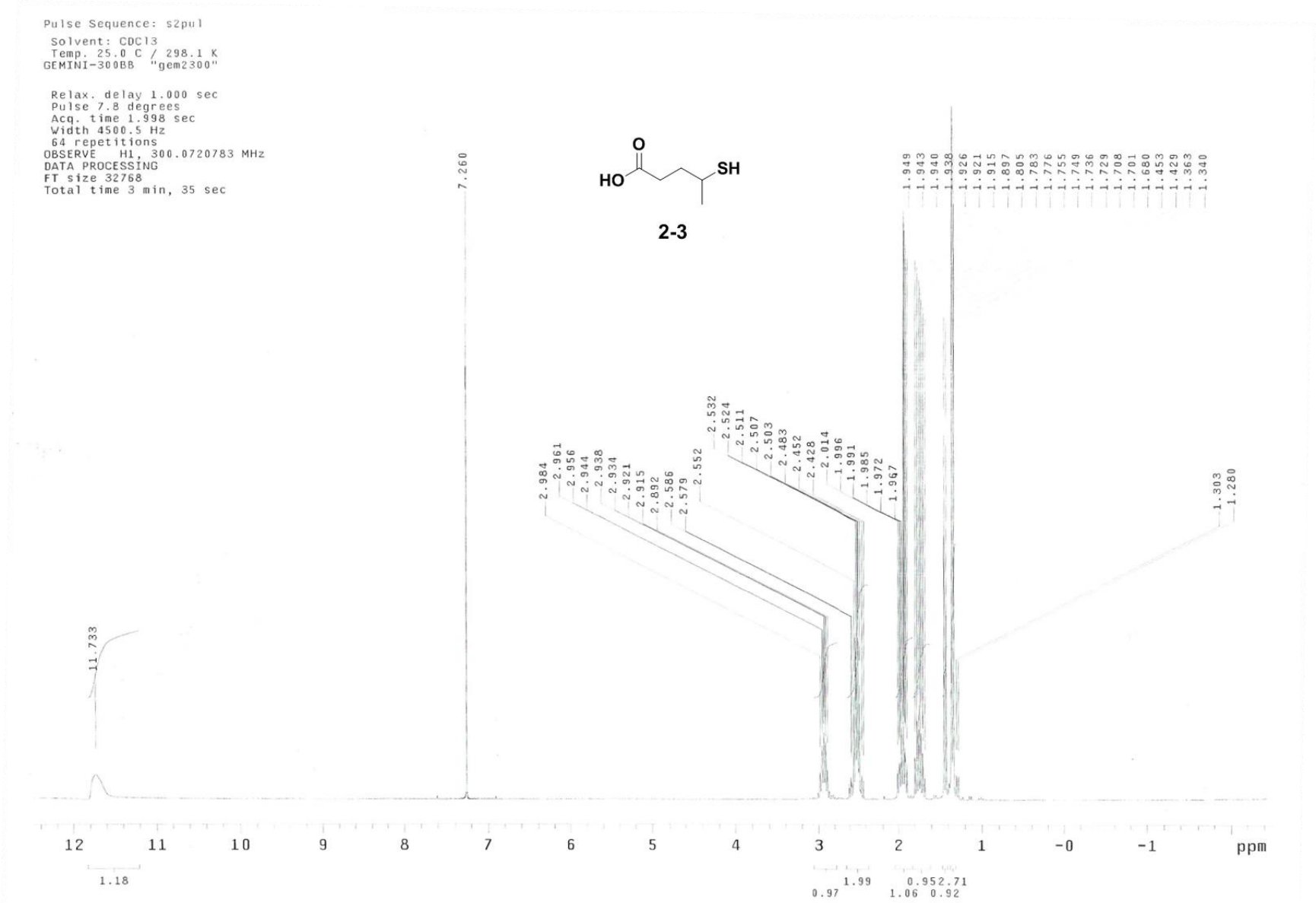
Pulse Sequence: s2pul
Solvent: CDCl3
Temp. 25.0 C / 298.1 K
GEMINI-300BB "gem2300"
Relax. delay 1.000 sec
Pulse 7.8 degrees
Acq. time 1.998 sec
Width 4500.5 Hz
64 repetitions
OBSERVE H1, 300.0720783 MHz
DATA PROCESSING
FT size 32768
Total time 3 min, 35 sec
HO
O
SH
2-3
7.260
11.733
2.984
2.961
2.956
2.944
2.938
2.934
2.921
2.915
2.892
2.586
2.579
2.552
2.532
2.524
2.511
2.507
2.503
2.483
2.452
2.428
2.014
1.996
1.991
1.985
1.972
1.967
1.949
1.943
1.940
1.938
1.926
1.921
1.915
1.897
1.805
1.783
1.776
1.755
1.749
1.736
1.729
1.708
1.701
1.680
1.453
1.429
1.363
1.340
1.303
1.280
12
11
10
9
8
7
6
5
4
3
2
1
-0
-1
ppm
1.18
0.97
1.99
1.06
0.95
0.92
2.71

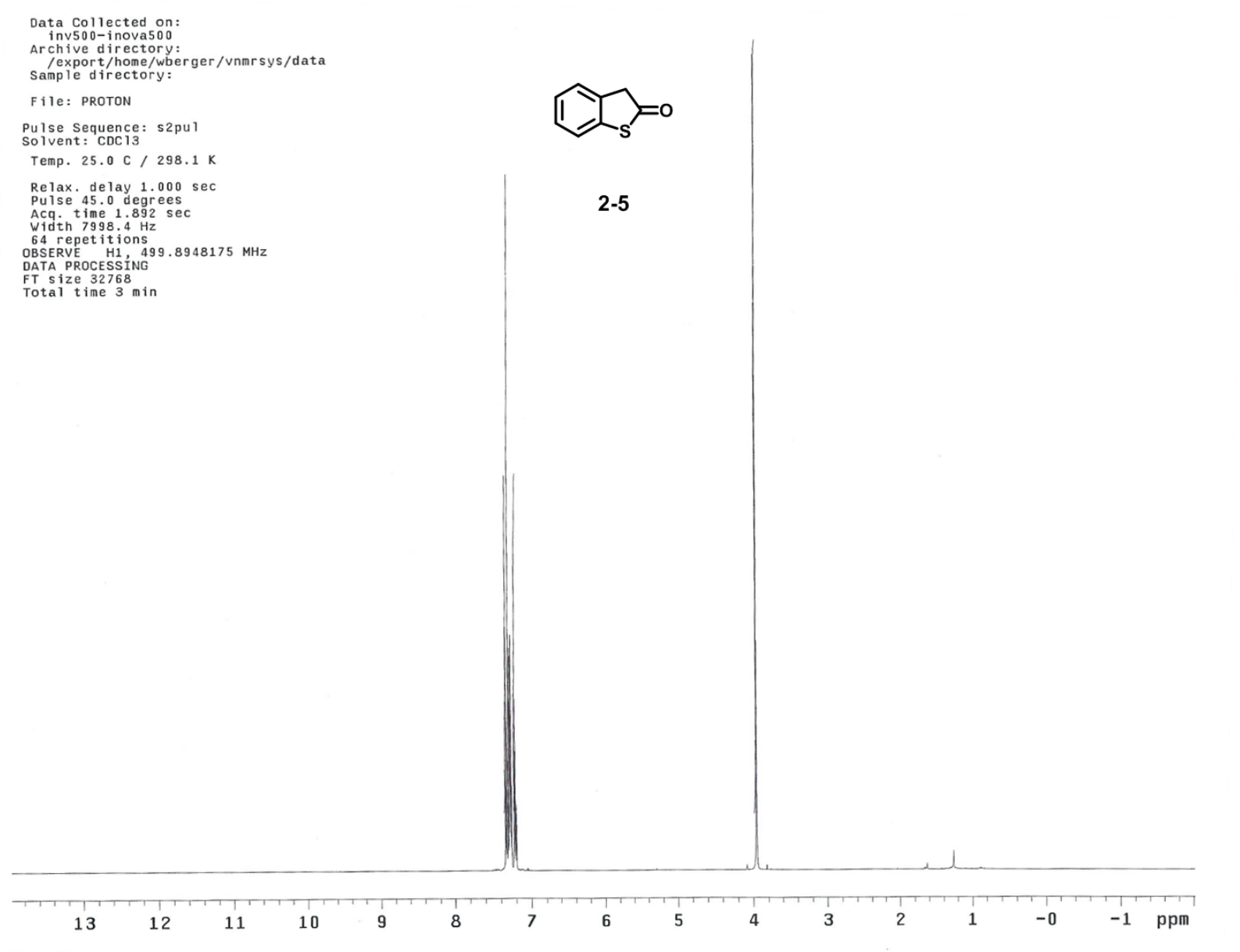
Data Collected on:
inv500-inova500
Archive directory:
/export/home/wberger/vnmrsys/data
Sample directory:
File: PROTON
Pulse Sequence: s2pul
Solvent: CDCl3
Temp. 25.0 C / 298.1 K
Relax. delay 1.000 sec
Pulse 45.0 degrees
Acq. time 1.892 sec
Width 7998.4 Hz
64 repetitions
OBSERVE H1, 499.8948175 MHz
DATA PROCESSING
FT size 32768
Total time 3 min
O
S
2-5
13
12
11
10
9
8
7
6
5
4
3
2
1
-0
-1
ppm

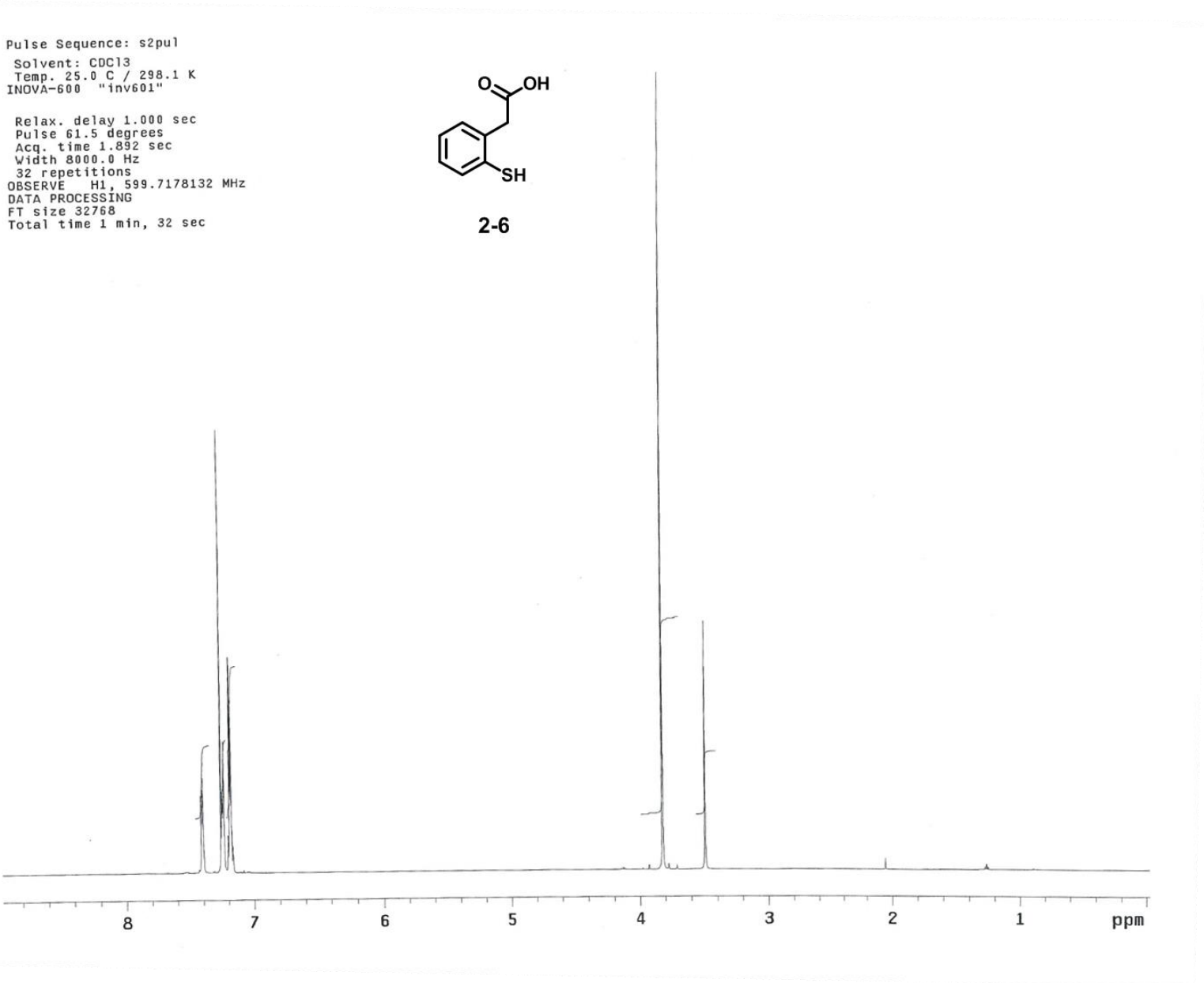
Pulse Sequence: s2pul
Solvent: CDCl3
Temp. 25.0 C / 298.1 K
INOVA-600 "inv601"
Relax. delay 1.000 sec
Pulse 61.5 degrees
Acq. time 1.892 sec
Width 8000.0 Hz
32 repetitions
OBSERVE H1, 599.7178132 MHz
DATA PROCESSING
FT size 32768
Total time 1 min, 32 sec
O
OH
SH
2-6
8
7
6
5
4
3
2
1
ppm

Pulse Sequence: s2pul
Solvent: CDCl3
Temp. 25.0 C / 298.1 K
GEMINI-300BB "gem2300"

Relax. delay 1.000 sec
Pulse 7.8 degrees
Acq. time 1.998 sec
Width 4500.5 Hz
32 repetitions
OBSERVE H1, 300.0720783 MHz
DATA PROCESSING
FT size 32768
Total time 1 min, 47 sec

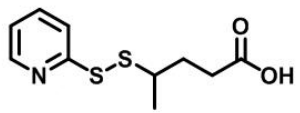

2-7

Pulse Sequence: s2pul
Solvent: CDCl3
Temp. 25.0 C / 298.1 K
INOVA-600 "inv601"

Relax. delay 1.000 sec
Pulse 61.5 degrees
Acq. time 1.892 sec
Width 8000.0 Hz
32 repetitions
OBSERVE H1, 599.7178142 MHz
DATA PROCESSING
FT size 32768
Total time 1 min, 32 sec

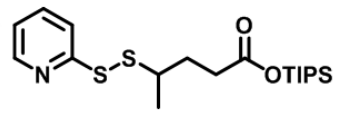

2-8

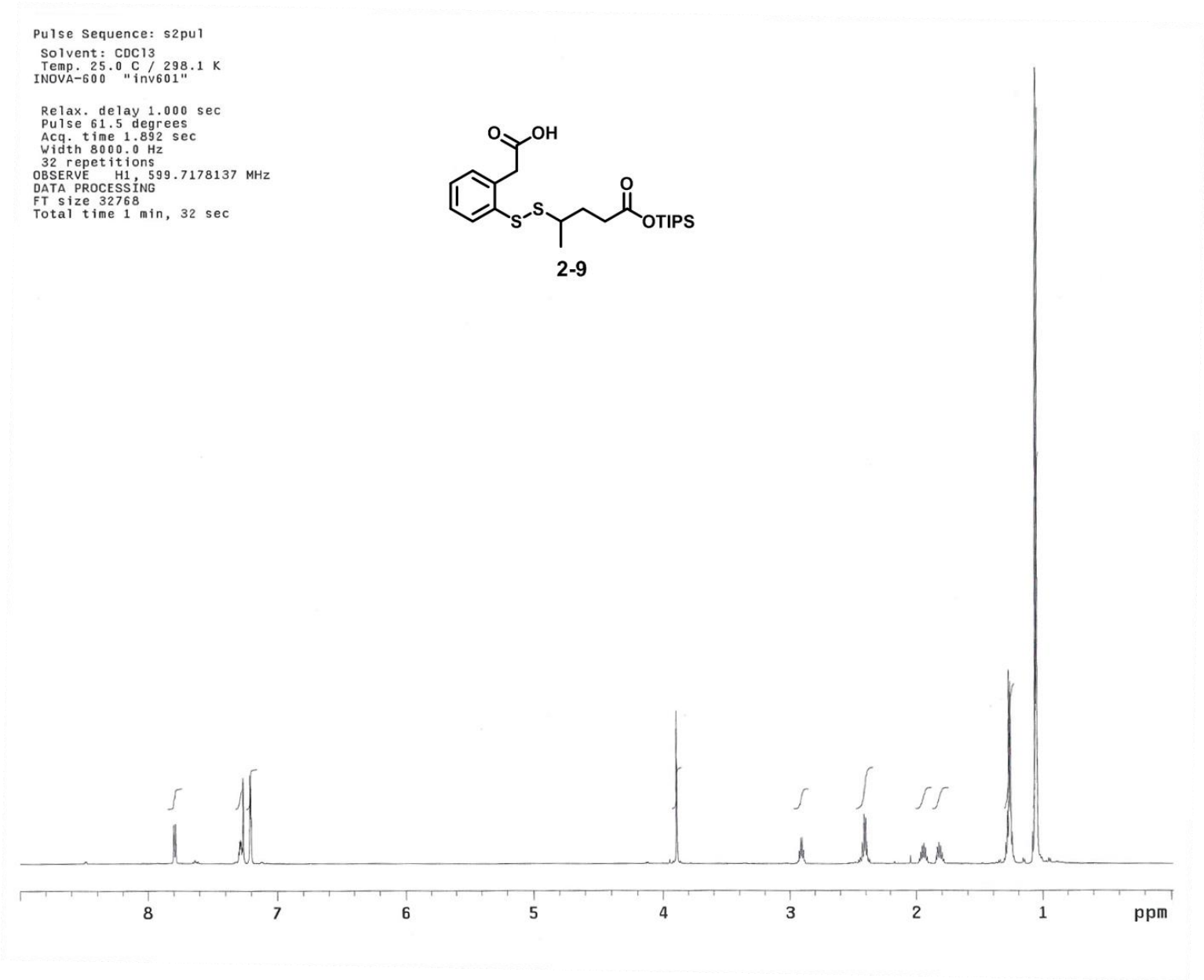
Pulse Sequence: s2pul
Solvent: CDCl3
Temp. 25.0 C / 298.1 K
INOVA-600 "inv601"
Relax. delay 1.000 sec
Pulse 61.5 degrees
Acq. time 1.892 sec
Width 8000.0 Hz
32 repetitions
OBSERVE H1, 599.7178137 MHz
DATA PROCESSING
FT size 32768
Total time 1 min, 32 sec
O
OH
S
S
O
OTIPS
2-9
8
7
6
5
4
3
2
1
ppm

```
Data Collected on:
  inv500-inova500
Archive directory:
  /export/home/wberger/vnmrsys/data
Sample directory:

File: PROTON

Pulse Sequence: s2pul
Solvent: CDCl3
Temp. 25.0 C / 298.1 K

Relax. delay 1.000 sec
Pulse 45.0 degrees
Acq. time 1.892 sec
Width 7998.4 Hz
120 repetitions
OBSERVE   H1, 499.8948175 MHz
DATA PROCESSING
FT size 32768
Total time 24 min
```

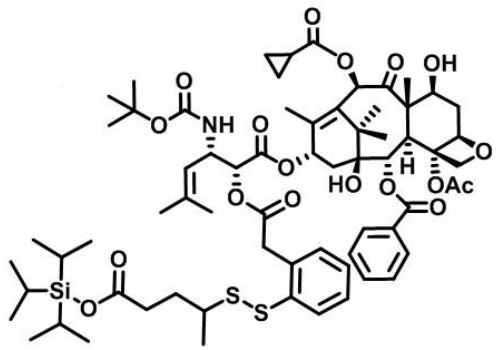

2-10

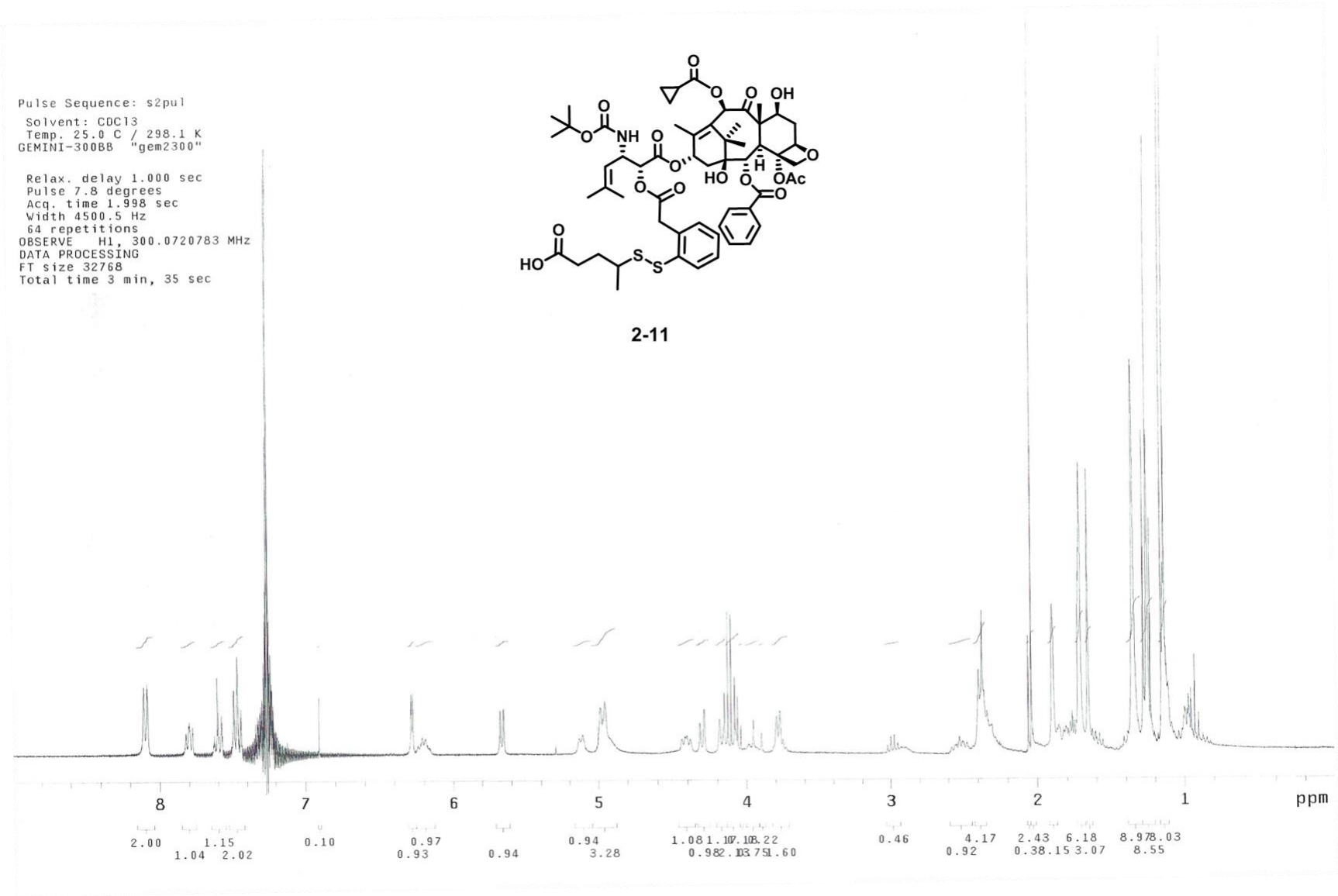
Pulse Sequence: s2pul
Solvent: CDCl3
Temp. 25.0 C / 298.1 K
GEMINI-300BB "gem2300"
Relax. delay 1.000 sec
Pulse 7.8 degrees
Acq. time 1.998 sec
Width 4500.5 Hz
64 repetitions
OBSERVE H1, 300.0720783 MHz
DATA PROCESSING
FT size 32768
Total time 3 min, 35 sec
2-11
8
7
6
5
4
3
2
1
ppm
2.00 1.15 1.04 2.02 0.10 0.97 0.93 0.94 0.94 3.28 1.08 1.10 7.10 3.22 0.98 2.10 3.75 1.60 0.46 4.17 0.92 2.43 0.38 6.18 5.15 3.07 8.97 8.03 8.55

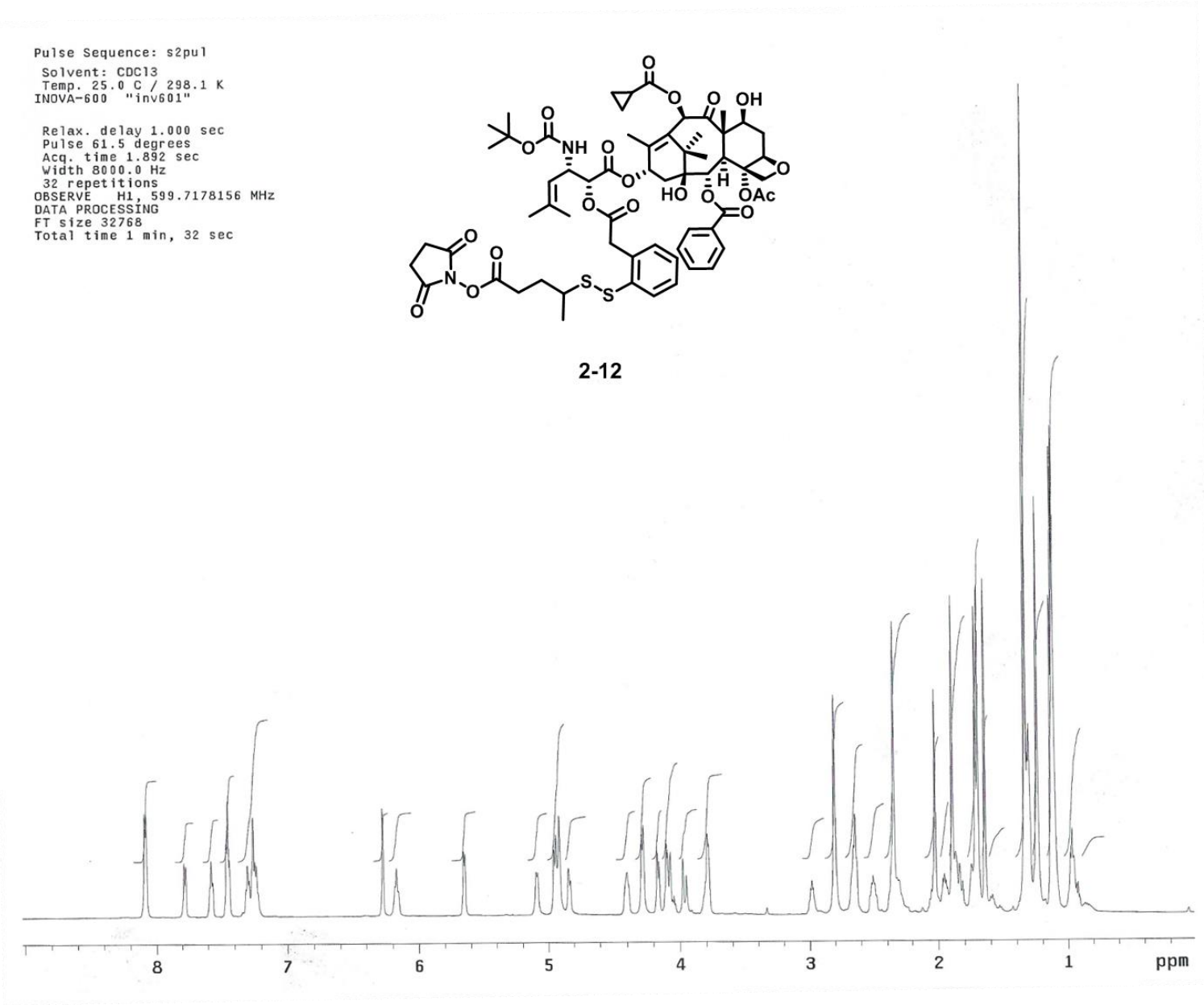
Pulse Sequence: s2pul
Solvent: CDCl3
Temp. 25.0 C / 298.1 K
INOVA-600 "inv601"
Relax. delay 1.000 sec
Pulse 61.5 degrees
Acq. time 1.892 sec
Width 8000.0 Hz
32 repetitions
OBSERVE H1, 599.7178156 MHz
DATA PROCESSING
FT size 32768
Total time 1 min, 32 sec
2-12
8
7
6
5
4
3
2
1
ppm

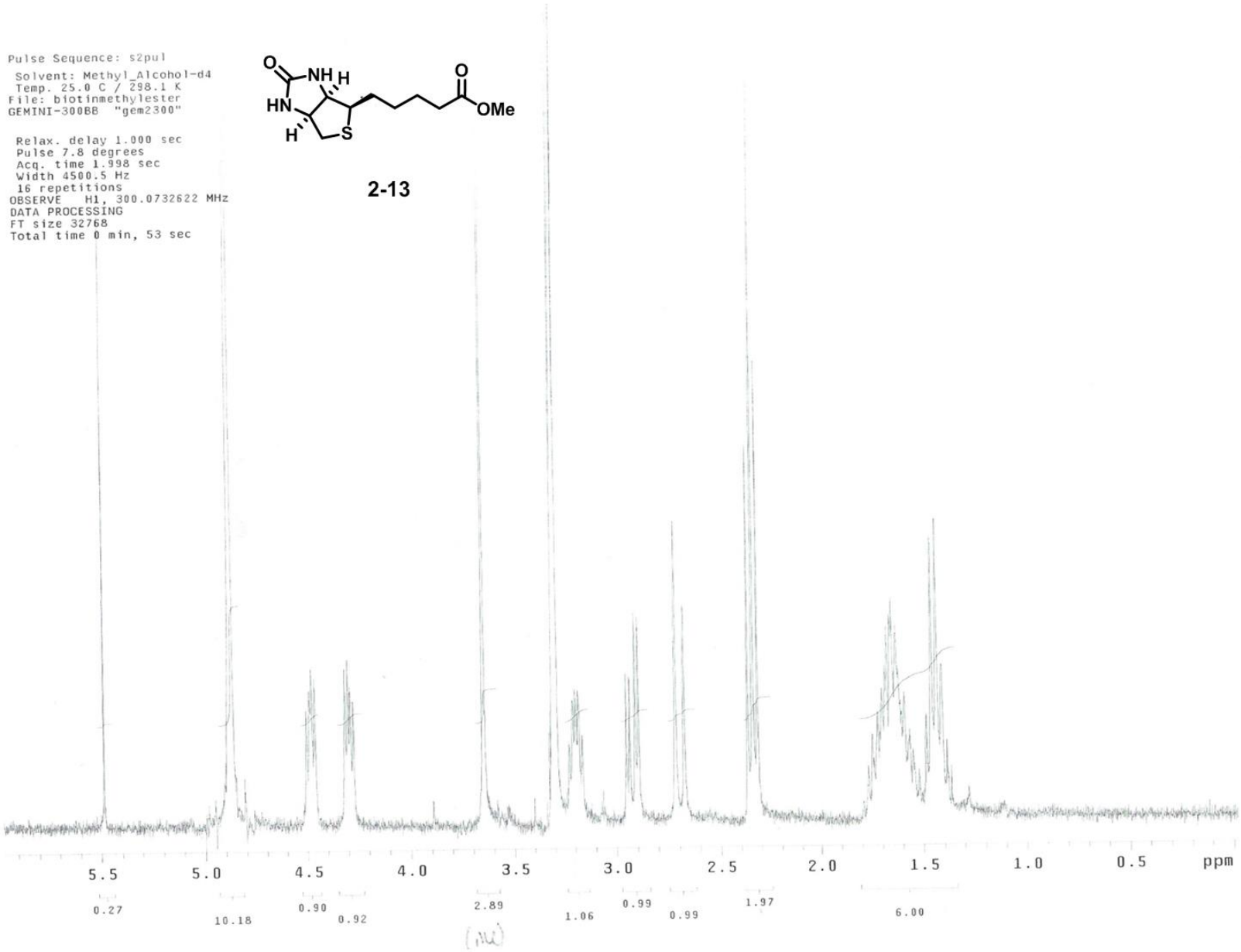
Pulse Sequence: s2pul
Solvent: Methyl_Alcohol-d4
Temp. 25.0 C / 298.1 K
File: biotinmethylester
GEMINI-300BB "gem2300"
Relax. delay 1.000 sec
Pulse 7.8 degrees
Acq. time 1.998 sec
Width 4500.5 Hz
16 repetitions
OBSERVE H1, 300.0732622 MHz
DATA PROCESSING
FT size 32768
Total time 0 min, 53 sec
O
NH
H
HN
H
S
O
OMe
2-13
5.5
5.0
4.5
4.0
3.5
3.0
2.5
2.0
1.5
1.0
0.5
ppm
0.27
10.18
0.90
0.92
2.89
1.06
0.99
0.99
1.97
6.00

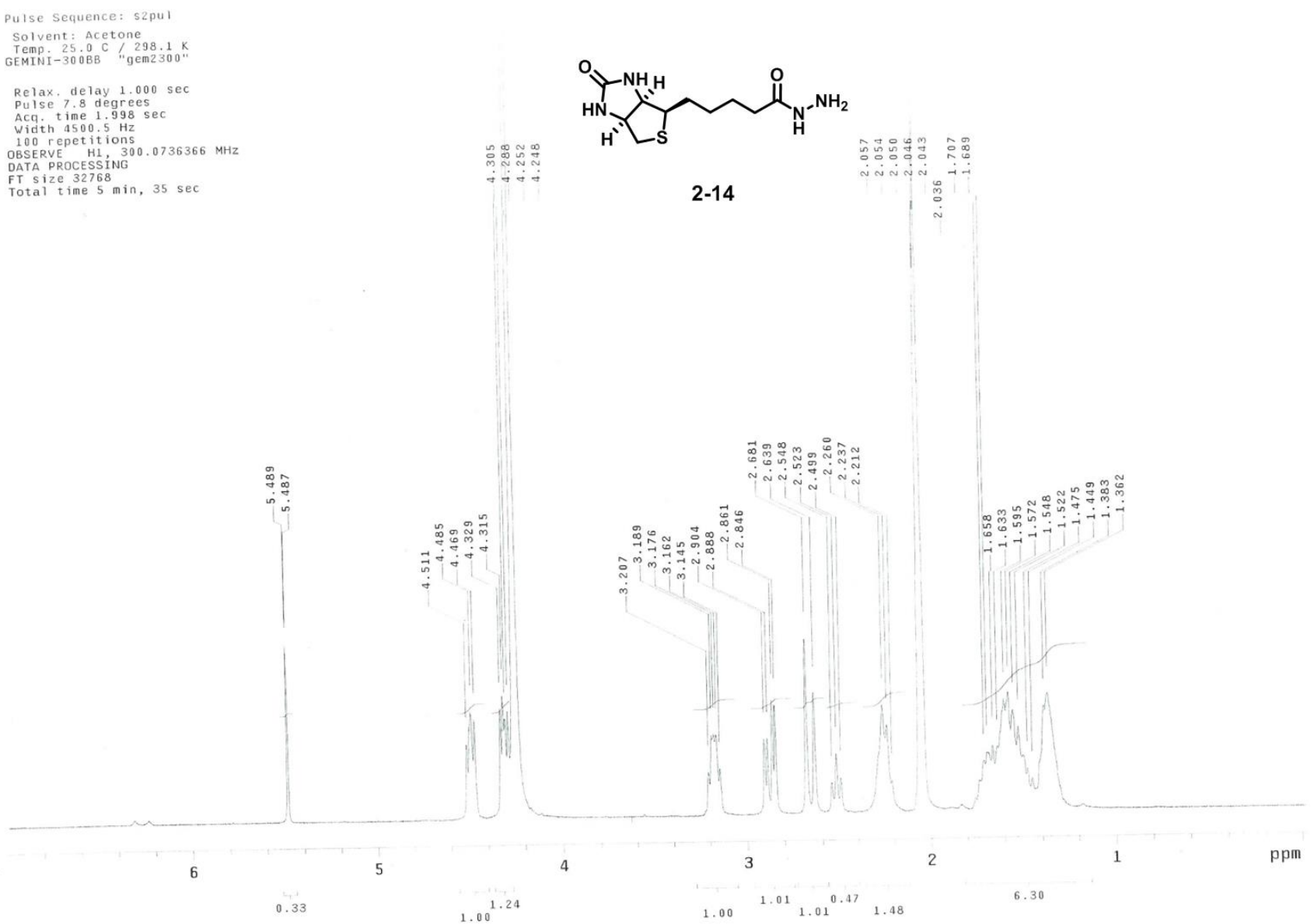
Pulse Sequence: s2pul
Solvent: Acetone
Temp. 25.0 C / 298.1 K
GEMINI-300BB "gem2300"
Relax. delay 1.000 sec
Pulse 7.8 degrees
Acq. time 1.998 sec
Width 4500.5 Hz
100 repetitions
OBSERVE H1, 300.0736366 MHz
DATA PROCESSING
FT size 32768
Total time 5 min, 35 sec
2-14
5.489
5.487
4.511
4.485
4.469
4.329
4.315
4.305
4.288
4.252
4.248
3.207
3.189
3.176
3.162
3.145
2.904
2.888
2.861
2.846
2.681
2.639
2.548
2.523
2.499
2.260
2.237
2.212
2.057
2.054
2.050
2.046
2.043
2.036
1.707
1.689
1.658
1.633
1.595
1.572
1.548
1.522
1.475
1.449
1.383
1.362
6
5
4
3
2
1
ppm
0.33
1.00
1.24
1.00
1.01
0.47
1.01
1.48
6.30

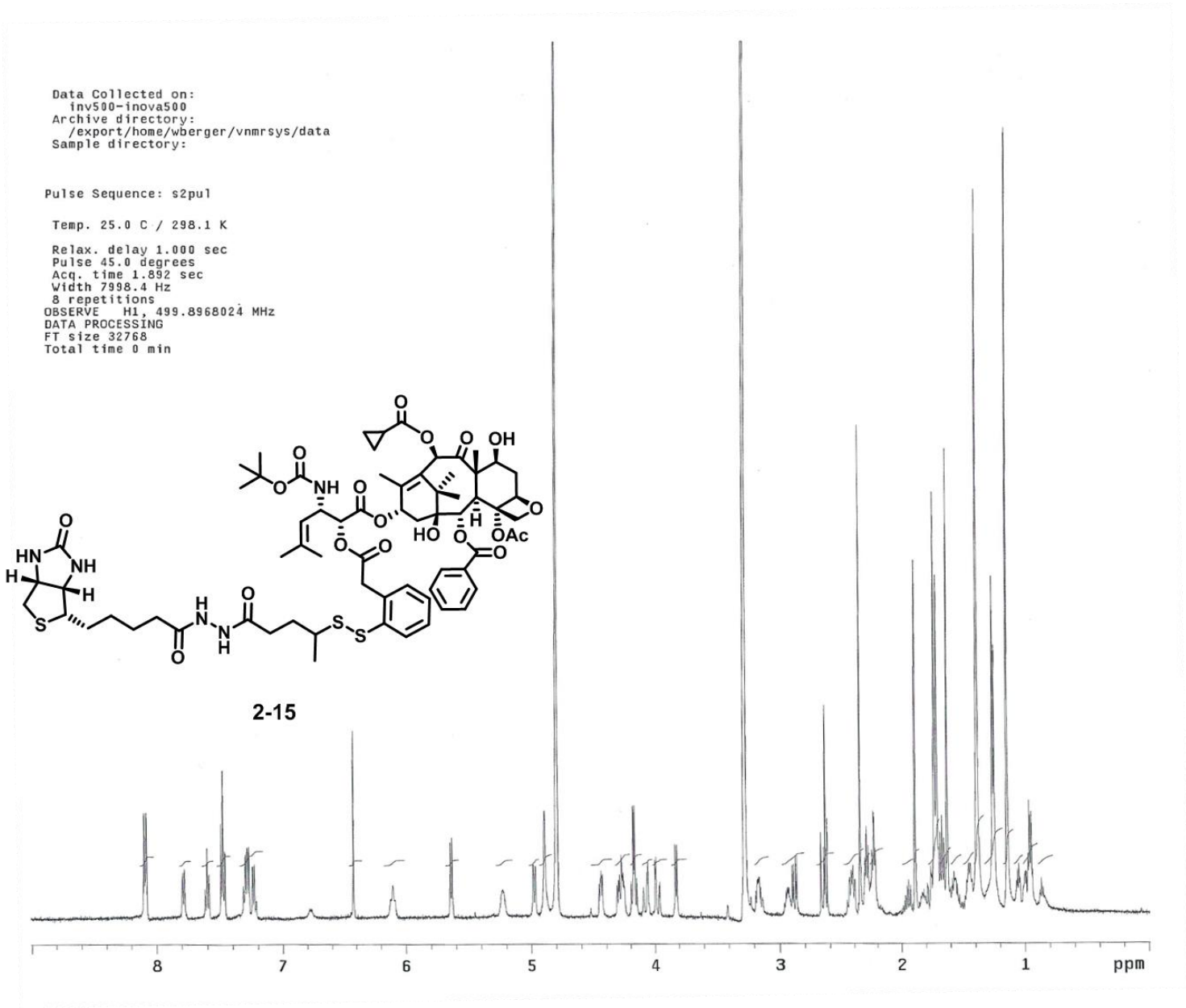
Data Collected on:
inv500-inova500
Archive directory:
/export/home/wberger/vnmrsys/data
Sample directory:
Pulse Sequence: s2pul
Temp. 25.0 C / 298.1 K
Relax. delay 1.000 sec
Pulse 45.0 degrees
Acq. time 1.892 sec
Width 7998.4 Hz
8 repetitions
OBSERVE H1, 499.8968024 MHz
DATA PROCESSING
FT size 32768
Total time 0 min
2-15
8
7
6
5
4
3
2
1
ppm

Pulse Sequence: s2pul
Solvent: CDCl3
Temp. 25.0 C / 298.1 K
GEMINI-300BB "gem2300"

Relax. delay 1.000 sec
Pulse 7.8 degrees
Acq. time 1.998 sec
Width 4500.5 Hz
100 repetitions
OBSERVE H1, 300.0720778 MHz
DATA PROCESSING
FT size 32768
Total time 5 min, 35 sec

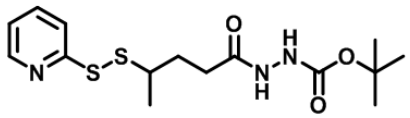

2-16

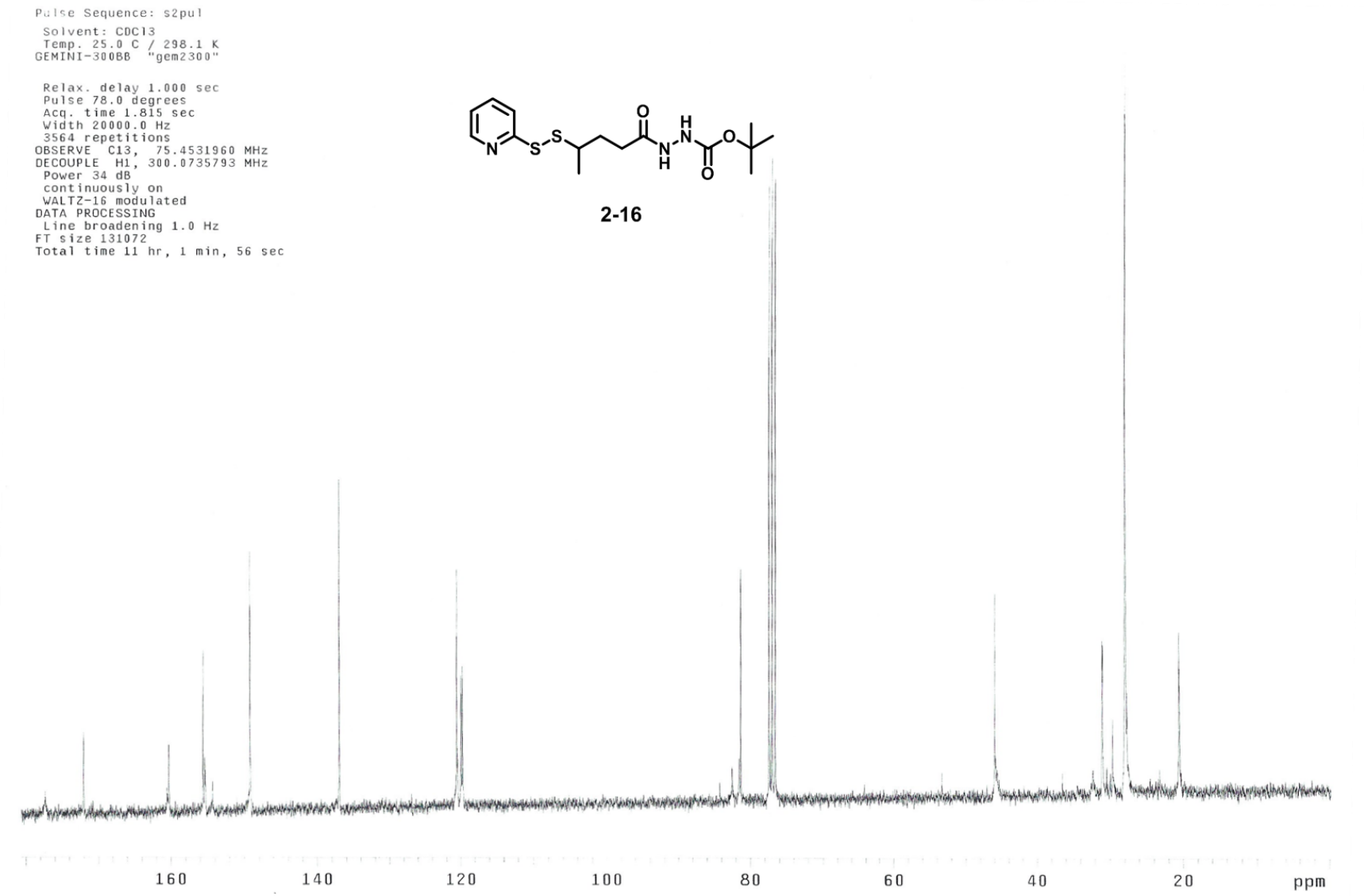
Pulse Sequence: s2pul
Solvent: CDCl3
Temp. 25.0 C / 298.1 K
GEMINI-300BB "gem2300"
Relax. delay 1.000 sec
Pulse 78.0 degrees
Acq. time 1.815 sec
Width 20000.0 Hz
3564 repetitions
OBSERVE C13, 75.4531960 MHz
DECOUPLE H1, 300.0735793 MHz
Power 34 dB
continuously on
WALTZ-16 modulated
DATA PROCESSING
Line broadening 1.0 Hz
FT size 131072
Total time 11 hr, 1 min, 56 sec
2-16
160
140
120
100
80
60
40
20
ppm

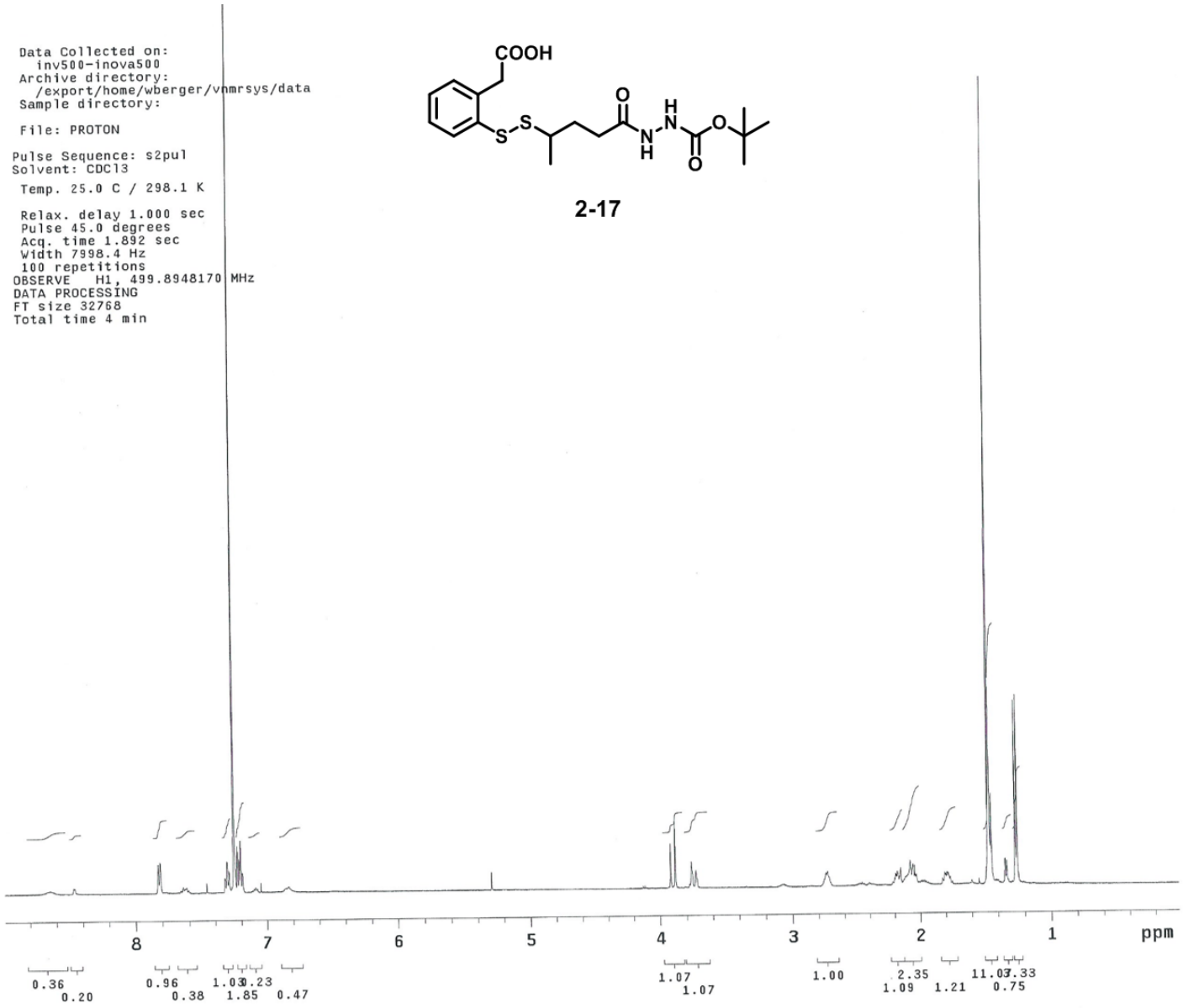
Data Collected on:
inv500-inova500
Archive directory:
/export/home/wberger/vnmrsys/data
Sample directory:
File: PROTON
Pulse Sequence: s2pul
Solvent: CDCl3
Temp. 25.0 C / 298.1 K
Relax. delay 1.000 sec
Pulse 45.0 degrees
Acq. time 1.892 sec
Width 7998.4 Hz
100 repetitions
OBSERVE H1, 499.8948170 MHz
DATA PROCESSING
FT size 32768
Total time 4 min
COOH
O
H
N
N
H
S
S
O
O
2-17
8
7
6
5
4
3
2
1
ppm
0.36
0.20
0.96
0.38
1.03
1.85
0.23
0.47
1.07
1.07
1.00
2.35
1.09
1.21
11.03
0.75
3.33

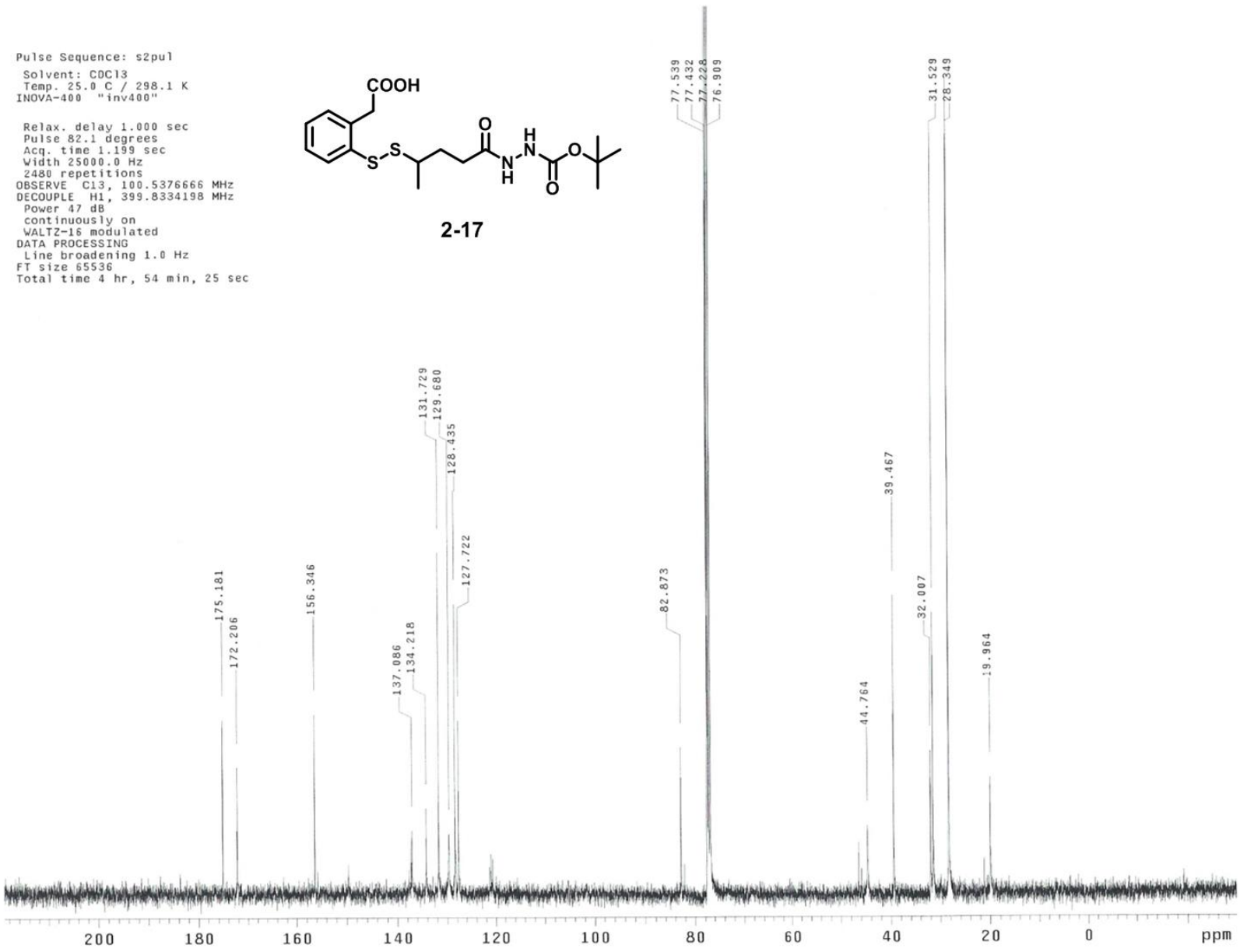
Pulse Sequence: s2pul
Solvent: CDCl3
Temp. 25.0 C / 298.1 K
INOVA-400 "inv400"
Relax. delay 1.000 sec
Pulse 82.1 degrees
Acq. time 1.199 sec
Width 25000.0 Hz
2480 repetitions
OBSERVE C13, 100.5376666 MHz
DECOUPLE H1, 399.8334198 MHz
Power 47 dB
continuously on
WALTZ-16 modulated
DATA PROCESSING
Line broadening 1.0 Hz
FT size 65536
Total time 4 hr, 54 min, 25 sec
COOH
S
S
O
N
H
N
H
O
O
2-17
77.539
77.432
77.228
76.909
31.529
28.349
175.181
172.206
156.346
137.086
134.218
131.729
129.680
128.435
127.722
82.873
44.764
39.467
32.007
19.964
200
180
160
140
120
100
80
60
40
20
0
ppm

Pulse Sequence: s2pul
Solvent: DMSO
Temp. 25.0 C / 298.1 K
File: nevenbiotin
GEMINI-300BB "gem2300"

Relax. delay 1.000 sec
Pulse 7.8 degrees
Acq. time 1.998 sec
Width 4500.5 Hz
32 repetitions
OBSERVE H1, 300.0734978 MHz
DATA PROCESSING
FT size 32768
Total time 1 min, 47 sec

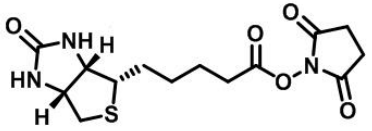

2-18

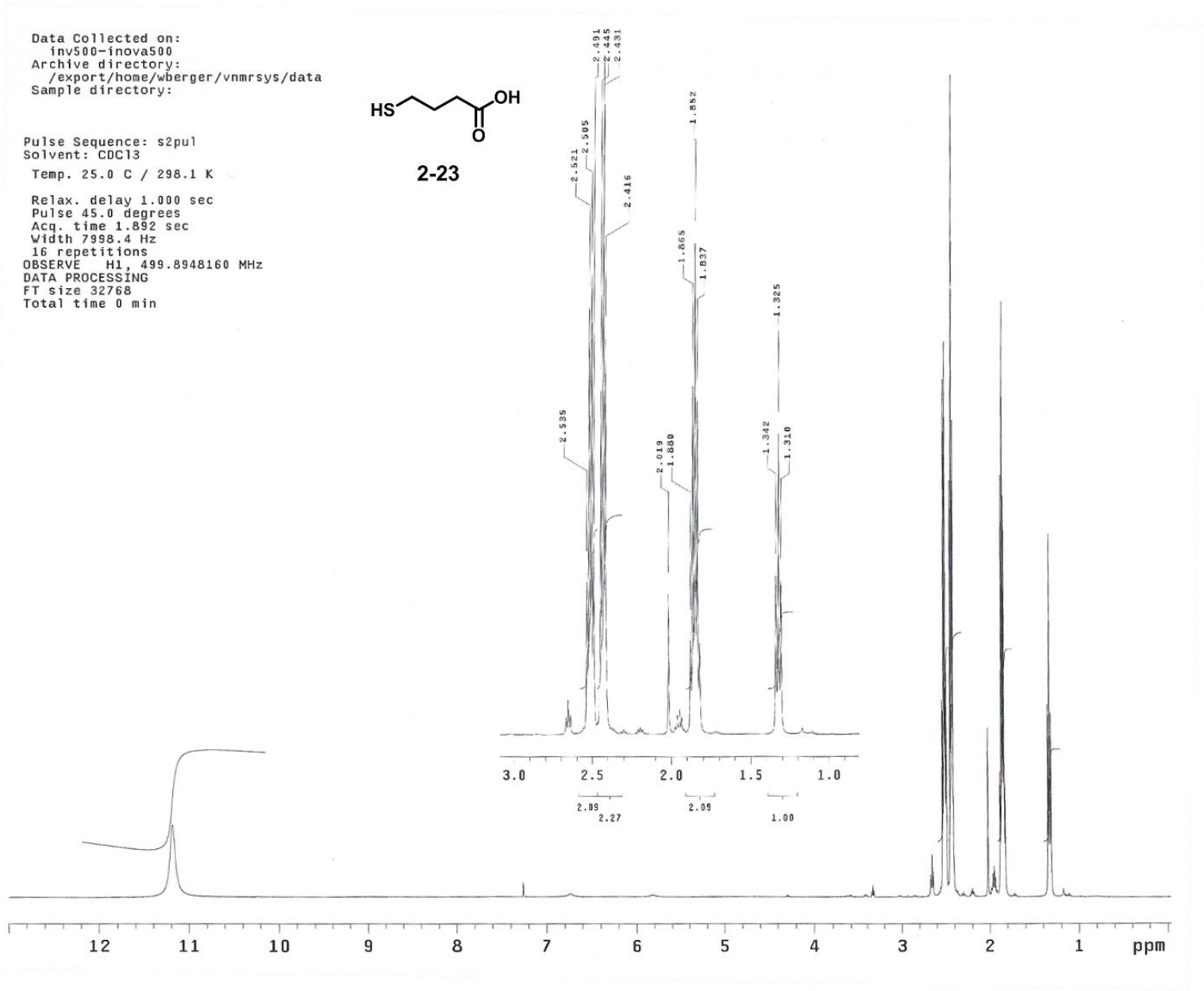
Data Collected on:
inv500-inova500
Archive directory:
/export/home/wberger/vnmrsys/data
Sample directory:
Pulse Sequence: s2pul
Solvent: CDCl3
Temp. 25.0 C / 298.1 K
Relax. delay 1.000 sec
Pulse 45.0 degrees
Acq. time 1.892 sec
Width 7998.4 Hz
16 repetitions
OBSERVE H1, 499.8948160 MHz
DATA PROCESSING
FT size 32768
Total time 0 min
HS
OH
O
2-23
2.491
2.445
2.431
2.521
2.505
2.416
1.852
1.865
1.837
1.325
2.535
2.019
1.880
1.342
1.310
3.0
2.5
2.0
1.5
1.0
2.09
2.27
2.09
1.00
12
11
10
9
8
7
6
5
4
3
2
1
ppm

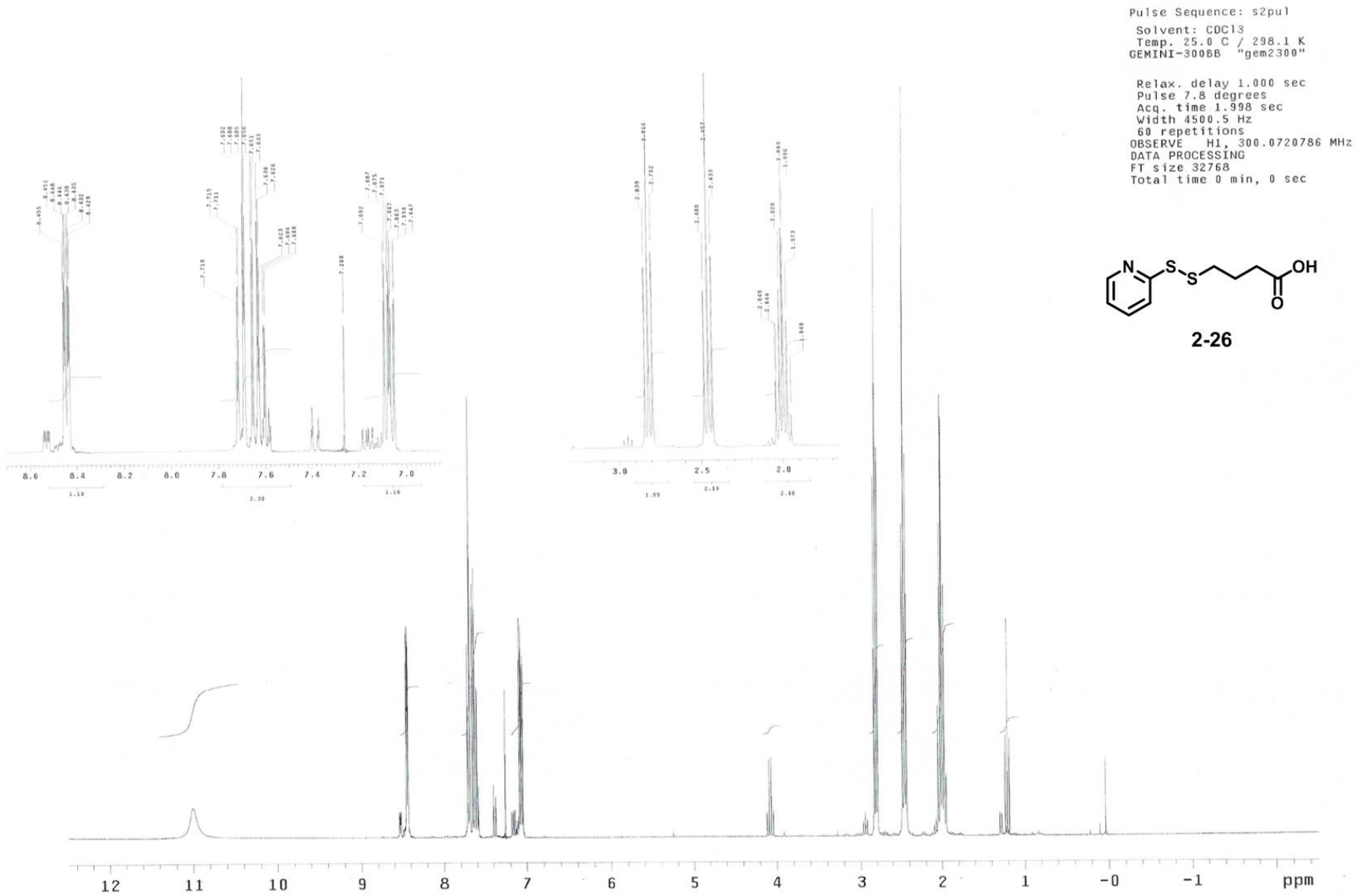
Pulse Sequence: s2pul
Solvent: CDCl3
Temp. 25.0 C / 298.1 K
GEMINI-300BB "gem2300"
Relax. delay 1.000 sec
Pulse 7.8 degrees
Acq. time 1.998 sec
Width 4500.5 Hz
60 repetitions
OBSERVE H1, 300.0720786 MHz
DATA PROCESSING
FT size 32768
Total time 0 min, 0 sec
N
S
S
OH
O
2-26
12
11
10
9
8
7
6
5
4
3
2
1
-0
-1
ppm

Pulse Sequence: s2pul
Solvent: CDCl3
Temp. 25.0 C / 298.1 K
INOVA-600 "inv601"

Relax. delay 1.000 sec
Pulse 61.5 degrees
Acq. time 1.892 sec
Width 8000.0 Hz
Single scan
OBSERVE H1, 599.7178127 MHz
DATA PROCESSING
FT size 32768
Total time 0 min, 2 sec

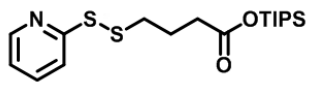

2-27

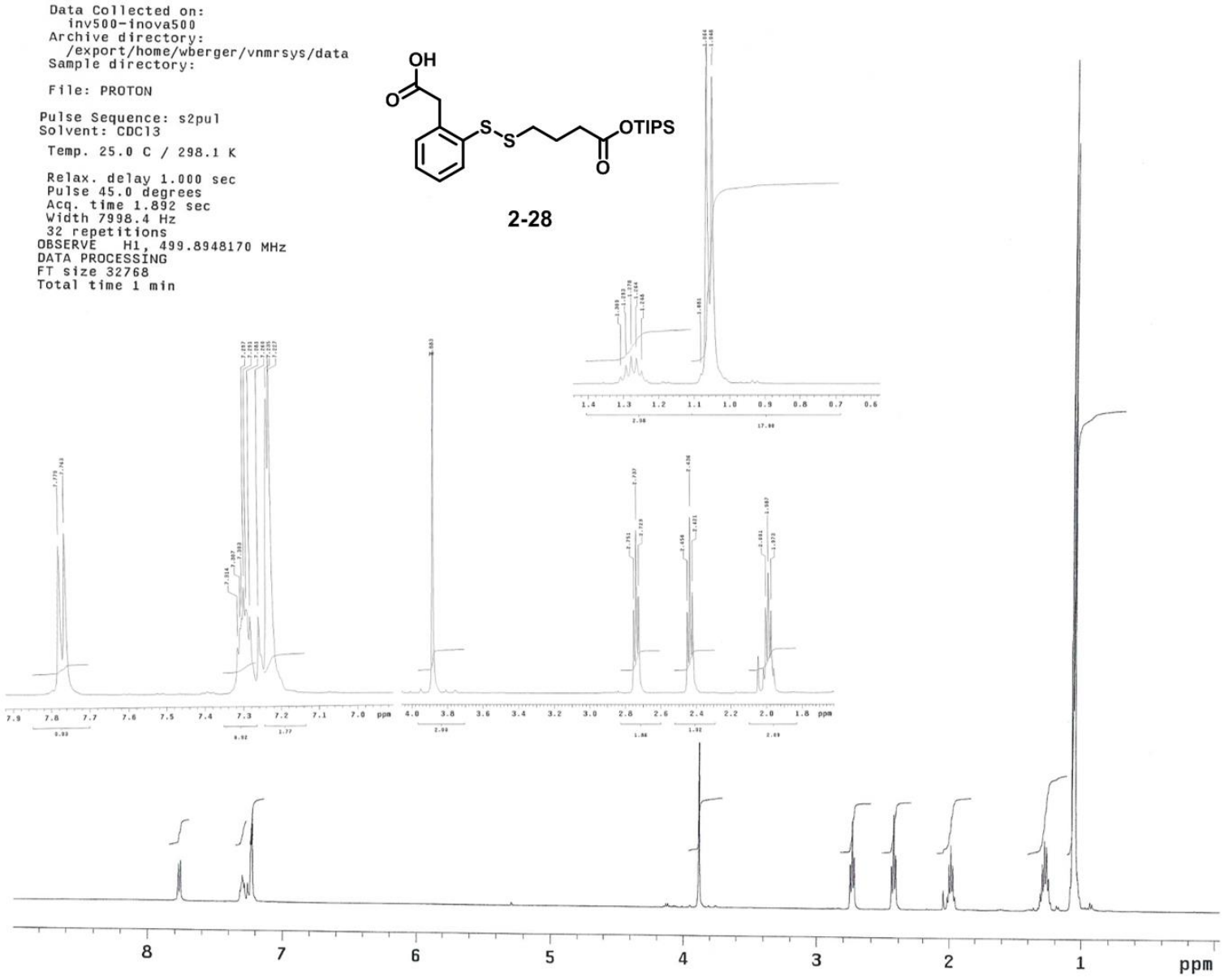
Data Collected on:
inv500-inova500
Archive directory:
/export/home/wberger/vnmrsys/data
Sample directory:
File: PROTON
Pulse Sequence: s2pul
Solvent: CDCl3
Temp. 25.0 C / 298.1 K
Relax. delay 1.000 sec
Pulse 45.0 degrees
Acq. time 1.892 sec
Width 7998.4 Hz
32 repetitions
OBSERVE H1, 499.8948170 MHz
DATA PROCESSING
FT size 32768
Total time 1 min
OH
O
S
S
OTIPS
O
2-28
8
7
6
5
4
3
2
1
ppm

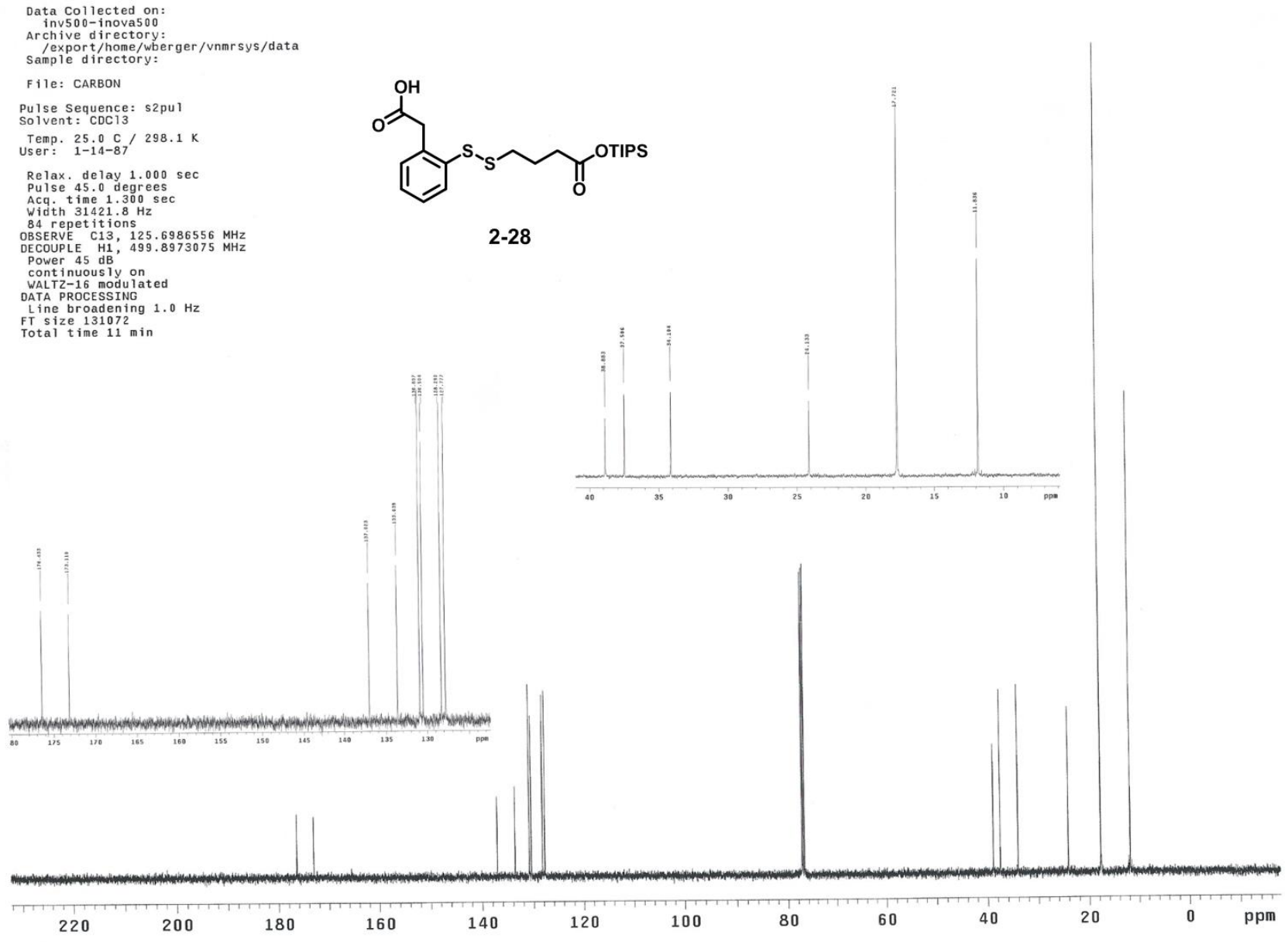
Data Collected on:
inv500-inova500
Archive directory:
/export/home/wberger/vnmrsys/data
Sample directory:
File: CARBON
Pulse Sequence: s2pul
Solvent: CDCl3
Temp. 25.0 C / 298.1 K
User: 1-14-87
Relax. delay 1.000 sec
Pulse 45.0 degrees
Acq. time 1.300 sec
Width 31421.8 Hz
84 repetitions
OBSERVE C13, 125.6986556 MHz
DECOUPLE H1, 499.8973075 MHz
Power 45 dB
continuously on
WALTZ-16 modulated
DATA PROCESSING
Line broadening 1.0 Hz
FT size 131072
Total time 11 min
OH
O
S
S
OTIPS
O
2-28
ppm

Pulse Sequence: s2pul
Solvent: CDCl3
Temp. 25.0 C / 298.1 K
INOVA-600 "inv601"

Relax. delay 1.000 sec
Pulse 61.5 degrees
Acq. time 1.892 sec
Width 8000.0 Hz
32 repetitions
OBSERVE H1, 599.7178132 MHz
DATA PROCESSING
FT size 32768
Total time 1 min, 32 sec

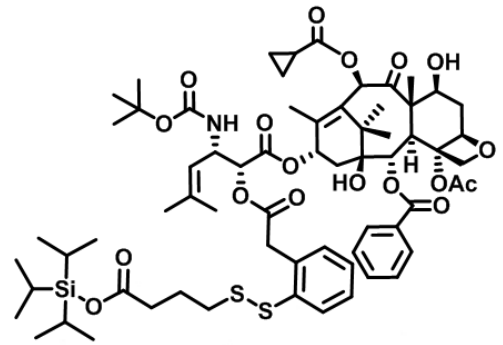

2-29

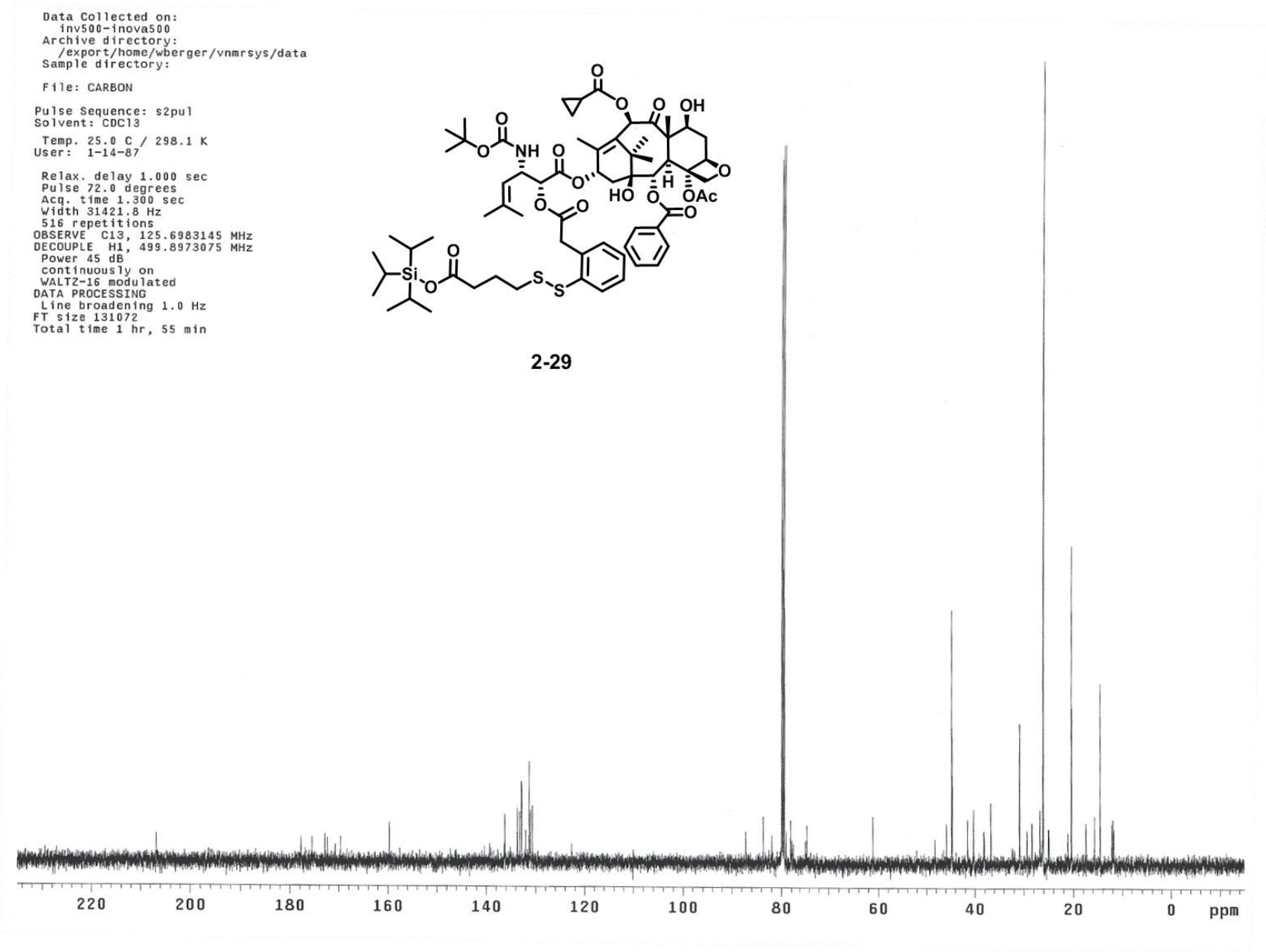
Data Collected on:
inv500-inova500
Archive directory:
/export/home/wberger/vnmrsys/data
Sample directory:
File: CARBON
Pulse Sequence: s2pul
Solvent: CDCl3
Temp. 25.0 C / 298.1 K
User: 1-14-87
Relax. delay 1.000 sec
Pulse 72.0 degrees
Acq. time 1.300 sec
Width 31421.8 Hz
516 repetitions
OBSERVE C13, 125.6983145 MHz
DECOUPLE H1, 499.8973075 MHz
Power 45 dB
continuously on
WALTZ-16 modulated
DATA PROCESSING
Line broadening 1.0 Hz
FT size 131072
Total time 1 hr, 55 min
220
200
180
160
140
120
100
80
60
40
20
0
ppm

2-29

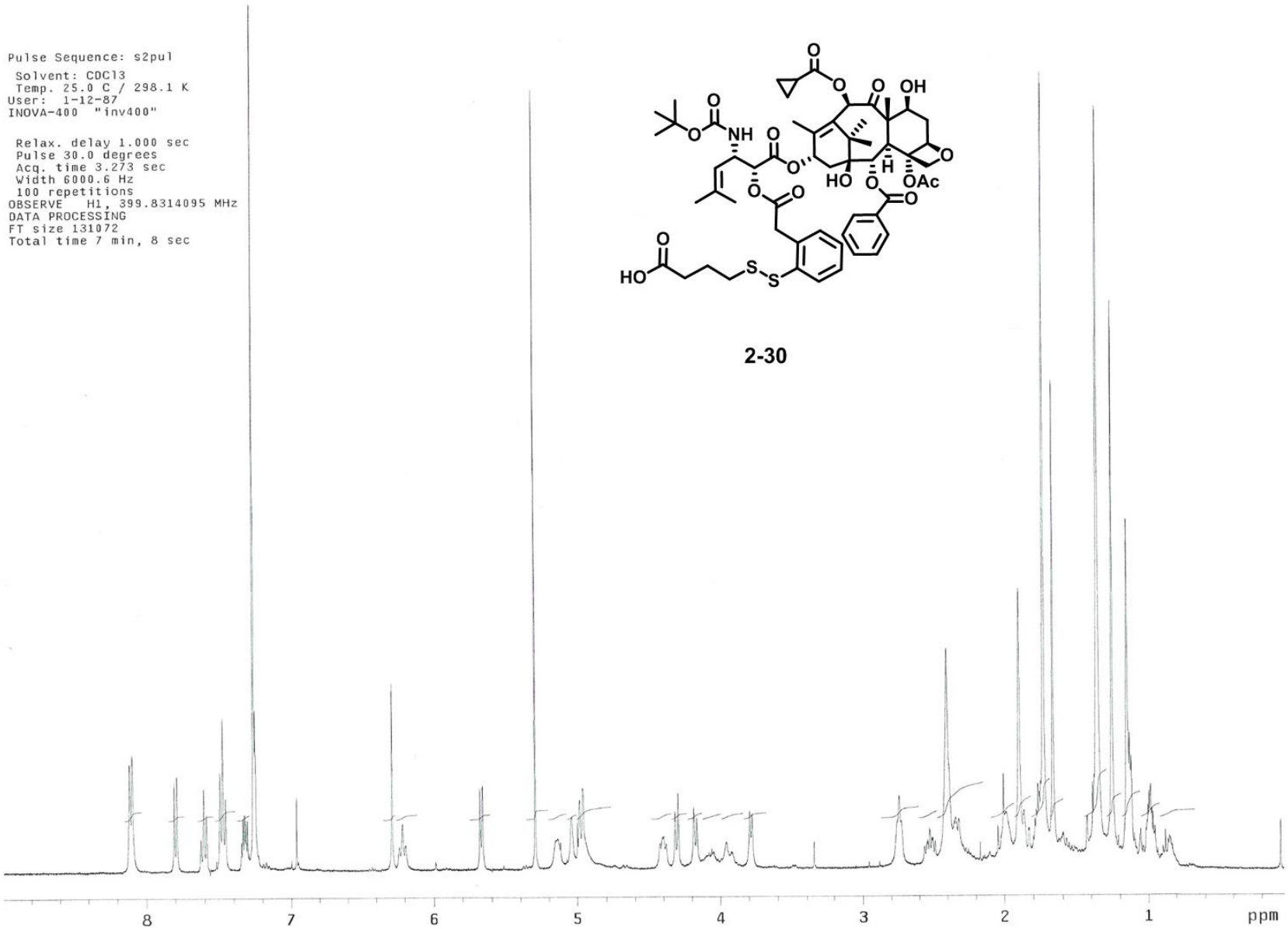
Pulse Sequence: s2pul
Solvent: CDCl3
Temp. 25.0 C / 298.1 K
User: 1-12-87
INOVA-400 "inv400"
Relax. delay 1.000 sec
Pulse 30.0 degrees
Acq. time 3.273 sec
Width 6000.6 Hz
100 repetitions
OBSERVE H1, 399.8314095 MHz
DATA PROCESSING
FT size 131072
Total time 7 min, 8 sec
8
7
6
5
4
3
2
1
ppm

2-30

Data Collected on:
inv500-inova500
Archive directory:
/export/home/wberger/vnmrsys/data
Sample directory:

File: PROTON

Pulse Sequence: s2pul
Solvent: CDCl3

Temp. 25.0 C / 298.1 K

Relax. delay 1.000 sec
Pulse 45.0 degrees
Acq. time 1.892 sec
Width 7998.4 Hz
92 repetitions
OBSERVE H1, 499.8948175 MHz
DATA PROCESSING
FT size 32768
Total time 4 min

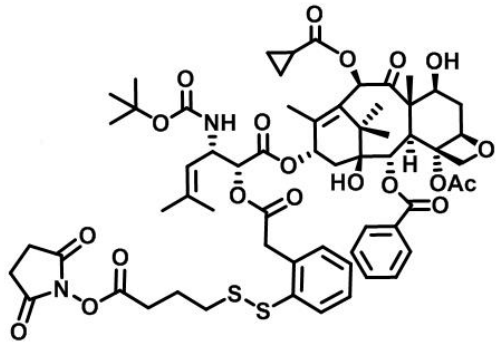

2-30

Data Collected on:
inv500-inova500
Archive directory:
/export/home/wberger/vnmrsys/data
Sample directory:

File: CARBON

Pulse Sequence: s2pul
Solvent: CDCl3

Temp. 25.0 C / 298.1 K
User: 1-14-87

Relax. delay 1.000 sec
Pulse 45.0 degrees
Acq. time 1.300 sec
Width 31421.8 Hz
3000 repetitions
OBSERVE C13, 125.6983145 MHz
DECOUPLE H1, 499.8973075 MHz
Power 45 dB
continuously on
WALTZ-16 modulated
DATA PROCESSING
Line broadening 1.0 Hz
FT size 131072
Total time 1 hr, 55 min

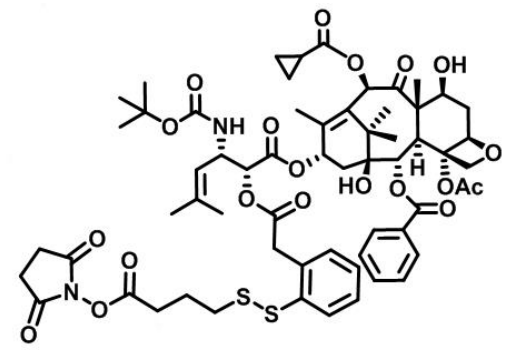

2-30

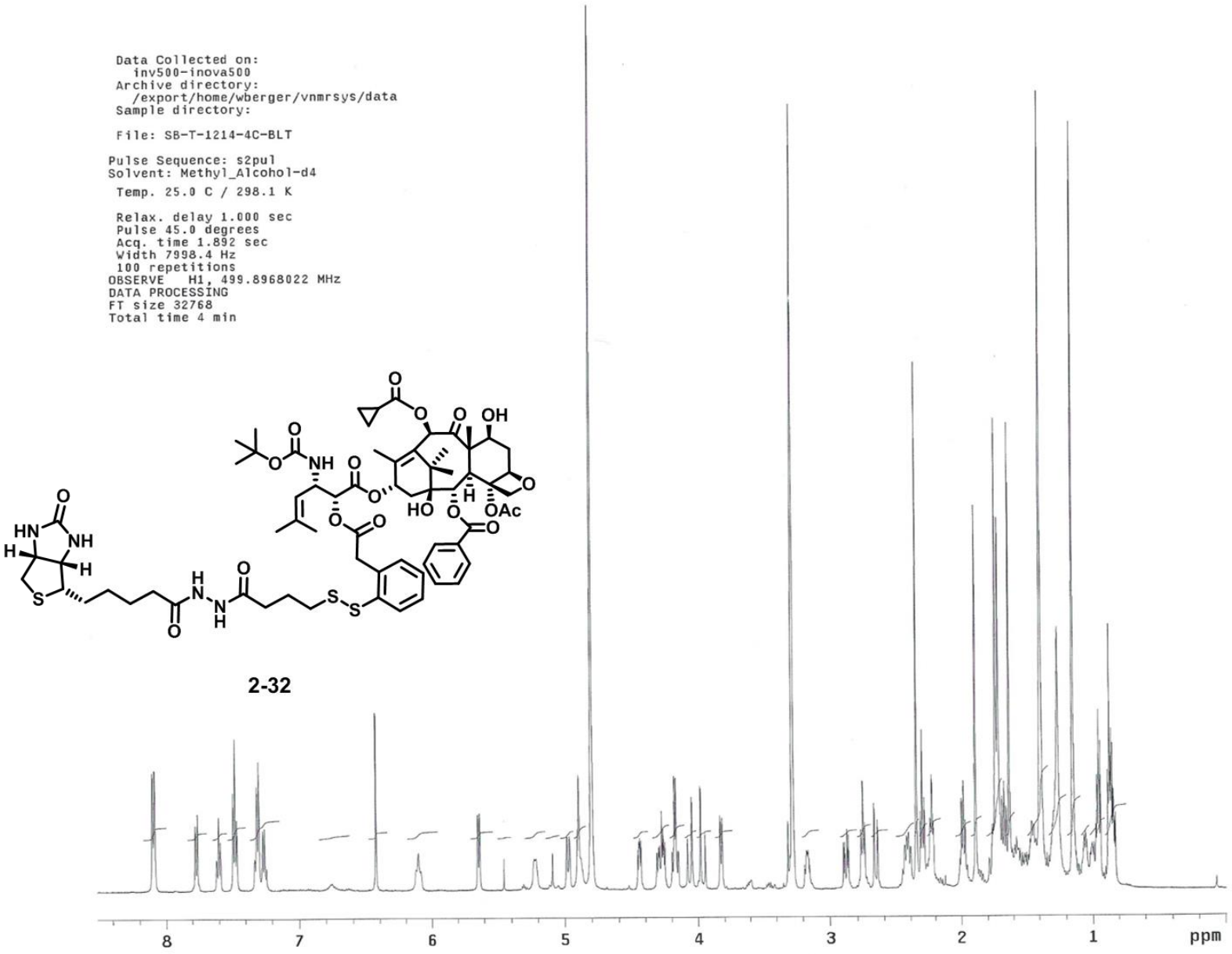
Data Collected on:
inv500-inova500
Archive directory:
/export/home/wberger/vnmrsys/data
Sample directory:
File: SB-T-1214-4C-BLT
Pulse Sequence: s2pul
Solvent: Methyl_Alcohol-d4
Temp. 25.0 C / 298.1 K
Relax. delay 1.000 sec
Pulse 45.0 degrees
Acq. time 1.892 sec
Width 7998.4 Hz
100 repetitions
OBSERVE H1, 499.8968022 MHz
DATA PROCESSING
FT size 32768
Total time 4 min
2-32
8
7
6
5
4
3
2
1
ppm

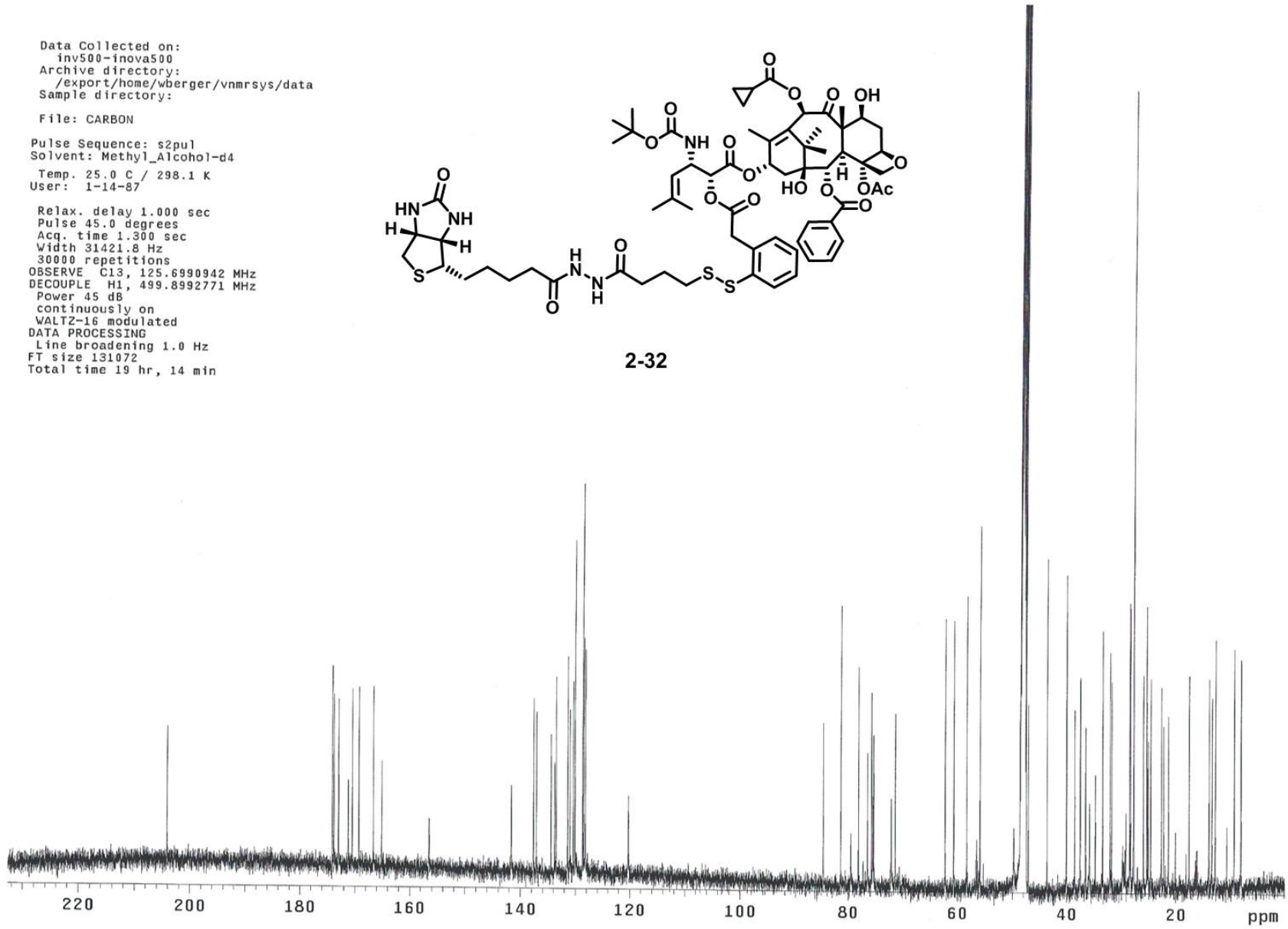
Data Collected on:
inv500-inova500
Archive directory:
/export/home/wberger/vnmrsys/data
Sample directory:
File: CARBON
Pulse Sequence: s2pul
Solvent: Methyl_Alcohol-d4
Temp. 25.0 C / 298.1 K
User: 1-14-87
Relax. delay 1.000 sec
Pulse 45.0 degrees
Acq. time 1.300 sec
Width 31421.8 Hz
30000 repetitions
OBSERVE C13, 125.6990942 MHz
DECOUPLE H1, 499.8992771 MHz
Power 45 dB
continuously on
WALTZ-16 modulated
DATA PROCESSING
Line broadening 1.0 Hz
FT size 131072
Total time 19 hr, 14 min
2-32
220
200
180
160
140
120
100
80
60
40
20
ppm

Appendix Chapter 3

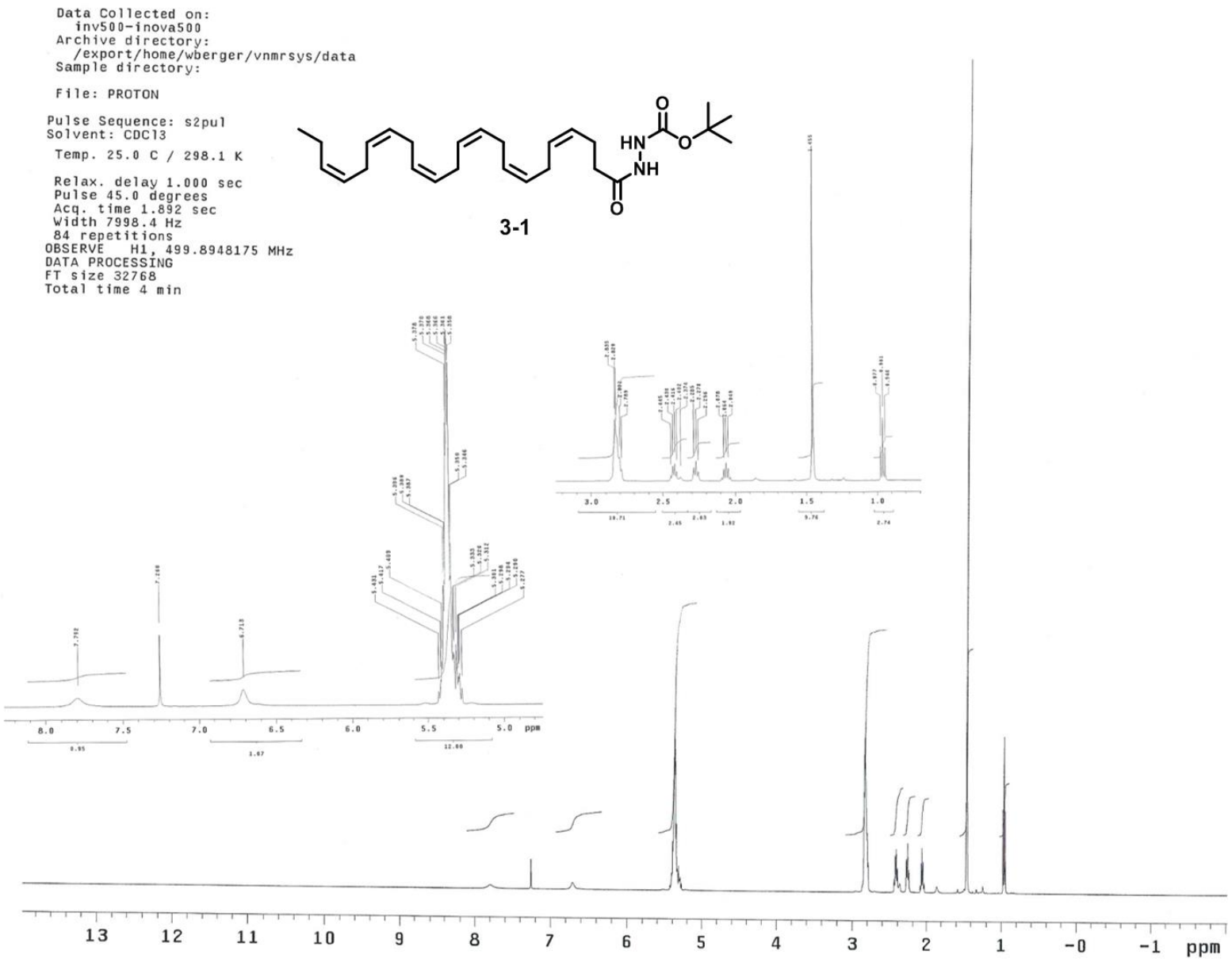
Data Collected on:
inv500-inova500
Archive directory:
/export/home/wberger/vnmrsys/data
Sample directory:
File: PROTON
Pulse Sequence: s2pul
Solvent: CDCl3
Temp. 25.0 C / 298.1 K
Relax. delay 1.000 sec
Pulse 45.0 degrees
Acq. time 1.892 sec
Width 7998.4 Hz
84 repetitions
OBSERVE H1, 499.8948175 MHz
DATA PROCESSING
FT size 32768
Total time 4 min
HN
NH
O
O
O
3-1
ppm

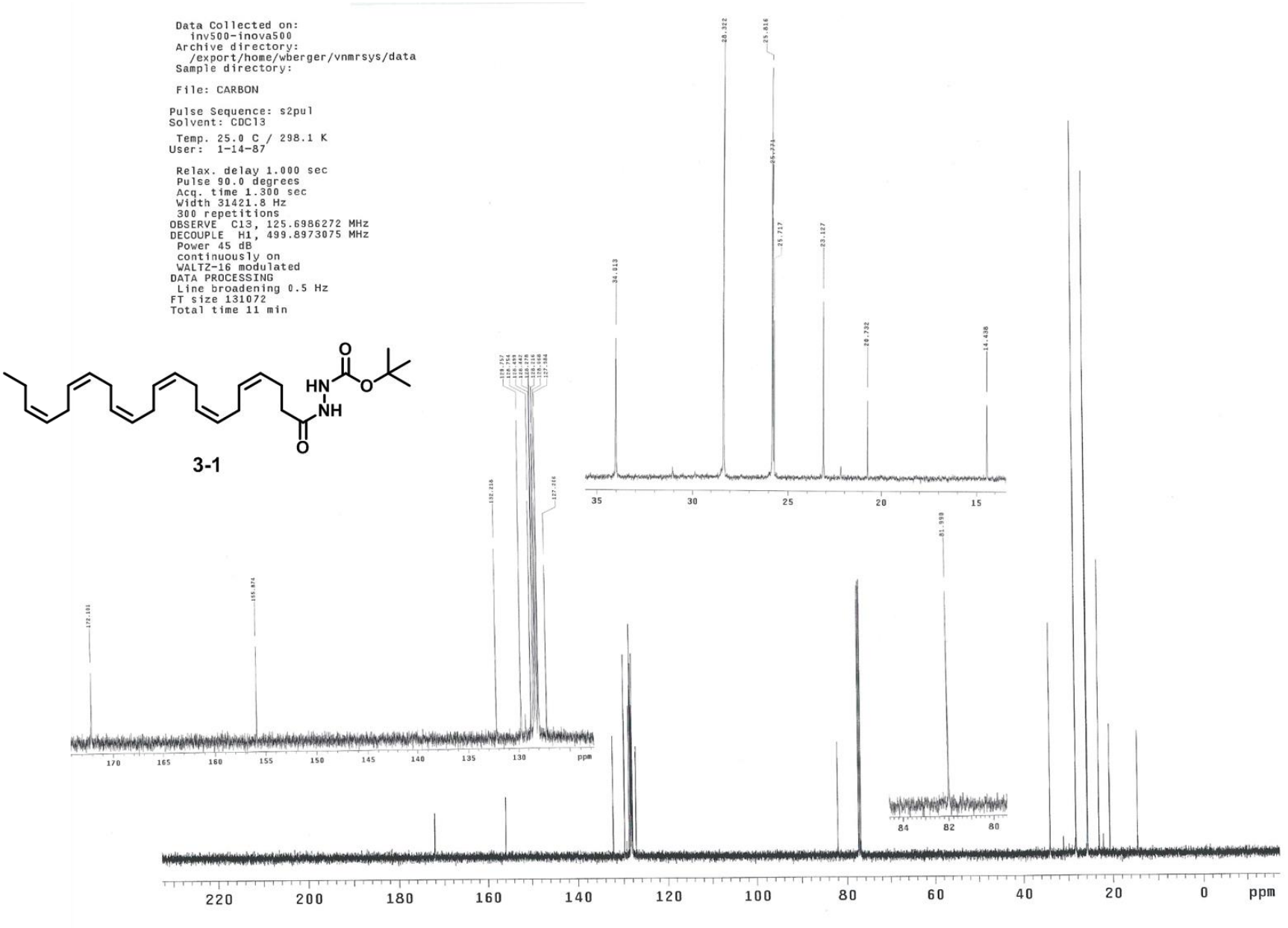
Data Collected on:
inv500-inova500
Archive directory:
/export/home/wberger/vnmrsys/data
Sample directory:
File: CARBON
Pulse Sequence: s2pul
Solvent: CDCl3
Temp. 25.0 C / 298.1 K
User: 1-14-87
Relax. delay 1.000 sec
Pulse 90.0 degrees
Acq. time 1.300 sec
Width 31421.8 Hz
300 repetitions
OBSERVE C13, 125.6986272 MHz
DECOUPLE H1, 499.8973075 MHz
Power 45 dB
continuously on
WALTZ-16 modulated
DATA PROCESSING
Line broadening 0.5 Hz
FT size 131072
Total time 11 min
HN
NH
O
O
O
3-1
ppm

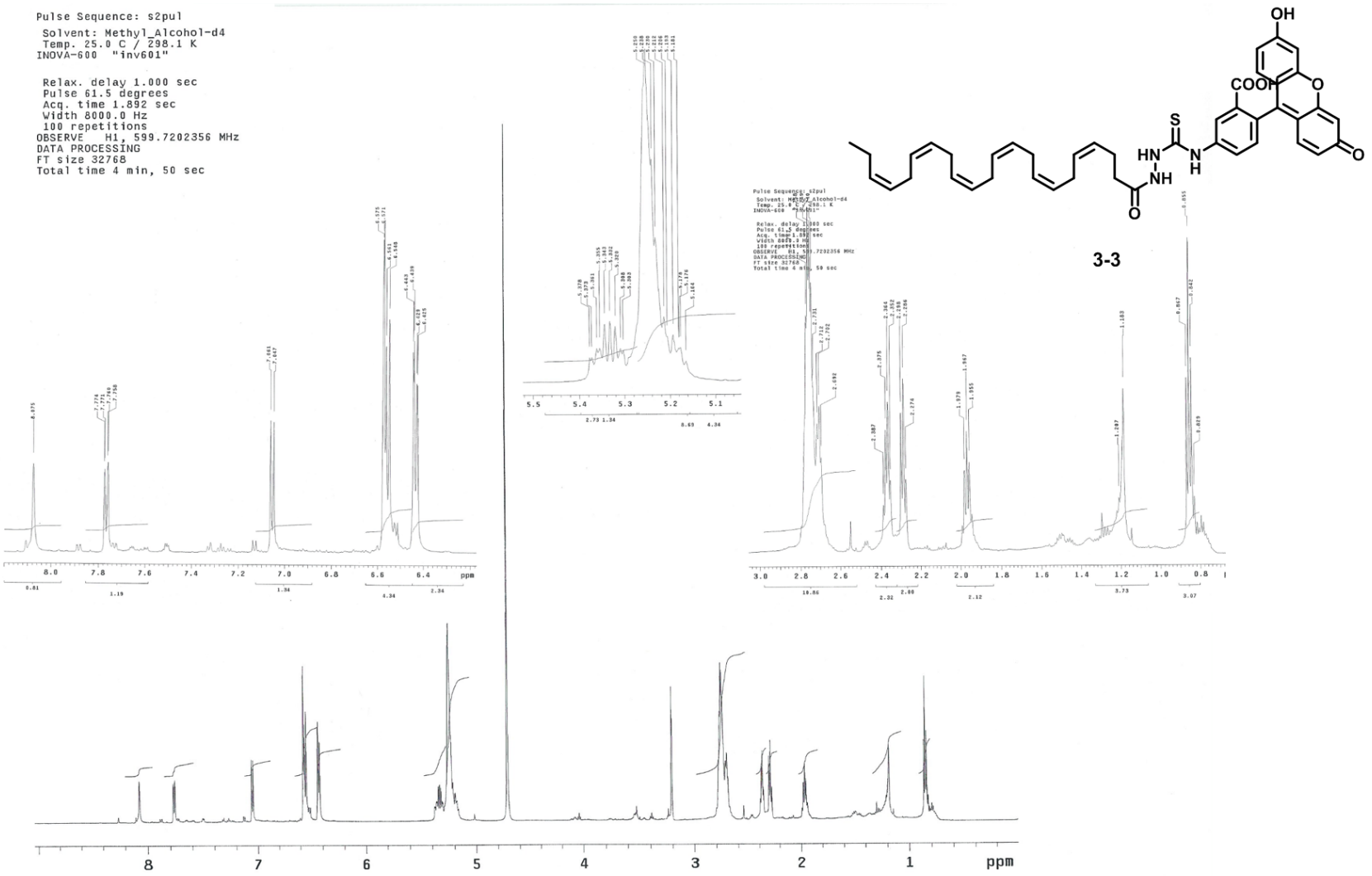
Pulse Sequence: s2pul
Solvent: Methyl_Alcohol-d4
Temp. 25.0 C / 298.1 K
INOVA-600 "inv601"
Relax. delay 1.000 sec
Pulse 61.5 degrees
Acq. time 1.892 sec
Width 8000.0 Hz
100 repetitions
OBSERVE H1, 599.7202356 MHz
DATA PROCESSING
FT size 32768
Total time 4 min, 50 sec
OH
COOH
O
S
HN
N
H
NH
O
O
3-3
ppm

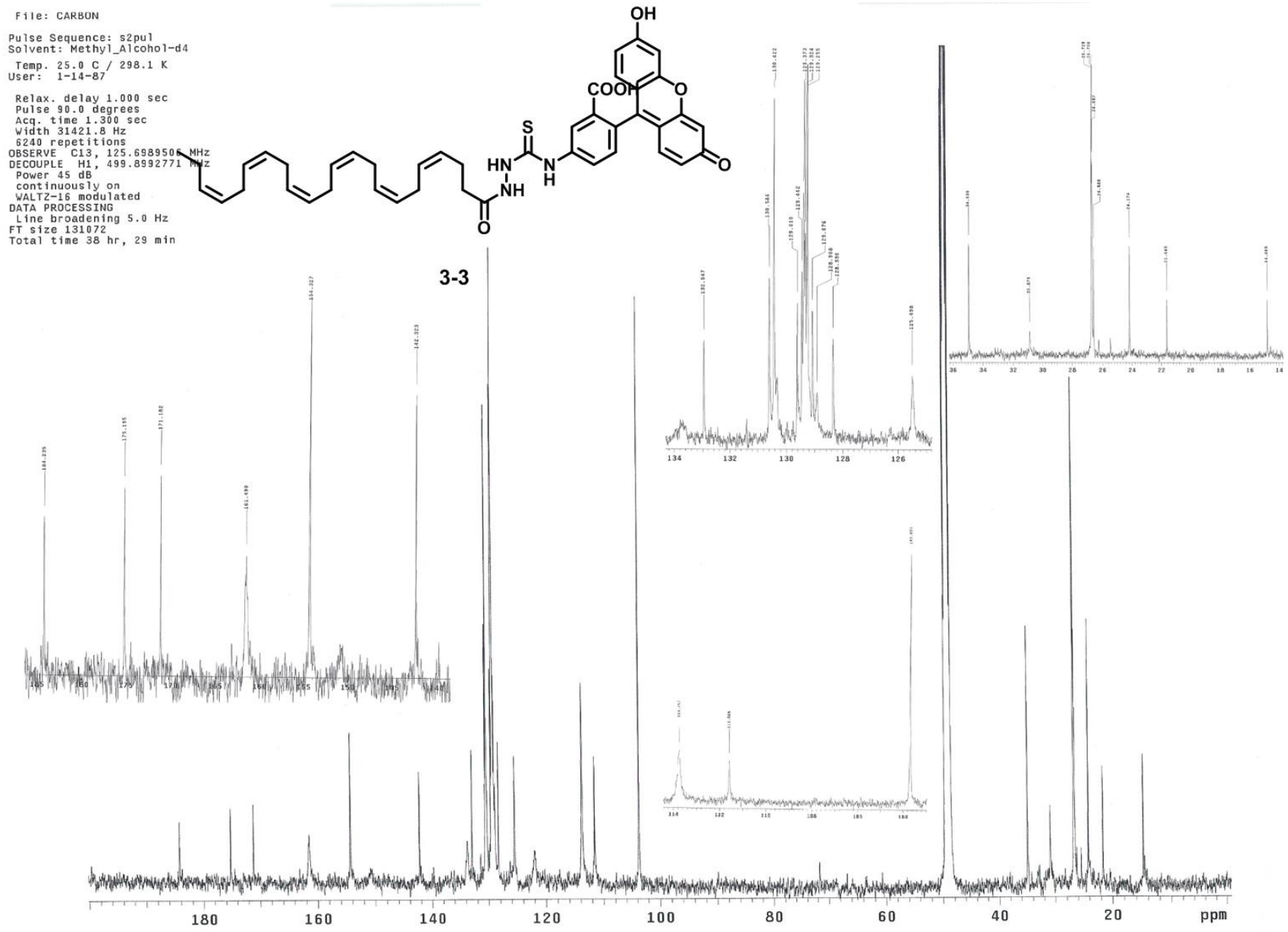
File: CARBON
Pulse Sequence: s2pul
Solvent: Methyl_Alcohol-d4
Temp. 25.0 C / 298.1 K
User: 1-14-87
Relax. delay 1.000 sec
Pulse 90.0 degrees
Acq. time 1.300 sec
Width 31421.8 Hz
6240 repetitions
OBSERVE C13, 125.6989506 MHz
DECOUPLE H1, 499.8992771 MHz
Power 45 dB
continuously on
WALTZ-16 modulated
DATA PROCESSING
Line broadening 5.0 Hz
FT size 131072
Total time 38 hr, 29 min
OH
COOH
O
S
HN
N
H
NH
O
O
3-3
180
160
140
120
100
80
60
40
20
ppm

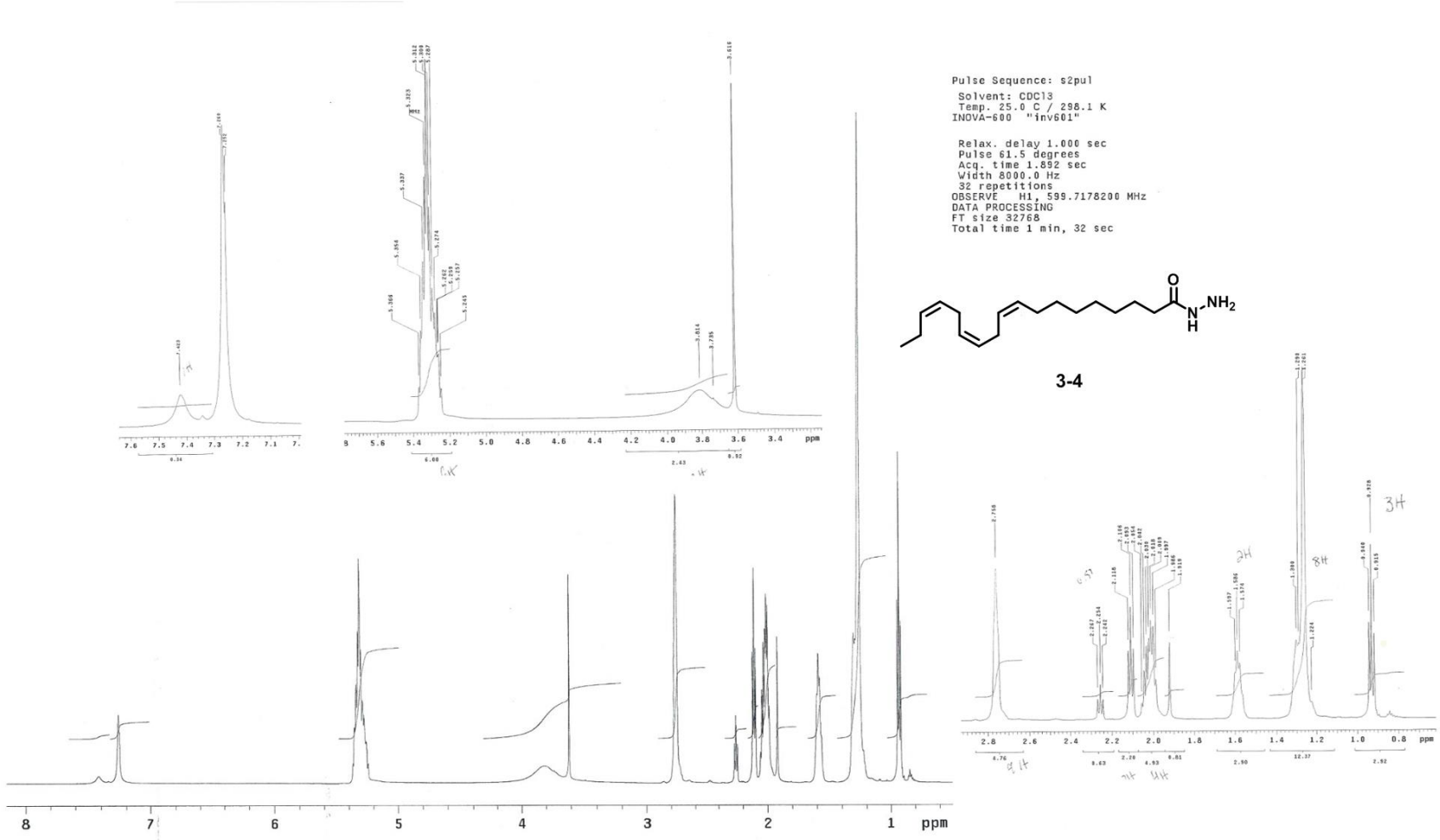
Pulse Sequence: s2pul
Solvent: CDCl3
Temp. 25.0 C / 298.1 K
INOVA-600 "inv601"
Relax. delay 1.000 sec
Pulse 61.5 degrees
Acq. time 1.892 sec
Width 8000.0 Hz
32 repetitions
OBSERVE H1, 599.7178200 MHz
DATA PROCESSING
FT size 32768
Total time 1 min, 32 sec
O
N
NH2
H
3-4
ppm

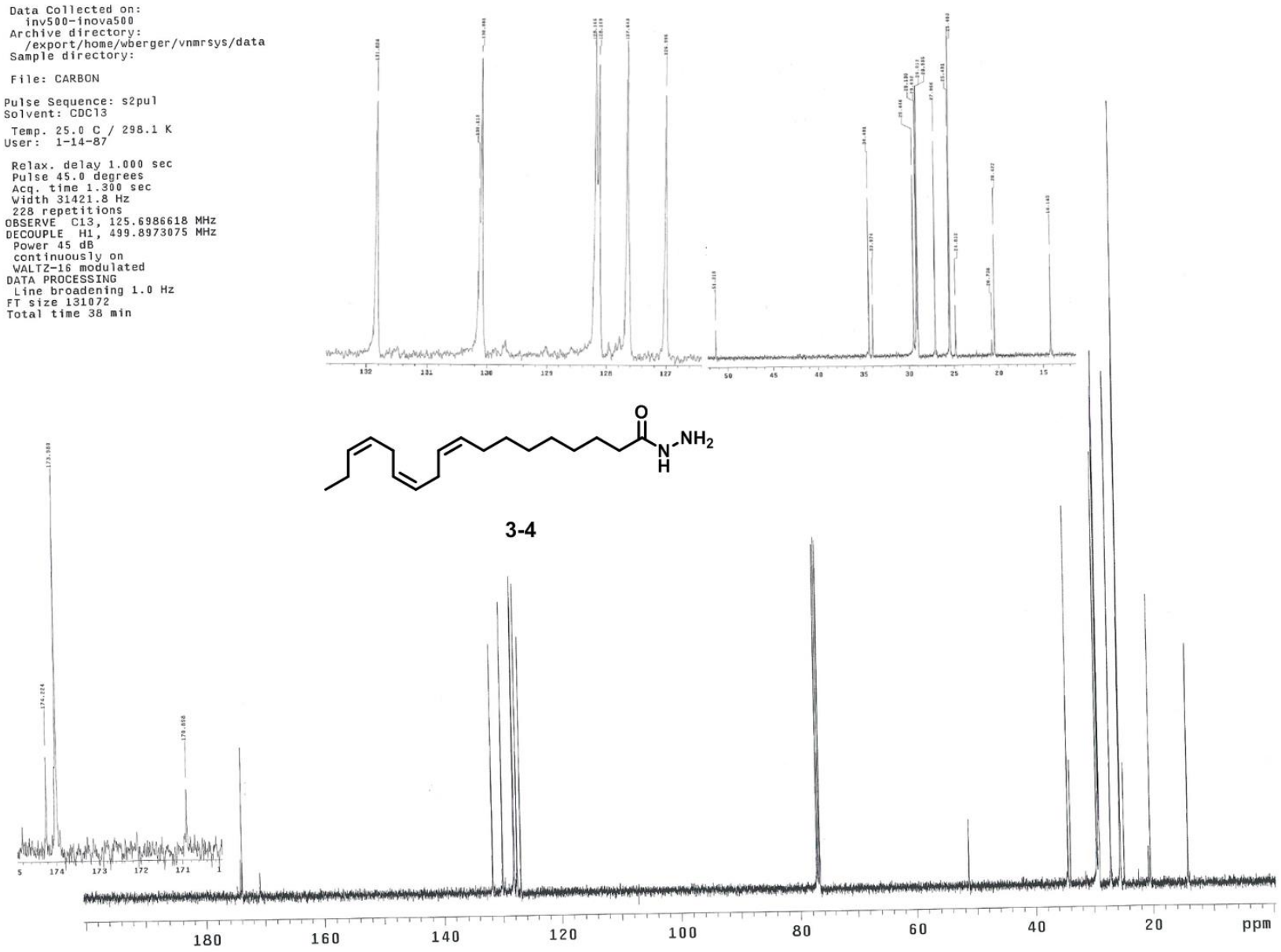
Data Collected on:
inv500-inova500
Archive directory:
/export/home/wberger/vnmrsys/data
Sample directory:
File: CARBON
Pulse Sequence: s2pul
Solvent: CDCl3
Temp. 25.0 C / 298.1 K
User: 1-14-87
Relax. delay 1.000 sec
Pulse 45.0 degrees
Acq. time 1.300 sec
Width 31421.8 Hz
228 repetitions
OBSERVE C13, 125.6986618 MHz
DECOUPLE H1, 499.8973075 MHz
Power 45 dB
continuously on
WALTZ-16 modulated
DATA PROCESSING
Line broadening 1.0 Hz
FT size 131072
Total time 38 min
O
N
H
NH2
3-4
ppm

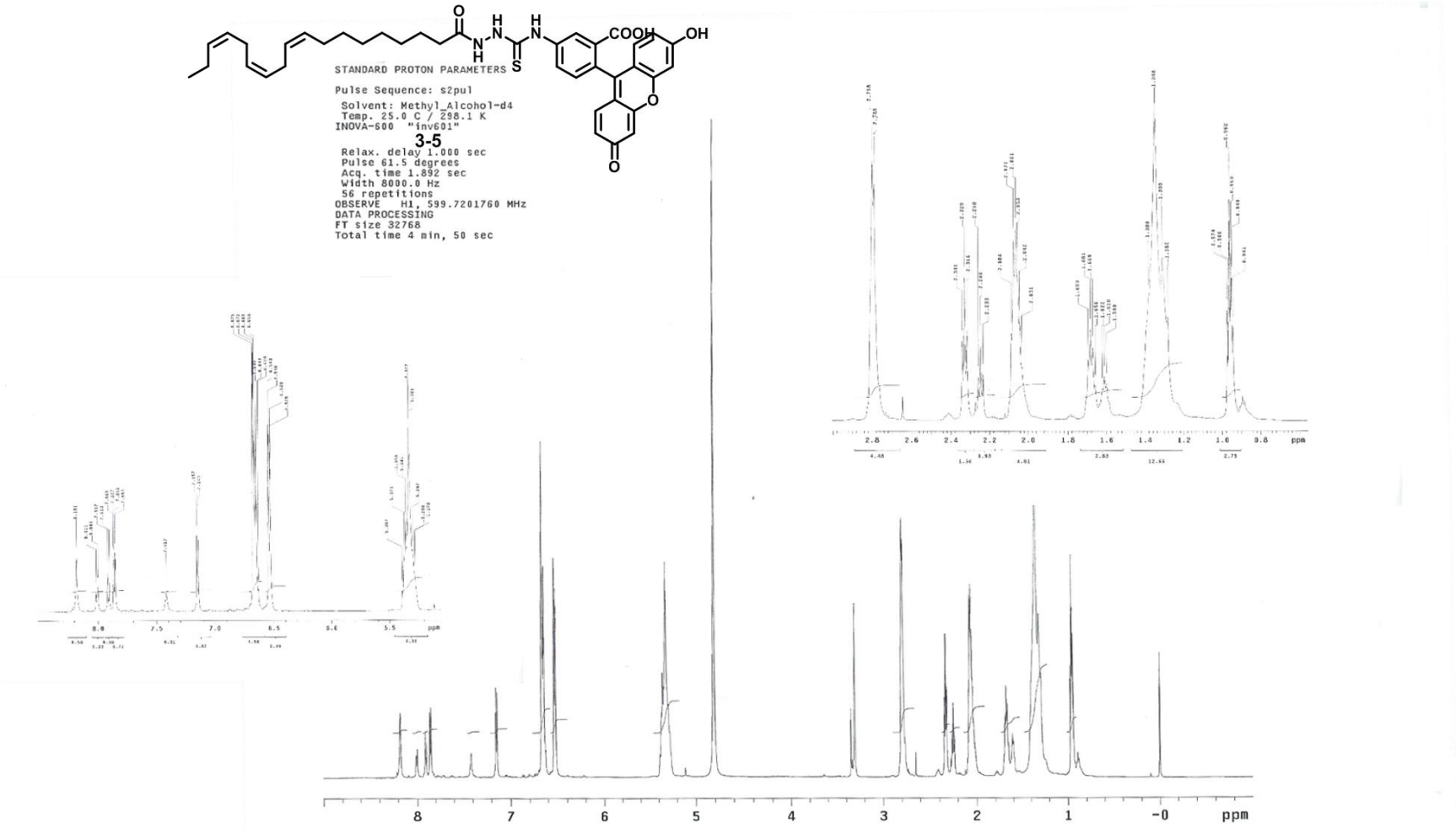
STANDARD PROTON PARAMETERS
Pulse Sequence: s2pul
Solvent: Methyl_Alcohol-d4
Temp. 25.0 C / 298.1 K
INOVA-600 "inv601"
3-5
Relax. delay 1.000 sec
Pulse 61.5 degrees
Acq. time 1.892 sec
Width 8000.0 Hz
56 repetitions
OBSERVE H1, 599.7201760 MHz
DATA PROCESSING
FT size 32768
Total time 4 min, 50 sec
COOH
OH
ppm

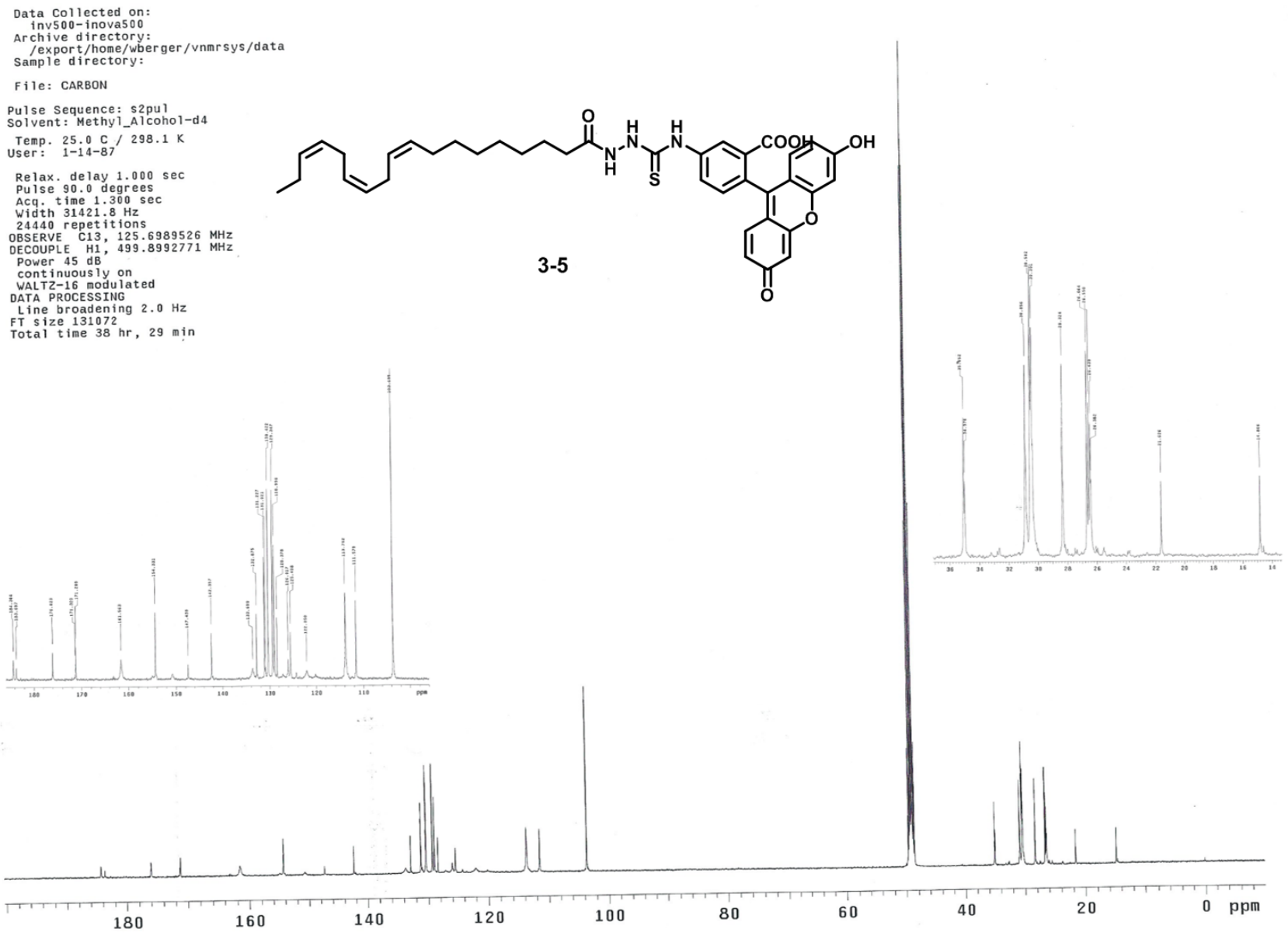
Data Collected on:
inv500-inova500
Archive directory:
/export/home/wberger/vnmrsys/data
Sample directory:
File: CARBON
Pulse Sequence: s2pul
Solvent: Methyl_Alcohol-d4
Temp. 25.0 C / 298.1 K
User: 1-14-87
Relax. delay 1.000 sec
Pulse 90.0 degrees
Acq. time 1.300 sec
Width 31421.8 Hz
24440 repetitions
OBSERVE C13, 125.6989526 MHz
DECOUPLE H1, 499.8992771 MHz
Power 45 dB
continuously on
WALTZ-16 modulated
DATA PROCESSING
Line broadening 2.0 Hz
FT size 131072
Total time 38 hr, 29 min
3-5
COOH
OH
180
160
140
120
100
80
60
40
20
0 ppm

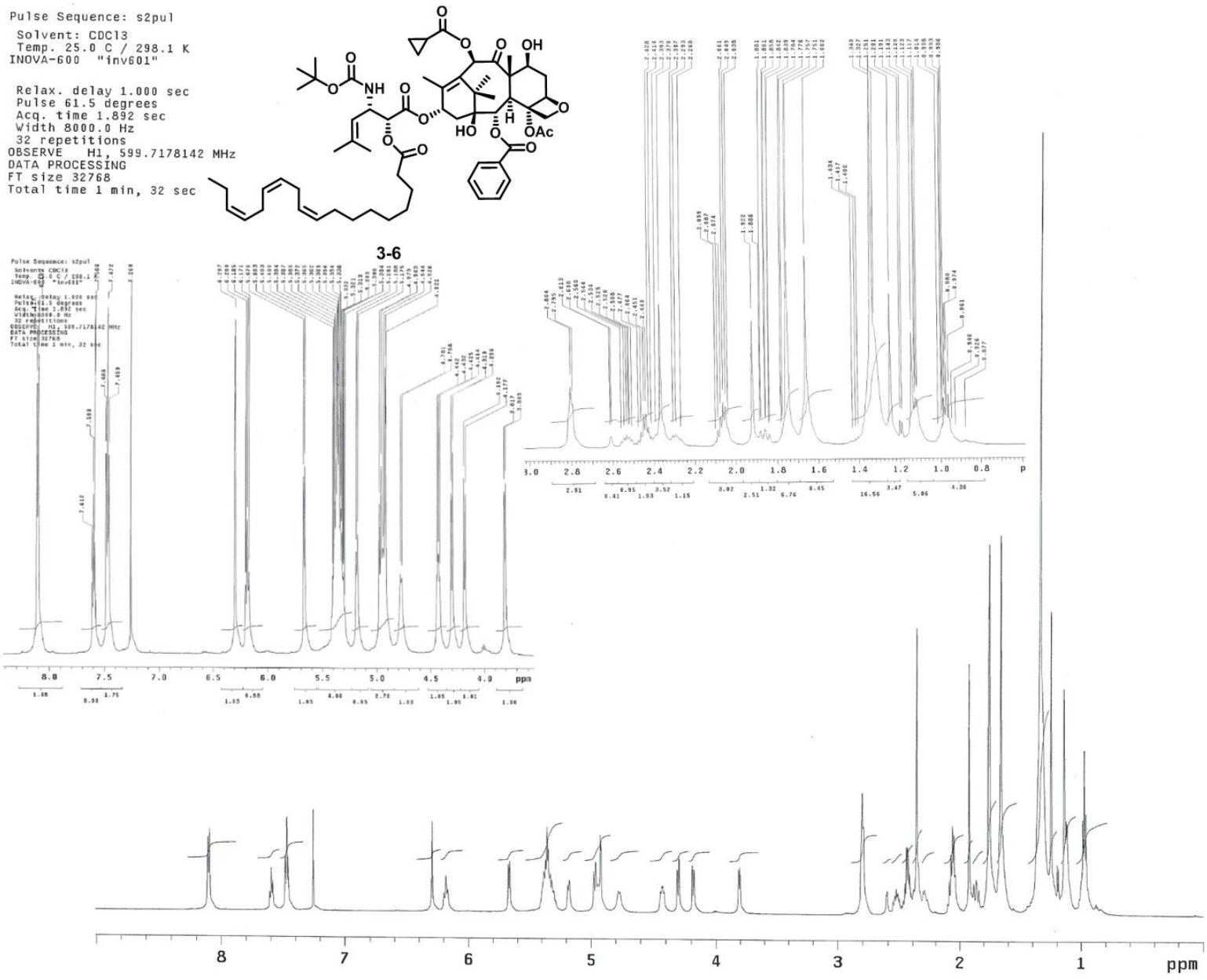
Pulse Sequence: s2pul
Solvent: CDCl3
Temp. 25.0 C / 298.1 K
INOVA-600 "inv601"
Relax. delay 1.000 sec
Pulse 61.5 degrees
Acq. time 1.892 sec
Width 8000.0 Hz
32 repetitions
OBSERVE H1, 599.7178142 MHz
DATA PROCESSING
FT size 32768
Total time 1 min, 32 sec
3-6
ppm

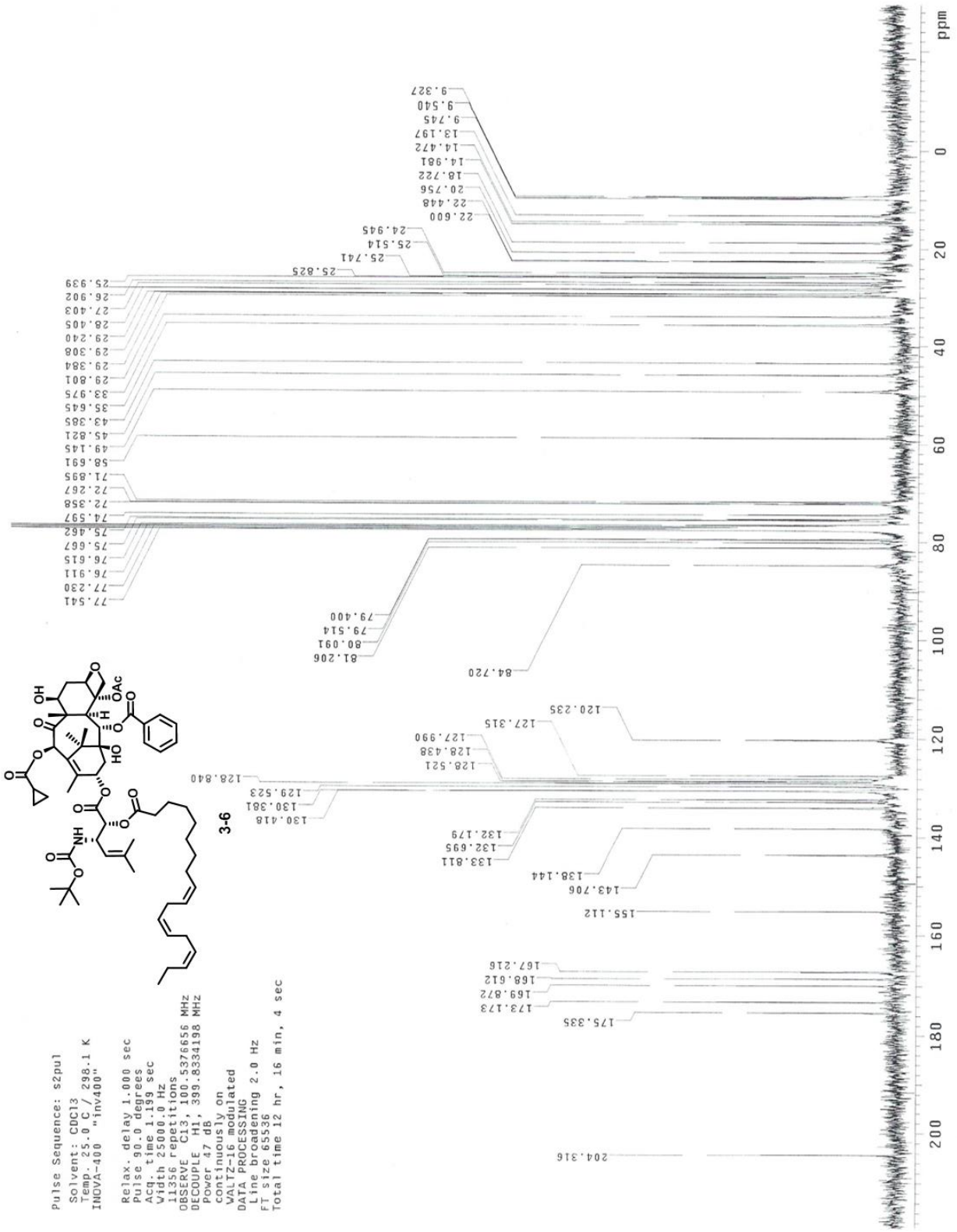
3-6
Pulse Sequence: s2pul
Solvent: CDCl3
Temp. 25.0 C / 298.1 K
INOVA-400 "inv400"
Relax. delay 1.000 sec
Pulse 90.0 degrees
Acq. time 1.199 sec
Width 25000.0 Hz
11356 repetitions
OBSERVE C13, 100.5376656 MHz
DECOUPLE H1, 399.8334198 MHz
Power 47 dB
continuously on
WALTZ-16 modulated
DATA PROCESSING
Line broadening 2.0 Hz
FT size 65536
Total time 12 hr, 16 min, 4 sec
9.327
9.540
9.745
13.197
14.472
14.981
18.722
20.756
22.448
22.600
24.945
25.514
25.741
25.825
25.939
26.902
27.403
28.405
29.240
29.308
29.384
29.801
33.975
35.645
43.385
45.821
49.145
58.691
71.895
72.267
72.358
74.597
75.462
75.667
76.615
76.911
77.230
77.541
79.400
79.514
80.091
81.206
84.720
120.235
127.315
127.990
128.438
128.521
128.840
129.523
130.361
130.418
132.179
132.695
133.811
138.144
143.706
155.112
167.216
168.612
169.872
173.173
175.335
204.316
ppm

Appendix Chapter 4

Data Collected on:
inv500-inova500
Archive directory:
/export/home/wberger/vnmrsys/data
Sample directory:

File: PROTON

Pulse Sequence: s2pul
Solvent: Methyl_Alcohol-d4

Temp. 25.0 C / 298.1 K

Relax. delay 1.000 sec
Pulse 45.0 degrees
Acq. time 1.892 sec
Width 7998.4 Hz
100 repetitions
OBSERVE H1, 499.8968012 MHz
DATA PROCESSING
FT size 32768
Total time 4 min

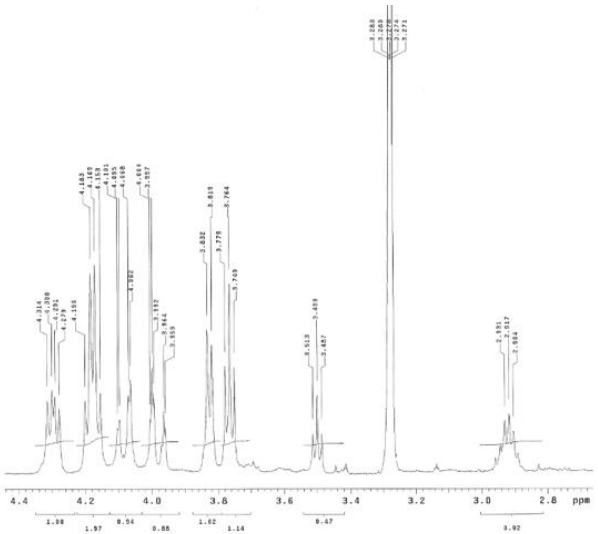

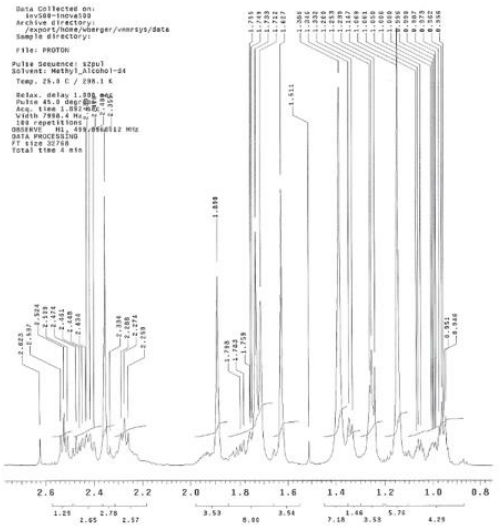

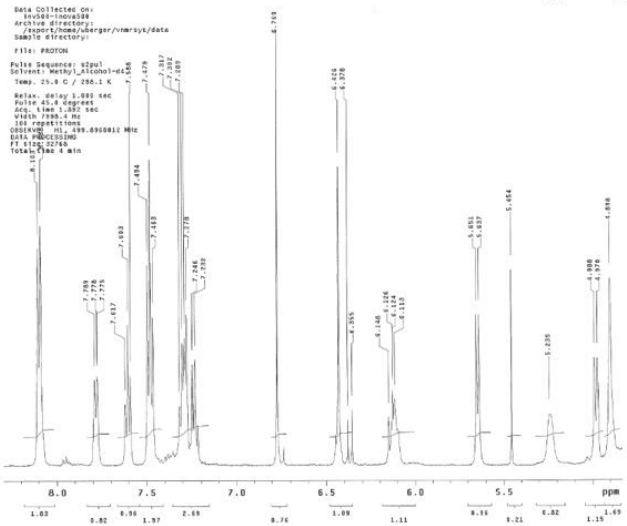

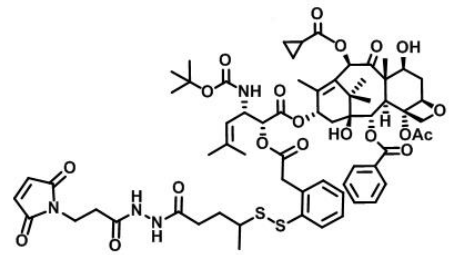

4-1

Data Collected on:
inv500-inova500
Archive directory:
/export/home/wberger/vnmrsys/data
Sample directory:

File: CARBON

Pulse Sequence: s2pul
Solvent: Methyl_Alcohol-d4

Temp. 25.0 C / 298.1 K
User: 1-14-87

Relax. delay 1.000 sec
Pulse 45.0 degrees
Acq. time 1.300 sec
Width 31421.8 Hz
6072 repetitions
OBSERVE C13, 125.6989506 MHz
DECOUPLE H1, 499.8992771 MHz
Power 45 dB
continuously on
WALTZ-16 modulated
DATA PROCESSING
Line broadening 3.0 Hz
FT size 131072
Total time 6 hr, 24 min

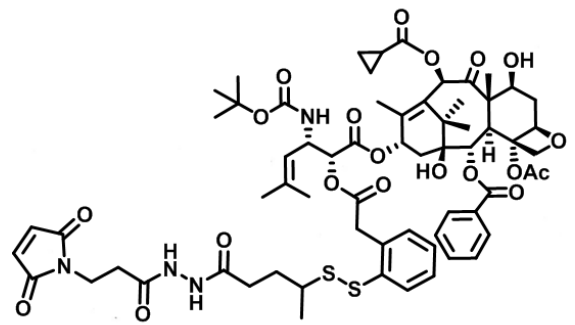

4-1

Pulse Sequence: s2pul
Solvent: CDCl3
Temp. 25.0 C / 298.1 K
User: l-12-87
INOVA-400 "inv400"
Relax. delay 1.000 sec
Pulse 6.7 degrees
Acq. time 3.273 sec
Width 6000.6 Hz
64 repetitions
OBSERVE H1, 399.8314085 MHz
DATA PROCESSING
Line broadening 1.0 Hz
FT size 32072
Total time 4 min, 34 sec
4-4
HO
O
N
O
O
7.260
6.684
3.544
3.531
3.495
3.513
2.356
2.338
2.319
2.156
1.689
1.671
1.652
1.632
1.625
1.606
1.587
1.568
1.373
1.352
1.334
1.314
1.295
ppm
1
2
3
4
5
6
7
8
9
10
11
1.77
0.91
2.14
1.99
3.97
2.13

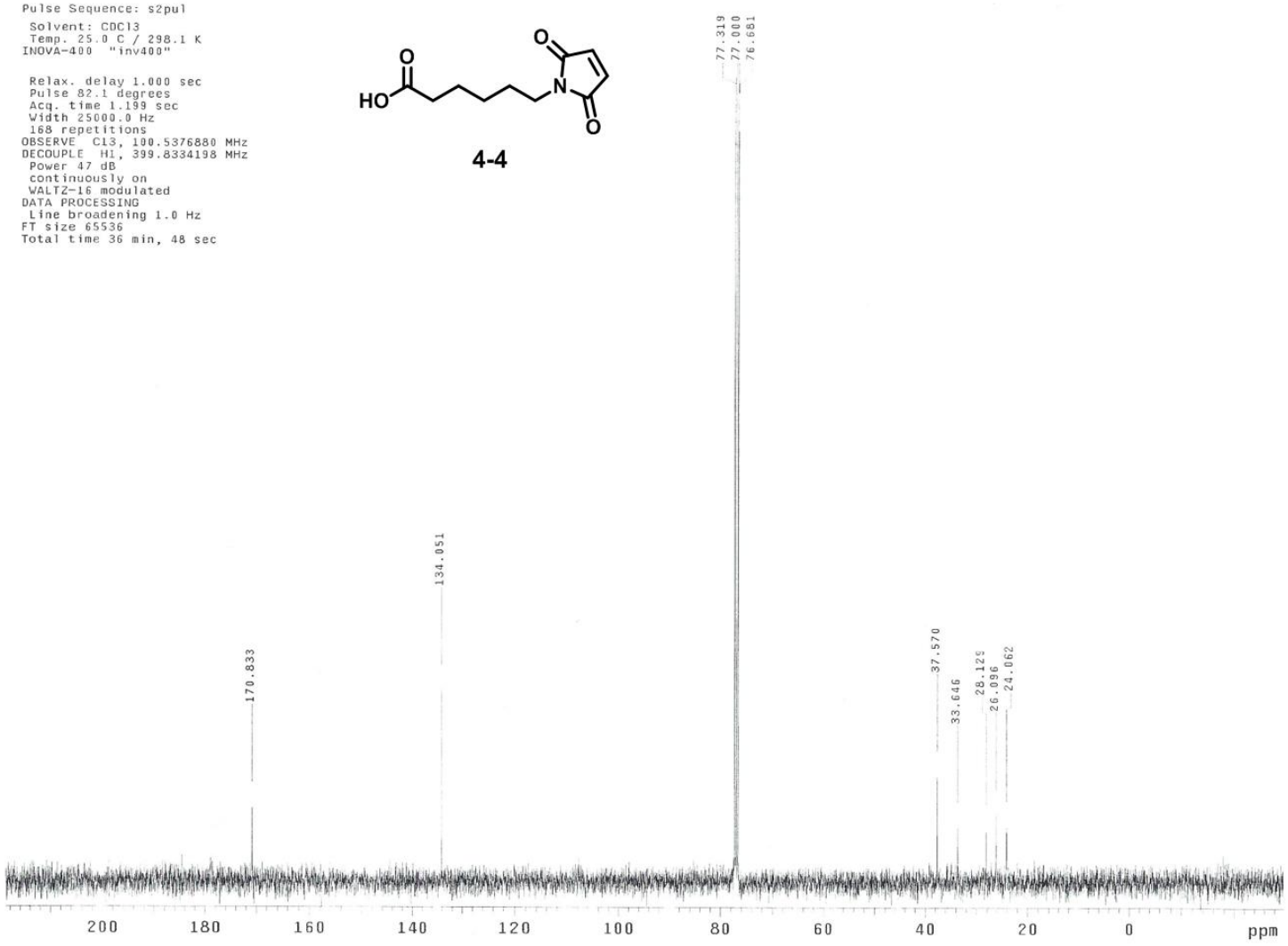
Pulse Sequence: s2pul
Solvent: CDCl3
Temp. 25.0 C / 298.1 K
INOVA-400 "inv400"
Relax. delay 1.000 sec
Pulse 82.1 degrees
Acq. time 1.199 sec
Width 25000.0 Hz
168 repetitions
OBSERVE C13, 100.5376880 MHz
DECOUPLE H1, 399.8334198 MHz
Power 47 dB
continuously on
WALTZ-16 modulated
DATA PROCESSING
Line broadening 1.0 Hz
FT size 65536
Total time 36 min, 48 sec
HO
O
O
N
O
4-4
77.319
77.000
76.681
170.833
134.051
37.570
33.646
28.125
26.096
24.062
200
180
160
140
120
100
80
60
40
20
0
ppm

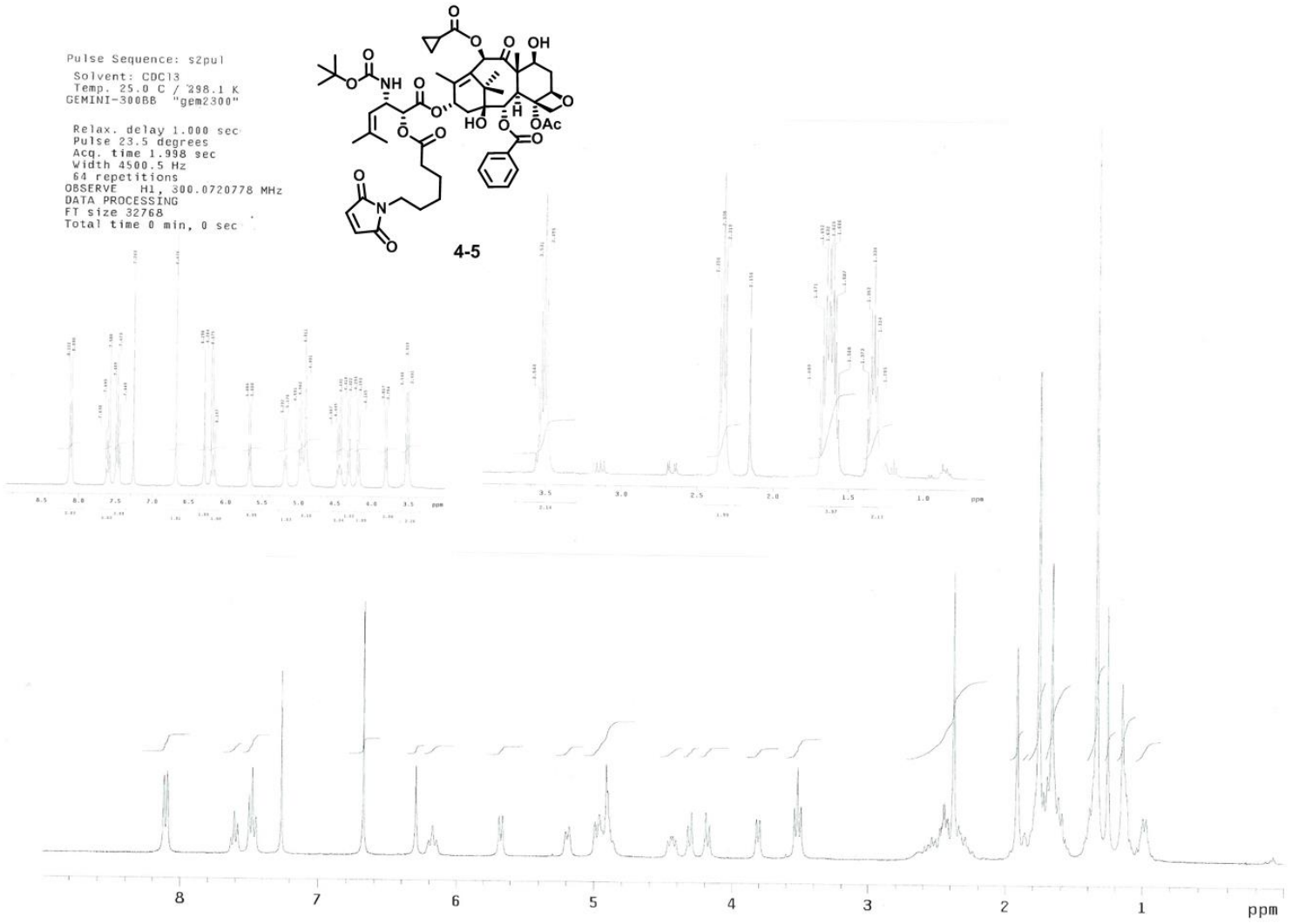
Pulse Sequence: s2pul
Solvent: CDCl3
Temp. 25.0 C / 298.1 K
GEMINI-300BB "gem2300"
Relax. delay 1.000 sec
Pulse 23.5 degrees
Acq. time 1.998 sec
Width 4500.5 Hz
64 repetitions
OBSERVE H1, 300.0720778 MHz
DATA PROCESSING
FT size 32768
Total time 0 min, 0 sec
4-5
ppm

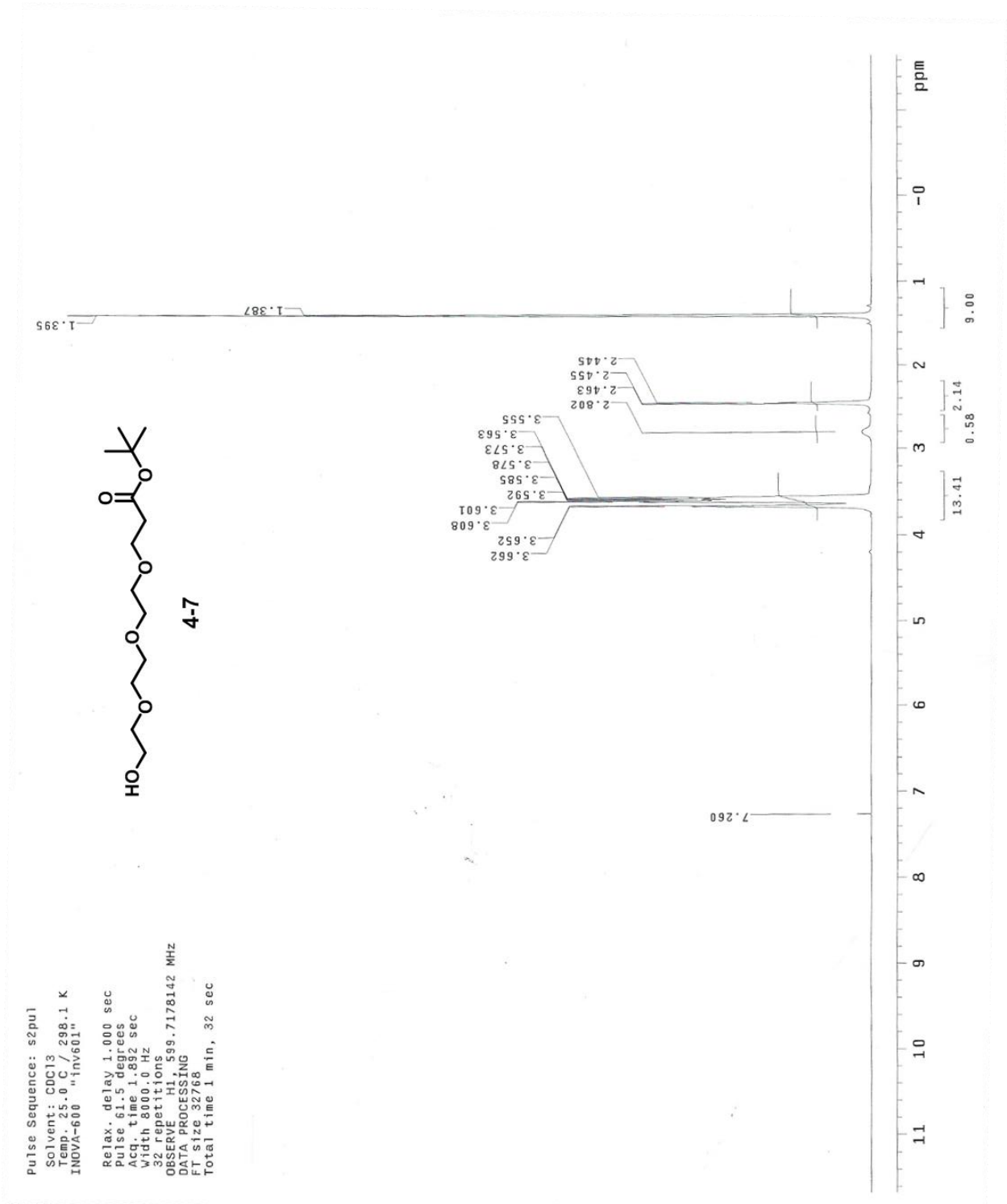
Pulse Sequence: s2pul
Solvent: CDCl3
Temp. 25.0 C / 298.1 K
INOVA-600 "inv601"
Relax. delay 1.000 sec
Pulse 61.5 degrees
Acq. time 1.892 sec
Width 8000.0 Hz
32 repetitions
OBSERVE H1, 599.7178142 MHz
DATA PROCESSING
FT size 32768
Total time 1 min, 32 sec
HO
4-7
1.395
1.387
2.802
2.463
2.455
2.445
3.662
3.652
3.608
3.601
3.592
3.585
3.578
3.573
3.563
3.555
7.260
13.41
2.14
0.58
9.00
ppm

Pulse Sequence: s2pul
Solvent: CDCl3
Temp. 25.0 C / 298.1 K
GEMINI-300BB "gem2300"

Relax. delay 1.000 sec
Pulse 7.8 degrees
Acq. time 1.998 sec
Width 4500.5 Hz
52 repetitions
OBSERVE H1, 300.0720781 MHz
DATA PROCESSING
FT size 32768
Total time 0 min, 0 sec

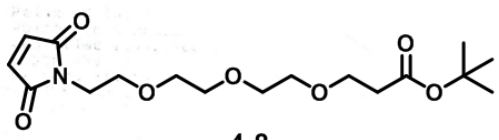

4-8

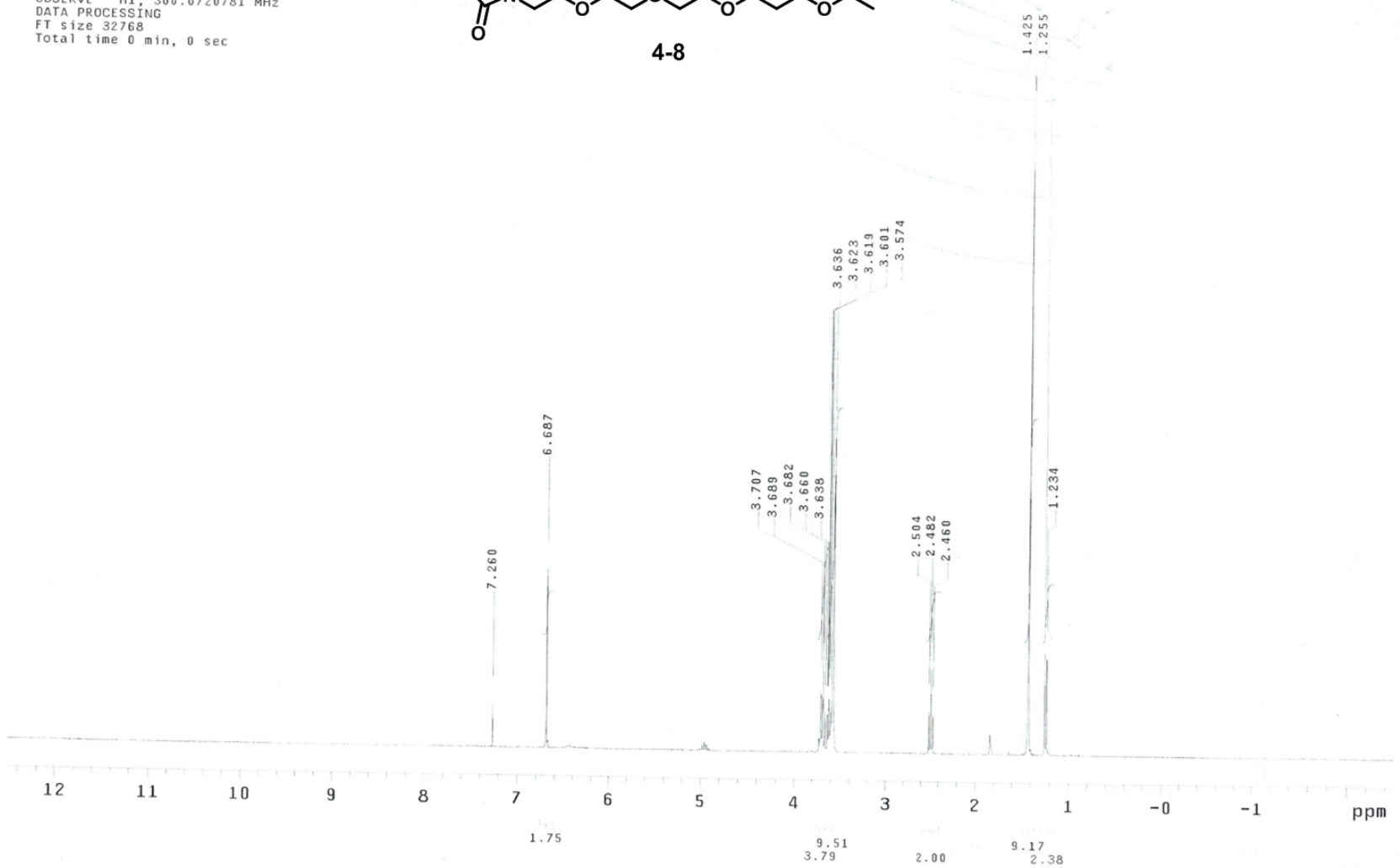

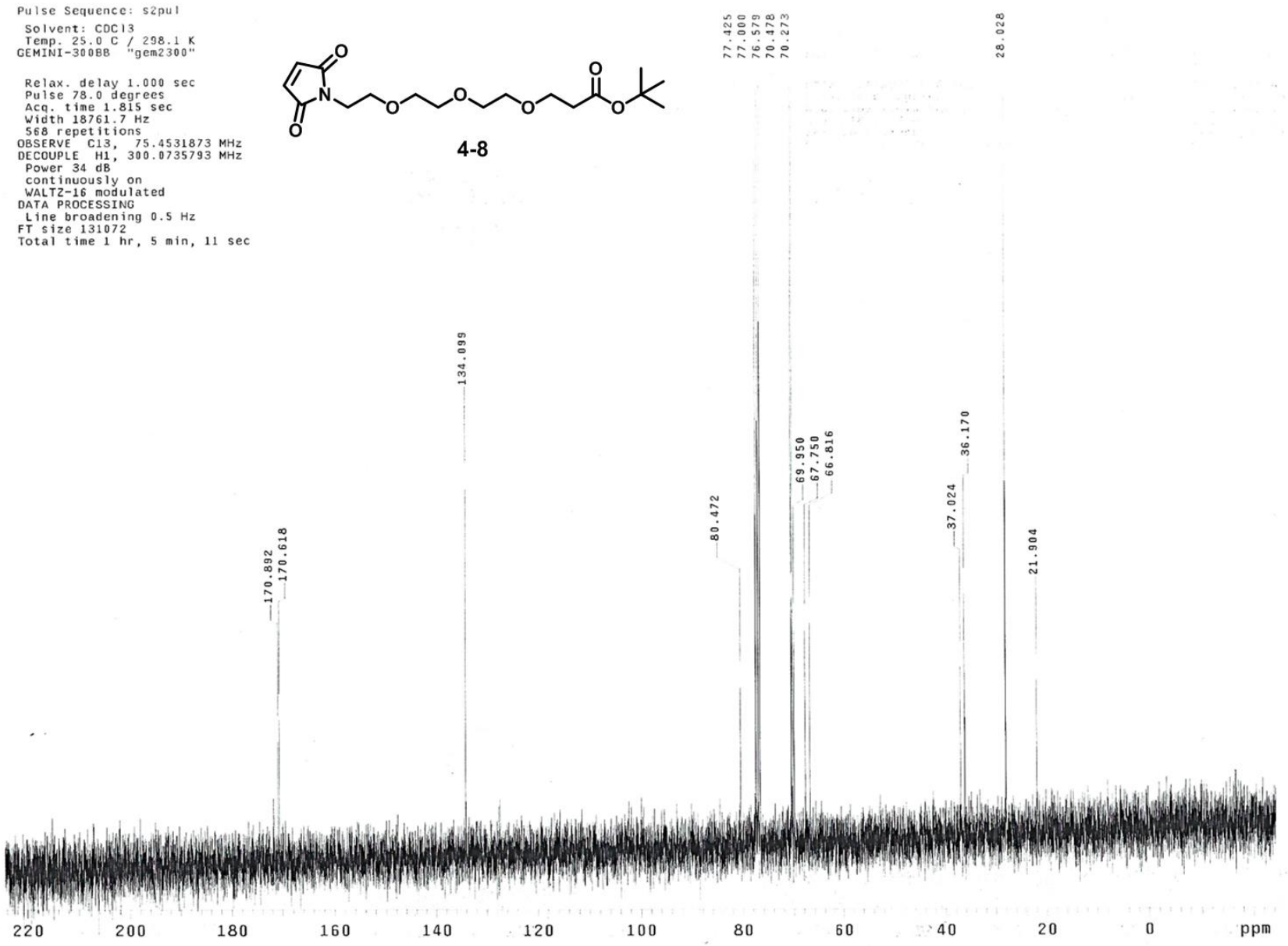
Pulse Sequence: s2pul
Solvent: CDCl3
Temp. 25.0 C / 298.1 K
GEMINI-300BB "gem2300"
Relax. delay 1.000 sec
Pulse 78.0 degrees
Acq. time 1.815 sec
Width 18761.7 Hz
568 repetitions
OBSERVE C13, 75.4531873 MHz
DECOUPLE H1, 300.0735793 MHz
Power 34 dB
continuously on
WALTZ-16 modulated
DATA PROCESSING
Line broadening 0.5 Hz
FT size 131072
Total time 1 hr, 5 min, 11 sec
4-8
77.425
77.000
76.579
70.478
70.273
28.028
170.892
170.618
134.099
80.472
69.950
67.750
66.816
37.024
36.170
21.904
220
200
180
160
140
120
100
80
60
40
20
0
ppm

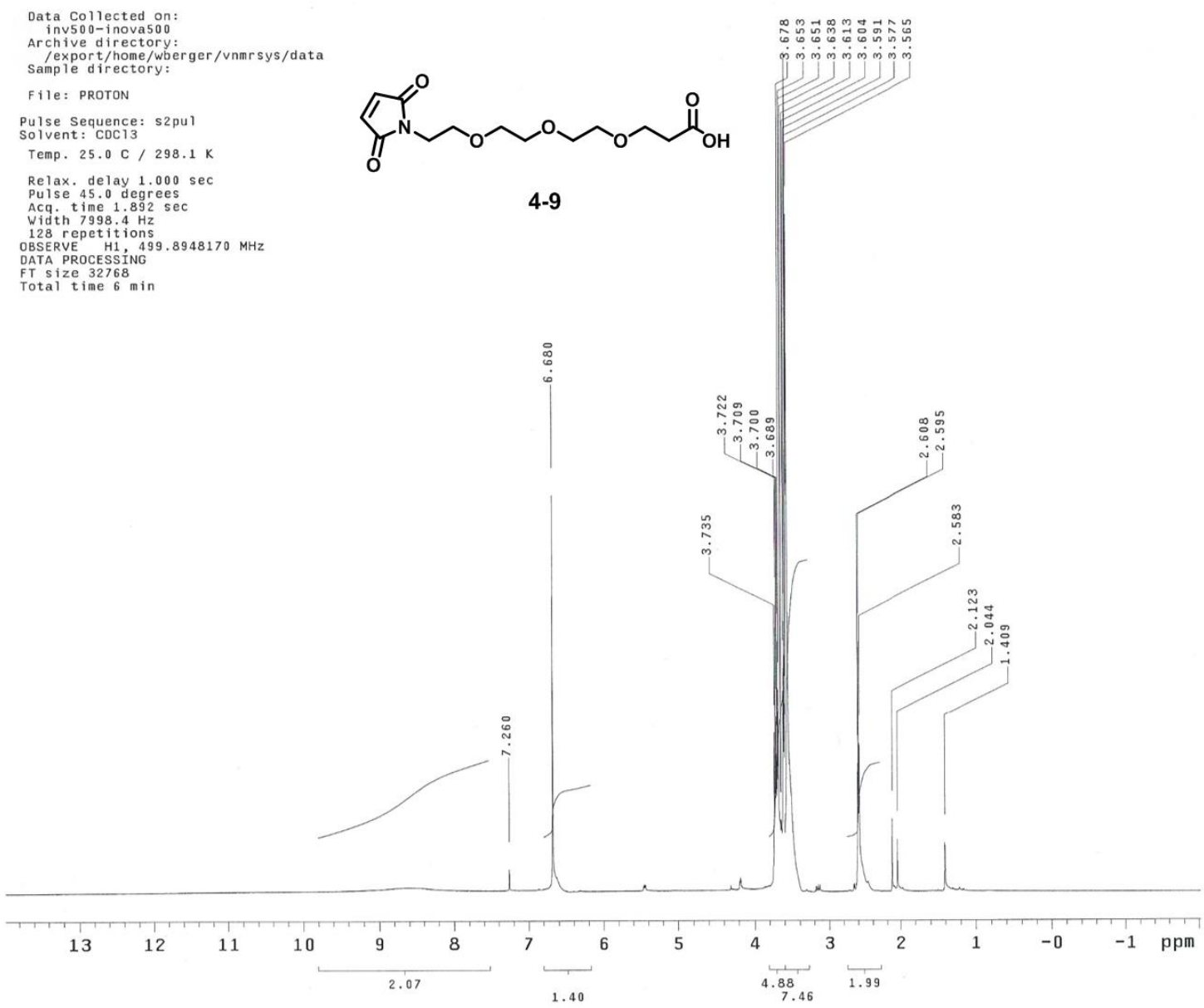
Data Collected on:
inv500-inova500
Archive directory:
/export/home/wberger/vnmrsys/data
Sample directory:
File: PROTON
Pulse Sequence: s2pul
Solvent: CDCl3
Temp. 25.0 C / 298.1 K
Relax. delay 1.000 sec
Pulse 45.0 degrees
Acq. time 1.892 sec
Width 7998.4 Hz
128 repetitions
OBSERVE H1, 499.8948170 MHz
DATA PROCESSING
FT size 32768
Total time 6 min
4-9
3.678
3.653
3.651
3.638
3.613
3.604
3.591
3.577
3.565
6.680
3.722
3.709
3.700
3.689
2.608
2.595
3.735
2.583
2.123
2.044
1.409
7.260
13
12
11
10
9
8
7
6
5
4
3
2
1
-0
-1
ppm
2.07
1.40
4.88
7.46
1.99

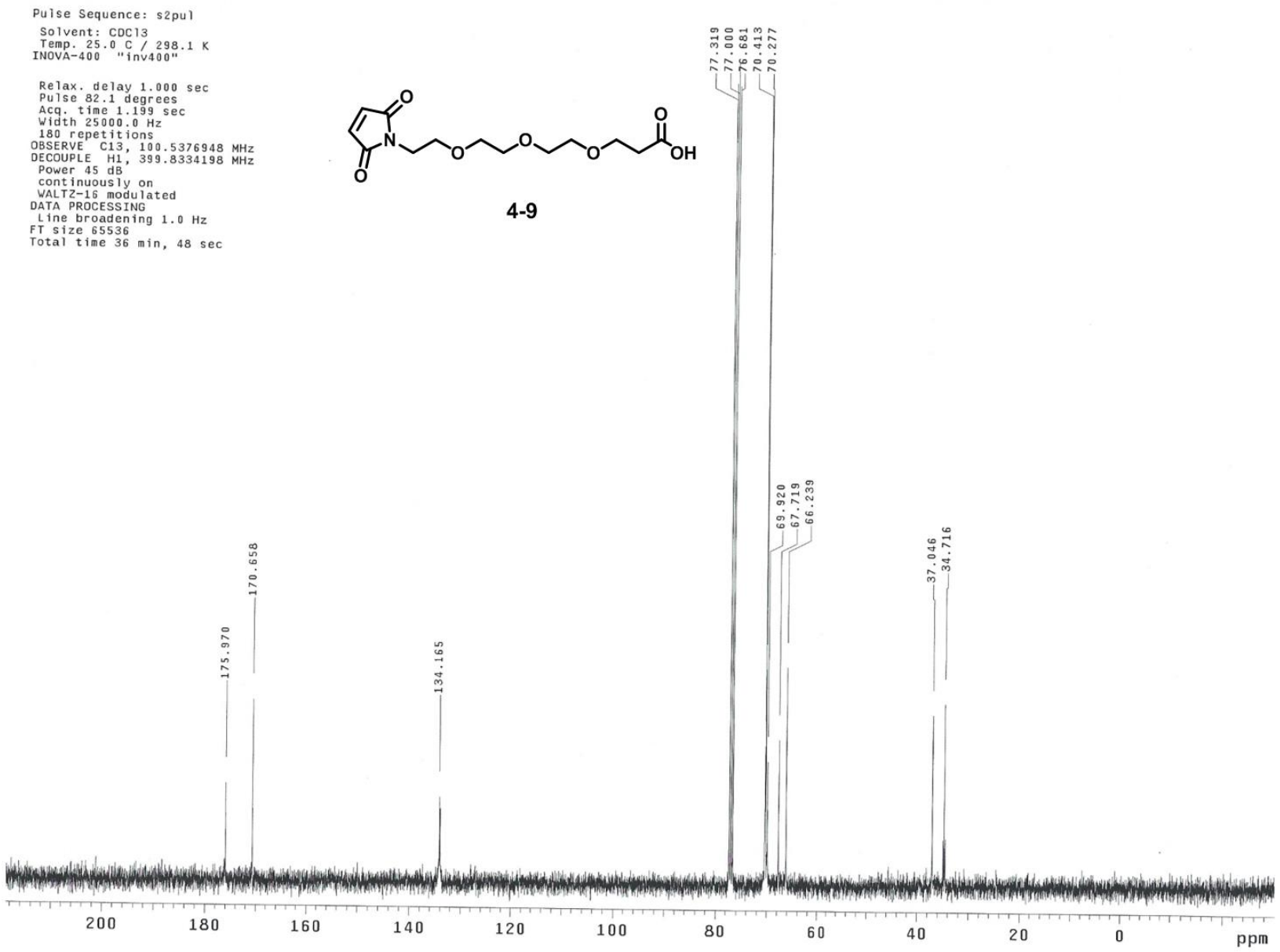
Pulse Sequence: s2pul
Solvent: CDCl3
Temp. 25.0 C / 298.1 K
INOVA-400 "inv400"
Relax. delay 1.000 sec
Pulse 82.1 degrees
Acq. time 1.199 sec
Width 25000.0 Hz
180 repetitions
OBSERVE C13, 100.5376948 MHz
DECOUPLE H1, 399.8334198 MHz
Power 45 dB
continuously on
WALTZ-16 modulated
DATA PROCESSING
Line broadening 1.0 Hz
FT size 65536
Total time 36 min, 48 sec
4-9
77.319
77.000
76.681
70.413
70.277
69.920
67.719
66.239
37.046
34.716
175.970
170.658
134.165
200
180
160
140
120
100
80
60
40
20
0
ppm

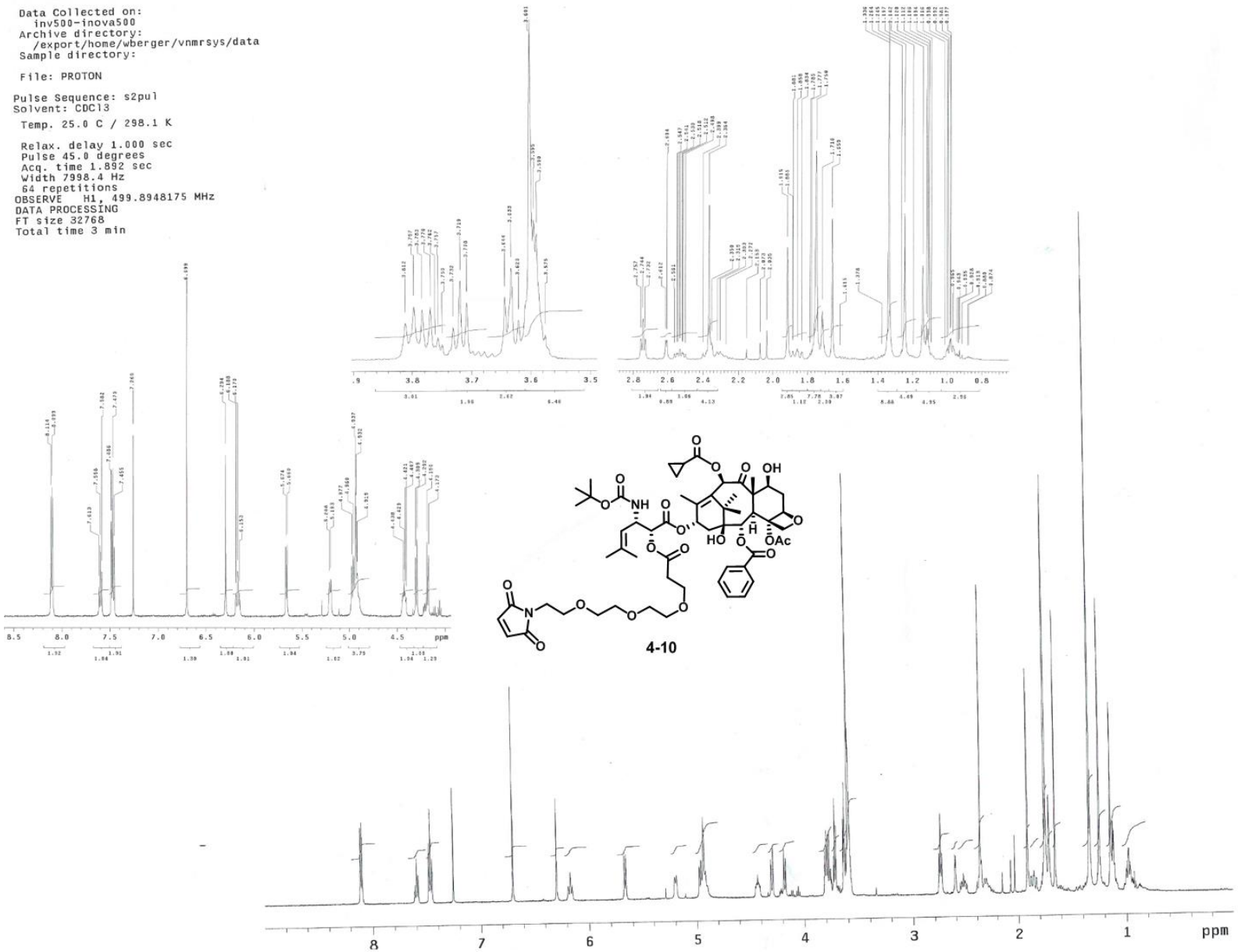
Data Collected on:
inv500-inova500
Archive directory:
/export/home/wberger/vnmrsys/data
Sample directory:
File: PROTON
Pulse Sequence: s2pul
Solvent: CDCl3
Temp. 25.0 C / 298.1 K
Relax. delay 1.000 sec
Pulse 45.0 degrees
Acq. time 1.892 sec
Width 7998.4 Hz
64 repetitions
OBSERVE H1, 499.8948175 MHz
DATA PROCESSING
FT size 32768
Total time 3 min
4-10
ppm

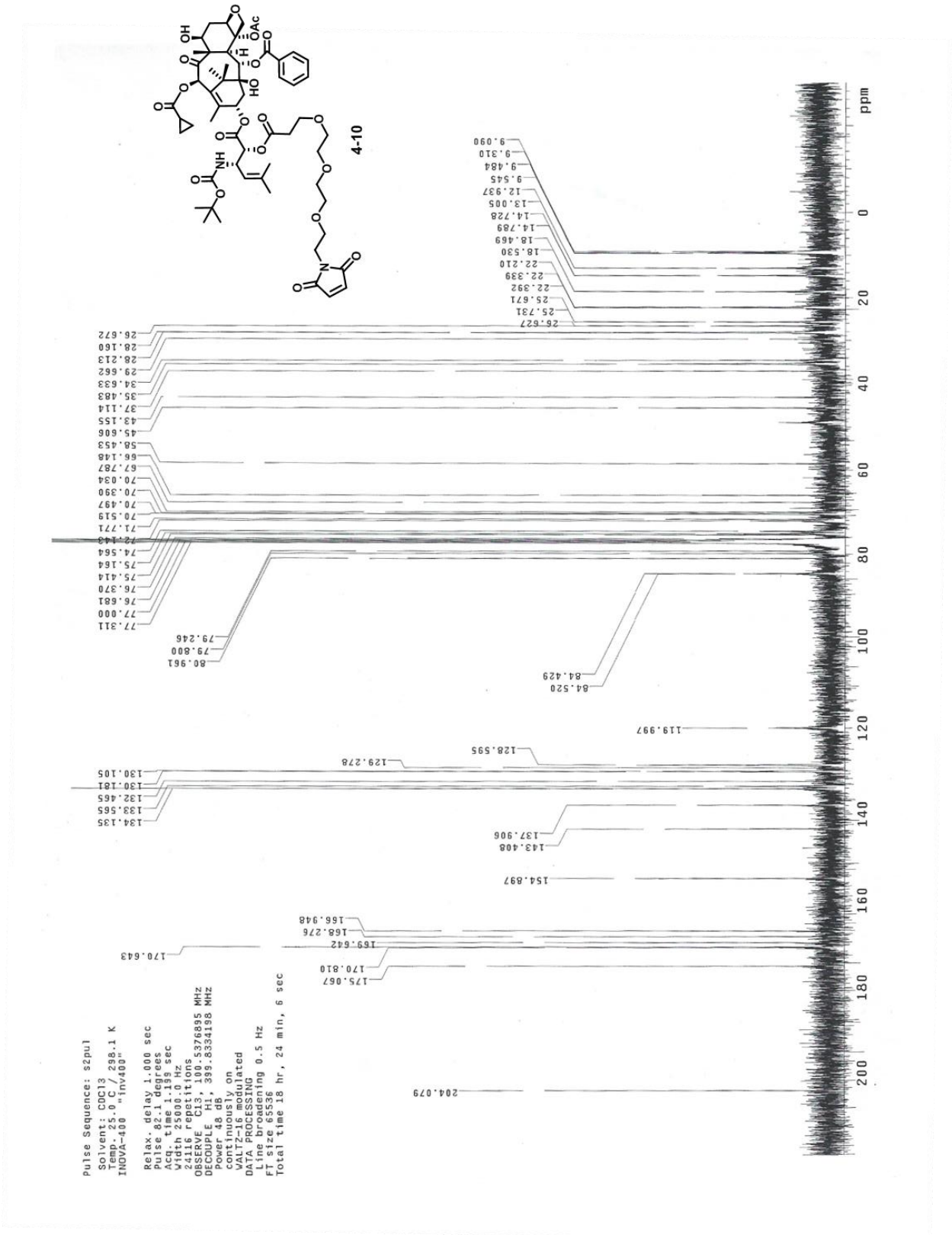
4-10
Pulse Sequence: s2pul
Solvent: CDCl3
Temp: 25.0 C / 298.1 K
INOVA-400 "inv400"
Relax. delay 1.000 sec
Pulse 82.1 degrees
Acq. time 1.199 sec
Width 25000.0 Hz
24116 repetitions
OBSERVE C13, 100.5376895 MHz
DECOUPLE H1, 399.8334198 MHz
Power 48 dB
continuously on
WALTZ16 modulated
DATA PROCESSING
Line broadening 0.5 Hz
FT size 65536
Total time 18 hr, 24 min, 6 sec
ppm

Appendix Chapter 5

STANDARD PROTON PARAMETERS

Data Collected on:
inv500-inova500
Archive directory:
/export/home/wberger/vnmrsys/data
Sample directory:

File: PROTON

Pulse Sequence: s2pul
Solvent: DMSO
Ambient temperature

Relax. delay 1.000 sec
Pulse 45.0 degrees
Acq. time 1.892 sec
Width 7998.4 Hz
64 repetitions
OBSERVE H1, 499.8971889 MHz
DATA PROCESSING
FT size 32768
Total time 4 min

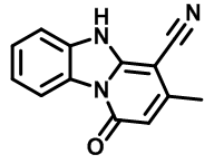

5-1

WB-6-21-12-SB11proton

Pulse Sequence: s2pul

Solvent: CDCl3
Temp. 25.0 C / 298.1 K
GEMINI-300BB "gem2300"

Relax. delay 1.000 sec
Pulse 23.5 degrees
Acq. time 1.998 sec
Width 4500.5 Hz
84 repetitions
OBSERVE H1, 300.0720783 MHz
DATA PROCESSING
FT size 32768
Total time 0 min, 0 sec

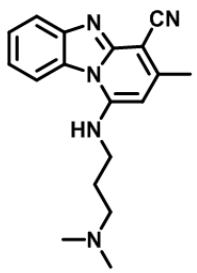

5-3

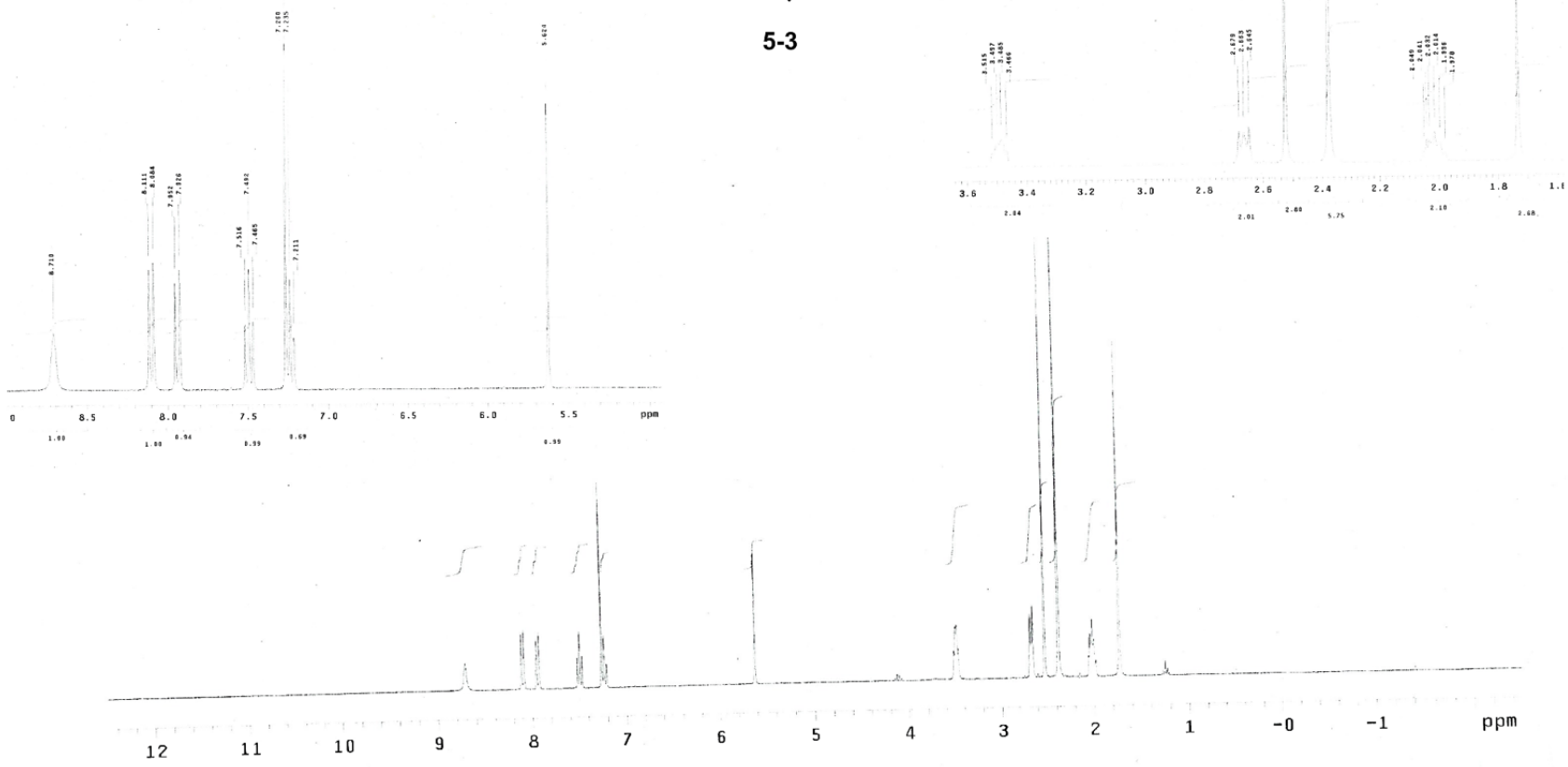

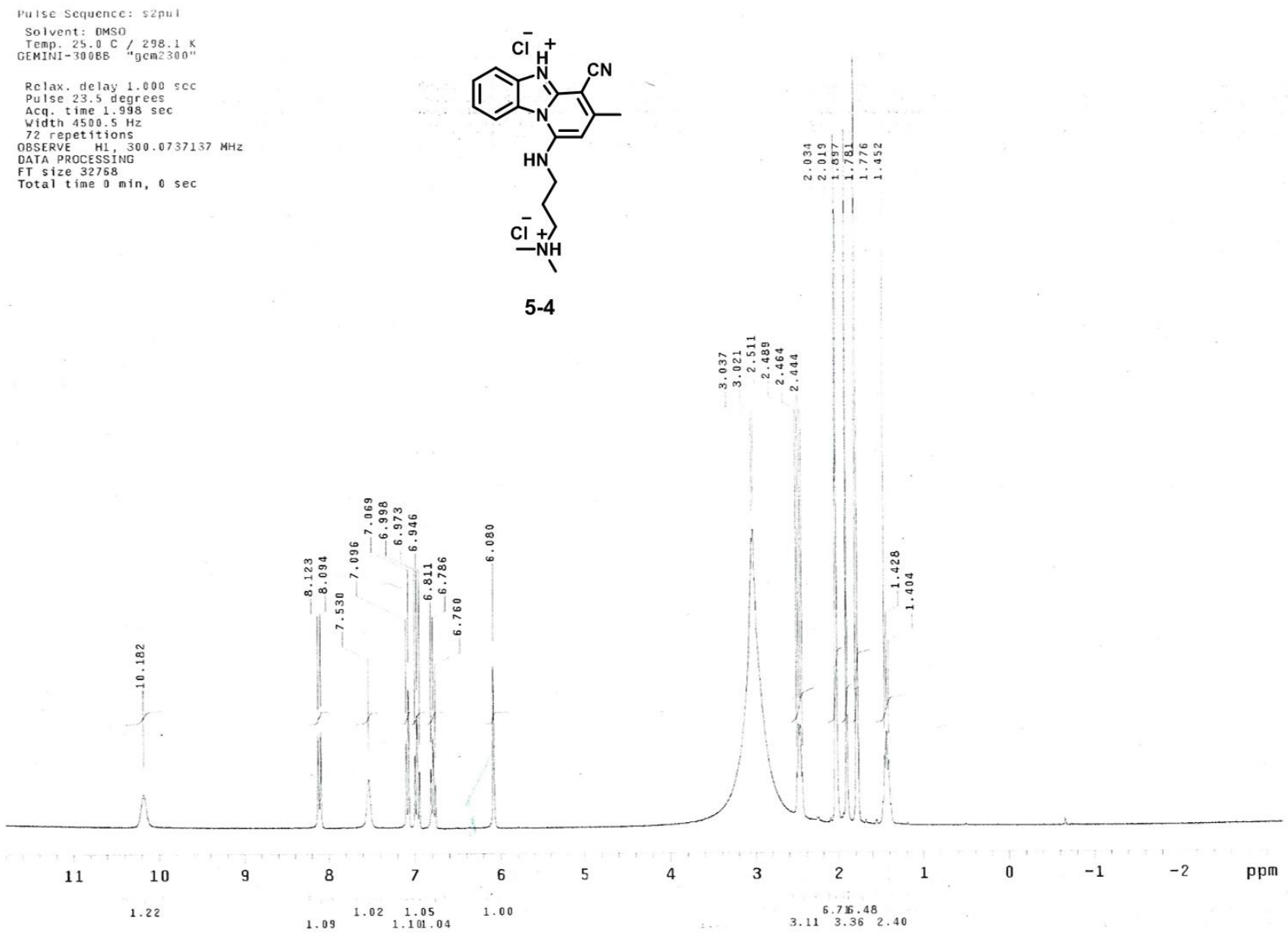
Pulse Sequence: s2pul
Solvent: DMSO
Temp. 25.0 C / 298.1 K
GEMINI-300BB "gem2300"
Relax. delay 1.000 sec
Pulse 23.5 degrees
Acq. time 1.998 sec
Width 4500.5 Hz
72 repetitions
OBSERVE H1, 300.0737137 MHz
DATA PROCESSING
FT size 32768
Total time 0 min, 0 sec
Cl
H
N
CN
N
HN
Cl
NH
5-4
10.182
8.123
8.094
7.530
7.096
7.069
6.998
6.973
6.946
6.811
6.786
6.760
6.080
3.037
3.021
2.511
2.488
2.464
2.444
2.034
2.019
1.697
1.781
1.776
1.452
1.428
1.404
11
10
9
8
7
6
5
4
3
2
1
0
-1
-2
ppm
1.22
1.09
1.02
1.05
1.10
1.04
1.00
6.71
6.48
3.11
3.36
2.40

2,4-dichlorocinnamic hydroxamate

Pulse Sequence: s2pul

Solvent: DMSO
Temp. 25.0 C / 298.1 K
GEMINI-300BB "gem2300"

Relax. delay 1.000 sec
Pulse 23.5 degrees
Acq. time 1.998 sec
Width 4500.5 Hz
92 repetitions
OBSERVE H1, 300.0735008 MHz
DATA PROCESSING
FT size 32768
Total time 5 min, 35 sec

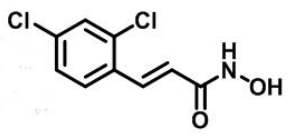

5-5

Appendix Chapter 6

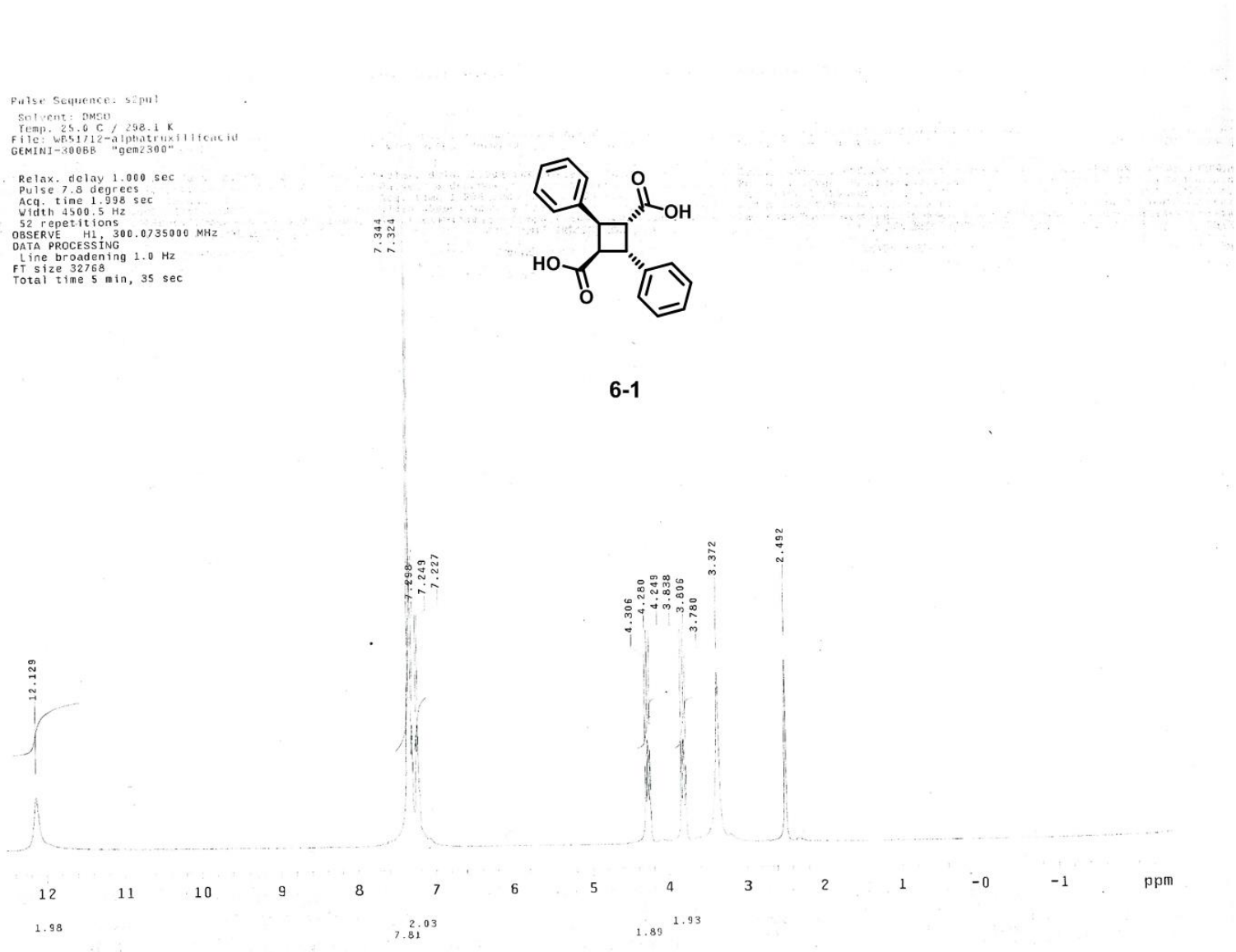
Pulse Sequence: s2pul
Solvent: DMSO
Temp. 25.0 C / 298.1 K
File: WB51712-alphatruxillicacid
GEMINI-300BB "gem2300"
Relax. delay 1.000 sec
Pulse 7.8 degrees
Acq. time 1.998 sec
Width 4500.5 Hz
52 repetitions
OBSERVE H1, 300.0735000 MHz
DATA PROCESSING
Line broadening 1.0 Hz
FT size 32768
Total time 5 min, 35 sec
HO
O
OH
O
6-1
12.129
7.344
7.324
7.298
7.249
7.227
4.306
4.280
4.249
3.838
3.806
3.780
3.372
2.492
12
11
10
9
8
7
6
5
4
3
2
1
-0
-1
ppm
1.98
2.03
7.81
1.89
1.93

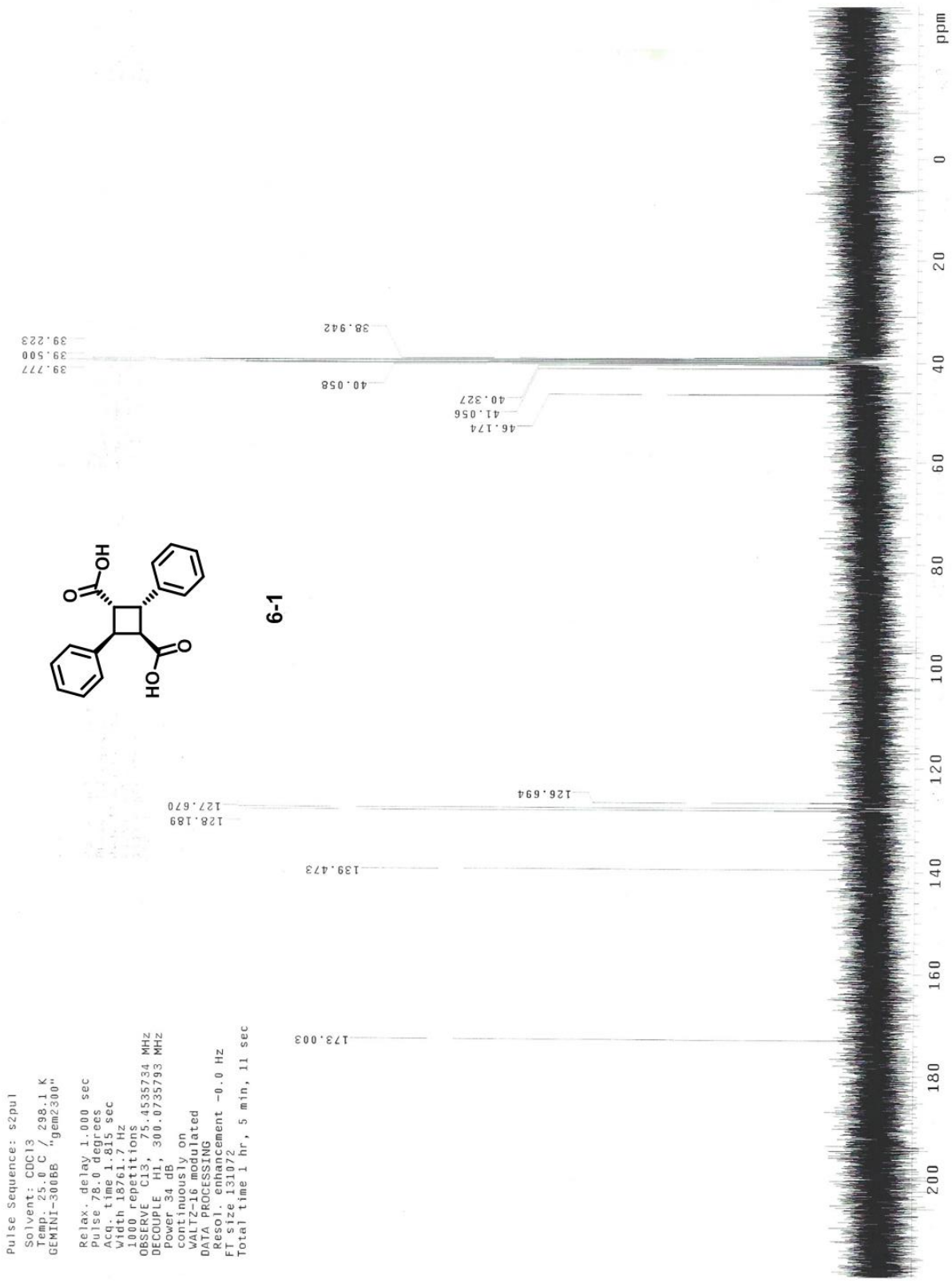
Pulse Sequence: s2pul
Solvent: CDCl3
Temp. 25.0 C / 298.1 K
GEMINI-300BB "gem2300"
Relax. delay 1.000 sec
Pulse 78.0 degrees
Acq. time 1.815 sec
Width 18761.7 Hz
1000 repetitions
OBSERVE C13, 75.4535734 MHz
DECOUPLE H1, 300.0735793 MHz
Power 34 dB
continuously on
WALTZ-16 modulated
DATA PROCESSING
Resol. enhancement -0.0 Hz
FT size 131072
Total time 1 hr, 5 min, 11 sec
OH
O
HO
O
6-1
173.003
139.473
128.189
127.670
126.694
46.174
41.056
40.327
40.058
38.942
39.777
39.500
39.223
ppm
200
180
160
140
120
100
80
60
40
20
0

Data Collected on:
inv500-inova500
Archive directory:
/export/home/wberger/vnmrsys/data
Sample directory:

File: PROTON

Pulse Sequence: s2pul
Solvent: DMSO

Relax. delay 1.000 sec
Pulse 45.0 degrees
Acq. time 1.892 sec
Width 7998.4 Hz
100 repetitions
OBSERVE H1, 499.8971889 MHz
DATA PROCESSING
FT size 32768
Total time 4 min

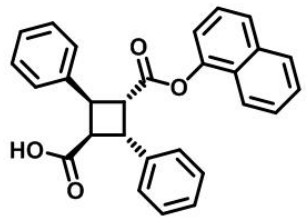

6-2

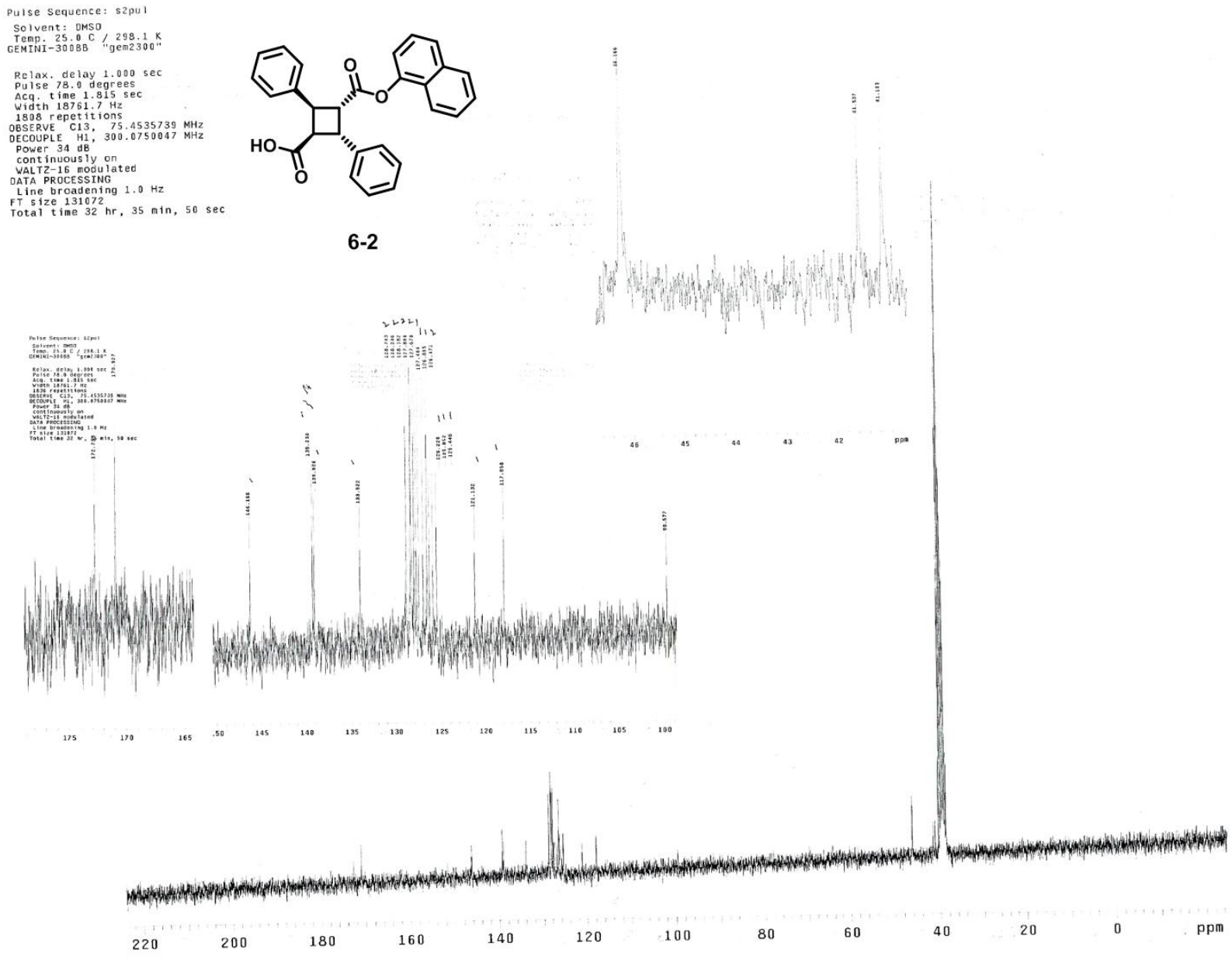
Pulse Sequence: s2pul
Solvent: DMSO
Temp. 25.0 C / 298.1 K
GEMINI-300BB "gem2300"
Relax. delay 1.000 sec
Pulse 78.0 degrees
Acq. time 1.815 sec
Width 18761.7 Hz
1808 repetitions
OBSERVE C13, 75.4535739 MHz
DECOUPLE H1, 300.0750047 MHz
Power 34 dB
continuously on
WALTZ-16 modulated
DATA PROCESSING
Line broadening 1.0 Hz
FT size 131072
Total time 32 hr, 35 min, 50 sec
HO
O
O
O
6-2
ppm

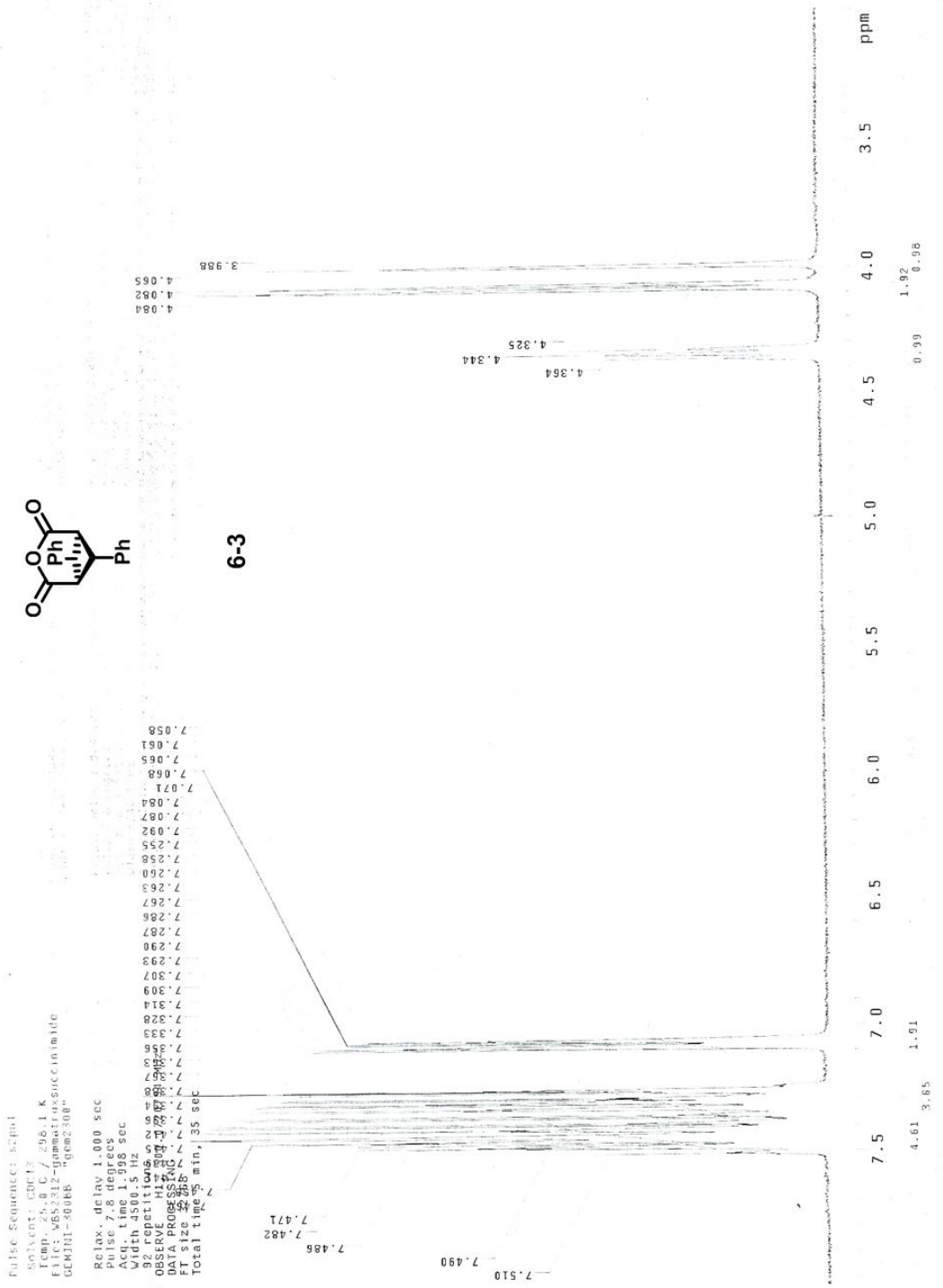
6-3
Ph
Ph
O
O
O
Pulse Sequence: s2pul
Solvent: CDCl3
Temp. 25.0 C / 298.1 K
File: W652312-gammatruxsuccinimide
GEMINI-300BB "gem2300"
Relax. delay 1.000 sec
Pulse 7.8 degrees
Acq. time 1.998 sec
Width 4500.5 Hz
92 repetitions
OBSERVE H1, 300.1 MHz
DATA PROCESSING
FT size 65536
Total time 5 min, 35 sec
7.058
7.061
7.065
7.068
7.071
7.084
7.087
7.092
7.255
7.258
7.260
7.263
7.267
7.286
7.287
7.290
7.293
7.307
7.309
7.314
7.328
7.333
7.486
7.482
7.471
7.490
7.510
4.084
4.082
4.065
3.988
4.364
4.344
4.325
7.5
7.0
6.5
6.0
5.5
5.0
4.5
4.0
3.5
ppm
4.61
3.65
1.91
0.99
1.92
0.98

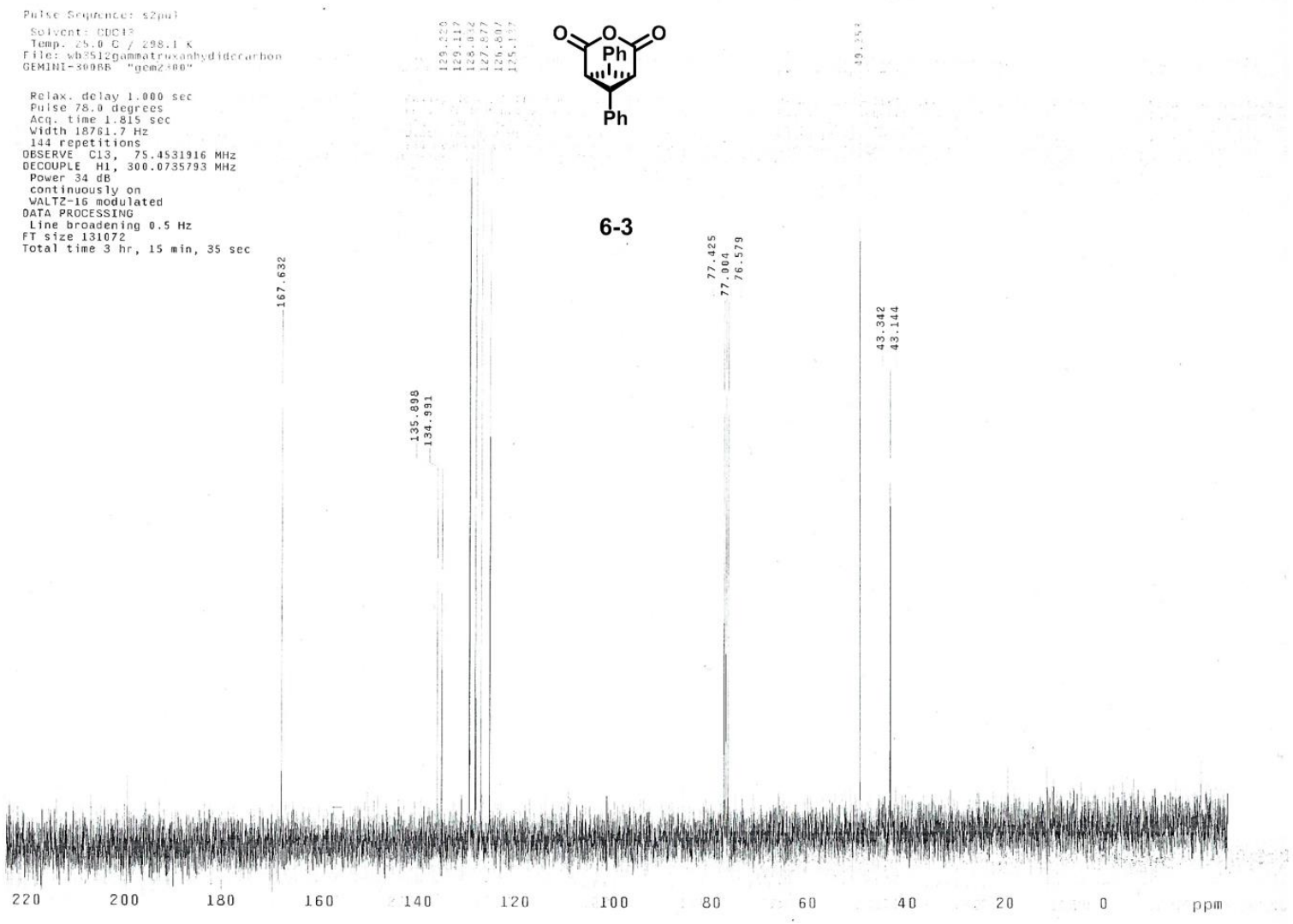
Pulse Sequence: s2pul
Solvent: CDCl3
Temp. 25.0 C / 298.1 K
File: wb2512gammatruxanhydridecarbon
GEMINI-300BB "gemz300"
Relax. delay 1.000 sec
Pulse 78.0 degrees
Acq. time 1.815 sec
Width 18761.7 Hz
144 repetitions
OBSERVE C13, 75.4531916 MHz
DECOUPLE H1, 300.0735793 MHz
Power 34 dB
continuously on
WALTZ-16 modulated
DATA PROCESSING
Line broadening 0.5 Hz
FT size 131072
Total time 3 hr, 15 min, 35 sec
O
O
O
Ph
Ph
6-3
167.632
135.898
134.991
129.220
129.117
128.034
127.877
126.807
125.197
77.425
77.004
76.579
49.352
43.342
43.144
220
200
180
160
140
120
100
80
60
40
20
0
ppm

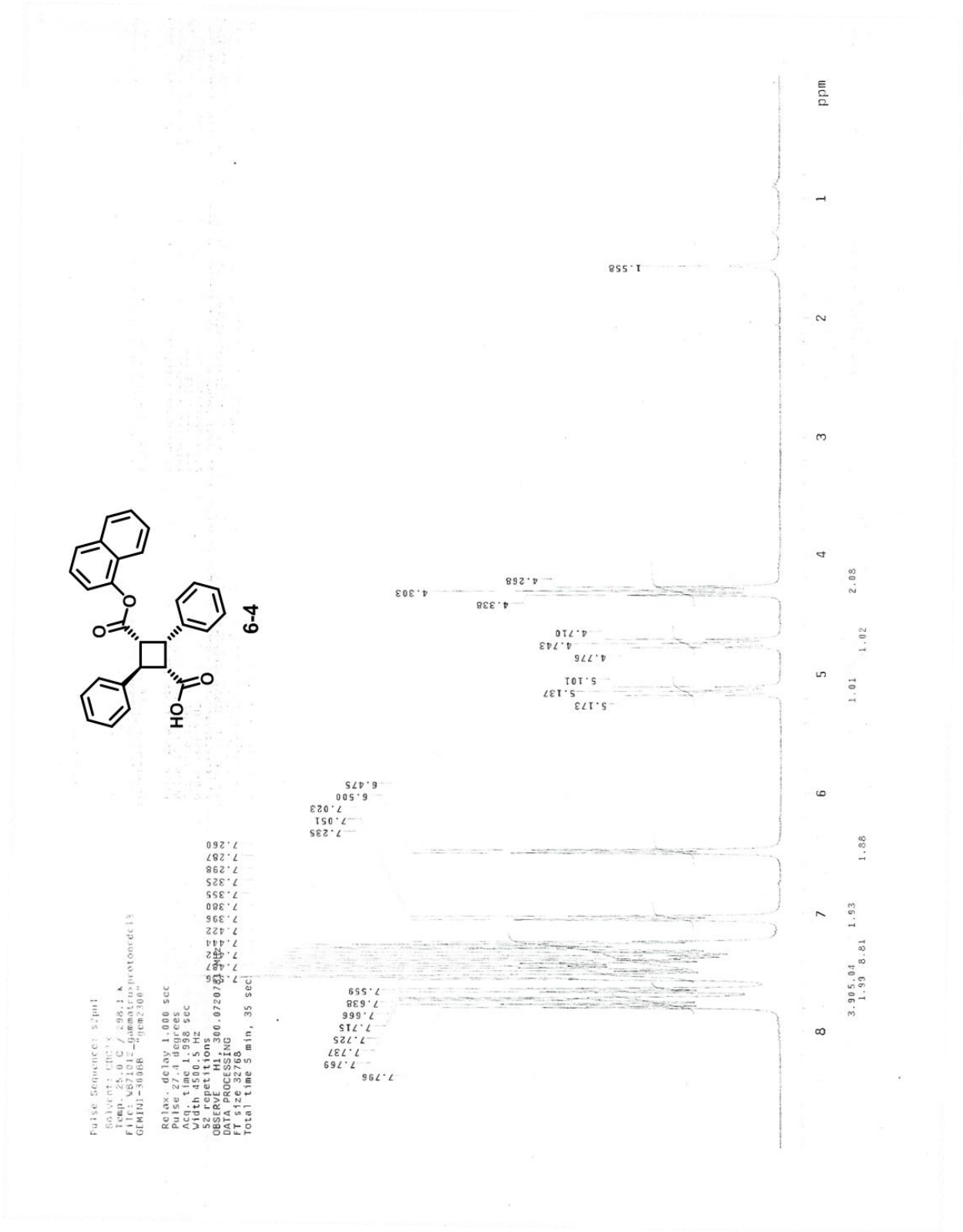
6-4
HO
O
Pulse Sequence: s2pul
Solvent: CDCl3
Temp. 25.0 C / 298.1 K
File: WB71012_gammatrans4ketoacid3
GEMINI-300BB "gem2300"
Relax. delay 1.000 sec
Pulse 27.4 degrees
Acq. time 1.998 sec
Width 4500.5 Hz
52 repetitions
OBSERVE H1, 300.0720783 MHz
DATA PROCESSING
FT size 32768
Total time 5 min, 35 sec
7.795
7.769
7.737
7.725
7.715
7.666
7.638
7.559
7.447
7.422
7.396
7.380
7.355
7.325
7.298
7.287
7.260
7.235
7.051
7.023
6.500
6.475
5.173
5.137
5.101
4.776
4.743
4.710
4.338
4.303
4.268
1.558
3.90 5.04
1.99 8.81
1.93
1.88
1.01
1.02
2.08
ppm

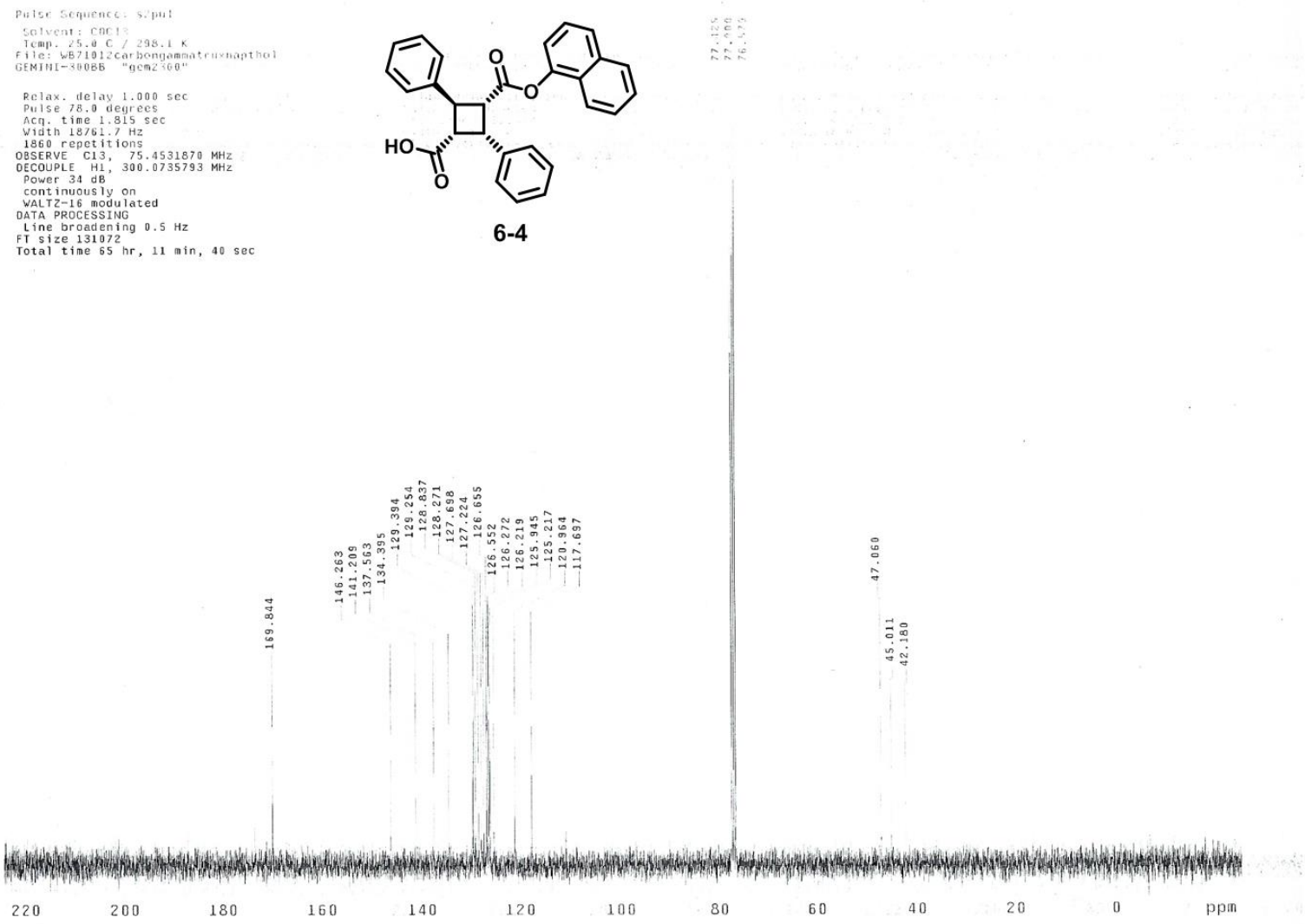
Pulse Sequence: s2pul
Solvent: CDCl3
Temp. 25.0 C / 298.1 K
File: WB71012carbongammatrexnapthol
GEMINI-300BB "gem2300"
Relax. delay 1.000 sec
Pulse 78.0 degrees
Acq. time 1.815 sec
Width 18761.7 Hz
1860 repetitions
OBSERVE C13, 75.4531870 MHz
DECOUPLE H1, 300.0735793 MHz
Power 34 dB
continuously on
WALTZ-16 modulated
DATA PROCESSING
Line broadening 0.5 Hz
FT size 131072
Total time 65 hr, 11 min, 40 sec
HO
O
O
O
6-4
77.325
77.060
76.479
169.844
146.263
141.209
137.563
134.395
129.394
129.254
128.837
128.271
127.698
127.224
126.655
126.552
126.272
126.219
125.945
125.217
120.964
117.697
47.060
45.011
42.180
220
200
180
160
140
120
100
80
60
40
20
0
ppm